frontiers | Research Topics

The function of Schwann cells in peripheral nervous system

Edited by
Bo He, Ji-Fan Hu and Zhaowei Zhu

Published in
Frontiers in Cellular Neuroscience

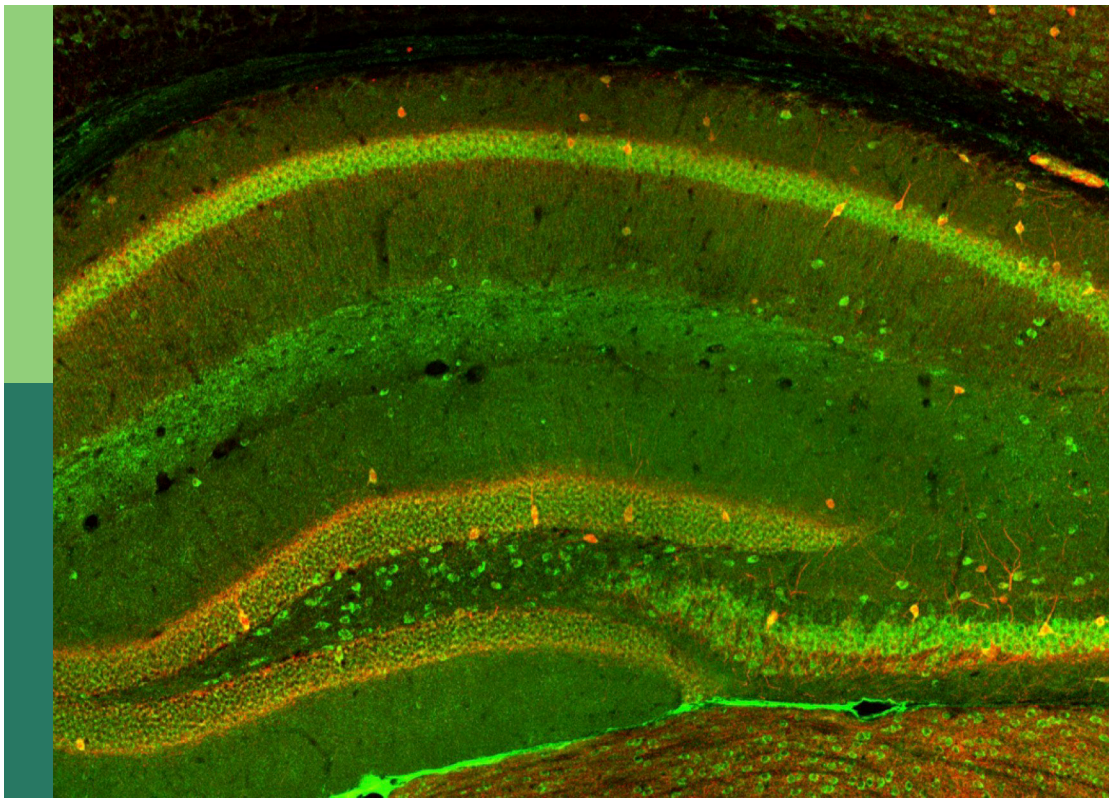

ISSN 1664-8714
ISBN 978-2-83251-399-6
DOI 10.3389/978-2-83251-399-6

About Frontiers

Frontiers is more than just an open access publisher of scholarly articles: it is a pioneering approach to the world of academia, radically improving the way scholarly research is managed. The grand vision of Frontiers is a world where all people have an equal opportunity to seek, share and generate knowledge. Frontiers provides immediate and permanent online open access to all its publications, but this alone is not enough to realize our grand goals.

Frontiers journal series

The Frontiers journal series is a multi-tier and interdisciplinary set of open-access, online journals, promising a paradigm shift from the current review, selection and dissemination processes in academic publishing. All Frontiers journals are driven by researchers for researchers; therefore, they constitute a service to the scholarly community. At the same time, the *Frontiers journal series* operates on a revolutionary invention, the tiered publishing system, initially addressing specific communities of scholars, and gradually climbing up to broader public understanding, thus serving the interests of the lay society, too.

Dedication to quality

Each Frontiers article is a landmark of the highest quality, thanks to genuinely collaborative interactions between authors and review editors, who include some of the world's best academicians. Research must be certified by peers before entering a stream of knowledge that may eventually reach the public - and shape society; therefore, Frontiers only applies the most rigorous and unbiased reviews. Frontiers revolutionizes research publishing by freely delivering the most outstanding research, evaluated with no bias from both the academic and social point of view. By applying the most advanced information technologies, Frontiers is catapulting scholarly publishing into a new generation.

What are Frontiers Research Topics?

Frontiers Research Topics are very popular trademarks of the *Frontiers journals series*: they are collections of at least ten articles, all centered on a particular subject. With their unique mix of varied contributions from Original Research to Review Articles, Frontiers Research Topics unify the most influential researchers, the latest key findings and historical advances in a hot research area.

Find out more on how to host your own Frontiers Research Topic or contribute to one as an author by contacting the Frontiers editorial office: frontiersin.org/about/contact

The function of Schwann cells in peripheral nervous system

Topic editors

Bo He — Third Affiliated Hospital of Sun Yat-sen University, China

Ji-Fan Hu — Jilin University, China

Zhaowei Zhu — The First Affiliated Hospital of Sun Yat-sen University, China

Citation

He, B., Hu, J.-F., Zhu, Z., eds. (2023). *The function of Schwann cells in peripheral nervous system*. Lausanne: Frontiers Media SA. doi: 10.3389/978-2-83251-399-6

Table of contents

frontiers | Frontiers in Cellular Neuroscience

TYPE Editorial
PUBLISHED 09 January 2023
DOI 10.3389/fncel.2022.1129560

OPEN ACCESS

EDITED AND REVIEWED BY
Yannick Poitelon,
Albany Medical College, United States

*CORRESPONDENCE
Bo He
✉ hebodoc@aliyun.com

SPECIALTY SECTION
This article was submitted to Non-Neuronal Cells, a section of the journal Frontiers in Cellular Neuroscience

RECEIVED 22 December 2022
ACCEPTED 23 December 2022
PUBLISHED 09 January 2023

CITATION
He B, Hu J and Zhu Z (2023) Editorial: The function of Schwann cells in peripheral nervous system. *Front. Cell. Neurosci.* 16:1129560. doi: 10.3389/fncel.2022.1129560

Editorial: The function of Schwann cells in peripheral nervous system

Bo He[1]*, Jifan Hu[2,3] and Zhaowei Zhu[4]

[1]Joint and Orthopaedics Trauma, Department of Orthopedics, The Third Affiliated Hospital of Sun Yat-sen University, Guangzhou, China, [2]VA Palo Alto Health Care System, Stanford University Medical School, Palo Alto, CA, United States, [3]Key Laboratory of Organ Regeneration and Transplantation of Ministry of Education, Cancer Center, The First Hospital of Jilin University, Changchun, Jilin, China, [4]Department of Plastic Surgery, The First Affiliated Hospital of Sun Yat-sen University, Guangzhou, China

KEYWORDS

Schwann cells, Schwann-like cells, peripheral nerve, nerve regeneration, nerve injury, stem cells, tissue engineering

Editorial on the Research Topic
The function of Schwann cells in peripheral nervous system

It is generally believed that the decline in the capacity of peripheral nerve regeneration relies on the slow regeneration of neuronal axons. However, Painter et al. believed that the key factor that affects mammalian peripheral nerve regeneration was not the neuron itself. Instead, Schwann Cells (SCs) played an important role in the process of nerve regeneration after peripheral nerve injury. First of all, SCs are necessary for successful nerve regeneration. After injury, they become partially de-differentiated, with increased expression of nerve regeneration genes and secretion of neurotrophic factors, including GDNF, NGF, BDNF, and CNTF. The proximal ends of peripheral nerves formed growth cones facilitating regeneration of nerve fiber. Secondly, SCs guide the orderly extension of nerve axons by organizing suitable scaffolds. Thirdly, SCs clear the myelin sheath fragments produced by Wallerian degeneration of injured nerves, thus removing obstacles on the regeneration channels. In order to solve shortage of primary SCs, researchers also explored the substitutes of SCs by inducing stem cells into Schwann-like cells (SLCs). Both SCs and SLCs are indispensable and ideal seed cells for tissue engineering.

Our Research Topic aimed to investigate the regulatory roles of Schwann Cells and Schwann-like cells in peripheral nervous systems. We are very grateful to the 145 contributors from 15 different countries participating in current Research Topic with six abstracts, four review articles and six original research papers. These publications discussed from different angles of the current challenges to the field. It could be summarized into the following three aspects: (1) Important genes or proteins of SCs during peripheral nerves regeneration; (2) Scaffolds or stem cells exploration in peripheral nerves; (3) SCs related Reviews.

After peripheral nerve injury, SCs, vascular endothelial cells and blood derived macrophages reacted and conducted Wallerian deformation process. He et al. performed transcriptome sequencing and qPCR verification on the sciatic nerves of rats 4 and 7 days after the clamp injury. They found that Notch1 might act as a coordinator among the processes of vascular endothelial cell regeneration, macrophage recruitment and nerve regeneration.

Shen et al. transfected CD146 siRNA into primary rat SCs, and found that cell proliferation rate decreased significantly with increased migration. These results implied that CD146, as an important cell adhesion molecule, might have a significant impact on regulating biological behavior of SCs.

Ulrichsen et al. found that Sortilin could affect Remak bundle formation. When they cultured Sort1 -/- Schwann cells *in vitro*, they found SCs lost the ability to migrate and myelination.

Chen et al. combined mesenchymal stem cell transplantation and electric acupuncture to treat acute sciatic nerve contusion in rats. After assessment of MRI, they found that the neural function recovery speed of the experimental group was much faster than that of control group.

Zhong et al. collected numerous transaction figures of peripheral nerves and established mathematical models to reproduce the contour of functional bundles inside nerves. What's more, they attempted to predict the spatial continuity of axons to the distal. Fang and Zou found that Col6, as component of extracellular matrix in nerves, could promote the formation of axon bundles. Considering safer clinical application, Col6α2 seemed able to promote orderly axon formation through NCAM1 guided pathway with lower immunogenicity than Col6 complex *in vivo*.

Manganas et al. reviewed relevant literature about how SCs adapted to mechanical properties of their external micro-environment. Rao et al. compared the survival of SCs and/or SLCs when repairing peripheral nerve injury, and their performance changes when encountering different biomaterials used in tissue engineering nerve grafts. Wei et al. summarized outcomes of transplantation of SCs and SLCs in different peripheral neuropathies, and importance of SCs in the process of repairing nerves. Su et al. discussed construction of tissue engineering nerve grafts with SCs. They compared not only the advantages of nerve scaffolds loaded with SCs, but also the related problems of SCLs induced by stem cells. In conclusion, all these publications largely enriched theoretical knowledge of importance of SCs and nerve regeneration, and proposed a new treatment strategy for better application of SCs and SLCs to peripheral nerve injury repair in the future.

In recent years, many studies have been focused on understanding the process of PNS repair and reconstruction after injury and aim to find novel clinical therapeutical methods. The advancement of genomics, epigenomics and proteomics research methods has made it possible to study the regulation of transcription, post-transcriptional modification and translation in SCs and SLCs derived from stem cells, as well as the biological roles of these cells in PNS regulation, but many cellular and molecular mechanisms are still unclear and need to be farther investigated. We hope these precious achievements could bring greater breakthroughs in the future.

We, as the guest editors group, appreciate all authors once more for their valuable contributions. It is our honor that all readers of this Research Topic will enjoy these expert opinions and excellent research results.

Author contributions

BH, JH, and ZZ have connected them all within the editorial. All authors have contributed to this editorial and writing comments to the different articles.

Conflict of interest

The authors declare that the research was conducted in the absence of any commercial or financial relationships that could be construed as a potential conflict of interest.

Publisher's note

frontiers in Cellular Neuroscience

ORIGINAL RESEARCH
published: 04 October 2021
doi: 10.3389/fncel.2021.717209

Interactions Among Nerve Regeneration, Angiogenesis, and the Immune Response Immediately After Sciatic Nerve Crush Injury in Sprague-Dawley Rats

Bo He[1,2†], Vincent Pang[2†], Xiangxia Liu[2,3†], Shuqia Xu[2], Yi Zhang[2], David Djuanda[2], Guanggeng Wu[2], Yangbin Xu[1*] and Zhaowei Zhu[1*]*

[1] Department of Orthopaedics, The Third Affiliated Hospital, Sun Yat-sen University, Guangzhou, China, [2] Department of Plastic Surgery, The First Affiliated Hospital, Sun Yat-sen University, Guangzhou, China, [3] Department of Plastic Surgery, University of Tennessee Health Science Center, Memphis, TN, United States

OPEN ACCESS

Edited by:
Maria Dolores Ganfornina, University of Valladolid, Spain

Reviewed by:
Ashutosh Kumar, National Institute of Pharmaceutical Education and Research (NIPER-Kolkata), India
Sergio Diez-Hermano, University of Valladolid, Spain

***Correspondence:**
Zhaowei Zhu
nmtmemoir@aliyun.com
Yangbin Xu
xuyangbin@hotmail.com
Bo He
hebodoc@aliyun.com

† These authors have contributed equally to this work and share first authorship

Specialty section:
This article was submitted to Non-Neuronal Cells, a section of the journal Frontiers in Cellular Neuroscience

Received: 30 May 2021
Accepted: 08 September 2021
Published: 04 October 2021

Citation:
He B, Pang V, Liu X, Xu S, Zhang Y, Djuanda D, Wu G, Xu Y and Zhu Z (2021) Interactions Among Nerve Regeneration, Angiogenesis, and the Immune Response Immediately After Sciatic Nerve Crush Injury in Sprague-Dawley Rats. Front. Cell. Neurosci. 15:717209. doi: 10.3389/fncel.2021.717209

To preliminarily explore the primary changes in the expression of genes involved in peripheral nerve processes, namely, regeneration, angiogenesis, and the immune response, and to identify important molecular therapeutic targets, 45 Sprague-Dawley (SD) rats were randomly divided into a control group and an injury group. In the injury group, tissue samples were collected at 4 and 7 days after the injury for next-generation sequencing (NGS) analysis combined with gene ontology (GO) analysis, Kyoto Encyclopedia of Genes and Genomes (KEGG) analysis and Venn diagram construction to identify the differentially expressed mRNAs (DEmRNAs) associated with regeneration, angiogenesis, and the immune response of the nerve. The expression of genes in the distal and proximal ends of the injured nerve after injury was analyzed by qRT-PCR. NGS revealed that compared with the control group, the injury group had 4020 DEmRNAs 4 days after injury and 3278 DEmRNAs 7 days after injury. A bioinformatics analysis showed that C-C chemokine receptor type 5 (CCR5), Thy1 cell surface antigen (Thy1), Notch homolog 1 (Notch1), and semaphorin 4A (Sema4A) were all associated with regeneration, angiogenesis, and the immune response of the nerve at both 4 and 7 days after injury, but qPCR revealed no significant difference in the expression of Thy1 ($P = 0.29$) or Sema4A ($P = 0.82$) in the proximal end, whereas a significant difference was observed in CCR5 and Notch1 ($P < 0.05$). The trend in the Notch1 change was basically consistent with the RNA-seq result after injury, which implied its indispensable role during endothelial cell proliferation and migration, macrophage recruitment, and neurotrophic factor secretion.

Keywords: peripheral nerve injury, SD rats, transcriptome, bioinformatic, immune response

BACKGROUND

Peripheral nerve regeneration is a complex process. Active Schwann cells (SCs) play an important role in nerve repair process. They not only allow the myelin sheath debris of the axon that disintegrates due to Wallerian degeneration to be cleared quickly but also attract immunocytes migrating to the injured site; this allows the regenerating axons to grow smoothly into the bands of Büngner and eventually improves the efficacy of neurological functional recovery

(Bozkurt et al., 2009). We also found in our research that efficacy of peripheral nerve defect repair is related to the blood supply within the graft (Zhu et al., 2017). Vascularized nerve grafting maintains the continuity of the blood supply during nerve transplantation, ensures the activity of SCs, and leads to continuous neurotrophic factor secretion. Due to local ischemia, SCs become necrotic and replaced by fibroblasts, which results in an excessively low concentration of neurotrophic factors secreted by local SCs and slow remyelination of regenerating axons; this is unfavorable for the ingrowth and maturation of regenerating axons (He et al., 2014). Many angiogenic factors are involved in the repair process. Among them, endothelial growth factor (VEGF) and angiopoietin (Ang) are the two most important proangiogenic factors, as they act synergistically in angiogenesis. Studies have shown that VEGF promotes axonal growth through angiogenesis (Ebenezer et al., 2012). In a previous study involving *in vivo* experiments in rats, we found that COMP-Ang1, an angiogenic factor, was able to promote early angiogenesis in nerve repair scaffolds and the proliferation of SCs in peripheral nerves (Qiu et al., 2015). Besides, immune response provided significant assistance, especially during the early phrase after nerve injury. The myelin sheath debris is phagocytosed and removed by macrophages, which are brought in by the blood supply, and local SCs. At the same time, immune cells also secrete some cytokines that promote proximal nerve fiber growth to form growth cones (Lindborg et al., 2018).

Although axonogenesis, angiogenesis and the immune response are three different processes, they have numerous interactions after nerve injury (Cattin et al., 2015). Many cytokines and genes are involved in the mutual regulation of regeneration, angiogenesis, and the immune response in the peripheral nerve, but the specific mechanism remains unclear. To further study the molecular mechanisms of regeneration, angiogenesis, and the immune response in the nerve after peripheral nerve injury, this study aimed to perform transcriptome analysis of injured nerves in a rat model of sciatic nerve crush injury induced by clamping. We preliminarily explored the primary changes in gene expression that are involved in regeneration, angiogenesis, and the immune response of the peripheral nerve and provide a scientific basis for more effective treatment of peripheral nerve injury by identifying important molecular therapeutic targets.

MATERIALS AND METHODS

Animal Selection and Sample Collection

Forty-Five healthy male Sprague-Dawley (SD) rats weighing approximately 150–200 g were chosen and randomly separated into three groups as follows: control, 4-day injury, and 7-day injury groups (15 rats per group). This study was approved by the Experimental Animal Administration Committee of Sun Yat-sen University. Efforts were taken to minimize animal suffering during the experiment. The study design is presented in **Figure 1**.

Abbreviations: SD rats, Sprague-Dawley rats; SCs, Schwann cells; NGS, next-generation sequencing; FPKM, fragments per kilobase of transcript per million mapped reads; TMM, trimmed mean of *M* values; FDR, false discovery rate; GO, Gene Ontology; KEGG, Kyoto Encyclopedia of Genes and Genomes; DEmRNAs, differentially expressed mRNAs; FC, fold change; RF, rich factor; DRG, dorsal root ganglion; ECs, endothelial cells; VEGF, vascular endothelial growth factor; ECM, extracellular matrix; ACTM, acellular tissue matrix; Ang, angiopoietin; FGF, fibroblast growth factor; IOD, integrated optical density.

Sciatic Nerve Damage Model and Sampling

Experimental rats (injured for 4 days and injured for 7 days) were anesthetized by intraperitoneal injection of 10% chloral hydrate (0.3 ml/100 g) (Sinopharm Chemical Reagent Co., Ltd., Shanghai, China) and were subjected to sciatic nerve crush injury according to a previously published procedure (Zhu et al., 2017). Under aseptic conditions, the skin of the left leg was cut parallel to the femur, and the sciatic nerve was exposed by splitting the superficial gluteus muscle. The middle segment of the left sciatic nerve was clamped with hemostatic forceps for approximately 30 s. Subsequently, they were released, and the wound was closed, after which the animals were kept in a quiet and comfortable environment with a temperature between 20 and 25°C and humidity between 50 and 65%, and enough food and water were ensured. We also offered light for 14 h to maintain the normal circadian rhythm of each animal. The condition of the animals and the wounds were observed regularly.

Immunofluorescence

Three rats were randomly selected from each group. In the 4-day and 7-day injury groups, the nerve was completely cut at the lesion site at each selected observation time, and samples were obtained 1 cm proximal to the lesion and 1 cm distal to the lesion. The nerve samples were fixed in 4% paraformaldehyde at 4°C for 24 h. Subsequently, the nerve was placed in 20% sucrose for 24 h for the first round of dehydration, which was followed by placement in 30% sucrose for 24 h for the second round of dehydration. Ten-micrometer-thick sections of the middle segment of the nerve were cut using a cryostat and placed on a coverslip; immunofluorescence staining was then performed with a rabbit anti-mouse NF-200 antibody (Sigma-Aldrich, Tokyo, Japan, 1:400), a CD31 antibody (Sigma-Aldrich, Tokyo, Japan, 1:400), and a FITC-conjugated goat anti-rabbit IgG secondary antibody (TCS Biologicals, Botolph Clayton, United Kingdom; 1:200). Antibodies were diluted in PBS containing 3% rat serum, 3% goat serum, and 0.02% sodium azide (Sigma-Aldrich, Tokyo, Japan) to reduce background staining.

For image study, photos were taken under the same condition as previously described (Zhu et al., 2015). For the determination of NF200 and CD31 expression, the integrated optical density (IOD) of positive staining was assessed using Image-Pro Plus. For each animal and for each stain, calculations were made on three randomly chosen sections, and the results were averaged.

Library Preparation and RNA Sequencing

Two rats were randomly selected from each group, and the injured nerves were harvested as samples for next-generation RNA sequencing (NGS). All sequencing programs

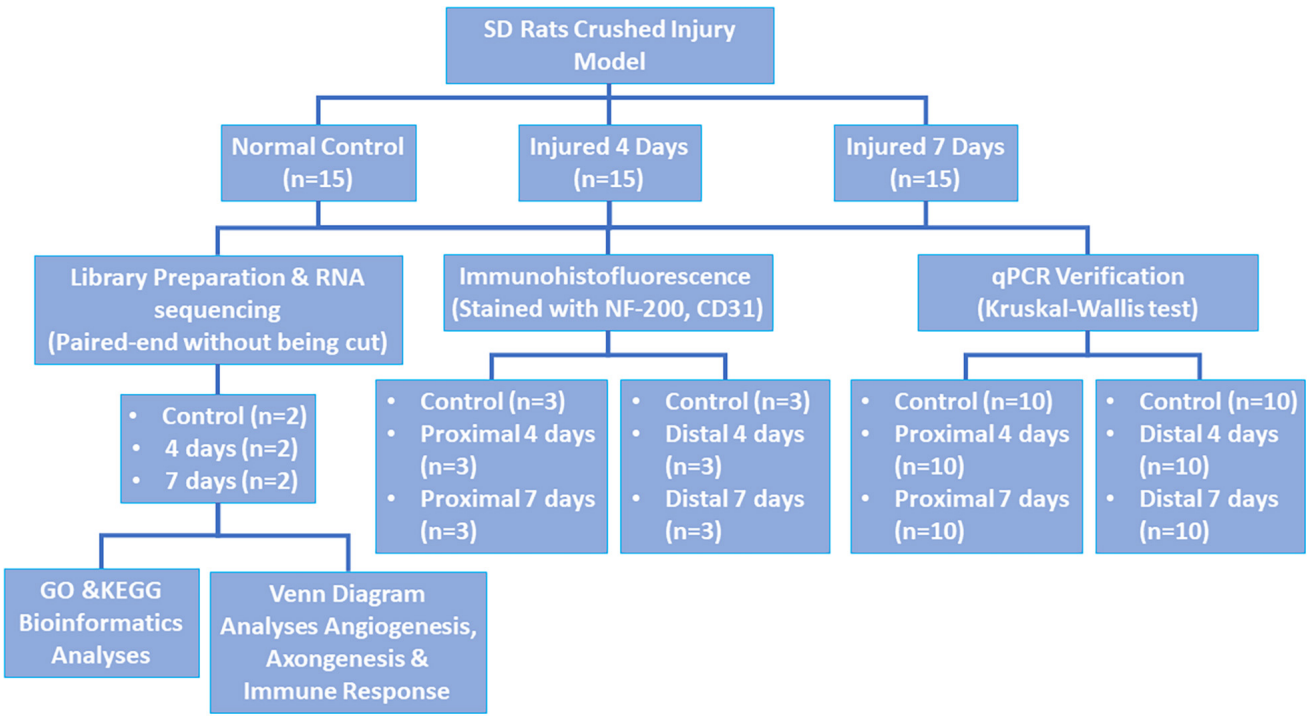

FIGURE 1 | Study design.

were performed by Shanghai Biotechnology Corporation (Shanghai, China).

During transcriptome sequencing, to enable comparability of gene expression levels among different genes and different samples, the reads were converted into FPKM (fragments per kilobase of transcript per million mapped reads) to normalize the gene expression level (Mortazavi et al., 2008). We first applied Stringtie (version: 1.3.0) (Pertea et al., 2015; Pertea et al., 2016) to count the number of fragments for each gene after HisAT2 alignment, and then we used the TMM (trimmed mean of *M* values) (Robinson and Oshlack, 2010) method for normalization; finally, we used Perl script to calculate the FPKM value for each gene.

Bioinformatics Analyses

EdgeR (Robinson et al., 2010) was used to perform the differential gene analysis between samples. After the *P*-value was derived, multiple hypothesis testing correction was performed, and the threshold of the *p*-value was determined by controlling the FDR (false discovery rate) (Benjamini et al., 2001); the corrected *p*-value is the *q*-value. Moreover, we calculated the fold differential expression based on the FPKM values, namely, the fold change. Differential gene screening conditions were set at a q-value ≤ 0.05 and a fold change ≥ 2. Both gene ontology (GO) analysis[1] and KEGG pathway analysis[2] were performed to determine the roles of the differentially expressed mRNAs. Fisher's exact test was used to test the significance of GO terms and KEGG pathway identifier enrichment in the differentially expressed gene list. RNA sequencing and bioinformatics analyses were carried out by Shanghai Biotechnology Corporation (Shanghai, China).

We defined axonogenesis, angiogenesis, and immune response by GO categories, whose item numbers were 0007409, 0001525, and 0006955, respectively. The upregulated differentially expressed mRNAs (DEmRNAs) related to these three items were analyzed, and a Venn diagram was generated by web tools[3].

Quantitative Real-Time RT-PCR

Ten rats were randomly selected from each group. In the 4-day and 7-day injury groups, the nerve was completely transected at the lesion site, and samples were obtained 1 cm proximal to the lesion and 1 cm distal to the lesion. Quantitative analysis of the targeted mRNA expression was performed using real-time RT-PCR as previously described (Djuanda et al., 2021). The RNA concentration and purity were detected using a NanoDrop 2000, and RNA with an excessively high concentration was diluted appropriately to a final concentration of 200 ng/μl. One microgram of each specimen was used for RNA reverse transcription using the RevertAid First Strand cDNA Synthesis Kit (Thermo, MA, United States). An appropriate amount of cDNA was amplified using FastStart Universal SYBR Green Master Mix (Roche, Basel, Switzerland)

[1]http://www.geneontology.org
[2]http://www.genome.jp/kegg/
[3]http://bioinformatics.psb.ugent.be/webtools/Venn/

in a fluorescence quantitative PCR machine (StepOne Plus, Thermo, MA, United States). For the specific procedure, please refer to the product manual. This experiment was repeated three times for each specimen. GAPDH expression was used to normalize the expression of mRNAs, and information about the genes to be tested and their primers is shown in **Table 1**. The specificity of real-time PCR was confirmed via routine agarose gel electrophoresis and melting-curve analysis. The $2^{-\Delta\Delta Ct}$ method was used to calculate relative gene expression. GAPDH served as the reference gene.

Gene Interaction Analysis

Network software built by Cytoscape (version: 3.7.1[4]) with the GeneMania plug-in (version: 3.5.1[5]) was used to analyze the interactions between genes sorted by the Venn diagram. *Rattus norvegicus* was chosen, and the parameter was set to the top 20 related genes using automatic weight. Through the score ranking of each gene, the network of genes interacting with the sorted genes was obtained.

Statistical Analysis

The RT-PCR data are presented as the mean ± SD as described previously (Liu et al., 2018). SPSS 16.0 software (SPSS, Chicago, IL, United States) was used to analyze quantitative RT-PCR results. Statistical analysis was performed with Kruskal–Wallis test to determine the significant differences between the groups. $\alpha < 0.05$ was considered statistically significant.

RESULTS

Staining of Nerve and Blood Vessel Markers in the Sciatic Nerve of Sprague-Dawley Rats After Injury

The sciatic nerves of SD rats in the control group and those of SD rats at 4 and 7 days after injury were obtained to examine the expression of the nerve axon marker NF-200 and the vascular endothelial cell marker CD31. The results showed that NF200 expression was negatively correlated with time and that its expression gradually changed from a line-like distribution to a punctate scattered distribution, as observed by microscopy; however, CD31 expression was positively correlated with time, and multiple small luminal structures were observed inside the nerve at day 7 (see **Figure 2**). Additionally, we found that compared to control group, the injury group had a decrease in NF200-positive fibers after injury, and on day 7, most NF200-positive staining had disappeared. These phenomena suggested that Wallerian degeneration of sciatic nerves after injury was ongoing and that our crush models were established successfully. In contrast to the transection models, the crush models still had some NF200 + axon fibers after injury, which were evident by immunofluorescence staining at day 7.

Analysis of IOD demonstrated that the expression of NF200 was higher in control group (12262 ± 2863), and decreased gradually after injury in day 4 (7478 ± 1603) and day 7 (4061 ± 2933). Same trend appeared in CD31 expression, which showed highest in control group (12043 ± 2849), then decrease in day 4 (1374 ± 848) and day 7 (3595 ± 2011).

[4]http://www.cytoscape.org/

[5]http://apps.cytoscape.org/apps/GeneMania

TABLE 1 | List of qRT-PCR primers.

Gene name	Sequence
GAPDH	Forward: 5′-TTCCTACCCCCAATGTATCCG-3′ Reverse: 5′-CATGAGGTCCACCACCCTGTT-3′
CCR5	Forward: 5′-CCTAAATCACTGAGGCGGTCAG-3′ Reverse: 5′-TGGCCACTTACCACAGAGCTA-3′
Thy1	Forward: 5′-CATGACCAGCTCGCAGACCTA-3′ Reverse: 5′-CTGGAGTGGGAGGAAGAGGTAA-3′
Notch1	Forward: 5′-TGTCGCTGGGTACAAATGCAA-3′ Reverse: 5′-A CGGTAGCTGCCATTGGTGTTC-3′
Sema4A	Forward: 5′-TGTCGCTGGGTACAAATGCAA-3′ Reverse: 5′-A CGGTAGCTGCCATTGGTGTTC-3′

Transcriptome Analysis After Clamp-Induced Sciatic Nerve Crush Injury in Sprague-Dawley Rats

We used NGS to analyze the expression of genes in the transcriptome at 4 and 7 days after clamp-induced sciatic nerve crush injury in SD rats, and the distribution of differentially expressed mRNAs (DEmRNAs) is shown in heat maps (**Figure 3**). In all, 30,957 mRNAs were detected by RNA-seq and were screened according to the criteria of a fold change ≥ 2.0 and $q < 0.05$. Compared with the control rats, rats examined 4 days after clamp-induced crush injury had 4020 DEmRNAs, with the expression of 2500 being upregulated and 1520 being downregulated. Four days after injury, 137 mRNAs were activated in the experimental group, and of these, the most obvious change was in Hmga2 (FPKM = 0 vs. 16.42, $q < 0.05$). Sixty-four genes were silenced, and the greatest change was seen in fgf4 (FPKM = 4.00 vs. 0, $q < 0.05$). The top 10 DEmRNAs that were activated or silenced are shown in **Table 2**. In addition, among the mRNAs that were expressed in both the control and experimental groups, the mRNA with the most significant increase was Tyrp1 (log2FC = 9.75, $q < 0.05$), whereas the one with the largest decrease was Sec14l5 (log2FC = −11.16, $q < 0.05$). The top 10 DEmRNAs that were the most significantly upregulated or downregulated are shown in **Table 3**. Seven days after injury, there were 3278 DEmRNAs; expression of 1977 mRNAs was upregulated, and expression of 1301 mRNAs were downregulated. Among them, 88 mRNAs were activated, and the most obvious change was seen in Apoc1 (FPKM = 0 vs. 5.96, $P < 0.05$); 35 mRNAs were silenced, and the most obvious change was seen in Hapln2 (FPKM = 4.26 vs. 0, $P < 0.05$). The top 10 DEmRNAs that were activated or silenced are shown in **Table 4**. In addition, among the mRNAs that were expressed in both the control and the experimental groups, the mRNA with the largest increase was tyrosinase-related protein 1 (Tyrp1) (log2FC = 10.92, $P < 0.05$),

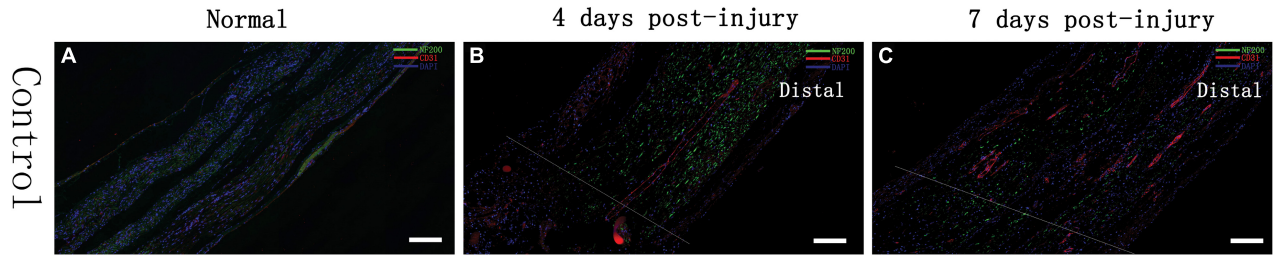

FIGURE 2 | Immunofluorescence assessment of the sciatic nerve in SD rats Changes in the expression of an axon-associated protein (NF-200) and a vascular endothelial cell protein (CD31) in the early stage of a contusion injury (4 days, 7 days) compared with controls. The scale bar represents 200 μm. **(A)** Normal rat sciatic nerve; **(B)** 4 days after injury, rat sciatic nerve injury and beyond; **(C)** 7 days after injury, rat sciatic nerve injury and beyond.

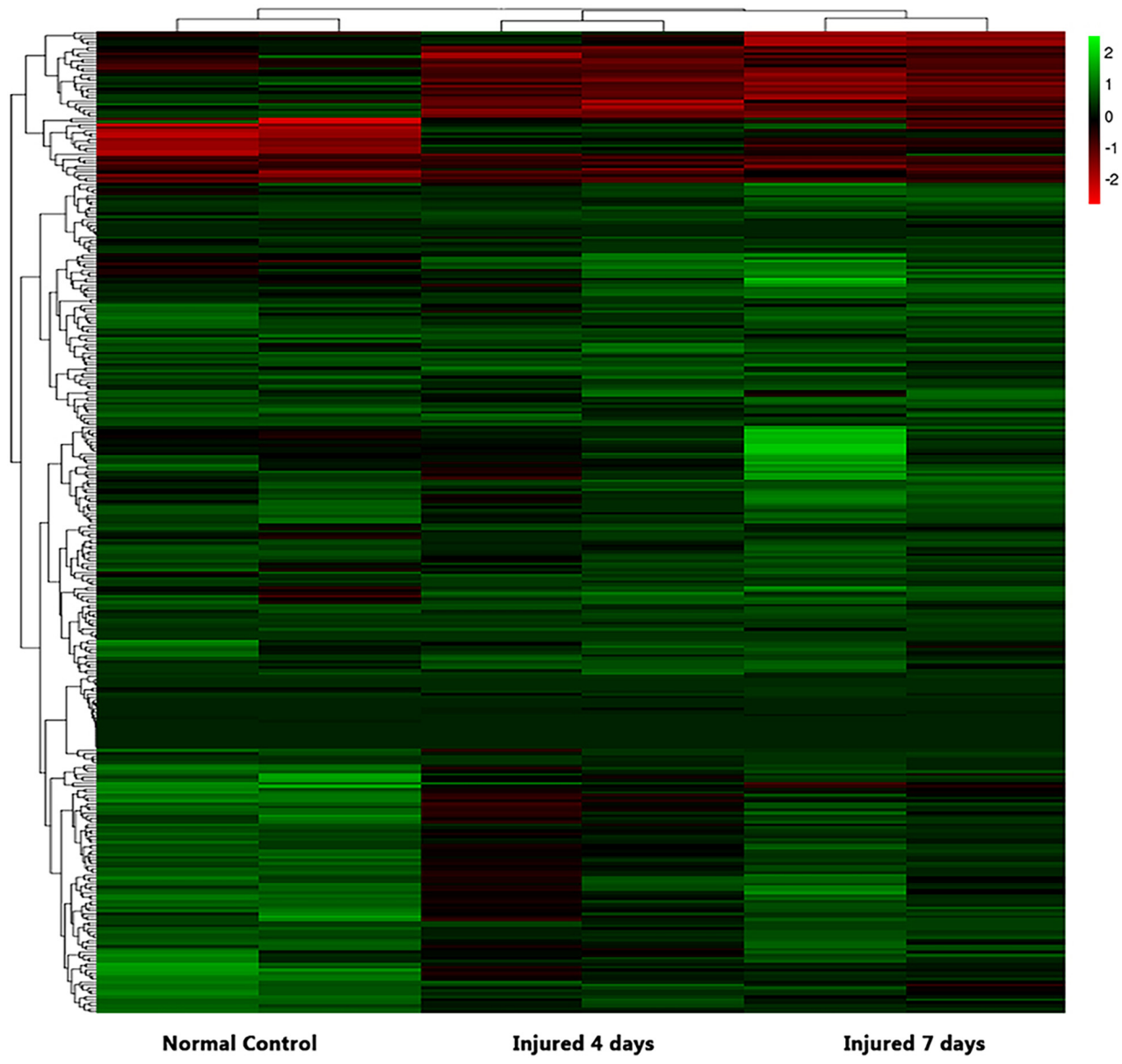

FIGURE 3 | Heatmap of differential mRNA expression after RNA sequencing at different times (4 and 7 days after injury) soon after sciatic nerve contusion in SD rats. Black indicates no significant fold change in mRNA expression between the groups, green indicates increased expression, and red indicates decreased expression.

TABLE 2 | Top 10 DEmRNAs only expressed 4 days after crush injury (Post-Injury 4 days, PI-4 d) or only expressed in normal sciatic nerves.

	Gene name	Control	PI-4d	*P*-value	*q*-value
Only in PI-4d	Hmga2	0	16.42365	1.10E-40	9.60E-39
	Draxin	0	4.227762	6.20E-21	1.79E-19
	Pth2r	0	2.709091	1.31E-22	4.29E-21
	Podnl1	0	2.029091	9.10E-17	1.94E-15
	U4	0	1.946587	0.008691	0.028003
	AABR07030791.1	0	1.931831	1.98E-10	2.41E-09
	SNORA26	0	1.701125	0.013095	0.039665
	Apoc1	0	1.623794	5.68E-09	5.87E-08
	Mmp7	0	1.524575	2.90E-05	0.000173
	Mar11	0	1.373298	6.41E-13	9.82E-12
Only in control group	Fgf4	3.996402849	0	7.56E-16	1.49E-14
	SNORA24	3.248064983	0	0.000219535	0.001086115
	C1qtnf4	2.995813298	0	3.86E-13	6.03E-12
	SNORA17	2.137505294	0	0.003996423	0.014321861
	7SK	1.846016982	0	7.86E-06	5.18E-05
	Mobp	1.845934814	0	6.50E-21	1.87E-19
	Omg	1.460558332	0	1.71E-16	3.57E-15
	AABR07030053.1	1.124891401	0	0.000367528	0.001730692
	Fam163b	1.039812773	0	4.98E-15	9.22E-14
	AABR07043929.1	1.029593343	0	0.003062435	0.011285335

TABLE 3 | Top 10 up/down regulated DEmRNAs 4 days after crush injury.

	Gene name	Control	PI-4d	log2FC	*P*-value	q-value
Up	Tyrp1	0.044697	38.389	9.74631	7.74E-151	2.88E-147
	Tnn	0.006946	4.546313	9.35422	2.66E-24	9.86E-23
	Mmp12	0.014896	4.753194	8.31787	3.46E-11	4.59E-10
	Gpr83	0.102426	30.33552	8.21029	4.74E-99	3.39E-96
	Ucn2	0.135147	36.98082	8.0961	4.40E-75	1.34E-72
	Gdnf	0.171444	36.09137	7.71778	2.13E-57	3.89E-55
	Mrap2	0.010181	2.045476	7.65046	1.04E-17	2.38E-16
	Fam132b	0.021671	4.319474	7.63894	2.13E-19	5.65E-18
	Fgf5	0.222784	39.20535	7.45926	3.66E-62	7.74E-60
	Cabp2	0.016972	2.560325	7.23702	2.74E-18	6.54E-17
Down	Sec14l5	20.16116	0.00883	–11.15691	1.45E-111	1.35E-108
	B3galt2	6.578876	0.004418	–10.54028	1.59E-77	5.49E-75
	LOC688613	13.08011	0.023957	–9.092689	2.49E-40	2.13E-38
	4932411E22Rik	16.50995	0.032553	–8.986331	7.87E-54	1.25E-51
	Lect1	189.2592	0.667838	–8.14665	1.18E-141	3.65E-138
	Ncmap	560.4528	2.046832	–8.097057	4.11E-140	1.09E-136
	Slco4c1	1.55139	0.008964	–7.435194	6.11E-31	3.26E-29
	Dcdc2	3.533837	0.020657	–7.418444	2.33E-67	5.71E-65
	Slc9a3	18.51888	0.116726	–7.309727	4.92E-128	8.30E-125
	Asb15	1.636855	0.010325	–7.308676	1.15E-27	5.15E-26

whereas the one with the largest decrease was Rn60_10_0890.5 (log2FC = −8.63, $P < 0.05$). The top 10 DEmRNAs that were the most significantly upregulated or downregulated are shown in **Table 5**.

Gene Ontology Analysis and Kyoto Encyclopedia of Genes and Genomes Analysis of DEmRNAs

Clustering analysis of DEmRNAs can help to identify the function of unknown transcripts or the unknown function of known transcripts by gathering similar expression patterns or similar genes to a class (Yao et al., 2012). The results showed that at 4 days after injury, DEmRNAs were enriched mainly in mitotic chromosome condensation [Rich factor (RF) = 5.52, $q < 0.05$], protein binding involved in cell-cell adhesion (RF = 5.52, $q < 0.05$), and condensed chromosome outer kinetochore (RF = 5.06, $q < 0.05$). However, 7 days after injury, DEmRNAs were enriched mainly in the G protein-coupled receptor signaling pathway involved in heart processes (RF = 6.14, $q < 0.05$), condensed chromosome outer kinetochores (RF = 5.62, $q < 0.05$),

TABLE 4 | Top 10 DEmRNAs only expressed 7 days after crush injury (Post-Injury 7 days, PI-7d) or only expressed in normal sciatic nerves.

	Gene name	Control	PI-7d	*P*-value	*q*-value
Only in PI-7d	Apoc1	0	5.970197	4.70E-17	2.95E-15
	Apoc4	0	5.188777	1.76E-13	6.82E-12
	AABR07030791.1	0	4.193796	1.22E-17	8.19E-16
	Hmga2	0	4.171533	4.29E-14	1.78E-12
	Pth2r	0	2.709295	2.96E-20	2.65E-18
	SNORA17	0	2.637213	0.004973	0.024347
	Mmp7	0	2.629549	5.82E-11	1.64E-09
	LOC683295	0	2.378256	7.81E-15	3.53E-13
	Draxin	0	1.958597	2.17E-11	6.48E-10
	Pnlip	0	1.601258	3.65E-11	1.06E-09
Only in normal nerves	Hapln2	4.256182914	0	1.07E-21	1.13E-19
	AABR07034833.1	3.00758614	0	3.20E-07	4.82E-06
	RGD1309651	1.150919443	0	0.002781747	0.014995912
	AABR07043929.1	1.029593343	0	0.003365706	0.017661869
	AABR07069211.1	0.971437254	0	0.000191145	0.001516581
	AABR07044148.1	0.743679909	0	0.000472723	0.003320686
	AABR07059527.1	0.647496594	0	0.005470721	0.026331135
	AABR07061178.1	0.611046904	0	0.000170623	0.001376103
	AABR07042654.1	0.595353922	0	0.006749527	0.03130678
	Htr3b	0.554774052	0	9.43E-06	0.000105647

TABLE 5 | Top 10 up/down regulated DEmRNAs 7 days after crush injury.

	Gene name	Control	PI-7d	log2FC	*P*-value	*q*-value
Up	Tyrp1	0.044697	86.81279	10.9235	1.40E-103	2.61E-99
	Gpr83	0.102426	62.51478	9.25348	3.13E-70	1.16E-66
	Mmp12	0.014896	3.421537	7.84362	7.88E-18	5.36E-16
	Mrap2	0.010181	1.772636	7.44392	1.35E-14	5.92E-13
	Tnn	0.006946	1.147016	7.36741	3.74E-19	2.95E-17
	Mmp8	0.038257	5.635753	7.20274	1.44E-21	1.49E-19
	Ucn2	0.135147	19.90056	7.20214	8.34E-37	4.69E-34
	Fgf5	0.222784	27.30074	6.93715	5.94E-40	4.80E-37
	Cabp2	0.016972	1.920472	6.82216	1.78E-13	6.88E-12
	Tfap2c	0.024944	2.734148	6.77627	5.83E-17	3.61E-15
Down	Rn60_10_0890.5	6.734551	0.017053	–8.625381	7.44E-05	0.000669
	Myh7	1.921069	0.025591	–6.23013	3.68E-25	6.57E-23
	Krt5	0.485026	0.006569	–6.206171	8.18E-10	1.91E-08
	Slco4c1	1.55139	0.021535	–6.170702	4.23E-24	6.05E-22
	Ninj2	0.921764	0.016422	–5.810661	6.83E-09	1.39E-07
	C1qtnf4	2.995813	0.054888	–5.770303	2.65E-09	5.68E-08
	Fgf4	3.996403	0.085413	–5.548109	1.21E-11	3.73E-10
	Slc46a2	0.517902	0.013404	–5.271998	4.39E-07	6.42E-06
	Fam163b	1.039813	0.027344	–5.248954	3.61E-11	1.05E-09
	4932411E22Rik	16.50995	0.466168	–5.146343	2.05E-32	8.08E-30

and MHC class II protein complexes (RF = 5.62, $q < 0.05$). The GO enrichment diagram and the distribution of GO entries enriched in the top 10 are shown in **Figures 4A1,B1** and **Table 6**.

Pathway enrichments was performed by means of KEGG analysis to determine the pathways in which DEmRNAs are involved during the early stage after injury to understand the molecular interactions after injury. The results showed that the top three pathways enriched were steroid biosynthesis (3.84 vs. 4.33, $q < 0.05$), DNA replication (3.15 vs. 3.39, $q < 0.05$), and *Staphylococcus aureus* infection (2.75 vs. 3.11, $q < 0.05$) at both 4 and 7 days after injury. The KEGG enrichment diagram and the distribution of the top 10 GO entries enriched are shown in **Figures 4A2,B2** and **Table 7**.

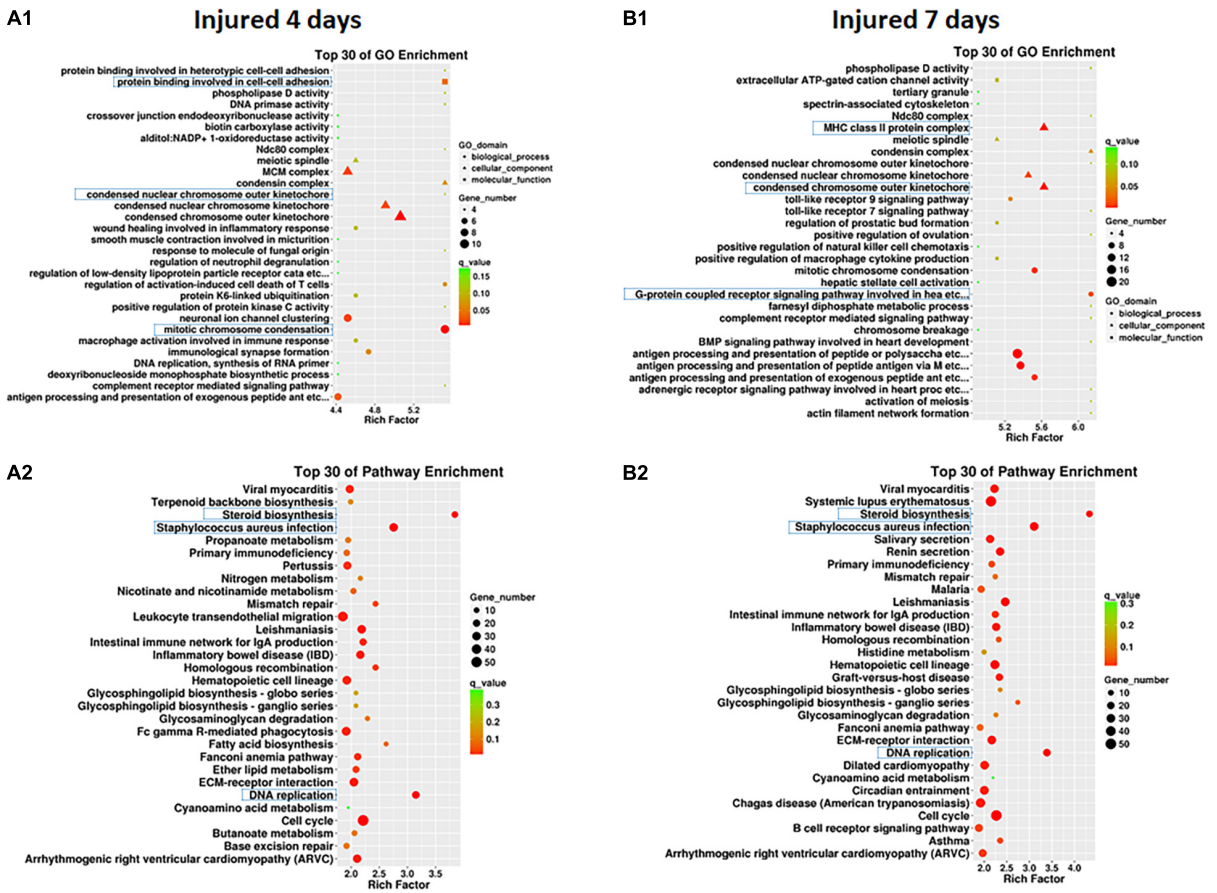

FIGURE 4 | GO enrichment map **(A1,B1)** and KEGG pathway enrichment map **(A2,B2)** of differentially expressed mRNAs in SD rats 4 and 7 days after sciatic nerve injury compared with rats without injury during the early stage after sciatic nerve contusion. **(A1)** GO gene enrichment map at 4 days after injury; **(B1)** GO gene enrichment map at 7 days after injury. The different shapes in the figure represent different categories, with circles representing biological processes, triangles representing cellular components, and squares representing molecular functions. A larger shape area indicates a greater number of DEmRNAs in that category. The significant differences in the distribution of DEmRNAs in different subcategories between the two groups are indicated by different colors, where green indicates q-values > 0.15, yellow indicates that q-values are between 0.10 and 0.15, orange indicates that q-values are between 0.05 and 0.10, and red indicates q-values < 0.05. The test criterion was set at 0.05. **(A2)** KEGG gene enrichment map at 4 days after injury; **(B2)** KEGG gene enrichment map at 7 days after injury. A larger graphical area in the figure indicates a higher number of DEmRNAs in that channel. The significant differences in the distribution of DEmRNAs in different channels between the two groups are indicated by different colors, where green indicates q-values > 0.3, yellow indicates that q-values are between 0.2 and 0.3, orange indicates that q-values are between 0.1 and 0.2, and red indicates q-values < 0.1. The test criterion was 0.1.

Triple Intersection of Nerve Regeneration, Angiogenesis and Immune Response Among Upregulated DEmRNAs at 4 and 7 Days After Injury and Validation by qPCR

At 4 days after injury, 6 DEmRNAs were found to be involved in both nerve regeneration and angiogenesis: semaphorin 3E (Sema3e), fibroblast growth factor 8 (Fgf8), neural cell adhesion molecule (Ncam), ephrin type-B receptor 3 (Ephb3), Sonic hedgehog (Shh), and TNF receptor superfamily member 12A (Tnfrsf12a). At 7 days after injury, increased expression in only Sema3e, Ephb3, Shh, and Tnfrsf12a was maintained ($P < 0.05$). At 4 and 7 days after injury, 2 DEmRNAs were found to be involved in both regeneration and the immune response of the nerve: nerve growth factor receptor (Ngfr) and Sema7a ($P < 0.05$).

A Venn diagram was used to perform the three-intersection analysis of the DEmRNA-associated signaling pathways of regeneration, angiogenesis, and the immune response of the nerve, and the intersection of the upregulated DEmRNAs at 4 and 7 days after injury is shown in **Figure 5**. The results showed that the intersecting mRNAs of regeneration, angiogenesis, and the immune response of the nerve at 4 and 7 days after injury included C-C chemokine receptor type 5 (Ccr5), Thy1 cell surface antigen (Thy1), Notch homolog 1 (Notch1), and Sema4A, and the expression levels of all but Thy1 were significantly increased compared with the control group ($P < 0.05$).

As shown in **Figure 6**, In the proximal ends of the injured nerve between the experimental group and the control group, the qPCR results revealed no significant difference in the expression

TABLE 6 | The classification corresponding to the top 10 DEmRNAs at 4 and 7 days after sciatic nerve crush injury in SD rats in the GO analysis.

	GO_ID	GO_term	Rich factor	*P*-value	*q*-value
4 Days	GO:0007076	Mitotic chromosome condensation	5.522492	0.000172	0.004143
	GO:0098632	Protein binding involved in cell–cell adhesion	5.522492	0.002896	0.040288
	GO:0000940	Condensed chromosome outer kinetochore	5.062285	0.000148	0.003641
	GO:0000778	Condensed nuclear chromosome kinetochore	4.908882	0.001208	0.020329
	GO:0042555	MCM complex	4.518403	0.000984	0.017223
	GO:0045161	Neuronal ion channel clustering	4.518403	0.000984	0.017223
	GO:0019886	Antigen processing and presentation of exogenous peptide antigen via MHC class II	4.417994	0.001983	0.029688
	GO:0006270	DNA replication initiation	4.417994	2.03E-05	0.000666
	GO:0002504	Antigen processing and presentation of peptide or polysaccharide antigen via MHC class II	4.321951	8.20E-06	0.000304
	GO:0042613	MHC class II protein complex	4.141869	0.001556	0.02449
7 Days	GO:0086103	G-protein coupled receptor signaling pathway involved in heart process	6.136293	0.000758	0.014837
	GO:0000940	Condensed chromosome outer kinetochore	5.624935	5.94E-05	0.001758
	GO:0042613	MHC class II protein complex	5.624935	5.94E-05	0.001758
	GO:0019886	Antigen processing and presentation of exogenous peptide antigen via MHC class II	5.522664	0.000278	0.006433
	GO:0007076	Mitotic chromosome condensation	5.522664	0.000278	0.006433
	GO:0000778	Condensed nuclear chromosome kinetochore	5.454483	0.000607	0.012311
	GO:0002495	Antigen processing and presentation of peptide antigen via MHC class II	5.369256	1.01E-05	0.000372
	GO:0002504	Antigen processing and presentation of peptide or polysaccharide antigen via MHC class II	5.335907	1.79E-07	1.18E-05
	GO:0034162	Toll-like receptor 9 signaling pathway	5.25968	0.002935	0.043712
	GO:0008331	High voltage-gated calcium channel activity	4.772672	0.002204	0.03514

TABLE 7 | The classification corresponding to the top 10 DEmRNAs at 4 and 7 days after sciatic nerve crush injury in SD rats in the KEGG analysis.

	Pathway_ID	Pathway description	Rich factor	*P*-value	*q*-value
4 Days	rno00100	Steroid biosynthesis	3.841198	7.69E-06	0.000448
	rno03030	DNA replication	3.148276	2.90E-06	0.000281
	rno05150	*Staphylococcus aureus* infection	2.754066	1.12E-06	0.000163
	rno03430	Mismatch repair	2.432759	0.005113	0.035425
	rno03440	Homologous recombination	2.432759	0.002673	0.025091
	rno04672	Intestinal immune network for IgA production	2.211599	0.000987	0.013053
	rno04110	Cell cycle	2.211599	1.59E-07	4.61E-05
	rno05140	Leishmaniasis	2.185957	7.34E-05	0.003562
	rno05321	Inflammatory bowel disease (IBD)	2.162452	0.000184	0.005962
	rno03460	Fanconi anemia pathway	2.115442	0.001708	0.017138
	rno00100	Steroid biosynthesis	4.331055	1.72E-06	9.89E-05
7 Days	rno03030	DNA replication	3.388414	1.47E-06	0.000141
	rno05150	*Staphylococcus aureus* infection	3.105285	9.14E-08	2.63E-05
	rno00604	Glycosphingolipid biosynthesis – ganglio series	2.743002	0.009715	0.049089
	rno05140	Leishmaniasis	2.464726	7.54E-06	0.00031
	rno04924	Renin secretion	2.351144	5.96E-05	0.001561
	rno05310	Asthma	2.351144	0.004946	0.031656
	rno05332	Graft-versus-host disease	2.334469	0.000499	0.006537
	rno03440	Homologous recombination	2.321001	0.007416	0.043586
	rno04110	Cell cycle	2.266943	2.71E-07	3.91E-05

of Thy1 ($P > 0.05$) or Sema4A ($P > 0.05$), whereas a significant difference was observed in CCR5 and Notch1 ($P < 0.05$); however, the trends in CCR5 was not completely consistent with the RNA-seq results. At 4 days after injury, the expression of CCR5 was significantly reduced (FC = 0.66 ± 0.02, $P < 0.01$), gradually increased and then remained lower than that of the control group at day 7 (FC = 0.80 ± 0.03, $P < 0.01$). The trend in the Notch1 change was basically consistent with the RNA-seq result after injury. In the proximal ends of injured nerves, Notch1 expression showed significant changes 4 days after the operation and continued to increase at day 7.

In distal ends of the injured nerves, the results of the three-intersection analyses in the control group, the 4-day injury group, and the 7-day injury group showed no significant difference in the expression of CCR5 ($P > 0.05$), but significant differences were observed in the expression of Thy1, Notch1, and Sema4A

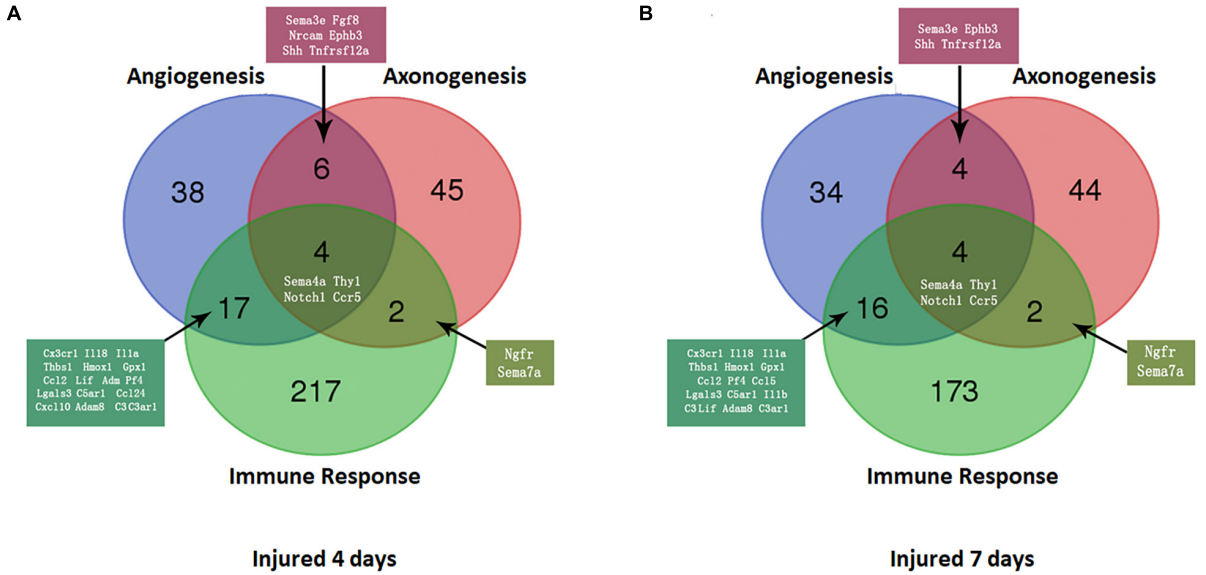

FIGURE 5 | Venn diagram of mRNAs with increased expression at the intersection of angiogenesis, axonal regeneration, and the immune response at different time points. **(A)** 4 days after sciatic nerve crush injury; **(B)** 7 days after sciatic nerve crush injury. The number and names of intersecting genes are indicated in the figure.

between the groups ($P < 0.05$). Compared with that in the control group, the expression of Thy1 was not significantly different in the day-4 (FC = 0.74 ± 0.16) or day-7 injury group (FC = 1.31 ± 0.18, $P > 0.05$), but Thy1 expression was significantly higher at day 7 than at day 4 ($P < 0.05$). Four days after injury, Notch1 expression was significantly lower than that in the control group (FC = 0.68 ± 0.10, $P < 0.01$); however, Notch1 expression then gradually increased and became significantly higher than that in the control group by day 7 ($P < 0.01$). Four days after injury, Sema4A expression was significantly reduced compared with that in the control group (FC = 0.48 ± 0.05, $P < 0.01$), and its expression gradually increased thereafter (FC = 0.86 ± 0.16, $P > 0.05$).

Analysis of the Intersecting Genes and Their Interactions With Related Genes

The gene network of the mutual intersections among the 21 genes with the highest correlation with Ccr5, Thy1, Notch1, and Sema4A is shown in **Figure 7** and **Supplementary Tables 1**, **2**. The results revealed a total of 47 links, of which co-expression accounted for 42.55%, predicted links accounted for 29.79%, and physical interactions accounted for 8.51%. Higher scores of the nodes indicate better correlation with the screened genes. The three nodes with the highest scores were X-linked inhibitor of apoptosis (Xiap, score: 0.012), F-box and WD repeat domain containing 7 (Fbxw7, score: 0.009) and Jagged 2 (Jag2, score: 0.008), and 8 were associated with the Notch signaling pathway.

DISCUSSION

Axonogenesis, angiogenesis and the immune response have numerous interactions after nerve injury (Cattin et al., 2015). In order to better verified cell clusters involved in the nerve injury and repair process, Kalinski et al. (2020) performed single-cell RNA sequencing in mice sciatic nerves after crush injury models. After being injured for 3 days, 24 different cell clusters were identified. The most prominently featured are immune cells, especially innate immune cells (Itgam/CD11b^{+}). Other abundantly featured cell types include mesenchymal progenitor cells, Schwann cells and nerve vasculature cells. The early pathophysiological changes after peripheral nerve injury are reflected in Wallerian degeneration of the distal end and part of the proximal end of the nerve. The myelin sheath debris is phagocytosed and removed by macrophages, which are brought in by the blood supply, and local SCs. As we found in our research that at the very beginning after injury, NF-200 positive fibers were fragmented and finally disappeared, while CD31 positive vasculature was immediately established. At the same time, cells also secrete some cytokines that promote proximal nerve fiber growth to form growth cones. Only when the proximal regenerating axons pass through the site of injury, regenerate distally, and innervate the target organ is the process of nerve regeneration ultimately completed (Sayad Fathi and Zaminy, 2017). During this process, a series of signaling pathways regulate the local microenvironment inside the nerve until nerve regeneration is completed (Kato et al., 2013; Liu et al., 2015, 2016; **Figure 8**).

In the adult mammalian peripheral nervous system, injured axons maintain the capacity to regenerate spontaneously and provide the possibility for functional recovery post-peripheral nerve injury (Dickson, 2002; Abe and Cavalli, 2008). Peripheral nerve regeneration is accompanied by activation of various complicated molecular pathways and cellular events, which are motivated by differentially expressed genes and significantly changed pathways postinjury. Li et al. (2013) previously profiled

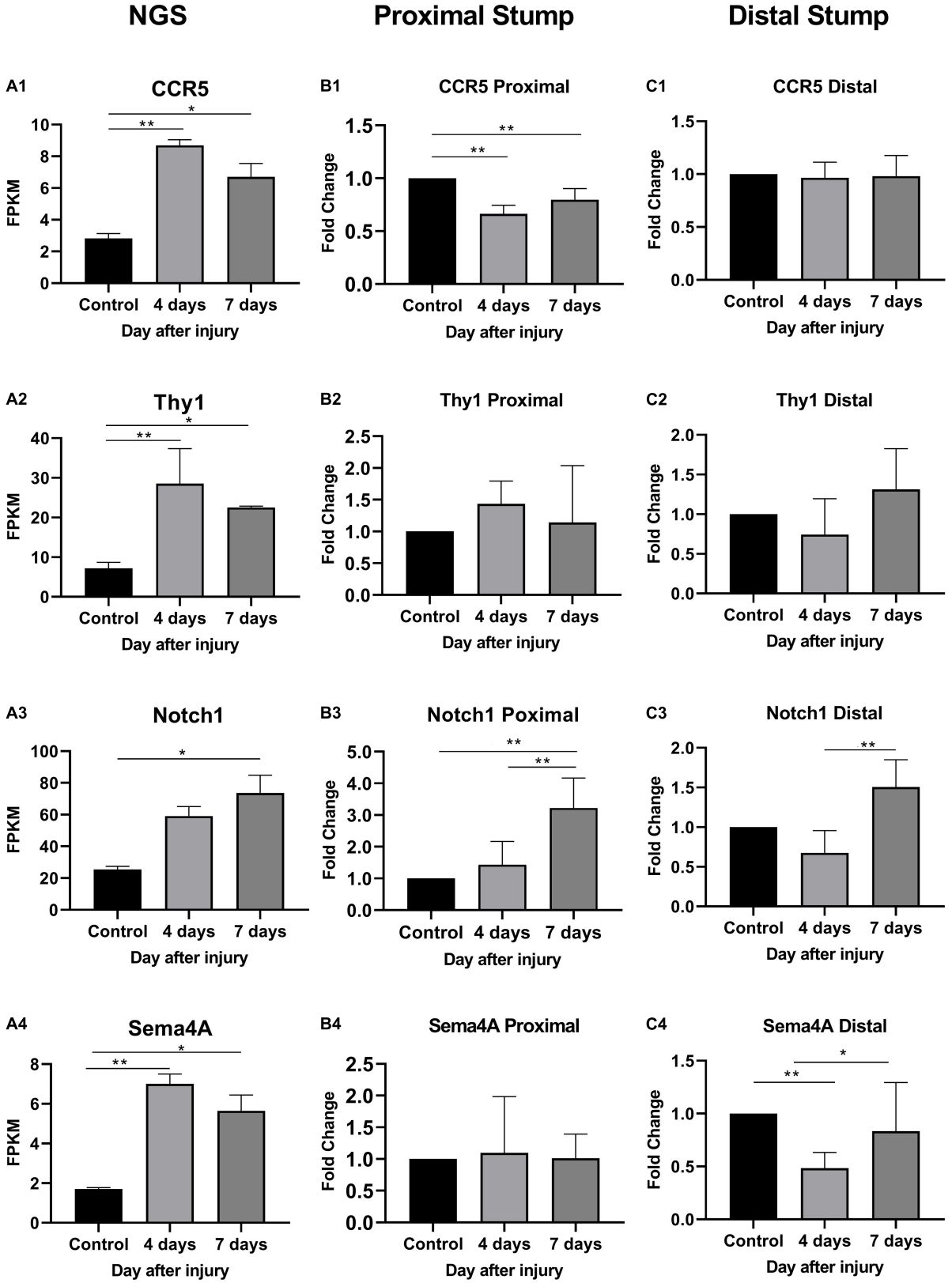

FIGURE 6 | Expression levels of DEmRNAs common to angiogenesis, axonal regeneration and immune response. **(A)** NGS results; **(B)** qRT-PCR expression of genes in proximal part after injury; **(C)** qRT-PCR expression of genes in distal part after injury. **(A1–C1)** CCR5 expression; **(A2–C2)** Thy1 expression; **(A3–C3)** Notch1 expression; **(A4–C4)** Sema4a expression. * denotes $P < 0.05$ compared with the control group, and ** denotes $P < 0.01$ compared with the control group.

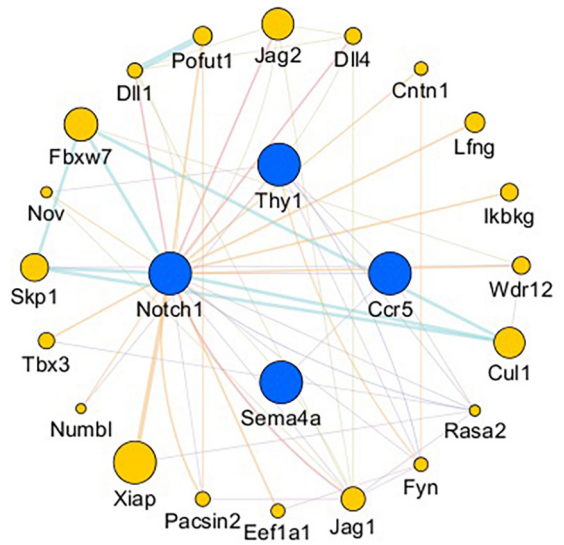

FIGURE 7 | Gene interaction network. Blue nodes: Genes related to axonogenesis, angiogenesis, and the immune response. Yellow nodes: Genes that interacted with CCR5, Thy1, Notch1, and Sema4A. The node size is based on the score. The larger the node is, the higher the score will be.

global mRNA expression changes in proximal nerve segments, focusing on dynamic changes in the crucial biological processes, and they noted the time-dependent expression of key regulatory genes after sciatic nerve transection. The peripheral nerve injury response leads to the upregulation of various genes required for initiating, guiding, and sustaining axonal growth. Guo et al. (2018) tried to identify specific genes related to the immune response and axon regeneration after peripheral nerve injury. They found six genes, namely, Alcam, Nrp1, Nrp2, Rac1, Creb1, and Runx3, in rat models of sciatic nerve transection, and these genes were found to be partially localized to the axons, especially in the regenerative axons (Guo et al., 2018). Injury to peripheral nerves can activate innate and acquired immune responses. Of note, the success or failure of the regeneration process has been interfered with by the interaction and overlap mechanisms of the nervous and immune systems after nerve injury (Gaudet et al., 2011; Rotshenker, 2011; Xanthos and Sandkühler, 2014). We suggested that regeneration, angiogenesis, and the immune response of the nerve interact and affect each other, and the results of their interaction directly affect the functional recovery of target organs after nerve repair (Yao et al., 2012; Cattin et al., 2015; Guo et al., 2018). Therefore, in this study, we investigated the transcriptome of SD rats in a model of sciatic nerve crush injury induced by clamping and combined the results of our GO and KEGG analyses to identify four genes related to nerve regeneration, angiogenesis, and the immune response: CCR5, Thy1, Notch1, and Sema4A. Among them, only change of Notch1 was basically consistent with the RNA-seq result after injury, which may be responsible for coordinating this process and promote peripheral nerve regeneration.

The DLL4/Notch1/Akt pathway is principally related to angiogenesis because it regulates the proliferation and migration of ECs in both normal conditions and in malignancies (Jones and Li, 2007; Sun et al., 2018; Tian et al., 2018). Inhibition of the Notch1 pathway suppresses ECs proliferation (Sun et al., 2018; Tian et al., 2018). It has also been reported that VEGF triggers DLL4 expression in tip cells to promote migration and activation of stalk cell proliferation via the Notch pathway (Jones and Li, 2007; Hasan et al., 2017; Park et al., 2018). Additionally, components of the Notch1 pathway are highly expressed in arteries but not in veins (Park et al., 2018), where it limits proliferation to prevent an excessively branched vasculature. Notch signaling can activate macrophage mobilization (Bai et al., 2018; Hossain et al., 2018) and promote neural stem and progenitor cell proliferation (Wang et al., 2018). On the one hand, enhancing arterial ECs proliferation and tube formation via the Notch1 pathway is important in angiogenesis during regeneration. On the other hand, the Notch1 pathway modulates artery formation by controlling ECs proliferation. The combination of the effects on immunology and neural cells suggests the importance of Notch1 in neural regeneration after damage. In the current study, we found that Notch1 expression showed significant change at both ends between 4 and 7 days after crush injury. The trend in the Notch1 change was basically consistent with the RNA-seq result after injury. In the proximal

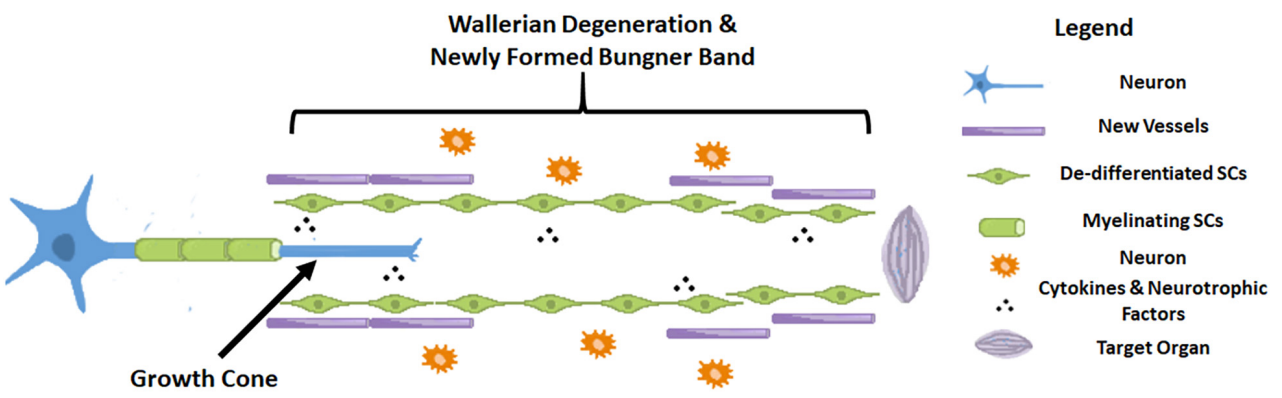

FIGURE 8 | Schematic diagram of a nerve after injury.

ends of injured nerves, Notch1 expression showed significant changes 4 days after the operation and continued to increase at day 7. But in the distal end, 4 days after injury, Notch1 expression was significantly lower than that in the control group, then gradually increased and became significantly higher than that in the control group by day 7 ($P < 0.01$). Furthermore, when we investigated interactions with related genes, we found eight important genes were associated with the Notch signaling pathway, most of which were indispensable in regeneration process of axons or vasculature.

Gene expression of CCR5, Thy1, and Sema4A showed either no changes or changes in the opposite direction, which implied that these three genes didn't not pass validation. However, it might be because of sites of samples were different between RNA-seq and qPCR analysis.

CONCLUSION

After peripheral nerve injury, CCR5, Thy1, Notch1, and Sema4A could be identified by bioinformatics analysis and transcriptional gene screening and found associated with regeneration, angiogenesis, and the immune response. Among them, the Notch1 change was basically consistent with the RNA-seq result after injury, which may be responsible for coordinating this process and promote peripheral nerve regeneration.

DATA AVAILABILITY STATEMENT

The datasets presented in this study can be found in online repositories. The names of the repository/repositories and accession number(s) can be found below: https://www.ncbi.nlm.nih.gov/, GSE162548.

ETHICS STATEMENT

The animal study was reviewed and approved by Experimental Animal Administration Committee of Sun Yat-sen University.

AUTHOR CONTRIBUTIONS

BH, ZZ, and YX designed the study. VP established the animal models. XL, SX, and YZ analysed and interpreted the experimental data. DD and GW were responsible for the bioinformatics analysis. ZZ and VP generated the graphs. YX, ZZ, and BH edited and revised the manuscript. All authors read and approved the final manuscript.

FUNDING

This research was supported by the Natural Science Foundation of Guangdong Province (2021A1515010471) and the National Natural Science Foundation of China (81901024).

SUPPLEMENTARY MATERIAL

The Supplementary Material for this article can be found online at: https://www.frontiersin.org/articles/10.3389/fncel.2021.717209/full#supplementary-material

REFERENCES

Abe, N., and Cavalli, V. (2008). Nerve injury signaling. *Curr. Opin. Neurobiol.* 18, 276–83. doi: 10.1016/j.conb.2008.06.005

Bai, X., Zhang, J., Cao, M., Han, S., Liu, Y., Wang, K., et al. (2018). MicroRNA-146a protects against LPS-induced organ damage by inhibiting Notch1 in macrophage. *Int. Immunopharmacol.* 63, 220–226. doi: 10.1016/j.intimp.2018.07.040

Benjamini, Y., Drai, D., Elmer, G., Kafkafi, N., and Golani, I. (2001). Controlling the false discovery rate in behavior genetics research. *Behav. Brain Res.* 125, 279–284. doi: 10.1016/S0166-4328(01)00297-2

Bozkurt, A., Deumens, R., Beckmann, C., Olde Damink, L., Schugner, F., Heschel, I., et al. (2009). In vitro cell alignment obtained with a Schwann cell enriched microstructured nerve guide with longitudinal guidance channels. *Biomaterials* 30, 169–179. doi: 10.1016/j.biomaterials.2008.09.017

Cattin, A. L., Burden, J. J., Van Emmenis, L., Mackenzie, F. E., Hoving, J. J., Garcia Calavia, N., et al. (2015). Macrophage-Induced blood vessels guide schwann cell-mediated regeneration of peripheral nerves. *Cell* 162, 1127–1139. doi: 10.1016/j.cell.2015.07.021

Dickson, B. J. (2002). Molecular mechanisms of axon guidance. *Science* 298, 1959–1964. doi: 10.1126/science.1072165

Djuanda, D., He, B., Liu, X., Xu, S., Zhang, Y., Xu, Y., et al. (2021). Comprehensive analysis of age-related changes in lipid metabolism and myelin sheath formation in sciatic nerves. *J. Mol. Neurosci. [Online ahead of print]* doi: 10.1007/s12031-020-01768-5

Ebenezer, G. J., McArthur, J. C., Polydefkis, M., Dorsey, J. L., O'Donnell, R., Hauer, P., et al. (2012). SIV-induced impairment of neurovascular repair: a potential role for VEGF. *J. Neurovirol.* 18, 222–230. doi: 10.1007/s13365-012-0102-5

Gaudet, A. D., Popovich, P. G., and Ramer, M. S. (2011). Wallerian degeneration: gaining perspective on inflammatory events after peripheral nerve injury. *J. Neuroinflammation*, 8:110. doi: 10.1186/1742-2094-8-110

Gorin, C., Rochefort, G. Y., Bascetin, R., Ying, H., Lesieur, J., Sadoine, J., et al. (2016). Priming dental pulp stem cells with fibroblast growth Factor-2 increases angiogenesis of implanted tissue-engineered constructs through hepatocyte growth factor and vascular endothelial growth factor secretion. *Stem. Cells Transl. Med.* 5, 392–404. doi: 10.5966/sctm.2015-0166

Guo, Q., Zhu, H., Wang, H., Zhang, P., Wang, S., Sun, Z., et al. (2018). Transcriptomic landscapes of immune response and axonal regeneration by integrative analysis of molecular pathways and interactive networks post-sciatic nerve transection. *Front. Neurosci.* 12:457. doi: 10.3389/fnins.2018.00457

Hasan, S. S., Tsaryk, R., Lange, M., Wisniewski, L., Moore, J. C., Lawson, N. D., et al. (2017). Endothelial Notch signalling limits angiogenesis via control of artery formation. *Nat. Cell Biol.* 19, 928–940. doi: 10.1038/ncb3574

He, B., Zhu, Z., Zhu, Q., Zhou, X., Zheng, C., Li, P., et al. (2014). Factors predicting sensory and motor recovery after the repair of upper limb peripheral nerve injuries. *Neural. Regen. Res.* 9, 661–672. doi: 10.4103/1673-5374.130094

Hossain, F., Majumder, S., Ucar, D. A., Rodriguez, P. C., Golde, T. E., Minter, L. M., et al. (2018). Notch signaling in myeloid cells as a regulator of tumor immune responses. *Front. Immunol.* 9:1288. doi: 10.3389/fimmu.2018.01288

Jones, C. A., and Li, D. Y. (2007). Common cues regulate neural and vascular patterning. *Curr. Opin. Genet. Dev.* 17, 332–336. doi: 10.1016/j.gde.2007.07.004

Kalinski, A. L., Yoon, C., Huffman, L. D., Duncker, P. C., Kohen, R., Passino, R., et al. (2020). Analysis of the immune response to sciatic nerve injury identifies efferocytosis as a key mechanism of nerve debridement. *eLife* 9:e60223. doi: 10.7554/eLife.60223

Kato, S., Matsukawa, T., Koriyama, Y., Sugitani, K., and Ogai, K. (2013). A molecular mechanism of optic nerve regeneration in fish: the retinoid signaling pathway. *Prog. Retin. Eye Res.* 37, 13–30. doi: 10.1016/j.preteyeres.2013.07.004

Konofaos, P., and Ver Halen, J. P. (2013). Nerve repair by means of tubulization: past, present, future. *J. Reconstr. Microsurg.* 29, 149–164. doi: 10.1055/s-0032-1333316

Kumar, V., Sachan, T., Natrajan, M., and Sharma, A. (2014). High resolution structural changes of Schwann cell and endothelial cells in peripheral nerves across leprosy spectrum. *Ultrastruct. Pathol.* 38, 86–92. doi: 10.3109/01913123.2013.870273

Li, S., Liu, Q., Wang, Y., Gu, Y., Liu, D., Wang, C., et al. (2013). Differential gene expression profiling and biological process analysis in proximal nerve segments after sciatic nerve transection. *PLoS One*, 8:e57000. doi: 10.1371/journal.pone.0057000

Lindborg, J. A., Niemi, J. P., Howarth, M. A., Liu, K. W., Moore, C. Z., Mahajan, D., et al. (2018). Molecular and cellular identification of the immune response in peripheral ganglia following nerve injury. *J. Neuroinflamm.* 15:192. doi: 10.1186/s12974-018-1222-5

Liu, D., Liang, X., and Zhang, H. (2016). Effects of high glucose on cell viability and differentiation in primary cultured schwann cells: potential role of ERK signaling pathway. *Neurochem. Res.* 41, 1281–1290. doi: 10.1007/s11064-015-1824-6

Liu, J., Wang, H. W., Liu, F., and Wang, X. F. (2015). Antenatal taurine improves neuronal regeneration in fetal rats with intrauterine growth restriction by inhibiting the Rho-ROCK signal pathway. *Metab. Brain Dis.* 30, 67–73. doi: 10.1007/s11011-014-9572-x

Liu, J. H., Tang, Q., Liu, X. X., Qi, J., Zeng, R. X., Zhu, Z. W., et al. (2018). Analysis of transcriptome sequencing of sciatic nerves in Sprague-Dawley rats of different ages. *Neural. Regen. Res.* 13, 2182–2190. doi: 10.4103/1673-5374.241469

Mortazavi, A., Williams, B. A., McCue, K., Schaeffer, L., and Wold, B. (2008). Mapping and quantifying mammalian transcriptomes by RNA-Seq. *Nat. Methods* 5, 621–628. doi: 10.1038/nmeth.1226

Park, J. K., Lee, T. W., Do, E. K., Moon, H. J., and Kim, J. H. (2018). Role of Notch1 in the arterial specification and angiogenic potential of mouse embryonic stem cell-derived endothelial cells. *Stem Cell Res. Ther.* 9:197. doi: 10.1186/s13287-018-0945-7

Pertea, M., Kim, D., Pertea, G. M., Leek, J. T., and Salzberg, S. L. (2016). Transcript-level expression analysis of RNA-seq experiments with HISAT, StringTie and Ballgown. *Nat. Protoc.* 11, 1650–1667. doi: 10.1038/nprot.2016.095

Pertea, M., Pertea, G. M., Antonescu, C. M., Chang, T. C., Mendell, J. T., and Salzberg, S. L. (2015). StringTie enables improved reconstruction of a transcriptome from RNA-seq reads. *Nat. Biotechnol.* 33, 290–295. doi: 10.1038/nbt.3122

Qiu, L., He, B., Hu, J., Zhu, Z., Liu, X., and Zhu, J. (2015). Cartilage oligomeric matrix protein Angiopoeitin-1 provides benefits during nerve regeneration in vivo and in vitro. *Ann. Biomed. Eng.* 43, 2924–2940.

Robinson, M. D., McCarthy, D. J., and Smyth, G. K. (2010). edgeR: a Bioconductor package for differential expression analysis of digital gene expression data. *Bioinformatics* 26, 139–140.

Robinson, M. D., and Oshlack, A. (2010). A scaling normalization method for differential expression analysis of RNA-seq data. *Genome Biol.* 11:R25.

Roth, L., Koncina, E., Satkauskas, S., Cremel, G., Aunis, D., and Bagnard, D. (2009). The many faces of semaphorins: from development to pathology. *Cell. Mol. Life Sci.* 66, 649–666.

Rotshenker, S. (2011). Wallerian degeneration: the innate-immune response to traumatic nerve injury. *J. Neuroinflammation* 8:109. doi: 10.1186/1742-2094-8-109

Sayad Fathi, S., and Zaminy, A. (2017). Stem cell therapy for nerve injury. *World J. Stem. Cells* 9, 144–151.

Sun, B., Dong, C., Lei, H., Gong, Y., Li, M., Zhang, Y., et al. (2018). Propranolol inhibits proliferation and invasion of hemangioma-derived endothelial cells by suppressing the DLL4/Notch1/Akt pathway. *Chem. Biol. Interact.* 294, 28–33.

Tessier-Lavigne, M., and Goodman, C. S. (1996). The molecular biology of axon guidance. *Science* 274, 1123–1133.

Tian, D., Zeng, X., Wang, W., Wang, Z., Zhang, Y., and Wang, Y. (2018). Protective effect of rapamycin on endothelial-to-mesenchymal transition in HUVECs through the Notch signaling pathway. *Vascul, Pharmacol.* 113, 20–26.

Wang, R., Zhao, C., Li, J., Li, Y., Liu, Y., Dong, H., et al. (2018). Notch1 promotes mouse spinal neural stem and progenitor cells proliferation via p-p38-pax6 induced cyclin D1 activation. *Exp. Cell Res.* 373, 80–90.

Xanthos, D. N., and Sandkühler J. (2014). Neurogenic neuroinflammation: inflammatory CNS reactions in response to neuronal activity. *Nat. Rev. Neurosci.* 15, 43–53. doi: 10.1038/nrn3617

Yao, D., Li, M., Shen, D., Ding, F., Lu, S., Zhao, Q., et al. (2012). Gene expression profiling of the rat sciatic nerve in early Wallerian degeneration after injury. *Neural. Regen. Res.* 7, 1285–1292.

Zhou, Y., Gunput, R. A., and Pasterkamp, R. J. (2008). Semaphorin signaling: progress made and promises ahead. *Trends Biochem. Sci.* 33, 161–170.

Zhu, Z., Huang, Y., Zou, X., Zheng, C., Liu, J., Qiu, L., et al. (2017). The vascularization pattern of acellular nerve allografts after nerve repair in Sprague-Dawley rats. *Neurol. Res.* 39, 1014–1021.

Zhu, Z., Zhou, X., He, B., Dai, T., Zheng, C., Yang, C., et al. (2015). Ginkgo biloba extract (EGb 761) promotes peripheral nerve regeneration and neovascularization after acellular nerve allografts in a rat model. *Cell Mol. Neurobiol.* 35, 273–282. doi: 10.1007/s10571-014-0122-1

Conflict of Interest: The authors declare that the research was conducted in the absence of any commercial or financial relationships that could be construed as a potential conflict of interest.

Publisher's Note: All claims expressed in this article are solely those of the authors and do not necessarily represent those of their affiliated organizations, or those of the publisher, the editors and the reviewers. Any product that may be evaluated in this article, or claim that may be made by its manufacturer, is not guaranteed or endorsed by the publisher.

frontiers in Cellular Neuroscience

ORIGINAL RESEARCH
published: 14 October 2021
doi: 10.3389/fncel.2021.743532

Up-Regulation of CD146 in Schwann Cells Following Peripheral Nerve Injury Modulates Schwann Cell Function in Regeneration

Yinying Shen[1†], Jun Zhu[2†], Qianyan Liu[1], Shiyan Ding[3], Xinpeng Dun[1] and Jianghong He[1*]*

[1] Key Laboratory of Neuroregeneration of Jiangsu and Ministry of Education, National Medical Products Administration (NMPA) Key Laboratory for Research and Evaluation of Tissue Engineering Technology Products, Co-innovation Center of Neuroregeneration, Nantong University, Nantong, China, [2] Department of Thoracic Surgery, Affiliated Hospital of Nantong University, Nantong, China, [3] Key Laboratory of Acupuncture and Medicine Research of Ministry of Education, School of Medicine and Holistic Integrative Medicine, Nanjing University of Chinese Medicine, Nanjing, China

OPEN ACCESS

Edited by:
Bo He,
Third Affiliated Hospital of Sun Yat-sen University, China

Reviewed by:
Jianlong Zou,
Guangzhou Medical University, China
Amol K. Bhandage,
Stockholm University, Sweden
Min Li,
Sun Yat-sen University Cancer Center (SYSUCC), China

****Correspondence:***
Xinpeng Dun
xinpengdun@hotmail.com
Jianghong He
hejh@ntu.edu.cn

[†] These authors have contributed equally to this work

Specialty section:
This article was submitted to Non-Neuronal Cells, a section of the journal Frontiers in Cellular Neuroscience

Received: *22 July 2021*
Accepted: *23 September 2021*
Published: *14 October 2021*

Citation:
Shen Y, Zhu J, Liu Q, Ding S, Dun X and He J (2021) Up-Regulation of CD146 in Schwann Cells Following Peripheral Nerve Injury Modulates Schwann Cell Function in Regeneration. Front. Cell. Neurosci. 15:743532. doi: 10.3389/fncel.2021.743532

CD146 is cell adhesion molecule and is implicated in a variety of physiological and pathological processes. However, the involvement of CD146 in peripheral nerve regeneration has not been studied yet. Here, we examine the spatial and temporal expression pattern of CD146 in injured mouse sciatic nerve via high-throughput data analysis, RT-PCR and immunostaining. By microarray data analysis and RT-PCR validation, we show that CD146 mRNA is significantly up-regulated in the nerve bridge and in the distal nerve stump following mouse sciatic nerve transection injury. By single cell sequencing data analysis and immunostaining, we demonstrate that CD146 is up-regulated in Schwann cells and cells associated with blood vessels following mouse peripheral nerve injury. Bioinformatic analysis revealed that CD146 not only has a key role in promoting of blood vessel regeneration but also regulates cell migration. The biological function of CD146 in Schwann cells was further investigated by knockdown of CD146 in rat primary Schwann cells. Functional assessments showed that knockdown of CD146 decreases viability and proliferation of Schwann cells but increases Schwann cell migration. Collectively, our findings imply that CD146 could be a key cell adhesion molecule that is up-regulated in injured peripheral nerves to regulate peripheral nerve regeneration.

Keywords: CD146, peripheral nerve injury, up-regulation, Schwann cells, blood vessels, regeneration

INTRODUCTION

Successful peripheral regeneration requires the co-ordination of injured neurons and multiple cell types in the distal nerve stump (Chen et al., 2007; Zigmond and Echevarria, 2019; Min et al., 2020). Damaged neurons shift from action potential transduction mode to a growth mode while Schwann cells, resident macrophages and endoneurial fibroblasts in the distal nerve stump undergo remarkable phenotypic changes in order to create a growth permissive environment for axon

regeneration (Weng et al., 2018; Jessen and Arthur-Farraj, 2019; Zigmond and Echevarria, 2019; Toma et al., 2020). Both myelinating and non-myelinating Schwann cells from injured site to the entire distal nerve stump dedifferentiate and proliferate to become mesenchymal-like repair cells and support axon elongation (Jessen and Mirsky, 2016). In the case of nerve transection injury, Schwann cells from both nerve ends migrate into the nerve gap and build Schwann cell cord to guide regenerating axons across the nerve gap (Parrinello et al., 2010; Clements et al., 2017; Chen et al., 2019; Min et al., 2020). The high plasticity of Schwann cells is one of the key reasons that the peripheral nervous system is superior over the central nervous system in regeneration following damage (Vargas and Barres, 2007; Chen et al., 2007; Jessen and Mirsky, 2016). Many neurotrophins, growth factors and cell adhesion molecules have been discovered to be differentially expressed in Schwann cells after peripheral nerve injury, and they have been demonstrated as important modulators of Schwann cell phenotype and peripheral nerve regeneration (Madduri and Gander, 2012; Jessen and Mirsky, 2016; Zhang et al., 2019). For instance, vascular endothelial growth factor stimulates the survival and proliferation of Schwann cells (Sondell et al., 1999). Nerve growth factor (NGF) promotes sensory axon regeneration while brain-derived neurotrophic factor (BDNF) and glial cell line-derived neurotrophic factor (GDNF) promote motor axon regeneration (Hoyng et al., 2014; Min et al., 2020). In contrast, neuregulin and betacellulin enhance Schwann cell proliferation, migration and remeylination (Li et al., 2015; Yi et al., 2016; Vallieres et al., 2017; Wang et al., 2021).

CD146, a cell surface protein encoded by MCAM (melanoma cell adhesion molecule), not only acts as a cell adhesion molecule but also is a signaling receptor of many extracellular matrix-related proteins and growth factors (Wang and Yan, 2013; Wang Z. et al., 2020). CD146 mediates multiple activities of various cell types including endothelial cells, epithelial cells, macrophages and T cells, and participates in miscellaneous biological processes such as development, angiogenesis and immune responses (Chen et al., 2017; Luo et al., 2017; Leroyer et al., 2019). The expression of CD146 is low in adult tissues but is highly expressed under various pathological conditions, especially carcinoma (Shih, 1999; Luo et al., 2012; Yawata et al., 2019). Previously, we performed sequencing analysis and studied the time course of gene expression profile in rat sciatic nerves (SRP113121) (Yi et al., 2015). Sequencing data analysis identified CD146 as one of differentially expressed molecules following peripheral nerve injury. To understand the expression pattern and a possible function of CD146 in peripheral nerve regeneration, in this study, we examined the dynamic changes of CD146 expression in injured mouse sciatic nerve, and investigated cell type specific distributions of CD146. We identified that CD146 is up-regulated in Schwann cells and cells associated with blood vessels in the nerve bridge and the distal nerve stump. Using cultured rat primary Schwann cells with siRNA transfection against CD146, we further demonstrated the regulatory role of CD146 in Schwann cell viability, proliferation and migration.

MATERIALS AND METHODS

Computational Analysis of Microarray and Single Cell Sequencing Data Sets

Microarray data of mouse distal sciatic nerves at 0, 3, 7, and 14 days after sciatic nerve crush injury were downloaded from NCBI GEO database GSE74087 (Pan et al., 2017) and GSE22291 (Barrette et al., 2010). Normalized data was applied to determine the fold changes of CD146 in the injured mouse sciatic nerves. Single cell sequencing data for intact mouse sciatic nerve and for the distal nerve at day 3 after sciatic nerve transection injury were downloaded from GSE147285 (Toma et al., 2020). Single cell sequencing data for mouse distal nerve at day 9 after sciatic nerve transection injury were downloaded from GSE120678 (Carr et al., 2019). Data were analyzed using Seurat v.3.2.1[1] and sctransform v.0.3 R packages v.4.0.2 as previously described (Chen et al., 2021). CD146 dotplot, tSNE and violinplot were created using Seurat specific function.

Animal Surgery

Animal experiments were ethical approved by the Administration Committee of Experimental Animals, China. Experimental procedures were carried out according to Institutional Animal Care Guidelines of Nantong University. Adult (2 month old) proteolipid protein (PLP)-GFP mice (Mallon et al., 2002) and C57BL/6 mice were subjected to sciatic nerve transection injury as previously described (Dun and Parkinson, 2018). Briefly, after isoflurane anesthetization and sciatic nerve exposure, sciatic nerve was transected at approximately 0.5 cm proximal to the nerve trifurcation site. Muscles were closed with sutures and skin was closed with Autoclips. Mice were given post-operative analgesia and sacrificed by CO_2 at 7 days after surgery. In total, 12 C57BL/6 mice and 3 PLP-GFP mice were used in this study.

Immunostaining

Sciatic nerves were collected and fixed with 4% paraformaldehyde overnight at 4°C. Fixed nerves were washed with PBS and dehydrated with 30% sucrose, and then embedded in OCT medium. Embedded nerves were sectioned on a cryostat at a thickness of 12 μm. Nerve sections were permeabilized with 0.25% Triton X-100 containing 1% BSA in PBS, blocked with blocking buffer (0.05% Triton X-100 containing3% BSA in PBS), and incubated with primary antibodies and species-specific secondary antibodies plus Hoechst 33342 nuclear dye diluted in blocking buffer. Primary antibodies neurofilament heavy chain (ab4680) and CD146 (ab75769) were purchased from Abcam (Cambridge, United Kingdom), CD31 (#5550274) was purchased from BD Pharmingen, NeuN was purchased from Merck Millipore (ABN91). Alexa Fluor 488 or 568 dye-conjugated donkey anti-rabbit and goat anti-chicken secondary antibodies and Hoechst 33342 nuclear dye (H3570) were purchased from Thermo Scientific (Basingstoke, United Kingdom). Stained nerve sections were mounted with Citifluor (Agar

[1]https://satijalab.org/seurat/

Scientific, R1320) and images were taken using a Leica SPE confocal microscope.

Bioinformatic Analysis

Functional pathways of CD146 were revealed using Ingenuity pathway analysis (IPA; Ingenuity Systems Inc., Redwood City, CA, United States) according to the build-in Ingenuity Pathways Knowledge Base (Yi et al., 2015). Interaction network of CD146, interacted factors and Gene Ontology (GO) biological processes were obtained using the ClueGo plug-in in the Cytoscape software.

Schwann Cell Culture and siRNA Transfection

Schwann cells were isolated from neonatal rat sciatic nerves, purified with anti-Thy1.1 (1:1,000, M7898, Sigma, St. Louis, MO, United States) and rabbit complement (Invitrogen, Carlsbad, CA, United States). Purified Schwann cells were cultured in DMEM (10-013-CVR, Corning, NY, United States) supplemented with 10% FBS (10099141c, Gibco, Grand Island, NY, United States). Cultured cells were transfected with CD146 siRNA (sequence: TAGTCAAGGAGGACAAAGA) or control siRNA (random sequence; RiboBio, Guangzhou, Guangdong, China) using Lipofectamine RNAiMAX transfection reagent (Invitrogen).

RT-PCR

Total mRNA was extracted from dissected left side sciatic nerve (control), nerve bridge and the distal nerve using a miRNeasy Mini Kit (Qiagen, Hilden, Germany) and first stand cDNA was synthesized with M-MLV reverse transcriptase (Promega, Southampton, United Kingdom) using random hexamer primers (Promega). Total mRNA was isolated from cultured cells using RNA-Quick Purification Kit (Yishan Biotechnology Co., Shanghai, China), reversely transcribed using HiScript III RT SuperMix for qPCR (+ gDNA wiper) (Vazyme, Nanjing, Jiangsu, China), and applied to a StepOne Real-time PCR System (Applied Biosystems, Foster City, CA, United States) with ChamQ SYBR qPCR Master Mix (Vazyme, Nanjing, Jiangsu, China). The sequences of primer pairs were as follows: CD146 (forward: 5′-AGGACCTTGAGTTTGAGTGG-3′; reverse: 5′-CAGTGGTTTGGCTGGAGT-3′), P0 (forward: 5′-CGTGATCG GTGGCATCCTC-3′; reverse: 5′- GGCATACAGCACTGGCG TCT-3′), p75 (forward: 5′-CTGCTGATTCTAGGGATGTCCT-3′; reverse: 5′-ATGTAACACTGTCCAGGCAGG-3′), GAPDH (forward: 5′-ACAGCAACAGGGTGGTGGAC-3′; reverse: 5′-TTTGAGGGTGCAGCGAACTT-3′), and 18 s (forward: 5′-GAGAAACGGCTACCACATCC-3′; reverse: 5′-GGACACT CAGCTAAGAGCATCG-3′). The $\Delta\Delta$Ct method was applied to quantify the relative abundances of CD146, P0, and p75 with GAPDH or 18 s as the reference gene.

Cell Viability Assay

Schwann cells transfected with CD146 siRNA or control siRNA for 36 h were seeded on 96-well plates at a density of 2×10^5 cells/ml and exposed to 10 μl of CCK8 using Cell Counting Kit-8 (Beyotime, Shanghai, China). After 2 h culture, cell viability was measured spectrophotometrically at 450 nm using a Synergy^{TM} 2 Multi-Mode Microplate Reader (BioTek, Burlington, VT, United States). Experiment was conducted four times using independent cultures, each tested induplicate.

Cell Proliferation Assay

Transfected Schwann cells were seeded onto 96-well plates at a density of 2×10^5 cells/ml and exposed to 50 μM EdU for 14 h using Cell-Light EdU DNA Cell Proliferation Kit (Ribibio). After additional 24 h, cells were fixed with 4% paraformaldehyde and stained with EdU and Hoechst 33342. Images were taken under Leica Model DMi8 (Leica Microsystems CMS GmbH, Bensheim, Germany). Experiment was conducted three times using independent cultures, each tested induplicate.

Cell Migration Assay

A 6.5 mm Transwell chamber with 8 μm pores (Costar, Cambridge, MA, United States) was applied to determine cell migration ability. The upper chamber was filled with transfected Schwann cells suspended in 100 μl DMEM at a density of 4×10^5 cells/ml. The bottom chamber was filled with 500 μl FBS containing cell culture medium. After 24 h culture, non-migrated Schwann cells on the upper surface of each membrane were cleaned with a cotton swab while migrated Schwann cells adhering to the bottom surface were stained with 0.1% crystal violet. Images were taken under Leica Model DMI3000B (Leica Microsystems). Experiment was conducted three times using independent cultures, each tested in triplicate.

A mold chamber with a 1 mm wide insert placed in the middle of the chamber was also applied. Transfected Schwann cells were seeded onto the two rectangular culture spaces in the mold chamber at a density of 2×10^5 cells/ml. Schwann cells were cultured for additional 9 h after cell confluence and insert removal. Remaining blank space was measured using Image-Pro Plus (Media Cybernetics, Silver Spring, MD, United States). Images were taken under Leica Model DMI3000B. Experiment was conducted three times using independent cultures, each tested induplicate or triplicate.

Statistical Analysis

Summarized data were presented as means ± SEM. Statistical significance was analyzed using student's *t*-test or one-way ANOVA followed by Dunnett's multiple comparisons test. Graphs and statistical tests were performed with GraphPad Prism 6.0 (GraphPad Software, Inc., La Jolla, CA, United States).

RESULTS

Enhanced Expression of CD146 After Peripheral Nerve Injury

To examine CD146 expression in the distal nerve stump following mouse sciatic nerve injury, we first analyzed two published microarray data sets, GSE74087 (Pan et al., 2017) and GSE22291 (Barrette et al., 2010). Both data sets have studied gene expression profile in the distal nerve at 0, 3, 7 and 14 days

following mouse sciatic nerve crush injury. Consistently, both data set revealed that CD146 was significantly up-regulated in the distal nerve at 3, 7 and 14 days following mouse sciatic nerve crush injury (**Figures 1A,B**). In microarray dataset GSE74087 (Pan et al., 2017), CD146 showed approximately 1.8 fold up-regulation at day 3 after injury as compared with its expression in uninjured mouse sciatic nerve (0 day). CD146 expression increased to an even higher level at day 7 and day 14 (**Figure 1A**). Similarly, data set GSE22291 (Barrette et al., 2010) showed approximately 1.7 fold up-regulation at day 3 after injury as compared with its expression in uninjured mouse sciatic nerve (0 day). CD146 up-regulation peaks at day 7 post-injury with both data set showing around fourfold up-regulation (**Figures 1A,B**). At day 14 post-injury, CD146 is slightly down-regulated compared with its up-regulation at day 7 post-injury but remain more than threefold up-regulation (**Figures 1A,B**). Because both data sets show the highest fold change of CD146 at day 7 post-injury, we performed RT-PCR study and validated our analysis using nerve bridge tissue and the distal nerve samples at day 7 after mouse sciatic nerve transection injury with left site uninjured sciatic nerve acting as control samples. In line with these observations by microarray data analysis, our RT-PCR results showed significant CD146 up-regulation in the nerve bridge and in the distal nerve stump at day 7 post-injury (**Figure 1C**). Our RT-PCR results also showed that CD146 is expressed in intact mouse sciatic nerves and it is further up-regulated in response to injury.

Next, we examined cell type specific expression of CD146 in both intact and injured mouse sciatic nerves with analyzed single cell RNA sequencing data GSE147285, which studied cell types and gene expression in intact mouse sciatic nerve and in the distal sciatic nerve at day 3 after sciatic nerve transection injury (Toma et al., 2020; Chen et al., 2021), and GSE120678 which studied cell types and gene expression in the distal sciatic nerves at day 9 after sciatic nerve transection injury (Carr et al., 2019; Chen et al., 2021). Single cell transcriptomics analysis demonstrated that CD146 is expressed in non-myelinating Schwann cells, vasculature-associated smooth muscle (VSM) cells and pericytes of intact mouse sciatic nerve (**Figure 2** and **Table 1**). Following injury, CD146 is strongly up-regulated in Schwann cells, VSM cells and pericytes of the distal nerve. It is also up-regulated in endoneurial fibroblasts and endothelial cells (**Figure 2** and **Table 1**). Thus, the single cell transcriptomics analysis demonstrated that CD146 is highly expressed in Schwann cells of the distal nerve and cells associated with blood vessels in the distal nerve stump.

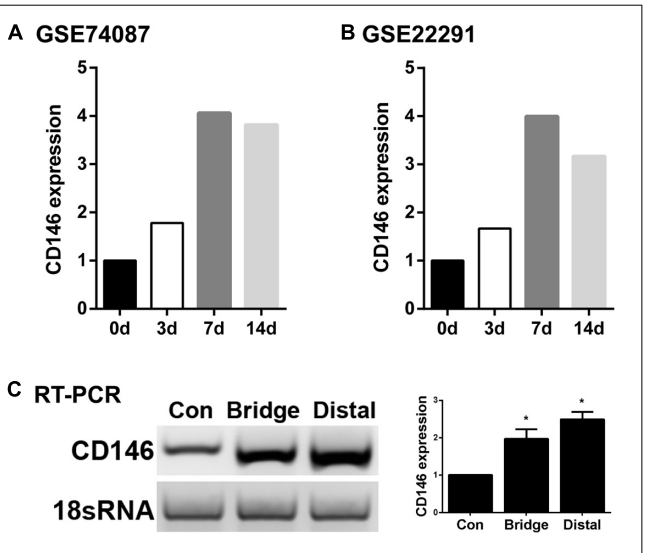

FIGURE 1 | Up-regulation of CD146 in injured mouse peripheral nerves. **(A,B)** CD146 fold changes in the distal nerve at 3, 7, and 14 days after mouse sciatic nerve injury, data was analyzed from microarray datasets GSE74087 **(A)** and GSE22291 **(B)**. **(C)** RT-PCR detection of CD146 expressions in intact mouse sciatic nerve (con), and in the nerve bridge and the distal nerve at day 7 after mouse sciatic nerve transection injury. Biological replicates $n = 3$, $^*p$-value < 0.05.

Expression of CD146 in Cells of Injured Mouse Sciatic Nerve

The expression of CD146 in cells of the injured mouse sciatic nerve was further investigated by immunohistochemistry after sciatic nerve transection injury. First, we double stained CD146 with an axon marker, neurofilament heavy chain, to reveal CD146 expression in transected mouse sciatic nerve at day 7 post-injury. The staining results revealed that CD146 doesn't co-localize with axons in the proximal nerve stump, indicating that regenerating axons don't express CD146 (**Figure 3C**). To confirm that regenerating axons don't express CD146, we double stained CD146 with a neuronal marker NeuN on sections of both spinal cord and dorsal root ganglion (DRG) after sciatic nerve transection injury. The staining confirmed that cell bodies of both motor neurons in the ventral horn of spinal cord (**Figures 3G–I**) and sensory neurons in DRG don't express CD146 (**Figures 3D–F**). At day 7 post-injury, regenerating axons have extended into the middle of the nerve bridge (**Figure 3A**). Interestingly, CD146staining signal partially co-localizes with regenerating axons in the nerve bridge (**Figures 3A–C**) although neurons do not express CD146. Regenerating axons in the nerve bridge are known to attach migrating Schwann cells for elongation (Chen et al., 2019; Min et al., 2020), indicating that CD146 could be expressed in migrating Schwann cells inside the nerve bridge. This staining also showed that CD146 is highly expressed in the distal nerve stump (**Figure 3B**).

To reveal CD146 up-regulation in Schwann cells, we stained CD146 on sciatic nerve sections at day 7 post-injury from PLP-GFP mice which Schwann cells are labeled with GFP (Mallon et al., 2002; Dun et al., 2019). As revealed by the single cell sequencing data analysis that CD146 is up-regulated in Schwann cells, strong CD146 immunostaining signals not only could be observed in GFP positive Schwann cells of the distal nerve stump (**Figures 4**, **5A–D**) but also could be observed in GFP positive Schwann cells inside the nerve bridge (**Figures 4**, **5E–H**). The staining results confirmed that Schwann cells in the distal nerve stump and migrating Schwann cells inside the nerve bridge express high level of CD146.

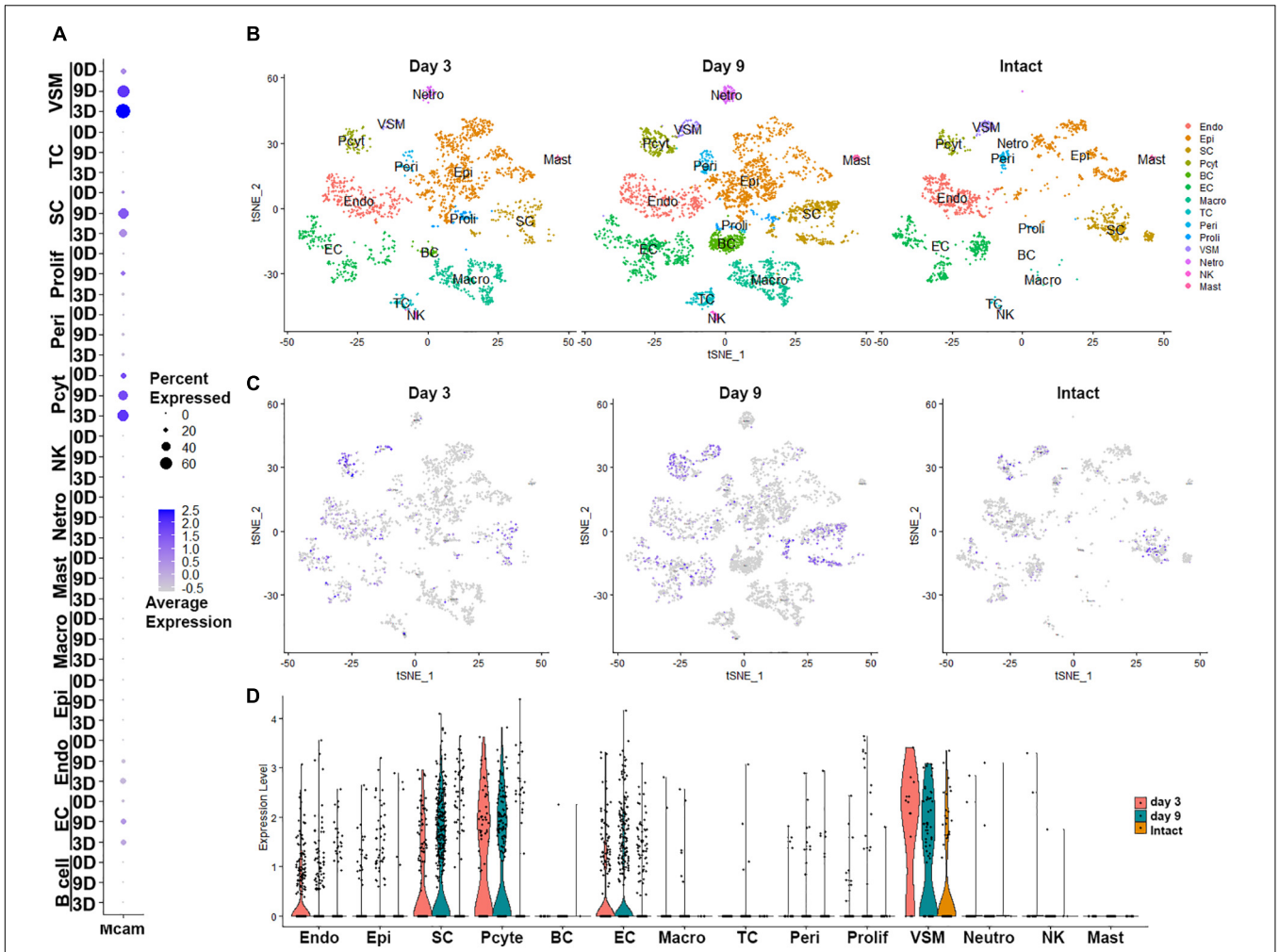

FIGURE 2 | Cell type specific expression of CD146 in intact and injured mouse sciatic nerve. **(A)** Dot plot showing CD146 up-regulation Schwann cells, VSM cells, pericytes and endothelial cells. **(B–D)** tSNE and violin plot showing Cell type specific expression of CD146 in intact and injured mouse sciatic nerve. Single cell sequencing data sets were analyzed from GSE147285 and GSE120678. EC, Endothelial cells; VSM, Vascular smooth muscle cells; Pcyt, Pericytes; Endo, Endoneurial fibroblasts; Peri, Perineurial fibroblasts; Epi, Epineurial fibroblasts; SC, Schwann cells; Macro, Macrophages; Neutro, Neutrophils; Mast, Mast cells; TC, T cells; NK, NK cells.

TABLE 1 | Expression levels of CD146 in cells of intact and injured mouse sciatic nerve.

	Schwann cells		VSM		Pericytes		Endothelial cells		Endoneurial cells	
	%	AE	%	AE	%	AE	%	AE	%	AE
Intact	13.65	1.02	25.88	1.16	23.47	1.61	13.53	0.45	6.22	0.23
Day 3	36.96	1.13	71.43	2.23	54.05	1.75	26.32	0.83	31.49	0.6
Day 9	49.66	1.55	57.14	1.74	48	1.64	25.86	1.03	16.54	0.47
	Perineurial cells		**Epineurial cells**		**neutrophils**		**NK cells**		**T cells**	
	%	AE	%	AE	%	AE	%	AE	%	AE
Intact	9.86	0.44								
Day 3	14.81	0.45	2.69	0.09	4.55	0.45	7.41	0.87		
Day 9	11.49	0.47	5.61	0.23			2.44	0.11	2.45	0.17

VSM, Vasculature-associated smooth muscle cells; AE, average expression.

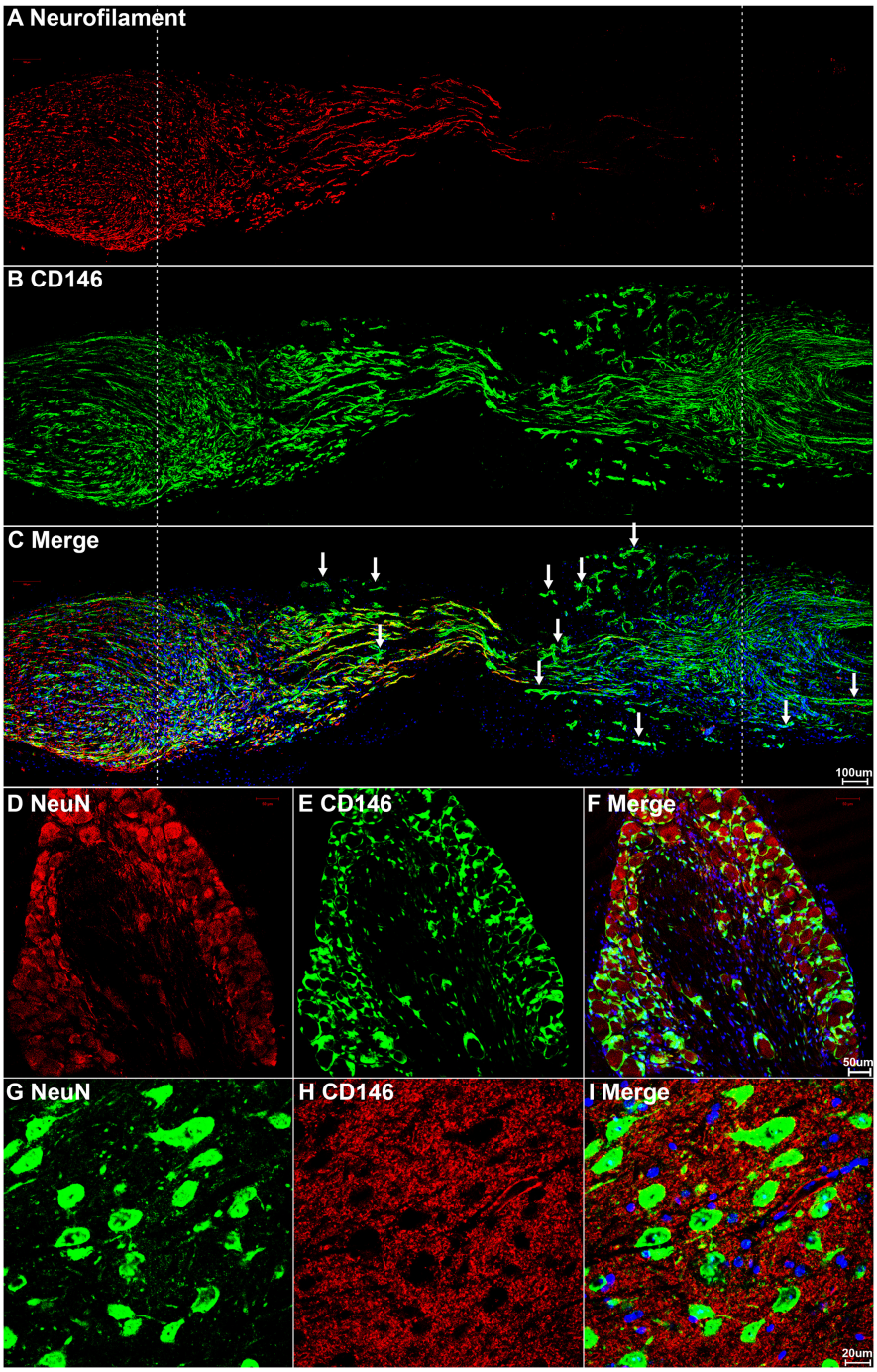

FIGURE 3 | CD146 expression in mouse peripheral nervous system following sciatic nerve transection injury. **(A–C)** Neurofilament and CD146 double staining on day 7 sciatic nerve longitudinal sections showing that CD146 is not expressed in regenerating axons. Scale bar in **(C)** 200 μm. Proximal nerve is located on the left and distal nerve is located on the right. Nerve bridge is located between two dished lines. **(D–F)** NeuN and CD146 double staining showing that CD146 is not expressed in sensory neurons of DRG. Scale bar in **(F)** 50 μm. **(G–I)** NeuN and CD146 double staining showing that CD146 is not expressed in motor neurons of spinal cord. Scale bar in **(I)** 20 μm. Biological replicates $n = 3$.

Above neurofilament double staining as well as CD146 staining in the PLP-GFP mice also showed that CD146 is strongly expressed in another population cells in the nerve bridge and in the distal nerve stump (indicated by arrows in **Figures 3C**, **4C**). Morphologically, these cells are associated with blood vessels. Our single cell sequencing data analysis showed that CD146 is highly up-regulated in VSM cells, pericytes and endothelial cells (**Figure 2** and **Table 1**). Due to the limitation

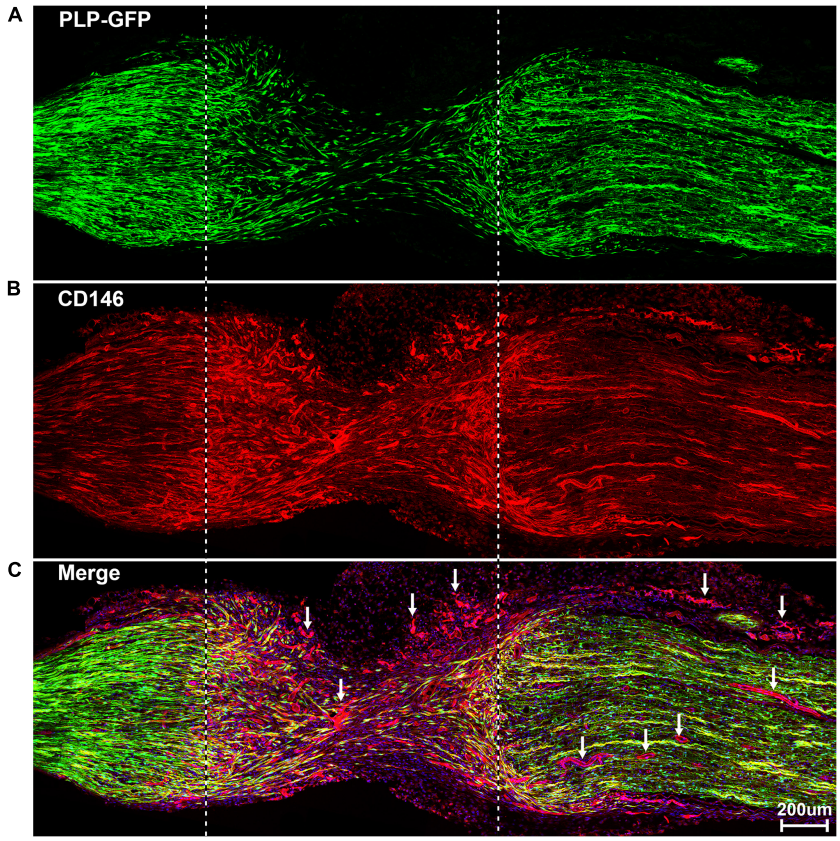

FIGURE 4 | Staining of CD146 on longitudinal sciatic nerve sections of PLP-GFP mice at day 7 after sciatic nerve transection injury showing CD146 expression in Schwann cells of the nerve bridge and the distal nerve stump. **(A)** PLP-GFP signal in Schwann cells. **(B)** CD146 staining in red. **(C)** Merged signals including Hoechst staining. Proximal nerve is located on the left and distal nerve is located on the right. Nerve bridge is located between two dished lines. Arrows in **(C)** indicated CD146 expression in blood vessels. Scale bar in **(C)** 200 μm. Biological replicates $n = 3$.

of available antibodies for double immunostaining, we therefore double stained CD146 with an endothelial cell marker CD31 to reveal CD146 expression in blood vessels. In consistent with our single cell sequencing data analysis, CD146 is highly expressed in cells associated with blood vessels (**Figures 5I–L**). Thus, our immunostaining results confirmed our single cell sequencing data analysis that, following peripheral nerve injury, CD146 is highly expressed in Schwann cells and cells associated with blood vessels.

Identifying Interaction Network of CD146

To gain insight into the biological function of CD146 up-regulation in injured peripheral nerves, the functional networks were investigated according to our sequencing data of injured rat sciatic nerves (Yi et al., 2015). Significant up-regulated genes were categorized based on the biological functions of CD146 using Gene Ontology (**Figure 6**). The functional network analysis revealed two important biological functions for CD146 in peripheral nerve regeneration. One biological function for CD146 is to promote angiogenesis (**Figure 6**). The up-regulation of CD146 in cells associated with regenerating blood vessels in the nerve bridge and the network analysis results indicate that CD146 could take part blood vessel regeneration in the nerve bridge by interacting with VEGF and FGF2 signaling pathways (**Figure 6**). In line with this finding, CD146 has a well characterized function in promoting angiogenesis and vascular development (St Croix, 2015; Tu et al., 2015). The other biological function for CD146 is to regulate cell migration (**Figure 6**). In view of the high abundance of CD146 in Schwann cells after peripheral nerve injury and the essential roles of migrating Schwann cells in the nerve bridge to direct axon regeneration, the biological functions of CD146 on Schwann cells were further examined in the following studies.

Biological Functions of CD146 in Schwann Cells

CD146 is highly expressed in Schwann cells of the injured peripheral nerves. Cultured Schwann cells are known to express similar gene as Schwann cells in the distal nerve stump (Jessen and Mirsky, 2016). Our qPCR result also confirmed that cultured rat primary Schwann cells express high level of CD146 (**Figure 7A**). We therefore took an *in vitro* approach to investigate CD146 function by knockdown CD146 with CD146 siRNA in cultured rat primary Schwann cells. The

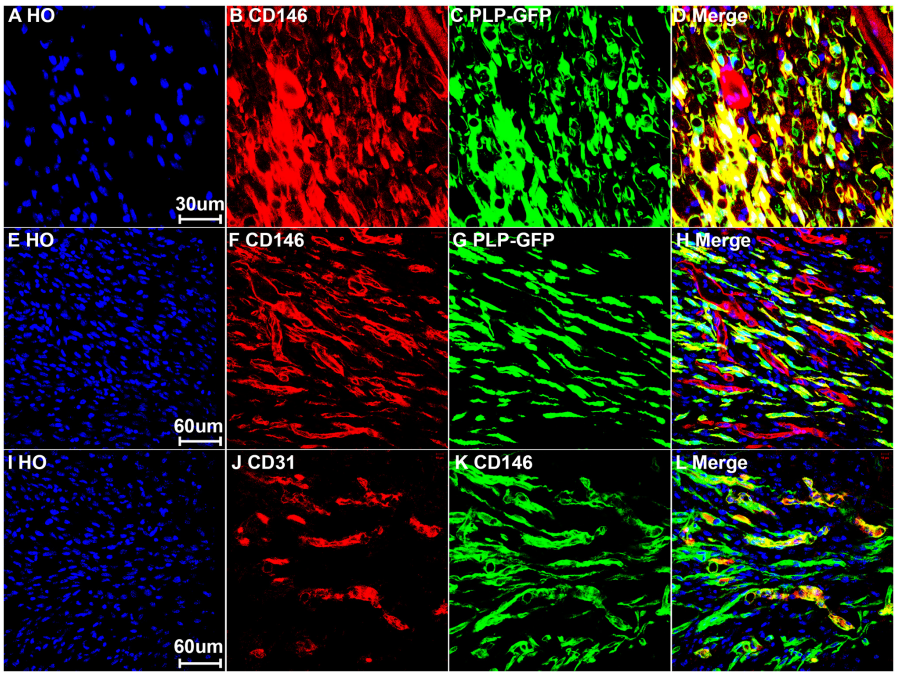

FIGURE 5 | Expression of CD146 in Schwann cells and cells associated with blood vessels of mouse sciatic nerve at day 7 post-injury. **(A–D)** Staining CD146 on distal nerve transverse sections. **(E–H)** CD146 on longitudinal nerve bridge sections from PLP-GFP mice at day 7 day after sciatic nerve transection injury showing migrating Schwann cells in the nerve bridge express CD146. Scale bar in **(E)** 60 μm. **(I–L)** Double staining CD146 with CD31 on longitudinal nerve bridge sections from C57BL/6 mice at day 7 after transection injury showing cells associated with blood vessels express CD146. Scale bar in **(I)** 60 μm. Biological replicates $n = 3$.

efficiency of CD146 knockdown was validated by qPCR to compare CD146 mRNA levels between control siRNA and CD146 siRNA transfected Schwann cells. qPCR results show that CD146 was effectively knocked down in Schwann cells following CD146 siRNA transfection (**Figure 7A**). After the validation of effective CD146 knockdown in Schwann cells, the function of CD146 on Schwann cell viability, proliferation and migration was investigated. CCK8 experiments showed that Schwann cells with attenuated CD146 expression exhibited relatively lower cell viability (**Figure 7B**). EdU proliferation assay demonstrated that after transfection with CD146 siRNA, the number of EdU-labeled proliferating cells and the ratio of proliferating cells to total cells were robustly reduced (**Figure 7C**). These findings indicate that knockdown of CD146 impairs the viability and proliferation of Schwann cells.

The high level of CD146 expression in migratory Schwann cells in the nerve bridge indicates that CD146 could regulate Schwann cell migration. Finally, we examined the effect of CD146 on Schwann cell migration by Transwell migration assay and wound healing assay. In control siRNA transfected Schwann cells after 24 h culture, a large amount of Schwann cells could be detected that have migrated across the upper surface (**Figure 8A**). In contrast, in CD146 siRNA transfected Schwann cells, significant more Schwann cells could be detected in the bottom surface of Transwell, suggesting that CD146 knockdown stimulates Schwann cell migration (**Figure 8A**). In line with the finding of Transwell migration assay, wound healing assay also showed enhanced Schwann cell migration following CD146 knockdown (**Figure 8B**).

DISCUSSION

CD146 (cluster of differentiation 146) is a cell adhesion molecule and it belongs to the immunoglobulin superfamily (Wang and Yan, 2013). It was initially identified as a tumor marker for melanoma with strong expression on metastatic lesions and advanced primary tumors, but its expression was rarely detected in benign lesions (Lehmann et al., 1987). Later studies have demonstrated that CD146 is highly expressed on a variety of carcinomas in addition to melanoma, and therefore CD146 has been suggested as a potential marker for tumor diagnosis, prognosis and treatment (Wang and Yan, 2013). However, recent reports have shown that CD146 not only just acts as a cell adhesion molecule to mediate cell-cell interaction and cell-matrix adhesion, it also acts as a cell surface receptor to transduce extracellular signals (St Croix, 2015; Tu et al., 2015). It is actively involved in many physiological processes such as organ development, cell migration, angiogenesis, immune response and tissue repair (St Croix, 2015; Tu et al., 2015).

In the central nervous system, CD146 has been identified as a recruiter of T cells and it is associated with multiple sclerosis, a central nervous system auto-inflammatory disease (Breuer et al., 2018; Zondler et al., 2020). Elevated soluble CD146 in the cerebrospinal fluid is considered as a biomarker of

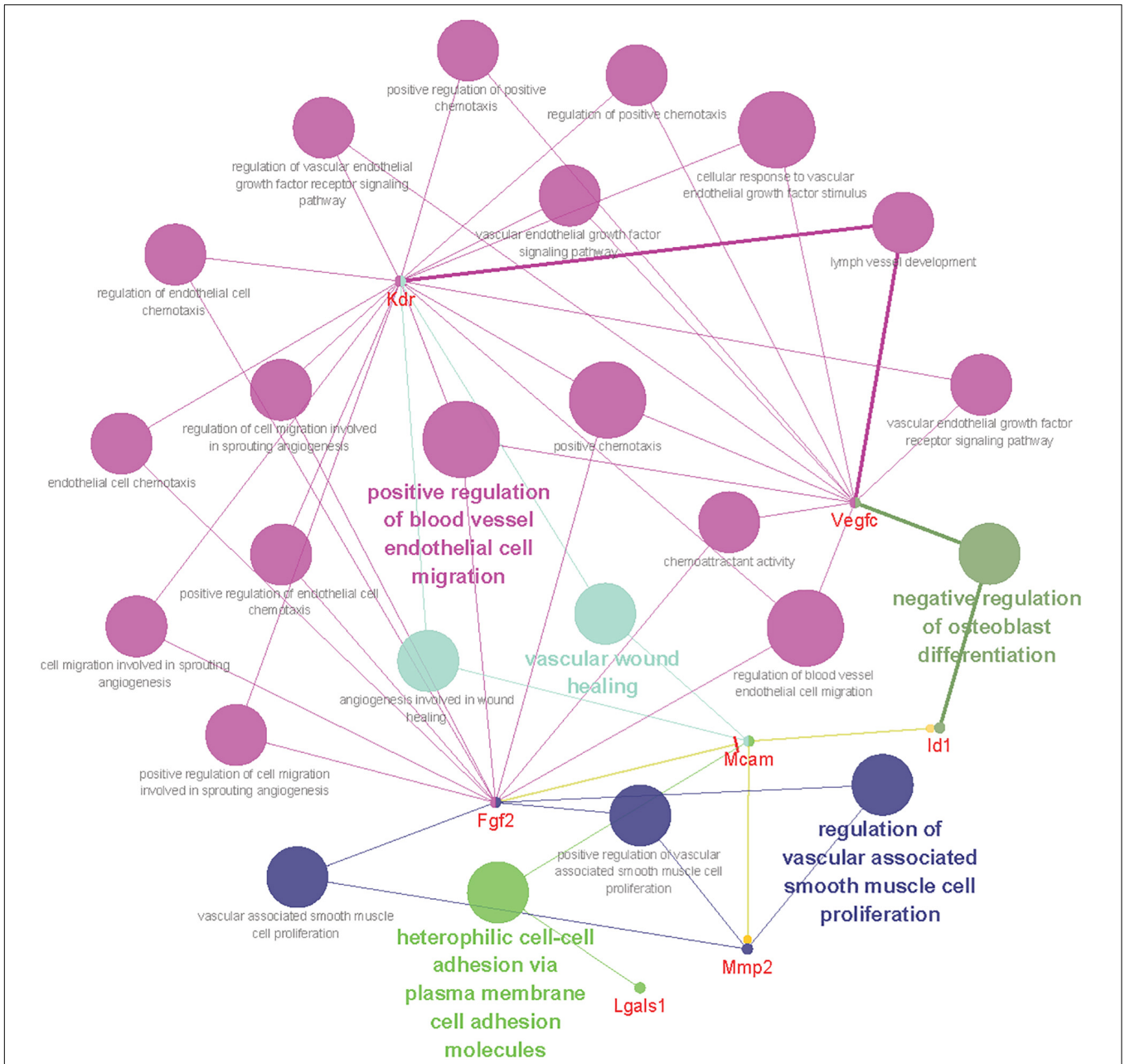

FIGURE 6 | Bioinformatic analysis showing CD146 functional network during peripheral nerve regeneration. Different colors of network nodes, respectively, represent different GO (Gene Ontology), with rose red representing GO:0043536 positive regulation of blood vessel endothelial cell migration, bright green representing GO:0007157 heterophilic cell-cell adhesion via plasma membrane cell adhesion molecules, dark green representing GO:0045668 negative regulation of osteoblast differentiation, light green representing GO:0061042 vascular wound healing, and blue representing GO: 1904705 regulation of vascular associated smooth muscle cell proliferation. The size of the nodes represents *p*-value.

neuroinflammation and blood-brain barrier dysfunction (Duan et al., 2013; Wang D. et al., 2020). Knockout CD146 in the central nervous system impaired mouse appetite, locomotion and spatial learning abilities (Tu et al., 2013). Expression of CD146 mRNA is increased in the spinal cord following spinal cord injury and it promotes neurogenesis and angiogenesis (Liu et al., 2016). Inhibition of CD146 function down-regulated the expression of angiogenesis-related factors such as VEGFR-2, p-p38 and p-AKT, and the inflammatory factors TNF-a, IL-1b, and IL-8, indicating that the up-regulation of CD146 has a beneficial role in the recovery from spinal cord injury (Liu et al., 2016). These studies revealed an important function of CD146 to promote the repair of central nervous system following injury or nerve degeneration.

Peripheral nerve injury induces vigorous gene expression changes not only in injured neurons but also in cells of the distal nerve stump (Jessen and Mirsky, 2016; Renthal et al., 2020;

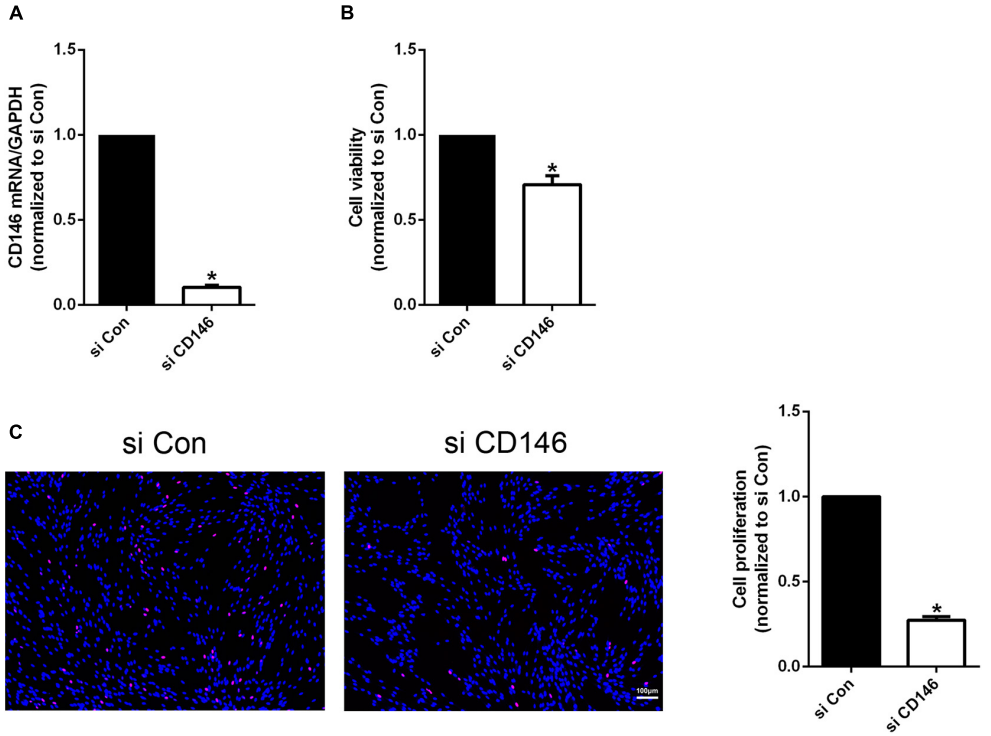

FIGURE 7 | Effects of CD146 on Schwann cell viability, proliferation and differentiation. **(A)** Efficiency of CD146 siRNA on CD146 expression in culture rat primary Schwann cells. Biological replicates $n = 3$. **(B)** Reduced Schwann cell viability after CD146 siRNA transfection. Biological replicates $n = 4$. **(C)** Proliferation rate of Schwann cells after CD146 siRNA transfection. Scale bar in C 100 μm. Biological replicates $n = 3$. The statistical differences were analyzed by student's *t*-test for comparisons between two groups or one-way analysis of variance (ANOVA) followed by Dunnett's multiple comparisons test for comparisons between multiple groups using GraphPad Prism 6.0 software (GraphPad Software, La Jolla, CA). *p-value < 0.05.

Toma et al., 2020; Chen et al., 2021). Previously, we studied gene expression changes in both DRG and the distal nerve stump in the rat by microarray analysis, and identified CD146 as one of DEGs in the distal nerve stump (Yi et al., 2015). However, the biological functions of CD146 in peripheral nerve regeneration remain undetermined. In this report, we examined cell type specific up-regulation of CD146 in injured mouse peripheral nervous system. We observed enhanced expression of CD146 in the nerve bridge and in the distal nerve stump after mouse sciatic nerve transection injury. We identified Schwann cells and cells associated with blood vessels expressing high level of CD146 in injured mouse peripheral nerves. An earlier study demonstrated that CD146 knockdown caused cell cycle arrest and induced the growth inhibition of glioma stem cells (Yawata et al., 2019). Similar to the function of CD146 in glioma stem cell proliferation, here, our CCK8 and EdU results showed that silencing of CD146 led to decreased cell viability and proliferation rate of cultured rat primary Schwann cells. Therefore, up-regulated CD146 in Schwann cells after nerve injury may contribute to the enlargement of Schwann cell population to promote peripheral nerve regeneration.

Our bioinformatic and functional pathway analysis revealed that CD146 has an important role in regulating cell migration, and our immunostaining results showed that CD146 is highly expressed on migrating Schwann cells of the nerve bridge, suggesting that CD146 could regulate Schwann cell migration in the nerve bridge following peripheral nerve transection injury. However, both Transwell migration assay and wound healing assay confirmed that knockdown of CD146 in cultured Schwann cells enhanced the speed of their migration, suggesting that CD146 mediated Schwann cell-Schwann cell adhesion could slows down Schwann cell migration in the nerve bridge. Previous studies also reported an opposite effects of CD146 on cell migration, which depends on the cell types of CD146 expression. For instance, it is reported that CD146 motivates the migration of endothelial cells (Zhang et al., 2018) and neuroendocrine carcinoma cells (Piao et al., 2019) but suppresses the migration of pancreatic cancer-associated fibroblasts (Zheng et al., 2016). Schwann cell migration in the nerve bridge is a highly coordinated process. They attach to each other through long bipolar processes and form chains migrating toward the middle of the nerve bridge (Chen et al., 2019, 2020; Min et al., 2020). Cell adhesion molecules play a key role in Schwann cell-Schwann cell interaction and Schwann cell chain migration in the nerve bridge (Parrinello et al., 2010). Thus, despite CD146 mediated Schwann cell adhesion slows down the speed of Schwann cell migration, it could be a key mediator for the formation of Schwann cell chains in the nerve bridge, but this remains to be investigated *in vivo*.

In this study, we show that CD146 is highly up-regulated in Schwann cells and cells associated with blood vessels following

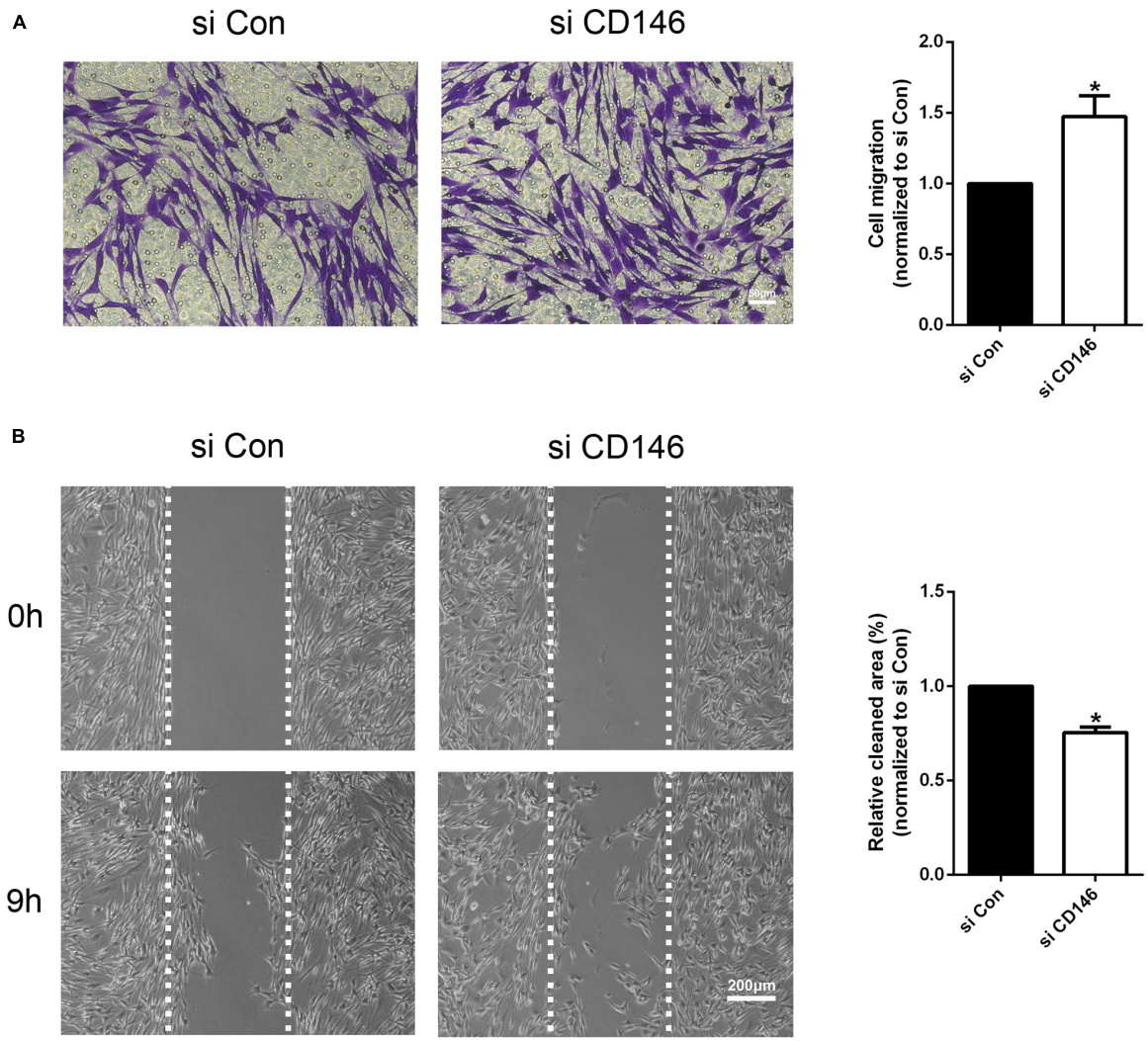

FIGURE 8 | Effects of CD146 on Schwann cell migration. **(A)** The Transwell-crossing migration ability of Schwann cells after CD146 siRNA transfection. Scale bar indicates 50 μm. Biological replicates $n = 3$. **(B)** The wound healing ability of Schwann cells after CD146 siRNA transfection. Scale bar indicates 200 μm. Biological replicates $n = 3$. The statistical differences were analyzed by student's *t*-test for comparisons between two groups or one-way analysis of variance (ANOVA) followed by Dunnett's multiple comparisons test for comparisons between multiple groups using GraphPad Prism 6.0 software (GraphPad Software, La Jolla, CA). *p-value < 0.05.

peripheral nerve injury. Previously, Nerve growth factor (NGF) has been shown to induce CD146 expression in Schwann cells (Hiroi et al., 2005; Taira et al., 2005). However, any other signals that could directly up-regulate CD146 expression in cells of the distal nerve have not been investigated. Evidence of CD146 expression in other tissue indicates that pro-inflammatory cytokines could also regulate CD146 up-regulation in the distal nerve stump. The production of pro-inflammatory cytokines is induced at the injury site and in the distal nerve stump following peripheral nerve injury (Cheepudomwit et al., 2008; Gaudet et al., 2011; Rotshenker, 2011). Reports have shown that some pro-inflammatory cytokines are able to induce CD146 expression, both tumor necrosis factor-alpha (TNFα) and interleukin-1a (IL1a) could significantly up-regulate CD146 expression in luteinizing granulosa cells (Melnikova et al., 2009; Wang and Yan, 2013). Transforming growth factor-beta (TGFβ) has been shown to up-regulate CD146 expression in hepatocytes (Tsuchiya et al., 2007). IL13 has been reported to induce CD146 expression in airway epithelial cells, this process could promote bacterial adherence to human bronchial epithelial cells (Simon et al., 2011). In addition, reports have shown that endothelin-1 and endothelin-3could enhance CD146 expression in melanocytes (Mangahas et al., 2004; Williams et al., 2014). Thus, growth factors and pro-inflammatory cytokines that are up-regulated in the injured peripheral nerve could regulate CD146 expression in Schwann cells and cells associated with blood vessels.

Taken together, we systematically studied the up-regulation of CD146 in injured mouse peripheral nervous system, and demonstrated that CD146 is up-regulated in Schwann cells

and cells associated with blood vessels. We further investigated the biological functions of CD146 on Schwann cell viability, proliferation and migration, and indicate that CD146 could play an essential role in peripheral nerve regeneration.

DATA AVAILABILITY STATEMENT

The original contributions presented in the study are included in the article/supplementary material, further inquiries can be directed to the corresponding author/s.

ETHICS STATEMENT

The animal study was reviewed and approved by Lab Animal Ethical Committee of Nantong University, and Administration Committee of Experimental Animals, Jiangsu, China. Written informed consent was obtained from the owners for the participation of their animals in this study.

AUTHOR CONTRIBUTIONS

XD and JH conceived, analyzed the data, contributed reagents, materials, and analysis tools, wrote the manuscript, and designed the experiments. YS, JZ, QL, SD, and XD performed the experiments. All authors contributed to the article and approved the submitted version.

FUNDING

This work was supported by the National Natural Science Foundation of China (No. 31971276) and the Natural Science Foundation of Jiangsu Higher Education Institutions of China (Major Program) (No. 19KJA320005) to JH.

REFERENCES

Barrette, B., Calvo, E., Vallieres, N., and Lacroix, S. (2010). Transcriptional profiling of the injured sciatic nerve of mice carrying the Wld(S) mutant gene: identification of genes involved in neuroprotection, neuroinflammation, and nerve regeneration. *Brain Behav. Immun.* 24, 1254–1267. doi: 10.1016/j.bbi.2010.07.249

Breuer, J., Korpos, E., Hannocks, M. J., Schneider-Hohendorf, T., Song, J., Zondler, L., et al. (2018). Blockade of MCAM/CD146 impedes CNS infiltration of T cells over the choroid plexus. *J. Neuroinflammation* 15:236. doi: 10.1186/s12974-018-1276-4

Carr, M. J., Toma, J. S., Johnston, A. P. W., Steadman, P. E., Yuzwa, S. A., Mahmud, N., et al. (2019). Mesenchymal precursor cells in adult nerves contribute to mammalian tissue repair and regeneration. *Cell Stem Cell* 24, 240-256.e9. doi: 10.1016/j.stem.2018.10.024

Cheepudomwit, T., Guzelsu, E., Zhou, C., Griffin, J. W., and Hoke, A. (2008). Comparison of cytokine expression profile during Wallerian degeneration of myelinated and unmyelinated peripheral axons. *Neurosci. Lett.* 430, 230–235. doi: 10.1016/j.neulet.2007.11.003

Chen, B., Banton, M. C., Singh, L., Parkinson, D. B., and Dun, X. P. (2021). Single cell transcriptome data analysis defines the heterogeneity of peripheral nerve cells in homeostasis and regeneration. *Front. Cell. Neurosci.* 15:624826. doi: 10.3389/fncel.2021.624826

Chen, B., Chen, Q., Parkinson, D. B., and Dun, X. P. (2019). Analysis of schwann cell migration and axon regeneration following nerve injury in the sciatic nerve bridge. *Front. Mol. Neurosci.* 12:308. doi: 10.3389/fnmol.2019.00308

Chen, B., Hu, R., Min, Q., Li, Y., Parkinson, D. B., and Dun, X. P. (2020). FGF5 regulates schwann cell migration and adhesion. *Front. Cell. Neurosci.* 14:237. doi: 10.3389/fncel.2020.00237

Chen, J., Luo, Y., Hui, H., Cai, T., Huang, H., Yang, F., et al. (2017). CD146 coordinates brain endothelial cell-pericyte communication for blood-brain barrier development. *Proc. Natl. Acad. Sci. U.S.A.* 114, E7622–E7631. doi: 10.1073/pnas.1710848114

Chen, Z. L., Yu, W. M., and Strickland, S. (2007). Peripheral regeneration. *Annu. Rev. Neurosci.* 30, 209–233. doi: 10.1146/annurev.neuro.30.051606.094337

Clements, M. P., Byrne, E., Camarillo Guerrero, L. F., Cattin, A. L., Zakka, L., Ashraf, A., et al. (2017). The wound microenvironment reprograms schwann cells to invasive mesenchymal-like cells to drive peripheral nerve regeneration. *Neuron* 96, 98-114.e7. doi: 10.1016/j.neuron.2017.09.008

Duan, H., Luo, Y., Hao, H., Feng, L., Zhang, Y., Lu, D., et al. (2013). Soluble CD146 in cerebrospinal fluid of active multiple sclerosis. *Neuroscience* 235, 16–26. doi: 10.1016/j.neuroscience.2013.01.020

Dun, X. P., Carr, L., Woodley, P. K., Barry, R. W., Drake, L. K., Mindos, T., et al. (2019). Macrophage-derived slit3 controls cell migration and axon pathfinding in the peripheral nerve bridge. *Cell Rep.* 26, 1458-1472.e4. doi: 10.1016/j.celrep.2018.12.081

Dun, X. P., and Parkinson, D. B. (2018). Transection and crush models of nerve injury to measure repair and remyelination in peripheral nerve. *Methods Mol. Biol.* 1791, 251–262. doi: 10.1007/978-1-4939-7862-5_20

Gaudet, A. D., Popovich, P. G., and Ramer, M. S. (2011). Wallerian degeneration: gaining perspective on inflammatory events after peripheral nerve injury. *J. Neuroinflammation* 8:110. doi: 10.1186/1742-2094-8-110

Hiroi, S., Taira, E., Ogawa, K., and Tsukamoto, Y. (2005). Neurite extension of DRG neurons by gicerin expression is enhanced by nerve growth factor. *Int. J. Mol. Med.* 16, 1009–1014.

Hoyng, S. A., De Winter, F., Gnavi, S., de Boer, R., Boon, L. I., Korvers, L. M., et al. (2014). A comparative morphological, electrophysiological and functional analysis of axon regeneration through peripheral nerve autografts genetically modified to overexpress BDNF, CNTF, GDNF, NGF, NT3 or VEGF. *Exp. Neurol.* 261, 578–593. doi: 10.1016/j.expneurol.2014.08.002

Jessen, K. R., and Arthur-Farraj, P. (2019). Repair schwann cell update: adaptive reprogramming. *Glia* 67, 421–437. doi: 10.1002/glia.23532

Jessen, K. R., and Mirsky, R. (2016). The repair Schwann cell and its function in regenerating nerves. *J. Physiol.* 594, 3521–3531. doi: 10.1113/JP270874

Lehmann, J. M., Holzmann, B., Breitbart, E. W., Schmiegelow, P., Riethmuller, G., and Johnson, J. P. (1987). Discrimination between benign and malignant cells of melanocytic lineage by two novel antigens, a glycoprotein with a molecular weight of 113,000 and a protein with a molecular weight of 76,000. *Cancer Res.* 47, 841–845.

Leroyer, A. S., Blin, M. G., Bachelier, R., Bardin, N., Blot-Chabaud, M., and Dignat-George, F. (2019). CD146 (Cluster of Differentiation 146). *Arterioscler. Thromb. Vasc. Biol.* 39, 1026–1033. doi: 10.1161/ATVBAHA.119.312653

Li, S., Wang, X., Gu, Y., Chen, C., Wang, Y., Liu, J., et al. (2015). Let-7 microRNAs regenerate peripheral nerve regeneration by targeting nerve growth factor. *Mol. Ther.* 23, 423–433. doi: 10.1038/mt.2014.220

Liu, C. J., Xie, L., Cui, C., Chu, M., Zhao, H. D., Yao, L., et al. (2016). Beneficial roles of melanoma cell adhesion molecule in spinal cord transection recovery in adult zebrafish. *J. Neurochem.* 139, 187–196. doi: 10.1111/jnc.13707

Luo, Y., Duan, H., Qian, Y., Feng, L., Wu, Z., Wang, F., et al. (2017). Macrophagic CD146 promotes foam cell formation and retention during atherosclerosis. *Cell Res.* 27, 352–372. doi: 10.1038/cr.2017.8

Luo, Y., Zheng, C., Zhang, J., Lu, D., Zhuang, J., Xing, S., et al. (2012). Recognition of CD146 as an ERM-binding protein offers novel mechanisms for melanoma cell migration. *Oncogene* 31, 306–321. doi: 10.1038/onc.2011.244

Madduri, S., and Gander, B. (2012). Growth factor delivery systems and repair strategies for damaged peripheral nerves. *J. Control. Release* 161, 274–282. doi: 10.1016/j.jconrel.2011.11.036

Mallon, B. S., Shick, H. E., Kidd, G. J., and Macklin, W. B. (2002). Proteolipid promoter activity distinguishes two populations of NG2-positive cells throughout neonatal cortical development. *J. Neurosci.* 22, 876–885.

Mangahas, C. R., dela Cruz, G. V., Schneider, R. J., and Jamal, S. (2004). Endothelin-1 upregulates MCAM in melanocytes. *J. Invest. Dermatol.* 123, 1135–1139. doi: 10.1111/j.0022-202X.2004.23480.x

Melnikova, V. O., Balasubramanian, K., Villares, G. J., Dobroff, A. S., Zigler, M., Wang, H., et al. (2009). Crosstalk between protease-activated receptor 1 and platelet-activating factor receptor regulates melanoma cell adhesion molecule (MCAM/MUC18) expression and melanoma metastasis. *J. Biol. Chem.* 284, 28845–28855. doi: 10.1074/jbc.M109.042150

Min, Q., Parkinson, D. B., and Dun, X. P. (2020). Migrating Schwann cells direct axon regeneration within the peripheral nerve bridge. *Glia* 69, 235-254. doi: 10.1002/glia.23892

Pan, B., Zhou, H. X., Liu, Y., Yan, J. Y., Wang, Y., Yao, X., et al. (2017). Time-dependent differential expression of long non-coding RNAs following peripheral nerve injury. *Int. J. Mol. Med.* 39, 1381–1392. doi: 10.3892/ijmm.2017.2963

Parrinello, S., Napoli, I., Ribeiro, S., Wingfield Digby, P., Fedorova, M., Parkinson, D. B., et al. (2010). EphB signaling directs peripheral nerve regeneration through Sox2-dependent Schwann cell sorting. *Cell* 143, 145–155. doi: 10.1016/j.cell.2010.08.039

Piao, Y., Guo, H., Qu, Z., Zheng, B., and Gao, Y. (2019). CD146 promotes migration and proliferation in pulmonary large cell neuroendocrine carcinoma cell lines. *Oncol. Lett.* 17, 2075–2080. doi: 10.3892/ol.2018.9830

Renthal, W., Tochitsky, I., Yang, L., Cheng, Y. C., Li, E., Kawaguchi, R., et al. (2020). Transcriptional reprogramming of distinct peripheral sensory neuron subtypes after axonal injury. *Neuron* 108, 128-144.e9. doi: 10.1016/j.neuron.2020.07.026

Rotshenker, S. (2011). Wallerian degeneration: the innate-immune response to traumatic nerve injury. *J. Neuroinflammation* 8:109. doi: 10.1186/1742-2094-8-109

Shih, I. M. (1999). The role of CD146 (Mel-CAM) in biology and pathology. *J. Pathol.* 189, 4–11. doi: 10.1002/(SICI)1096-9896(199909)189:1 <4::AID-PATH332>3.0.CO;2-P

Simon, G. C., Martin, R. J., Smith, S., Thaikoottathil, J., Bowler, R. P., Barenkamp, S. J., et al. (2011). Up-regulation of MUC18 in airway epithelial cells by IL-13: implications in bacterial adherence. *Am. J. Respir. Cell Mol. Biol.* 44, 606–613. doi: 10.1165/rcmb.2010-0384OC

Sondell, M., Lundborg, G., and Kanje, M. (1999). Vascular endothelial growth factor has neurotrophic activity and stimulates axonal outgrowth, enhancing cell survival and Schwann cell proliferation in the peripheral nervous system. *J. Neurosci.* 19, 5731–5740.

St Croix, B. (2015). CD146: the unveiling of a pro-angiogenic netrin receptor. *Cell Res.* 25, 533–534. doi: 10.1038/cr.2015.42

Taira, E., Kohama, K., Tsukamoto, Y., Okumura, S., and Miki, N. (2005). Gicerin/CD146 is involved in neurite extension of NGF-treated PC12 cells. *J. Cell. Physiol.* 204, 632–637. doi: 10.1002/jcp.20365

Toma, J. S., Karamboulas, K., Carr, M. J., Kolaj, A., Yuzwa, S. A., Mahmud, N., et al. (2020). Peripheral nerve single-cell analysis identifies mesenchymal ligands that promote axonal growth. *eNeuro* 7:ENEURO.0066-20.2020. doi: 10.1523/ENEURO.0066-20.2020

Tsuchiya, S., Tsukamoto, Y., Taira, E., and LaMarre, J. (2007). Involvement of transforming growth factor-beta in the expression of gicerin, a cell adhesion molecule, in the regeneration of hepatocytes. *Int. J. Mol. Med.* 19, 381–386.

Tu, T., Gao, Q., Luo, Y., Chen, J., Lu, D., Feng, J., et al. (2013). CD146 deletion in the nervous system impairs appetite, locomotor activity and spatial learning in mice. *PLoS One* 8:e74124. doi: 10.1371/journal.pone.0074124

Tu, T., Zhang, C., Yan, H., Luo, Y., Kong, R., Wen, P., et al. (2015). CD146 acts as a novel receptor for netrin-1 in promoting angiogenesis and vascular development. *Cell Res.* 25, 275–287. doi: 10.1038/cr.2015.15

Vallieres, N., Barrette, B., Wang, L. X., Belanger, E., Thiry, L., Schneider, M. R., et al. (2017). Betacellulin regulates schwann cell proliferation and myelin formation in the injured mouse peripheral nerve. *Glia* 65, 657–669. doi: 10.1002/glia.23119

Vargas, M. E., and Barres, B. A. (2007). Why is Wallerian degeneration in the CNS so slow? *Annu. Rev. Neurosci.* 30, 153–179. doi: 10.1146/annurev.neuro.30.051606.094354

Wang, D., Duan, H., Feng, J., Xiang, J., Feng, L., Liu, D., et al. (2020). Soluble CD146, a cerebrospinal fluid marker for neuroinflammation, promotes blood-brain barrier dysfunction. *Theranostics* 10, 231–246. doi: 10.7150/thno.37142

Wang, Y., Zhang, F., Zhang, Y., Shan, Q., Liu, W., Zhang, F., et al. (2021). Betacellulin regulates peripheral nerve regeneration by affecting Schwann cell migration and axon elongation. *Mol. Med.* 27:27. doi: 10.1186/s10020-021-00292-5

Wang, Z., Xu, Q., Zhang, N., Du, X., Xu, G., and Yan, X. (2020). CD146, from a melanoma cell adhesion molecule to a signaling receptor. *Signal Transduct. Target Ther.* 5:148. doi: 10.1038/s41392-020-00259-8

Wang, Z., and Yan, X. (2013). CD146, a multi-functional molecule beyond adhesion. *Cancer Lett.* 330, 150–162. doi: 10.1016/j.canlet.2012.11.049

Weng, Y. L., Wang, X., An, R., Cassin, J., Vissers, C., Liu, Y., et al. (2018). Epitranscriptomic m(6)A regulation of axon regeneration in the adult mammalian nervous system. *Neuron* 97, 313-325.e6. doi: 10.1016/j.neuron.2017.12.036

Williams, B., Schneider, R. J., and Jamal, S. (2014). Akt and PI3K-dependent but CREB-independent upregulation of MCAM by endothelin-3 in human melanocytes. *Melanoma Res.* 24, 404–407. doi: 10.1097/CMR.0000000000000077

Yawata, T., Higashi, Y., Kawanishi, Y., Nakajo, T., Fukui, N., Fukuda, H., et al. (2019). CD146 is highly expressed in glioma stem cells and acts as a cell cycle regulator. *J. Neurooncol.* 144, 21–32. doi: 10.1007/s11060-019-03200-4

Yi, S., Yuan, Y., Chen, Q., Wang, X., Gong, L., Liu, J., et al. (2016). Regulation of Schwann cell proliferation and migration by miR-1 targeting brain-derived neurotrophic factor after peripheral nerve injury. *Sci. Rep.* 6:29121. doi: 10.1038/srep29121

Yi, S., Zhang, H., Gong, L., Wu, J., Zha, G., Zhou, S., et al. (2015). Deep sequencing and bioinformatic analysis of lesioned sciatic nerves after crush injury. *PLoS One* 10:e0143491. doi: 10.1371/journal.pone.0143491

Zhang, R., Zhang, Y., and Yi, S. (2019). Identification of critical growth factors for peripheral nerve regeneration. *RSC Adv.* 9, 10760-10765.

Zhang, Z., Zheng, Y., Wang, H., Zhou, Y., and Tai, G. (2018). CD146 interacts with galectin-3 to mediate endothelial cell migration. *FEBS Lett.* 592, 1817–1828. doi: 10.1002/1873-3468.13083

Zheng, B., Ohuchida, K., Chijiiwa, Y., Zhao, M., Mizuuchi, Y., Cui, L., et al. (2016). CD146 attenuation in cancer-associated fibroblasts promotes pancreatic cancer progression. *Mol. Carcinog.* 55, 1560–1572. doi: 10.1002/mc.22409

Zigmond, R. E., and Echevarria, F. D. (2019). Macrophage biology in the peripheral nervous system after injury. *Prog. Neurobiol.* 173, 102–121. doi: 10.1016/j.pneurobio.2018.12.001

Zondler, L., Herich, S., Kotte, P., Korner, K., Schneider-Hohendorf, T., Wiendl, H., et al. (2020). MCAM/CD146 signaling via plcgamma1 leads to activation of beta1-integrins in memory t-cells resulting in increased brain infiltration. *Front. Immunol.* 11:599936. doi: 10.3389/fimmu.2020.599936

Conflict of Interest: The authors declare that the research was conducted in the absence of any commercial or financial relationships that could be construed as a potential conflict of interest.

Publisher's Note: All claims expressed in this article are solely those of the authors and do not necessarily represent those of their affiliated organizations, or those of the publisher, the editors and the reviewers. Any product that may be evaluated in this article, or claim that may be made by its manufacturer, is not guaranteed or endorsed by the publisher.

frontiers in Cellular Neuroscience

ORIGINAL RESEARCH
published: 23 December 2021
doi: 10.3389/fncel.2021.816781

Recombinant COL6 α2 as a Self-Organization Factor That Triggers Orderly Nerve Regeneration Without Guidance Cues

Zhou Fang[1,2] *and Jian-Long Zou*[1,2]*

[1] *Institute of Neuroscience and the Second Affiliated Hospital of Guangzhou Medical University, Key Laboratory of Neurogenetics and Channelopathies of Guangdong Province and the Ministry of Education of China, Guangzhou, China,* [2] *Key Laboratory of Neurological Function and Health, School of Basic Medical Sciences, Guangzhou Medical University, Guangzhou, China*

Collagen VI (COL6) in the microenvironment was recently identified as an extracellular signal that bears the function of promoting orderly axon bundle formation. However, the large molecular weight of COL6 (≈2,000 kDa) limits its production and clinical application. It remains unclear whether the smaller subunit α chains of COL6 can exert axon bundling and ordering effects independently. Herein, based on a dorsal root ganglion (DRG) *ex vivo* model, the contributions of three main COL6 α chains on orderly nerve bundle formation were analyzed, and COL6 α2 showed the largest contribution weight. A recombinant COL6 α2 chain was produced and demonstrated to promote the formation of orderly axon bundles through the NCAM1-mediated pathway. The addition of COL6 α2 in conventional hydrogel triggered orderly nerve regeneration in a rat sciatic nerve defect model. Immunogenicity assessment showed weaker immunogenicity of COL6 α2 compared to that of the COL6 complex. These findings suggest that recombinant COL6 α2 is a promising material for orderly nerve regeneration.

Keywords: peripheral nerve injury, nerve bundle formation, self-organization, COL6 α2, immunogenicity, myelination

OPEN ACCESS

Edited by:
Ji-Fan Hu,
Jilin University, China

Reviewed by:
Jianghui Liu,
The First Affiliated Hospital of Sun Yat-sen University, China
Liumin He,
Sun Yat-sen University, China

***Correspondence:**
Jian-Long Zou
zou_jianlong@gzhmu.edu.cn

Specialty section:
This article was submitted to Non-Neuronal Cells, a section of the journal Frontiers in Cellular Neuroscience

Received: *17 November 2021*
Accepted: *06 December 2021*
Published: *23 December 2021*

Citation:
Fang Z and Zou J-L (2021) Recombinant COL6 α2 as a Self-Organization Factor That Triggers Orderly Nerve Regeneration Without Guidance Cues. Front. Cell. Neurosci. 15:816781. doi: 10.3389/fncel.2021.816781

INTRODUCTION

Peripheral nerve injury is a common disease for which there exist a large number of nerve repair strategies, including end-to-end neurorrhaphy, nerve grafting, gene therapy, and electrical stimulation. These medical and engineering approaches have shown effectiveness in promoting peripheral nerves regeneration (Gordon and English, 2016; Eggers et al., 2020; Raza et al., 2020). However, the disorganization of regenerated nerve fibers is still an important factor that leads to a mismatch between nerve fibers and target organs and restricts functional recovery from peripheral nerve injury (Robinson and Madison, 2004; English, 2005; de Ruiter et al., 2014).

The introduction of extrinsic guidance signals in nerve grafts is an effective strategy for orderly axon regeneration (Krick et al., 2011; Liu et al., 2018). However, these approaches require the anisotropic distribution of guidance signals, such as gradient-distributed biochemical cues or well-aligned physical cues, within small nerve grafts (Handarmin et al., 2011; Oh et al., 2018; Hsu et al., 2019). Hence, their axon-ordering effects are severely limited by the development of manufacturing techniques.

The concept of axonal self-organization without guidance cues may overcome this limitation. A previous study reported a unique phenomenon whereby dorsal root ganglion (DRG) axons tended to gather into straight bundles in the peripheral nerve extracellular matrix (ECM)-derived homogeneous hydrogel environment (Zou et al., 2018a). Collagen VI (COL6), an ECM protein abundant in various tissues, was subsequently identified as a microenvironmental cue that induced the formation of parallel nerve bundles through the neural cell adhesion molecule 1 (NCAM1)-mediated pathway (Sun et al., 2022).

In peripheral nerves, the COL6 is mainly secreted by Schwann cells, which in turn regulates the structure and function of Schwann cell. Lack of COL6 in the peripheral nervous system leads to increased myelin thickness and impaired motor coordination in mice (Cescon et al., 2015). Among the 28 types of identified collagens, COL6 is composed of COL6 α1, COL6 α2, and COL6 α3 chains, which undergo a unique process of supramolecular assembly leading to the formation of extremely large COL6 tetramers (molecular mass, ≈2,000 kDa) (Cescon et al., 2015). Due to the complicated assembly process and large molecular weight of COL6, it is difficult to prepare the whole COL6 protein using the recombinant protein technique. At the same time, the high molecular weight of COL6 also increases its immunogenicity (Lynn et al., 2004; Boeer et al., 2014). In general, whole proteins are not suitable drug candidates for several reasons, including susceptibility to proteolytic degeneration, antigenicity, and high associated costs. Therefore, some protein subunits or peptides are typically produced to achieve functional specificity, low immunogenicity, and to make drug candidates less costly (Ullrich et al., 1983; Lau and Dunn, 2018).

Encouraged by the results of these studies, here, we present a comparative study on the function and immunogenicity of recombinant COL6 α chains, which aimed to determine the independent effect of COL6 subunit chains on axonal self-organization with potential application in peripheral nerve injury.

MATERIALS AND METHODS

Animals

Three to five day old Sprague–Dawley rats (with randomized sex; weights, 10–12 g) and 2-month-old Sprague–Dawley rats (female, ≈220 g) were purchased from the Animal Center Laboratory of Sun Yat-sen University (license no. SCXK (Yue) 2016-0029). All rats were housed under specific pathogen-free conditions. All animal experiments in this study were carried out per the ethical standards of the Animal Ethics Committee of Guangzhou Medical University (approval no. GY2019048) on April 30, 2019.

Reagents

Human native COL6 protein (cat# 354261) and Matrigel (cat# 356230, growth factor reduced) were purchased from Corning Inc. (NY, USA). Pentobarbital (cat# P3761), Triton X-100 (cat# T8787), anti-neurofilament 200 (NF200) antibody (mouse monoclonal, cat# SAB4200705), anti-COL6 α3 antibody (rabbit polyclonal, cat# HPA010080), radioimmunoprecipitation assay (RIPA) buffer (cat# R0278) were purchased from Sigma–Aldrich (San Francisco, CA, USA). B27 (cat# 17504044) and L-glutamine (cat# 25030081) were purchased from Gibco (Grand Island, NY, USA). β-nerve growth factor (cat# 450-01) was purchased from Peprotech (Rocky Hill, NJ, USA). Anti-COL6 α1 antibody (rabbit monoclonal, cat# ab182744), anti-NCAM1 antibody (rabbit monoclonal, cat# ab220360), and rat IgM SimpleStep enzyme-linked immunosorbent assay (ELISA®) Kit (cat# ab215085) were purchased from Abcam (Cambridge, MA, USA). Anti-COL6 α2 antibody (mouse monoclonal, cat# sc-374566) was purchased from Santa Cruz Biotechnology, Inc. (Dallas, TX, USA). Anti-glyceraldehyde 3-phosphate dehydrogenase (anti-GAPDH) antibody (rabbit monoclonal, cat# AF1186), Cy3-conjugated goat anti-rabbit IgG (cat# A0516), Alexa Fluor 488-conjugated goat anti-mouse IgG (cat# A0428), bicinchoninic acid (BCA) protein assay kits (cat# P0009), horseradish peroxidase (HRP)-conjugated goat anti-mouse IgG (cat# A0216), HRP-conjugated goat anti-rabbit IgG (cat# A0208), anti-β-actin antibody (mouse monoclonal, cat# AA128), and fast silver stain kit (cat# P0017S) were purchased from Beyotime Biotechnology (Shanghai, China). Normal goat serum (cat# 31873) was purchased from Invitrogen (Carlsbad, CA, USA). Mounting medium containing 4′, 6-diamidino-2-phenylindole (DAPI) (cat# S36973), MAX Efficiency™ DH5α cells (cat# 18258012), and a protein ladder (cat# 26625) were purchased from Thermo Fisher Scientific (Waltham, MA, USA). Myc-DDK-tagged human COL6 α2 open reading frame (ORF) clone (cat# RC209476) was purchased from OriGene Technologies Inc. (Rockville, MD, USA). HEK293 cells were purchased from the American Type Culture Collection (Manassas, VA, USA). Anti-Myc tag affinity gel (cat# IP0097) was purchased from Dia-An Biotechnology Co., Ltd. (Wuhan, Hubei, China). Protease/phosphatase inhibitor cocktail (cat# 5872S) was purchased from Cell Signaling Technology (Danvers, MA, USA). Sodium dodecyl sulfate-polyacrylamide gel electrophoresis (SDS-PAGE; cat# 4568123) was purchased from Bio-Rad (Hercules, CA, USA). Isoflurane (cat# R510-22-8) and a small animal anesthesia machine (R540) were purchased from RWD Life Science Co. Ltd. (Shenzhen, China). A silicone catheter (with diameter 1.2 mm) was purchased from Merck KGaA (Darmstadt, Germany).

Coating of the Cell Culture Plates

In coating the culture plates with COL6, human native COL6 was dissolved in cold saline to obtain a 20 μg/ml COL6 solution before coating. The COL6 solution was added to the culture dishes at 2 μg/cm^2. The culture dishes were placed at 37°C for 2 h and washed once with the culture medium before DRG implantation. Using the same procedure described above, the plates used in the COL6 α2 treatment group were precoated with a solution consisting of 1 mg/ml Matrigel and 10 μg/ml COL6 α2 in cold saline, and the plates used in the vehicle group were precoated with a solution containing 1 mg/ml Matrigel in cold saline.

DRG *ex vivo* Preparation

Neonatal rats were deeply anesthetized via intraperitoneal injection with pentobarbital (200 mg/kg) before dissection of the DRG tissue blocks. The DRGs were then seeded

onto protein-precoated dishes and immersed in Neurobasal-A medium containing 2% B27, 0.5 mM L-glutamine, and 50 ng/ml β-nerve growth factor. The dishes were placed in an incubator with a temperature of 37°C with the medium changed every 2 days.

Antibody Blocking Assay

To block the function of COL6 subunit chains, the DRGs seeded on the COL6-precoated surface were incubated with function-blocking antibodies to COL6 α1, α2, and α3, respectively, at 37°C for 48 h. In other experiments, the DRGs growing on the Matrigel and COL6 α2-precoated surface were treated with an NCAM1 antibody for 48 h; then, the DRGs were fixed and examined by microscopy. An antibody against GAPDH was used as a control. All antibodies were applied at the same concentration (1 μg/ml) in this assay.

Immunofluorescence Staining

After a period of incubation, the DRG tissue blocks were fixed with 4% paraformaldehyde for 2 h and thoroughly rinsed with phosphate-buffered saline for 30 min. The membrane was permeabilized by incubation in 0.3% Triton X-100 for 10 min, and non-specific antigens were blocked by incubation for 30 min with 10% normal goat serum. The specimens were then incubated with anti-NF200 antibody (1:200) or anti-NCAM1 antibody (1:300) at 37°C for 3 h, followed by incubation with Cy3-conjugated secondary antibody (1:500) or Alexa Fluor 488-conjugated secondary antibody (1:500) at 37°C for 1 h. The nuclei were visualized using a mounting medium containing DAPI.

Measurement of Axon Diameter

In a subset of DRG *ex vivo* preparations, DRG tissue blocks with regenerated axons were photographed using a microscope at a magnification of 400×. The region of interest (ROI) was defined as a square with a length of 200 μm and randomly set at a distance of 500 μm from the DRG tissue block. Within the ROI, the diameter of each axon or bundle was measured, and six ROIs were recorded in each culture well; five biological replicates were performed for each group and the average diameter of the axon bundle in each group was calculated.

Evaluation of Axon Directional Stability

Based on the micrographs of DRG *ex vivo* preparations, a 20 μm wide stripe was masked along the initial direction of the axon or axon bundle. The distance at which the axon or bundle first crossed the boundary of the stripe was measured, and a longer distance reflected better directional stability of the regenerating axon. The data for 20 axons were randomly recorded in each culture well and five biological replicates were performed for each group.

Recombinant Protein Expression and Purification

The plasmid of the Myc-DDK-tagged human COL6 α2 ORF clone was purchased from OriGene. The product manual (https://cdn.origene.com/assets/documents/trueorf/trueorfapplicationguide.pdf) describes the protein expression method in detail. Briefly, the plasmid was first amplified in DH5α cells and then used to infect HEK293 cells to produce the Myc-DDK-tagged COL6 α2 chain. Seventy-two hours after transduction, the cells were harvested and lysed in a lysis buffer containing 150 mM sodium chloride, 50 mM tris(hydroxymethyl)aminomethane hydrochloride, 1% Triton X-100, and 5 mM ethylenediaminetetraacetic acid. The Myc-DDK-tagged COL6 α2 was separated via incubation with the anti-Myc tag affinity gel at room temperature for 2 h and then eluted using 0.15 M glycine hydrochloride buffer (pH 3.0). The purity of COL6 α2 in the eluent was detected by silver staining, and the pH of the COL6 α2 eluent was neutralized by dialysis against distilled water at 4°C overnight. After freeze-drying, the purified COL6 α2 was collected and stored as a lyophilized powder.

Silver Staining of SDS-PAGE Gel

The following steps were performed according to the instructions of the fast silver stain kit. Briefly, after electrophoresis, the gel was rinsed with distilled water. We then fixed the gel in a fixation solution (50% v/v ethanol, 10% v/v acetic acid, 40% v/v ultrapure water) for 20 min and washed the gel in 30% ethanol while shaking for 10 min. The gel was rinsed with ultrapure water for 10 min. The gel was incubated in sensitizer solution for 1 min, followed by rinsing with two changes of ultrapure water for 1 min each, after which we incubated the gel in staining solution for 10 min. The gel was washed with two changes of ultrapure water while shaking for 20 s each. The developer solution was immediately added and incubated at room temperature while shaking until protein bands appeared (approximately 2–3 min). When the desired band intensity was reached, the developer working solution was replaced with a stop solution.

Western Blot Analysis of NCAM1

In brief, DRGs were lysed in RIPA buffer containing 1% protease/phosphatase inhibitor cocktail. The protein concentration of the lysate was determined using the BCA assay. Protein samples (20 μg per well) were loaded onto an SDS-PAGE gel. After electrophoresis and transfer, the membrane was incubated with anti-NCAM1 antibody (1:1,000) and anti-β-actin antibody (1:1,000) overnight at 4°C, followed by incubation with HRP-conjugated goat anti-rabbit IgG (1:1,000), and HRP-conjugated goat anti-mouse IgG (1:1,000) for 1 h at room temperature. The protein bands were detected via electrochemiluminescence using a JS-M6 Chemiluminescence Imaging System (Peiqing Science and Technology Co. Ltd., Shanghai, China). The Image Lab software (version 6.0; Bio-Rad) was used to quantify the protein expression levels. The proteins of interest were normalized to β-actin. A protein ladder was used to determine the molecular weights.

Sciatic Nerve Defect and Repair Model

Adult rats were anesthetized with isoflurane (2%, 0.6 L/min) using a small animal anesthesia machine (R540; RWD Life Science Co. Ltd.). The sciatic nerve on the right side was exposed

and transected twice to create an 8 mm defect in the nerve trunk. The stumps were then bridged with a silicone catheter (with diameter 1.2 mm) filled with different types of hydrogels. In the COL6 α2 treatment group, the hydrogel was composed of 10 mg/ml Matrigel and 20 μg/ml COL6 α2, whereas in the vehicle group, the hydrogel was composed of 10 mg/ml Matrigel and an equal volume of saline. After surgery, the rats were housed under specific pathogen-free conditions at a temperature of 22 ± 1°C.

Morphological Analysis of Sciatic Nerve Regeneration

Eight weeks postoperatively, the rats were euthanized with an overdose of isoflurane. Sciatic nerves were dissected from the animals and fixed in 4% paraformaldehyde for 48 h. Gradient sucrose dehydration and cryo-sectioning were performed to prepare longitudinal slices of the sciatic nerve at a thickness of 20 μm. Immunofluorescence staining of NF200 and NCAM1 was performed on these slices, as described above. Based on the fluorescence images, the density of axons along the transverse line was calculated, and the continuous length of axons was also measured and compared between different groups.

Functional Experiments on the Regenerated Sciatic Nerves

The animals were anesthetized with isoflurane after 8 weeks of regeneration, and the catheter-bridged sciatic nerve and sham-operated sciatic nerve were carefully exposed. Using the BL-420 biological function experiment system (Techman Software Co. Ltd., Chengdu, China), a recording electrode was inserted into the gastrocnemius, and a stimulating electrode was placed sequentially at the proximal and distal parts of the injured nerve trunk, across the catheter. The electrical impulses were set at 8 V and 30 Hz, and traces of compound muscle action potential (CMAP) were recorded in different groups. The amplitude recovery was calculated by dividing the maximum amplitude in the experimental group by the maximum amplitude in the sham group. The motor nerve conduction velocity was calculated by dividing the difference between the latency of the proximal stimulus and the latency of the distal stimulus by the distance between the proximal and distal stimuli.

Transmission Electron Micrography

Sciatic nerve tissues were fixed with 0.2 M phosphate buffer containing 2% paraformaldehyde and 2% glutaraldehyde, embedded in EPON-812. Transverse sections of sciatic nerve tissues were prepared via ultramicrotomy. After lead-uranium staining, the sections were mounted and photographed using a transmission electron microscope (Philips XL30 FEG; Philips, Eindhoven, The Netherlands). The density of myelinated axons was calculated, and the degree of myelination was evaluated using the axon-to-fiber diameter ratio, with a smaller ratio representing a higher degree of myelination.

Immunogenicity Assessment of COL6 α2

To characterize the effect of human COL6 α2 on the production of inflammation-related cytokines in rats, the animals were immunized with COL6 α2 via subcutaneous injection of COL6 α2 (100 μg/ml, 0.5 ml) at the dorsal sites. After immunization for 3, 7, and 14 days, the tails were incised to collect 0.5 ml blood in a 1.5 ml Eppendorf tube. After 3 h of coagulation at room temperature, the serum was collected by centrifugation at 800 × g for 5 min. The sera collected before immunization were defined as the 0 day group. The levels of plasma cytokines (IL-1α, IL-1β, IL-2, IL-4, IL-5, IL-6, IL-7, IL-10, IL-12, IL-13, IL-17A, IL-18, GM-CSF, GRO/KC, IFN-γ, MCP-1, MIP-1α, MIP-3α, RANTES, TNF-α, VEGF, G-CSF, and M-CSF) were measured using the Rat Cytokine 23-Plex Assays panel and the Bio-Plex MAGPIX System (Bio-Rad) according to the manufacturer's instructions. Serum samples from COL6 (100 μg/ml, 0.5 ml) immunized rats were used as controls for comparison.

The primary humoral immune response was determined using the Rat IgM SimpleStep ELISA Kit according to the manufacturer's instructions. In brief, rat serum was diluted (1:10,000) with sample diluent, 50 μl of each sample was added to the wells, followed by mixing with 50 μl of the antibody cocktail. After 1 h incubation at room temperature, each well was washed with Wash Buffer and repeated three times. we added 100 μl of 3,3′, 5,5′-tetramethylbenzidine development solution to each well and incubated for 10 min on a plate shaker set to 400 rpm, then 100 μl of stop solution was added. The optical density of each well was recorded at 450 nm using an Infinite M200 PRO microplate reader (TECAN, Männedorf, Zürich, Switzerland).

Heatmap Plotting

Matrix data of cytokine expressions were analyzed via an online heatmap plotting software (https://international.biocloud.net/en/software/tools/detail/small/305). The data were normalized by column, and we take the logarithm of the data (log base 10) for heatmap output.

Statistical Analysis

Continuous variables were compared between the two groups using an unpaired *t*-test if the data had a Gaussian distribution and had the same standard deviation, or a ratio paired *t*-test if the ratios of paired values were consistent. Differences among three or more groups were compared via one-way analysis of variance, followed by Tukey's multiple comparison tests. All statistical tests were performed and plots were generated using the GraphPad Prism version 8 (GraphPad Software, LLC, San Diego, CA, USA). Analysis items with a two-tailed p-value < 0.05 were considered statistically significant.

RESULTS

Contributions of COL6 Subunits in the COL6-Induced Orderly Axon Bundle Formation

Dorsal root ganglions seeded on the COL6-coated substrate gradually exhibited well-aligned axon bundles after 48 h of incubation (**Supplementary Video 1**). The effects of function-blocking antibodies against different COL6 α chains on nerve bundle formation were examined. The control antibody against GAPDH did not hinder the formation of orderly nerve

bundles. In contrast, the formation of orderly axon bundles was specifically inhibited by antibodies against COL6 α1 and COL6 α2; the antibody to COL6 α3 also exhibited a relatively weak inhibitory effect on the fasciculation and alignment of axons (**Figure 1A**). Morphological analysis showed that compared with the control antibody to GAPDH, the function-blocking antibodies to COL6 α1, α2, and α3 reduced the diameter of the bundle by 38, 60, and 22%, respectively (**Figure 1B**), and the directional stability of axons were decreased by 55, 65, and 41% in the COL6 α1, α2, and α3 blocking groups, respectively (**Figure 1C**). These results suggested that there were differences in the contribution of COL6 subunit chains to axon bundle formation, with COL6 α2 having the largest contribution weight.

Expression of Recombinant Proteins of Human COL6 α2 Chain

To investigate the independent functions of COL6 α2 in nerve bundle formation, a recombinant human COL6 α2 full-length chain was produced using a TrueORF clone among HEK293T cells. The amino acid sequence and major domains of the recombinant COL6 α2 protein are shown in **Figure 2A**. A Myc-DDK tag was added at the C-terminal of COL6 α2 to facilitate subsequent purification and identification of this protein (**Figure 2B**). The purity of this fusion protein was over 85% after purification with anti-Myc agarose under denaturing conditions, as determined via silver staining of SDS-PAGE gel (**Figures 2C,D**).

Axon Clustering and Straightening Effects of Recombinant Human COL6 α2

As described previously, a Matrigel-coated substrate was used to induce regeneration of dispersed and curved axons (Sun et al., 2022). The addition of COL6 α2 (10 μg/ml) to the solution of Matrigel (1 mg/ml) for coating led to the formation of orderly axon bundles, while the addition of a vehicle (an equal volume of saline) to Matrigel still resulted in disordered axons (**Figure 3A**).

Morphological analysis revealed approximately three times the average diameter of bundles in the COL6 α2 group (2.51 ± 0.25 μm) compared with that in the vehicle group (0.93 ± 0.11 μm, **Figure 3B**). The directional stability of axons in the

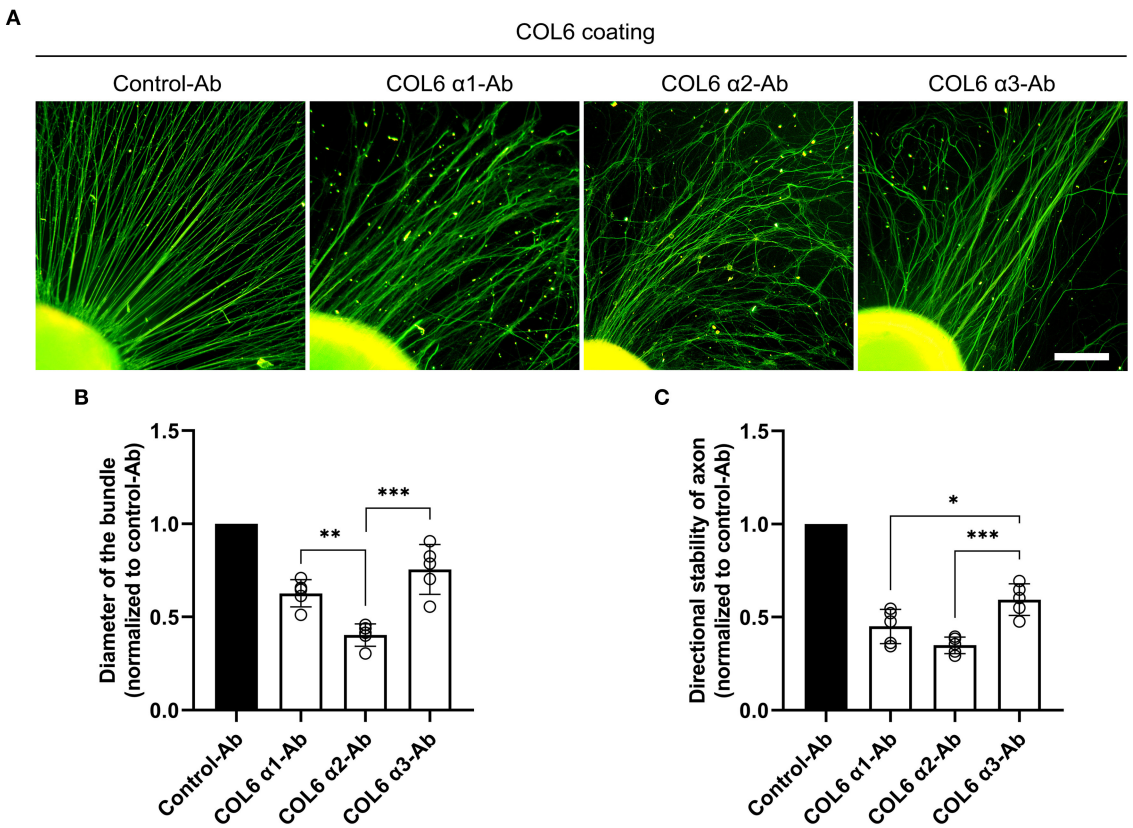

FIGURE 1 | Function-blocking of different COL6 α chains hinders nerve bundle formation in various degrees. DRGs cultured on the COL6-coated surface were subjected to an antibody-blocking assay. **(A)** DRGs treated with control-antibody (an antibody against GAPHD) exhibited radially aligned axon bundles. The antibodies to different COL6 α chains gave rise to disorganized axons in varying degrees. **(B)** The relative values of axon bundle diameters are compared among different experimental groups ($n = 5$ independent biological experiments, $^{**}p = 0.0074$, $^{***}p = 0.0002$, one-way ANOVA followed by Tukey's multiple comparison tests). **(C)** Histogram showing the relative values of directional stability of axons in different groups ($n = 5$ independent biological experiments, $^{*}p = 0.0287$, $^{***}p = 0.0008$, one-way ANOVA followed by Tukey's multiple comparisons tests). Scale bar = 200 μm.

COL6 α2 group was significantly better than that in the vehicle group (**Figure 3C**). The increase in axon bundle diameter with COL6 α2 occurred in a dose-dependent manner (**Figure 3D**).

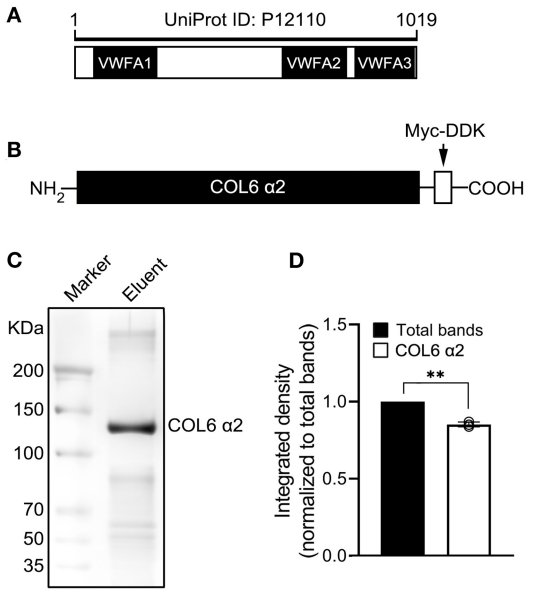

FIGURE 2 | Schematic diagram of the COL6 α2 chain domains and the recombinant COL6 α2 protein used in this study. **(A)** The scale of amino acid is shown on the top. The COL6 α2 full-length chain (UniProt ID: P12110) is mainly composed of VWFA1, VWFA2, and VWFA3 domains. **(B)** Schematic diagram of the recombinant COL6 α2 full-length chain. A Myc-DDK tag was added at the C-terminal of the COL6 α2 chain. **(C)** After purification, the purity of the Myc-DDK-tagged COL6 α2 was analyzed via SDS-PAGE and visualized by silver staining. **(D)** The statistical analysis based on optical density of the protein bands determined that the purity of the recombinant COL6 α2 was 85.24 ± 1.56% ($n = 3$ independent biological experiments, $^{**}p = 0.0043$, ratio paired *t*-test).

These results demonstrated an independent role of the recombinant COL6 α2 chain in axonal self-organization.

Involvement of NCAM1 in the COL6 α2-Induced Axonal Alignment and Fasciculation

NCAM1 has been demonstrated to mediate axon bundle formation (Sun et al., 2022). We speculated that COL6 α2-induced axonal self-organization may also require the participation of NCAM1.

Immunofluorescent staining of DRG *ex vivo* preparations showed higher axonal NCAM1 expression in the COL6 α2 group than in the vehicle group (**Figure 4A**). Consistent with the results of the immunofluorescence assay, western blot assays confirmed the upregulation of three NCAM1 isoforms (NCAM180, NCAM140, and NCAM120) in the COL6 α2 treatment group compared with the vehicle group (**Figures 4B,C**). Antibody blocking assays showed that compared with the control antibody to GAPDH, the function-blocking antibodies to NCAM1 significantly hindered the formation of axon bundles induced by COL6 α2 (**Figures 4D,E**).

In vivo Functions of Recombinant COL6 α2 Chain

Next, the function of the recombinant COL6 α2 protein was tested in a rat sciatic nerve defect model. Silicone catheters filled with Matrigel (10 mg/ml) were used to bridge the nerve stumps. An additional COL6 α2 (20 μg/ml) was mixed with Matrigel in the COL6 α2 treatment group, and an equal volume of saline was mixed with Matrigel in the vehicle group.

After 8 weeks of repair, immunofluorescent staining showed that the NF200-positive axons were fasciculated and evenly distributed in the longitudinal sections from the COL6 α2 group. In contrast, axons were scattered and laterally distributed in the vehicle group (**Figure 5A**). The regenerated sciatic nerve tissues

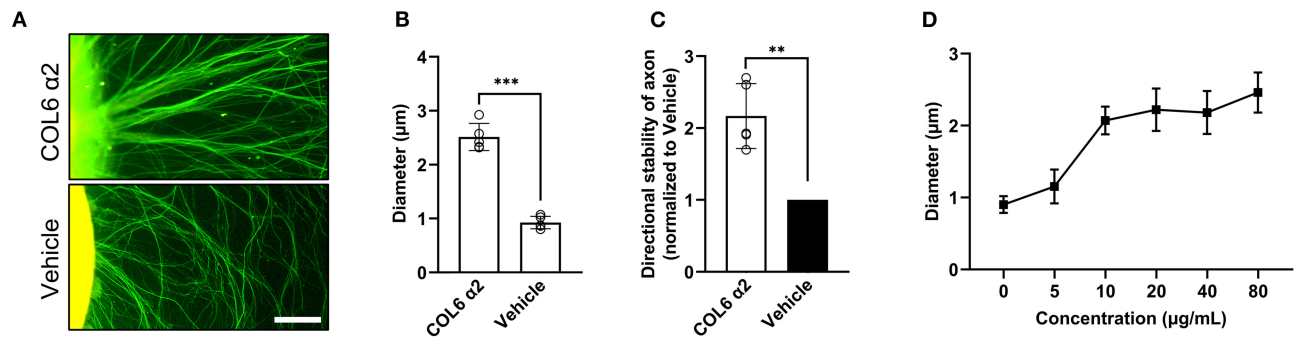

FIGURE 3 | COL6 α2 treatment increases the diameter and directional stability of axon bundle in Matrigel. In the COL6 α2 group, DRGs were seeded on a surface precoated with normal saline solution containing Matrigel (1 mg/ml) and COL6 α2 (10 μg/ml), and in the vehicle group, the surface for DRG seeding was precoated with normal saline solution containing only Matrigel (1 mg/ml). (**A**) Representative immunofluorescence images of DRG axons (labeled with NF200, green, stained with Alexa Fluor 488) in different groups. **(B)** Histogram of average diameter showing increased axon bundle diameter in the COL6 α2, compared with that in the vehicle group ($n = 5$ independent biological experiments, $^{***}p < 0.0001$, unpaired *t*-test). **(C)** Histogram showing more than twice the directional stability of axons in the COL6 α2 group compared to the vehicle group ($n = 5$ independent biological experiments, $^{**}p = 0.0012$, ratio paired *t*-test). (**D**) Different concentrations of COL6 α2 were tested for coating in the COL6 α2 group. The dose-dependent curve shows that the axon bundle diameter increased with increasing COL6 α2 concentrations ($n = 5$ independent biological experiments). Scale bar = 20 μm in **(A)**.

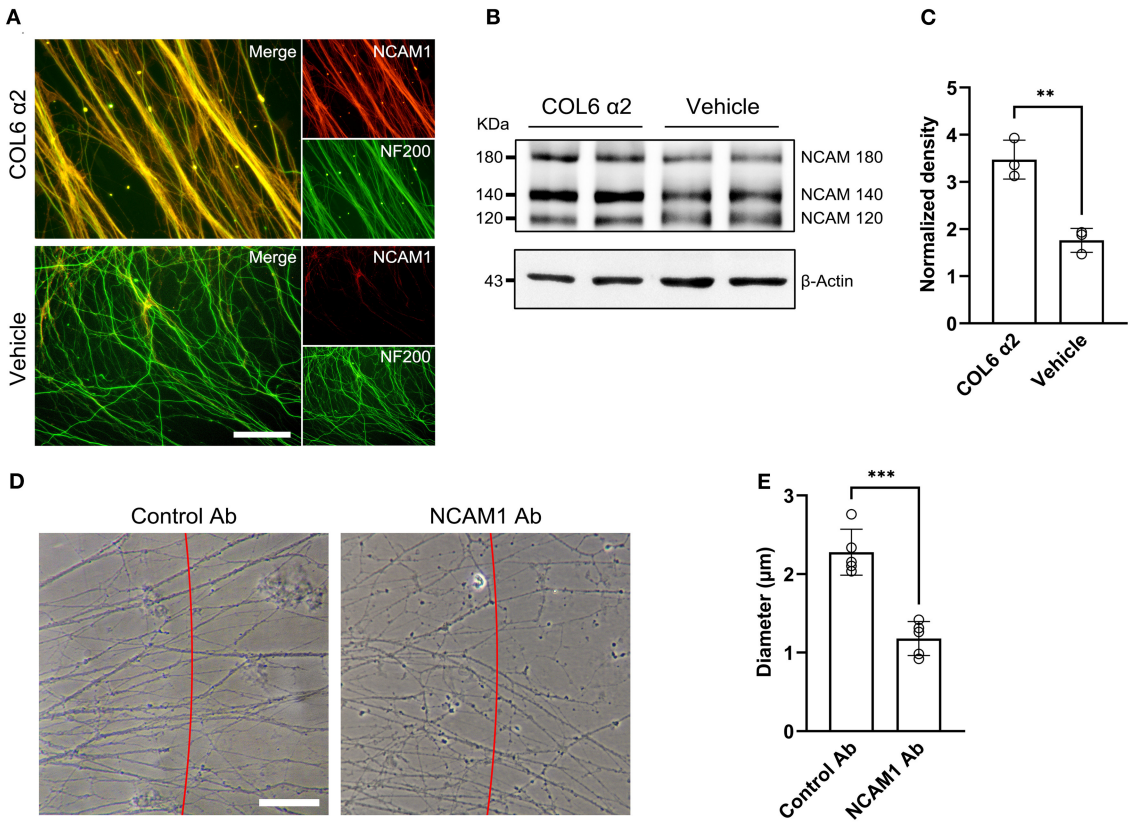

FIGURE 4 | COL6 α2 promotes axonal clustering through the NCAM1-mediated pathway. **(A)** Representative immunofluorescence images showing the expression of NCAM1 (red) in axons (labeled with NF200, green). The fluorescence signal of NCAM1 was stronger in the COL6 α2 group than in the vehicle group. **(B)** Immunoblotting exhibited the NCAM1 (NCAM120, NCAM140, and NCAM180) bands together with the β-actin bands in the COL6 α2 and vehicle groups. **(C)** Histogram of the normalized density showing an upregulated NCAM1 expression in the COL6 α2 group, compared with the vehicle group ($n = 3$ independent experiments, $^{**}p = 0.0036$, unpaired t-test; the expression of NCAM1 was normalized to β-actin). **(D)** Microscopy of axon bundles growing on the COL6 α2-coated substrate followed by control-antibody (GAPDH-Ab) or NCAM1-antibody blocking for 48 h. The red line indicates a 500 μm distance from the DRG tissue block. The diameter of each bundle across the red line was measured. **(E)** Histogram showing a significantly decreased axon bundle diameter with NCAM1-antibody treatment, compared with the control-antibody ($n = 5$ independent biological experiments, $^{***}p < 0.0001$, unpaired t-test). Scale bar = 20 μm in **(A)**.

also exhibited higher levels of NCAM1 expression in the COL6 α2 group than in the vehicle group.

Morphological analysis based on the immunofluorescence images showed that COL6 α2 treatment resulted in more than 1.3 times the axon density observed with vehicle treatment (**Figure 5B**). The mean continuous length of axons was 158 ± 25.97 μm in the COL6 α2 group vs. 24.17 ± 7.36 μm in the vehicle group (**Figure 5C**), which represented increased stability of axon direction with COL6 α2 treatment.

Functionally, vehicle treatment led to a 26.19 ± 2.65% recovery in sciatic nerve CMAP following 8 weeks of regeneration, and the addition of 20 μg/ml COL6 α2 to Matrigel enhanced the recovery of CMAP by up to 49.55 ± 4.73% (**Figures 5D,E**). However, the motor nerve conduction velocities were not significantly changed by COL6 α2 administration (**Figure 5F**). Consistent with this, transmission electron microscopy revealed a comparable level of myelination in the regenerated nerve tissues between the COL6 α2 and vehicle groups (**Figures 5G–I**).

Comparison of the Immunogenicity of COL6 α2 and COL6

To assess the immunogenicity of human COL6 α2 and COL6 in rats, the release of 23 inflammatory cytokines in rat serum was examined using a Luminex system, following subcutaneous injection of COL6 α2 and COL6. A heat map showed that the overall expression levels of pro-inflammatory factors were relatively lower, and the levels of anti-inflammatory factors were relatively higher in the COL6 α2 group than in the COL6 group (**Figure 6A**). Among them, there were significant differences in four down-regulated (IL-2, IL-17A, IL-18, and MIP-1α) and two up-regulated (IL-1α and TNF-α) pro-inflammatory factors, and four up-regulated (IL-4, IL-5, IL-10, and M-CSF) and one down-regulated (G-CSF) anti-inflammatory factors (**Figure 6B**). It is noteworthy that among all pro-inflammatory factors detected, IL-17A showed the highest increase after 14 days of immunization, 3.22 ± 1.70 and 2.70 ± 1.26 times higher than those recorded before immunization in the COL6 and COL6 α2 groups, respectively. In terms of anti-inflammatory factors, IL-10

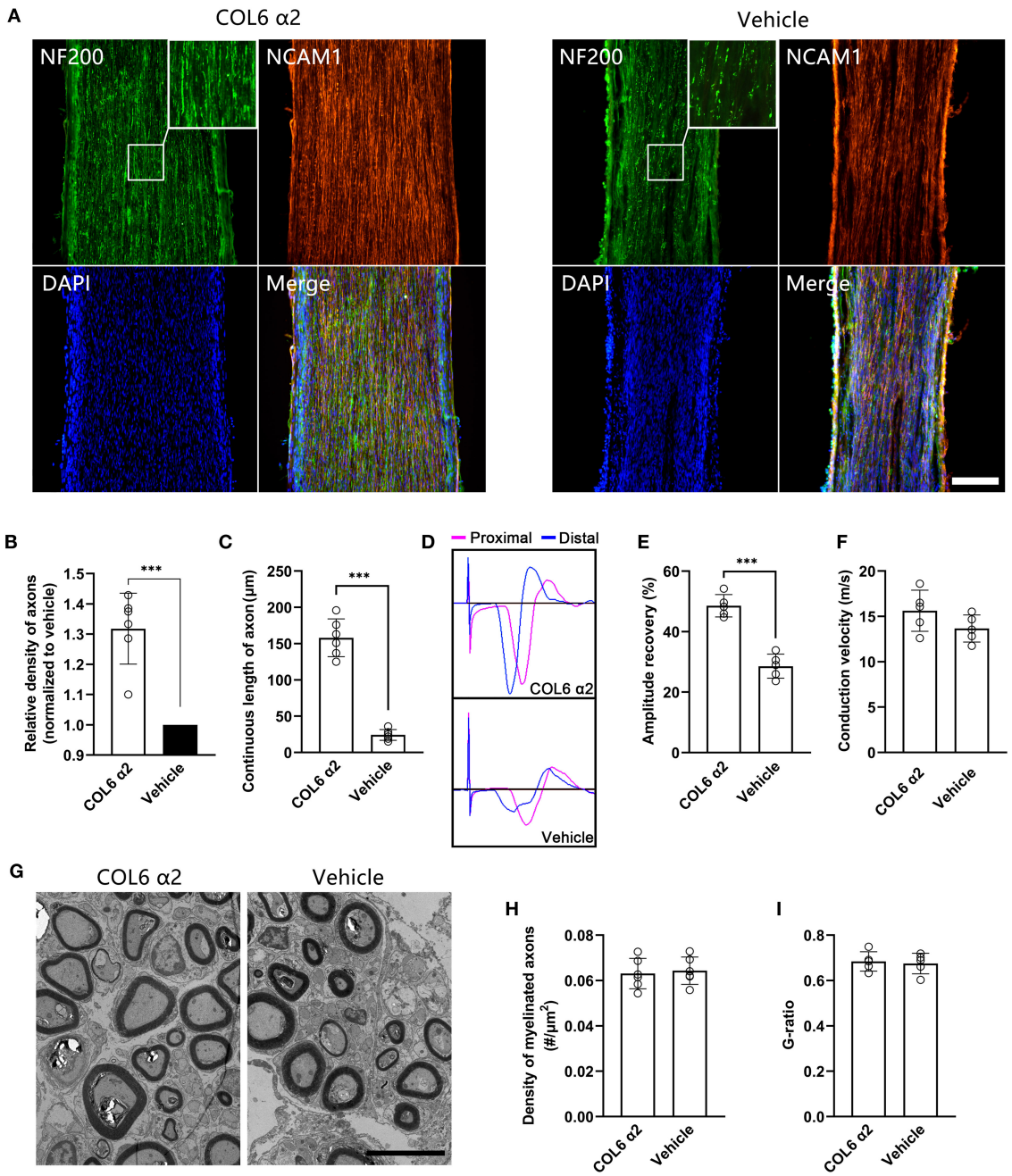

FIGURE 5 | Addition of COL6 α2 in Matrigel improves the regeneration of sciatic nerve defect. Based on a rat sciatic nerve defect model, the nerve stumps were bridged with a catheter filled with 10 mg/ml Matrigel as the carrier. 20 μg/ml COL6 α2 and an equal volume of saline were added to the Matrigel in the COL6 α2 and vehicle groups, respectively. **(A)** After 8 weeks of repair, the longitudinal sections with immunofluorescence staining showed regenerated nerve tissues from the COL6 α2 and vehicle groups. **(B)** Histogram showing an increased density of axons in the COL6 α2 group compared to the vehicle group ($n = 6$ animals, $^{***}p = 0.0009$, ratio paired t-test, normalized to vehicle). **(C)** The continuous length of axons was measured and compared between the two groups ($n = 6$ animals, $^{***}p < 0.0001$, unpaired t-test). **(D)** Panels showing representative traces of CMAP in the COL6 α2 and vehicle groups (magenta trace, the stimulating electrode was placed at the proximal of the nerve trunk; blue trace, the stimulating electrode was placed distal to the nerve trunk). **(E)** Histogram showing the amplitude recovery of the injured sciatic nerve in the COL6 α2 and vehicle groups ($n = 5$, $^{***}p < 0.0001$, unpaired t-test). **(F)** Histogram showing the motor nerve conduction velocities of the COL6 α2 and vehicle groups; no statistical difference was detected between the two groups ($n = 5$, $p = 0.1449$, unpaired t-test). **(G)** Representative TEM images of sciatic nerve cross-sections showing myelinated axons after 8 weeks of regeneration. **(H)** Histogram showing the density of myelinated axons in the COL6 α2 and vehicle groups ($n = 6$ visual fields from three animals, $p = 0.7378$, unpaired t-test). **(I)** The degree of myelination was evaluated between groups using the axon-to-fiber diameter ratio (G-ratio; $n = 5$ visual fields, $p = 0.7442$, unpaired t-test). Scale bars = 200 μm in **(A)** and 5 μm in **(G)**.

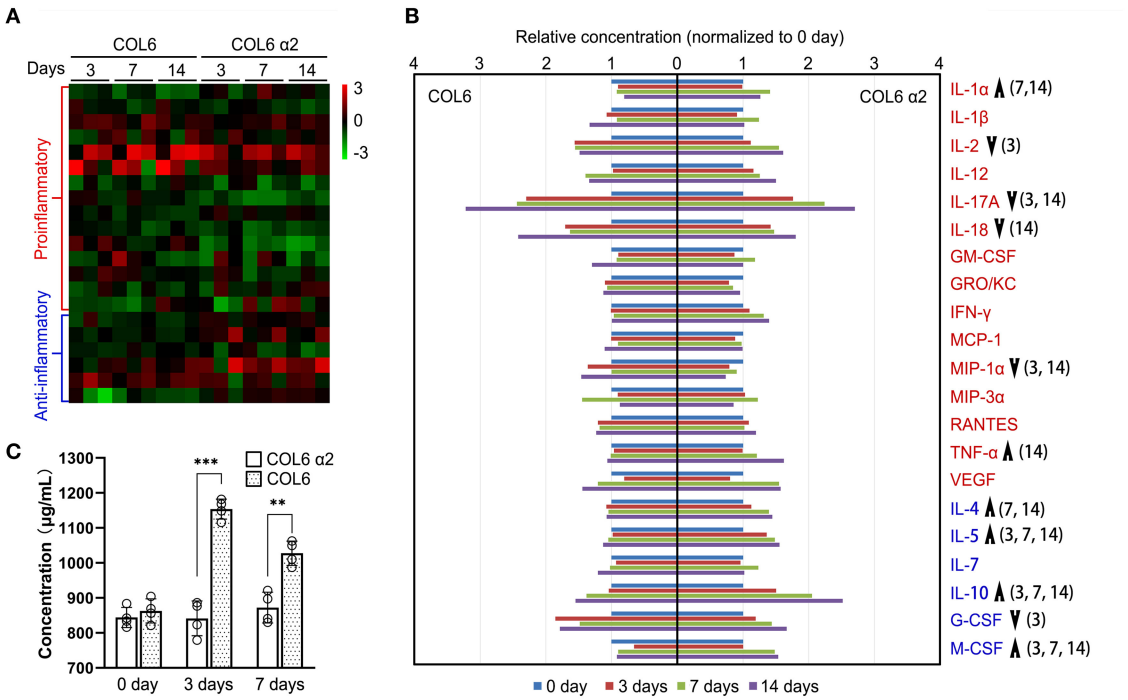

FIGURE 6 | Immunogenicity assessment of human-sourced COL6 α2 and COL6 among rats. **(A)** Heatmap of cytokine expressions in COL6 and COL6 α2 immunized rat serum at 3, 7, and 14 days; the order of cytokines was consistent with that in **(B)**. **(B)** Relative expression levels of each pro-inflammatory cytokine (red font) and anti-inflammatory cytokine (blue font) were compared between COL6 and COL6 α2. Up and down arrows respectively indicate higher and lower levels of cytokine in COL6 α2, compared with COL6. The numbers in brackets indicate statistical differences between the groups on specific days [three independent biological experiments were performed in **(A)** and **(B)**]. **(C)** Concentration of serum IgM at various time points, detected via ELISA ($n = 4$ independent biological experiments, $^{***}p < 0.0001$, $^{**}p = 0.0015$ unpaired t-test).

showed the highest increase (2.52 ± 0.75 times that obtained before immunization) after subcutaneous injection of COL6 α2 for 14 days. IL-6 and IL-13 were excluded from the comparison because their concentrations were lower than the detection range of the standard curve.

ELISA revealed a significantly higher level of IgM, the main serum immunoglobulin prominent in the early immune response, at 3 and 7 days following subcutaneous injection of COL6, while subcutaneous injection of COL6 α2 resulted in no significant change in IgM within 7 days (**Figure 6C**).

DISCUSSION

The data from this study revealed that COL6 α2, one of the three subunit chains of COL6, plays an important role in the induction of orderly axon bundle formation. A recombinant protein of the human COL6 α2 full-length chain recapitulated the axon clustering and ordering effects of COL6, in that compared with COL6 complex, the COL6 α2 chain triggered a weaker immune response.

In the dynamic sense, the organization of orderly axon bundles can be divided into hetero-organization and self-organization. Hetero-organization is defined as the process of constructing system patterns according to pattern information introduced from outside the system (Wu and Nan, 2019). For example, the process by which axons grow along the parallel topology provided by a multichannel nerve catheter (Mobasseri et al., 2015; Chang et al., 2018; Song et al., 2020), and the growth cone turns in response to the spatiotemporal distribution patterns of biochemical guidance cues (Tang et al., 2013; Zou et al., 2018b). The most attractive advantage of hetero-organization in nerve repair is the customizable nerve regeneration route. However, sophisticated extrinsic pattern information is usually vulnerable to complex microenvironments *in vivo*, such as the destruction of the material structure by enzymes, and the deposition of ECM on the surface of the material may destroy the pattern information originally carried in the nerve grafts.

Self-organization, on the contrary, refers to a process in which the system spontaneously forms an internal orderly structure through interactions among its components rather than through external intervention or instruction (Haken and Portugali, 2017). Examples of this process include the generation of patterns on animal furs, fish skins, and butterfly wings (Liu et al., 2006; Werner et al., 2010; Konow et al., 2021); the development of fertilized eggs and embryos (Niu et al., 2019; Xiang et al., 2020); and the orderly axon bundle formation in the homogeneous, COL6- or COL6 α2-containing microenvironment without any guidance cues. This concept greatly simplifies the strategy for ordering nerve regeneration;

however, it also has some limitations in precisely guiding the direction of axonal regeneration.

According to synergetics, the main component of self-organization theory, the synergy of elements inside the system comprises the basis of self-organization (Corning, 1995; Kröger, 2015). A previous study demonstrated that extracellular COL6 can directly bind to the fibronectin type 3 domain of NCAM1, resulting in the accumulation of NCAM1 molecules on axolemma, promoting axon bundle formation through their homophilic (NCAM–NCAM) binding activity (Sun et al., 2022). Therefore, the synergy between COL6 and NCAM1 is regarded as the key to the self-organization of the nerve bundle structure. The results of this study showed that the COL6 α2 chain uses the same NCAM1-mediated mechanism pathway as COL6.

In addition to the interaction of COL6 α1, α2, and α3 chains to form COL6 tetramers, the assembly of protein complex is a ubiquitous phenomenon in organisms. The united proteins can act in coordination to generate functions of which the individual proteins are incapable (Berg et al., 2002). On the other hand, some protein subunits such as β-NGF have been demonstrated to exert biological activities ascribed to the NGF complex in the development and preservation of the sensory and sympathetic nervous systems (Castellanos et al., 2003; Perrard and Durand, 2009). The PPFLMLLKGSTR motif within the laminin-5 α3 chain inherits the cell adhesion function of laminin-5 (Kim et al., 2005). These findings are in line with the results of the present study as they showed that the COL6 α2 chain had an independent function in orderly axon bundle formation.

To improve the efficiency of protein purification, we used a denaturing buffer during the purification of recombinant human COL6 α2 chains. Even after denaturation, COL6 α2 still maintained the ability to trigger axonal self-organization, which demonstrates a strong resistance of the recombinant COL6 α2 chain to environmental interference. In addition to nerve bundle formation, the number of axons in the regenerated nerve tissue was also increased by COL6 α2 treatment, indicating that COL6 α2 may also inherit other neuroprotective and immunomodulatory effects from COL6 (Urciuolo et al., 2013; Chen et al., 2015; Cescon et al., 2016).

In the peripheral nervous system, COL6 exhibits a dual myelination activity in a dose-dependent manner, the lack of COL6 in *Col6a1*$^{-/-}$ mice causes hypermyelination (Chen et al., 2014), while a high concentration of COL6 in the microenvironment leads to the detachment of Schwann cells and axons (Sun et al., 2022). It is reasonable to consider that the addition of COL6 α2, a functional subunit of COL6, in the microenvironment may affect axonal myelination, and data from transmission electron microscopy and motor nerve conduction velocity assessment showed that the addition of 20 μg/ml COL6 α2 to Matrigel had no adverse effects on axonal myelination.

The present study detected lower levels of IgM secretion with COL6 α2 immunization compared to COL6 immunization, which points to a weaker humoral immune response to COL6 α2. Following subcutaneous injection of COL6 and COL6 α2, the pro-inflammatory factor IL-17A showed the most significant change among all the 21 inflammatory factors detected, suggesting that IL-17A can be used as an important index in evaluating the immune response induced by COL6 and COL6 α2. On the other hand, the increased expressions of several anti-inflammatory factors (particularly, IL-10) in the COL6 α2 treated group, indicated an advanced anti-inflammatory effect of COL6 α2 in comparison with the COL6 complex.

In terms of methodology, gene knockout strategies are widely used to study loss-of-function phenotypes (Zare et al., 2018; Freund et al., 2020; Paul et al., 2021). However, this approach is not suitable for determining the functional differences among COL6 subunit chains, because the COL6 α1, α2, and α3 chains must be assembled into COL6 tetramers in the cytoplasm before they can be secreted into the ECM. Knockout of the gene encoding any one of the COL6 α chains will result in the simultaneous disappearance of all three COL6 α chains in the ECM (Bonaldo et al., 1998; Irwin et al., 2003). Hence, an antibody blocking assay was preferred in the present study. In the section on immunogenicity assessment, considering that the inflammatory responses caused by the surgery and carrier material (Matrigel) may conceal the differences in immunogenicity between COL6 and COL6 α2, we performed subcutaneous injections to eliminate these interfering factors.

This study exhibits two distinct dynamics of axon clustering and straightening during axon self-organization, the homophilic binding of NCAM1 could explain the dynamic of axon clustering, but the detailed molecular mechanisms underlying axonal straightening remain to be further studied. The recombinant human COL6 α2 shows relatively low immunogenicity in rat, but we cannot completely rule out its potential allogeneic immunogenicity in human. Considering that COL6 is mainly secreted by Schwann cells and has regulatory effects on myelination, it may be a better solution to modulate the production of endogenous COL6 in the early stage of peripheral nerve injury through genetic engineering.

Collectively, the present study demonstrated the role of COL6 α2 in axonal self-organization, which leads to the formation of orderly axon bundles and promotes peripheral nerve regeneration. Based on the data presented, the recombinant COL6 α2 showed better feasibility and lower immunogenicity than the COL6 complex in practical applications, which indicates a promising prospect for clinical transformation.

DATA AVAILABILITY STATEMENT

The datasets generated or analyzed for this study can be found in the Google Drive, https://drive.google.com/drive/folders/1iHJS02jkUxQQhwza_PCW8-B3KmHMl6Be?usp=sharing.

ETHICS STATEMENT

The animal study was reviewed and approved by Animal Ethics Committee of Guangzhou Medical University (approval no. GY2019048).

AUTHOR CONTRIBUTIONS

ZF and J-LZ designed the experiments and wrote the manuscript. ZF conducted the experiments and analyzed

the data. All authors contributed to the article and approved the submitted version.

FUNDING

This study was supported by grants from National Natural Science Foundation of China, No. 31800892 (to J-LZ).

SUPPLEMENTARY MATERIAL

The Supplementary Material for this article can be found online at: https://www.frontiersin.org/articles/10.3389/fncel.2021.816781/full#supplementary-material

Supplementary Video 1 | Axonal self-organization on the COL6-coated substrate.

REFERENCES

Berg, J. M., Tymoczko, J. L., and Stryer, L. (2002). "Chapter 3: Protein structure and function," in *Biochemistry. 5th Edn*. (New York, NY: WH Freeman). Available online at: https://www.ncbi.nlm.nih.gov/books/NBK21177/ (accessed November 14, 2021).

Boeer, U., Buettner, F. F., Klingenberg, M., Antonopoulos, G. C., Meyer, H., Haverich, A., et al. (2014). Immunogenicity of intensively decellularized equine carotid arteries is conferred by the extracellular matrix protein collagen type VI. *PLoS ONE* 9, e105964. doi: 10.1371/journal.pone.0105964

Bonaldo, P., Braghetta, P., Zanetti, M., Piccolo, S., Volpin, D., and Bressan, G. M. (1998). Collagen VI deficiency induces early onset myopathy in the mouse: an animal model for Bethlem myopathy. *Hum. Mol. Genet.* 7, 2135–2140. doi: 10.1093/hmg/7.13.2135

Castellanos, M. R., Aguiar, J., Fernández, C. I., Almaguer, W., Mejias, C., and Varela, A. (2003). Evaluation of the neurorestorative effects of the murine beta-nerve growth factor infusions in old rat with cognitive deficit. *Biochem. Biophys. Res. Commun.* 312, 867–872. doi: 10.1016/j.bbrc.2003.10.198

Cescon, M., Chen, P., Castagnaro, S., Gregorio, I., and Bonaldo, P. (2016). Lack of collagen VI promotes neurodegeneration by impairing autophagy and inducing apoptosis during aging. *Aging (Albany NY)* 8, 1083–1101. doi: 10.18632/aging.100924

Cescon, M., Gattazzo, F., Chen, P., and Bonaldo, P. (2015). Collagen VI at a glance. *J. Cell Sci.* 128, 3525–3531. doi: 10.1242/jcs.169748

Chang, W., Shah, M. B., Lee, P., and Yu, X. (2018). Tissue-engineered spiral nerve guidance conduit for peripheral nerve regeneration. *Acta Biomater.* 73, 302–311. doi: 10.1016/j.actbio.2018.04.046

Chen, P., Cescon, M., Megighian, A., and Bonaldo, P. (2014). Collagen VI regulates peripheral nerve myelination and function. *FASEB J.* 28, 1145–1156. doi: 10.1096/fj.13-239533

Chen, P., Cescon, M., Zuccolotto, G., Nobbio, L., Colombelli, C., Filaferro, M., et al. (2015). Collagen VI regulates peripheral nerve regeneration by modulating macrophage recruitment and polarization. *Acta Neuropathol.* 129, 97–113. doi: 10.1007/s00401-014-1369-9

Corning, P. A. (1995). Synergy and self-organization in the evolution of complex systems. *Syst. Res.* 12, 89–121. doi: 10.1002/sres.3850120204

de Ruiter, G. C., Spinner, R. J., Verhaagen, J., and Malessy, M. J. (2014). Misdirection and guidance of regenerating axons after experimental nerve injury and repair. *J. Neurosurg.* 120, 493–501. doi: 10.3171/2013.8.JNS122300

Eggers, R., de Winter, F., Tannemaat, M. R., Malessy, M. J. A., and Verhaagen, J. (2020). GDNF gene therapy to repair the injured peripheral nerve. *Front. Bioeng. Biotechnol.* 8, 583184. doi: 10.3389/fbioe.2020.583184

English, A. W. (2005). Enhancing axon regeneration in peripheral nerves also increases functionally inappropriate reinnervation of targets. *J. Comp. Neurol.* 490, 427–441. doi: 10.1002/cne.20678

Freund, E. C., Lock, J. Y., Oh, J., Maculins, T., Delamarre, L., Bohlen, C. J., et al. (2020). Efficient gene knockout in primary human and murine myeloid cells by non-viral delivery of CRISPR-Cas9. *J. Exp. Med.* 217, e20191692. doi: 10.1084/jem.20191692

Gordon, T., and English, A. W. (2016). Strategies to promote peripheral nerve regeneration: electrical stimulation and/or exercise. *Eur. J. Neurosci.* 43, 336–350. doi: 10.1111/ejn.13005

Haken, H., and Portugali, J. (2017). Information and self-organization. *Entropy.* 19, 18. doi: 10.3390/e19010018

Handarmin, Tan, G. J., Sundaray, B., Marcy, G. T., and Goh, E. L., Chew, S. Y. (2011). Nanofibrous scaffold with incorporated protein gradient for directing neurite outgrowth. *Drug Deliv. Transl. Res.* 1, 147–160. doi: 10.1007/s13346-011-0017-3

Hsu, R. S., Chen, P. Y., Fang, J. H., Chen, Y. Y., Chang, C. W., Lu, Y. J., et al. (2019). Adaptable microporous hydrogels of propagating NGF-gradient by injectable building blocks for accelerated axonal outgrowth. *Adv. Sci.* 6, 1900520. doi: 10.1002/advs.201900520

Irwin, W. A., Bergamin, N., Sabatelli, P., Reggiani, C., Megighian, A., Merlini, L., et al. (2003). Mitochondrial dysfunction and apoptosis in myopathic mice with collagen VI deficiency. *Nat. Genet.* 35, 367–371. doi: 10.1038/ng1270

Kim, J. M., Park, W. H., and Min, B. M. (2005). The PPFLMLLKGSTR motif in globular domain 3 of the human laminin-5 alpha3 chain is crucial for integrin alpha3beta1 binding and cell adhesion. *Exp. Cell Res.* 304, 317–327. doi: 10.1016/j.yexcr.2004.11.009

Konow, C., Li, Z., Shepherd, S., Bullara, D., and Epstein, I. R. (2021). Influence of survival, promotion, and growth on pattern formation in zebrafish skin. *Sci. Rep.* 11:9864. doi: 10.1038/s41598-021-89116-4

Krick, K., Tammia, M., Martin, R., Höke, A., and Mao, H. Q. (2011). Signaling cue presentation and cell delivery to promote nerve regeneration. *Curr. Opin. Biotechnol.* 22, 741–746. doi: 10.1016/j.copbio.2011.04.002

Kröger, B. (2015). *Theories of Self-organization: The Role of Synergetics*. Cham: Springer. doi: 10.1007/978-3-319-11689-1_9

Lau, J. L., and Dunn, M. K. (2018). Therapeutic peptides: historical perspectives, current development trends, and future directions. *Bioorg. Med. Chem.* 26, 2700–2707. doi: 10.1016/j.bmc.2017.06.052

Liu, D., Mi, D., Zhang, T., Zhang, Y., Yan, J., Wang, Y., et al. (2018). Tubulation repair mitigates misdirection of regenerating motor axons across a sciatic nerve gap in rats. *Sci. Rep.* 8:3443. doi: 10.1038/s41598-018-21652-y

Liu, R. T., Liaw, S. S., and Maini, P. K. (2006). Two-stage Turing model for generating pigment patterns on the leopard and the jaguar. *Phys. Rev. E Stat. Nonlin. Soft Matter Phys.* 74, 011914. doi: 10.1103/PhysRevE.74.011914

Lynn, A. K., Yannas, I. V., and Bonfield, W. (2004). Antigenicity and immunogenicity of collagen. *J. Biomed. Mater. Res. B Appl. Biomater.* 71, 343–354. doi: 10.1002/jbm.b.30096

Mobasseri, A., Faroni, A., Minogue, B. M., Downes, S., Terenghi, G., and Reid, A. J. (2015). Polymer scaffolds with preferential parallel grooves enhance nerve regeneration. *Tissue Eng. A* 21, 1152–1162. doi: 10.1089/ten.TEA.2014.0266

Niu, Y., Sun, N., Li, C., Lei, Y., Huang, Z., Wu, J., et al. (2019). Dissecting primate early post-implantation development using long-term *in vitro* embryo culture. *Science* 366, eaaw5754. doi: 10.1126/science.aaw5754

Oh, S. H., Kang, J. G., Kim, T. H., Namgung, U., Song, K. S., Jeon, B. H., et al. (2018). Enhanced peripheral nerve regeneration through asymmetrically porous nerve guide conduit with nerve growth factor gradient. *J. Biomed. Mater. Res. A* 106, 52–64. doi: 10.1002/jbm.a.36216

Paul, A., Anand, R., Karmakar, S. P., Rawat, S., Bairagi, N., and Chatterjee, S. (2021). Exploring gene knockout strategies to identify potential drug targets using genome-scale metabolic models. *Sci. Rep.* 11, 213. doi: 10.1038/s41598-020-80561-1

Perrard, M. H., and Durand, P. (2009). Redundancy of the effect of TGFbeta1 and beta-NGF on the second meiotic division of rat spermatocytes. *Microsc. Res. Tech.* 72, 596–602. doi: 10.1002/jemt.20706

Raza, C., Riaz, H. A., Anjum, R., and Shakeel, N. U. A. (2020). Repair strategies for injured peripheral nerve: review. *Life Sci.* 243, 117–308. doi: 10.1016/j.lfs.2020.117308

Robinson, G. A., and Madison, R. D. (2004). Motor neurons can preferentially reinnervate cutaneous pathways. *Exp. Neurol.* 190, 407–413. doi: 10.1016/j.expneurol.2004.08.007

Song, S., Wang, X., Wang, T., Yu, Q., Hou, Z., Zhu, Z., et al. (2020). Additive manufacturing of nerve guidance conduits for regeneration of injured peripheral nerves. *Front. Bioeng. Biotechnol.* 8, 590596. doi: 10.3389/fbioe.2020.590596

Sun, J. H., Huang, M., Fang, Z., Li, T. X., Wu, T. T., Chen, Y., et al. (2022). Nerve bundle formation during the promotion of peripheral nerve regeneration: collagen VI-neural cell adhesion molecule 1 interaction. *Neural Regen. Res.* 17, 1023–1033. doi: 10.4103/1673-5374.324861

Tang, S., Zhu, J., Xu, Y., Xiang, A. P., Jiang, M. H., and Quan, D. (2013). The effects of gradients of nerve growth factor immobilized PCLA scaffolds on neurite outgrowth in vitro and peripheral nerve regeneration in rats. *Biomaterials* 34, 7086–7096. doi: 10.1016/j.biomaterials.2013.05.080

Ullrich, A., Gray, A., Berman, C., and Dull, T. J. (1983). Human beta-nerve growth factor gene sequence highly homologous to that of mouse. *Nature* 303, 821–825. doi: 10.1038/303821a0

Urciuolo, A., Quarta, M., Morbidoni, V., Gattazzo, F., Molon, S., Grumati, P., et al. (2013). Collagen VI regulates satellite cell self-renewal and muscle regeneration. *Nat. Commun.* 4:1964. doi: 10.1038/ncomms2964

Werner, T., Koshikawa, S., Williams, T. M., and Carroll, S. B. (2010). Generation of a novel wing colour pattern by the Wingless morphogen. *Nature* 464, 1143–1148. doi: 10.1038/nature08896

Wu, K., and Nan, Q. (2019). Information characteristics, processes, and mechanisms of self-organization evolution. *Complexity* 2019, 5603685. doi: 10.1155/2019/5603685

Xiang, L., Yin, Y., Zheng, Y., Ma, Y., Li, Y., Zhao, Z., et al. (2020). A developmental landscape of 3D-cultured human pre-gastrulation embryos. *Nature* 577, 537–542. doi: 10.1038/s41586-019-1875-y

Zare, K., Shademan, M., Ghahramani Seno, M. M., and Dehghani, H. (2018). CRISPR/Cas9 knockout strategies to ablate CCAT1 lncRNA gene in cancer cells. *Biol. Proced. Online* 20, 21. doi: 10.1186/s12575-018-0086-5

Zou, J. L., Liu, S., Sun, J. H., Yang, W. H., Xu, Y. W., Rao, Z. L., et al. (2018a). Peripheral nerve-derived matrix hydrogel promotes remyelination and inhibits synapse formation. *Adv. Funct. Mater.* 28, 1705739. doi: 10.1002/adfm.201705739

Zou, J. L., Sun, J. H., Qiu, S., Chen, S. H., He, F. L., Li, J. C., et al. (2018b). Spatial distribution affects the role of CSPGs in nerve regeneration via the actin filament-mediated pathway. *Exp. Neurol.* 307, 37–44. doi: 10.1016/j.expneurol.2018.05.023

Conflict of Interest: The authors declare that the research was conducted in the absence of any commercial or financial relationships that could be construed as a potential conflict of interest.

Publisher's Note: All claims expressed in this article are solely those of the authors and do not necessarily represent those of their affiliated organizations, or those of the publisher, the editors and the reviewers. Any product that may be evaluated in this article, or claim that may be made by its manufacturer, is not guaranteed or endorsed by the publisher.

frontiers in Cellular Neuroscience

REVIEW
published: 08 March 2022
doi: 10.3389/fncel.2022.836931

The Effect of Schwann Cells/Schwann Cell-Like Cells on Cell Therapy for Peripheral Neuropathy

Qian Wang[1†], Fang-Yu Chen[1†], Zhuo-Min Ling[2], Wen-Feng Su[1], Ya-Yu Zhao[1], Gang Chen[1,2,3] and Zhong-Ya Wei[1*]*

[1] Key Laboratory of Neuroregeneration of Jiangsu and Ministry of Education, Jiangsu Clinical Medicine Center of Tissue Engineering and Nerve Injury Repair, Co-innovation Center of Neuroregeneration, Nantong University, Nantong, China, [2] Medical School of Nantong University, Nantong, China, [3] Department of Anesthesiology, Affiliated Hospital of Nantong University, Nantong, China

OPEN ACCESS

Edited by:
Zhaowei Zhu,
The First Affiliated Hospital of Sun Yat-sen University, China

Reviewed by:
Nicolas Guérout,
Université de Rouen, France
Yong Ho Kim,
Gachon University, South Korea
Yunxiang Luo,
The First Affiliated Hospital of Sun Yat-sen University, China

***Correspondence:**
Gang Chen
chengang6626@ntu.edu.cn
Zhong-Ya Wei
weizhongya08yan@126.com

[†] These authors have contributed equally to this work

Specialty section:
This article was submitted to Non-Neuronal Cells, a section of the journal Frontiers in Cellular Neuroscience

Received: 16 December 2021
Accepted: 02 February 2022
Published: 08 March 2022

Citation:
Wang Q, Chen F-Y, Ling Z-M, Su W-F, Zhao Y-Y, Chen G and Wei Z-Y (2022) The Effect of Schwann Cells/Schwann Cell-Like Cells on Cell Therapy for Peripheral Neuropathy. Front. Cell. Neurosci. 16:836931. doi: 10.3389/fncel.2022.836931

Peripheral neuropathy is a common neurological issue that leads to sensory and motor disorders. Over time, the treatment for peripheral neuropathy has primarily focused on medications for specific symptoms and surgical techniques. Despite the different advantages of these treatments, functional recovery remains less than ideal. Schwann cells, as the primary glial cells in the peripheral nervous system, play crucial roles in physiological and pathological conditions by maintaining nerve structure and functions and secreting various signaling molecules and neurotrophic factors to support both axonal growth and myelination. In addition, stem cells, including mesenchymal stromal cells, skin precursor cells and neural stem cells, have the potential to differentiate into Schwann-like cells to perform similar functions as Schwann cells. Therefore, accumulating evidence indicates that Schwann cell transplantation plays a crucial role in the resolution of peripheral neuropathy. In this review, we summarize the literature regarding the use of Schwann cell/Schwann cell-like cell transplantation for different peripheral neuropathies and the potential role of promoting nerve repair and functional recovery. Finally, we discuss the limitations and challenges of Schwann cell/Schwann cell-like cell transplantation in future clinical applications. Together, these studies provide insights into the effect of Schwann cells/Schwann cell-like cells on cell therapy and uncover prospective therapeutic strategies for peripheral neuropathy.

Keywords: Schwann cells, Schwann cell-like cells, myelination, regeneration, peripheral neuropathy

INTRODUCTION

Peripheral neuropathies are commonly encountered disorders that result from a great number of etiologies, including trauma and side effects of diseases and treatments (Hughes, 2002). Although there is no standard method to diagnose peripheral neuropathy, the development of imaging and laboratory tests has aided in primary diagnosis, and electromyography and nerve conduction tests are especially beneficial for allowing doctors to narrow down the category and the management of peripheral neuropathies (Barrell and Smith, 2019). The categories used to be mononeuropathies,

multifocal neuropathies and polyneuropathies. However, these categories are frequently further divided into axonal, demyelinating, or mixed according to a systematic approach, which is vital for treatment (Hanewinckel et al., 2016). The symptoms often include sensory and motor dysfunctions, including numbness, pain, weakness and paresthesia due to damage to sensory, motor and autonomic fibers. Treatments for peripheral neuropathy are primarily dependent on the subtype and cause of underlying disease, such as grafts for traumatic nerve injury (Baradaran et al., 2021) and metabolic control for diabetic neuropathy (Cernea and Raz, 2021; Holmes and Hastings, 2021). Recently, with insights into cell-based therapy for diseases, emerging evidence has revealed the benefits of cell transplantation in peripheral neuropathic conditions (Hopf et al., 2020; Monje, 2020).

Peripheral neuropathies are affected by disorders of peripheral nerve fibers and cells (Hughes, 2002; Hanewinckel et al., 2016; Barrell and Smith, 2019; Hammi and Yeung, 2021). Schwann cells, which are the primary glial cells in the peripheral nervous system, are predominantly subdivided into myelinating and non-myelinating Schwann cells, both of which are associated with axons through physical support and the release of a variety of neurotrophins and many other signaling molecules during development (Kidd et al., 2013). Relatively large-diameter axons from most motor axons, some sensory axons and are enwrapped by Schwann cells, resulting in the establishment of compact myelin at a ratio of 1:1, which is needed for fast nerve conduction. Other small-diameter axons from autonomous and many sensory neurons, which are known as Remak bundles, are wrapped only by Schwann cells and are not myelinated (Griffin and Thompson, 2008). Schwann cells are recognized as flexible cells due to their capability for rapid transformation after injury (Jessen and Mirsky, 2016). In the injured microenvironment, myelinating Schwann cells and non-myelinating Remak Schwann cells coordinate to repair Schwann cells, resembling the developmental stage through the self-renewal and release of a variety of neurotrophic factors and signaling molecules involved in motor and sensory functional recovery (Stassart and Woodhoo, 2021). Therefore, the role of Schwann cells is pivotal for axonal functions both in physiological and pathological conditions, which leads to increasing attempts to prevent malfunction in Schwann cells or the supply Schwann cells/Schwann cell-like cells for the treatment of peripheral neuropathies (Brewer et al., 2016; Sayad Fathi and Zaminy, 2017; Wing et al., 2017; Al-Massri et al., 2020; Hopf et al., 2020; Monje, 2020). Schwann cells are known to originate from neural crest cells, which can be found in other tissues, such as the epidermis and hair follicle, and have great potential to generate Schwann cell-like cells (McKenzie et al., 2006; Lin et al., 2011). Moreover, with technical innovations in related stem cells, many types of stem cells can differentiate into Schwann cell-like cells or target the regulation of Schwann cells for motor and sensory functional recovery (Caddick et al., 2006; Park et al., 2010; Ma et al., 2015; Cai et al., 2017; Hopf et al., 2020). Thus, in this review, we will primarily discuss the potential applications of Schwann cells/Schwann cell-like cells in peripheral neuropathies induced by common disorders, including peripheral nerve injury, diabetes and chemotherapy, and the challenges for future clinical treatments (**Figure 1**).

PERIPHERAL NERVE INJURY-INDUCED NEUROPATHY

Peripheral nerve injury is a common disease that results from trauma or disease and leads to damage to motor and sensor functions. Although the peripheral nervous system has the potential to self-repair nerve injury, peripheral nerve injury-induced neuropathy and lifelong disabilities for patients are common (Menorca et al., 2013). Insights into cellular and molecular mechanisms have revealed that modulating axons and Schwann cells are effective strategies for peripheral nerve injury-induced neuropathy. After injury, injured axons break and form debris in the distal stump, which is called Wallerian degeneration. This debris is segmented and incorporated by Schwann cells, and then phagocytized with the aid with the recruited macrophages (Nazareth et al., 2021). Once this debris is cleaned, the proximal stump will begin to outgrow. During this process, Schwann cells play an important role in the repair of peripheral nerve injury-induced neuropathy. Once axonal injury occurs, activated Schwann cells transform into a dedifferentiated state by expressing developmental genes, releasing various neurotrophic factors to create a reparative environment, and forming Büngner bands, which are a longitudinal column for guiding axonal regrowth through proliferation in the distal stump (Stassart and Woodhoo, 2021). However, this self-repair method is unable to guide axonal outgrowth and target innerved muscles due to a lack of an advantageous environment, which includes the dysfunction of Schwann cells (Lehmann and Hoke, 2016). Therefore, emerging evidence is focused on cell transplantation to supply Schwann cells or repair Schwann cells to promote axonal growth and motor and sensory restoration (Lehmann and Hoke, 2016; Hopf et al., 2020). Among these strategies, cell transplantation in combination with nerve scaffolds is a promising treatment for peripheral nerve injury-induced neuropathy (Rodriguez et al., 2000; Kornfeld et al., 2019). In the case of peripheral nerve injury, the gold standard treatment is end-to-end suturing of the proximal and distal parts by neurosurgical methods. However, this method is only useful for short gaps (<3 mm), and for longer gaps, a nerve or conduit graft is required to bridge the gap (Hopf et al., 2020). Thus, autologous Schwann cell transplantation is the best choice for treatment. However, these cells must be collected from healthy peripheral nerves and harvested in a time-consuming manner, and all of these limitations constrain their wide applications (Sullivan et al., 2016; Baradaran et al., 2021). Therefore, attention has moved toward the use of allogeneic Schwann cells and Schwann cell-like cells from stem cells to promote axonal regeneration and repair peripheral nerve injury-induced neuropathy (Sayad Fathi and Zaminy, 2017; Hopf et al., 2020; Kubiak et al., 2020). Here, we review current developments in Schwann cell or Schwann cell-like cell transplantations

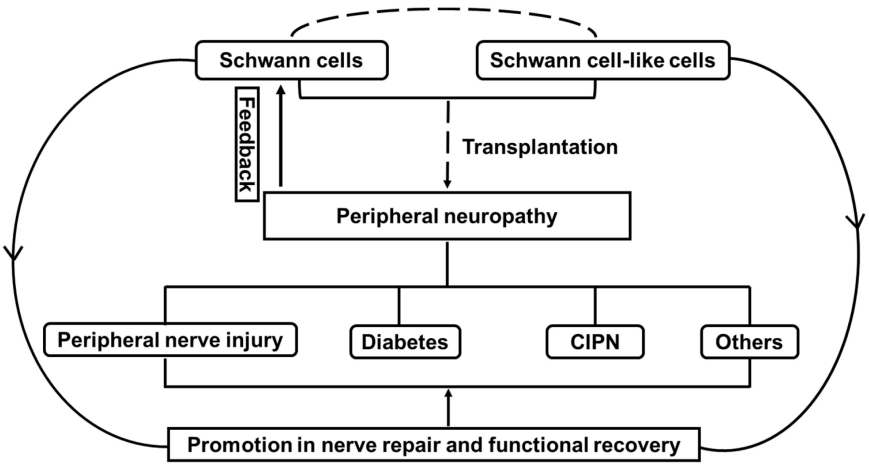

FIGURE 1 | The effect of Schwann cells and Schwann cell-like cells on cell therapy for peripheral neuropathy. Note that peripheral neuropathies induced by peripheral nerve injury, diabetes and chemotherapy-induced peripheral neuropathy (CIPN) often leads to the malfunctional change in Schwann cells. Transplantation with Schwann cells or Schwann cell-like cells (from different sources) attempts to promote nerve repair and functional recovery through the effect of Schwann cells for the treatment of peripheral neuropathies.

for the repair of peripheral nerve injury-induced neuropathy (**Tables 1**, **2**).

Schwann Cell Transplantation in Peripheral Nerve Injury-Induced Neuropathy

In 1992, a study of the transplantation of autologous Schwann cells derived from adult nerves in permselective guidance channels to repair 8 mm nerve gaps in transected rat sciatic nerves indicated that this combination supported extensive regeneration and myelination. In contrast, a strong immune reaction occurred when heterologous Schwann cells were seeded, resulting in the prevention of nerve regeneration (Guenard et al., 1992). To avoid immune reactions, an immune-deficient rat was used, and the functional capacity of human Schwann cells in an 8 mm gap of transected sciatic nerves was evaluated. The outcomes showed that human Schwann cells could survive and effectively promote axonal regrowth and myelination but were less successful than allogeneic Schwann cells (Levi et al., 1994). A study aimed to evaluate the effect of allogeneic Schwann cell transplantation following rat sciatic nerve injury with a 10 mm gap and showed that compared with syngenetic Schwann cells, allogeneic Schwann cells also promoted axonal regeneration and myelination, but the effect was less than that of syngenetic Schwann cells, and an immune response occurred at 6 weeks post-transplantation when there was no use of immunosuppressive therapy (Mosahebi et al., 2002). In addition, a decellularizing approach has been developed to prevent rejection when allogeneic nerve grafts are applied to injured nerve repair (Hudson et al., 2004). However, due to the loss of Schwann cells, this method is less effective for nerve repair than contact nerves (Hoben et al., 2015). Of note, decellularized nerve conduits combined with Schwann cells to repair peripheral nerve injury obtained good results in non-human primate 6 cm ulnar nerve defects (Hess et al., 2007) and rat sciatic nerve defects (Aszmann et al., 2008; Sun et al., 2009; Hoben et al., 2015) and were demonstrated to be a better therapy than the addition of vascular endothelial growth factor to improve axonal regrowth (Hoben et al., 2015). In human studies (Levi et al., 2016; Gersey et al., 2017), Schwann cells were isolated from sural nerve biopsies and traumatized sciatic nerve stumps. After purification and proliferation, the cells were combined with sural nerve grafts to repair two cases of a 7.5 cm defect (case 1 with complete transection of sciatic nerves by a boat propeller injury) and a 5 cm defect (case two with partial damage of the tibial division of sciatic nerves by a gun wound of the leg). Follow-up was 36 months for the patient in case 1, and the patient regained proximal sensory recovery, including neuropathic pain, and motor function recovery in the common peroneal and tibial distribution (Levi et al., 2016). Twelve months post-operation, the patient in case 2 exhibited recovery of complete motor function and partial sensation in the tibial distribution (Gersey et al., 2017). Despite the fact that after injury, neurotrophic factor release from activated Schwann cells is beneficial for nerve regeneration and functional recovery, a study of allogeneic nerve grafts with Schwann cells overexpressing glial cell line-derived neurotrophic factors resulted in limited axonal regeneration and poor functional recovery (Santosa et al., 2013). Indeed, the timing, volume and distribution of these neurotrophic factors associated with postinjury Schwann cell behavior are critical for the rate of axonal regrowth and functional recovery (Kidd et al., 2013; Jessen and Mirsky, 2016). Due to the difficulty of harvesting human nerve-derived Schwann cells, skin-derived Schwann cells from patients were collected, and gene expression was characterized in human nerve-derived Schwann cells, and the feasibility of transplantation into injured mouse sciatic nerves was evaluated. The results demonstrated that adult human skin-derived Schwann cells were similar to human nerve-derived Schwann cells genetically and phenotypically,

TABLE 1 | The effect of Schwann cell therapy on peripheral nerve injury-induced neuropathy.

Model	Schwann cell source	Outcomes	Notes
Rat sciatic nerve defect with an 8 mm gap	Autologous	Extensive peripheral nerve regeneration and myelination	• A strong immune reaction occurred when seeding with heterologous Schwann cells; • Seeding density of Schwann cells should be considered (Guenard et al., 1992)
Sciatic nerve defect with a 5 mm gap in immune-deficient rats	Allogeneic, from human nerves	Promotion of axonal regeneration and myelination	Repair outcomes were better than the channels with Matrigel solution alone (Levi et al., 1994)
Human sciatic nerve defect with a 7.5 cm gap	Autologous	Proximal sensory recovery, including neuropathic pain, and motor function recovery in the common peroneal and tibial distribution	The patient suffered complete transection of sciatic nerves by a boat propeller injury (Levi et al., 2016)
Human sciatic nerve defect with a 5 cm gap	Autologous	Recovery of complete motor function and partial sensation in the tibial distribution	The patient suffered partial damage of the tibial division of sciatic nerves by a gun wound to the leg (Gersey et al., 2017)
Mouse sciatic nerve crush	Allogeneic, from human skin	Promotion of axonal regrowth and myelination	• Adult human skin-derived Schwann cells were similar to human nerve-derived Schwann cells in genetical and phenotypical characterization; • Highly accessible source of autologous skin-derived Schwann cells was a substitute for nerve-derived Schwann cells for injured nerve repair (Stratton et al., 2017)
Rat sciatic nerve defect with a 10 mm gap	Allogeneic, from neonatal rat sciatic nerves	Improvement in axonal regeneration	• The quantity of regenerated axons was less than that induced by treatment with syngeneic Schwann cells; • Immune response occurred at 6 weeks post-transplantation in the absence of immunosuppressive therapy (Mosahebi et al., 2002)
Rat sciatic nerve defect with a 20 mm gap (Hoben et al., 2015), 10 mm gap (Sun et al., 2009) and 14 mm gap (Santosa et al., 2013)	Allogeneic, from neonatal (Sun et al., 2009; Hoben et al., 2015)/adult (Santosa et al., 2013) rat sciatic nerves	Improvement in axonal regeneration (Sun et al., 2009; Santosa et al., 2013; Hoben et al., 2015) and myelination (Sun et al., 2009)	• Acellular nerve allografts combined with allogeneic Schwann cells obtained the same outcomes as the isograft group (Hoben et al., 2015); • Adding vascular endothelial growth factor alone (Hoben et al., 2015) or Schwann cells overexpressing glial cell-derived neurotrophic factor (Santosa et al., 2013) in acellular nerve allografts had reduced effects on improving axonal regeneration
Rat sciatic nerve injury with a 3 cm gap	Autologous, from the proximal stump neuroma	Regenerative fibers crossing the entire distance but no motor and poor sensory function recovery	It is challenging to regenerate axons with a 3 cm gap defect with only grafts (Aszmann et al., 2008)
Primate ulnar nerve defect with a 6 cm gap	Autologous, from the sural nerve fascicles	Low immune response and significant regeneration	Cold-preserved allografts combined with autologous Schwann cells was a potentially safe and effective alternative to autografts (Hess et al., 2007)
Rabbit peroneal nerve defect with a 6 cm gap	Autologous, from the contralateral peroneal nerve	Excellent growth of axons targeting the distal end	Autologous Schwann cells break the limit of nerve regeneration by an empty autogenous venous nerve conduit (Strauch et al., 2001)
Rat sciatic nerve defect with a 10 mm gap (Mosahebi et al., 2002) and 1 cm gap (Bryan et al., 2000; Tohill et al., 2004; di Summa et al., 2011)	Allogeneic, from rat sciatic nerves	Improvements in axonal regrowth and fiber myelination	Combination with allogeneic Schwann cells obtained better outcomes in synthetic grafts, such as polyhydroxybutyrate conduits (Mosahebi et al., 2002; Tohill et al., 2004), fibrin conduits (di Summa et al., 2011) and poly (lactic-co-glycolic) acid conduits (Bryan et al., 2000)

which indicates that a highly accessible source of autologous skin-derived Schwann cells may be a substitute for nerve-derived Schwann cells for injured nerve repair (Stratton et al., 2017). Both autogenous and allogenous nerve transplantation require nerve supply from the donor, which leads to donor-site morbidity resulting from the loss of nerves (Kim et al., 2020). A variety of conduits have been developed, including veins and synthetic grafts. Several studies (Chiu et al., 1982; Strauch et al., 1996) have used autogenous venous nerve conduits to successfully support axonal regeneration for short distances (less than a 3 cm gap). Moreover, conduit supplementation with autologous Schwann cells rapidly grew 6 cm peroneal nerve defect-injured nerves compared with treatment alone (Strauch et al., 2001). In addition, Schwann cells in a polyhydroxybutyrate conduit (Mosahebi et al., 2002; Tohill et al., 2004), fibrin conduit (di Summa et al., 2011) and poly (lactic-co-glycolic) acid conduit (Bryan et al., 2000) display more improvements in axonal regrowth and fiber myelination than the use of conduits alone. Based on a study comparing green fluorescent protein-labeled Schwann cells with non-transduced Schwann cells in bioengineered nerve conduits,

TABLE 2 | The effect of Schwann cell-like cells on cell therapy for peripheral nerve injury-induced neuropathy.

Model	Cell source	Grafts	Outcomes	Notes
Rat sciatic nerve transection with a 12 mm gap (Mimura et al., 2004; Ao et al., 2011), 10 mm gap (Shimizu et al., 2007); Rabbit facial nerve buccal branch transection with a 1 cm gap (Wang et al., 2011)	BMSC-derived Schwann cells from rats (Mimura et al., 2004; Ao et al., 2011), humans (Shimizu et al., 2007), rabbits (Wang et al., 2011)	Hollow fiber (Mimura et al., 2004) Transpermeable tube (Shimizu et al., 2007) Chitosan nerve conduits (Ao et al., 2011), autogenous vein (Wang et al., 2011)	Improvements in regenerative axon populations (Mimura et al., 2004; Shimizu et al., 2007; Ao et al., 2011; Wang et al., 2011), motor functions and reconstruction of Ranvier nodes and myelination (Mimura et al., 2004; Ao et al., 2011; Wang et al., 2011)	• No tumor formation within 6 months (Mimura et al., 2004) • Human BMSCs were used in rat sciatic nerve repair with immunosuppressants (Shimizu et al., 2007) • No significant outcomes compared with sciatic nerve-derived Schwann cells (Ao et al., 2011)
Rat sciatic nerve transection with a 1 cm gap (di Summa et al., 2010, 2011; Orbay et al., 2012; Kingham et al., 2014) and 15 mm gap (Georgiou et al., 2015); Tibial nerve crush in athymic nude rats (Tomita et al., 2013)	ASC-derived Schwann cell-like cells from rats (di Summa et al., 2010, 2011; Orbay et al., 2012; Georgiou et al., 2015) and humans (Tomita et al., 2013; Kingham et al., 2014)	Nerve fibrin conduits (di Summa et al., 2010, 2011; Kingham et al., 2014) Silicone (Orbay et al., 2012) Aligned collagen matrix (Georgiou et al., 2015)	Improvements in axonal regeneration (di Summa et al., 2010, 2011; Orbay et al., 2012; Tomita et al., 2013; Kingham et al., 2014; Georgiou et al., 2015) and myelination (Orbay et al., 2012; Tomita et al., 2013), as well as a reduction in muscle atrophy (di Summa et al., 2011); neurotrophic factor release (Kingham et al., 2014), and glial cell differentiation (Tomita et al., 2013); an increase in conduit vascularity (Kingham et al., 2014)	• Differentiated ASC transplantation obtained similar outcomes as that with differentiated MSCs at 2 weeks (di Summa et al., 2010), but the treatment was more effective than differentiated MSCs in a long-term experiment of 16 weeks (di Summa et al., 2011); • Differentiated and undifferentiated rat ASCs had a similar effect on nerve reconstruction 6 months after transplantation (Orbay et al., 2012); • Differentiated human ASCs had a potent effect on neurotrophic factors release and axonal regeneration (Tomita et al., 2013)
Rat sciatic nerve transection with an 8 mm gap (Matsuse et al., 2010)	Schwann cells differentiated from human umbilical cord-derived MSCs	Matrigel-transplanted graft	Promotion of nerve regeneration and myelination	• FK506 was used to avoid immunorejection; • The effect was comparable to treatment with human Schwann cells
Mouse sciatic nerve crush (McKenzie et al., 2006); Rat sciatic nerve crush (Kumar et al., 2016; Stratton et al., 2016; Wu et al., 2020); Rat sciatic nerve transection with a 5 mm gap (Shakhbazau et al., 2014; Zhang et al., 2014), 10 mm gap (Khuong et al., 2014; Zhu et al., 2018)	SKP-derived precursor Schwann cells from mice (McKenzie et al., 2006) and rats (Khuong et al., 2014; Shakhbazau et al., 2014; Zhang et al., 2014; Kumar et al., 2016; Stratton et al., 2016; Zhu et al., 2018; Wu et al., 2020; Cong et al., 2021)	Silicon tube (Shakhbazau et al., 2014) Decellularized nerve grafts (Khuong et al., 2014) Artificial guidance channels (Zhang et al., 2014) Chitosan nerve guidance conduits and silk fibroin filamentous fillers (Zhu et al., 2018)	Improvements in axonal regeneration (McKenzie et al., 2006; Zhang et al., 2014), and myelination (Kumar et al., 2016; Zhu et al., 2018), sensory functional recovery (Shakhbazau et al., 2014), motoneuron and sensory neuron regrowth (Wu et al., 2020; Cong et al., 2021), behavioral recovery (Khuong et al., 2014), surrounding immunological properties to accelerate myelin debris clearance (Stratton et al., 2016)	• The probability of myelination with SKP-derived Schwann cells was higher than with naïve SKPs at 2 weeks post-transplantation, but they had similar profiles at 4 weeks (McKenzie et al., 2006); • Cells in supporting sensory functional recovery is similar to treatment with isogenic Schwann cells (Shakhbazau et al., 2014); • Cells improved behavioral recovery in both acute and chronic nerve injury, but the medium and the dead cells had fewer effects (Khuong et al., 2014); • The immunomodulatory role of SKP-derived precursor Schwann cells on peripheral neuropathy included macrophage recruitment and inflammatory factor expression (Stratton et al., 2016); • Transplantation with adult SKP-derived Schwann cells produced the same outcome that of acutely injured Schwann cells, but chronically denervated Schwann cells were less effective (Kumar et al., 2016); • Acellular matrix from SKP-derived Schwann cells combined with chitosan/silk scaffolds was beneficial for nerve repair (Zhu et al., 2018);

(Continued)

TABLE 2 | (Continued)

Model	Cell source	Grafts	Outcomes	Notes
				• Extracellular vesicles from SKP-derived Schwann cells were responsible for axonal regrowth of motoneurons and sensory neurons (Wu et al., 2020; Cong et al., 2021)
Mouse sciatic nerve transection with a 2–3 mm gap (Kim et al., 2017)	Schwann cell-like cells from human pluripotent stem cells	Matrigel	Improvements in nerve regeneration and myelination	Cells derived from human pluripotent stem cells *via* self-renewing Schwann cell precursors under sequential treatments with cultured medium
Mouse sciatic nerve transection with a 5 mm gap (Sowa et al., 2017)	Schwann cell-like cells from direct conversion from human fibroblast	Gelatin hydrogel	Improvements in myelin formation, axonal regrowth and motor functional recovery	The effect of cells in axonal regrowth and motor functional recovery was comparable to that of treatment with Schwann cells from peripheral nerves
Rat sciatic nerve transection with a 15 mm or 12 mm (Verdú et al., 1999; You et al., 2011; Zhang et al., 2019), and 20 mm gap (Guérout et al., 2011; Boecker et al., 2018); Rat facial nerve transection with a 5 mm gap (Guntinas-Lichius et al., 2001) or end-to-end suture (Guntinas-Lichius et al., 2002); Rat sciatic nerve transection with microsurgical nerve repair (Radtke et al., 2009a); Rat sciatic nerve crush lesion (Dombrowski et al., 2006); Mouse sciatic nerve transection with a 3 mm gap (Goulart et al., 2016)	Olfactory bulb ensheathing cells (Verdú et al., 1999; Guntinas-Lichius et al., 2001; Dombrowski et al., 2006; Radtke et al., 2009a; You et al., 2011; Goulart et al., 2016; Boecker et al., 2018; Zhang et al., 2019); Olfactory mucosa (Guntinas-Lichius et al., 2002)	Silicone tube prefilled with a laminin gel (Verdú et al., 1999); Microporous poly acid conduit (You et al., 2011); Tubular conduit (Goulart et al., 2016); Nerve guide Perimaix (Boecker et al., 2018); Nerve conduits (Zhang et al., 2019)	Improvements in regenerative axon populations (Verdú et al., 1999); Stimulation on collateral sprouting (Guntinas-Lichius et al., 2001); Promotion in the accuracy of target reinnervation and the vibrissae motor performance (Guntinas-Lichius et al., 2002); Improvements in axonal regeneration and functional outcomes (Radtke et al., 2009a; Guérout et al., 2011); Improvements in myelination and nodal formation of regenerative peripheral nerve fibers (Dombrowski et al., 2006); Synergistical improvements in Schwann cells-mediated sciatic nerve repair (You et al., 2011); Improvements in sciatic nerve functional and morphological recovery (Goulart et al., 2016; Boecker et al., 2018); The increase of the level of brain derived factor and nerve growth factor (Zhang et al., 2019)	• It is a powerful tool for severe nerve injury (2 months between injury and repair) (Guntinas-Lichius et al., 2001); • Transplantation of olfactory mucosa significantly improves nerve regeneration (Guntinas-Lichius et al., 2002); • No olfactory ensheathing cells are present in the sciatic nerves 3 months post-transplantation (Guérout et al., 2011); • Olfactory ensheathing cells with the nerve guide Perimaix has local effects on nerve regeneration, but not for traversing the lesion gap (Boecker et al., 2018); • Epidermal neural crest stem cell and olfactory ensheathing cell co-transplantation effectively repairs peripheral nerve injury (Zhang et al., 2019)

the outcomes showed that both of treatments had similar growth characteristics (Tohill et al., 2004). Fluorescently labeled Schwann cells will be beneficial for monitoring Schwann cell behaviors and interactions with axons in bioengineered systems.

The Effect of Schwann Cell-Like Cells on Cell Therapies for Peripheral Neuropathy

Schwann cells are primary glial cells in the peripheral nervous system, and autologous and allogeneic Schwann cells are thought to be good choices for the repair of injured nerves. However, because acquiring these Schwann cells from nerves is time-consuming and has secondary morbidity at the donor site, it is desirable to explore cell sources with similar potential to produce Schwann cells. Stem cells with wide distribution, multilineage potential and self-renewal capacity are highly suitable as alternative cell sources for Schwann cells (Sayad Fathi and Zaminy, 2017). Here, we emphasize the effect of stem cell-derived Schwann cell-like cells on cell therapy for peripheral neuropathy.

A major source of Schwann cell-like cells is mesenchymal stem/stromal cells (MSCs), which are readily isolated from a variety of tissues, including bone marrow, skin, adipose tissue and umbilical cord tissue (Sayad Fathi and Zaminy, 2017;

Hopf et al., 2020). Bone marrow stromal cell (BMSC)-derived Schwann cells from rats (Mimura et al., 2004; Ao et al., 2011), humans (Shimizu et al., 2007) and rabbits (Wang et al., 2011) may mediate improvements in regenerative axon populations, motor functions and the reconstruction of Ranvier nodes and myelination in rat sciatic nerve transection with a 12 mm gap and a 10 mm gap, as well as in rabbit facial nerve buccal branch transection within a 1 cm gap. Moreover, tumor formation was not detected within 6 months (Mimura et al., 2004), and no significant outcomes occurred compared with treatment with sciatic nerve-derived Schwann cells (Ao et al., 2011). Differentiated adipose-derived stem cells (ASCs) are primarily derived from rats (di Summa et al., 2010, 2011; Orbay et al., 2012; Georgiou et al., 2015) and humans (Tomita et al., 2013; Kingham et al., 2014). Transplantation with these cells in nerve fibrin conduits, silicone or aligned collagen matrix has a potential role in the repair of peripheral neuropathy to improve neurotrophic factor release, axonal regrowth (di Summa et al., 2010, 2011; Orbay et al., 2012; Tomita et al., 2013; Kingham et al., 2014; Georgiou et al., 2015), myelination (Orbay et al., 2012; Tomita et al., 2013) and vascularity (Kingham et al., 2014), as well as reduce muscle atrophy (di Summa et al., 2011). Notably, differentiated and undifferentiated rat ASCs combined with silicone in rat sciatic nerve transection with a 1 cm gap had a similar effect on nerve reconstruction within 6 months (Orbay et al., 2012). However, transplantation with differentiated human ASCs in a nude rat tibial nerve crush model obtained a better outcome than the use of undifferentiated cells (Tomita et al., 2013). In contrast to the effect of undifferentiated ASCs, differentiated ASCs had a similar effect at 2 weeks post-transplantation but were more effective in a long-term experiment of 16 weeks (di Summa et al., 2010, 2011). Although there is no direct evidence of human umbilical cord blood-MSC-derived Schwann cell-like cells for treating peripheral neuropathy (Weiss and Troyer, 2006), Schwann cell-like cells obtained from the mesenchymal tissue surrounding umbilical cord vessels (Wharton jelly) were combined with Matrigel-transplanted grafts to repair rat sciatic nerve transection with an 8 mm gap with the immunosuppressor FK506. The effect was comparable to that of using human Schwann cells to promote nerve regeneration and myelination (Matsuse et al., 2010). Compared with other stem cells, skin-derived precursor cells (SKPs) are more accessible and readily differentiate into Schwann cells, and much more attention has been given to investigating their potential role in cell therapy in peripheral nerve injury-induced neuropathy. These cells are widely used to repair rodent sciatic nerve crush or transection with 5 or 10 mm gaps combined with different kinds of grafts, including silicon tubes (Shakhbazau et al., 2014), decellularized nerve grafts (Khuong et al., 2014), artificial guidance channels (Zhang et al., 2014), and chitosan/silk scaffolds (Zhu et al., 2018). After transplantation, these cells improve sensory functional and behavioral recovery in both acute (4 weeks) and chronic (17 weeks) nerve injury (Khuong et al., 2014; Shakhbazau et al., 2014), axonal regeneration and myelination *in vivo* (McKenzie et al., 2006; Zhang et al., 2014; Kumar et al., 2016; Zhu et al., 2018), and motoneuron and sensory neuron regrowth *in vitro* (Wu et al., 2020; Cong et al., 2021). Moreover, they can adjust surrounding immunological properties to accelerate myelin debris clearance by recruiting many more macrophages and enhancing inflammatory factor expression (Stratton et al., 2016). The myelination of these cells is higher than that of naïve SKPs in the early stage (McKenzie et al., 2006), and their ability to support sensory functional recovery is equal to or better than that of treatments with isogenic Schwann cells (Shakhbazau et al., 2014). In addition to the great effect of the cells by themselves, acellular matrix and extracellular vesicles from SKP-derived cells are also responsible for neuronal regrowth *in vitro* (Wu et al., 2020; Cong et al., 2021), but dead cells or the medium was less effective on nerve repair *in vivo* (Khuong et al., 2014). Although great improvements have been obtained with rat/mouse SKP-derived Schwann cell-like cells, the clinical application of human SKPs still needs many more studies to test the utility of cells from different anatomical regions (Dai et al., 2018). In addition, human pluripotent stem cells can be differentiated into Schwann cell-like cells *via* self-renewing Schwann cell precursor cells through sequential treatment with conditioned medium *in vitro*, and the combination with Matrigel successfully improves axonal regeneration and myelin repair (Kim et al., 2017). Another interesting source of Schwann cell-like cells is human fibroblasts, which can be converted with a cellular reprogramming strategy. *In vitro* and *in vivo* experiments with gelatin hydrogel showed a potential role of converted Schwann cells in significantly enhancing axonal regrowth, myelin repair and motor functional recovery, which is comparable to treatment with Schwann cells from peripheral nerves (Sowa et al., 2017).

In addition to these Schwann cell-like cells, olfactory ensheathing cells from olfactory bulb and mucosa share many properties with Schwann cells which include the support of axonal regeneration and myelination (Doucette, 1990). They also exhibit great potentials for nerve repair in peripheral nerve injury-induced neuropathy (Radtke et al., 2009b, 2011; Radtke and Kocsis, 2012, 2014). Olfactory bulb ensheathing cells from mouse (Goulart et al., 2016) and rat mediate improvements in axonal regeneration, myelination and sciatic nerve functional recovery in mouse sciatic nerve transection with a 3 mm gap, and in rat sciatic nerve transection with a 15 or 12 mm gap (Verdú et al., 1999; You et al., 2011; Zhang et al., 2019), and 20 mm gap (Guérout et al., 2011; Boecker et al., 2018), and with microsurgical nerve repair (Radtke et al., 2009a) and in rat sciatic nerve crush lesion (Dombrowski et al., 2006), as well as in rat facial nerve transection with a 5 mm gap (Guntinas-Lichius et al., 2001). As well, transplantation of olfactory mucosa significantly increases the accuracy of target reinnervation and accelerates the vibrissae movements (Guntinas-Lichius et al., 2002). Notably, olfactory ensheathing cell and Schwann cell, or and epidermal neural crest stem cell co-transplantation effectively enhance anatomical and functional repair after sciatic nerve injury in rats (You et al., 2011; Zhang et al., 2019) through enhancing the level of brain derived factor and nerve growth factor, which indicates that cells co-transplantation may serve as a new method for PNI in future therapies.

DIABETIC NEUROPATHY

Diabetic neuropathy is one of the most common complications of diabetic patients. With the incidences of diabetes increasing annually, especially in type 2 diabetes, studies are focused on understanding the pathogenic mechanisms, most of which are associated with neurons and vessels (Kim et al., 2012). However, accumulating evidence indicates the effect on morphological alterations and dysfunction in Schwann cells following diabetic neuropathy (Mizisin, 2014; Naruse, 2019). Studies on the sural nerves of rodents, cats and patients with diabetic neuropathy indicate that an apparently normal axon is wrapped by an abnormal myelin sheath resulting from segmental demyelination and remyelination (Thomas and Lascelles, 1965; Sima et al., 1988; Malik et al., 2005; Lennertz et al., 2011). In addition, the ultrastructure of abnormal Schwann cells showed mitochondrial enlargement with numerous vacuoles, cytoplasmic expansion, glycogen inclusion, and hyperplasia of the basement membrane (Yagihashi and Matsunaga, 1979; Chowdhury et al., 2013; Mizisin, 2014). Metabolic and molecular perturbations of Schwann cells in diabetic neuropathy include high activity of aldose reductase-mediated polyol pathway flux, oxidative stress and inflammation, as well as damage associated with microvascular changes in Schwann cells, all of which result in decreased neurotrophic factors release and the accumulation of neurotoxic intermediates leading to the dysfunction of interactions between Schwann cells and axons and diabetic neuropathy (Gonçalves et al., 2017, 2018; Naruse, 2019). Therefore, treating Schwann cells offers a potential strategy for diabetic neuropathy. Here, we primarily review the role of Schwann cells in cell therapy for diabetic neuropathy.

As shown in **Table 3**, different sources of stem cells exhibit potential of treating diabetic neuropathy and have an effect on the function of Schwann cells. BM-derived cells, endothelial progenitor cells (EPCs), and mononuclear cells (MNCs) can effectively reverse the symptoms of diabetic neuropathy through neuroprotective effects and neovascularization (Naruse et al., 2005; Hasegawa et al., 2006; Jeong et al., 2009; Kim et al., 2009). During this process, these neurotrophic and angiogenic factors suppress Schwann cell apoptosis and enhance Schwann cell proliferation and myelination (Jeong et al., 2009; Kim et al., 2012). In addition, treatment with BMSCs in hindlimb muscles, which can be differentiated into Schwann cell-like cells (Caddick et al., 2006), can ameliorate diabetic neuropathy symptoms, such as dysfunction of sensory and motor nerves, as well as demyelination in streptozotocin (STZ)-induced diabetic rats (Han et al., 2016). In addition to BMSCs, ASCs were transplanted by intramuscular injection and had a positive effect on the repair of STZ-induced diabetic neuropathy through the regulation of Schwann cell-related neurotrophic factor expression and remyelination (Yigitturk et al., 2021). Compared with stem cell-based treatment for diabetic neuropathy, additional studies have been performed with dental pulp stem cells (DPSCs). After human DPSCs were injected into the hindlimb skeletal muscle of diabetic mice, increases in vascular endothelial growth factor and nerve growth factor were detected at the injection site, while antibody neutralization reversed the effect of human DPSCs (Hata et al., 2020). Moreover, in STZ-induced diabetic rats, rat DPSCs ameliorated long-term (52 weeks) diabetic neuropathy (Omi et al., 2017). Although GFP-labeled rat DPSCs did not differentiate into Schwann cells after being injected into skeletal muscles (Hata et al., 2015), they had a beneficial effect on Schwann cells, including increasing Schwann cell viability and myelin formation (Omi et al., 2017). Of note, there was no difference in the therapeutic effect on diabetic neuropathy between the injection of rat DPSC-secreted factors and DPSCs (Kanada et al., 2020), and DPSC-secreted factors promoted Schwann cell proliferation and myelin formation (Omi et al., 2017). Conditioned medium from ASCs was also beneficial in preventing foot ulcer formation, ameliorating diabetic neuropathy in diabetic BKS *db*/*db* mice, and blocking diabetes-induced Schwann cell apoptosis (De Gregorio et al., 2020). Human DPSCs were used to treat a rat model of diabetic neuropathy through intramuscular or intravenous administration of one or two rounds of transplantation were helpful in contributing to functional recovery, but repeated doses *via* the intramuscular route was the most effective (Datta et al., 2017), which indicates that different routes and doses produce different effects. Neural crest can differentiate into multiple types of cells, including Schwann cells and peripheral neurons (Bronner and LeDouarin, 2012). However, there has only been one study using neural crest-like cells derived from induced pluripotent stem cells to treat STZ-induced diabetic mice, and the transplanted cells differentiated into Schwann cell-like cells or vascular smooth muscle cells to effectively improve the impaired vascular and neuronal functions (Okawa et al., 2013). Although the effect of Schwann cells as a cell therapy needs further study, Schwann cells are a key player in the treatment of diabetic neuropathy through cell transplantation.

CHEMOTHERAPY-INDUCED PERIPHERAL NEUROPATHY

Chemotherapy-induced peripheral neuropathy (CIPN) is the most common secondary effect in cancer patients who receive chemotherapy treatment. Signs of damage to peripheral nerves in CIPN are associated with sensory abnormalities, including allodynia (loss of touch sensation, numbness) or hyperalgesia (pin sensation and tingling), and often manifest as glove-stocking distributions (Bobylev et al., 2015). Some patients also exhibit motor nerve damage and altered musculoskeletal adverse effects (Ibrahim and Ehrlich, 2020). With the increasing numbers of cancer survivors and no ways to predict who will develop symptoms or when, there are no effective approved drugs to prevent or reduce CIPN (Carozzi et al., 2015; Jordan et al., 2019). Therefore, the management of CIPN is still a major challenge for clinical treatment. Despite the lack of direct evidence to illustrate the role of Schwann cell transplantation in CIPN, more attention has been given to the impairment of Schwann cells by chemotherapeutic agents and stem cell therapy for CIPN (**Table 4**; Al-Massri et al., 2020; Ibrahim and Ehrlich, 2020).

TABLE 3 | The effect of different cell therapies on Schwann cells for diabetic neuropathy.

Stem cell type	Cell source	Effect on Schwann cells	Notes
MNCs	Bone marrow/peripheral blood	Increased angiogenic and neurotrophic factor release (Hasegawa et al., 2006; Kim et al., 2009)	• Implantation into hindlimb muscles in STZ-induced diabetic rats; • Improvement in vascularity and motor nerve conduction velocity
EPCs	Bone marrow (Jeong et al., 2009)/ cord blood (Naruse et al., 2005)	• Decreased Schwann cells apoptosis and enhanced proliferation (Naruse et al., 2005; Jeong et al., 2009)	• Cell were injected into the hindlimb of STZ-induced diabetic mice or rats; • Enhancement in neural neovascularization and neuroprotective effects
BMSCs	Bone marrow	• Differentiation into Schwann cell-like cells and the upregulation of neurotrophic factors and myelination-related genes (Han et al., 2016)	• Injection into the hindlimb muscles of STZ-induced diabetic rats; • Increases in angiogenesis, neural function and myelination
ASCs	Adipose tissue	• Effects on the Schwann cell signal network, including neurotrophic effects and the restoration of myelination (Yigitturk et al., 2021)	• Injection into the thigh and lower hind-leg muscles of STZ-induced diabetic mice; • Restoration of neural structure and function
		• Reduced Schwann cell apoptosis with ASCs-conditioned medium (De Gregorio et al., 2020)	• Systemic administration in diabetic BKS *db/db* mice; • Avoiding foot ulcer formation and ameliorating polyneuropathy
DPSCs	Teeth	• Increased viability and myelin-related protein expression in Schwann cells (Omi et al., 2017) • Promotion of Schwann cells proliferation and myelin formation (Omi et al., 2017)	• Transplantation of human DPSCs into the hindlimb skeletal muscles of STZ-induced diabetic nude mice; • Treatment of diabetic polyneuropathy *via* the angiogenic and neurotrophic mechanism of hDPSC-secreted factors (Hata et al., 2020)
			• Transplantation of rat DPSCs into the hindlimb skeletal muscles of STZ-induced diabetic rats; • Improvements in long-term diabetic polyneuropathy (Omi et al., 2017)
			• Transplantation of freshly isolated and cryopreserved rat DPSCs into the hindlimb skeletal muscles of STZ-induced diabetic rats; • Amelioration of diabetic polyneuropathy (Hata et al., 2015)
			• Transplantation of rat DPSCs or administration of secreted factors into the hindlimb skeletal muscles of STZ-induced diabetic rats; • Amelioration of diabetic polyneuropathy with either treatment (Kanada et al., 2020)
			• Transplantation into STZ-induced neuropathic rats through the intramuscular or intravenous route *via* a single or two repeat doses; • Contribution to functional recovery with all treatments, but repeated doses *via* the intramuscular route was the most effective (Datta et al., 2017)
Neural crest cells	Induced pluripotent stem cells	Differentiation into Schwann cell-like cells (Bronner and LeDouarin, 2012)	• Transplantation into the hindlimb skeletal muscles of STZ-diabetic mice; • Improvement in impaired vascular and neuronal functions (Okawa et al., 2013)

TABLE 4 | The effect of chemotherapy on Schwann cells.

Anticancer agents	Symptoms	Effect on Schwann cells	Notes
Bortezomib	Severe sensory ataxia	Myelin damage (Filosto et al., 2007) Acute and transient endoplasmic reticulum damage to Schwann cells, abnormal myelination of Remak bundles and downregulation of myelin-related genes (Shin et al., 2010)	*In vitro* and *in vivo* experiments demonstrated the side effect of bortezomib on Schwann cells (Filosto et al., 2007; Shin et al., 2010)
Oxaliplatin, cisplatin, paclitaxel	Numbness, dysesthesia, paresthesia and muscle weakness	Disruption of myelin formation and mitochondrial dysfunction in Schwann cells	The cytotoxicity-induced by these drugs requires a lower dose in Schwann cells than in the dorsal root ganglion; The effect of these drugs on Schwann cells are different (Imai et al., 2017)
Epirubicin/docetaxel	Pain	Improvements in Schwann cell dedifferentiation	The side effect was suppressed by concomitant treatment with duloxetine and allopregnanolone (Matta et al., 2020)

Bortezomib, a proteasome inhibitor, is widely used in the treatment of multiple myeloma and induces axonal-dependent sensory damage and pathological responses in Schwann cells. Bortezomib-treated Schwann cells were analyzed by gene expression microarray, and the results indicated endoplasmic reticulum damage to Schwann cells accompanied by the downregulation of myelin-related genes, which was verified in a patient with high-dose bortezomib-induced peripheral neuropathy (Filosto et al., 2007; Shin et al., 2010). In contrast, compared with that in dorsal rooting ganglion neurons, a lower dose of oxaliplatin, cisplatin or paclitaxel is required in cultured Schwann cells because of cytotoxicity, and these drugs have a negative effect on myelin formation in cocultures but do not affect neurons, which indicates that Schwann cells are more susceptible to CIPN than other cells. Surprisingly, mitochondrial dysfunction occurs in cisplatin- and oxaliplatin-treated Schwann cells but not in paclitaxel-treated Schwann cells, while only paclitaxel induces Schwann cell dedifferentiation (Imai et al., 2017). Consistently, Schwann cell dedifferentiation occurs in epirubicin-docetaxel-induced CIPN, and this effect is suppressed by concomitant duloxetine-allopregnanolone treatment (Matta et al., 2020).

Mesenchymal stem/stromal cell therapy, which is a potential strategy for CIPN treatment, has a beneficial effect on improving symptoms (Al-Massri et al., 2020). MSC treatment could protect both sensory and motor neurons and enhance the efficacy of pregabalin in paclitaxel-induced peripheral neuropathy (Al-Massri et al., 2019). Notably, nasal administration of MSC-based therapy reverses cisplatin- or paclitaxel-induced peripheral neuropathy by Boukelmoune et al. (2021). In addition, ASCs also have a positive role in alleviating oxaliplatin-induced peripheral neuropathy (Di Cesare Mannelli et al., 2018). Induced pluripotent stem cells (iPSCs) can serve as a new method to estimate the neurotoxicity associated with chemotherapy treatment (Wheeler et al., 2015; Wing et al., 2017). The mechanisms of MSC-based therapies, including whether MSCs can differentiate into Schwann-like cells, need further study. MSC-based cell therapy may be a promising strategy for patients suffering from the adverse effects of cancer treatment.

CONCLUSION AND FUTURE PERSPECTIVES

Emerging evidence has demonstrated the important role of Schwann cell/Schwann cell-like cell therapy in alleviating peripheral neuropathy, but a variety of challenges still need to be investigated. The source of both autological and allogenic Schwann cells are primarily nerve biopsies and traumatized nerve stumps, all of which will result in the innervation of anatomical regions for the donor and undesired morbidities. Moreover, nerve-derived Schwann cells need a long expansion time *in vitro* to produce a large number of cells. The time between injury and transplantation with Schwann cells should be minimized to protect patients from a series of secondary injuries, including muscle degeneration and functional loss. Given these limitations, Schwann cell-like cells from stem cells have become a relatively robust alternative cell for the repair of peripheral neuropathy. The therapeutic application of pluripotent stem cells is associated with safety and technical and ethical constraints compared with other stem cell types, such as BM-MSCs, dM-MSCs and SKPs. However, these cells have a long differentiation time after isolation and can delay treatment, resulting in further damage to the patient. Highly efficient methods for *in vitro* differentiation and characterization of Schwann cell-like cells may support future clinical applications. On the other hand, direct transplantation with these stem cells, followed by *in vivo* differentiation associated with the pathological stage of peripheral neuropathy, may become a promising and attractive therapeutic strategy. In addition, in patients transplanted with allogenic Schwann cells or Schwann cell-like cells, drugs still need to be used to avoid immune rejection and potential side effects.

Although there is a large amount of evidence on the role of Schwann cell-like cells in peripheral neuropathy in rodent animal models, including peripheral nerve injury, diabetes and chemotherapy, until now, no direct clinical trials have been developed with these cells. However, for spinal cord injury, several studies reported the therapeutic benefits of treatment with these cells. Most studies have been focused on evaluating safety and adverse events after transplantation (Yazdani et al., 2013; Mendonca et al., 2014; Anderson et al., 2017; Gant et al., 2021). Notably, single MSC administration is safe but less effective than combination treatment with autologous Schwann cells (Oh et al., 2016), which improves sensory and motor functional recovery to some extent, as well as bladder compliance (Oraee-Yazdani et al., 2016, 2021). In addition, the administration of these cells by intravenous infusion, intrathecal administration or direct injection into spinal lesions, and the injury level and size may lead to different outcomes. Due to the effect of advanced age (Tong et al., 2015; Liu et al., 2018) and sexual dimorphism (Magnaghi et al., 2006; Stenberg and Dahlin, 2014) on the characterization of Schwann cells, these factors need to be taken into consideration when choosing a therapeutic strategy. Therefore, many more preclinical studies with cell therapies are needed prior to clinical application.

Schwann cells release a variety of signaling molecules under both physiological and pathological conditions to promote neuronal development and postinjury regeneration (Monje, 2020). Therefore, whether appropriate signaling molecules or drugs are administered in combination with transplanted Schwann cells still needs to be carefully assessed (Balakrishnan et al., 2020). In addition to the variability in the repair response between rodent and human models, relatively long-distance transection or injury occurs in humans compared with rodent models, and a slow rate of nerve regeneration requires a longer time for transplanted Schwann cells or Schwann cell-like cells to support and remyelinate the regenerated axons (Balakrishnan et al., 2020).

In summary, although a great number of challenges remain to be addressed, a growing body of evidence demonstrates the beneficial therapeutic roles of Schwann cells and Schwann cell-like cells in peripheral neuropathy. With deeper insights into the pathology of peripheral neuropathy-related disorders, including

peripheral nerve injury, diabetes and chemotherapy, as well as the development of bioengineering systems, Schwann cell-based therapy will soon be a more attractive and effective strategy for treating peripheral neuropathy.

AUTHOR CONTRIBUTIONS

Z-YW and GC conceptualized the topics. Z-YW, QW, Z-ML, F-YC, W-FS, and Y-YZ wrote and revised the manuscript. All authors contributed to the article and approved the submitted version.

FUNDING

This study was supported by National Natural Science Foundation of China (31900718 and 32070998), Basic Research Program of the Education Department of Jiangsu Province (19KJB180024), Postdoctoral Science Foundation of China (2019M651925); The Key Research and Development of Jiangsu Province (BE2020667); The Foundation of Jiangsu Province "333 Project High-level Talents" (BRA2020076), and Priority Academic Program Development of Jiangsu Higher Education Institutions (PAPD).

REFERENCES

Al-Massri, K. F., Ahmed, L. A., and El-Abhar, H. S. (2019). Mesenchymal stem cells therapy enhances the efficacy of pregabalin and prevents its motor impairment in paclitaxel-induced neuropathy in rats: role of Notch1 receptor and JAK/STAT signaling pathway. *Behav. Brain Res.* 360, 303–311. doi: 10.1016/j.bbr.2018.12.013

Al-Massri, K. F., Ahmed, L. A., and El-Abhar, H. S. (2020). Mesenchymal stem cells in chemotherapy-induced peripheral neuropathy: a new challenging approach that requires further investigations. *J. Tissue Eng. Regen. Med.* 14, 108–122. doi: 10.1002/term.2972

Anderson, K. D., Guest, J. D., Dietrich, W. D., Bartlett Bunge, M., Curiel, R., Dididze, M., et al. (2017). Safety of autologous human schwann cell transplantation in subacute thoracic spinal cord injury. *J. Neurotrauma* 34, 2950–2963. doi: 10.1089/neu.2016.4895

Ao, Q., Fung, C. K., Tsui, A. Y., Cai, S., Zuo, H. C., Chan, Y. S., et al. (2011). The regeneration of transected sciatic nerves of adult rats using chitosan nerve conduits seeded with bone marrow stromal cell-derived Schwann cells. *Biomaterials* 32, 787–796. doi: 10.1016/j.biomaterials.2010.09.046

Aszmann, O. C., Korak, K. J., Luegmair, M., and Frey, M. (2008). Bridging critical nerve defects through an acellular homograft seeded with autologous schwann cells obtained from a regeneration neuroma of the proximal stump. *J. Reconstr. Microsurg.* 24, 151–158. doi: 10.1055/s-2008-1076091

Balakrishnan, A., Belfiore, L., Chu, T. H., Fleming, T., Midha, R., Biernaskie, J., et al. (2020). Insights into the role and potential of schwann cells for peripheral nerve repair from studies of development and injury. *Front. Mol. Neurosci.* 13:608442. doi: 10.3389/fnmol.2020.608442

Baradaran, A., El-Hawary, H., Efanov, J. I., and Xu, L. (2021). Peripheral nerve healing: so near and yet so far. *Semin. Plast. Surg.* 35, 204–210. doi: 10.1055/s-0041-1731630

Barrell, K., and Smith, A. G. (2019). Peripheral Neuropathy. *Med. Clin. North Am.* 103, 383–397. doi: 10.1016/j.mcna.2018.10.006

Bobylev, I., Elter, T., Schneider, C., Wunderlich, G., Zimmer, P., Streckmann, F., et al. (2015). [Chemotherapy-induced Peripheral Neuropathy]. *Fortschr. Neurol. Psychiatr.* 83, 427–436. doi: 10.1055/s-0035-1553475

Boecker, A. H., Bozkurt, A., Kim, B. S., Altinova, H., Tank, J., Deumens, R., et al. (2018). Cell-enrichment with olfactory ensheathing cells has limited local extra beneficial effects on nerve regeneration supported by the nerve guide Perimaix. *J. Tissue Eng. Regen. Med.* 12, 2125–2137. doi: 10.1002/term.2731

Boukelmoune, N., Laumet, G., Tang, Y., Ma, J., Mahant, I., Singh, S. K., et al. (2021). Nasal administration of mesenchymal stem cells reverses chemotherapy-induced peripheral neuropathy in mice. *Brain Beha. Immun.* 93, 43–54. doi: 10.1016/j.bbi.2020.12.011

Brewer, J. R., Morrison, G., Dolan, M. E., and Fleming, G. F. (2016). Chemotherapy-induced peripheral neuropathy: current status and progress. *Gynecol. Oncol.* 140, 176–183. doi: 10.1016/j.ygyno.2015.11.011

Bronner, M. E., and LeDouarin, N. M. (2012). Development and evolution of the neural crest: an overview. *Dev. Biol.* 366, 2–9. doi: 10.1016/j.ydbio.2011.12.042

Bryan, D. J., Holway, A. H., Wang, K. K., Silva, A. E., Trantolo, D. J., Wise, D., et al. (2000). Influence of glial growth factor and Schwann cells in a bioresorbable guidance channel on peripheral nerve regeneration. *Tissue Eng.* 6, 129–138. doi: 10.1089/107632700320757

Caddick, J., Kingham, P. J., Gardiner, N. J., Wiberg, M., and Terenghi, G. (2006). Phenotypic and functional characteristics of mesenchymal stem cells differentiated along a Schwann cell lineage. *Glia* 54, 840–849. doi: 10.1002/glia.20421

Cai, S., Tsui, Y. P., Tam, K. W., Shea, G. K., Chang, R. S., Ao, Q., et al. (2017). Directed differentiation of human bone marrow stromal cells to fate-committed schwann cells. *Stem Cell Rep.* 9, 1097–1108. doi: 10.1016/j.stemcr.2017.08.004

Carozzi, V. A., Canta, A., and Chiorazzi, A. (2015). Chemotherapy-induced peripheral neuropathy: What do we know about mechanisms? *Neurosci. Lett.* 596, 90–107. doi: 10.1016/j.neulet.2014.10.014

Cernea, S., and Raz, I. (2021). Management of diabetic neuropathy. *Metabolism* 123:154867. doi: 10.1016/j.metabol.2021.154867

Chiu, D. T., Janecka, I., Krizek, T. J., Wolff, M., and Lovelace, R. E. (1982). Autogenous vein graft as a conduit for nerve regeneration. *Surgery* 91, 226–233.

Chowdhury, S. K., Smith, D. R., and Fernyhough, P. (2013). The role of aberrant mitochondrial bioenergetics in diabetic neuropathy. *Neurobiol. Dis.* 51, 56–65. doi: 10.1016/j.nbd.2012.03.016

Cong, M., Shen, M., Wu, X., Li, Y., Wang, L., He, Q., et al. (2021). Improvement of sensory neuron growth and survival via negatively regulating PTEN by miR-21-5p-contained small extracellular vesicles from skin precursor-derived Schwann cells. *Stem Cell Res. Ther.* 12:80. doi: 10.1186/s13287-020-02125-4

Dai, R., Hua, W., Xie, H., Chen, W., Xiong, L., and Li, L. (2018). The human skin-derived precursors for regenerative medicine: current state, challenges, and perspectives. *Stem Cells Int.* 2018, 1–11. doi: 10.1155/2018/8637812

Datta, I., Bhadri, N., Shahani, P., Majumdar, D., Sowmithra, S., Razdan, R., et al. (2017). Functional recovery upon human dental pulp stem cell transplantation in a diabetic neuropathy rat model. *Cytotherapy* 19, 1208–1224. doi: 10.1016/j.jcyt.2017.07.009

De Gregorio, C., Contador, D., Diaz, D., Carcamo, C., Santapau, D., Lobos-Gonzalez, L., et al. (2020). Human adipose-derived mesenchymal stem cell-conditioned medium ameliorates polyneuropathy and foot ulceration in diabetic BKS db/db mice. *Stem Cell Res. Ther.* 11:168. doi: 10.1186/s13287-020-01680-0

Di Cesare Mannelli, L., Tenci, B., Micheli, L., Vona, A., Corti, F., Zanardelli, M., et al. (2018). Adipose-derived stem cells decrease pain in a rat model of oxaliplatin-induced neuropathy: role of VEGF-A modulation. *Neuropharmacology* 131, 166–175. doi: 10.1016/j.neuropharm.2017.12.020

di Summa, P. G., Kalbermatten, D. F., Pralong, E., Raffoul, W., Kingham, P. J., and Terenghi, G. (2011). Long-term in vivo regeneration of peripheral nerves through bioengineered nerve grafts. *Neuroscience* 181, 278–291. doi: 10.1016/j.neuroscience.2011.02.052

di Summa, P. G., Kingham, P. J., Raffoul, W., Wiberg, M., Terenghi, G., and Kalbermatten, D. F. (2010). Adipose-derived stem cells enhance peripheral nerve regeneration. *J. Plast. Reconstr. Aesthet. Surg.* 63, 1544–1552. doi: 10.1016/j.bjps.2009.09.012

Dombrowski, M. A., Sasaki, M., Lankford, K. L., Kocsis, J. D., and Radtke, C. (2006). Myelination and nodal formation of regenerated peripheral nerve fibers

following transplantation of acutely prepared olfactory ensheathing cells. *Brain Res.* 1125, 1–8. doi: 10.1016/j.brainres.2006.09.089

Doucette, R. (1990). Glial influences on axonal growth in the primary olfactory system. *Glia* 3, 433–449. doi: 10.1002/glia.440030602

Filosto, M., Rossi, G., Pelizzari, A. M., Buzio, S., Tentorio, M., Broglio, L., et al. (2007). A high-dose bortezomib neuropathy with sensory ataxia and myelin involvement. *J. Neurol. Sci.* 263, 40–43. doi: 10.1016/j.jns.2007.05.023

Gant, K. L., Guest, J. D., Palermo, A. E., Vedantam, A., Jimsheleishvili, G., Bunge, M. B., et al. (2021). Phase 1 safety trial of autologous human schwann cell transplantation in chronic spinal cord injury. *J. Neurotrauma* 39, 285–299. doi: 10.1089/neu.2020.7590

Georgiou, M., Golding, J. P., Loughlin, A. J., Kingham, P. J., and Phillips, J. B. (2015). Engineered neural tissue with aligned, differentiated adipose-derived stem cells promotes peripheral nerve regeneration across a critical sized defect in rat sciatic nerve. *Biomaterials* 37, 242–251. doi: 10.1016/j.biomaterials.2014.10.009

Gersey, Z. C., Burks, S. S., Anderson, K. D., Dididze, M., Khan, A., Dietrich, W. D., et al. (2017). First human experience with autologous Schwann cells to supplement sciatic nerve repair: report of 2 cases with long-term follow-up. *Neurosurg. Focus.* 42:E2. doi: 10.3171/2016.12.FOCUS16474

Gonçalves, N. P., Vægter, C. B., Andersen, H., Østergaard, L., Calcutt, N. A., and Jensen, T. S. (2017). Schwann cell interactions with axons and microvessels in diabetic neuropathy. *Nat. Rev. Neurol.* 13, 135–147. doi: 10.1038/nrneurol.2016.201

Gonçalves, N. P., Vægter, C. B., and Pallesen, L. T. (2018). Peripheral glial cells in the development of diabetic neuropathy. *Front. Neurol.* 9:268. doi: 10.3389/fneur.2018.00268

Goulart, C. O., Ângelo Durço, D. F., de Carvalho, L. A., Oliveira, J. T., Alves, L., Cavalcante, L. A., et al. (2016). Olfactory ensheathing glia cell therapy and tubular conduit enhance nerve regeneration after mouse sciatic nerve transection. *Brain Res.* 1650, 243–251. doi: 10.1016/j.brainres.2016.09.021

Griffin, J. W., and Thompson, W. J. (2008). Biology and pathology of nonmyelinating Schwann cells. *Glia* 56, 1518–1531. doi: 10.1002/glia.20778

Guenard, V., Kleitman, N., Morrissey, T. K., Bunge, R. P., and Aebischer, P. (1992). Syngeneic Schwann cells derived from adult nerves seeded in semipermeable guidance channels enhance peripheral nerve regeneration. *J. Neurosci.* 12, 3310–3320. doi: 10.1523/JNEUROSCI.12-09-03310.1992

Guérout, N., Duclos, C., Drouot, L., Abramovici, O., Bon-Mardion, N., Lacoume, Y., et al. (2011). Transplantation of olfactory ensheathing cells promotes axonal regeneration and functional recovery of peripheral nerve lesion in rats. *Muscle Nerve* 43, 543–551. doi: 10.1002/mus.21907

Guntinas-Lichius, O., Angelov, D. N., Tomov, T. L., Dramiga, J., Neiss, W. F., and Wewetzer, K. (2001). Transplantation of olfactory ensheathing cells stimulates the collateral sprouting from axotomized adult rat facial motoneurons. *Exp. Neurol.* 172, 70–80. doi: 10.1006/exnr.2001.7774

Guntinas-Lichius, O., Wewetzer, K., Tomov, T. L., Azzolin, N., Kazemi, S., Streppel, M., et al. (2002). Transplantation of olfactory mucosa minimizes axonal branching and promotes the recovery of vibrissae motor performance after facial nerve repair in rats. *J. Neurosci.* 22, 7121–7131. doi: 10.1523/JNEUROSCI.22-16-07121.2002

Hammi, C., and Yeung, B. (2021). *Neuropathy. StatPearls*. Treasure Island, FL: StatPearls Publishing.

Han, J. W., Choi, D., Lee, M. Y., Huh, Y. H., and Yoon, Y. S. (2016). Bone marrow-derived mesenchymal stem cells improve diabetic neuropathy by direct modulation of both angiogenesis and myelination in peripheral nerves. *Cell Transplant.* 25, 313–326. doi: 10.3727/096368915X688209

Hanewinckel, R., Ikram, M. A., and Van Doorn, P. A. (2016). Peripheral neuropathies. *Handb. Clin. Neurol.* 138, 263–282. doi: 10.1016/B978-0-12-802973-2.00015-X

Hasegawa, T., Kosaki, A., Shimizu, K., Matsubara, H., Mori, Y., Masaki, H., et al. (2006). Amelioration of diabetic peripheral neuropathy by implantation of hematopoietic mononuclear cells in streptozotocin-induced diabetic rats. *Exp. Neurol.* 199, 274–280. doi: 10.1016/j.expneurol.2005.11.001

Hata, M., Omi, M., Kobayashi, Y., Nakamura, N., Miyabe, M., Ito, M., et al. (2020). Transplantation of human dental pulp stem cells ameliorates diabetic polyneuropathy in streptozotocin-induced diabetic nude mice: the role of angiogenic and neurotrophic factors. *Stem Cell Res. Ther.* 11:236. doi: 10.1186/s13287-020-01758-9

Hata, M., Omi, M., Kobayashi, Y., Nakamura, N., Tosaki, T., Miyabe, M., et al. (2015). Transplantation of cultured dental pulp stem cells into the skeletal muscles ameliorated diabetic polyneuropathy: therapeutic plausibility of freshly isolated and cryopreserved dental pulp stem cells. *Stem Cell Res Ther.* 6:162. doi: 10.1186/s13287-015-0156-4

Hess, J. R., Brenner, M. J., Fox, I. K., Nichols, C. M., Myckatyn, T. M., Hunter, D. A., et al. (2007). Use of cold-preserved allografts seeded with autologous Schwann cells in the treatment of a long-gap peripheral nerve injury. *Plast. Reconstr. Surg.* 119, 246–259. doi: 10.1097/01.prs.0000245341.71666.97

Hoben, G., Yan, Y., Iyer, N., Newton, P., Hunter, D. A., Moore, A. M., et al. (2015). Comparison of acellular nerve allograft modification with Schwann cells or VEGF. *Hand* 10, 396–402. doi: 10.1007/s11552-014-9720-0

Holmes, C. J., and Hastings, M. K. (2021). The application of exercise training for diabetic peripheral neuropathy. *J. Clin. Med.* 10:5042. doi: 10.3390/jcm10215042

Hopf, A., Schaefer, D. J., Kalbermatten, D. F., Guzman, R., and Madduri, S. (2020). Schwann cell-like cells: origin and usability for repair and regeneration of the peripheral and central nervous system. *Cells* 9:1990. doi: 10.3390/cells9091990

Hudson, T. W., Zawko, S., Deister, C., Lundy, S., Hu, C. Y., Lee, K., et al. (2004). Optimized acellular nerve graft is immunologically tolerated and supports regeneration. *Tissue Eng.* 10, 1641–1651. doi: 10.1089/ten.2004.10.1641

Hughes, R. A. (2002). Peripheral neuropathy. *BMJ* 324, 466–469. doi: 10.1136/bmj.324.7335.466

Ibrahim, E. Y., and Ehrlich, B. E. (2020). Prevention of chemotherapy-induced peripheral neuropathy: a review of recent findings. *Crit. Rev. Oncol. Hematol.* 145:102831. doi: 10.1016/j.critrevonc.2019.102831

Imai, S., Koyanagi, M., Azimi, Z., Nakazato, Y., Matsumoto, M., Ogihara, T., et al. (2017). Taxanes and platinum derivatives impair Schwann cells via distinct mechanisms. *Sci. Rep.* 7:5947. doi: 10.1038/s41598-017-05784-1

Jeong, J. O., Kim, M. O., Kim, H., Lee, M. Y., Kim, S. W., Ii, M., et al. (2009). Dual angiogenic and neurotrophic effects of bone marrow-derived endothelial progenitor cells on diabetic neuropathy. *Circulation* 119, 699–708. doi: 10.1161/CIRCULATIONAHA.108.789297

Jessen, K. R., and Mirsky, R. (2016). The repair Schwann cell and its function in regenerating nerves. *J. Physiol.* 594, 3521–3531. doi: 10.1113/JP270874

Jordan, B., Jahn, F., Sauer, S., and Jordan, K. (2019). Prevention and management of chemotherapy-induced polyneuropathy. *Breast Care* 14, 79–84. doi: 10.1159/000499599

Kanada, S., Makino, E., Nakamura, N., Miyabe, M., Ito, M., Hata, M., et al. (2020). Direct comparison of therapeutic effects on diabetic polyneuropathy between transplantation of dental pulp stem cells and administration of dental pulp stem cell-secreted factors. *Int. J. Mol. Sci.* 21:6064. doi: 10.3390/ijms21176064

Khuong, H. T., Kumar, R., Senjaya, F., Grochmal, J., Ivanovic, A., Shakhbazau, A., et al. (2014). Skin derived precursor Schwann cells improve behavioral recovery for acute and delayed nerve repair. *Exp. Neurol.* 254, 168–179. doi: 10.1016/j.expneurol.2014.01.002

Kidd, G. J., Ohno, N., and Trapp, B. D. (2013). Biology of Schwann cells. *Handb. Clin. Neurol.* 115, 55–79. doi: 10.1016/B978-0-444-52902-2.00005-9

Kim, H., Kim, J. J., and Yoon, Y. S. (2012). Emerging therapy for diabetic neuropathy: cell therapy targeting vessels and nerves. *Endocr. Metab. Immune. Disord. Drug Targets* 12, 168–178. doi: 10.2174/187153012800493486

Kim, H., Park, J. S., Choi, Y. J., Kim, M. O., Huh, Y. H., Kim, S. W., et al. (2009). Bone marrow mononuclear cells have neurovascular tropism and improve diabetic neuropathy. *Stem Cells* 27, 1686–1696. doi: 10.1002/stem.87

Kim, H. S., Kim, J. Y., Song, C. L., Jeong, J. E., and Cho, Y. S. (2020). Directly induced human Schwann cell precursors as a valuable source of Schwann cells. *Stem Cell Res. Ther.* 11:257. doi: 10.1186/s13287-020-01772-x

Kim, H. S., Lee, J., Lee, D. Y., Kim, Y. D., Kim, J. Y., Lim, H. J., et al. (2017). Schwann cell precursors from human pluripotent stem cells as a potential therapeutic target for myelin repair. *Stem Cell Rep.* 8, 1714–1726. doi: 10.1016/j.stemcr.2017.04.011

Kingham, P. J., Kolar, M. K., Novikova, L. N., Novikov, L. N., and Wiberg, M. (2014). Stimulating the neurotrophic and angiogenic properties of human adipose-derived stem cells enhances nerve repair. *Stem Cells Dev.* 23, 741–754. doi: 10.1089/scd.2013.0396

Kornfeld, T., Vogt, P. M., and Radtke, C. (2019). Nerve grafting for peripheral nerve injuries with extended defect sizes. *Wien Med. Wochenschr.* 169, 240–251. doi: 10.1007/s10354-018-0675-6

Kubiak, C. A., Grochmal, J., Kung, T. A., Cederna, P. S., Midha, R., and Kemp, S. W. P. (2020). Stem-cell-based therapies to enhance peripheral nerve regeneration. *Muscle Nerve* 61, 449–459. doi: 10.1002/mus.26760

Kumar, R., Sinha, S., Hagner, A., Stykel, M., Raharjo, E., Singh, K. K., et al. (2016). Adult skin-derived precursor Schwann cells exhibit superior myelination and regeneration supportive properties compared to chronically denervated nerve-derived Schwann cells. *Exp. Neurol.* 278, 127–142. doi: 10.1016/j.expneurol.2016.02.006

Lehmann, H. C., and Hoke, A. (2016). Use of engineered Schwann cells in peripheral neuropathy: hopes and hazards. *Brain Res.* 1638(Pt A), 97–104. doi: 10.1016/j.brainres.2015.10.040

Lennertz, R. C., Medler, K. A., Bain, J. L., Wright, D. E., and Stucky, C. L. (2011). Impaired sensory nerve function and axon morphology in mice with diabetic neuropathy. *J. Neurophysiol.* 106, 905–914. doi: 10.1152/jn.01123.2010

Levi, A. D., Burks, S. S., Anderson, K. D., Dididze, M., Khan, A., and Dietrich, W. D. (2016). The use of autologous schwann cells to supplement sciatic nerve repair with a large gap: first in human experience. *Cell Transplant.* 25, 1395–1403. doi: 10.3727/096368915X690198

Levi, A. D., Guenard, V., Aebischer, P., and Bunge, R. P. (1994). The functional characteristics of Schwann cells cultured from human peripheral nerve after transplantation into a gap within the rat sciatic nerve. *J. Neurosci.* 14(3 Pt 1), 1309–1319. doi: 10.1523/JNEUROSCI.14-03-01309.1994

Lin, H., Liu, F., Zhang, C., Zhang, Z., Kong, Z., Zhang, X., et al. (2011). Characterization of nerve conduits seeded with neurons and Schwann cells derived from hair follicle neural crest stem cells. *Tissue Eng. Part A* 17, 1691–1698. doi: 10.1089/ten.tea.2010.0514

Liu, J. H., Tang, Q., Liu, X. X., Qi, J., Zeng, R. X., Zhu, Z. W., et al. (2018). Analysis of transcriptome sequencing of sciatic nerves in Sprague-Dawley rats of different ages. *Neural Regen. Res.* 13, 2182–2190. doi: 10.4103/1673-5374.241469

Ma, M. S., Boddeke, E., and Copray, S. (2015). Pluripotent stem cells for Schwann cell engineering. *Stem Cell Rev. Rep.* 11, 205–218. doi: 10.1007/s12015-014-9577-1

Magnaghi, V., Veiga, S., Ballabio, M., Gonzalez, L. C., Garcia-Segura, L. M., and Melcangi, R. C. (2006). Sex-dimorphic effects of progesterone and its reduced metabolites on gene expression of myelin proteins by rat Schwann cells. *J. Peripher. Nerv. Syst.* 11, 111–118. doi: 10.1111/j.1085-9489.2006.00075.x

Malik, R. A., Tesfaye, S., Newrick, P. G., Walker, D., Rajbhandari, S. M., Siddique, I., et al. (2005). Sural nerve pathology in diabetic patients with minimal but progressive neuropathy. *Diabetologia* 48, 578–585. doi: 10.1007/s00125-004-1663-5

Matsuse, D., Kitada, M., Kohama, M., Nishikawa, K., Makinoshima, H., Wakao, S., et al. (2010). Human umbilical cord-derived mesenchymal stromal cells differentiate into functional Schwann cells that sustain peripheral nerve regeneration. *J. Neuropathol. Exp. Neurol.* 69, 973–985. doi: 10.1097/NEN.0b013e3181eff6dc

Matta, C., Meyer, L., Mensah-Nyagan, A. G., and Taleb, O. (2020). Behavioral, electrophysiological, and histological characterization of a new rat model for neoadjuvant chemotherapy-induced neuropathic pain: therapeutic potential of duloxetine and allopregnanolone concomitant treatment. *Neurotox. Res.* 38, 145–162. doi: 10.1007/s12640-020-00176-2

McKenzie, I. A., Biernaskie, J., Toma, J. G., Midha, R., and Miller, F. D. (2006). Skin-derived precursors generate myelinating Schwann cells for the injured and dysmyelinated nervous system. *J. Neurosci.* 26, 6651–6660. doi: 10.1523/JNEUROSCI.1007-06.2006

Mendonca, M. V., Larocca, T. F., de Freitas Souza, B. S., Villarreal, C. F., Silva, L. F., Matos, A. C., et al. (2014). Safety and neurological assessments after autologous transplantation of bone marrow mesenchymal stem cells in subjects with chronic spinal cord injury. *Stem Cell Res. Ther.* 5:126. doi: 10.1186/scrt516

Menorca, R. M., Fussell, T. S., and Elfar, J. C. (2013). Nerve physiology: mechanisms of injury and recovery. *Hand Clin.* 29, 317–330. doi: 10.1016/j.hcl.2013.04.002

Mimura, T., Dezawa, M., Kanno, H., Sawada, H., and Yamamoto, I. (2004). Peripheral nerve regeneration by transplantation of bone marrow stromal cell-derived Schwann cells in adult rats. *J. Neurosurg.* 101, 806–812. doi: 10.3171/jns.2004.101.5.0806

Mizisin, A. P. (2014). Mechanisms of diabetic neuropathy: schwann cells. *Handb. Clin. Neurol.* 126, 401–428. doi: 10.1016/B978-0-444-53480-4.00029-1

Monje, P. V. (2020). Schwann cell cultures: biology, technology and therapeutics. *Cells* 9:1848. doi: 10.3390/cells9081848

Mosahebi, A., Fuller, P., Wiberg, M., and Terenghi, G. (2002). Effect of allogeneic Schwann cell transplantation on peripheral nerve regeneration. *Exp. Neurol.* 173, 213–223. doi: 10.1006/exnr.2001.7846

Naruse, K. (2019). Schwann cells as crucial players in diabetic neuropathy. *Adv. Exp. Med. Biol.* 1190, 345–356. doi: 10.1007/978-981-32-9636-7_22

Naruse, K., Hamada, Y., Nakashima, E., Kato, K., Mizubayashi, R., Kamiya, H., et al. (2005). Therapeutic neovascularization using cord blood-derived endothelial progenitor cells for diabetic neuropathy. *Diabetes* 54, 1823–1828. doi: 10.2337/diabetes.54.6.1823

Nazareth, L., St John, J., Murtaza, M., and Ekberg, J. (2021). Phagocytosis by peripheral glia: importance for nervous system functions and implications in injury and disease. *Front. Cell Dev. Biol.* 9:660259. doi: 10.3389/fcell.2021.660259

Oh, S. K., Choi, K. H., Yoo, J. Y., Kim, D. Y., Kim, S. J., and Jeon, S. R. (2016). A phase III clinical trial showing limited efficacy of autologous mesenchymal stem cell therapy for spinal cord injury. *Neurosurgery* 78, 436–447; discussion 447. doi: 10.1227/NEU.0000000000001056

Okawa, T., Kamiya, H., Himeno, T., Kato, J., Seino, Y., Fujiya, A., et al. (2013). Transplantation of neural crest-like cells derived from induced pluripotent stem cells improves diabetic polyneuropathy in mice. *Cell Transplant.* 22, 1767–1783. doi: 10.3727/096368912X657710

Omi, M., Hata, M., Nakamura, N., Miyabe, M., Ozawa, S., Nukada, H., et al. (2017). Transplantation of dental pulp stem cells improves long-term diabetic polyneuropathy together with improvement of nerve morphometrical evaluation. *Stem Cell Res. Ther.* 8:279. doi: 10.1186/s13287-017-0729-5

Oraee-Yazdani, S., Akhlaghpasand, M., Golmohammadi, M., Hafizi, M., Zomorrod, M. S., Kabir, N. M., et al. (2021). Combining cell therapy with human autologous Schwann cell and bone marrow-derived mesenchymal stem cell in patients with subacute complete spinal cord injury: safety considerations and possible outcomes. *Stem Cell Res. Ther.* 12:445. doi: 10.1186/s13287-021-02515-2

Oraee-Yazdani, S., Hafizi, M., Atashi, A., Ashrafi, F., Seddighi, A. S., Hashemi, S. M., et al. (2016). Co-transplantation of autologous bone marrow mesenchymal stem cells and Schwann cells through cerebral spinal fluid for the treatment of patients with chronic spinal cord injury: safety and possible outcome. *Spinal Cord* 54, 102–109. doi: 10.1038/sc.2015.142

Orbay, H., Uysal, A. C., Hyakusoku, H., and Mizuno, H. (2012). Differentiated and undifferentiated adipose-derived stem cells improve function in rats with peripheral nerve gaps. *J. Plast. Reconstr. Aesthet. Surg.* 65, 657–664. doi: 10.1016/j.bjps.2011.11.035

Park, H. W., Lim, M. J., Jung, H., Lee, S. P., Paik, K. S., and Chang, M. S. (2010). Human mesenchymal stem cell-derived Schwann cell-like cells exhibit neurotrophic effects, via distinct growth factor production, in a model of spinal cord injury. *Glia* 58, 1118–1132. doi: 10.1002/glia.20992

Radtke, C., Aizer, A. A., Agulian, S. K., Lankford, K. L., Vogt, P. M., and Kocsis, J. D. (2009a). Transplantation of olfactory ensheathing cells enhances peripheral nerve regeneration after microsurgical nerve repair. *Brain Res.* 1254, 10–17. doi: 10.1016/j.brainres.2008.11.036

Radtke, C., Kocsis, J. D., and Vogt, P. M. (2009b). Chapter 22: transplantation of olfactory ensheathing cells for peripheral nerve regeneration. *Int. Rev. Neurobiol.* 87, 405–415. doi: 10.1016/S0074-7742(09)87022-0

Radtke, C., and Kocsis, J. D. (2012). Peripheral nerve injuries and transplantation of olfactory ensheathing cells for axonal regeneration and remyelination: fact or fiction? *Int. J. Mol. Sci.* 13, 12911–12924. doi: 10.3390/ijms131012911

Radtke, C., and Kocsis, J. D. (2014). Olfactory-ensheathing cell transplantation for peripheral nerve repair: update on recent developments. *Cells Tissues Organs* 200, 48–58. doi: 10.1159/000369006

Radtke, C., Wewetzer, K., Reimers, K., and Vogt, P. M. (2011). Transplantation of olfactory ensheathing cells as adjunct cell therapy for peripheral nerve injury. *Cell Transplant.* 20, 145–152. doi: 10.3727/096368910X522081

Rodriguez, F. J., Verdu, E., Ceballos, D., and Navarro, X. (2000). Nerve guides seeded with autologous schwann cells improve nerve regeneration. *Exp. Neurol.* 161, 571–584. doi: 10.1006/exnr.1999.7315

Santosa, K. B., Jesuraj, N. J., Viader, A., MacEwan, M., Newton, P., Hunter, D. A., et al. (2013). Nerve allografts supplemented with schwann cells overexpressing glial-cell-line-derived neurotrophic factor. *Muscle Nerve* 47, 213–223. doi: 10.1002/mus.23490

Sayad Fathi, S., and Zaminy, A. (2017). Stem cell therapy for nerve injury. *World J. Stem Cells* 9, 144–151. doi: 10.4252/wjsc.v9.i9.144

Shakhbazau, A., Mohanty, C., Kumar, R., and Midha, R. (2014). Sensory recovery after cell therapy in peripheral nerve repair: effects of naive and skin precursor-derived Schwann cells. *J. Neurosurg.* 121, 423–431. doi: 10.3171/2014.5.JNS132132

Shimizu, S., Kitada, M., Ishikawa, H., Itokazu, Y., Wakao, S., and Dezawa, M. (2007). Peripheral nerve regeneration by the in vitro differentiated-human bone marrow stromal cells with Schwann cell property. *Biochem. Biophys. Res. Commun.* 359, 915–920. doi: 10.1016/j.bbrc.2007.05.212

Shin, Y. K., Jang, S. Y., Lee, H. K., Jung, J., Suh, D. J., Seo, S. Y., et al. (2010). Pathological adaptive responses of Schwann cells to endoplasmic reticulum stress in bortezomib-induced peripheral neuropathy. *Glia* 58, 1961–1976. doi: 10.1002/glia.21065

Sima, A. A., Bril, V., Nathaniel, V., McEwen, T. A., Brown, M. B., Lattimer, S. A., et al. (1988). Regeneration and repair of myelinated fibers in sural-nerve biopsy specimens from patients with diabetic neuropathy treated with sorbinil. *N. Engl. J. Med.* 319, 548–555. doi: 10.1056/NEJM198809013190905

Sowa, Y., Kishida, T., Tomita, K., Yamamoto, K., Numajiri, T., and Mazda, O. (2017). Direct conversion of human fibroblasts into schwann cells that facilitate regeneration of injured peripheral nerve in vivo. *Stem Cells Translat. Med.* 6, 1207–1216. doi: 10.1002/sctm.16-0122

Stassart, R. M., and Woodhoo, A. (2021). Axo-glial interaction in the injured PNS. *Dev. Neurobiol.* 81, 490–506. doi: 10.1002/dneu.22771

Stenberg, L., and Dahlin, L. B. (2014). Gender differences in nerve regeneration after sciatic nerve injury and repair in healthy and in type 2 diabetic Goto-Kakizaki rats. *BMC Neurosci.* 15:107. doi: 10.1186/1471-2202-15-107

Stratton, J. A., Kumar, R., Sinha, S., Shah, P., Stykel, M., Shapira, Y., et al. (2017). Purification and characterization of schwann cells from adult human skin and nerve. *Eneuro* 4:ENEURO.0307-16.2017. doi: 10.1523/ENEURO.0307-16.2017

Stratton, J. A., Shah, P. T., Kumar, R., Stykel, M. G., Shapira, Y., Grochmal, J., et al. (2016). The immunomodulatory properties of adult skin-derived precursor Schwann cells: implications for peripheral nerve injury therapy. *Eur. J. Neurosci.* 43, 365–375. doi: 10.1111/ejn.13006

Strauch, B., Ferder, M., Lovelle-Allen, S., Moore, K., Kim, D. J., and Llena, J. (1996). Determining the maximal length of a vein conduit used as an interposition graft for nerve regeneration. *J. Reconstr. Microsurg.* 12, 521–527. doi: 10.1055/s-2007-1006624

Strauch, B., Rodriguez, D. M., Diaz, J., Yu, H. L., Kaplan, G., and Weinstein, D. E. (2001). Autologous Schwann cells drive regeneration through a 6-cm autogenous venous nerve conduit. *J Reconstr Microsurg* 17, 589–595; discussion 96–97. doi: 10.1055/s-2001-18812

Sullivan, R., Dailey, T., Duncan, K., Abel, N., and Borlongan, C. V. (2016). Peripheral nerve injury: stem cell therapy and peripheral nerve transfer. *Int. J. Mol. Sci.* 17:2101. doi: 10.3390/ijms17122101

Sun, X. H., Che, Y. Q., Tong, X. J., Zhang, L. X., Feng, Y., Xu, A. H., et al. (2009). Improving nerve regeneration of acellular nerve allografts seeded with SCs bridging the sciatic nerve defects of rat. *Cell. Mol. Neurobiol.* 29, 347–353. doi: 10.1007/s10571-008-9326-6

Thomas, P. K., and Lascelles, R. G. (1965). Schwann-cell abnormalities in diabetic neuropathy. *Lancet* 1, 1355–1357. doi: 10.1016/S0140-6736(65)92154-9

Tohill, M. P., Mann, D. J., Mantovani, C. M., Wiberg, M., and Terenghi, G. (2004). Green fluorescent protein is a stable morphological marker for schwann cell transplants in bioengineered nerve conduits. *Tissue Eng.* 10, 1359–1367. doi: 10.1089/ten.2004.10.1359

Tomita, K., Madura, T., Sakai, Y., Yano, K., Terenghi, G., and Hosokawa, K. (2013). Glial differentiation of human adipose-derived stem cells: implications for cell-based transplantation therapy. *Neuroscience* 236, 55–65. doi: 10.1016/j.neuroscience.2012.12.066

Tong, L. L., Ding, Y. Q., Jing, H. B., Li, X. Y., and Qi, J. G. (2015). Differential motor and sensory functional recovery in male but not female adult rats is associated with remyelination rather than axon regeneration after sciatic nerve crush. *Neuroreport* 26, 429–437. doi: 10.1097/WNR.0000000000000366

Verdú, E., Navarro, X., Gudiño-Cabrera, G., Rodríguez, F. J., Ceballos, D., Valero, A., et al. (1999). Olfactory bulb ensheathing cells enhance peripheral nerve regeneration. *Neuroreport* 10, 1097–1101. doi: 10.1097/00001756-199904060-00035

Wang, X., Luo, E., Li, Y., and Hu, J. (2011). Schwann-like mesenchymal stem cells within vein graft facilitate facial nerve regeneration and remyelination. *Brain Res.* 1383, 71–80. doi: 10.1016/j.brainres.2011.01.098

Weiss, M. L., and Troyer, D. L. (2006). Stem cells in the umbilical cord. *Stem Cell Rev.* 2, 155–162. doi: 10.1007/s12015-006-0022-y

Wheeler, H. E., Wing, C., Delaney, S. M., Komatsu, M., and Dolan, M. E. (2015). Modeling chemotherapeutic neurotoxicity with human induced pluripotent stem cell-derived neuronal cells. *PLoS One* 10:e0118020. doi: 10.1371/journal.pone.0118020

Wing, C., Komatsu, M., Delaney, S. M., Krause, M., Wheeler, H. E., and Dolan, M. E. (2017). Application of stem cell derived neuronal cells to evaluate neurotoxic chemotherapy. *Stem Cell Res.* 22, 79–88. doi: 10.1016/j.scr.2017.06.006

Wu, X., Wang, L., Cong, M., Shen, M., He, Q., Ding, F., et al. (2020). Extracellular vesicles from skin precursor-derived Schwann cells promote axonal outgrowth and regeneration of motoneurons via Akt/mTOR/p70S6K pathway. *Ann. Transl. Med.* 8:1640. doi: 10.21037/atm-20-5965

Yagihashi, S., and Matsunaga, M. (1979). Ultrastructural pathology of peripheral nerves in patients with diabetic neuropathy. *Tohoku J. Exp. Med.* 129, 357–366. doi: 10.1620/tjem.129.357

Yazdani, S. O., Hafizi, M., Zali, A. R., Atashi, A., Ashrafi, F., Seddighi, A. S., et al. (2013). Safety and possible outcome assessment of autologous Schwann cell and bone marrow mesenchymal stromal cell co-transplantation for treatment of patients with chronic spinal cord injury. *Cytotherapy* 15, 782–791. doi: 10.1016/j.jcyt.2013.03.012

Yigitturk, G., Erbas, O., Karabay Yavasoglu, N. U., Acikgoz, E., Buhur, A., Gokhan, A., et al. (2021). The neuro-restorative effect of adipose-derived mesenchymal stem cell transplantation on a mouse model of diabetic neuropathy. *Neurol. Res.* doi: 10.1080/01616412.2021.1967679 [Online ahead of print].

You, H., Wei, L., Liu, Y., Oudega, M., Jiao, S. S., Feng, S. N., et al. (2011). Olfactory ensheathing cells enhance Schwann cell-mediated anatomical and functional repair after sciatic nerve injury in adult rats. *Exp. Neurol.* 229, 158–167. doi: 10.1016/j.expneurol.2010.08.034

Zhang, L., Li, B., Liu, B., and Dong, Z. (2019). Co-transplantation of epidermal neural crest stem cells and olfactory ensheathing cells repairs sciatic nerve defects in rats. *Front. Cell. Neurosci.* 13:253. doi: 10.3389/fncel.2019.00253

Zhang, P., Lu, X., Chen, J., and Chen, Z. (2014). Schwann cells originating from skin-derived precursors promote peripheral nerve regeneration in rats. *Neural Regen. Res.* 9, 1696–1702. doi: 10.4103/1673-5374.141805

Zhu, C., Huang, J., Xue, C., Wang, Y., Wang, S., Bao, S., et al. (2018). Skin derived precursor Schwann cell-generated acellular matrix modified chitosan/silk scaffolds for bridging rat sciatic nerve gap. *Neurosci. Res.* 135, 21–31. doi: 10.1016/j.neures.2017.12.007

Conflict of Interest: The authors declare that the research was conducted in the absence of any commercial or financial relationships that could be construed as a potential conflict of interest.

Publisher's Note: All claims expressed in this article are solely those of the authors and do not necessarily represent those of their affiliated organizations, or those of the publisher, the editors and the reviewers. Any product that may be evaluated in this article, or claim that may be made by its manufacturer, is not guaranteed or endorsed by the publisher.

frontiers | Frontiers in Cellular Neuroscience

REVIEW
published: 06 May 2022
doi: 10.3389/fncel.2022.865266

Engineered Schwann Cell-Based Therapies for Injury Peripheral Nerve Reconstruction

Qisong Su[1,2,3†], Moussa Ide Nasser[1,2†], Jiaming He[4†], Gang Deng[2,5], Qing Ouyang[2,5], Donglin Zhuang[1,6], Yuzhi Deng[2,7], Haoyun Hu[2,7], Nanbo Liu[1,3], Zhetao Li[1,8], Ping Zhu[1,2,3,5,7,8,9] and Ge Li[1,2,3,9*]*

[1] Medical Research Center, Guangdong Provincial People's Hospital, Guangdong Academy of Medical Sciences, Guangzhou, China, [2] Guangdong Provincial People's Hospital, Guangdong Cardiovascular Institute, Guangzhou, China, [3] School of Biology and Biological Engineering, South China University of Technology, Guangzhou, China, [4] School of Basic Medical Science, Shandong University, Jinan, China, [5] School of Medicine, South China University of Technology, Guangzhou, China, [6] Fuwai Hospital, Chinese Academy of Medical Sciences and Peking Union Medical College, Beijing, China, [7] The First Clinical College, Guangdong Medical University, Zhanjiang, China, [8] The Second School of Clinical Medicine, Southern Medical University, Guangzhou, China, [9] Guangdong Provincial Key Laboratory of Structural Heart Disease, Guangzhou, China

OPEN ACCESS

Edited by:
Ji-Fan Hu,
Jilin University, China

Reviewed by:
Yunxiang Luo,
The First Affiliated Hospital of Sun Yat-sen University, China
Bing Han,
Chinese Academy of Medical Sciences and Peking Union Medical College, China

***Correspondence:**
Ping Zhu
zhuping@gdph.org.cn
Ge Li
lige@gdph.org.cn

[†] These authors have contributed equally to this work

Specialty section:
This article was submitted to Non-Neuronal Cells, a section of the journal Frontiers in Cellular Neuroscience

Received: 29 January 2022
Accepted: 04 April 2022
Published: 06 May 2022

Citation:
Su Q, Nasser MI, He J, Deng G, Ouyang Q, Zhuang D, Deng Y, Hu H, Liu N, Li Z, Zhu P and Li G (2022) Engineered Schwann Cell-Based Therapies for Injury Peripheral Nerve Reconstruction. Front. Cell. Neurosci. 16:865266. doi: 10.3389/fncel.2022.865266

Compared with the central nervous system, the adult peripheral nervous system possesses a remarkable regenerative capacity, which is due to the strong plasticity of Schwann cells (SCs) in peripheral nerves. After peripheral nervous injury, SCs de-differentiate and transform into repair phenotypes, and play a critical role in axonal regeneration, myelin formation, and clearance of axonal and myelin debris. In view of the limited self-repair capability of SCs for long segment defects of peripheral nerve defects, it is of great clinical value to supplement SCs in necrotic areas through gene modification or stem cell transplantation or to construct tissue-engineered nerve combined with bioactive scaffolds to repair such tissue defects. Based on the developmental lineage of SCs and the gene regulation network after peripheral nerve injury (PNI), this review summarizes the possibility of using SCs constructed by the latest gene modification technology to repair PNI. The therapeutic effects of tissue-engineered nerve constructed by materials combined with Schwann cells resembles autologous transplantation, which is the gold standard for PNI repair. Therefore, this review generalizes the research progress of biomaterials combined with Schwann cells for PNI repair. Based on the difficulty of donor sources, this review also discusses the potential of "unlimited" provision of pluripotent stem cells capable of directing differentiation or transforming existing somatic cells into induced SCs. The summary of these concepts and therapeutic strategies makes it possible for SCs to be used more effectively in the repair of PNI.

Keywords: Schwann cells, peripheral nervous system, transcriptional regulators, tissue-engineered nerve graft, directed reprogramming

INTRODUCTION

Mechanical trauma, for example, as sustained in an industrial or traffic accident, is the most frequent cause of peripheral nervous system injury (Faroni et al., 2015). Approximately five million peripheral nerve injuries occur each year with 500,000 surgical operations performed in the United States alone, generating $1.5 billion for the nerve repair industry (Meena et al., 2021). Peripheral nerve injury (PNI) may result in permanent motor and sensory disabilities, and most individuals cannot return to regular employment immediately after injury. Additionally, recovery is poor because of the limited therapeutic impact, which affects patients' quality of life and imposes a significant economic burden on society and families (Slavin et al., 2021). In contrast to the central nervous system (CNS), the adult peripheral nervous system (PNS) maintains considerable regenerative capacity even after serious injury (Chen et al., 2007). The considerable regeneration capability of the PNS is demonstrated by the capability of injured peripheral axons to regenerate and target their destinations, a process facilitated by the high plasticity of Schwann cells (SCs) in the PNS (Kim et al., 2013; Jessen et al., 2015).

SCs are a critical component of the PNS. Nerves in the periphery are composed of myelinated and unmyelinated fibers. Myelin sheaths, axons, and nerve membranes comprise nerve fibers. The larger axons establish a 1:1 connection with myelinated SCs, whereas the non-myelinated SCs bundle the smaller axons to form Remak bundles (Napoli et al., 2012). Peripheral nerve fibroblasts subsequently facilitate the formation of axon group bundles enclosed by SCs, and larger nerves consist of many bundles wrapped in the epineurium. Primary injury to these neural structures is often induced by direct forces, such as abrupt extension, tears, or compression, and the subsequent vascular ischemia exacerbates the primary injury, resulting in secondary injury (Sullivan et al., 2016). Within 12–24 h of PNS injury, calcium influx activates proteases, resulting in cytoskeleton rupture, axon membrane breakdown, and myelin degradation within 2 days (Schlaepfer and Bunge, 1973; Stoll et al., 1989). SCs dedifferentiate into a repair phenotype as a result of axonal breakdown and myelinolysis (Hall, 2005; Arthur-Farraj et al., 2017). Not only can repair SCs contribute to the clearance of axon and myelin-derived debris but they may also multiply to fill the empty endoneurial tube and create a strip-like column in the basal layer, called Büngner bands (Li et al., 2005; Murinson et al., 2005; Gomez-Sanchez et al., 2015). SCs in Büngner bands release neurotrophic factors that nourish injured neurons and promote axonal regeneration and myelination (Madduri and Gander, 2010; Jessen and Mirsky, 2016). The healing of PNS injury by SCs is outlined in **Figure 1**. To summarize, SCs are essential for the healing process after PNI. It is critical to study the many identities of SCs that rely on various important chemicals throughout the development, injury, and repair of the PNS to achieve more effective treatment methods for preventing or removing micro-environmental problems in myelination injury.

Given the critical role of SCs in the healing process of PNI, this article presents a comprehensive analysis of the major molecular regulatory networks of SCs involved in the treatment of PNI over the last decade to identify significant targets for increasing SC repair efficiency. Using existing genetic modification of SCs and induced Schwann-like cells (iSCs), their applications in the repair of PNI are summarized, and gene editing using cutting-edge technology to enhance the effect of SC repair possibilities is explored. An "unlimited" supply potential of pluripotent stem cell directional differentiation or conversion of available class cells to iSCs can occur and is explained in this review. The comprehensive review of these studies has enabled researchers to make new advancements from conventional SC transplantation treatment to SC engineering and manufacture and to provide new ideas for stimulating related research.

Abbreviations: PNI, Peripheral nerve injury; PNS, peripheral nervous system; SCs, Schwann cells; iSCs, induced Schwann-like cells; NCCs, neural crest cells; SCPs, Schwann cell precursors; BL, basal layer; D4, day 4; D7, day 7; lncRNAs, long non-coding RNAs; TGF-β, transforming growth factor-β; NRG1, Neuregulin 1; αBC, AlphaB-crystallin; Notch, Neurogenic locus Notch homolog protein; DRG, dorsal root ganglions; HIF-1α, hypoxia inducible factor −1α; VEGF, vascular endothelial growth factor; WD, Wallerian degeneration; NGF, nerve growth factor; AMPK, AMP-activated protein kinase; mTOR, mammalian target of rapamycin; PIGF, placental growth factor; VEGFR1, vascular endothelial growth factor receptor 1; CNTF, Ciliary neurotrophic factor; STAT3, signal transducer and activator of transcription 3; IL-6, interleukin 6; CRISPR, clustered regularly spaced short palindromic repeats; HDAC, Histone deacetylase; Zeb2, Zinc-finger e-box-binding Homeobox 2; HDAC1/2-NuRD, HDAC1 and 2 and nucleosome remodeling and histone deacetylation; NFs, neurotrophic factors; GDNF, glial cell line-derived neurotrophic factor; BDNF, brain-derived neurotrophic factor; LIF, leukemia inhibitory factor; FGF-2, Fibroblast growth factor-2; NT-3, Neurotrophin-3; ANG, acellular nerve graft; COMP, cartilage oligomeric matrix protein; Ang1, angiopoietin1; EGb 761, extract 761; NGC, nerve-guided catheter; PGA, polyglycolic acid; GO, Graphene oxide; MWCNT, multi-walled carbon nanotubes; MSCs, mesenchymal stem cells; TIPS, thermally-induced phase separation; NYs, nanofiber yarns; PPDO, poly(p-dioxanone); CNT, carbon nanotubes; ES, electrical stimulation; EGF, epidermal growth factor; HGF, hepatocyte growth factor; ADMSCs, adipose-derived mesenchymal stem cells; ESCs, embryonic stem cells; iPSCs, induced pluripotent stem cells; FGFs, Fibroblast growth factors; NLCs, neural lineage-like cells; bFGF, basic-FGF; PDGF, platform-derived growth factor; GFP, green fluorescent protein; PBMSCs, peripheral blood-derived mesenchymal stem cells.

DEVELOPMENTAL LINEAGE AND POST-INJURY GENE REGULATION NETWORK OF SCHWANN CELLS

Schwann Cells Are Derived From Ectodermal Neural Crest Cells

SCs are derived from neural crest cells (NCCs), which ultimately create myelin sheaths through two intermediate stages: (1) Schwann cell precursors (SCPs) and (2) immature SCs, which provide nutritional support for the development of peripheral nerve axons (**Figure 2A**). NCCs develop throughout the PNS growth process by forming new peripheral axons with strong proliferative capabilities and high pluripotency (Muppirala et al., 2021). The first stable branch separates the sensory lineage from the common progenitor cells of the autonomic and mesenchymal branches during the migration of NCCs. The second stable branch divides the production of autonomic neurons, and the remaining branches can be attributed to glial differentiation owing to their expression of the transcription markers for early glial cells (*Mpz, Fabp7, Zfp488, Plp1, Sox10*) and transcriptional

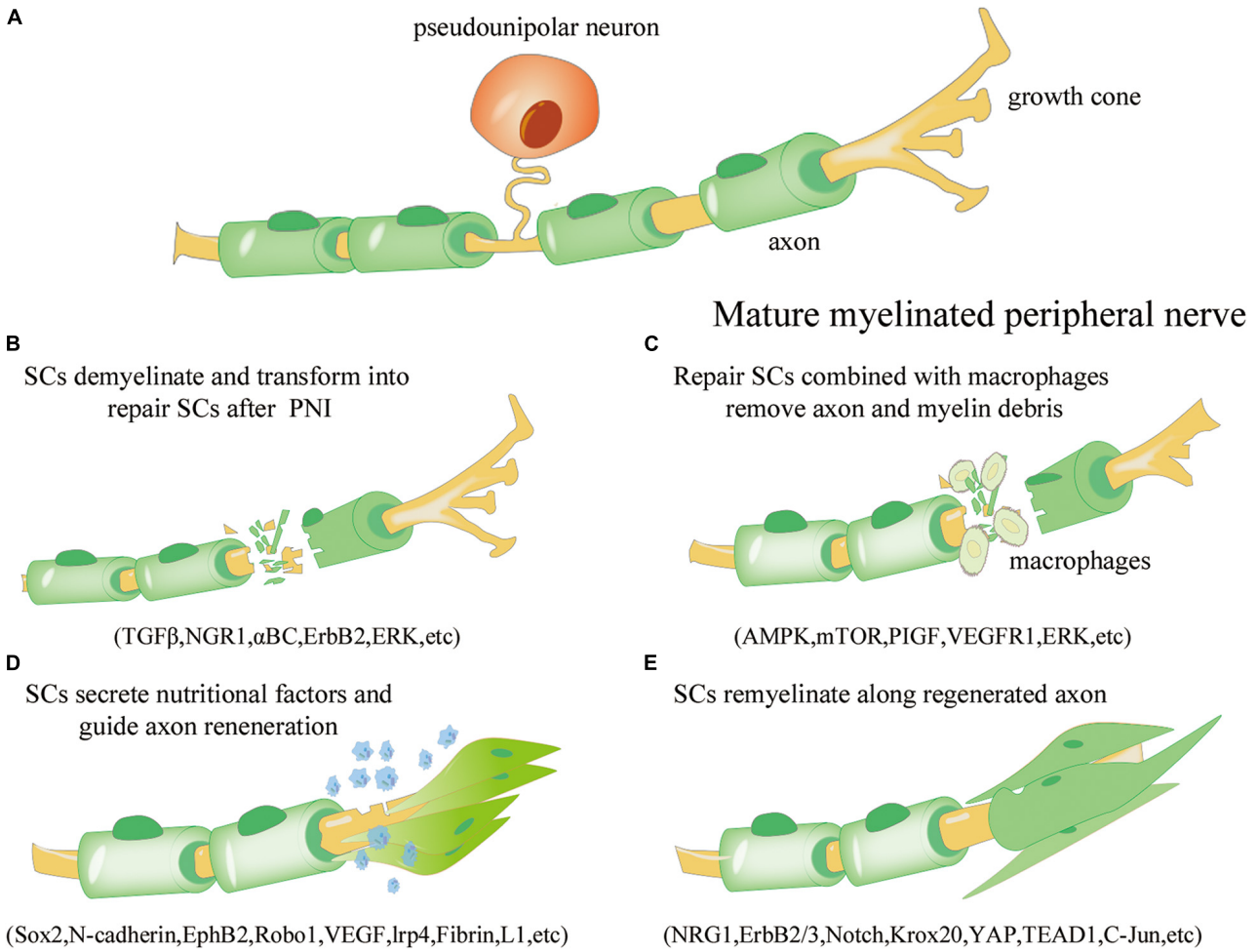

FIGURE 1 | Overview of the repair process of Schwann cells (SCs) after peripheral nerve injury. **(A)** Under normal physiological conditions, mature myelinated peripheral nerve processes (yellow) are surrounded by the myelin sheath formed by SCs (green). **(B)** Axonal rupture and myelin disintegration due to peripheral nerve injury. SCs are activated, dedifferentiate, and transform into the repair phenotype. The involved signaling pathways include transforming growth factor beta (TGF-β), neuroregulin 1 (NGR1), αBC transporter, ErbB2, and extracellular signal receptor-kinase (ERK). **(C)** Repair SCs proliferate and fill the empty endoneurial canal, working with macrophages to remove axonal and myelin-derived debris; the involved signaling pathways include AMP activated protein kinase (AMPK), mammalian target of rapamycin (mTOR), placental growth factor (PIGF), vascular endothelial growth factor receptor 1 (VEGFR1), and ERK. **(D)** SCs are arranged along axons to form Büngner bands and secrete neurotrophic factors to improve the microenvironment and guide axon regeneration; the involved regulators include Sox1, N-cadherin, EphB2, Robo1, VEGF, lrp4, Fibrin, and L1. **(E)** SCs are re-myelinated along the regenerated axons to promote neural information transmission; the involved regulators include NRG1, ErbB2/3, Notch, Krox20, yes-associated protein (YAP), transcriptional enhance factor domain transcription factor 4 (TEAD1), and c-Jun.

markers of SCPs (Soldatov et al., 2019). SCP migration starts with the formation of a basal layer (BL) and the process of wrapping the axons during the juvenile SC stage. When immature SCs are wrapped in a 1:1 manner throughout the radial separation phase, proliferation of the immature SCS slows, and definitive differentiation begins. This phase of differentiation is controlled by the BL, which facilitates an increase in the expression of myelination genes. After differentiation, the juvenile SC skeleton progressively grows until its membrane wraps around the axon and produces a myelin sheath. Following the completion of the package, myelin is compressed to create a mature myelin sheath. Stable and mature SCs are then formed through active signaling pathways.

SCs exhibit distinct gene regulatory networks after PNI when compared with SC development (**Figure 2B**). According to Chen et al. (2021), the cells in normal and injured peripheral nerves may be functionally classified as SCs, neurofibroblasts, immune cells, and vascular-related cells. SCs and neurofibroblasts are critical for the regeneration of peripheral nerves. Zhang et al. (2021) discovered four distinct phenotypes in SCs in newborn rats using single-cell transcriptome analysis, namely, SC subtype 1 resembling connective tissue cells expressing *LOC100134871* and *Hbb*, and highly mature SC subtype 2, expressing *Cldn19* and *Emid1*. *Timp3* and *Col5a3* were found to be expressed in subtype 3, which is involved in tissue development and differentiation into other SC subtypes, whereas *Cenpf* and *Mki67*

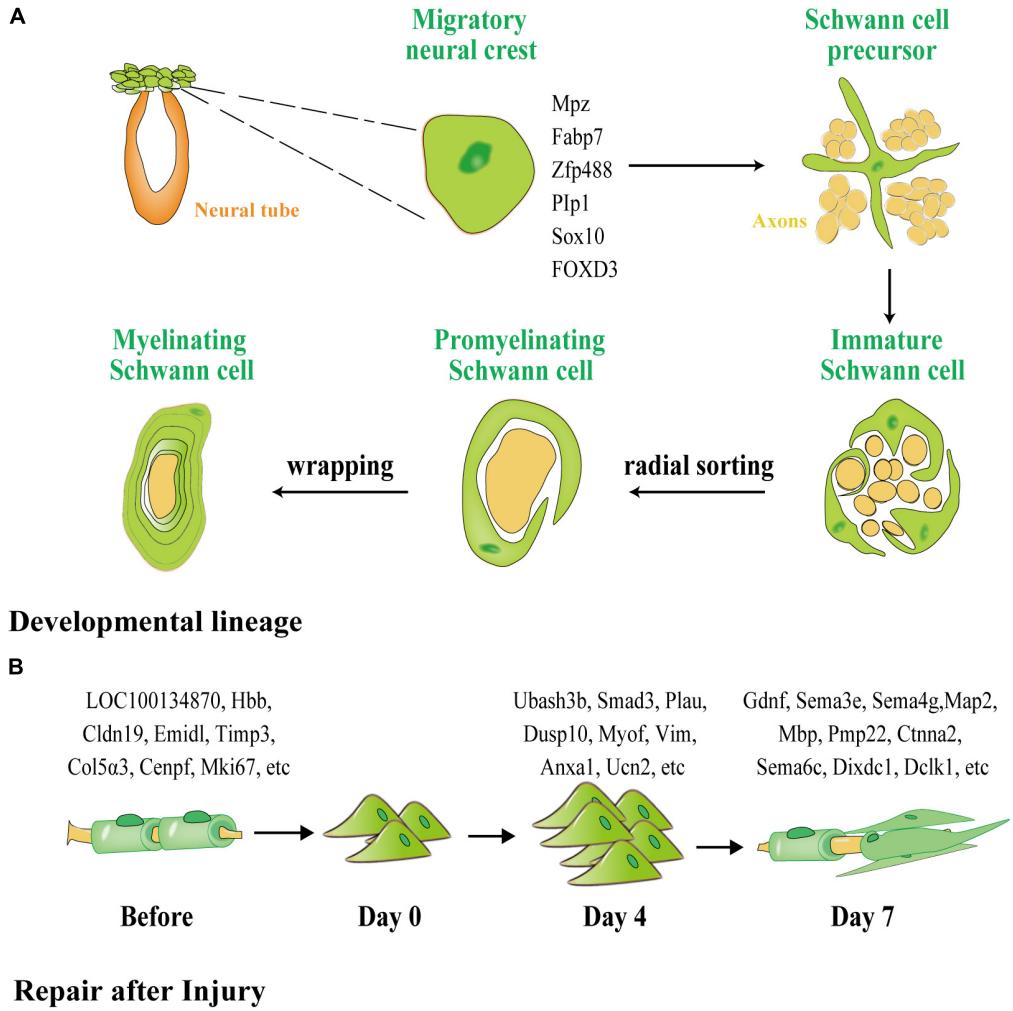

FIGURE 2 | The different processes of myelination of SCs during development and after peripheral nerve injury (PNI). **(A)** SCs generated from neural crests create myelin sheaths in the PNS. Green represents glial cells and precursors, and orange represents the neural tube and yellow represents neurons and their axons. SCPs are neural crest cells that detach from the neural tube and migrate along the nascent peripheral axons, expressing the early glial markers Mpz, Fabp7, Zfp488, Plp1, Sox10, and forkhead box D3 FOXD3. SCPs differentiate into immature SCs, which, *via* cytoplasmic extension, enclose the axon bundle. Finally, radial sorting is used to choose a single axon for wrapping. SCs that have been myelinated enclosed axon segments, forming myelin sheaths. **(B)** Dedifferentiation and remyelination of SCs after PNI. Normal SCs form a myelin sheath around axons with one of four phenotypes: subtype 1 expressing LOC100134871 and Hbb, subtype 2 expressing Cldn19 and Emid1, subtype 3 expressing Timp3 and Col5a3, and subtype 4 expressing Cenpf and Mki67. After PNI, SCs transform into a homogenous phenotype and participate in proliferation and phagocytosis. On the fourth day after injury, 776 lncRNAs were unique to the proliferation of SCs. After day 7, 317 lncRNAs were unique to the remyelination of SCs.

were found to be expressed in subtype 4, which is related to cell division, peripheral nerve development, and regeneration. Zhang et al. (2021) used second-generation sequencing to perform deep sequencing in rats on days 4 and 7 (D4 and D7) respectively after sciatic nerve injury, and discovered that 776 long non-coding RNAs (lncRNAs), such as *Ubash3b, Smad3, Plau*, and others, are unique to D4. Most of these RNAs are related to wound healing, phosphatase binding, and the mitogen-activated protein kinase (MAPK) signaling cascade. *Gdnf, Sema3e, Sema4g*, and others were found on D7 and appear to be associated with axon regeneration and cell cycle. Throughout development and repair, these diverse expression regulatory networks indicate that separate neural regulation methods for differentiation and induction of iSCs and the mobilization of repair following injury can be used.

Key Signaling Pathways Involved in Migration, Proliferation, and Axon Guidance of Schwann Cells After Peripheral Nerve Injury

Following PNI, mature SCs may undergo de-differentiation through various pathways, migrate to the wounded area, stimulate nerve remyelination, and play a role in directing axon regeneration. Wang et al. (2012) investigated the intrinsic migration characteristics of SCs using single-cell migration

experiments and discovered that de-differentiated SCs first develop long protuberances, during which the nucleus was shown to move forward to the front of the cell and then retract to the back of the protuberances after which the protuberances extended again. Numerous studies have shown links between transforming growth factor beta (TGF-β), Slit-Robo, ErbB2 receptor, Hippo and Notch, extracellular signal -related kinase (ERK), and vascular endothelial growth factor (VEGF) signaling pathways and migration, proliferation, and axon guidance of SCs after PNI (**Table 1**).

Figure 3 depicts a schematic representation of the many signaling pathways involved in the migration of SCs after PNS injury.

TARGETING GENETICALLY ENGINEERED SCHWANN CELLS TO IMPROVE THE REPAIR EFFICIENCY OF PERIPHERAL NERVE INJURY

Numerous studies have shown that SCs are capable of successfully facilitating PNI repair. Through genetic engineering, the native genes of SCs may be up- or down-regulated, and the natural products required for peripheral nerve regeneration can be generated in a controlled manner. SCs may be genetically modified using various tools and methods that introduce specific genes or sequences into the genome, such as viral vectors, non-viral transfection systems, and clustered regularly spaced short palindromic repeats (CRISPR)/Cas9 gene-editing approaches.

Intervention With Histone Deacetylase Affects the Maturation and Myelination of Schwann Cells Through Notch-Hey2 Signaling

Histone deacetylase (HDAC) is a significant epigenetic regulator of the Notch–Hey2 signaling pathway, which is required for myelination in the peripheral nervous system. Two groups of HDACs, HDAC1 and 2, both of which are involved in the myelination of SCs and HDAC3, which is involved in maintaining myelin homeostasis have been found. Jacob et al. (2011) used lentiviral transfection to selectively knockdown HDAC1 and 2 in SCs, a process leading to a substantial decrease in the expression of SOX10 and Krox20, the main transcriptional regulators of myelination in SCs. HDAC1 and 2 have been shown to have distinct main roles in SCs, with HDAC2 cooperating with Sox10 to initiate the myelination transcriptional process. Concurrently, HDAC1 regulates SC survival by controlling the amount of active β-catenin.

Likewise, Chen et al. (2011) discovered that the absence of HDAC1 and 2 prevented the NF-κB protein complex from binding to p300 and HDAC1/2, resulting in significant acetylation of NF-κB p65, reduction in the positive regulators of myelin development, and activation of differentiation inhibitors. In addition, development of SCs stalled during the immature stage. Interestingly, Brügger et al. (2017) discovered that early treatment with HDAC1/2 inhibitors caused an increase in the production of repair SCs and improvement in axonal regeneration and functional recovery but also led to impaired myelin regeneration. This process raises the possibility of adjusting the expression period of HDAC1 and 2 in SCs after injury during clinical transformation to improve peripheral nerve regeneration. Rosenberg et al. (2018) demonstrated the unique effects of HDAC3, another class of protein deacetylases involved in the Notch-Hey2 signaling pathway, on SCs *via* gene knockout. These authors demonstrated that although HDAC3 was not found to be necessary for the formation of myelinated SCs, once myelinated SCs are formed, HDAC3 appears to be required for their stability. He et al. (2018) discovered that HDAC3 caused suppression of the neuroregulin/phosphoinositide 3-kinase/protein kinase B (NRG1/PI3K/Akt) signaling pathway and its downstream myelination process, ensuring correct myelination and preventing peripheral myelin expansion *in vivo*.

Additionally, HDAC3 may bind the p300 histone acetyltransferase and control the expression of the transcriptional enhance factor domain transcription factor 4 (TEAD4) gene thus activating the inhibitory network of myelin development. Zinc-finger e-box-binding Homeobox 2 (Zeb2) is another important regulator of the Notch–Hey2 signaling cascade. Wu et al. (2016) generated Zeb2-defective SCs by non-viral transfection and discovered that Zeb2 regulated the start of SC development by recruiting the co-inhibitory histone

TABLE 1 | Key signaling pathways involved in migration, proliferation and axon guidance of SCs after PNI.

Signaling pathways	Factors	Function	References
TGF-β	TGF-β, N-cadherin, EphB2, SOX2	Dedifferentiation, sorting and migration of SCs, axon regeneration	Parrinello et al., 2010; Clements et al., 2017
Slit-Robo	Slit,Slit2,Slit3	Axon pathfinding, migration of SCs	Blockus and Chédotal, 2016; Dun et al., 2019
ErbB2 Receptor	NRG1, αBC	Proliferation of SCs, axon wrapping and myelination	Garratt et al., 2000; Hendry et al., 2016; Lim et al., 2017
Notch and Hippo	Notch, NICD, Krox20, TEAD1, YAP, TAZ	Proliferation and myelination of SCs	Ghislain and Charnay, 2006; Woodhoo et al., 2009; Hansen et al., 2015; Grove et al., 2017
ERK	Raf, fibrin, ERK, c-Jun	Dedifferentiation and myelination of SCs.	Akassoglou et al., 2002; Harrisingh et al., 2004; Syed et al., 2010; Napoli et al., 2012
VEGF	HIF-1α, VEGF	Proliferation and migration of SCs	Sondell et al., 1999; Cattin et al., 2015

TGF-β, transforming growth factor-β; NRG1, Neuregulin 1; αBC, AlphaB-crystallin; Notch, Neurogenic locus Notch homolog protein; HIF-1α, hypoxia inducible factor −1α; VEGF, vascular endothelial growth factor.

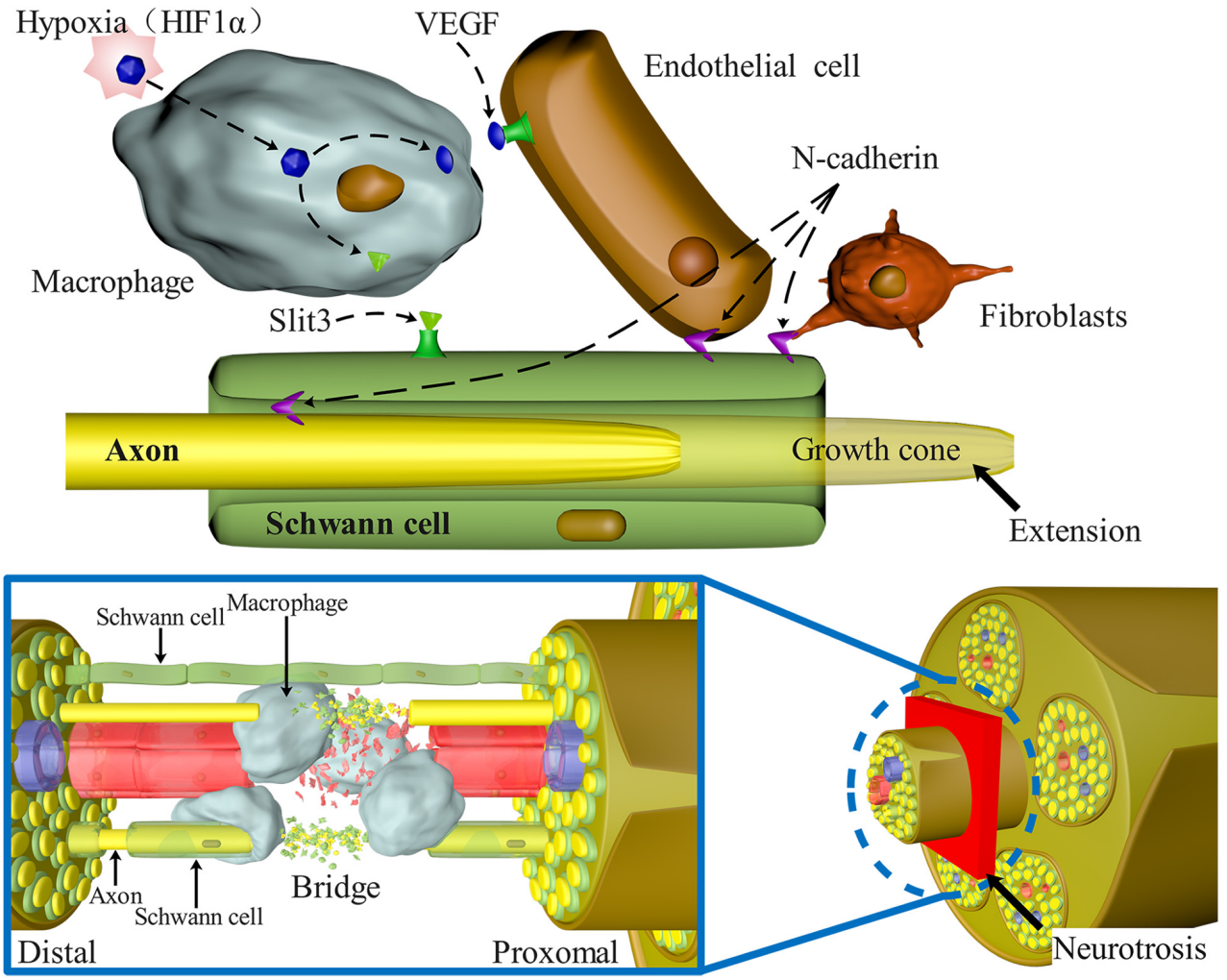

FIGURE 3 | Signaling pathways involved in SC migration, proliferation, and axon guidance in nerve bridges after peripheral nerve injury. N-Cadherin increases the adhesion between SCs, fibroblasts, and endothelial cells, causing SCs to migrate to the outside of the nerve stump and guiding axons to reorient growth at the injury site. Macrophages enter the nerve space and secrete Slit3, which binds with SCs expressing Robo1 to control the formation of correct nerve bridges and promote SC migration and axon guidance. Macrophages in the nerve bridges detect hypoxia and enhance the amount of VEGF-induced blood vessel regeneration, alleviating hypoxia, and acting as an important medium to guide axon regeneration.

deacetylases, HDAC1 and 2, and nucleosome remodeling and histone deacetylation (HDAC1/2-NuRD). Hey2 appears to limit differentiation of SCs by preventing differentiation and promoting their proliferation, whereas Zeb2 seems to promote the maturation and myelination of SCs by directly inhibiting Hey2 and regulating the Notch–Hey2 signaling pathway.

Intervention of Mitogen-Activated Protein Kinase and Hippo Signaling Pathways to Promote the Proliferation and Myelin Regeneration of Schwann Cells

Moesin-ezrin-radixin-like protein (Merlin) tumor suppressors contribute to cell signaling, contact-mediated proliferation, and tumorigenesis. Loss of Merlin was found to disrupt the MAPK and Hippo signaling pathways, leading to enhanced activity of the Hippo effectors, yes-associated protein 1 and (YAP) and related protein, TAZ (Ammoun et al., 2008; Cooper and Giancotti, 2014). Merlin deficiency results in a significant increase in SC proliferation, macrophage infiltration, severe injury to axons and myelin regeneration, decreased induction of c-Jun, dysregulation of the MAPK signaling pathway, and activation of the Hippo signaling pathway following injury (Mindos et al., 2017). Previous studies have demonstrated that silencing YAP in SCs could functionally restore both axon and myelin sheath regeneration caused by Merlin loss and restore the expression of c-Jun and neurotrophic factors in addition to axon regeneration and functional recovery following injury. Deng and coworkers (Deng et al., 2017) showed that activating the Hippo signaling pathway led to an increase in SC proliferation, while TAZ inhibited the Gnas gene, which produces the GαS protein. Gnas

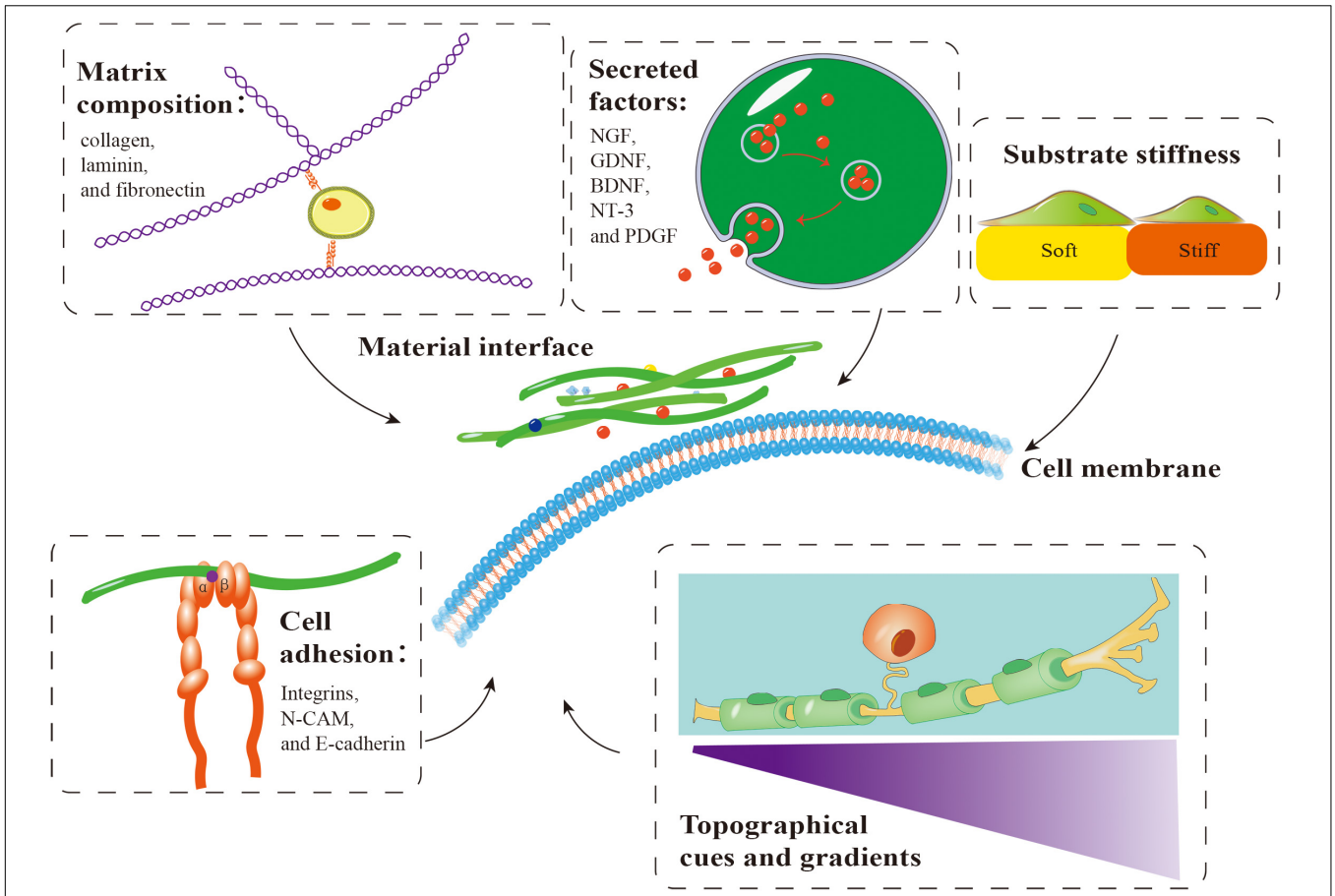

FIGURE 4 | Important factors involved in the application of biomaterials in combination with Schwann cells (SCs) in peripheral nerve regeneration. Matrix components, secreted factors, cell adhesion, substrate stiffness and topographical cues and gradients influence the behavior of SCs on biomaterials, which is crucial for peripheral nerve regeneration. NGF, nerve growth factor; GDNF, glial-derived neurotrophic factor; BDNF, brain-derived neurotrophic factor; NT-3, neurotrophin-3; PDGF, platelet-derived growth factor.

deficiency resulted in a dramatic increase in the proliferation of SCs. Consequently, it was hypothesized that Gnas control may aid in limiting SC growth. However, Grove et al. (2020) showed that knock down of YAP/TAZ does not impair the proliferation of SCs or enhance transition of SCs into repair SCs. However, axon sorting and myelin degeneration are impaired in the absence of YAP/TAZ (Poitelon et al., 2016; Grove et al., 2017, 2020). This process occurs because growing SCs need YAP/TAZ to enter the S phase and generate sufficient SCs for correct axon sorting. Concurrently, YAP/TAZ is needed for TEAD1 to activate Krox20, which regulates myelination (Grove et al., 2017).

Activation of c-Jun and Overexpression of Neurotrophic Factors in Schwann Cells Regulate Neural Regeneration Potential

Activation of the transcription factor c-Jun in SCs acts as a global regulator of Waller's degeneration and regulates the expression of nutrient factors, adhesion molecules, regeneration locus formation, and myelin clearance. In addition to activating repair programs in SCs, this factor contributes to generating cells specifically designed for regeneration, thereby regulating the regeneration potential of peripheral nerves (Arthur-Farraj et al., 2012). c-Jun deficiency results in the development of defective repair SCs, impairs functional recovery, and results in neuronal death. c-Jun overexpression can effectively lead to an increase in expression and secretion of a variety of neurotrophic factors (NFs), including glial cell line-derived neurotrophic factor (GDNF), brain-derived neurotrophic factor (BDNF), artemin, leukemia inhibitory factor (LIF), and nerve growth factor (NGF), thereby promoting the migration of SCs. In addition, c-Jun overexpression enhances local proliferation of SCs and neurite development in the presence of axons (Huang L. et al., 2015). Lackington and colleagues (Lackington et al., 2018) created plasmid-carrying nanoparticles and transfected SCs to overexpress nerve growth factor (NGF), glial cell line-derived neurotrophic factor (GDNF), and c-Jun. A comparative study revealed that all three types of cells could promote neurite development; however, SCs overexpressing c-Jun had the highest capacity for cell regeneration.

SCs produced an increase in the expression of several axon-regenerating NFs in response to PNI (Hammarberg et al., 1996; Höke et al., 2000; Eggers et al., 2010). By targeting NFs expression with advanced genetic engineering methods, SC repair efficiency after injury could be substantially increased. Shakhbazau et al. (2012) transfected SCs with either NGF or GDNF and discovered that SCs overexpressing NGF enhanced axonal regeneration to a much greater degree. However, NGF and GDNF overexpression may have various consequences on sensory and motor regenerating neurons. The increase in NGF and GDNF levels did not affect the number of regenerated sensory neurons at 1 cm from the distal end of the injury at 4 weeks after injury. GDNF overexpression was found to promote long-distance axon development and nerve re-innervation of the target muscle in motor neurons, whereas NGF had little impact on these parameters (Tannemaat et al., 2008). However, axon regeneration is sluggish and requires considerable time to complete. Marquardt et al. (2015) developed a system for controlling GDNF release over time and in space *via* lentiviral transfection of SCs and combining this system with biomaterials. They discovered that GDNF overexpression at 4–8 weeks promoted axon regeneration and muscle mass recovery, but that too short a delivery time (4 weeks) prevented axon extension and that too long a delivery time (> 8 weeks) could also result in axon regeneration failure.

Fibroblast growth factor 2 (FGF-2) is a neurotrophic factor produced by fibroblasts and SCs. This factor plays a critical role in SC proliferation and migration (Chen et al., 2010). FGF-2 subtype differences may have a profound impact on nerve regeneration. By comparing SCs overexpressing 18 kDa FGF-2 to SCs overexpressing 21/23 kDa FGF-2, Haastert et al. (2006) discovered that 18 kDa FGF-2 hinders the myelination of regenerated axons. However, 21/23 kDa FGF-2 enhanced the early recovery of sensory function and the myelination of long-distance axons in regenerated axons. Allodi et al. (2014) transplanted SCs overexpressing 18 kDa FGF-2 into a rat model of sciatic nerve injury and observed that nerve reinnervation of the hind limb muscles was accelerated and more obvious following transplantation. The number of motor and sensory neurons reaching the distal nerve increases at the end of follow-up, a process that is conducive to injury repair.

Studies have shown that neurotrophin-3 (NT-3) is a neurotrophic factor that helps reduce inflammatory responses and promotes cell survival and migration in poor microenvironments after injury (Randolph et al., 2007; Li et al., 2016, 2021a). Woolley et al. (2008) discovered that loss of NT-3 led to enhancement of caspase-3 protein production in SCs, suggesting that NT-3 is required for proper SC survival and differentiation. Additionally, NT-3 released by SCs at the axon–glial interface may act on axons and promote release of neuroregulatory proteins, which subsequently signal SCs to accelerate myelination. Zong et al. (2013) implanted SCs into a rat model of sciatic nerve injury. They found that SCs overexpressing NT-3 caused a decrease in motor neuron apoptosis in the injured sciatic nerve, accelerated nerve and axon regeneration, and enhanced the function of the injured nerve.

RECONSTRUCTION OF PERIPHERAL NERVE TISSUE MORPHOLOGY AND FUNCTION BASED ON A COMBINATION OF SCHWANN CELLS AND BIOMATERIALS

Repair of PNI with a long-distance nerve deficit present a significant challenge. The gold standard for PNI healing has always been autologous nerve tissue transplantation. Autologous transplantation at the donor site may result in pathological alterations, such as sensory abnormalities, neuroma, infection, and other potential complications. Additionally, autografts are only available in a limited quantity (Lee and Wolfe, 2000). As a result, it is critical to create efficient nerve healing methods to circumvent autologous transplantation restrictions. Similarly, various biomaterials have been used to treat PNI. These biomaterials can provide favorable conditions for peripheral nerve regeneration by simulating the microenvironment through matrix components, secreted factors, cell adhesion, substrate stiffness, and topographical cues and gradients (**Figure 4**). These biomaterials may be roughly classified into natural and synthetic biomaterials, each with clear benefits. Synthetic biomaterials can adjust material properties to meet various repair needs, such as enhancement of cell adhesion and regulation of mechanical characteristics (Li et al., 2015; Mobasseri et al., 2015; Shahriari et al., 2017). In contrast to synthetic biomaterials, natural materials (such as autografts, allografts, and acellular grafts) generate non-toxic degradation products, possess intrinsic cell-binding domains, and can efficiently activate natural tissue remodeling and repair pathways (Bonnans et al., 2014; Nicolas et al., 2020).

Natural Acellular Grafts and Schwann Cells

He et al. (2015) created a human acellular nerve graft (ANG) to replace autologous nerves and showed that ANG was safe and efficient for nerve deficits ranging in size from 1 to 5 cm. By obliterating antigenic biological components, ANGs, in comparison to allografts, can lead to a decrease in the immune responses. The impact of ANGs on long and massive nerve deficits, in contrast, is far from acceptable. As a result, Qiu et al. (2015) modified ANGs using the cartilage oligomeric matrix protein (COMP)-angiopoietin-1 (Ang1). COMP-Ang1 was found to enhance early neovascularization followed by rapid nerve regeneration, thus significantly increasing the effectiveness of ANGs in healing peripheral nerve lesions in clinical studies. Zhu et al. (2015) used Ginkgo biloba extract 761 (EGb 761) after ANG transplantation in rats with sciatic nerve injury. They discovered that ANG repair treated with EGb 761 showed the same effects on peripheral nerve regeneration and vascularization as autograft repair and was superior to ANG repair alone. However, ANGs are always deficient in the SCs required for nerve regeneration, limiting nerve regeneration in pure ANGs and rendering them inferior to autografts or allografts (Bunge, 1994; Whitlock et al., 2009). By transplanting SCs into ANGs,

Jesuraj et al. (2014) discovered that SCs could enhance growth factor expression in ANGs and exhibit equivalent muscular strength and nerve fiber regeneration to allografts, thus boosting peripheral nerve regeneration and functional recovery.

In conclusion, ANG may facilitate more complete removal of cells, myelin sheaths, and other components associated with immune rejection from the grafts, thus lowering the risk of immunological rejection and increasing histocompatibility. In addition, ANGs preserve the nerve's original structure and efficiently direct the regenerated axons to their target organs. Sun et al. (2020) showed that decellularization selectively removes axon-suppressing molecules, such as myelin associated glycoproteins and chondroitin sulfate proteoglycans present in normal nerves and retains axon-promoted extracellular matrix (ECM) proteins, including collagen IV and laminin. The preserved extracellular matrix components create a milieu similar to peripheral nerve tissue for SC adhesion and proliferation (Carriel et al., 2014). In their latest study, Wang et al. (2022) found that components and spatial organization of the extracellular matrix secreted by bone marrow MSCs closely resemble the acellular nerve and have stronger expression of factors related to nerve regeneration and lower immune responses; therefore, MSCs may be more likely to provide potential alternatives for clinical repair of peripheral nerve defects.

Synthetic Neural Catheter and Swann Cells

The synthetic nerve-guided catheter (NGC) is another method of replacing autologous nerves. In contrast to allogeneic acellular nerve, NGCs have no donor restriction and are simpler to manufacture on a large scale. The tubular structure of the NGCs bridges the nerve stump and prevents the regenerated nerve from being influenced by the surrounding tissue while concurrently directing the regenerated axon to the distal stump properly. By creating a polyglycolic acid (PGA) multi-channel guidance scaffold, Hu et al. (2008) recruited and directed endogenous SCs to move along the PGA wire and form a cell column comparable with Büngner bands involved in PNI repair. However, nerve regeneration involves cell interactions, the extracellular matrix, and growth factors. Consequently, nerve injury repair methods have evolved from simple nerve catheters to sophisticated tissue engineering approaches that closely resemble the complex milieu seen in autografts. Chitosan has excellent biocompatibility, permeability, plasticity, and biodegradability, making it a suitable candidate material for the construction of artificial nerve grafts (Nawrotek et al., 2016). Chitosan-based nerve grafts mediate a novel molecular mechanism of nerve regeneration in that chitosan degrades into chitosan oligosaccharides following transplantation. This process was found to lead to a decrease in the expression of miR-327 in SCs and increase in CCL2 expression, thereby inducing macrophage infiltration, rebuilding of the microenvironment at the site of injury, and promotion of nerve regeneration (Zhao et al., 2017). Graphene oxide (GO) is a nanomaterial with extraordinary physical and chemical characteristics. Polycaprolactone (PCL) is a biocompatible polymer scaffold with an appropriate hardness. The nano-scaffolds prepared using GO and PCL are beneficial for the proliferation, survival, adhesion, and maintenance of neural properties in SCs. They can effectively promote functional and morphological recovery of peripheral nerves, which is promising for tissue engineering (Qian et al., 2018). Zhang et al. (2020) demonstrated that micropatterning on the inner wall of NGCs constructed with GO was conducive for promoting SCs to secrete neurotrophic factors, such as NGF and BDNF, guiding the direction of axons, inducing macrophage M2 differentiation, and promoting nerve regeneration and the recovery of normal functions. Fadia et al. (2020) created PCL nerve conduits implanted with GDNF microspheres and discovered that they could cause a substantial increase in SC proliferation and nerve conduction when compared with autografts but had no meaningful effect on functional function recovery.

Manipulating the microstructure and mechanical characteristics of biological scaffold materials can alter the differentiation efficiency of Schwann cell-like cells. Electrospinning fibers can be arranged, stacked, or folded to form organized arrays or layered structure and effectively direct axon regeneration (Xie et al., 2010; Huang C. et al., 2015; Xue et al., 2017a). Furthermore, they can efficiently stimulate the development of mesenchymal stem cells (MSCs) into SCs and control the morphology and arrangement of source cells (Xue et al., 2017b). Hu et al. (2020) showed that the combination of amine-functionalized multi-walled carbon nanotubes (MWCNT) with PCL and gelatin and preparation of directional or random conductive nanofibers by electrostatic spinning could lead to a significant improvement in the differentiation efficiency of BMSCs into SCs. This process could also promote axon regrowth in the peripheral nervous system. This research indicates a good solution to address the difficulties associated with the source of SCs and required improvements in the differentiation and functionalization of stem cells to SCs. Thermally-induced phase separation (TIPS) technology has the potential to influence the efficiency of MSCs to transdifferentiate into SC-like phenotypes by causing alterations in the microstructure and mechanical properties of the nanofibers and macroporous and ladder-like structures found in gelatin-based three-dimensional (3D) tubes (Ma and Zhang, 1999; Zeng et al., 2014). Uz et al. (2017) demonstrated that the conduit structure with macroporous and ladder 3D structures could enhance the attachment, proliferation, and diffusion of MSCs to create an interconnected cell network with many living cells and achieve an optimal microenvironment for the transformation of MSCs into SC-like phenotypes. Wu et al. (2020) synthesized composite nanofiber yarns (NYs) from poly(p-dioxanone) (PPDO) and carbon nanotubes (CNT). CNTs are added to NYs to improve their mechanical characteristics and electrical conductivity. Further electrical stimulation (ES) can lead to a substantial increase in expression levels of *S100B*, *GFAP*, *NGFR*, *MBP*, and *MPZ*, which are associated with myelination in SCs and an increase in NGF production, EGF, and hepatocyte growth factor (HGF). This process can also promote differentiation of human adipose-derived mesenchymal stem cells (hADMSCs) into SC-like cells. By constructing a biological

scaffold to promote stem cell differentiation into SC-like cells and establishing a milieu favorable to SC-like cell differentiation, the risk to the host from viral transfection or drug induction may be significantly minimized. Li et al. (2021b) demonstrated that using electrostatic spinning, micro-nano processing, and biomaterial surface biologization techniques, the constructed neural regeneration micro-environment scaffold with anisotropic micro-nano composite topology could effectively induce directed SC growth. The Wnt/-catenin, ERK2/MAP, and TGF-pathways upregulate the expression of myelination-related genes and proteins, offering an essential approach to the development of a new generation of functional artificial neural implants.

Biomaterial and Schwann Cell-Based Engineered Nerve Tissue

The idea of neural tissue engineering focuses on repair of PNI that is different than a single bridging mechanism and leans toward a more biomimetic and bioactive environment that promotes nerve regeneration and axon development. NGCs manufactured using SCs have been demonstrated to stimulate peripheral nerve regeneration. However, as SCs are inaccessible, and cells placed on NGCs are unable to fully cover the catheter surface, long-distance nerve regeneration fails, and motor function recovery becomes compromised. NGCs implanted into bone marrow stromal cells demonstrate more uniform cell dispersion with the assistance of NGF and rotary cell culture systems, which is favorable for establishing a stable 3D bionic environment, enhancing proliferation and differentiation of bone marrow stromal cells into SC-like cells in a substantial manner, and stimulating long-distance peripheral nerve regeneration (Zhou et al., 2020). Georgiou et al. (2015) converted adipose-derived stem cells into an SC cell-like phenotype *in vitro* and then implanted the differentiated cells into type 1 collagen gel, which had been stabilized to produce artificial neural tissue. When the designed nerve tissue generated from ASCs was transplanted into a rat model of sciatic nerve injury, it was shown that this engineered nerve tissue possessed a high capacity for nerve regeneration *in vivo*. Adipose stem cells (ASCs) are a potential cellular vectors because they have the capability of creating cell sheets consisting of cells, intercellular junctions, and extracellular matrix (Yeh et al., 2014). Hsu et al. (2019) prepared functionally enhanced engineered nerves by using ASCs overexpressing BDNF, GDNF, and NGF. This cell plates were shown to be capable of stimulating SC migration, neuron proliferation, and axon development *in vitro* and enhancing the functional recovery, nerves, axons, and myelin sheath regeneration after sciatic nerve injury.

The combination of engineered peripheral nerve tissue with SCs and biomaterials closely mimics the cell composition, extracellular matrix microenvironment, and three-dimensional space structure of the peripheral nerve, resulting in a graft that is closely resembles autologous nerves and has a broad market application potential. Concurrently, as neurological organ technology advances, peripheral nerve tissue engineered from the combination of SCs and biological materials, will also undergo continuous iteration. Not only will this process improve the effect of PNI replacement, but also will help develop a type of peripheral nerve tissue *in vitro* for neurogenesis, repair, and drug screening prior to basic and clinical research. Thibodeau et al. (2022) prepared a new type of tissue-engineered neural catheter. The neural conduit consists of a deactivated hollow tube on the outside and a living fibroblast sheet, which is infused with endothelial cells, rolled into concentric layers on the inside to facilitate the formation of a network containing capillary-like structures for rapid binding to the host neuromicrovascular system after transplantation. When this system in combination with SCs was transplanted into rats, this combination was found to have a higher rates of nerve regeneration than the material-only group.

REPAIR OF PERIPHERAL NERVE INJURY BASED ON SCHWANN-LIKE CELL OF NEW SOURCE

SCs play a critical role in the PNI healing process, but their usage is limited by the difficulty of cell acquisition and its amplification. In addition, isolating, cultivating, and purifying fiber cells, which often multiply quickly in cultured cells, is very challenging (Rutkowski et al., 1995; Andersen et al., 2016; Stratton et al., 2017). To address these obstacles, scientists are investigating safer and more reliable methods for reprogramming various cell sources into induced Schwann-like cells (iSCs) as shown in **Table 2**.

Numerous studies have shown that embryonic stem cells (ESCs) and adult stem cells, such as those found in bone marrow, fat, and the umbilical cord, may develop into iSCs (McKenzie et al., 2006; Kingham et al., 2007; Peng et al., 2011; Ziegler et al., 2011; Cai et al., 2017). Although embryonic stem cells proliferate rapidly, their use is controversial and raises ethical questions (Biswas and Hutchins, 2007; Zakrzewski et al., 2019). When ESCs are transplanted into the body, the chance of developing teratomas, localized overgrowth, or cancer increases (Martin et al., 2020). Adult stem cells grow slowly and are often obtained invasively, which limits their therapeutic use (Huang Z. et al., 2020). The development of induced pluripotent stem cells (iPSCs) addresses several constraints associated with stem cells as potential sources of SCs. iPSCs may be isolated from fibroblasts in the skin, peripheral blood mononuclear cells, or even umbilical cord blood cells (Huang et al., 2019). iPSCs have a high capacity for self-renewal and a high rate of proliferation, and they can develop into any type of cell in the endoderm, mesoderm, or ectoderm (Takahashi et al., 2007; Martin et al., 2020). Khuong et al. (2014) utilized lentivirus to promote iSC transformation by driving the expression of two transcription factors, Sox10 and Egr2, in skin fibroblasts. Immunofluorescence research revealed that iSCs, as with primary SCs, exhibited high expression of SC markers, glial fibrillary acidic protein and myelin basic proteins (GFAP and MBP, respectively). *In vitro*, these iSCs form tight myelin sheaths with regular node patterns around axons. Fibroblast growth factors (FGFs) control brain development and cell fate determination during embryonic development by directing cells to differentiate

TABLE 2 | The methods used in recent years to reprogram cells from different sources into iSCs are summarized.

Original cell	Induction factors	Phenotypic Markers	Animal model	Result	References
BMSCs	BME, RA, FSK, rbFGF, PDGF and HRG	p75,S-100,GFAP and O4	Sciatic nerve injury	The GFP expressing MSCs differentiated into myelin cells and supported the regrowth of nerve fibers within 3 weeks after surgery.	Dezawa et al., 2001
BMSCs	BME, RA, FSK, bFGF, PDGF and HRG	P0 and MAG	Sciatic nerve injury	ISCs-derived artificial grafts have a strong potential to promote peripheral nerve regeneration and can be used to reconstruct long distance gaps in difficult peripheral nerves.	Mimura et al., 2004
BMSCs	BME, RA, FSK, bFGF, PDGF and HRG	PMP22,P0 and MBP	Facial nerve injury	Compared with BMSCs, iSCs provide a faster rate of axon extension and better quality of myelination for peripheral nerve regeneration.	Wang et al., 2011
BMSCs	BME, RA, FSK, bFGF, PDGF and HRG, PROG, insulin and GLUCs.	GFAP, S100B, P0, and PMP22	Sciatic nerve injury	The combined application of PROG, GLUC and insulin significantly improved the differentiation and culture conditions of classical iSCs, and enhanced the stability of morphology, phenotype and functional characteristics of iSCs *in vitro*, as well as the ability of axon growth and endogenous myelin sheath formation *in vivo*.	Liu et al., 2016
ADSCs	engineered substrates with imprinted cell-like topographies	S100b, $p75^{NTR}$, and Sox10	–	Specific cell-like topography and associated micromechanical cues can directly differentiate ADSCs into Schwann cells.	Moosazadeh Moghaddam et al., 2019
ADSCs	BME, RA, FSK, bFGF, PDGF and HRG	GFAP, S100 and p75	–	Adipose stem cells can transdifferentiate into iSCs, which may be beneficial for the treatment of peripheral nerve injury.	Kingham et al., 2007
ADSCs	BME, RA, FSK, bFGF, PDGF and HRG	GFAP, S100 and p75	Common peroneal nerve injury	DASCs can be used as a substitute for autologous SCs to form myelin sheaths wrapped with axons *in vivo*, providing nutritional support for axons and promoting peripheral nerve regeneration.	Tomita et al., 2012
ADSCs	BME, RA, FSK, bFGF, PDGF and HRG	S-100, p75 and integrin β4	Sciatic nerve injury	DASCs can accelerate nerve conduction velocity, increase nerve fiber density and myelinated/unmyelinated fiber ratio, and rebuild nerves.	Orbay et al., 2012
ADSCs	BME, RA, FSK, bFGF, PDGF and HRG, PROG, insulin and GLUCs.	S100B, GFAP, PMP22 and P0	Sciatic nerve injury	The combined application of PROG, GLUC and insulin significantly improved the differentiation and culture conditions of classical iSCs, and enhanced the stability of morphology, phenotype and functional characteristics of iSCs *in vitro*, as well as the ability of nerve regeneration and functional recovery *in vivo*.	Kang et al., 2019
MSCs	electrical stimulation by graphene electrodes	p75,α-S100 and α-S100β	–	MSCs can be transdifferentiated into Schwann cell-like phenotypes by electrical stimulation alone without additional chemical growth factors.	Das et al., 2017
UCB-MSCs	BME, RA, FSK, bFGF, PDGF and HRG	GFAP and S-100	–	*In vitro*, UCB-MSCs can differentiate into cells that resemble Schwann cells in morphology, phenotype, and function.	Zhang et al., 2009
hESCs	N2, glutamine, penicillin, streptomycin, bFGF, FSK, NRG1	GFAP, S100, HNK1, P75, MBP and PMP-22	–	HESCs derived neurosphere cells can efficiently differentiate into iSCs with expression of SCs markers.	Ziegler et al., 2011
Human pluripotent stem cells (hPSCs)	N2, B27, BSA, GlutaMAX, BME, CT 99021, SB431542, NRG1, forskolin, RA, PDGF-BB	S100B, NGFR, EGR2, and MPZ	Sciatic nerve injury	Two small molecules SB431542 (a TGF-β inhibitor) and CT99021 (GSK-3 inhibitor) and NRG1 were used and high-quality multipotent SCPs were produced. SCPs can be effectively differentiated into mature SCs with the functions of secreting GDNF, NGF, BDNF and NT-3, which can promote myelination of rat DRG axons *in vitro* and promote axonal regeneration of sciatic nerve injured mice *in vivo*.	Kim et al., 2017
Skin fibroblasts	Lentiviral vectors	Erbb2, Erbb3, Cnx32, Pmp22 and Mpz	–	By driving the expression of two transcription factors, Sox10 and Egr2, human fibroblasts can be successfully transformed into iSCs with unique molecules and functions.	Mazzara et al., 2017
SKIN fibroblasts	Retroviral vectors	S100B	Sciatic nerve injury	Transduction of SOX10 and Krox20 genes directly converts human fibroblasts into functional iSCs. ISCs can form myelin sheath and help mice recover from peripheral nerve injury.	Sowa et al., 2017

BMSCs, bone marrow mesenchymal cells; BME, beta-mercaptoethanol; RA, retinoic acid; FSK, forskolin; bFGF, basic-fibroblast growth factor PDGF, platelet derived growth factor; HRG, heregulin-beta1; GFP, green fluorescent protein; iSCs, induced Schwann-like cells; PROG, progesterone; GLUCs, glucocorticoids; ADSCs, adipose-derived stem cells; UCB-MSCs, umbilical cord blood-derived mesenchymal stromal cells; hESCs, human embryonic stem cells; NRG1, neuregulin-1; SCs, Schwann cells; MSCs, mesenchymal stem cells; hPSCs, human pluripotent stem cells; GSK-3, glycogen synthase kinase-3; GDNF, glial cell line-derived neurotrophic factor; NGF, nerve growth factor; BDNF, brain-derived neurotrophic factor; NT-3, neurotrophin-3; SCPs, Schwann cell precursors; DRG, dorsal root ganglion.

into neurons or glial cells (Mertens et al., 2016). Huang C.W. et al. (2020) seeded adipose-derived stem cells (ADSCs) onto chitosan-coated culture plates, causing the ADSCs to differentiate into a mixed population of neural lineage-like cells (NLCs) after which they then induced NLCs to differentiate into S100β- and GFAP-positive iSCs using FGF9. Wong et al. (2020) compared the effects of different induction times on the proliferation and secretion capacity of iSCs induced by ADSCs and discovered that while the proliferation capacity negatively correlated with induction time, the expression of SC marker proteins S100, MBP, p75, and GFAP positively correlated with induction time. MBP expression resemble normal SCs on day 19 after induction and substantially enhanced axon development compared with early induction. As a result, iSCs appear to be safe to use for 19 days following induction. Dezawa et al. (2001) used beta-mercaptoethanol, retinoic acid, forskolin, basic-FGF (bFGF), platform-derived growth factor (PDGF), and heregulin to induce BMSCs to differentiate into iSCs. The iSCs obtained presented an SC morphology and expressed p75, S100, GFAP, and O4. When retroviruses expressing green fluorescent protein (GFP) were genetically modified and implanted into a sciatic nerve injury model, extensive nerve fiber regeneration and myelination were found. Matsuse et al. (2010) showed that this technique was equally applicable to MSCs from the human umbilical cord. Liu et al. (2012) used conditioned medium to differentiate human hESCs and iPSCs into NCCs and subsequently into SCs from NCCs, establishing the first report on the myelination of human hESCs or iPSC-derived SCs. Subsequently, Kim et al. (2017) converted human iPSCs to self-renewing SCPs by utilizing inhibitors (SB431542 and CT99021) of the TGF-β and GSK-3 signaling pathways, respectively, in addition to using NRG1. Within 1 week, SCPs may differentiate into mature SCs capable of myelination and secreting neurotrophic factors, such as GDNF, NGF, BDNF, and NT-3. Pan and colleagues (Pan et al., 2017) discovered that peripheral blood-derived mesenchymal stem cells (PBMSCs) may generate iSCs that express SC-specific markers (S100, p75NTR, and CNPase) and functional factors (NGF, NT-3, c-fos, and Krox20). This finding solves the problem of the difficult source of tissue engineering seed cells (Schwann cells) after PNI. SCs encapsulating axons in injured sciatic nerves may function well after transplantation. In conclusion, focused modulation of critical molecules in the developmental gene regulatory network lineage of SCs may more effectively stimulate the creation of these various sources of iSCs, indicating a potential therapeutic application.

OUTLOOK

By describing the process through which SCs repair PNI, our ability to utilize viruses, non-viral vectors, or gene-editing technologies to alter the SC gene may be improved, enabling us to perform additional tasks favorable to peripheral nerve repair. As the safety and control of these methods are enhanced, genetically engineered SCs will have a broader potential for clinical application in peripheral nerve regeneration. The critical element of PNI is the rapid and precise targeting of axons, a process that may be accomplished by developing specialized biological scaffolding for neural bridging. Consequently, cell and biological scaffolding materials may be combined. At this stage, it is critical to develop a biological scaffolding material capable of more accurately simulating the natural milieu of SCs *in vivo*. The source of human SCs severely limits their therapeutic use; however, iSCs offer an excellent solution to this problem. However, an important issue to address throughout the iSC creation process is how to help the iSCs exhibit as many SCs characteristics as feasible while exhibiting as few properties of other cells as possible.

Gene modification can purposefully change the expression of certain genes in SCs thus making it easier to achieve therapeutic goals. However, the corresponding genetic modification also raises more unknown safety issues. After transplantation, SC or iSC survival is low due to the poor microenvironment. Through combinations of biological materials, the internal microenvironment of peripheral nerves was simulated to improve cell survival rate. However, some problems, such as uneven distribution, poor penetration and difficulty in stable release of transplanted cells in biological scaffold materials, exist. Therefore, it is urgent to develop biological scaffold materials that can overcome these shortcomings and achieve industrial mass production, which is of great significance for clinical applications. SC products obtained by tissue and/or genetic engineering and stem cell reprogramming have their own advantages and disadvantages, which can meet the needs of PNI treatment to a certain extent. With the advancement in tissue and genetic engineering, stem cell reprogramming, and other technologies, the purpose of SCs has been extended from simple transplantation to multi-functional complex engineered organogenesis therapeutics thus providing a new perspective on the treatment of PNI and organoid construction.

AUTHOR CONTRIBUTIONS

QS, MN, JH, GD, QO, DZ, YD, HH, NL, ZL, PZ, and GL performed the bibliographic research and drafted the manuscript. QS and YD created the table. GD, DZ, and GL prepared the figures. All authors read, approved the final manuscript, analyzed, discussed the literature, commenting on, and approving the manuscript.

FUNDING

This work was supported by the National Natural Science Foundation of China (82001301 and 81974019) to GL and PZ, the National Key Research and Development Program of China (2018YFA0108700 and 2017YFA0105602), NSFC Projects of International Cooperation and Exchanges (81720108004) to PZ, the Key Program of Guangzhou Science Research Plan (201904020047) to PZ, the Co-innovation Foundation of Guangzhou City (201704020221) to GL, and the Special Project of Dengfeng Program of Guangdong Provincial People's Hospital (KY0120220133, DFJHBF202111, KJ012020630, DFJH201812, KJ012019119, and KJ012019423) to GL and PZ.

REFERENCES

Akassoglou, K., Yu, W. M., Akpinar, P., and Strickland, S. (2002). Fibrin inhibits peripheral nerve remyelination by regulating Schwann cell differentiation. *Neuron* 33, 861–875. doi: 10.1016/s0896-6273(02)00617-7

Allodi, I., Mecollari, V., González-Pérez, F., Eggers, R., Hoyng, S., Verhaagen, J., et al. (2014). Schwann cells transduced with a lentiviral vector encoding Fgf-2 promote motor neuron regeneration following sciatic nerve injury. *Glia* 62, 1736–1746. doi: 10.1002/glia.22712

Ammoun, S., Flaiz, C., Ristic, N., Schuldt, J., and Hanemann, C. O. (2008). Dissecting and targeting the growth factor-dependent and growth factor-independent extracellular signal-regulated kinase pathway in human schwannoma. *Cancer Res.* 68, 5236–5245. doi: 10.1158/0008-5472.Can-07-5849

Andersen, N. D., Srinivas, S., Piñero, G., and Monje, P. V. (2016). A rapid and versatile method for the isolation, purification and cryogenic storage of Schwann cells from adult rodent nerves. *Sci. Rep.* 6:31781. doi: 10.1038/srep31781

Arthur-Farraj, P. J., Latouche, M., Wilton, D. K., Quintes, S., Chabrol, E., Banerjee, A., et al. (2012). c-Jun reprograms Schwann cells of injured nerves to generate a repair cell essential for regeneration. *Neuron* 75, 633–647. doi: 10.1016/j.neuron.2012.06.021

Arthur-Farraj, P. J., Morgan, C. C., Adamowicz, M., Gomez-Sanchez, J. A., Fazal, S. V., Beucher, A., et al. (2017). Changes in the coding and non-coding transcriptome and DNA methylome that define the schwann cell repair phenotype after nerve injury. *Cell Rep.* 20, 2719–2734. doi: 10.1016/j.celrep.2017.08.064

Biswas, A., and Hutchins, R. (2007). Embryonic stem cells. *Stem Cells Dev.* 16, 213–222. doi: 10.1089/scd.2006.0081

Blockus, H., and Chédotal, A. (2016). Slit-robo signaling. *Development* 143, 3037–3044. doi: 10.1242/dev.132829

Bonnans, C., Chou, J., and Werb, Z. (2014). Remodelling the extracellular matrix in development and disease. *Nat. Rev. Mol. Cell Biol.* 15, 786–801. doi: 10.1038/nrm3904

Brügger, V., Duman, M., Bochud, M., Münger, E., Heller, M., Ruff, S., et al. (2017). Delaying histone deacetylase response to injury accelerates conversion into repair Schwann cells and nerve regeneration. *Nat. Commun.* 8:14272. doi: 10.1038/ncomms14272

Bunge, R. P. (1994). The role of the Schwann cell in trophic support and regeneration. *J. Neurol.* 242, S19–S21. doi: 10.1007/bf00939235

Cai, S., Tsui, Y. P., Tam, K. W., Shea, G. K., Chang, R. S., Ao, Q., et al. (2017). Directed differentiation of human bone marrow stromal cells to fate-committed schwann cells. *Stem Cell Rep.* 9, 1097–1108. doi: 10.1016/j.stemcr.2017.08.004

Carriel, V., Alaminos, M., Garzón, I., Campos, A., and Cornelissen, M. (2014). Tissue engineering of the peripheral nervous system. *Expert Rev. Neurother.* 14, 301–318. doi: 10.1586/14737175.2014.887444

Cattin, A. L., Burden, J. J., Van Emmenis, L., Mackenzie, F. E., Hoving, J. J., Garcia Calavia, N., et al. (2015). Macrophage-induced blood vessels guide schwann cell-mediated regeneration of peripheral nerves. *Cell* 162, 1127–1139. doi: 10.1016/j.cell.2015.07.021

Chen, B., Banton, M. C., Singh, L., Parkinson, D. B., and Dun, X. P. (2021). Single cell transcriptome data analysis defines the heterogeneity of peripheral nerve cells in homeostasis and regeneration. *Front. Cell. Neurosci.* 15:624826. doi: 10.3389/fncel.2021.624826

Chen, H. T., Tsai, Y. L., Chen, Y. S., Jong, G. P., Chen, W. K., Wang, H. L., et al. (2010). Dangshen (*Codonopsis pilosula*) activates IGF-I and FGF-2 pathways to induce proliferation and migration effects in RSC96 Schwann cells. *Am. J. Chin. Med.* 38, 359–372. doi: 10.1142/s0192415x10007907

Chen, Y., Wang, H., Yoon, S. O., Xu, X., Hottiger, M. O., Svaren, J., et al. (2011). HDAC-mediated deacetylation of NF-κB is critical for Schwann cell myelination. *Nat. Neurosci.* 14, 437–441. doi: 10.1038/nn.2780

Chen, Z. L., Yu, W. M., and Strickland, S. (2007). Peripheral regeneration. *Annu. Rev. Neurosci.* 30, 209–233. doi: 10.1146/annurev.neuro.30.051606.094337

Clements, M. P., Byrne, E., Camarillo Guerrero, L. F., Cattin, A. L., Zakka, L., Ashraf, A., et al. (2017). The wound microenvironment reprograms schwann cells to invasive mesenchymal-like cells to drive peripheral nerve regeneration. *Neuron* 96, 98–114.e7. doi: 10.1016/j.neuron.2017.09.008

Cooper, J., and Giancotti, F. G. (2014). Molecular insights into NF2/Merlin tumor suppressor function. *FEBS Lett.* 588, 2743–2752. doi: 10.1016/j.febslet.2014.04.001

Das, S. R., Uz, M., Ding, S., Lentner, M. T., Hondred, J. A., Cargill, A. A., et al. (2017). Electrical differentiation of mesenchymal stem cells into schwann-cell-like phenotypes using inkjet-printed graphene circuits. *Adv. Healthc. Mater.* 6:1601087. doi: 10.1002/adhm.201601087

Deng, Y., Wu, L. M. N., Bai, S., Zhao, C., Wang, H., Wang, J., et al. (2017). A reciprocal regulatory loop between TAZ/YAP and G-protein Gαs regulates Schwann cell proliferation and myelination. *Nat. Commun.* 8:15161. doi: 10.1038/ncomms15161

Dezawa, M., Takahashi, I., Esaki, M., Takano, M., and Sawada, H. (2001). Sciatic nerve regeneration in rats induced by transplantation of in vitro differentiated bone-marrow stromal cells. *Eur. J. Neurosci.* 14, 1771–1776. doi: 10.1046/j.0953-816x.2001.01814.x

Dun, X. P., Carr, L., Woodley, P. K., Barry, R. W., Drake, L. K., Mindos, T., et al. (2019). Macrophage-derived slit3 controls cell migration and axon pathfinding in the peripheral nerve bridge. *Cell Rep.* 26, 1458–1472.e4. doi: 10.1016/j.celrep.2018.12.081

Eggers, R., Tannemaat, M. R., Ehlert, E. M., and Verhaagen, J. (2010). A spatio-temporal analysis of motoneuron survival, axonal regeneration and neurotrophic factor expression after lumbar ventral root avulsion and implantation. *Exp. Neurol.* 223, 207–220. doi: 10.1016/j.expneurol.2009.07.021

Fadia, N. B., Bliley, J. M., DiBernardo, G. A., Crammond, D. J., Schilling, B. K., Sivak, W. N., et al. (2020). Long-gap peripheral nerve repair through sustained release of a neurotrophic factor in nonhuman primates. *Sci. Transl. Med.* 12:eaav7753. doi: 10.1126/scitranslmed.aav7753

Faroni, A., Mobasseri, S. A., Kingham, P. J., and Reid, A. J. (2015). Peripheral nerve regeneration: experimental strategies and future perspectives. *Adv. Drug Deliv. Rev.* 8, 160–167. doi: 10.1016/j.addr.2014.11.010

Garratt, A. N., Britsch, S., and Birchmeier, C. (2000). Neuregulin, a factor with many functions in the life of a schwann cell. *Bioessays* 22, 987–996. doi: 10.1002/1521-1878(200011)22:11<987::AID-BIES5>3.0.CO;2-5

Georgiou, M., Golding, J. P., Loughlin, A. J., Kingham, P. J., and Phillips, J. B. (2015). Engineered neural tissue with aligned, differentiated adipose-derived stem cells promotes peripheral nerve regeneration across a critical sized defect in rat sciatic nerve. *Biomaterials* 37, 242–251. doi: 10.1016/j.biomaterials.2014.10.009

Ghislain, J., and Charnay, P. (2006). Control of myelination in Schwann cells: a Krox20 cis-regulatory element integrates Oct6, Brn2 and Sox10 activities. *EMBO Rep.* 7, 52–58. doi: 10.1038/sj.embor.7400573

Gomez-Sanchez, J. A., Carty, L., Iruarrizaga-Lejarreta, M., Palomo-Irigoyen, M., Varela-Rey, M., Griffith, M., et al. (2015). Schwann cell autophagy, myelinophagy, initiates myelin clearance from injured nerves. *J. Cell. Biol.* 210, 153–168. doi: 10.1083/jcb.201503019

Grove, M., Kim, H., Santerre, M., Krupka, A. J., Han, S. B., Zhai, J., et al. (2017). YAP/TAZ initiate and maintain Schwann cell myelination. *Elife* 6:e20982. doi: 10.7554/eLife.20982

Grove, M., Lee, H., Zhao, H., and Son, Y. J. (2020). Axon-dependent expression of YAP/TAZ mediates Schwann cell remyelination but not proliferation after nerve injury. *Elife* 9:e50138. doi: 10.7554/eLife.50138

Haastert, K., Lipokatic, E., Fischer, M., Timmer, M., and Grothe, C. (2006). Differentially promoted peripheral nerve regeneration by grafted Schwann cells over-expressing different FGF-2 isoforms. *Neurobiol. Dis.* 21, 138–153. doi: 10.1016/j.nbd.2005.06.020

Hall, S. (2005). The response to injury in the peripheral nervous system. *J. Bone Joint Surg. Br.* 87, 1309–1319. doi: 10.1302/0301-620x.87b10.16700

Hammarberg, H., Piehl, F., Cullheim, S., Fjell, J., Hökfelt, T., and Fried, K. (1996). GDNF mRNA in Schwann cells and DRG satellite cells after chronic sciatic nerve injury. *Neuroreport* 7, 857–860. doi: 10.1097/00001756-199603220-00004

Hansen, C. G., Moroishi, T., and Guan, K. L. (2015). YAP and TAZ: a nexus for Hippo signaling and beyond. *Trends Cell Biol.* 25, 499–513. doi: 10.1016/j.tcb.2015.05.002

Harrisingh, M. C., Perez-Nadales, E., Parkinson, D. B., Malcolm, D. S., Mudge, A. W., and Lloyd, A. C. (2004). The Ras/Raf/ERK signalling pathway drives Schwann cell dedifferentiation. *Embo J.* 23, 3061–3071. doi: 10.1038/sj.emboj.7600309

He, B., Zhu, Q., Chai, Y., Ding, X., Tang, J., Gu, L., et al. (2015). Safety and efficacy evaluation of a human acellular nerve graft as a digital nerve scaffold: a prospective, multicentre controlled clinical trial. *J. Tissue Eng. Regen. Med.* 9, 286–295. doi: 10.1002/term.1707

He, X., Zhang, L., Queme, L. F., Liu, X., Lu, A., Waclaw, R. R., et al. (2018). A histone deacetylase 3-dependent pathway delimits peripheral myelin growth and functional regeneration. *Nat. Med.* 24, 338–351. doi: 10.1038/nm.4483

Hendry, J. M., Alvarez-Veronesi, M. C., Placheta, E., Zhang, J. J., Gordon, T., and Borschel, G. H. (2016). ErbB2 blockade with Herceptin (trastuzumab) enhances peripheral nerve regeneration after repair of acute or chronic peripheral nerve injury. *Ann. Neurol.* 80, 112–126. doi: 10.1002/ana.24688

Höke, A., Cheng, C., and Zochodne, D. W. (2000). Expression of glial cell line-derived neurotrophic factor family of growth factors in peripheral nerve injury in rats. *Neuroreport* 11, 1651–1654. doi: 10.1097/00001756-200006050-00011

Hsu, M. N., Liao, H. T., Truong, V. A., Huang, K. L., Yu, F. J., Chen, H. H., et al. (2019). CRISPR-based activation of endogenous neurotrophic genes in adipose stem cell sheets to stimulate peripheral nerve regeneration. *Theranostics* 9, 6099–6111. doi: 10.7150/thno.36790

Hu, W., Gu, J., Deng, A., and Gu, X. (2008). Polyglycolic acid filaments guide Schwann cell migration in vitro and in vivo. *Biotechnol Lett.* 30, 1937–1942. doi: 10.1007/s10529-008-9795-1

Hu, X., Wang, X., Xu, Y., Li, L., Liu, J., He, Y., et al. (2020). Electric conductivity on aligned nanofibers facilitates the transdifferentiation of mesenchymal stem cells into schwann cells and regeneration of injured peripheral nerve. *Adv. Healthc. Mater.* 9:e1901570. doi: 10.1002/adhm.201901570

Huang, C., Ouyang, Y., Niu, H., He, N., Ke, Q., Jin, X., et al. (2015). Nerve guidance conduits from aligned nanofibers: improvement of nerve regeneration through longitudinal nanogrooves on a fiber surface. *ACS Appl. Mater. Interfaces* 7, 7189–7196. doi: 10.1021/am509227t

Huang, L., Quan, X., Liu, Z., Ma, T., Wu, Y., Ge, J., et al. (2015). c-Jun gene-modified Schwann cells: upregulating multiple neurotrophic factors and promoting neurite outgrowth. *Tissue Eng. Part A* 21, 1409–1421. doi: 10.1089/ten.TEA.2014.0416

Huang, C. W., Lu, S. Y., Huang, T. C., Huang, B. M., Sun, H. S., Yang, S. H., et al. (2020). FGF9 induces functional differentiation to Schwann cells from human adipose derived stem cells. *Theranostics* 10, 2817–2831. doi: 10.7150/thno.38553

Huang, Z., Powell, R., Phillips, J. B., and Haastert-Talini, K. (2020). Perspective on Schwann cells derived from induced pluripotent stem cells in peripheral nerve tissue engineering. *Cells* 9:2497. doi: 10.3390/cells9112497

Huang, C. Y., Liu, C. L., Ting, C. Y., Chiu, Y. T., Cheng, Y. C., Nicholson, M. W., et al. (2019). Human iPSC banking: barriers and opportunities. *J. Biomed. Sci.* 26:87. doi: 10.1186/s12929-019-0578-x

Jacob, C., Christen, C. N., Pereira, J. A., Somandin, C., Baggiolini, A., Lötscher, P., et al. (2011). HDAC1 and HDAC2 control the transcriptional program of myelination and the survival of Schwann cells. *Nat. Neurosci.* 14, 429–436. doi: 10.1038/nn.2762

Jessen, K. R., and Mirsky, R. (2016). The repair Schwann cell and its function in regenerating nerves. *J. Physiol.* 594, 3521–3531. doi: 10.1113/jp270874

Jessen, K. R., Mirsky, R., and Lloyd, A. C. (2015). Schwann cells: development and role in nerve repair. *Cold Spring Harb. Perspect. Biol.* 7:a020487. doi: 10.1101/cshperspect.a020487

Jesuraj, N. J., Santosa, K. B., Macewan, M. R., Moore, A. M., Kasukurthi, R., Ray, W. Z., et al. (2014). Schwann cells seeded in acellular nerve grafts improve functional recovery. *Muscle Nerve* 49, 267–276. doi: 10.1002/mus.23885

Kang, Y., Liu, Y., Liu, Z., Ren, S., Xiong, H., Chen, J., et al. (2019). Differentiated human adipose-derived stromal cells exhibit the phenotypic and functional characteristics of mature Schwann cells through a modified approach. *Cytotherapy* 21, 987–1003. doi: 10.1016/j.jcyt.2019.04.061

Khuong, H. T., Kumar, R., Senjaya, F., Grochmal, J., Ivanovic, A., Shakhbazau, A., et al. (2014). Skin derived precursor Schwann cells improve behavioral recovery for acute and delayed nerve repair. *Exp. Neurol.* 254, 168–179. doi: 10.1016/j.expneurol.2014.01.002

Kim, H. A., Mindos, T., and Parkinson, D. B. (2013). Plastic fantastic: Schwann cells and repair of the peripheral nervous system. *Stem Cells Transl. Med.* 2, 553–557. doi: 10.5966/sctm.2013-0011

Kim, H. S., Lee, J., Lee, D. Y., Kim, Y. D., Kim, J. Y., Lim, H. J., et al. (2017). Schwann cell precursors from human pluripotent stem cells as a potential therapeutic target for myelin repair. *Stem Cell Rep.* 8, 1714–1726. doi: 10.1016/j.stemcr.2017.04.011

Kingham, P. J., Kalbermatten, D. F., Mahay, D., Armstrong, S. J., Wiberg, M., and Terenghi, G. (2007). Adipose-derived stem cells differentiate into a Schwann cell phenotype and promote neurite outgrowth in vitro. *Exp. Neurol.* 207, 267–274. doi: 10.1016/j.expneurol.2007.06.029

Lackington, W. A., Raftery, R. M., and O'Brien, F. J. (2018). In vitro efficacy of a gene-activated nerve guidance conduit incorporating non-viral PEI-pDNA nanoparticles carrying genes encoding for NGF, GDNF and c-Jun. *Acta Biomater.* 75, 115–128. doi: 10.1016/j.actbio.2018.06.014

Lee, S. K., and Wolfe, S. W. (2000). Peripheral nerve injury and repair. *J. Am. Acad. Orthop. Surg.* 8, 243–252. doi: 10.5435/00124635-200007000-00005

Li, B., Qiu, T., Iyer, K. S., Yan, Q., Yin, Y., Xie, L., et al. (2015). PRGD/PDLLA conduit potentiates rat sciatic nerve regeneration and the underlying molecular mechanism. *Biomaterials* 55, 44–53. doi: 10.1016/j.biomaterials.2015.03.028

Li, G., Che, M. T., Zhang, K., Qin, L. N., Zhang, Y. T., Chen, R. Q., et al. (2016). Graft of the NT-3 persistent delivery gelatin sponge scaffold promotes axon regeneration, attenuates inflammation, and induces cell migration in rat and canine with spinal cord injury. *Biomaterials* 83, 233–248. doi: 10.1016/j.biomaterials.2015.11.059

Li, G., Zhang, B., Sun, J. H., Shi, L. Y., Huang, M. Y., Huang, L. J., et al. (2021a). An NT-3-releasing bioscaffold supports the formation of TrkC-modified neural stem cell-derived neural network tissue with efficacy in repairing spinal cord injury. *Bioact. Mater.* 6, 3766–3781. doi: 10.1016/j.bioactmat.2021.03.036

Li, G., Zheng, T., Wu, L., Han, Q., Lei, Y., Xue, L., et al. (2021b). Bionic microenvironment-inspired synergistic effect of anisotropic micro-nanocomposite topology and biology cues on peripheral nerve regeneration. *Sci. Adv.* 7:eabi5812. doi: 10.1126/sciadv.abi5812

Li, X., Gonias, S. L., and Campana, W. M. (2005). Schwann cells express erythropoietin receptor and represent a major target for Epo in peripheral nerve injury. *Glia* 51, 254–265. doi: 10.1002/glia.20202

Lim, E. F., Nakanishi, S. T., Hoghooghi, V., Eaton, S. E., Palmer, A. L., Frederick, A., et al. (2017). AlphaB-crystallin regulates remyelination after peripheral nerve injury. *Proc. Natl. Acad. Sci. U. S. A.* 114, E1707–E1716. doi: 10.1073/pnas.1612136114

Liu, Q., Spusta, S. C., Mi, R., Lassiter, R. N., Stark, M. R., Höke, A., et al. (2012). Human neural crest stem cells derived from human ESCs and induced pluripotent stem cells: induction, maintenance, and differentiation into functional schwann cells. *Stem Cells Transl. Med.* 1, 266–278. doi: 10.5966/sctm.2011-0042

Liu, Y., Chen, J., Liu, W., Lu, X., Liu, Z., Zhao, X., et al. (2016). A modified approach to inducing bone marrow stromal cells to differentiate into cells with mature schwann cell phenotypes. *Stem Cells Dev.* 25, 347–359. doi: 10.1089/scd.2015.0295

Ma, P. X., and Zhang, R. (1999). Synthetic nano-scale fibrous extracellular matrix. *J. Biomed. Mater. Res.* 46, 60–72. doi: 10.1002/(sici)1097-4636(199907)46:1<60::aid-jbm7>3.0.co;2-h

Madduri, S., and Gander, B. (2010). Schwann cell delivery of neurotrophic factors for peripheral nerve regeneration. *J. Peripher. Nerv. Syst.* 15, 93–103. doi: 10.1111/j.1529-8027.2010.00257.x

Marquardt, L. M., Ee, X., Iyer, N., Hunter, D., Mackinnon, S. E., Wood, M. D., et al. (2015). Finely tuned temporal and spatial delivery of GDNF promotes enhanced nerve regeneration in a long nerve defect model. *Tissue Eng. Part A* 21, 2852–2864. doi: 10.1089/ten.TEA.2015.0311

Martin, R. M., Fowler, J. L., Cromer, M. K., Lesch, B. J., Ponce, E., Uchida, N., et al. (2020). Improving the safety of human pluripotent stem cell therapies using genome-edited orthogonal safeguards. *Nat. Commun.* 11:2713. doi: 10.1038/s41467-020-16455-7

Matsuse, D., Kitada, M., Kohama, M., Nishikawa, K., Makinoshima, H., Wakao, S., et al. (2010). Human umbilical cord-derived mesenchymal stromal cells differentiate into functional Schwann cells that sustain peripheral nerve regeneration. *J. Neuropathol. Exp. Neurol.* 69, 973–985. doi: 10.1097/NEN.0b013e3181eff6dc

Mazzara, P. G., Massimino, L., Pellegatta, M., Ronchi, G., Ricca, A., Iannielli, A., et al. (2017). Two factor-based reprogramming of rodent and human fibroblasts into Schwann cells. *Nat. Commun.* 8:14088. doi: 10.1038/ncomms14088

McKenzie, I. A., Biernaskie, J., Toma, J. G., Midha, R., and Miller, F. D. (2006). Skin-derived precursors generate myelinating Schwann cells for the injured

and dysmyelinated nervous system. *J. Neurosci.* 26, 6651–6660. doi: 10.1523/jneurosci.1007-06.2006

Meena, P., Kakkar, A., Kumar, M., Khatri, N., Nagar, R. K., Singh, A., et al. (2021). Advances and clinical challenges for translating nerve conduit technology from bench to bed side for peripheral nerve repair. *Cell Tissue Res.* 383, 617–644. doi: 10.1007/s00441-020-03301-x

Mertens, J., Marchetto, M. C., Bardy, C., and Gage, F. H. (2016). Evaluating cell reprogramming, differentiation and conversion technologies in neuroscience. *Nat. Rev. Neurosci.* 17, 424–437. doi: 10.1038/nrn.2016.46

Mimura, T., Dezawa, M., Kanno, H., Sawada, H., and Yamamoto, I. (2004). Peripheral nerve regeneration by transplantation of bone marrow stromal cell-derived Schwann cells in adult rats. *J. Neurosurg.* 101, 806–812. doi: 10.3171/jns.2004.101.5.0806

Mindos, T., Dun, X. P., North, K., Doddrell, R. D., Schulz, A., Edwards, P., et al. (2017). Merlin controls the repair capacity of Schwann cells after injury by regulating Hippo/YAP activity. *J. Cell Biol.* 216, 495–510. doi: 10.1083/jcb.201606052

Mobasseri, A., Faroni, A., Minogue, B. M., Downes, S., Terenghi, G., and Reid, A. J. (2015). Polymer scaffolds with preferential parallel grooves enhance nerve regeneration. *Tissue Eng. Part A* 21, 1152–1162. doi: 10.1089/ten.TEA.2014.0266

Moosazadeh Moghaddam, M., Bonakdar, S., Shokrgozar, M. A., Zaminy, A., Vali, H., and Faghihi, S. (2019). Engineered substrates with imprinted cell-like topographies induce direct differentiation of adipose-derived mesenchymal stem cells into Schwann cells. *Artif Cells Nanomed. Biotechnol.* 47, 1022–1035. doi: 10.1080/21691401.2019.1586718

Muppirala, A. N., Limbach, L. E., Bradford, E. F., and Petersen, S. C. (2021). Schwann cell development: from neural crest to myelin sheath. *Wiley Interdiscip. Rev. Dev. Biol.* 10:e398. doi: 10.1002/wdev.398

Murinson, B. B., Archer, D. R., Li, Y., and Griffin, J. W. (2005). Degeneration of myelinated efferent fibers prompts mitosis in Remak Schwann cells of uninjured C-fiber afferents. *J. Neurosci.* 25, 1179–1187. doi: 10.1523/jneurosci.1372-04.2005

Napoli, I., Noon, L. A., Ribeiro, S., Kerai, A. P., Parrinello, S., Rosenberg, L. H., et al. (2012). A central role for the ERK-signaling pathway in controlling Schwann cell plasticity and peripheral nerve regeneration in vivo. *Neuron* 73, 729–742. doi: 10.1016/j.neuron.2011.11.031

Nawrotek, K., Tylman, M., Rudnicka, K., Gatkowska, J., and Wieczorek, M. (2016). Epineurium-mimicking chitosan conduits for peripheral nervous tissue engineering. *Carbohydr. Polym.* 152, 119–128. doi: 10.1016/j.carbpol.2016.07.002

Nicolas, J., Magli, S., Rabbachin, L., Sampaolesi, S., Nicotra, F., and Russo, L. (2020). 3D extracellular matrix mimics: fundamental concepts and role of materials chemistry to influence stem cell fate. *Biomacromolecules* 21, 1968–1994. doi: 10.1021/acs.biomac.0c00045

Orbay, H., Uysal, A. C., Hyakusoku, H., and Mizuno, H. (2012). Differentiated and undifferentiated adipose-derived stem cells improve function in rats with peripheral nerve gaps. *J. Plast. Reconstr. Aesthet. Surg.* 65, 657–664. doi: 10.1016/j.bjps.2011.11.035

Pan, M., Wang, X., Chen, Y., Cao, S., Wen, J., Wu, G., et al. (2017). Tissue engineering with peripheral blood-derived mesenchymal stem cells promotes the regeneration of injured peripheral nerves. *Exp. Neurol.* 292, 92–101. doi: 10.1016/j.expneurol.2017.03.005

Parrinello, S., Napoli, I., Ribeiro, S., Wingfield Digby, P., Fedorova, M., Parkinson, D. B., et al. (2010). EphB signaling directs peripheral nerve regeneration through Sox2-dependent Schwann cell sorting. *Cell* 143, 145–155. doi: 10.1016/j.cell.2010.08.039

Peng, J., Wang, Y., Zhang, L., Zhao, B., Zhao, Z., Chen, J., et al. (2011). Human umbilical cord Wharton's jelly-derived mesenchymal stem cells differentiate into a Schwann-cell phenotype and promote neurite outgrowth in vitro. *Brain Res. Bull.* 84, 235–243. doi: 10.1016/j.brainresbull.2010.12.013

Poitelon, Y., Lopez-Anido, C., Catignas, K., Berti, C., Palmisano, M., Williamson, C., et al. (2016). YAP and TAZ control peripheral myelination and the expression of laminin receptors in Schwann cells. *Nat. Neurosci.* 19, 879–887. doi: 10.1038/nn.4316

Qian, Y., Song, J., Zhao, X., Chen, W., Ouyang, Y., Yuan, W., et al. (2018). 3D fabrication with integration molding of a graphene oxide/polycaprolactone nanoscaffold for neurite regeneration and angiogenesis. *Adv. Sci.* 5:1700499. doi: 10.1002/advs.201700499

Qiu, L., He, B., Hu, J., Zhu, Z., Liu, X., and Zhu, J. (2015). Cartilage oligomeric matrix protein angiopoeitin-1 provides benefits during nerve regeneration in vivo and in vitro. *Ann. Biomed. Eng.* 43, 2924–2940. doi: 10.1007/s10439-015-1342-3

Randolph, C. L., Bierl, M. A., and Isaacson, L. G. (2007). Regulation of NGF and NT-3 protein expression in peripheral targets by sympathetic input. *Brain Res.* 1144, 59–69. doi: 10.1016/j.brainres.2007.01.099

Rosenberg, L. H., Cattin, A. L., Fontana, X., Harford-Wright, E., Burden, J. J., White, I. J., et al. (2018). HDAC3 regulates the transition to the homeostatic myelinating schwann cell state. *Cell Rep.* 25, 2755–2765.e5. doi: 10.1016/j.celrep.2018.11.045

Rutkowski, J. L., Kirk, C. J., Lerner, M. A., and Tennekoon, G. I. (1995). Purification and expansion of human Schwann cells in vitro. *Nat. Med.* 1, 80–83. doi: 10.1038/nm0195-80

Schlaepfer, W. W., and Bunge, R. P. (1973). Effects of calcium ion concentration on the degeneration of amputated axons in tissue culture. *J. Cell Biol.* 59, 456–470. doi: 10.1083/jcb.59.2.456

Shahriari, D., Shibayama, M., Lynam, D. A., Wolf, K. J., Kubota, G., Koffler, J. Y., et al. (2017). Peripheral nerve growth within a hydrogel microchannel scaffold supported by a kink-resistant conduit. *J. Biomed. Mater. Res. A* 105, 3392–3399. doi: 10.1002/jbm.a.36186

Shakhbazau, A., Kawasoe, J., Hoyng, S. A., Kumar, R., van Minnen, J., Verhaagen, J., et al. (2012). Early regenerative effects of NGF-transduced Schwann cells in peripheral nerve repair. *Mol. Cell. Neurosci.* 50, 103–112. doi: 10.1016/j.mcn.2012.04.004

Slavin, B. R., Sarhane, K. A., von Guionneau, N., Hanwright, P. J., Qiu, C., Mao, H. Q., et al. (2021). Insulin-like growth factor-1: a promising therapeutic target for peripheral nerve injury. *Front. Bioeng. Biotechnol.* 9:695850. doi: 10.3389/fbioe.2021.695850

Soldatov, R., Kaucka, M., Kastriti, M. E., Petersen, J., Chontorotzea, T., Englmaier, L., et al. (2019). Spatiotemporal structure of cell fate decisions in murine neural crest. *Science* 364:eaas9536. doi: 10.1126/science.aas9536

Sondell, M., Lundborg, G., and Kanje, M. (1999). Vascular endothelial growth factor has neurotrophic activity and stimulates axonal outgrowth, enhancing cell survival and Schwann cell proliferation in the peripheral nervous system. *J. Neurosci.* 19, 5731–5740. doi: 10.1523/jneurosci.19-14-05731.1999

Sowa, Y., Kishida, T., Tomita, K., Yamamoto, K., Numajiri, T., and Mazda, O. (2017). Direct conversion of human fibroblasts into schwann cells that facilitate regeneration of injured peripheral nerve in vivo. *Stem Cells Transl. Med.* 6, 1207–1216. doi: 10.1002/sctm.16-0122

Stoll, G., Griffin, J. W., Li, C. Y., and Trapp, B. D. (1989). Wallerian degeneration in the peripheral nervous system: participation of both Schwann cells and macrophages in myelin degradation. *J. Neurocytol.* 18, 671–683. doi: 10.1007/bf01187086

Stratton, J. A., Kumar, R., Sinha, S., Shah, P., Stykel, M., Shapira, Y., et al. (2017). Purification and characterization of schwann cells from adult human skin and nerve. *eNeuro* 4:ENEURO.0307-16.2017. doi: 10.1523/eneuro.0307-16.2017

Sullivan, R., Dailey, T., Duncan, K., Abel, N., and Borlongan, C. V. (2016). Peripheral nerve injury: stem cell therapy and peripheral nerve transfer. *Int. J. Mol. Sci.* 17:2101. doi: 10.3390/ijms17122101

Sun, J. H., Li, G., Wu, T. T., Lin, Z. J., Zou, J. L., Huang, L. J., et al. (2020). Decellularization optimizes the inhibitory microenvironment of the optic nerve to support neurite growth. *Biomaterials* 258:120289. doi: 10.1016/j.biomaterials.2020.120289

Syed, N., Reddy, K., Yang, D. P., Taveggia, C., Salzer, J. L., Maurel, P., et al. (2010). Soluble neuregulin-1 has bifunctional, concentration-dependent effects on Schwann cell myelination. *J. Neurosci.* 30, 6122–6131. doi: 10.1523/jneurosci.1681-09.2010

Takahashi, K., Tanabe, K., Ohnuki, M., Narita, M., Ichisaka, T., Tomoda, K., et al. (2007). Induction of pluripotent stem cells from adult human fibroblasts by defined factors. *Cell* 131, 861–872. doi: 10.1016/j.cell.2007.11.019

Tannemaat, M. R., Eggers, R., Hendriks, W. T., de Ruiter, G. C., van Heerikhuize, J. J., Pool, C. W., et al. (2008). Differential effects of lentiviral vector-mediated overexpression of nerve growth factor and glial cell line-derived neurotrophic factor on regenerating sensory and motor axons in the transected peripheral nerve. *Eur. J. Neurosci.* 28, 1467–1479. doi: 10.1111/j.1460-9568.2008.06452.x

Thibodeau, A., Galbraith, T., Fauvel, C. M., Khuong, H. T., and Berthod, F. (2022). Repair of peripheral nerve injuries using a prevascularized cell-based tissue-engineered nerve conduit. *Biomaterials* 280:121269. doi: 10.1016/j.biomaterials.2021.121269

Tomita, K., Madura, T., Mantovani, C., and Terenghi, G. (2012). Differentiated adipose-derived stem cells promote myelination and enhance functional recovery in a rat model of chronic denervation. *J. Neurosci. Res.* 90, 1392–1402. doi: 10.1002/jnr.23002

Uz, M., Büyüköz, M., Sharma, A. D., Sakaguchi, D. S., Altinkaya, S. A., and Mallapragada, S. K. (2017). Gelatin-based 3D conduits for transdifferentiation of mesenchymal stem cells into Schwann cell-like phenotypes. *Acta Biomater.* 53, 293–306. doi: 10.1016/j.actbio.2017.02.018

Wang, S., Zhu, C., Zhang, B., Hu, J., Xu, J., Xue, C., et al. (2022). BMSC-derived extracellular matrix better optimizes the microenvironment to support nerve regeneration. *Biomaterials* 280:121251. doi: 10.1016/j.biomaterials.2021.121251

Wang, X., Luo, E., Li, Y., and Hu, J. (2011). Schwann-like mesenchymal stem cells within vein graft facilitate facial nerve regeneration and remyelination. *Brain Res.* 1383, 71–80. doi: 10.1016/j.brainres.2011.01.098

Wang, Y., Teng, H. L., and Huang, Z. H. (2012). Intrinsic migratory properties of cultured Schwann cells based on single-cell migration assay. *PLoS One* 7:e51824. doi: 10.1371/journal.pone.0051824

Whitlock, E. L., Tuffaha, S. H., Luciano, J. P., Yan, Y., Hunter, D. A., Magill, C. K., et al. (2009). Processed allografts and type I collagen conduits for repair of peripheral nerve gaps. *Muscle Nerve* 39, 787–799. doi: 10.1002/mus.21220

Wong, C. W., Xu, Y., Liu, X., Xu, S., Zhang, Y., Zhu, Z., et al. (2020). Effect of induction time on the proliferation and differentiation of induced schwann-like cells from adipose-derived stem cells. *Cell Mol. Neurobiol.* 40, 1105–1116. doi: 10.1007/s10571-020-00795-5

Woodhoo, A., Alonso, M. B., Droggiti, A., Turmaine, M., D'Antonio, M., Parkinson, D. B., et al. (2009). Notch controls embryonic Schwann cell differentiation, postnatal myelination and adult plasticity. *Nat. Neurosci.* 12, 839–847. doi: 10.1038/nn.2323

Woolley, A. G., Tait, K. J., Hurren, B. J., Fisher, L., Sheard, P. W., and Duxson, M. J. (2008). Developmental loss of NT-3 in vivo results in reduced levels of myelin-specific proteins, a reduced extent of myelination and increased apoptosis of Schwann cells. *Glia* 56, 306–317. doi: 10.1002/glia.20614

Wu, L. M., Wang, J., Conidi, A., Zhao, C., Wang, H., Ford, Z., et al. (2016). Zeb2 recruits HDAC-NuRD to inhibit Notch and controls Schwann cell differentiation and remyelination. *Nat. Neurosci.* 19, 1060–1072. doi: 10.1038/nn.4322

Wu, S., Qi, Y., Shi, W., Kuss, M., Chen, S., and Duan, B. (2020). Electrospun conductive nanofiber yarns for accelerating mesenchymal stem cells differentiation and maturation into Schwann cell-like cells under a combination of electrical stimulation and chemical induction. *Acta Biomater.* 139, 91–104. doi: 10.1016/j.actbio.2020.11.042

Xie, J., MacEwan, M. R., Schwartz, A. G., and Xia, Y. (2010). Electrospun nanofibers for neural tissue engineering. *Nanoscale* 2, 35–44. doi: 10.1039/b9nr00243j

Xue, J., Xie, J., Liu, W., and Xia, Y. (2017a). Electrospun nanofibers: new concepts, materials, and applications. *Acc. Chem. Res.* 50, 1976–1987. doi: 10.1021/acs.accounts.7b00218

Xue, J., Yang, J., O'Connor, D. M., Zhu, C., Huo, D., Boulis, N. M., et al. (2017b). Differentiation of bone marrow stem cells into schwann cells for the promotion of neurite outgrowth on electrospun fibers. *ACS Appl. Mater. Interfaces* 9, 12299–12310. doi: 10.1021/acsami.7b00882

Yeh, T. S., Fang, Y. H., Lu, C. H., Chiu, S. C., Yeh, C. L., Yen, T. C., et al. (2014). Baculovirus-transduced, VEGF-expressing adipose-derived stem cell sheet for the treatment of myocardium infarction. *Biomaterials* 35, 174–184. doi: 10.1016/j.biomaterials.2013.09.080

Zakrzewski, W., Dobrzyński, M., Szymonowicz, M., and Rybak, Z. (2019). Stem cells: past, present, and future. *Stem Cell Res. Ther.* 10:68. doi: 10.1186/s13287-019-1165-5

Zeng, W., Rong, M., Hu, X., Xiao, W., Qi, F., Huang, J., et al. (2014). Incorporation of chitosan microspheres into collagen-chitosan scaffolds for the controlled release of nerve growth factor. *PLoS One* 9:e101300. doi: 10.1371/journal.pone.0101300

Zhang, D., Yao, Y., Duan, Y., Yu, X., Shi, H., Nakkala, J. R., et al. (2020). Surface-anchored graphene oxide nanosheets on cell-scale micropatterned Poly(d,l-lactide-co-caprolactone) conduits promote peripheral nerve regeneration. *ACS Appl. Mater. Interfaces* 12, 7915–7930. doi: 10.1021/acsami.9b20321

Zhang, H. T., Cheng, H. Y., Zhang, L., Fan, J., Chen, Y. Z., Jiang, X. D., et al. (2009). Umbilical cord blood cell-derived neurospheres differentiate into Schwann-like cells. *Neuroreport* 20, 354–359. doi: 10.1097/WNR.0b013e328323d74c

Zhang, Y., Zhu, Z., Liu, X., Xu, S., Zhang, Y., Xu, Y., et al. (2021). Integrated analysis of long noncoding RNAs and mRNA expression profiles reveals the potential role of lncRNAs in early stage of post-peripheral nerve injury in Sprague-Dawley rats. *Aging* 13, 13909–13925. doi: 10.18632/aging.202989

Zhao, Y., Wang, Y., Gong, J., Yang, L., Niu, C., Ni, X., et al. (2017). Chitosan degradation products facilitate peripheral nerve regeneration by improving macrophage-constructed microenvironments. *Biomaterials* 134, 64–77. doi: 10.1016/j.biomaterials.2017.02.026

Zhou, G., Chang, W., Zhou, X., Chen, Y., Dai, F., Anwar, A., et al. (2020). Nanofibrous nerve conduits with nerve growth factors and bone marrow stromal cells pre-cultured in bioreactors for peripheral nerve regeneration. *ACS Appl. Mater. Interfaces* 12, 16168–16177. doi: 10.1021/acsami.0c04191

Zhu, Z., Zhou, X., He, B., Dai, T., Zheng, C., Yang, C., et al. (2015). Ginkgo biloba extract (EGb 761) promotes peripheral nerve regeneration and neovascularization after acellular nerve allografts in a rat model. *Cell Mol. Neurobiol.* 35, 273–282. doi: 10.1007/s10571-014-0122-1

Ziegler, L., Grigoryan, S., Yang, I. H., Thakor, N. V., and Goldstein, R. S. (2011). Efficient generation of schwann cells from human embryonic stem cell-derived neurospheres. *Stem Cell Rev. Rep.* 7, 394–403. doi: 10.1007/s12015-010-9198-2

Zong, H., Zhao, H., Zhao, Y., Jia, J., Yang, L., Ma, C., et al. (2013). Nanoparticles carrying neurotrophin-3-modified Schwann cells promote repair of sciatic nerve defects. *Neural Regen. Res.* 8, 1262–1268. doi: 10.3969/j.issn.1673-5374.2013.14.002

Conflict of Interest: The authors declare that the research was conducted in the absence of any commercial or financial relationships that could be construed as a potential conflict of interest.

Publisher's Note: All claims expressed in this article are solely those of the authors and do not necessarily represent those of their affiliated organizations, or those of the publisher, the editors and the reviewers. Any product that may be evaluated in this article, or claim that may be made by its manufacturer, is not guaranteed or endorsed by the publisher.

frontiers | Frontiers in Cellular Neuroscience

ORIGINAL RESEARCH
published: 11 May 2022
doi: 10.3389/fncel.2022.856734

Sortilin Modulates Schwann Cell Signaling and Remak Bundle Regeneration Following Nerve Injury

*Maj Ulrichsen[1†], Nádia P. Gonçalves[1†], Simin Mohseni[2], Simone Hjæresen[3], Thomas L. Lisle[1], Simon Molgaard[4], Niels K. Madsen[1], Olav M. Andersen[1], Åsa F. Svenningsen[3], Simon Glerup[4], Anders Nykjær[1,5,6] and Christian B. Vægter[1]**

[1] Danish Research Institute of Translational Neuroscience – DANDRITE, Nordic EMBL Partnership for Molecular Medicine, Department of Biomedicine, Aarhus University, Aarhus, Denmark, [2] Department of Biomedical and Clinical Sciences, Linköping University, Linköping, Sweden, [3] Neurobiological Research, Faculty of Health Sciences, Department of Molecular Medicine, University of Southern Denmark, Odense, Denmark, [4] Department of Biomedicine, Aarhus University, Aarhus, Denmark, [5] Department of Neurosurgery, Aarhus University Hospital, Aarhus, Denmark, [6] Center of Excellence PROMEMO, Aarhus University, Aarhus, Denmark

OPEN ACCESS

Edited by:
Ji-Fan Hu,
Jilin University, China

Reviewed by:
Petr Dubový,
Masaryk University, Czechia
Jose Antonio Gomez-Sanchez,
Miguel Hernández University of Elche, Spain
Stefania Raimondo,
University of Turin, Italy

***Correspondence:**
Christian B. Vægter
cv@biomed.au.dk

[†]These authors share first authorship

Specialty section:
This article was submitted to Non-neuronal Cells, a section of the journal Frontiers in Cellular Neuroscience

Received: 17 January 2022
Accepted: 11 April 2022
Published: 11 May 2022

Citation:
Ulrichsen M, Gonçalves NP, Mohseni S, Hjæresen S, Lisle TL, Molgaard S, Madsen NK, Andersen OM, Svenningsen ÅF, Glerup S, Nykjær A and Vægter CB (2022) Sortilin Modulates Schwann Cell Signaling and Remak Bundle Regeneration Following Nerve Injury. Front. Cell. Neurosci. 16:856734. doi: 10.3389/fncel.2022.856734

Peripheral nerve regeneration relies on the ability of Schwann cells to support the regrowth of damaged axons. Schwann cells re-differentiate when reestablishing contact with the sprouting axons, with large fibers becoming remyelinated and small nociceptive fibers ensheathed and collected into Remak bundles. We have previously described how the receptor sortilin facilitates neurotrophin signaling in peripheral neurons *via* regulated trafficking of Trk receptors. This study aims to characterize the effects of sortilin deletion on nerve regeneration following sciatic crush injury. We found that *Sort1*$^{-/-}$ mice displayed functional motor recovery like that of WT mice, with no detectable differences in relation to nerve conduction velocities and morphological aspects of myelinated fibers. In contrast, we found abnormal ensheathment of regenerated C-fibers in injured *Sort1*$^{-/-}$ mice, demonstrating a role of sortilin for Remak bundle formation following injury. Further studies on Schwann cell signaling pathways showed a significant reduction of MAPK/ERK, RSK, and CREB phosphorylation in *Sort1*$^{-/-}$ Schwann cells after stimulation with neurotrophin-3 (NT-3), while Schwann cell migration and myelination remained unaffected. In conclusion, our results demonstrate that loss of sortilin blunts NT-3 signaling in Schwann cells which might contribute to the impaired Remak bundle regeneration after sciatic nerve injury.

Keywords: nerve injury, NT-3, TrkC, sortilin, Schwann cell, Remak bundle

HIGHLIGHTS

- Sortilin ablation results in Remak bundle pathology after nerve injury.
- *In vitro* studies demonstrate blunted NT-3 signaling in sortilin-deficient Schwann cells.

INTRODUCTION

Schwann cells are the axon-ensheathing glial cells of the peripheral nervous system (PNS), generally divided into myelinating and non-myelinating subtypes, both being essential for maintaining normal nerve functions. The myelinating Schwann cells form a multi-layered myelin sheath by spirally wrapping plasma membrane around a segment of a single caliber axon. In contrast, the non-myelinating Schwann cells surround and segregate groups of several small-diameter axons into Remak bundles (Jessen and Mirsky, 2002).

Following peripheral nerve injury, the process of Wallerian degeneration sets the stage for subsequent regeneration. This process is characterized by the morphological and molecular changes that occur in the distal part of an injured peripheral nerve, where the damaged axon and myelin debris become degraded. The Schwann cells dedifferentiate into their repair phenotype, and the macrophages infiltrate the injured nerve to partake in myelin degradation (Gaudet et al., 2011). A population of repair Schwann cells proliferate and migrate, forming the characteristic bands of Büngner to provide guidance and growth factor support (including secreted neurotrophins) for the regenerating axons, stimulate ensheathing of small-caliber fibers to reform Remak bundles, and facilitate remyelination of large-caliber axons (Gaudet et al., 2011; Jessen and Arthur-Farraj, 2019; Jessen and Mirsky, 2019, 2022). Neurotrophins elicit trophic signaling for sprouting axons but are also reported to regulate Schwann cell functions. Thus, *in vitro* studies have shown how neurotrophin-3 (NT-3) and brain-derived neurotrophic factor (BDNF) appear to have opposing effects on Schwann cell migration and myelin formation, with NT-3/TrkC enhancing Schwann cell migration but inhibiting myelin formation (Yamauchi et al., 2003, 2004, 2005b), whereas BDNF/$p75^{NTR}$ inhibits Schwann cell migration and enhance myelin formation (Cosgaya et al., 2002; Tolwani et al., 2004; Yamauchi et al., 2004).

Intracellular signaling pathways are activated upon binding of neurotrophins to their cognate Trk receptors, resulting in increased phosphorylation of downstream messengers such as protein kinase B (Akt) as well as the mitogen-activated protein kinase (MAPK/ERK). Transcriptional events are induced by MAPK/ERK *via* members of the ribosomal s6 kinase (RSK) family and CREB transcription, ultimately modulating the cell cycle, neurite outgrowth, and synaptic plasticity (Chao, 2003). The activation of MAPK/ERK can be observed early after injury (Sheu et al., 2000) and is implicated in the injury-induced dedifferentiation of Schwann cells (Harrisingh et al., 2004). Accordingly, MAPK/ERK activation in Schwann cells is sufficient to drive the dedifferentiation of myelinating Schwann cells to a progenitor-like state in peripheral adult nerves, causing severe loss of motor function with rapid remyelination and neurological recovery occurring after inhibition of the MAPK/ERK activation (Napoli et al., 2012). Of further support has been how sustained MAPK/ERK activation in Schwann cells resulted in delayed functional recovery and morphological defects in both myelinated and non-myelinated fibers after injury (Cervellini et al., 2017).

Sortilin is a member of the Vps10p sorting receptor family and is involved in the transport of a wide variety of intracellular proteins between several cellular compartments (Willnow et al., 2008; Nykjaer and Willnow, 2012). We have previously described how the sortilin receptor, abundantly expressed in the central nervous system and the PNS, facilitates the phosphorylation of MAPK/ERK in primary sensory neurons by associating with Trk receptors to mediate their subcellular trafficking (Vaegter et al., 2011). As Schwann cells express sortilin (Gonçalves et al., 2020) as well as TrkC receptors, we asked if sortilin is similarly involved in neurotrophin signaling in these cells, and more specifically if ablation of sortilin *in vivo* would affect the morphological and/or functional aspects of sciatic nerve regeneration. We have found that the lack of sortilin elicits a blunted NT-3 signaling in cultured Schwann cells, which might contribute to the impaired Remak Schwann cell regeneration following nerve injury.

MATERIALS AND METHODS

Primary Rat Schwann Cell Cultures

Primary Schwann cell cultures were prepared from neonatal rat sciatic nerves according to Kim and Maurel (2009) with few alterations. Pregnant wild-type (WT) Sprague–Dawley rats were obtained from Janvier Labs (France). *Sort1*$^{-/-}$ Sprague–Dawley rats were bred at Aarhus University (Gonçalves et al., 2020). In brief, sciatic nerves were dissected from P1-P3 Sprague–Dawley rat pups and placed in ice-cold Leibovitz's L-15 medium (Gibco, Cat. #11415). Following dissection, the harvested nerves were digested with 0.25% trypsin (Gibco, Cat. #25200-072) and 0.1% collagenase I (Sigma, Cat. #C9722) for 30 min at 37°C and dissociated by trituration in DMEM (Sigma, Cat. #D0819) containing 10% FBS (Thermo Fisher, Cat. #10270) before being plated on poly-L lysine-coated culture dishes in DMEM supplemented with 10% FBS and Primocin^{TM} (InvivoGen, Cat. #ant-pm-2). Contaminating fibroblasts were removed by 48 h incubation with the anti-metabolic agent Cytosine-ß-arabino furanoside hydrochloride (Ara-C; 10 μM final concentration, Sigma, Cat. #C1768), which kills mitotic cells. The cultures were washed twice with HBSS (Gibco, Cat. #14170-088) and the Schwann cells expanded in the growth medium [DMEM containing 10% FBS, recombinant human neuregulin-1-β1 EGF domain (10 ng/ml, R&D Systems, Cat. #396-HB-050) and forskolin (2.5 μM, Sigma, Cat. #F-6886)].

Mouse Model and Surgical Procedures

Sciatic nerve crush injury was performed in both 12-weeks-old WT mice (Janvier Labs, France) and *Sort1*$^{-/-}$ mice (Jansen et al., 2007). Mixed groups with both males and females were used throughout the experiments.

The animals were anesthetized with isoflurane (IsoFlo vet, Abbot). Eye ointment was applied to protect the eyes from drying during the procedure and a subcutaneous injection of buprenorphine (0.3 mg/ml; Temgesic, RB Pharmaceuticals, Cat. #521634) and ampicillin (0.25 mg/ml; Ampicillin PCD, PharmaCoDane, Cat. #175689) was administered before surgery, to minimize post-surgery pain and risk of infection. The thigh

and legs were shaved and disinfected before application of lidocaine (10 mg/ml; AstraZeneca, Cat. #PS02671) and exposure of the sciatic nerve at the mid-thigh level by separation of the biceps femoris and the gluteus superficialis. The left sciatic nerve was crushed with a non-serrated clamp for 30 s (Varejo et al., 2004; Ronchi et al., 2010). A sham surgery was performed on the contralateral side, where the sciatic nerve was exposed and the skin sutured immediately after. Care was taken to minimize damage to the musculature to guarantee ideal conditions for functional recovery. Post-surgery analgesic (0.006 mg/ml buprenorphine) was supplied in the drinking water for a minimum of 2 days. The mice were housed with littermates and cared for in a pathogen-free environment, in a 12 h light/dark cycle and with water and chow *ad libitum*. All experiments were approved by the Danish Animal Experiments Inspectorate under the Ministry of Justice (permission no. 2017-15-0201-01192) and carried out according to the European Council directive, and institutional and national guidelines.

Motor Analysis

Walking tract analysis (Mendes et al., 2015) was performed to access locomotor functional recovery before (0) and on days 3, 7, 9, 11, 18, 25, and 60 after injury (n = 6 mice per genotype). The mice were allowed to walk through a homemade catwalk consisting of a 50 cm × 5.5 cm corridor with a transparent Plexiglas floor to a box on the side of the catwalk containing bedding from their cages. Green light was sent horizontally through the Plexiglas floor and ambient red light was used to enhance contrast to the green light reflected down when the mouse placed a paw on the floor. The paw placement during walking was accurately determined from a video recorded with a camera below. A liner was placed on top of the Plexiglas floor. This way, the paw prints and gait could be analyzed in ImageJ by setting the scale accordingly to obtain print measurements.

The obtained footprints were then measured in ImageJ to calculate the sciatic functional index (SFI) using the empirical equation adapted for mice by Inserra et al. (1998): SFI = 118.9 × [(ETS-CTS)/CTS] − 51.2 × [(EPL-CPL)/CPL] − 7.5, where ETS represents operated experimental toe spread (distance between the first and fifth toes), CTS stands for control toe spread, EPL for operated experimental print length, and CPL for control print length. Footmarks made at the beginning of the trial were excluded and three analyzable walks were evaluated from each run for individual step parameter calculation. The pre-injured SFI values (time point = 0) were used as control for comparison. The SFI scores that we processed ranged from 0 to −130, with 0 representing normal or completely recovered nerve function and −100 or more, a non-functional nerve; thus, the mice who dragged their paws were arbitrarily assigned a value of −100.

The stride length and the step length (from the center of the right paws to the center of the left paws and vice versa) were measured in ImageJ from 3 consecutive steps. The step width and the angle of the paw to the mouse midline were additionally measured from the 3 consecutive steps. The mice who dragged their paws were arbitrarily assigned a value of 90°.

A grip strength test was performed after the walking tract analysis to evaluate the hind limb muscle strength as an indicator of motor regeneration and neuromuscular function before (0) and on days 3, 9, 11, 18, 25, 31, 38, 45, and 60 after injury. Combined hind limb grip strength was measured as tension force using the commercial grip strength meter from Bioseb (Chaville, France), which digitally displays the maximum force applied as the peak tension (in Newton) when the grasp is released. The mice were subjected to 5 consecutive trials and the maximum value was taken as an index of the hind limb strength.

Nerve Conduction Velocities

Motor (sciatic) and sensory (sural) nerve conduction velocities (MNCV, SNCV, respectively) were performed 60 days after crush injury according to Oh et al. (2010) using a Viking Quest apparatus (Natus Neurology Incorporated, United States) (n = 6 mice per group). NCV was measured from the crush-injured side and from the contralateral side, which was subjected to sham surgery. Briefly, for the sural nerve, recording electrodes were placed in the dorsal part of the foot, with supramaximal stimulation at the ankle. Sural sensory NCV (m/s) was calculated by dividing the distance between the recording and stimulating electrodes (mm) by the onset latency (ms) of the sensory nerve action potential after supramaximal antidromic stimulation. Sciatic-tibial motor NCV was recorded by placing electrodes dorsally in the foot and orthodromically stimulating first at the ankle, then at the sciatic notch. The distance between the two sites of stimulation (mm) was then divided by the difference between the two onset latencies (ankle distance and notch distance, ms) to calculate the final sciatic-tibial motor NCV (m/s).

Sciatic Nerve Histology and Axon Density Analysis

The operated mice (n = 6 per genotype) were euthanized 25 days after injury with intraperitoneal injections of pentobarbital (5 mg/ml). The mice were then transcardially perfused with ice-cold Tyrodes solution followed by fixation in ice-cold 5% glutaraldehyde in 300 mOsm phosphate buffer containing 0.1 M sucrose. The samples were postfixed in 1% osmium tetroxide for 1 h at 4°C and washed in the phosphate buffer. The samples were dehydrated in 50% ethanol and stained with 2% uranyl acetate in 50% ethanol. The samples were then dehydrated in a series of ascending concentrations of ethanol and 100% acetone. A three-step infiltration in a mixture of acetone-embedding medium (1:3, 1:1, 3:1) was performed before embedding (48 h at 60°C) in the Epoxy Embedding Medium Kit (Sigma-Aldrich, Sweden AB). The blocks were initially trimmed and sectioned using a Leica UC7 ultra microtome (Leica Microsystems GmbH, Vienna, Austria). Ultrathin sections (60 nm thickness) were collected onto formvar-coated copper slot grids, and counter-stained with uranyl acetate and lead citrate. Images were taken using a 100 kV transmission electron microscope (TEM, JEM 1230, JEOL Ltd., Tokyo, Japan). For each nerve, a panorama picture was created (x1,200) for orientation and quantification of myelinated fibers. For C-fiber quantification, 30 pictures

were randomly taken (each third window; x15,000), and fibers were counted and normalized against the area to obtain fiber density.

Immunohistochemistry

Sciatic nerves dissected 5 days after injury were fixed overnight with 4% PFA and cryoprotected in 25% (w/v) sucrose in DPBS. The tissue was embedded in OCT compound mounting medium (VWR, Cat. #361603E) and snap-frozen on dry ice using isopentane before sectioning with a Leica CM1900 cryostat. About 10 μm longitudinal sections were thawed at RT for 10 min and antigen retrieval was performed with Target Retrieval Solution (Dako, Cat. #S1699) for 30 min at 80°C. The sections were rinsed once in TBS (50 mM tris base and 150 mM NaCl, pH 7.4) and incubated in TBS containing 5% donkey serum and 0.3% Triton-X-100 to block the unspecific binding of antibodies. The sections were incubated with primary antibodies (**Table 1**) diluted in TBS containing 5% donkey serum overnight in a humidified chamber at 4°C. The following day, the sections were incubated for 4 h with secondary antibodies (**Table 1**) diluted in TBS containing 5% donkey serum and Hoechst 33258 was used for nuclear stain. The slides were mounted with Dako fluorescence mounting medium (Dako, Cat. #S3023), sealed with nail polish, and stored at 4°C.

Images were acquired with a Zeiss Axio Imager 2 microscope (Carl Zeiss, Germany) equipped with a Hamamatsu digital camera (ORCA-flash4.0 digital camera, model C11440-22CU, Hamamatsu Photonics Deutschland GmbH, Germany) and a Plan-Apochromat 20x/0.8 lens or the LSM 780 confocal microscope (Carl Zeiss) equipped with a 63x water-immersion objective or a 20x/0.8 M27 objective (Carl Zeiss). Subsequent image analysis was performed with ImageJ.

Immunocytochemistry

The Schwann cells were fixed for 10 min in 4% formaldehyde and permeabilized with DPBS containing 0.1% Triton-X-100 (PanReac Applichem, Cat. #A4975) 3 times for 10 min. Unspecific binding of antibodies was blocked by subsequent incubation in DPBS containing 5% donkey serum and 1% BSA (Sigma, Cat. #A8806). The cells were then incubated with primary antibodies (**Table 1**) diluted in DPBS and containing 1% BSA overnight at 4°C. The samples were left for 1 h at RT before being washed 3 times for 10 min in DPBS and then incubated for 4 h with the secondary antibodies (**Table 1**), diluted in 1% BSA. Hoechst 33258 was used for nuclear staining (1:10.000, Sigma). The sections were then mounted with Dako Fluorescent mounting medium (Dako, Cat. #S3023) and sealed with nail polish.

Western Blot Analysis

Sort1$^{-/-}$ and WT primary Schwann cells were lysed in ice-cold lysis buffer [10 mM Tris–HCl and 1 mM disodium EDTA, pH 8.0 (Sigma-Aldrich, Cat. #93283)] containing 1% IGEPAL (Sigma-Aldrich, Cat. #I8896), cOmplete Mini (Roche, Cat. # 4719956001), and PhosStop (Roche, 4906845001), incubated for 30 min on ice and frozen overnight at −20°C.

Naïve mice (day 0) or crush-injured mice were euthanized by decapitation after isoflurane gas-induced anesthesia at days 1, 7, or 25 post-injury (n = 3 animals per time point/group). The sciatic nerves were lysed in TNE buffer supplemented with protease (cOmplete Mini, Roche) and phosphatase inhibitors (PhosStop, Roche), after which a 10.000 g centrifugation for 10 min at 4°C was performed. The supernatant was stored at −20°C until use. A vacuum concentrator was used to increase protein concentration in the lysates, when necessary.

TABLE 1 | List of antibodies used.

Antibodies	Supplier, cat. no.	RRID	Dilution	Use
Mouse anti-βIII Tubulin	Promega, G7121	AB_430874	1:400	IF
Rabbit anti-Ki-67	Thermo Scientific, MA5-14520	AB_10979488	1:200	IF
Rabbit anti-S100β	Dako, Z0311	AB_10013383	1:400	IF/WB
Goat anti-sortilin	R&D Systems, AF2934	AB_2192424	1:100	IF
Donkey anti-rabbit IgG, Alexa Fluor 488	Invitrogen, A21206	AB_2535792	1:300	IF
Donkey anti-goat IgG, Alexa Fluor 488	Invitrogen, A11055	AB_2534102	1:300	IF
Donkey anti-sheep IgG, Alexa Fluor 488	Invitrogen, A11015	AB_141362	1:300	IF
Donkey anti-mouse IgG, Alexa Fluor 568	Invitrogen, A10037	AB_2534013	1:300	IF
Donkey anti-rabbit IgG, Alexa Fluor 647	Invitrogen, A31573	AB_2536183	1:300	IF
Mouse anti-β-Actin	Sigma, Cat. A5441	RRID:AB_476744	1:5,000	WB
Mouse anti-NTR3	BD Bioscience, 612100	AB_399471	1:1,000	WB
Rabbit anti-phospho-Akt (Ser473)	Cell signaling, 4060	AB_2315049	1:1,000	WB
Rabbit anti-phospho-p44/42 MAPK/ERK	Cell Signaling, 9101	AB_331646	1:1,000	WB
Rabbit anti-pRSK	Abcam, AB32413	AB_2181172	1:1,000	WB
Rabbit anti-pCREB	Cell Signaling, 9198	AB_2561044	1:1,000	WB
Rabbit anti-p75NTR	Abcam, 10494	AB_297233	1:1,000	WB
HRP swine anti-rabbit	Dako, P0217	AB_2728719	1:2,000	WB
HRP rabbit anti-mouse	Dako, P0260	AB_2636929	1:2,000	WB
HRP rabbit anti-goat	Dako, P0160	AB_2617143	1:200	WB
HRP rabbit anti-sheep	Dako, P0163		1:2,000	WB

Total protein concentration for both cell and tissue lysates was determined with the Bicinchoninic acid assay (Sigma, Cat. #BCA1-1KT). About 50 or 100 μg total protein was mixed with NuPAGE LDS sample buffer (Life Technologies, Cat. #NP0008) and a minimum of 10 mM dithioerythritol (DTE, AppliChem). The protein samples were separated on 4–12% Bis-Tris protein gels (Life technologies) in MOPS SDS running buffer (Thermo Fisher, Cat. #NP0001) containing NuPAGE Antioxidant (Invitrogen, Cat. #NP0005) and electroblotted with nitrocellulose iBlot Gel Transfer Stacks (Invitrogen, Cat. #IB301001) using the iBlot DryBlotting System (Invitrogen) according to manufactures guidelines. The membranes were subsequently blocked in TST buffer [50 mM Tris base, 500 mM NaCl, and 0.05% Tween-20 (PanReac Applichem, Cat. #A4974)] containing 2% skimmed milk powder and 2% Tween-20 and subsequently incubated with primary antibodies (**Table 1**), diluted in blocking buffer overnight at 4°C. The following day, the membranes were washed 3 times for 5 min in washing buffer (2 mM CaCl2, 1 mM MgCl2, 10 mM Hepes, and 140 mM NaCl) containing 0.2% skimmed milk powder and 0.05% Tween-20 and incubated for 1 h at RT with HRP conjugated secondary antibodies (**Table 1**). The membranes were then washed 3 times for 5 min and developed with Amersham ECL Prime Western Blotting Detection Reagent (GE Healthcare, Cat. #RPN2236). Fuji film LAS4000 was used for visualization and densitometry.

Viability Assay and Ki-67 Proliferation Assay

The viability of Schwann cells was assessed by seeding Schwann cells on poly-L lysine-coated coverslips (250.000 cells/ml) in DMEM containing 10% FBS, at 37°C and 5% CO_2. The following day, the medium was replaced with or without NT-3 (50 ng/ml, Sigma, Cat. #SRP3128). The viability assay was performed 24 h after stimulation, according to the manufacture's protocol (Live/Death Viability/Cytotoxicity Kit, Molecular Probes, Cat. #L3224). Calcein-positive (live) cells and ethidium homodimer-1 (dead) cells were counted and the percentage of live cells was calculated ($n = 4$ for each genotype).

The proliferation rate was assessed ($n = 3$ for each genotype) in parallel with the viability assay. The Schwann cells were fixed with 4% formaldehyde (Sigma, Cat. #158127) in Dulbecco's phosphate-buffered saline (DPBS, Sigma, Cat. #D8537) 48 h after stimulation, and immunostained with an antibody against Ki-67. The Ki-67 positive cells and total cells were counted using ImageJ and the percentage of Ki-67 positive cells was calculated.

Migration Assay

The scratch wound healing assay was used to examine the migration of *Sort1*$^{-/-}$ Schwann cells ($n = 3$ independent experiments). *Sort1*$^{-/-}$ or WT Schwann cells were seeded in an IncuCyte® 96 well ImageLock plate (Satorius, Cat. #4379) at 31,000 cells/cm^3 (10,000 cells/well) in Schwann cell growth media. The plate was incubated at RT for 20 min followed by incubation at 37°C. When the cells formed a confluent monolayer, the media was changed to starvation media (DMEM containing 2% B27 and 1% heat-inactivated FBS). The cells were starved for 18 h, after which a 700–800 μm scratch was induced using the 96-pin mechanical WoundMaker™ (Satorius, Cat. #4493). The media was replaced with either DMEM containing 2% B27, 1% FBS, 2.5 μM forskolin, and 10 ng/ml neuregulin-1 (negative control), DMEM containing 2% B27, 10% FBS, 2.5 μM forskolin, and 10 ng/ml neuregulin-1 (positive control), or DMEM containing 2% B27, 1% FBS, 2.5 μM forskolin, 10 ng/ml neuregulin-1, and 50 ng/ml of NT-3. The plates were then immediately placed in the IncuCyte Zoom Live-Cell Imaging System from Essen Bioscience and pictures were taken with the 10x objective every 3 h for 48 h. A cell mask was created and adjusted to fit the cell type after which the IncuCyte™ Scratch Wound Cell Migration Software Module (Essen BioScience) was used to calculate the Relative Wound Density (the Relative Wound Density is a measurement of the cell density in the wound area relative to the cell density in the non-wound area).

Schwann Cell-Dorsal Root Ganglia Neuron Co-cultures

Dorsal root ganglia (DRG) were dissected from neonatal WT rats on postnatal days 1–3 and dissociated with 0.25% trypsin for 30 min at 37°C before being seeded onto poly-L lysine and laminin (Sigma, Cat. #L2020)-coated coverslips. The DRG neurons were purified and maintained in the presence of NGF (100 ng/ml, Promega, Cat. #G514A) for 2 weeks with cycles of maintenance medium (MEM) (Sigma, Cat. #M2279) containing 10% FBS, Primocin (0.1 mg/ml), 0.4% glucose, and GlutaMAX (2 mM, Fisher Scientific, 35050-061), and anti-mitotic medium [DMEM containing Primocin (0.1 mg/ml), pyruvate (1 mM), rat transferrin (10 mg/L, Sigma, Cat. #SRP6513), progesterone (20 nM, Sigma, Cat. #P8783), putrescine (100 μM, Sigma, Cat. #P5780), insulin (5 mg/L, Sigma, Cat. #I6634) supplemented with FdU (10 μM, Sigma, Cat. #F0503), and uridine (10 μM, Sigma, Cat. #U3750)]. Purified *Sort1*$^{-/-}$ or WT Schwann cells were seeded onto the DRG neurons (100.000 cells/well) and allowed to proliferate for 1 week in a maintenance medium before the addition of ascorbic acid (50 μg/ml, Sigma, Cat. #A5960) to induce myelin formation, in the presence or absence of 50 ng/ml NT-3. The medium was changed every 2–3 days. The Schwann cell-DRG neuron co-cultures were fixed for 10 min with 4% formaldehyde in DPBS, 11 days after myelin induction. The cells were permeabilized and unspecific binding of antibodies was blocked with 0.3% Triton-X-100 and 10% FBS in DPBS for 1 h. Subsequently, the cells were incubated with mouse anti-Myelin Basic Protein (1:50, Sigma, Cat. #MAB381) and rabbit anti-neurofilament M (1:200, Millipore, Cat. #AB1987) overnight in a humified box at 4°C. The following day, the Schwann cells were washed 3 times for 10 min in DPBS before 4 h incubation at RT with Alexa Fluor 488 donkey anti-mouse IgG (1:300, Abcam, Cat. #AB150105) and Alexa Fluor 568 donkey anti-rabbit IgG (1:300, Abcam, Cat. #AB175470), diluted in blocking buffer, with Hoechst 33258 (1:10.000, Sigma) as a nuclear stain. The cells were washed and mounted with Fluorescent mounting medium (Dako), sealed with nail polish, and stored at 4°C until image acquisition with the LSM 780 laser scanning confocal microscope

(Carl Zeiss) equipped with a Plan-Apochromat 20x/0.8 lens objective (Carl Zeiss). The myelin segments were counted in ImageJ (n = 3 for each genotype, 6 images were acquired per coverslip for each experiment, and myelin segments per image averaged).

Statistical Analysis

Statistical comparison of data was accomplished using one-way or two-way ANOVA or multiple analysis and Bonferroni's or Bonferroni Holm's multiple comparisons *post hoc* test, with Graph Pad Prism software. Quantitative data are reported as mean ± SEM. Statistical significance was established for $^{*}p < 0.05$, $^{**}p < 0.01$, $^{***}p < 0.001$, and $^{****}p < 0.0001$.

RESULTS

Functional Parameters of Nerve Recovery After Sciatic Crush Injury Are Largely Unaffected in *Sort1*$^{-/-}$ Mice

The sciatic nerve crush model was chosen to investigate the role of sortilin on nerve regeneration. The crush injury model with the intact basal lamina, as opposed to a transection injury where the basal lamina is disrupted, provides a system to test if sortilin enhances or inhibits peripheral nerve regeneration without variables imposed by transection injuries [reviewed in Griffin et al. (2010)]. We have previously described the impact of sortilin on neuropathic pain (Richner et al., 2019), and herein, we focus on functional and morphometric analysis of the injured nerve. The overall functional recovery was evaluated over 60 days by the sciatic functional index (SFI), which is a metric tool to evaluate sciatic nerve function (Inserra et al., 1998). We found that at day 7 post-injury, there was a maximum reduction for WT mice, with a steady recovery over the next few weeks until reaching baseline level from day 25. Although *Sort1*$^{-/-}$ mice displayed a similar overall pattern, the SFI values were significantly reduced on days 25 and 60, relative to both WT and pre-injury baseline (**Figure 1A**). Next, the recovery was further examined by measuring the dynamic gait parameters (Mendes et al., 2015). Parameters such as stride and step length did not reveal any major altered patterns or endpoints between the genotypes (**Figures 1B–D**). However, the step width was significantly higher at the endpoint in WT as compared to the Sort1$^{-/-}$ mice (**Figure 1E**). The paw angle is the angle between the paw axis and the midline of the mouse body during movement and it can be affected by abnormalities of the muscles controlling the paw or the innervating nerves. We correspondingly observed increased paw angle 3 days after injury, which corroborates loss of motor and sensory nerve muscle innervation, but with no significant differences detected between the two genotypes (**Figure 1F**). Muscle strength was evaluated by the grip strength test at pre-injury baseline (day 0) and at different time intervals up to 60 days after nerve crush, with a recovery pattern for *Sort1*$^{-/-}$ mice indistinguishable from that of WT mice (**Figure 1G**).

Due to the reduced SFI recovery in *Sort1*$^{-/-}$ mice (**Figure 1A**), we finally assessed the nerve electrophysiological properties by measuring the motor and sensory nerve conduction velocities (MNCV and SNCV, respectively) at the terminal endpoint day 60. As expected, the injured WT mice displayed a significant reduction in both SNCV and MNCV as compared with pre-injury (**Figure 1H**). The corresponding parameters for *Sort1*$^{-/-}$ mice were identical to those of WT mice at both naïve or injury conditions (**Figure 1H**).

Abnormal Ensheathment of C-Fibers After Crush Injury in *Sort1*$^{-/-}$ Mice

Histological examination using electron microscopy analysis of the sciatic nerve transverse sections demonstrated overall normal histology of the sciatic nerve in naïve *Sort1*$^{-/-}$ mice (**Figure 2**). The endoneurium was occupied by myelinated fibers with different caliber sizes (**Figure 2A**) and unmyelinated axons (C-fibers) that appeared in large groups entailed by Schwann cell cytoplasm, forming Remak bundles (**Figure 2B**). No difference in myelinated or C-fiber densities was observed between *Sort1*$^{-/-}$ and WT sciatic nerve in naïve conditions (**Figures 2A,B**), per previous studies (Jansen et al., 2007; Vaegter et al., 2011). As expected, pathology was prominent in the injured tissue of WT mice 25 days after injury. Accordingly, axonal degeneration of myelinated axons and removal or degradation of myelin by Schwann cells was evident. These parameters were indistinguishable between the genotypes (**Figures 2A,B**), as were the levels of total fat droplets (**Figure 2C**), indicating that the *Sort1*$^{-/-}$ status did not affect lipid degeneration or reutilization after nerve crush. The densities of myelinated axons (**Figure 2A**) and C-fibers (**Figure 2B**), 25 days after injury were also identical between *Sort1*$^{-/-}$ and WT mice.

For both genotypes, we observed that C-fibers appeared in lower average numbers in the Remak bundles on the injured side as compared to the contralateral sham sciatic nerve (**Figure 2B**, bottom chart), with extensive Schwann cell cytoplasmic branches spreading throughout the endoneurium. Nonetheless, a prominent feature of the *Sort1*$^{-/-}$ mice entailed a more than twofold increase in the number of C-fibers only partially enclosed by Schwann cell cytoplasm with areas where the C-fiber was naked and not engulfed by the basement membrane (**Figures 3A,B**), demonstrating a potentially important role for sortilin in the Remak bundle formation following injury.

Neurotrophin-3 Signaling Is Decreased in *Sort1*$^{-/-}$ Primary Schwann Cells

The sortilin expression was confirmed by immunohistochemistry in Schwann cells of naïve WT murine sciatic nerves co-localizing with the Schwann cell marker S100β (**Figure 4A**). Furthermore, the sciatic crush injury resulted in considerably increased sortilin immunoreactivity in Schwann cells at 5 days post-injury (**Figure 4B**). These *in vivo* observations prompted us to investigate the potential involvement of sortilin on Schwann cell neurotrophin signaling using primary cell cultures. Immunofluorescence (**Figure 5A**) and WB

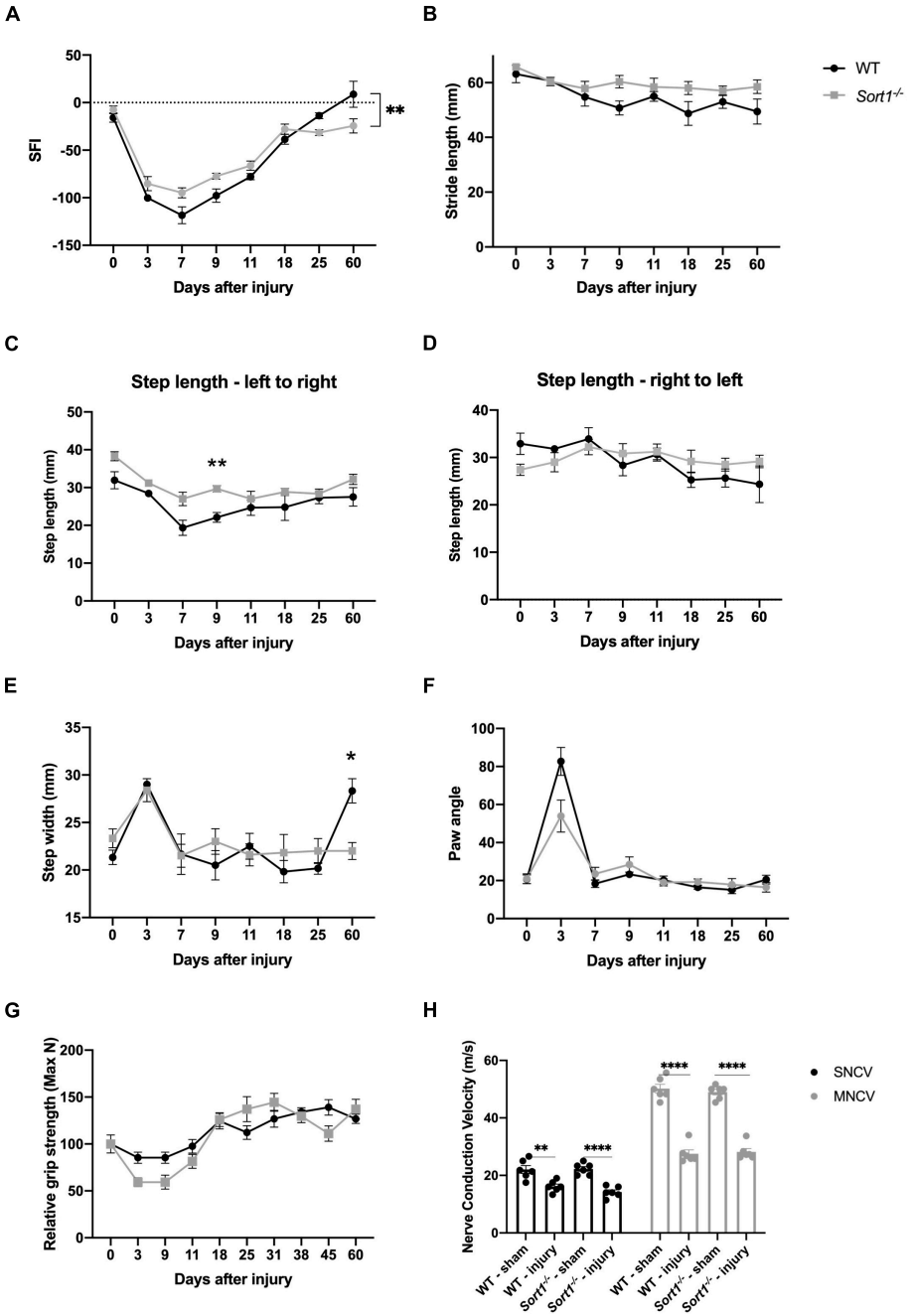

FIGURE 1 | Motor recovery after sciatic nerve crush injury. Motor function recovery of WT and *Sort1*$^{-/-}$ mice assessed by walking tract analysis and calculation of **(A)** SFI, **(B)** stride length, **(C,D)** step length, **(E)** step width, and **(F)** angle of paw placement to the midline, assessed at pre-treatment (time = 0), 3, 7, 9, 11, 18, 25, and 60 days after nerve crush injury. **(G)** Grip strength was additionally assessed at pre-treatment (time = 0), 3, 9, 11, 18, 25, 31, 38, 45, and 60 days after nerve crush injury. **(H)** Nerve conduction velocity analysis of sural (sensory; SNCV) and sciatic (motor; MNCV) nerves 60 days after injury on the ipsilateral and contralateral (sham) side. *N* = 6 WT mice or 6 *Sort1*$^{-/-}$ mice. Statistical significance was established with multiple measures test **(A–G)** or two-way ANOVA **(H)** and Bonferroni's multiple comparisons *post hoc* test (*$p < 0.05$, **$p < 0.01$, ****$p < 0.0001$).

analysis (**Figure 5B**) confirmed sortilin expression in cultured WT Schwann cells with no detectable sortilin in *Sort1*$^{-/-}$ Schwann cells. Quantification of viability and proliferation, as addressed by the live and death assay (**Figure 5C**) and the Ki67-positive cell percentages (**Figure 5D**), respectively, were indistinguishable between WT and *Sort1*$^{-/-}$ Schwann cells, indicating that *Sort1* expression is not essential for Schwann cell proliferation or viability.

We have previously demonstrated the involvement of sortilin in neurotrophin signaling in dorsal root ganglia neurons

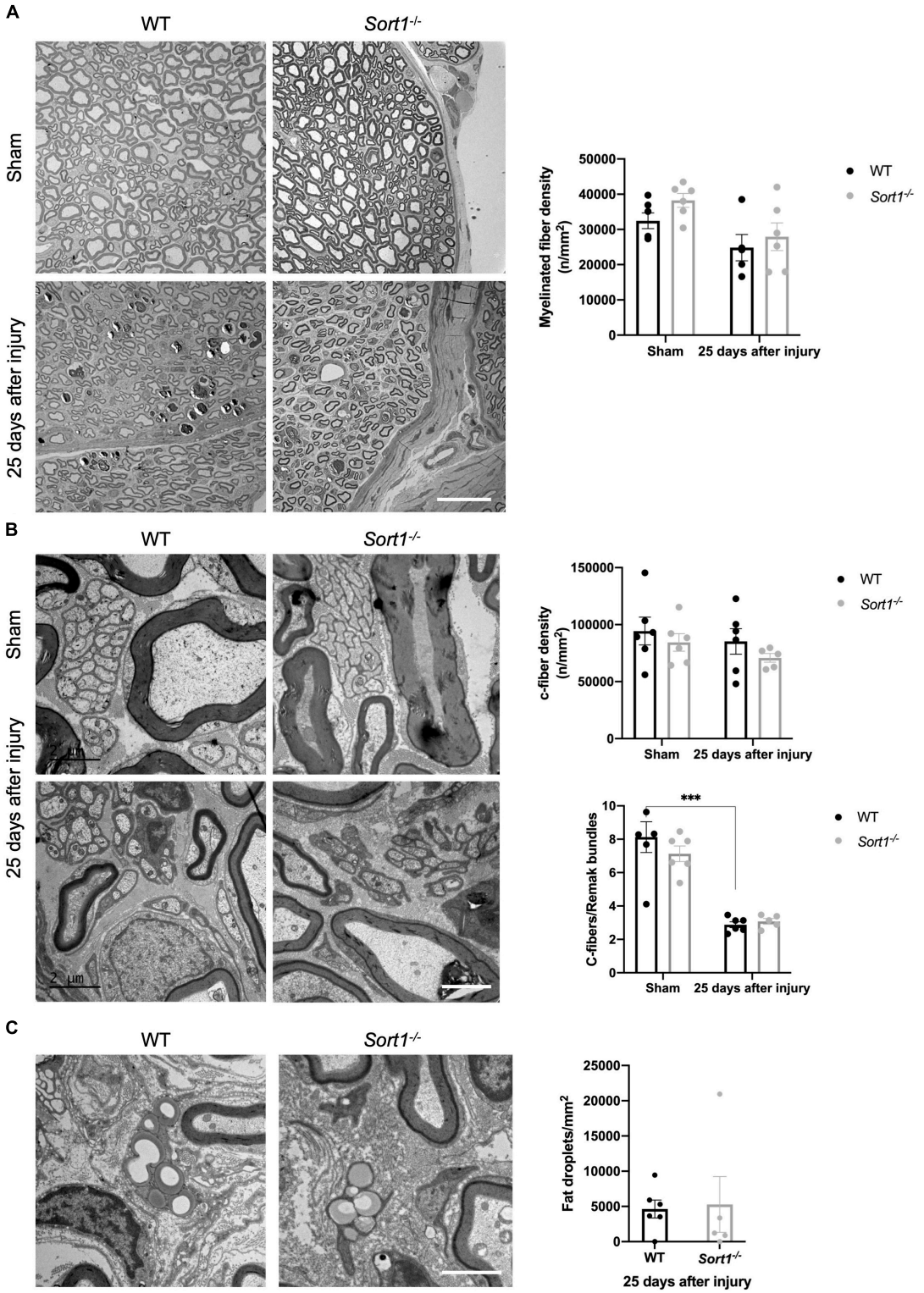

FIGURE 2 | Morphological and morphometrical analysis of crush-injured *Sort1*$^{-/-}$ sciatic nerve. **(A)** Myelinated and **(B)** C-fiber densities were similar between *Sort1*$^{-/-}$ mice and WT mice in the contralateral (sham) and 25 days after sciatic nerve crush injury. Representative EM images of thin transverse sections of sham contralateral or the distal stumps of crush-injured sciatic nerves 25 days after injury [scale bar **(A)**: 20 μm; **(B)**: 2 μm]. Bottom graph in panel **(B)** shows the average number of C-fibers/Remak bundle, which were significantly lower (***$p < 0.001$) in both crush-injured WT and *Sort1*$^{-/-}$ sciatic nerve compared to the contralateral sham control. **(C)** Representative images of fat droplets in thin transverse sections of injured WT or *Sort1*$^{-/-}$ sciatic nerve 25 days after sciatic nerve crush injury. The total number of fat droplets/mm^2 were similar between WT and *Sort1*$^{-/-}$.

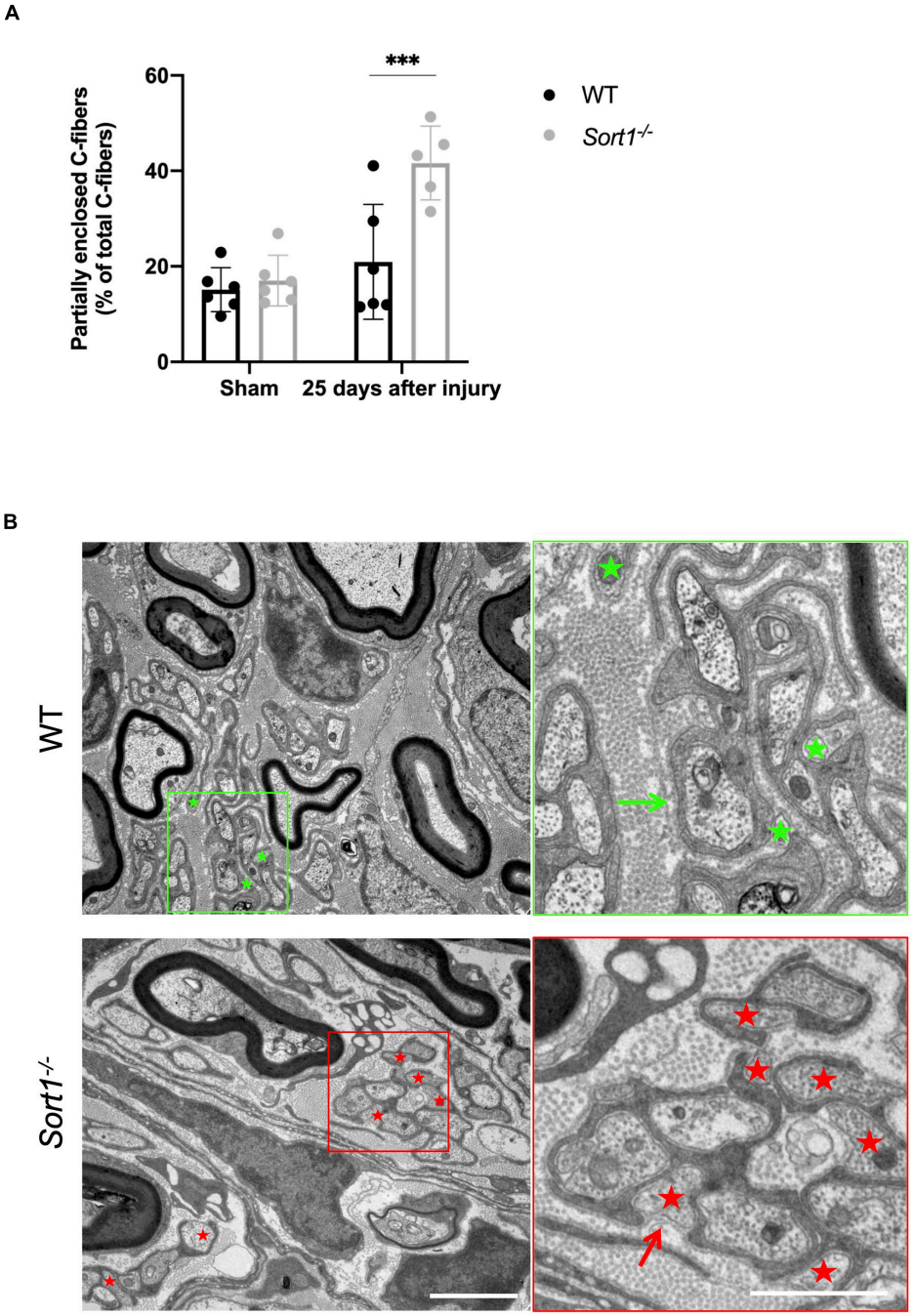

FIGURE 3 | Reduced axon ensheathment by Remak Schwann cells in regenerated *Sort1*$^{-/-}$ sciatic nerve. Significantly more partially enclosed C-fibers were observed in the injured *Sort1*$^{-/-}$ sciatic nerve compared to WT. Representative images showing normal Schwann cell ensheathment of C-fibers in injured WT sciatic nerve 25 days after crush injury (indicated by the green arrow) and only partly enclosure of C-fibers by Schwann cell cytoplasm and partly by only basement membrane 25 days after sciatic nerve crush injury in WT (green stars) and the *Sort1*$^{-/-}$ mouse (indicated by red stars and red arrows). Scale bars: left images 2 μm, right images (zoom of left) 1 μm. **(A,B)** *N* = 6 WT mice and 6 *Sort1*$^{-/-}$ mice. Statistical significance was established with two-way ANOVA and Bonferroni's multiple comparisons *post hoc* test (***$p < 0.001$).

(Vaegter et al., 2011). To further examine such a role in Schwann cells, primary WT and *Sort1*$^{-/-}$ cultures were stimulated with either BDNF or NT-3. Using WB analysis, we found that NT-3 stimulation significantly increased the pAKT, pMAPK/ERK, pRSK, and pCREB protein levels in WT Schwann cells (**Figure 6A**). In contrast, BDNF did not activate these pathways, confirming previous reports that Schwann cells do not express the full-length catalytically active form of the BDNF neurotrophin

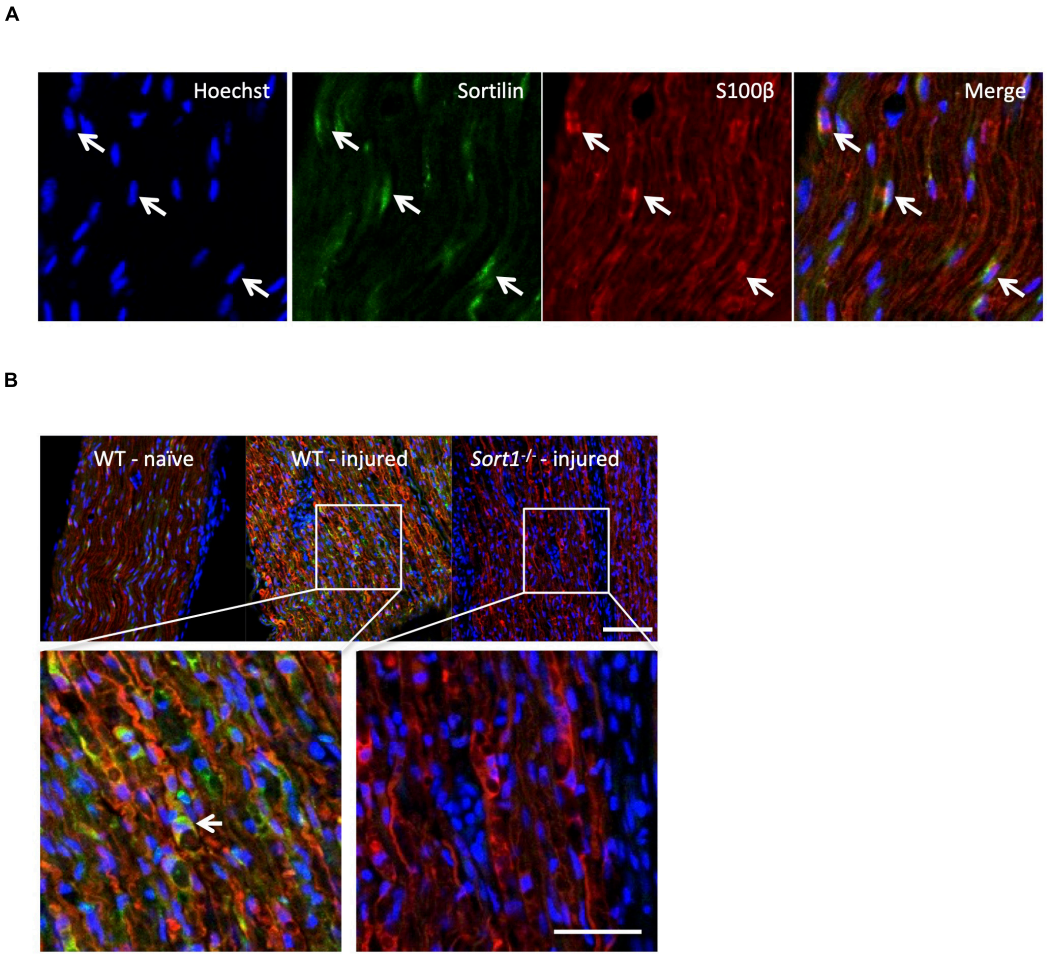

FIGURE 4 | Schwann cells of the sciatic nerve express sortilin. **(A)** Double-labeled immunofluorescence microscopy of sortilin (green) and s100β (red) in longitudinal sections of wild-type (WT) naïve sciatic nerve. Nuclei are labeled with Hoechst (blue). White arrows demonstrate Schwann cells expressing sortilin. Scale bar 50 μm. **(B)** Double-label immunofluorescence microscopy of sortilin (green) and s100β (red; Schwann cell marker) in longitudinal sections of naïve sciatic nerves and 5 days after crush injury in WT and *Sort1*$^{-/-}$ distal sciatic nerves. Nuclei are labeled with Hoechst (blue). The white arrow points to a sortilin-positive (green) s100β-positive (red) WT Schwann cell. Scale bar 100 μm upper images and 50 μm lower images.

receptor TrkB (Funakoshi et al., 1993). Interestingly, relative to WT, NT-3 stimulation of *Sort1*$^{-/-}$ Schwann cells significantly reduced the pMAPK/ERK response by 47 ± 10%, while the downstream mediators, pRSK and pCREB, were significantly reduced by 45 ± 15 and 35 ± 9%, respectively (**Figure 6A**). As NT-3 has been reported to facilitate Schwann cell migration (Yamauchi et al., 2003, 2005a), we compared WT and *Sort1*$^{-/-}$ Schwann cell migration in the scratch wound healing assay but observed similar migration rates between the two groups of primary Schwann cells (**Figure 6B**). NT-3 is furthermore described to inhibit myelination (Chan et al., 2001) and we compared the performance of WT and *Sort1*$^{-/-}$ Schwann cells in their ability to myelinate segments of WT dorsal root ganglia neurons in an *in vitro* co-culture system. While we obtained a similar degree of myelination for both genotypes in the absence of NT-3, we were also unable to confirm an inhibitory effect of NT-3 on myelination in either genotype but rather observed a (non-significant) trend toward a stimulatory effect (**Figure 6C**).

In conclusion, sortilin ablation in cultured primary Schwann cells reduced the activation of NT-3 stimulated intracellular signaling pathways. Surprisingly, we did not observe any NT-3-dependent cellular responses in either genotype on *in vitro* characteristics of proliferation, survival, migration, or myelination.

DISCUSSION

Sortilin facilitates neurotrophin signaling in DRG neurons by anterograde trafficking of Trk receptors and even though sortilin ablation does not seem to affect the development of the PNS (Jansen et al., 2007; Vaegter et al., 2011), a role of sortilin in nerve regeneration following, e.g., a crush injury, has not been studied. Here, we demonstrate that while nerve regeneration appears to be functionally normal following sciatic nerve crush in *Sort1*$^{-/-}$ mice, neuroanatomical examination

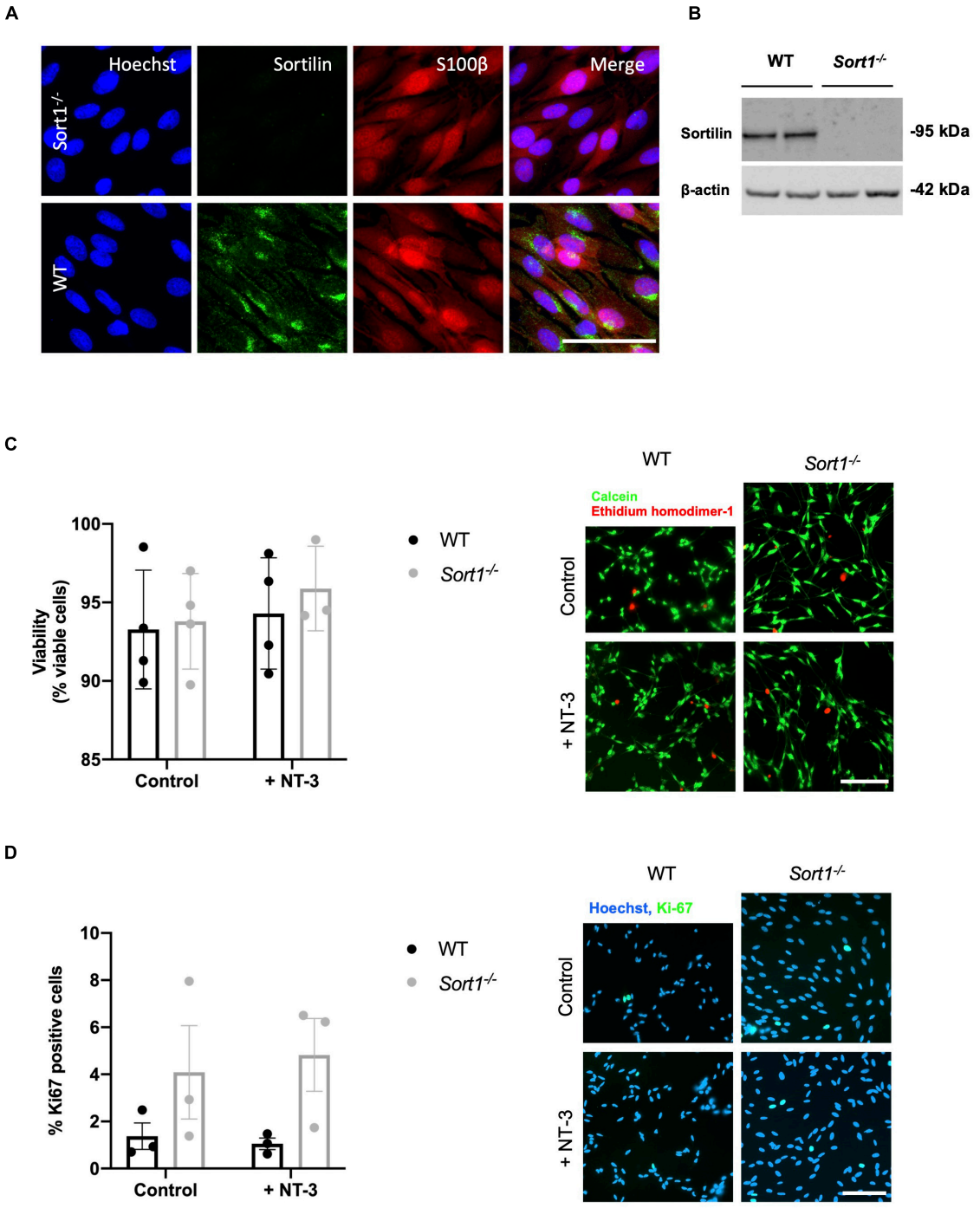

FIGURE 5 | Primary cultured Schwann cells express sortilin. **(A)** Double-labeled immunofluorescence microscopy of primary cultured Schwann cells show sortilin (green) in wild-type (WT) Schwann cells (red; identified by the Schwann cell marker s100β), but not in cells derived from *Sort1*$^{-/-}$ rat sciatic nerves. Nuclei are labeled with Hoechst (blue). Scale bar 50 μm. **(B)** Immunoblot analysis of sortilin in lysates of WT or *Sort1*$^{-/-}$ primary Schwann cells shows sortilin expression in WT. **(C)** The viability of *Sort1*$^{-/-}$ Schwann cells is like WT Schwann cells with (95.89 ± 1.55% vs. 94.30 ± 1.77%, $p > 0.99$) or without NT-3 stimulation (93.8 ± 1.52% vs. 93.29 ± 1.89%, $p > 0.99$). Viable cells were identified in Schwann cell cultures 24 h after stimulation with or without NT-3 by calcein (green) fluorescence, while dead cells were identified by ethidium homodimer-1 (red) fluorescence. Scale bar 100 μm. Viability reflects mean% calcein-positive cells ± SEM, $n = 4$. **(D)** Schwann cell proliferation (percentage of Ki-67% cells) was not significantly different in cultures of *Sort1*$^{-/-}$ Schwann cells compared to WT Schwann cell cultures with (4.82 ± 1.54% vs. 1.05 ± 0.25%, $p = 0.4381$) or without NT-3 stimulation (4.09 ± 1.98% vs. 1.37 ± 0.56%, $p > 0.99$). The proliferation marker, Ki-67 (green), was identified by immunofluorescence in Schwann cell cultures 48 h after stimulation with or without NT-3. Nuclei are labeled with Hoechst (blue). Scale bar 100 μm. Proliferation rates reflect% Ki-67 positive cells ± S.E.M., $n = 3$. Statistical significance was analyzed using two-way ANOVA with Bonferroni's multiple comparisons *post hoc* test.

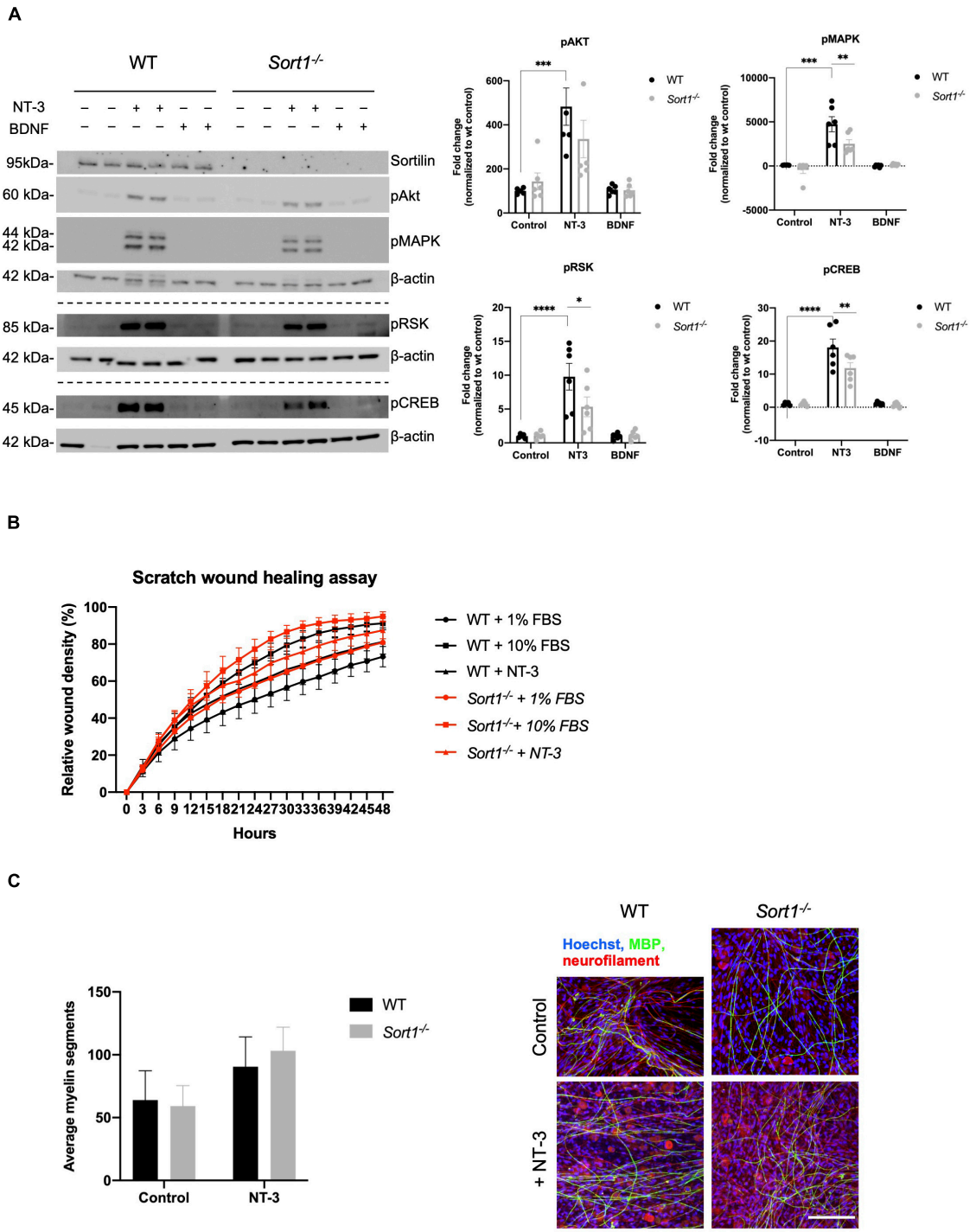

FIGURE 6 | Neurotrophin signaling is decreased in *Sort1*$^{-/-}$ Schwann cells. **(A)** pAkt, pMAPK, pRSK, and pCREB were quantified by densitometry of immunoblots from lysates of NT-3 or BDNF stimulated wild-type (WT) or *Sort1*$^{-/-}$ primary cultures of Schwann cells and normalized against β-actin. pMAPK, pRSK, and pCREB levels are significantly lower in *Sort1*$^{-/-}$ Schwann cells compared to WT Schwann cells. Data represent the mean ± SEM for $n = 3$. **(B)** The relative wound healing closure time was similar in *Sort1*$^{-/-}$ Schwann cells relative to WT Schwann cells with or without 10% FBS (positive control) or NT-3. Furthermore, the relative wound healing closure time indicates that NT-3 does not increase the relative wound healing closure time significantly in WT Schwann cells compared to unstimulated controls; 10% FBS significantly increased the relative wound healing closure time at 27–39 h (*$p < 0.05$). **(C)** *Sort1*$^{-/-}$ Schwann cells showed similar myelin formation relative to WT Schwann cells. Co-cultures of DRG neurons and Schwann cells were fixed 11 days after myelin induction with or without NT-3 stimulation. The myelin segments were identified with an antibody against myelin basic protein (MBP; green) and the neurites were identified with antibodies against neurofilament (red). Hoechst identifies nuclei (blue). Statistical significance was determined by two-way ANOVA with Bonferroni's multiple comparisons *post hoc* test. Data represents mean ± SEM, $n = 3$ (*$p < 0.05$, **$p < 0.005$, ***$p < 0.001$, ****$p < 0.0001$).

revealed abnormal structural regeneration demonstrated by the impaired embracing of C-fibers by the Remak Schwann cells. *In vitro* studies further demonstrated a decreased signaling response to NT-3 in primary cultures of *Sort1*$^{-/-}$ Schwann cells, with blunted activation (phosphorylation) of MAPK/ERK, RSK, and CREB. Naïve *Sort1*$^{-/-}$ mice display a normal response to acute mechanical and thermal stimuli (Vaegter et al., 2011), but the sensory phenotype of *Sort1*$^{-/-}$ mice is affected by changes in spinal plasticity (Richner et al., 2019). Consequently, a further investigation of a peripheral sensory recovery after nerve crush would likely be concealed by the spinal phenotype of *Sort1*$^{-/-}$ mice and was therefore not addressed in this study.

Schwann cells are remarkably plastic cells, with their Remak or myelin phenotypes highly depending on signals derived from the cellular environment. Furthermore, upon nerve injury and the conversion to a dedifferentiated/repaired Schwann cell type, it seems that the subsequent redifferentiation to a Remak or myelinating phenotype is independent of their prior identity. The MAPK/ERK pathway has a central role in these processes being required for processes in Wallerian degeneration and the subsequent Schwann cell differentiation and remyelination (Harrisingh et al., 2004; Napoli et al., 2012). Different levels or duration of MAPK/ERK activity may, however, elicit distinct responses. An example of this is a study by Cervellini et al. (2017), utilizing a mouse model with sustained MAPK/ERK activation in adult Schwann cells. Following crush injury, post-injury myelin clearance was accelerated while a delay in repair and functional recovery was observed. At 4 weeks following injury, myelinated axons in the transgenic mice demonstrated higher rates of myelin decompaction, a reduced number of Cajal bands, and decreased internodal length. Furthermore, the authors reported the presence of abnormal Remak bundle formations and a reduced number of C-fibers per Remak bundle in the regenerated nerve (Cervellini et al., 2017).

The neurotrophins NGF, BDNF, NT-3, and NT-4 are potent activators of the MAPK/ERK pathway *via* their cognate Trk tyrosine kinase receptors, and their effects on PNS development and signaling have been extensively studied (Chao, 2003; Reichardt, 2006). Schwann cells express TrkC, allowing for NT-3-mediated activation of downstream MAKP/ERK and AKT signaling pathways. They further express a truncated form of TrkB lacking the intracellular tyrosine kinase domain, rendering BDNF/TrkB unable to activate these same pathways. However, BDNF appears to induce signaling in these cells *via* the common neurotrophin receptor p75^{NTR}, activating downstream pathways distinct from those of TrkB (Cosgaya et al., 2002; Skeldal et al., 2011). *In vitro* studies have described how NT-3 enhances Schwann cell migration and proliferation (Yamauchi et al., 2003, 2004, 2005a,b), while inhibiting myelin formation in co-cultures of DRG neurons and Schwann cells (Chan et al., 2001; Ng et al., 2007). This is consistent with other reports of the MAPK/ERK pathway involvement in these events. Accordingly, stimulation of the MAPK/ERK pathways facilitated *in vitro* Schwann cell migration while application of MAPK/ERK inhibitor impaired migration (Meintanis et al., 2001). Inhibition of this pathway was also found to block Schwann cell proliferation *via* inhibition of cyclin/cdk activity (Lloyd et al., 1997). Intriguingly, while we observed robust MAPK/ERK activation in NT-3 stimulated cultures, we were unable to detect any effect on WT Schwann cell migration as well as on their rate of proliferation. However, our data seem consistent with a study by Woolley et al. (2008) examining NT-3-deficient mice. These authors found that ablation of NT-3 expression did not affect developmental myelination in terms of timing or structural features. Furthermore, from postnatal day 21 when myelination was complete, a reduction in MAG and P0 expression levels and myelin thickness were observed (Woolley et al., 2008), seemingly contradicting predictions based on *in vitro* studies that removal of an inhibitory NT-3 signal would have been expected to enhance myelination. Further support for a myelin-promoting role of NT-3 came from a study on NT-3 heterozygote mice subjected to a nerve crush injury, where reduced NT-3 expression was found to decrease myelination of regenerating axons (Sahenk et al., 2008). Graft implantation studies indicated that Schwann cell-secreted NT-3 is necessary for post-injury remyelination, apparently acting *via* an autocrine-signaling loop (Meier et al., 1999; Sahenk et al., 2008). In terms of Remak Schwann cells, NT-3/TrkC also seems to play a substantial role. Accordingly, it was found that the administration of activating anti-TrkC antibodies to a nerve crush model in trembler mice increased the presence of Remak fibers, as well as increased functional recovery measured by grip strength but with no impact on NCV (Sahenk et al., 2010). In another injury study, acellular nerve grafts populated with Schwann cells genetically modified to express NT-3 resulted in the presence of twice as many Remak bundles compared to grafts populated with WT Schwann cell controls, although a reduction in the number of axons per bundle was also found (Godinho et al., 2012). These latter studies point toward a stimulatory role of NT-3/TrkC on the regeneration of Remak bundles, which is consistent with our data presented here that loss of sortilin blunts NT-3 signaling in Schwann cells and impairs Remak bundle regeneration. Interestingly, we have previously described an effect of sortilin on the structural integrity of Remak bundles. Combined deletion of sortilin and p75^{NTR} (*Sort1*$^{-/-}$; *Ngfr*$^{-/-}$) displayed normal Remak bundle development at postnatal day 15 but later these structures underwent a marked degeneration. The mice with deletion of either receptor alone did not present any spontaneous Remak degenerative phenotype (Vaegter et al., 2011). It, therefore, seems that neurotrophin signaling in the PNS is governed by a rather robust system with significant buffer capacity as the system can be pressured without developmental consequences. This is further illustrated by the normal structural development of peripheral nerves in the mice heterozygous for TrkA, -B or -C (Klein et al., 1993; Ernfors et al., 1994b,a; Minichiello et al., 1995), or p75^{NTR} (Lee et al., 1992). The biological role of sortilin in neurotrophin signaling needs to be unmasked in situations where the system is closer to its limit, as exemplified here by nerve crush or in our previous study by p75^{NTR} deletion (Vaegter et al., 2011), both affecting the Remak bundle structure. The latter study further identified severe sympathetic neuropathy upon sortilin deletion in the TrkA heterozygous mice.

NT-3/TrkC stimulation as well as the temporal activation and intensity of MAPK/ERK activation seems essential to facilitate the regenerative process in terms of remyelination and formation of Remak bundles. Here, we describe how sortilin immunoreactivity is increased in the nerve shortly after injury and how sortilin ablation results in Remak pathology. The observation of blunted NT-3 signaling response in cultured *Sort1*$^{-/-}$ Schwann cells supports a function of sortilin in regulating NT-3 signaling in Remak Schwann cells following nerve injury.

DATA AVAILABILITY STATEMENT

The raw data supporting the conclusions of this article will be made available by the authors, without undue reservation.

ETHICS STATEMENT

The animal study was reviewed and approved by Danish Animal Experiments Inspectorate under the Ministry of Justice (permission no. 2017-15-0201-01192).

AUTHOR CONTRIBUTIONS

MU, NG, and CV designed the experiments and wrote the manuscript. MU, NG, SMoh, SH, TL, and NM performed the experiments. MU, NG, SMoh, SH, SMol, OA, ÅS, SG, AN, and CV interpreted the results, and contributed with reagents, materials, and analysis tools. All authors contributed to the article and approved the submitted version.

FUNDING

This study was funded by the Lundbeck Foundation R313-2019-606 (CV), Aarhus University Research Foundation AUFF-E-015-FLS-8-4 (CV), Aase and Ejnar Danielsens Fond (CV), and Dagmar Marshalls Fond (CV and NG), The Lundbeck Foundation R248-2017-431 (AN), DANDRITE-R248-2016-2518 (AN), and R90-2011-7723 (AN), and The Independent Research Fund Denmark DFF-7016-00261 (AN).

ACKNOWLEDGMENTS

We would like to thank Maria Ntzouni at the EM lab of Core Facility at the Faculty of Medicine and Health Sciences, Linköping University, Sweden, for electron microscopy sample preparation. We would also like to thank technicians, Marianne Lundsgaard and Sandra Bonnesen, for technical assistance. We would also further like to thank Anne Kathrine Sørensen for guidance on the catwalk assay.

REFERENCES

Cervellini, I., Galino, J., Zhu, N., Allen, S., Birchmeier, C., and Bennett, D. L. (2017). Sustained MAPK/ERK activation in adult Schwann cells impairs nerve repair. *J. Neurosci.* 38, 2255–2217. doi: 10.1523/jneurosci.2255-17.2017

Chan, J. R., Cosgaya, J. M., Wu, Y. J., and Shooter, E. M. (2001). Neurotrophins are key mediators of the myelination program in the peripheral nervous system. *Proc. Natl. Acad. Sci. U.S.A.* 98, 14661–14668. doi: 10.1073/pnas.251543398

Chao, M. V. (2003). Neurotrophins and their receptors: a convergence point for many signalling pathways. *Nat. Rev. Neurosci.* 4, 299–309. doi: 10.1038/nrn1078

Cosgaya, J. M., Chan, J. R., and Shooter, E. M. (2002). The neurotrophin receptor p75NTR as a positive modulator of myelination. *Science* 298, 1245–1248. doi: 10.1126/science.1076595

Ernfors, P., Lee, K.-F., and Jaenisch, R. (1994b). Mice lacking brain-derived neurotrophic factor develop with sensory deficits. *Nature* 368, 147–150. doi: 10.1038/368147a0

Ernfors, P., Lee, K. F., Kucera, J., and Jaenisch, R. (1994a). Lack of neurotrophin-3 leads to deficiencies in the peripheral nervous system and loss of limb proprioceptive afferents. *Cell* 77, 503–512. doi: 10.1016/0092-8674(94)90213-5

Funakoshi, H., Frisén, J., Barbany, G., Timmusk, T., Zachrisson, O., Verge, V. M., et al. (1993). Differential expression of mRNAs for neurotrophins and their receptors after axotomy of the sciatic nerve. *J. Cell Biol.* 123, 455–465. doi: 10.1083/jcb.123.2.455

Gaudet, A. D., Popovich, P. G., and Ramer, M. S. (2011). Wallerian degeneration: gaining perspective on inflammatory events after peripheral nerve injury. *J. Neuroinflamm.* 8:110. doi: 10.1186/1742-2094-8-110

Godinho, M. J., Teh, L., Pollett, M. A., Goodman, D., Hodgetts, S. I., Sweetman, I., et al. (2012). Immunohistochemical, Ultrastructural and Functional Analysis of Axonal Regeneration through Peripheral Nerve Grafts Containing Schwann Cells Expressing BDNF, CNTF or NT3. *PLoS One* 8:e69987. doi: 10.1371/journal.pone.0069987

Gonçalves, N. P., Yan, Y., Ulrichsen, M., Venø, M. T., Poulsen, E. T., Enghild, J. J., et al. (2020). Modulation of Small RNA Signatures in Schwann-Cell-Derived Extracellular Vesicles by the p75 Neurotrophin Receptor and Sortilin. *Biomedicines* 8:450. doi: 10.3390/biomedicines8110450

Griffin, J. W., Pan, B., Polley, M. A., Hoffman, P. N., and Farah, M. H. (2010). Measuring nerve regeneration in the mouse. *Exp. Neurol.* 223, 60–71. doi: 10.1016/j.expneurol.2009.12.033

Harrisingh, M. C., Perez-Nadales, E., Parkinson, D. B., Malcolm, D. S., Mudge, A. W., and Lloyd, A. C. (2004). The Ras/Raf/ERK signalling pathway drives Schwann cell dedifferentiation. *EMBO J.* 23, 3061–3071. doi: 10.1038/sj.emboj.7600309

Inserra, M. M., Bloch, D. A., and Terris, D. J. (1998). Functional indices for sciatic, peroneal, and posterior tibial nerve lesions in the mouse. *Microsurgery* 18, 119–124. doi: 10.1002/(sici)1098-2752199818:2<119::aid-micr10<3.0.co;2-0

Jansen, P., Giehl, K., Nyengaard, J. R., Teng, K., Lioubinski, O., Sjoegaard, S. S., et al. (2007). Roles for the pro-neurotrophin receptor sortilin in neuronal development, aging and brain injury. *Nat. Neurosci.* 10, 1449–1457. doi: 10.1038/nn2000

Jessen, K. R., and Arthur-Farraj, P. (2019). Repair Schwann cell update: adaptive reprogramming, EMT, and stemness in regenerating nerves. *Glia* 67, 421–437. doi: 10.1002/glia.23532

Jessen, K. R., and Mirsky, R. (2002). Signals that determine Schwann cell identity*. *J. Anat.* 200, 367–376. doi: 10.1046/j.1469-7580.2002.00046.x

Jessen, K. R., and Mirsky, R. (2019). The Success and Failure of the Schwann Cell Response to Nerve Injury. *Front. Cell. Neurosci.* 13:16. doi: 10.3389/fncel.2019.00033

Jessen, K. R., and Mirsky, R. (2022). The Role of c-Jun and Autocrine Signaling Loops in the Control of Repair Schwann Cells and Regeneration. *Front. Cell. Neurosci.* 15:820216. doi: 10.3389/fncel.2021.820216

Kim, H. A., and Maurel, P. (2009). "Primary Schwann Cell Cultures" in *Protocols for Neural Cell Culture*, Fourth Edition. Ed. L. Doering. (Berlin: Springer Protocols Handbooks). 253–268. doi: 10.1007/978-1-60761-292-6_15

Klein, R., Smeyne, R. J., Wurst, W., Long, L. K., Auerbach, B. A., Joyner, A. L., et al. (1993). Targeted disruption of the trkB neurotrophin receptor gene results in nervous system lesions and neonatal death. *Cell* 75, 113–122.

Lee, K. F., Li, E., Huber, L. J., Landis, S. C., Sharpe, A. H., Chao, M. V., et al. (1992). Targeted mutation of the gene encoding the low affinity NGF receptor p75 leads to deficits in the peripheral sensory nervous system. *Cell* 69, 737–749. doi: 10.1016/0092-8674(92)90286-l

Lloyd, A. C., Obermüller, F., Staddon, S., Barth, C. F., McMahon, M., and Land, H. (1997). Cooperating oncogenes converge to regulate cyclin/cdk complexes. *Gene Dev.* 11, 663–677. doi: 10.1101/gad.11.5.663

Meier, C., Parmantier, E., Brennan, A., Mirsky, R., and Jessen, K. R. (1999). Developing Schwann Cells Acquire the Ability to Survive without Axons by Establishing an Autocrine Circuit Involving Insulin-Like Growth Factor, Neurotrophin-3, and Platelet-Derived Growth Factor-BB. *J. Neurosci.* 19, 3847–3859. doi: 10.1523/jneurosci.19-10-03847.1999

Meintanis, S., Thomaidou, D., Jessen, K. R., Mirsky, R., and Matsas, R. (2001). The neuron–glia signal β−neuregulin promotes Schwann cell motility via the MAPK pathway. *Glia* 34, 39–51. doi: 10.1002/glia.1038

Mendes, C. S., Bartos, I., Márka, Z., Akay, T., Márka, S., and Mann, R. S. (2015). Quantification of gait parameters in freely walking rodents. *BMC Biol.* 13:50. doi: 10.1186/s12915-015-0154-0

Minichiello, L., Piehl, F., Vazquez, E., Schimmang, T., Hökfelt, T., Represa, J., et al. (1995). Differential effects of combined trk receptor mutations on dorsal root ganglion and inner ear sensory neurons. *Development* 121, 4067–4075. doi: 10.1242/dev.121.12.4067

Napoli, I., Noon, L. A., Ribeiro, S., Kerai, A. P., Parrinello, S., Rosenberg, L. H., et al. (2012). A Central Role for the ERK-Signaling Pathway in Controlling Schwann Cell Plasticity and Peripheral Nerve Regeneration In Vivo. *Neuron* 73, 729–742. doi: 10.1016/j.neuron.2011.11.031

Ng, B. K., Chen, L., Mandemakers, W., Cosgaya, J. M., and Chan, J. R. (2007). Anterograde Transport and Secretion of Brain-Derived Neurotrophic Factor along Sensory Axons Promote Schwann Cell Myelination. *J. Neurosci.* 27, 7597–7603. doi: 10.1523/jneurosci.0563-07.2007

Nykjaer, A., and Willnow, T. E. (2012). Sortilin: a receptor to regulate neuronal viability and function. *Trends Neurosci.* 35, 261–270. doi: 10.1016/j.tins.2012.01.003

Oh, S. S., Hayes, J. M., Sims-Robinson, C., Sullivan, K. A., and Feldman, E. L. (2010). The effects of anesthesia on measures of nerve conduction velocity in male C57Bl6/J mice. *Neurosci. Lett.* 483, 127–131. doi: 10.1016/j.neulet.2010.07.076

Reichardt, L. F. (2006). Neurotrophin-regulated signalling pathways. *Phil. Trans. R. Soc. Lond. Ser. B Biol. Sci.* 361, 1545–1564. doi: 10.1098/rstb.2006.1894

Richner, M., Pallesen, L. T., Ulrichsen, M., Poulsen, E. T., Holm, T. H., Login, H., et al. (2019). Sortilin gates neurotensin and BDNF signaling to control peripheral neuropathic pain. *Sci. Adv.* 5:eaav9946. doi: 10.1126/sciadv.aav9946

Ronchi, G., Raimondo, S., Varejão, A. S. P., Tos, P., Perroteau, I., and Geuna, S. (2010). Standardized crush injury of the mouse median nerve. *J. Neurosci. Meth.* 188, 71–75. doi: 10.1016/j.jneumeth.2010.01.024

Sahenk, Z., Galloway, G., Edwards, C., Malik, V., Kaspar, B. K., Eagle, A., et al. (2010). TrkB and TrkC agonist antibodies improve function, electrophysiologic and pathologic features in TremblerJ mice. *Exp. Neurol.* 224, 495–506. doi: 10.1016/j.expneurol.2010.05.013

Sahenk, Z., Oblinger, J., and Edwards, C. (2008). Neurotrophin-3 deficient Schwann cells impair nerve regeneration. *Exp. Neurol.* 212, 552–556. doi: 10.1016/j.expneurol.2008.04.015

Sheu, J. Y., Kulhanek, D. J., and Eckenstein, F. P. (2000). Differential Patterns of ERK and STAT3 Phosphorylation after Sciatic Nerve Transection in the Rat. *Exp. Neurol.* 166, 392–402. doi: 10.1006/exnr.2000.7508

Skeldal, S., Matusica, D., Nykjaer, A., and Coulson, E. J. (2011). Proteolytic processing of the p75 neurotrophin receptor: A prerequisite for signalling?: neuronal life, growth and death signalling are crucially regulated by intramembrane proteolysis and trafficking of p75(NTR). *Bioessays* 33, 614–625. doi: 10.1002/bies.201100036

Tolwani, R. J., Cosgaya, J. M., Cosgaya, J. M., Varma, S., Jacob, R., Kuo, L. E., et al. (2004). BDNF overexpression produces a long-term increase in myelin formation in the peripheral nervous system. *J. Neurosci. Res.* 77, 662–669. doi: 10.1002/jnr.20181

Vaegter, C. B., Jansen, P., Fjorback, A. W., Glerup, S., Skeldal, S., Kjolby, M., et al. (2011). Sortilin associates with Trk receptors to enhance anterograde transport and neurotrophin signaling. *Nat. Neurosci.* 14, 54–61. doi: 10.1038/nn.2689

Varejo, A. S. P., Cabrita, A. M., Meek, M. F., Bulas-Cruz, J., Melo-Pinto, P., Raimondo, S., et al. (2004). Functional and Morphological Assessment of a Standardized Rat Sciatic Nerve Crush Injury with a Non-Serrated Clamp. *J. Neurotraum.* 21, 1652–1670. doi: 10.1089/neu.2004.21.1652

Willnow, T. E., Petersen, C. M., and Nykjaer, A. (2008). VPS10P-domain receptors - regulators of neuronal viability and function. *Nat. Rev. Neurosci.* 9, 899–909. doi: 10.1038/nrn2516

Woolley, A. G., Tait, K. J., Hurren, B. J., Fisher, L., Sheard, P. W., and Duxson, M. J. (2008). Developmental loss of NT-3 in vivo results in reduced levels of myelin-specific proteins, a reduced extent of myelination and increased apoptosis of Schwann cells. *Glia* 56, 306–317. doi: 10.1002/glia.20614

Yamauchi, J., Miyamoto, Y., Tanoue, A., Shooter, E. M., and Chan, J. R. (2005b). Ras activation of a Rac1 exchange factor, Tiam1, mediates neurotrophin-3-induced Schwann cell migration. *Proc. Natl. Acad. Sci. U.S.A.* 102, 14889–14894. doi: 10.1073/pnas.0507125102

Yamauchi, J., Chan, J. R., Miyamoto, Y., Tsujimoto, G., and Shooter, E. M. (2005a). The neurotrophin-3 receptor TrkC directly phosphorylates and activates the nucleotide exchange factor Dbs to enhance Schwann cell migration. *Proc. Natl. Acad. Sci. U.S.A.* 102, 5198–5203. doi: 10.1073/pnas.0501160102

Yamauchi, J., Chan, J. R., and Shooter, E. M. (2003). Neurotrophin 3 activation of TrkC induces Schwann cell migration through the c-Jun N-terminal kinase pathway. *Proc. Natl. Acad. Sci. U.S.A.* 100, 14421–14426. doi: 10.1073/pnas.2336152100

Yamauchi, J., Chan, J. R., and Shooter, E. M. (2004). Neurotrophins regulate Schwann cell migration by activating divergent signaling pathways dependent on Rho GTPases. *Proc. Natl. Acad. Sci. U.S.A.* 101, 8774–8779. doi: 10.1073/pnas.0402795101

Conflict of Interest: The authors declare that the research was conducted in the absence of any commercial or financial relationships that could be construed as a potential conflict of interest.

Publisher's Note: All claims expressed in this article are solely those of the authors and do not necessarily represent those of their affiliated organizations, or those of the publisher, the editors and the reviewers. Any product that may be evaluated in this article, or claim that may be made by its manufacturer, is not guaranteed or endorsed by the publisher.

frontiers | Frontiers in Cellular Neuroscience

ORIGINAL RESEARCH
published: 13 May 2022
doi: 10.3389/fncel.2022.860103

Research on the Contour Modeling Method of Peripheral Nerve Internal Fascicular Groups During the Non-Splitting/Merging Phase and Distribution Rules of Model Parameters

Yingchun Zhong[1], *Zhihao Tian*[1], *Peng Luo*[2], *Siyu Sun*[1†] *and Shuang Zhu*[3*†]

[1] School of Automation, Guangdong University of Technology, Guangzhou, China, [2] Department of Bone and Joint Surgery, Shenzhen Sixth People's Hospital, Shenzhen, China, [3] Department of Pathophysiology, School of Basic Medical Sciences, Zhengzhou University, Zhengzhou, China

OPEN ACCESS

Edited by:
Ji-Fan Hu,
Jilin University, China

Reviewed by:
Hehai Pan,
Sun Yat-sen University, China
David S. Holder,
University College London,
United Kingdom
Enrico Ravagli,
University College London,
United Kingdom, in collaboration with reviewer DH
Yining Ma,
National University of Singapore, Singapore

***Correspondence:**
Shuang Zhu
38625267@qq.com

[†]These authors have contributed equally to this work

Specialty section:
This article was submitted to Non-Neuronal Cells, a section of the journal Frontiers in Cellular Neuroscience

Received: 22 January 2022
Accepted: 19 April 2022
Published: 13 May 2022

Citation:
Zhong Y, Tian Z, Luo P, Sun S and Zhu S (2022) Research on the Contour Modeling Method of Peripheral Nerve Internal Fascicular Groups During the Non-Splitting/Merging Phase and Distribution Rules of Model Parameters.
Front. Cell. Neurosci. 16:860103.
doi: 10.3389/fncel.2022.860103

Objectives: To investigate benchmark data for docking the same functional nerve bundles based on the mathematical contour model of peripheral nerve internal fascicular groups.

Materials and Methods: First, the discrete points of the original contours of nerve bundles were extracted into a dataset through the image process. Second, two indicators were employed to evaluate the modeling precision. Third, the dataset was modeled by the 3rd-order quasi-uniform B-spline method. Fourth, the dataset was modeled by the Fourier transform method. Fifth, all contours were modeled by the 4th-order Fourier method. Then, the histogram of each parameter from the Fourier model was calculated. Furthermore, the probability density function was fit to each parameter.

Results: First, the optimized sampling number of the 3rd-order quasi-uniform B-spline method is 21. The sampling number is the control point number of the 3rd-order quasi-uniform B-spline, which produces more than 63 parameters in the model. Second, when the Fourier transform model is employed to model the contour of nerve bundles, the optimized order number yields a 4th-order Fourier model, which has 16 parameters. Third, when all contours are modeled by the 4th-order Fourier model, the statistical analysis shows that (1) the pitch parameters a1 and d1 obey the mixed Gaussian distribution; (2) the harmonic parameter b3 obeys the normal distribution; and (3) the pitch parameters b1 and c1 and the remaining harmonic parameters obey the *t* distribution with position and scale.

Conclusion: This work paves the way for the exploration of the correlation between model parameters and spatial extension.

Keywords: peripheral nerve bundles in non-splitting and merging stage, Fourier, contour modeling, Hausdorff distance, peripheral nerve repair

INTRODUCTION

Peripheral nerve injury in the limbs is a common disease in surgical clinics (Sullivan et al., 2016; Zhu et al., 2018). Connecting nerve bundles according to the original anatomical structure will restore nerve conduction and function to the greatest extent during peripheral nerve repair (Zhong et al., 2015, 2020). The contour information of the nerve bundle can provide a positioning reference for the docking nerve (Zhuo et al., 2016; Zhong et al., 2020). At present, research on the modeling method of neural bundle contours is exceptionally scarce. Therefore, exploring the modeling method of the nerve bundle contour in the peripheral nerve and the rules of the model parameters is of great significance to the repair of peripheral nerve injury.

The contours of the nerve bundles are a series of irregular circular curves with different sizes and shapes in the MicroCT image. Zihao et al. (2016) proposed a contour fitting method based on a piecewise cubic polynomial Bezier curve using the modeling method of quasi-circular contours. The result has high accuracy and a good fitting effect. In addition, Zhong et al. (2021) proposed a tensor B-spline method with an arbitrary spline degree, taking advantage of its characteristics of excellent interpolation and approximation, multiscale representation, algorithm speed, and mesh-free construction. The problem of mathematical modeling in noninvasive medical imaging can be accurate and effective. Moreover, Chi et al. (2008) proposed a new CT image preprocessing method that uses a cubic spline curve to perform contour fitting on CT image data. This method has a good representation of detailed information. In addition, Albay and Kamaşak (2015) and Bahri et al. (2018) proposed a method based on Fourier and gradient histograms to realize human detection. This method can construct delicate human image contours in surveillance images.

Furthermore, (Albay and Kamaşak, 2015) applied Fourier descriptors to classify the extracted dermoscopic image lesion boundaries, which improved the diagnosis rate of the disease. Equally important, Serpa-Andrade et al. (2015) proposed an automated diagnosis system that uses the fast Fourier transform of shape features and the Hu moment descriptor to construct an esophageal image and uses the translation, rotation, and zoom invariance of the descriptor to transform the esophagus image. By classifying and using the irregularity of the z-line to describe the disease image, the method distinguishes a healthy esophagus from an esophagus with esophagitis. The literature review shows that the spline curve method and the Fourier method are two commonly used methods for modeling the contours of biological tissues.

In addition, Serpa-Andrade et al. (2015) proposed a local linear fitting function method combined with a DnCNN, which can improve the image quality and improve the results of medical image reconstruction. Although this method can suppress the error caused by noise, it is not suitable for the nerve bundle study conducted in this paper—research on the regularity of contour modeling and model parameters. Furthermore, Li (2019)proposed a multiple ellipse fitting framework suitable for densely connected contours. The framework decomposes complex multiellipse fitting tasks into single ellipse fitting, anomaly detection, and other easy-to-implement subtasks. The sliding window method and anomaly detection technology can extract multiple ellipses from the contour with good accuracy and efficiency. However, this method has two limitations: because the size of the sliding window is fixed, this method is not applicable when the size of the ellipse in the contour changes significantly; the frame cannot distinguish between an inner ellipse and an outer ellipse. Kapoor et al. (2019) used a polynomial curve to fit the contour of the iris, effectively realizing the positioning of the iris at any distance and direction. This method can be further extended to a mature iris recognition system to improve the efficiency of iris recognition, but there is no further explanation of the modeling effect of the iris contour.

On the basis of completing the acquisition and three-dimensional reconstruction of the nerve bundle contour in the peripheral nerve MicroCT image, in this paper, we constructed the mathematical model of the neural bundle contour in the framework of the Fourier transform and studied the statistical law of the parameters in the model. First, this paper constructed the neural bundle contour discrete point dataset; second, the quasi-uniform 3rd-order B-spline curve method and the Fourier transform method were used to construct the neural bundle contour model; third, the Dice coefficient was used as the evaluation index to explore the appropriate order in the established model based on the Fourier transform idea. The mathematical model built based on the appropriate order should make the Dice coefficient of all the modeled contours reach more than 95%. Fourth, the concept of the relative error of the Hausdorff distance was proposed and used to evaluate the contour modeling error of the nerve bundle.

METHODS AND RESULTS

Study Design

The studies involving human specimens were reviewed and approved by the institutional review board of the Shenzhen Sixth People's Hospital.

As shown in **Figure 1**, the research framework of this paper is divided into three stages: dataset preparation, model construction method research, and model parameter regularity exploration.

In the dataset preparation stage, a dataset of discrete points of nerve bundle contours was constructed based on segmenting nerve bundle contours.

In the research phase of the model construction method, the quasi-uniform 3rd-order B-spline curve method and the Fourier method were used to construct the nerve bundle contour. The two methods in terms of modeling method error, error, and adaptability to follow-up research were compared, and a more suitable modeling method was acquired.

In the exploration stage of the regularity of model parameters, according to the requirements of meeting the error requirements and the minimum model complexity, the lowest order of the model was obtained through experiments, and the probability density function of each model parameter was constructed by performing probability statistical analysis. The statistical law of each parameter was acquired.

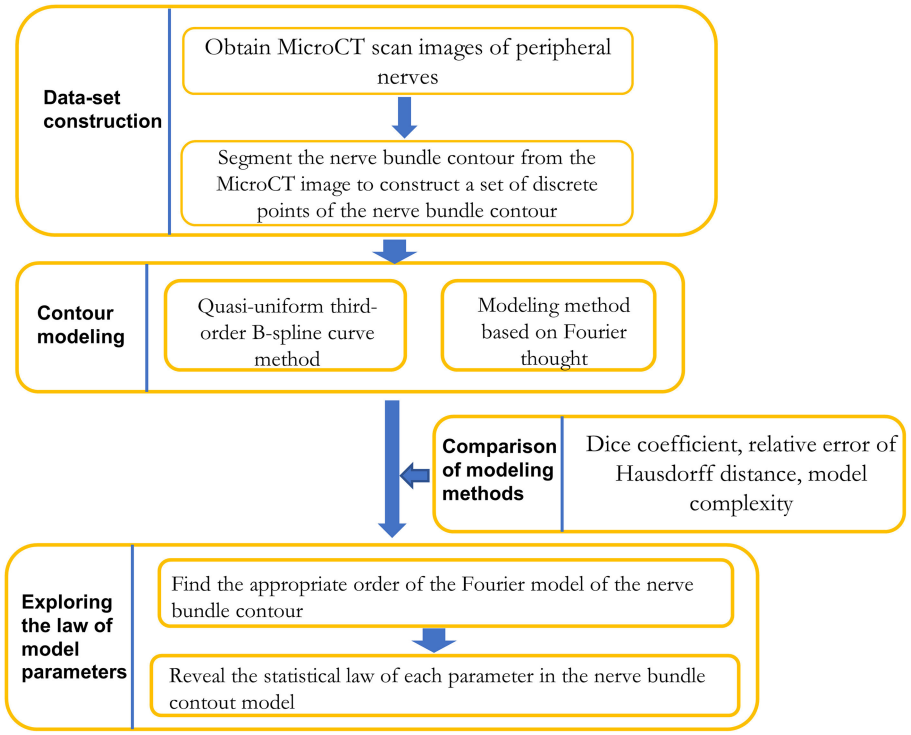

FIGURE 1 | Framework for contour modeling method research on nerve bundles.

Dataset Construction

To explore the modeling method suitable for the nerve bundle profile and the law of model parameters, the following material preparations were carried out.

Acquisition of specimens. The obtained peripheral nerves of the extremities are shown in **Figure 2a**. The peripheral nerves were dehydrated and frozen and then cut into multiple small sections with a length of ∼3 mm as specimens, as shown in **Figure 2b**.

The specimen shown in **Figure 2b** was freeze-dried at −80° for 48 h, and the second specimen was arbitrarily selected as a case.

The second specimen was scanned by the MicroCT device, and a total of 522 MicroCT scan images were obtained. The 10th scan result image selected arbitrarily is shown in **Figure 2c**. The scanning parameters of MicroCT can be found in the literature (Zhu et al., 2016).

Image processing and deep learning methods were utilized to obtain nerve bundle contours (Zhong et al., 2015). A total of 10,962 nerve bundle contours were obtained from the sequence of scanned images. Taking the 10th scan result image as an example, the contour acquisition results are shown in **Figure 2d**. For clarity of subsequent expression, the nerve bundles in **Figure 2d** are numbered. The result of the binarization of the nerve bundle region is shown in **Figure 2e**.

To avoid the influence of the position coordinates on the neural bundle contour modeling, the centroid of each nerve bundle contour image was used as the coordinate origin for unified processing. All the discrete point sets of nerve bundle contours were saved one by one until the nerve bundle contour coordinate data of all images were obtained, and the nerve bundle contour coordinate discrete point dataset required in this article was constructed.

According to the image binarization processing result of the nerve bundle region, the nerve bundle was reconstructed in three dimensions, and the result is shown in **Figure 2f**. **Figure 2f** shows that the spatial structure of the nerve bundle is highly complicated, and the nerve bundle will split/merge several times within a distance of 1–5 mm. For this reason, this article only focused on the modeling and model parameter law study of the nerve bundles in the non-splitting/merging phase.

Contour Modeling

Modeling Method of Nerve Tract Contour

Figures 2c–e shows that the contours of the nerve bundles in the peripheral nerves at the non-splitting/merging phase are circular-like figures with different areas, and the boundary contours are closed curves. According to the literature, the contour modeling of biological tissues usually adopts the B-spline curve method.

B-Spline Curve Modeling Method

The B-spline curve method is often used to construct curve models in computer-aided geometric design, which can

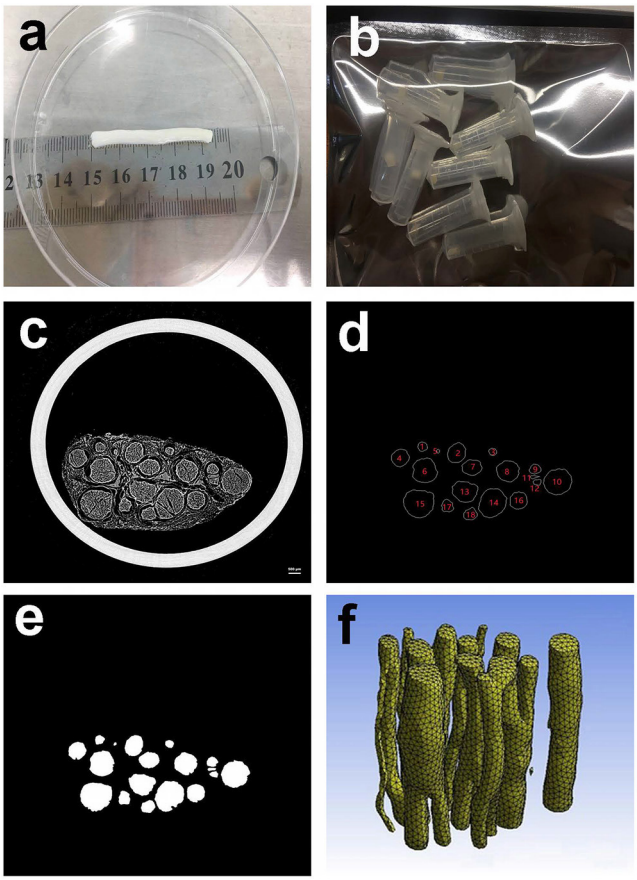

FIGURE 2 | Preparing materials. **(a)** Peripheral nerve; **(b)** Peripheral nerve specimens with a length of ∼3 mm; **(c)** 10th MicroCT image of the second specimen; **(d)** Contours of the nerve bundle from 10th MicroCT image; **(e)** Binary image of the nerve bundles from the 10th MicroCT image; **(f)** 3D reconstruction result of the second specimen.

effectively meet the requirements of graphic shape representation and geometric design, is convenient for shape information transmission and image shape mathematical modeling, and can solve the modeling problem of free-form curves. To construct a B-spline curve model, a starting point, an ending point, and multiple control points must be defined. By changing the coordinates of the vertices of the polygon inscribed in the contour (i.e., control points), the shape of the B-spline curve can be changed accordingly to realize nerve bundle contour modeling (Zhong et al., 2021).

The k-th B-spline model is:

$$c(u) = \sum_{i=0}^{n} \mathbf{P}_i \cdot N_{i,k}(u)\,, u \in [0,1] \tag{1}$$

where Pi(i = 0,1,2...n) represents the control point coordinates, and Ni, k(u)(i = 0,1,2...n) is the K-order canonical B-spline basis function. The basis function is a piecewise polynomial of K-order. The Cox-de Boor recurrence formula is usually used to express the B-spline basis function, which is defined as,

$$\begin{cases} N_{i,0}(u) = \begin{cases} 1, & u_i \le u < u_{i+1} \\ 0, & other \end{cases} \\ N_{i,k} = \dfrac{u - u_i}{u_{i+k} - u_i} N_{i,k-1}(u) + \dfrac{u_{i+k+1} - u}{u_{i+k+1} - u_{i+1}} N_{i+1,k-1}(u) \end{cases} \tag{2}$$

Definition: In the formula of , the first subscript i of the $N_{i,k}$ double subscript is the node number, the second subscript k is the number of the basis function, and the k-th B-spline curve is C^{k-r} continuous at the node where the repeatability is r.

In Formula 2, the meaning of u_i is as follows: suppose U is a set of n + k + 1 nondecreasing numbers ($\boldsymbol{U}$: $u_0 \le u_1 \le ... \le u_{n+k+1}$), ui is called a node, and set U is called a node vector. The interval $[u_i, u_{i+1}]$ is the i-th node interval. If a node appears r times, this node represents multiple nodes with a repeat degree of r, written as $u_i(r)$.

To obtain the result of the quantitative description of the closed B-spline curve, two control points, $\boldsymbol{P}_{n+1} = \boldsymbol{P}_1$ and $\boldsymbol{P}_{n+2} = P_2$, need to be added at the end of each contour dataset to make the curve connect end to end.

Based on the B-spline model, this paper used the quasi-uniform cubic B-spline curve method to describe the contour of the nerve bundle. The reasons are as follows:

(1) Selection of the order: take $k = 3$, and the nodes that satisfy the repetition degree of 1 ($r = 1$) are C^2 continuous; that is, the cubic B-spline curve is used.
(2) Selection of the node vector: The node vector $\boldsymbol{U}$ must take a strictly increasing sequence to satisfy the repetition degree at the node of 1 ($r = 1$). A uniform B-spline model can be used when the node vector is uniformly distributed along the parameter axis.
(3) Since the number of pixels forming the contour of the nerve bundle is not equal, to reduce the number of parameters/items of the model and obtain a description model with the same length of the number of parameters/items, a method of limiting the number of control points is adopted; that is, the dataset is sampled at equal intervals for a limited number of times. This method is a quasi-uniform sampling dataset method. In this paper, the quasi-uniform 3rd-order B-spline method is used to establish the model of the nerve bundle contour.

Modeling Method Based on the Fourier Transform

According to the idea of the Fourier transform, any periodic function can be expanded into the Fourier series of trigonometric functions, and each coefficient in the series determines the shape of the periodic function curve. Analyzing the contour of the nerve bundle shows that if the contour of the nerve bundle is converted to the complex plane, the contour is periodic in the complex plane, and the Fourier method can be used to construct the contour model. In this way, the follow-up exploration of the regularity of the nerve bundle profile is transformed into the exploration of the regularity of the Fourier model parameters.

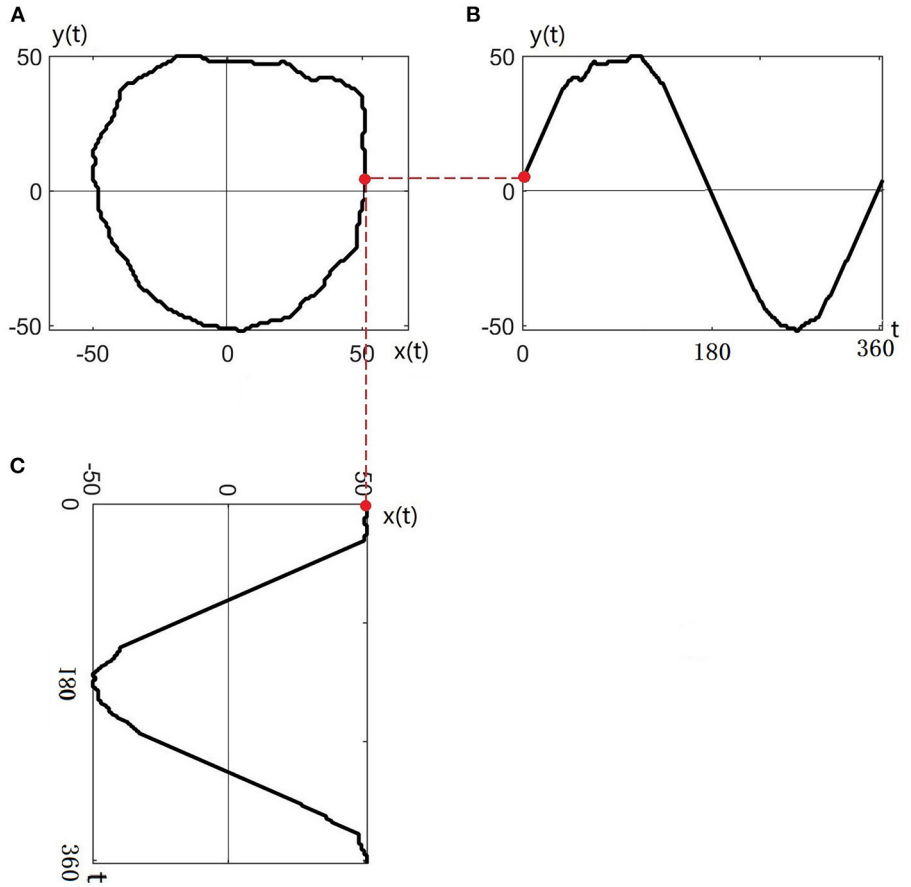

FIGURE 3 | Transferring the contour of the nerve bundle to the complex plane: **(A)** Original contour of the nerve bundle; **(B)** Contour profiled to the $y(t)$ plane; **(C)** Contour profiled to the $x(t)$ plane.

The contour of any nerve bundle is transformed to the complex plane and named $z(t)$, as shown in **Figure 3A**. Taking the centroid of the nerve bundle as the origin of the coordinate system, the nerve bundle contour $z(t)$ can be expressed in the complex plane as:

$$z(t) = x(t) + iy(t) \tag{3}$$

Where $x(t), y(t)$ are two parameter planes orthogonal to each other.

Taking the intersection of the nerve bundle contour and the real axis as the starting point, the nerve bundle contour is circled 360° in a counterclockwise direction to obtain the projection curve of the nerve bundle contour on the real plane $x(t)$ and imaginary plane $y(t)$, as shown in **Figures 3B,C**.

Since the nerve bundle contour curve $z(t)$ is a closed curve, the real and imaginary parts ($x(t)$ and $y(t)$, respectively) are periodic functions. Any periodic function can be represented by an infinite series composed of a sine function and a cosine function, so $z(t)$ is expanded in a triangular Fourier series within 1 cycle (360°):

$$\begin{bmatrix} x(t) \\ y(t) \end{bmatrix} = \begin{bmatrix} a_0 \\ c_0 \end{bmatrix} + \sum_{k=1}^{\infty} \begin{bmatrix} a_k & b_k \\ c_k & d_k \end{bmatrix} \begin{bmatrix} \cos \dfrac{2k\pi t}{T} \\ \sin \dfrac{2k\pi t}{T} \end{bmatrix} \tag{4}$$

$$\begin{cases} a_k = \dfrac{T}{2k^2\pi^2} \sum_{p=1}^{n} \dfrac{\Delta x_p}{\Delta t_p} (\cos \dfrac{2k\pi t_p}{T} - \cos \dfrac{2k\pi t_{p-1}}{T}); \\ b_k = \dfrac{T}{2k^2\pi^2} \sum_{p=1}^{n} \dfrac{\Delta x_p}{\Delta t_p} (\sin \dfrac{2k\pi t_p}{T} - \sin \dfrac{2k\pi t_{p-1}}{T}); \\ c_k = \dfrac{T}{2k^2\pi^2} \sum_{p=1}^{n} \dfrac{\Delta y_p}{\Delta t_p} (\cos \dfrac{2k\pi t_p}{T} - \cos \dfrac{2k\pi t_{p-1}}{T}); \\ d_k = \dfrac{T}{2k^2\pi^2} \sum_{p=1}^{n} \dfrac{\Delta y_p}{\Delta t_p} (\sin \dfrac{2k\pi t_p}{T} - \sin \dfrac{2k\pi t_{p-1}}{T}). \end{cases} \tag{5}$$

Therefore:

$$\begin{cases} a_0 = \frac{1}{T}\sum_{p=1}^{n}\left[\frac{\Delta x_p}{2\Delta t_p}(t_p^2 - t_{p-1}^2) + \xi_p(t_p - t_{p-1})\right]; \\ c_0 = \frac{1}{T}\sum_{p=1}^{n}\left[\sum\frac{\Delta y_p}{2\Delta t_p}(t_p^2 - t_{p-1}^2) + \delta_p(t_p - t_{p-1})\right]. \end{cases} \quad (6)$$

$$\begin{cases} \Delta t_p = \sqrt{\Delta x_p^2 + \Delta y_p^2};\ t_p = \sum_{i=1}^{p}\Delta t_i;\ \xi_1 = \delta_1 = 0; \\ \xi_p = \sum_{j=1}^{p-1}\Delta x_j - \frac{\Delta x_p}{\Delta t_p}\sum_{j=1}^{p-1}\Delta t_j;\ \delta_p = \sum_{j=1}^{p-1}\Delta y_j \\ \qquad\qquad -\frac{\Delta y_p}{\Delta t_p}\sum_{j=1}^{p-1}\Delta t_j. \end{cases} \quad (7)$$

where Δx_p is the change in the x-direction, Δy_p is the change in the y-direction, p is the current coordinate, and k is the order. In Formula 4, the model parameters a_0, c_0 represent the centroid coordinates of the nerve bundle contour; the model parameters a_k, b_k, c_k, d_k determine the shape, rotation angle, and scale of the nerve bundle contour. The parameter $k = 1$ is the fundamental frequency component, and $k \geq 2$ is the harmonic component. In the nerve bundle contour model based on the Fourier transform idea (the following is referred to as the Fourier model of the contour), the low-frequency component describes the main shape of the nerve bundle contour, and the high-frequency component describes the details of the nerve bundle contour. Under the premise of satisfying the description accuracy, a small number of parameters can be used to describe the nerve bundle contour.

Methods to Mine the Regularity of Model Parameters

Observing the contour shape of the nerve bundle in **Figure 2d**, it can be seen that the contours of the nerve bundles in the same tomographic image are different, and the contours of the same nerve bundle on different slices are also different. After turning the regularity research problem of nerve bundle contours into the regularity research problem of model parameters, it is necessary to determine the proper order of the model through experimental methods. The condition for the proper order of the model requires that the order should be as low as possible under the premise of meeting the accuracy; that is, the model parameters should be as few as possible.

In addition, the statistical analysis methods of each parameter in the model include evaluating the normal distribution, logistic distribution, and t distribution with scale/location. Based on constructing the probability density function of each parameter, the following will explore the law of model parameters extending in space to achieve the goal of describing the spatial change law of the nerve bundle contour with a small number of parameters.

Comparison of Modeling Methods and Exploring the Law of Model Parameters

Experimental Environment Configuration

In this paper, the software platform for constructing the neural tract contour model is JetBrains PyCharm Community Edition 2018.2.4 × 64 running on a Win10 64-bit operating system.

Evaluation Index

Overall Evaluation Index of the Contour Model: Dice Coefficient

The *Dice* coefficient is an evaluation index commonly used to compare the similarity of two samples (Roth et al., 2018), which is defined as:

$$Dice = \frac{2\,|S_A \cap S_B|}{|S_A| + |S_B|} \times 100\% \quad (8)$$

In this paper, represent the original contour of the nerve bundle and the area enclosed by the contour curve constructed by the mathematical model, respectively. The larger the Dice coefficient is, the more similar the two contours are on a macroscopic scale. The *Dice* coefficient is used to evaluate the approximation degree of the nerve bundle contour constructed by the quasi-uniform 3rd-order B-spline curve method and the Fourier method compared with the original contour from the overall perspective. In this article, it is required that the *Dice* coefficient of the modeled contour and the actual contour be no <95%.

Because the *Dice* coefficient lacks the evaluation of the contour boundary details when evaluating the modeling accuracy, we also introduce the relative error *H_E* of the Hausdorff distance as the evaluation criterion of the contour detail error.

Local Error Evaluation Index of the Contour Model: Relative Error H_E of the Hausdorff Distance

The Hausdorff distance H is a measure to describe the similarity between two sets of points (Kim et al., 2016) and is defined as:

There are two sets of discrete data points $A = \{a_1, a_2 a_2, \ldots, a_m\}$ and $B = \{b_1, b_2 b_2, \ldots, b_n\}$. In this paper, the discrete data point set A is the original contour discrete data point set, and point set B is a set of discrete data points of the reconstructed contour of the model. The Euclidean distance between point $b_x (x \in 1,2,\ldots,n)$ in dataset B and all the corresponding points in dataset A was found, and then the minimum value was taken. The shortest vertical distance between point b_x and the original contour was obtained, that is, the boundary error e:

$$e_x = min_{y \in 1,2,\ldots,m}(\|b_x - a_y\|) \quad (9)$$

The Hausdorff distance H is:

$$H = \max_{x \in 1,2,\ldots,n}(e_x) \quad (10)$$

Although the Hausdorff distance H can better evaluate the difference in contour details, the circumference of the nerve bundle contour is different. The same Hausdorff distance H has very different descriptions of nerve bundle contours with different circumferences. For this reason, this paper proposes using the relative error of the Hausdorff distance as the evaluation index.

Let the number of discrete points contained in a particular nerve bundle contour be N; then, the relative error of the Hausdorff distance *H_E* is defined as:

$$H\_E = \frac{H}{N} \times 100\% \quad (11)$$

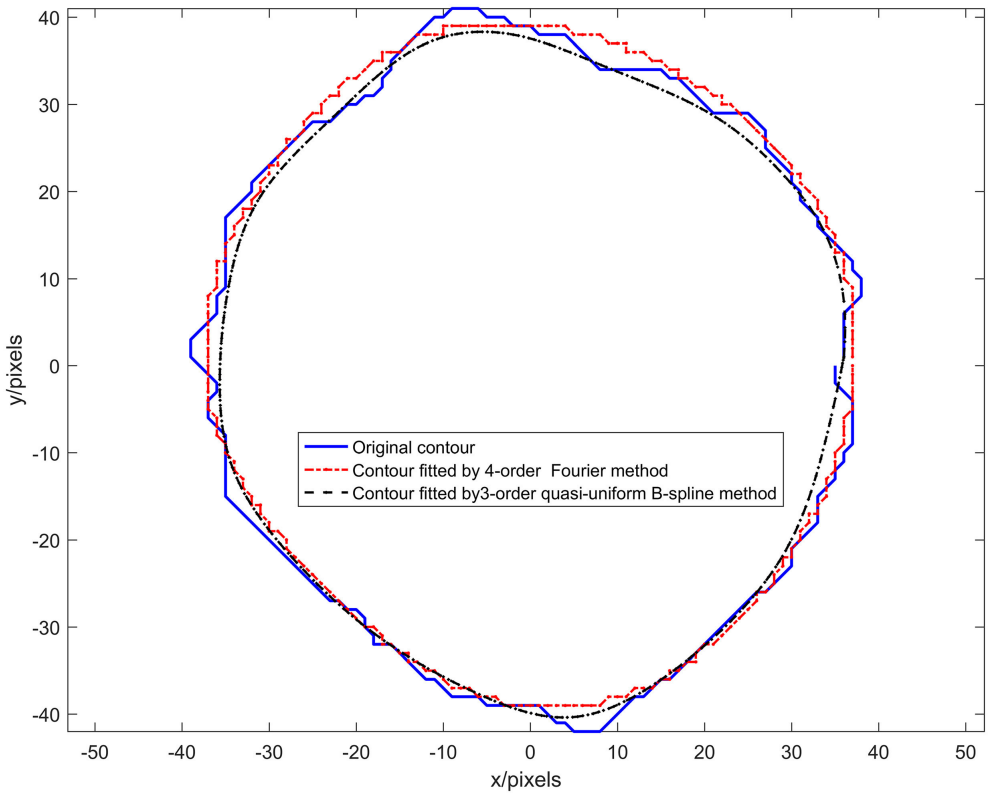

FIGURE 4 | Results of experiment 1.

In this article, the relative error H_E of the Hausdorff distance is required to be no more than 5%.

Experimental Plan Design

Experiment 1

The methods suitable for constructing a neural tract contour mathematical model were explored: the quasi-uniform 3rd-order B-spline curve modeling method and Fourier modeling method were used to construct the mathematical model of the nerve tract contour, and the advantages and disadvantages were compared and analyzed.

Experiment 2

The proper order of the Fourier model was investigated. The Fourier models of different orders were taken to model the nerve bundle contour, the evaluation index was used to evaluate it, and the lowest order that meets and was selected as the appropriate order of the Fourier model, which not only ensures the accuracy of the model but also makes the model parameters as few as possible.

Experiment 3

The statistical law of profile model parameters of the nerve bundle was revealed: the Fourier model parameters a_0, a_1,…, a_4, b_1,…, b_4, c_0, c_1,…, c_4, d_1,…, d_4 and those of other models. Statistical analysis of parameters was performed, the probability density distribution of each parameter was fitted, and the probability distribution and probability density function were obtained.

Experimental Results

Experiment 1: A Mathematical Model Suitable for Constructing Nerve Bundle Contours Was Explored

The quasi-uniform third-order B-spline curve method and the Fourier method were used to construct the neural bundle contour model, and the neural bundle numbered 8 in **Figure 2d** was used as a case to show the contour modeling results, as shown in **Figure 4**. It can be seen from **Figure 4** that:

The nerve bundle contour constructed by the quasi-uniform 3rd-order B-spline method with 21 control points and the nerve bundle contour constructed by the 4th-order Fourier method are very close to the original contour.

When the number of control points is 21, the quasi-uniform third-order B-spline curve method is used to construct the neural bundle contour with a *Dice* coefficient of 96.93%, and the Hausdorff distance is <5 pixels $H\_E \leq 0.5\%$.

The coefficient of the neural bundle profile constructed by the fourth-order Fourier method is 95.17%, and the Hausdorff distance is <4.27 pixels $H\_E \leq 0.77\%$.

The adjustable parameters modeled by the fourth-order Fourier method are 16 (excluding the constant term for locating the centroid coordinates of the nerve bundle), and the adjustable parameters modeled by the third-order quasi-uniform B-spline curve method are more than 64.

The control point coordinates modeled by the quasi-uniform 3rd-order B-spline curve method depend on the discrete point set of the nerve bundle contour. In particular, the perimeter of the nerve bundle contour is different since the data in the discrete point concentration are very different. Therefore, the data obtained by uniformly sampling 21 times in this discrete point concentration have no physical meaning. The model parameters modeled by the Fourier method represent the rotation process of a contour point in the complex plane $z(t)$ around the center of mass. The angle and period corresponding to the $x(t)$-plane and the $y(t)$-plane are not related to the contour circumference of the nerve bundle and have a clear physical significance. Moreover, using the Fourier method to construct a nerve bundle contour model can obtain a model with the same number of parameters when the nerve bundle contour circumference is different, which is extremely important for follow-up research.

Comprehensively comparing the above factors, we choose the Fourier method as the primary modeling method of nerve bundle contours.

Experiment 2: Finding a Suitable Fourier Model Order

The Fourier method with different orders has different accuracies in describing the contours of nerve bundles. The higher the order is, the higher the accuracy, the more the model parameters, and the higher the model complexity. The complexity of the model is too high, which is not conducive to the subsequent exploration of the regularity of model parameters. In this article, the specimen shown in **Figure 2c** is used as a case to illustrate the experimental process as follows.

The first and 46th images among the 522 scanned sequence images of the specimen were chosen, as shown in **Figures 5A,B**.

A nerve bundle is chosen in **Figures 5A,B**, the algorithm is used to extract its contour, and a binarized image is obtained, as shown in **Figures 5C,D**.

The contours of the two nerve bundles were modeled using the 2nd-, 4th-, and 8th-order Fourier methods, and the results are shown in **Figures 5E,F**.

From the modeling results in **Figures 5E,F**, it can be seen that the curve fitted by the second-order Fourier model has a relatively significant difference from the original contour. Moreover, the curve fitted by the fourth-order Fourier model has a relatively small difference from the original contour. The curve fitted by the eighth-order Fourier model is very close to the original contour.

The second-, fourth-, and eighth-order Fourier methods were used to model all nerve bundle profiles, and their average *Dice* coefficients, Hausdorff distance H, and Hausdorff distance relative error were calculated. The results are shown in **Table 1**.

Analysis of the data in **Table 1** shows the following:

(1) When the order of the Fourier method reaches or exceeds order 4, the *Dice* coefficient of the model is higher than 95%. Taking the 95% confidence level as the criterion, a Fourier model of order 4 or higher should be selected for neural bundle contour modeling.

(2) The relative error of the Hausdorff distance modeled by Fourier methods above the fourth order is <1%. In detail, the contours modeled by the Fourier method of each order are close to the actual contours.

(3) Comparing the data of the fourth-order model and the fifth-order model in **Table 1**, it is found that the Hausdorff distance of the two models is the same. Comparing the data of the 6th order and 7th order models in **Table 1**, it is found

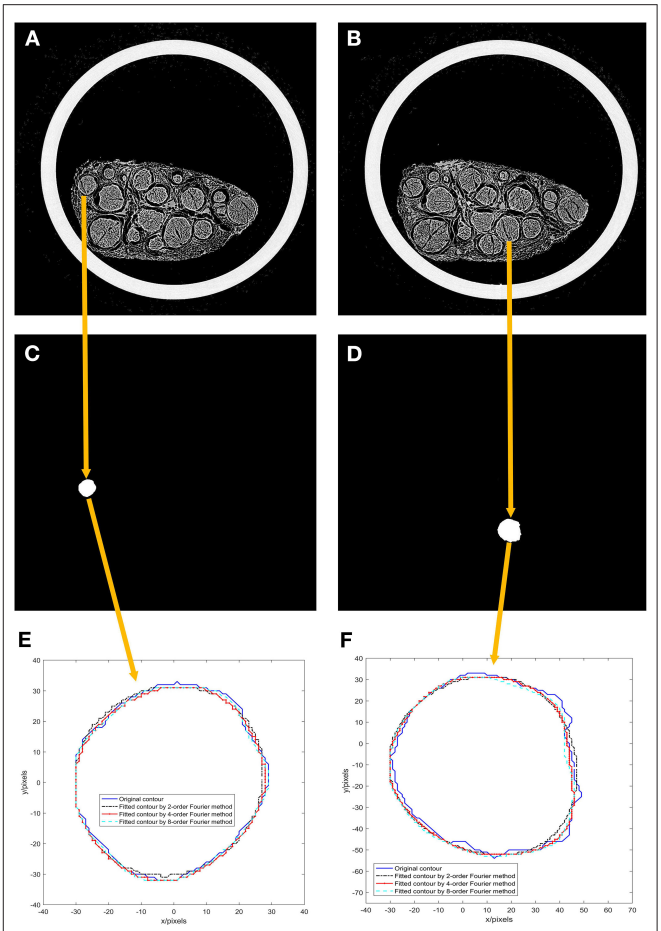

FIGURE 5 | Results of experiment 2. **(A)** 1st image of the 522 scanned sequence images of the specimen; **(B)** 46th image of the 522 scanned sequence images of the specimen; **(C)** A binarized image of the 1st scanned image; **(D)** a binarized image of the 46th scanned image; **(E)** Fourier models of the 1st scanned image; **(F)** Fourier models of the 46th scanned image.

TABLE 1 | Calculation results of evaluation indices by modeling different orders of the Fourier method.

Order (*k*)/	**1**	**2**	**3**	**4**	**5**	**6**	**7**
Dice (mean value)/%	93.29	94.20	94.73	95.17	95.55	95.95	96.22
Hausdorff distance H/pixel	11.70	7.81	7.07	5.83	5.83	5.10	5.38
Relative error *H_E*/%	1.07	0.93	0.84	0.77	0.71	0.64	0.61

that the Hausdorff distance of the 6th order model is lower than the Hausdorff distance of the 7th order model. It can be seen that the lower the order of the model is, the more minor the modeling error; that is, the order of the mathematical model and the Hausdorff distance is not monotonic.

In summary, we choose the 4th order as the appropriate Fourier model order, and the modeling contour is stable with $Dice \geq 95\%$ and $H\_E \leq 5\%$. This ensures the model's accuracy and makes the model parameters as few as possible and the model complexity as low as possible.

Experiment 3: Statistical Analysis of Model Parameters

The 4th-order Fourier model was used to model the contours of 10,962 nerve bundles in 552 scanned images, and data of 18 model parameters, such as a_0, a_1,…, a_4, b_1,…, b_4, c_0, c_1,…, c_4, d_1,…, d_4, etc., were obtained. Statistical analysis of the data for each parameter was performed, and the results are as follows.

The constant term parameters a_0 and c_0 are used to locate the center of mass coordinates of the nerve bundle contour area and have no effect on the contour shape of the nerve bundle.

The relevant results of the histogram of the parameters a_1 and d_1 and the probability density function are shown in **Figure 6**. **Figure 6** shows that parameter a_1 has three peaks, and parameter d_1 has four peaks. These two parameters obey the mixed Gaussian distribution. To this end, the Gaussian mixture model is used to construct the probability density functions of the parameters a_1 and d_1,

$$\begin{cases} \frac{1}{5\sqrt{2\pi}} e^{\frac{(x-14.11)^2}{50}} & (0 \leq x < 25) \\ \frac{1}{6.68\sqrt{2\pi}} e^{\frac{(x-36.51)^2}{89.2448}} & (25 \leq x < 50) \\ \frac{1}{3.86\sqrt{2\pi}} e^{\frac{(x-58.15)^2}{29.7992}} & (50 \leq x) \end{cases} \tag{12}$$

as shown in Formulas 12, 13:

$$f_{d_1}(x) = \begin{cases} \frac{1}{4.44\sqrt{2\pi}} e^{\frac{(x-14.4)^2}{39.4272}} & (0 \leq x < 25) \\ \frac{1}{1.77\sqrt{2\pi}} e^{\frac{(x-29.99)^2}{6.2658}} & (25 \leq x < 33) \\ \frac{1}{4.41\sqrt{2\pi}} e^{\frac{(x-41.57)^2}{38.8962}} & (33 \leq x < 50) \\ \frac{1}{3.75\sqrt{2\pi}} e^{\frac{(x-59.15)^2}{28.125}} & (50 \leq x) \end{cases} \tag{13}$$

The histogram and cumulative probability density function results of parameter b_3 are shown in **Figure 7**. **Figure 7** shows that the normal and logistic distributions fit the histogram of parameter c_1. The results show that parameter b_3 obeys the normal distribution of $N(0.03, 0.46^2)$.

The probability density functions of the remaining 13 Fourier model parameters a2,…, a4,…, b1,…, b2,…, b4,…, c1,…, c4,…, d2,…, d4 are constructed. The parameter c_1 is taken as a case description. The normal, logistic, and t distributions with scale/location were used to fit the histogram of parameter c_1, and the results are shown in **Figure 8**. **Figure 8** shows that the cumulative probability density function curve with the scale/location parameter t distribution is closest to the actual probability density curve. Therefore, parameter c_1 obeys the t distribution with scale/location parameters, and the probability density function is:

$$f_T(x) = \frac{\Gamma(\frac{\upsilon+1}{2})}{\sqrt{\upsilon\pi} \cdot \Gamma(\frac{\upsilon}{2})} (1 + \frac{t^2}{\upsilon})^{-\frac{\upsilon+1}{2}} \tag{14}$$

Among them is the gamma function.

The position, scale, and degree of freedom distribution of the 13 parameters a_2,…, a_4, b_1, b_2, b_4, c_1,…, c_4, d_2,… d_4 of the neural bundle profile Fourier model are shown in **Table 2**.

In **Table 2**, the parameters b_1 and c_1 are the parameters of the fundamental component in the Fourier model, and the other parameters are the corresponding parameters of the harmonic components in the Fourier model. By observing the scale σ row of **Table 2** and comparing the scale σ of the parameters b_1 and c_1 with the scale σ of other parameters, the findings indicate that the scale parameter σ value of the fundamental component is much larger than the scale parameter σ value of the harmonic component. This shows the probability of the parameters b_1 and c_1. The density function curve is relatively flat, and the probability density function curve of the harmonic component parameter value is sharp. The concentration of the harmonic component parameter value is much higher than the concentration of the parameters b_1 and c_1.

DISCUSSION

In repairing peripheral nerve injury, if the nerve bundle can be docked according to its original spatial structure, the disability rate will be significantly reduced. However, there are currently no technical means to achieve precise docking. Constructing a mathematical model of the inner nerve bundle contour of the peripheral nerve and studying the regularity of the model parameters is critical to achieve a precise connection of the peripheral nerve. To this end, Zhong et al. (2015) frozen the median nerve, followed by sectioning, microscopic imaging, registration, extraction of nerve bundle contours, and 3D reconstruction to obtain a visual model of the nerve bundle. Since this method requires slicing and registration, the efficiency and accuracy are not high. To this end, Zhu et al. (2016) used MicroCT to image peripheral nerves, and Zhong et al. (2021) used Mask RCNN method to extract nerve bundle contours from these images, and obtained long-segment inner nerve bundles Methods of 3D reconstruction. In order to explore the extension law of nerve bundles in space, Zhong et al. (2020) simplified the shape of nerve bundles in space to their centroid space curves, and used the Fourier method to build a mathematical model, and obtained the nerve bundles. The space shape law. In order to accurately connect the nerve bundles, it is necessary to know many key parameters of the nerve bundles, including: the morphological parameters of the nerve bundles and their spatial extension laws, and the mathematical model of the nerve bundle contours. To this end, Zhong et al. (2021) studied the statistical laws of core morphological parameters such as area, perimeter, and roundness of nerve bundles, as well as the laws of spatial extension. In this paper, by constructing a mathematical model of the nerve bundle

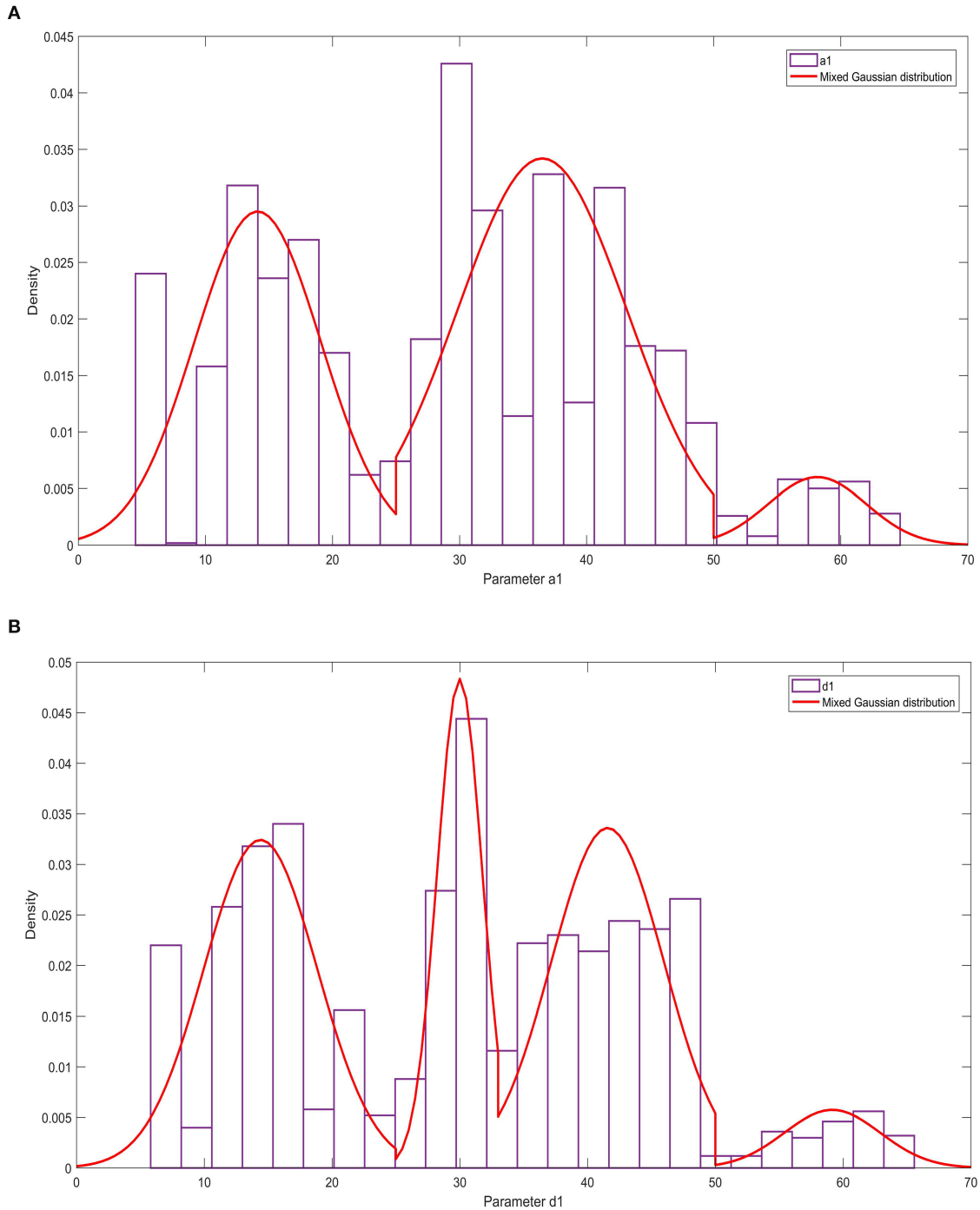

FIGURE 6 | The statistical law of parameters a1 and d1. **(A)** Histogram and probability density function of parameter a1; **(B)** Histogram and probability density function of parameter d1.

contour and obtaining the statistical law of the model parameters, it lays a key foundation for the accurate docking of the nerve bundle.

In this paper, the quasi-uniform third-order B-spline curve method and the Fourier transform method are used to construct the neural bundle contour model, and the regularity of the model parameters is studied. Experiment 1, shown in **Figure 5**, demonstrates that the quasi-uniform 3rd-order B-spline curve method used to construct the neural bundle contour has a coefficient of 96.93%, and the Hausdorff distance is less than 5 pixels. The coefficient of the neural bundle profile constructed by the fourth-order Fourier method is 95.17%, and the Hausdorff

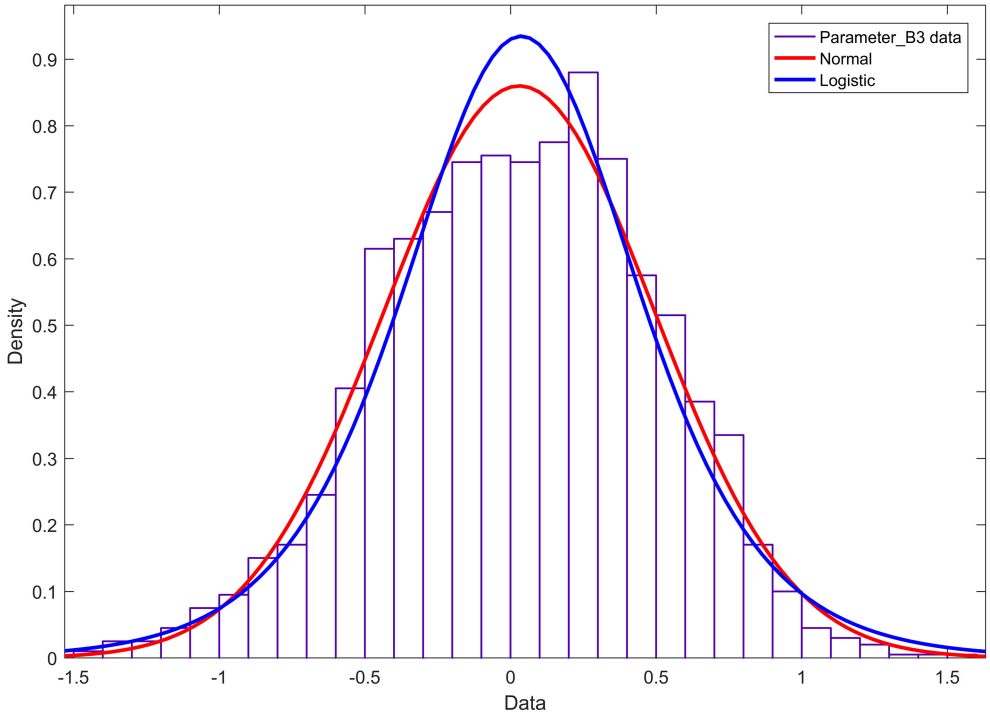

FIGURE 7 | Histogram and probability density function of parameter b3.

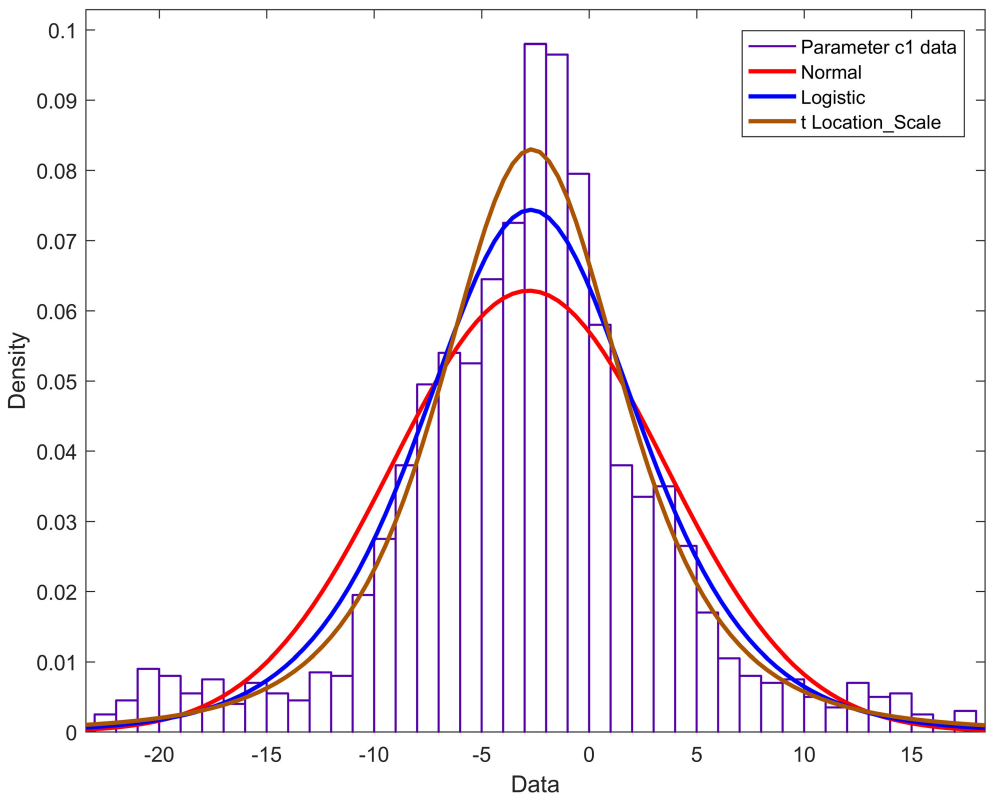

FIGURE 8 | Histogram and probability density function of parameter c1.

TABLE 2 | Calculation results of evaluation indices by modeling different orders of the Fourier method.

Parameter	a_2	a_3	a_4	b_1	b_2	b_4	c_1	c_2	c_3	c_4	d_2	d_3	d_4
Position μ	−0.08	−0.05	0.01	2.36	−0.03	0.02	−2.67	0.02	0.02	−0.01	0.04	0.18	0.11
Scale σ	0.66	0.49	0.36	4.45	0.49	0.40	4.48	0.47	0.47	0.30	0.62	0.40	0.36
Variance υ	5.43	5.7	7.17	2.85	2.62	4.84	3.45	2.37	16.71	3.18	4.44	5.39	4.33

distance is <4.27 pixels. It can be seen that (1) both the quasi-uniform 3rd-order B-spline curve method and the Fourier method can construct the nerve bundle contour model. (2) Although the modeling accuracy of the Fourier model is slightly lower than that of the quasi-uniform 3rd-order B-spline curve model, the complexity of the contour Fourier model is much lower than that of the quasi-uniform 3rd-order B-spline curve model. (3) The control point coordinates of the quasi-uniform 3rd-order B-spline curve model are obtained by uniformly sampling the original data and have no physical meaning; each parameter of the Fourier model expresses the detailed shape of the nerve bundle profile at different orders and has a clear physical meaning. Therefore, the Fourier method is more suitable for constructing nerve bundle contour models.

According to the results of Experiment 2, it can be seen that the Dice coefficient can reach more than 95% when the Fourier model of order four and above is used to construct the nerve bundle contour curve, and the relative error of the Hausdorff distance is <0.77%. There is no monotonic relationship between the Hausdorff distance and model order. Considering model complexity and modeling accuracy, it is appropriate to use the 4th-order Fourier method to construct the mathematical model of the nerve bundle contour.

According to the results of Experiment 3, the research in this paper shows that when the 4th-order Fourier model is used to model the nerve bundle profile, the two fundamental parameters a1 and d1 of the model obey the mixed Gaussian distribution, with a relatively obvious 3–4 a wave peak. The degree of freedom of the harmonic parameter b3 is much larger than that of other parameters, and it obeys the normal distribution. The peak of the probability density function is lower, and the two ends are slightly higher than other parameters. The other two fundamental wave parameters b1, c1, and other harmonic parameters in the model all obey the *t*-distribution with position/scale parameters, and the probability density function has a relatively sharp peak shape. On this basis, when we need 3D printing or 3D reconstruction of nerve bundles, the probability distribution corresponding to the parameters can be used to randomly generate an actual value. Substitute this value into the mathematical model constructed in this paper, and then we can obtain the nerve bundle with a difference of <5% from the original nerve bundle profile. It can be seen that the construction of the nerve bundle outline can provide a positioning reference for the docking nerve. It can provide a smooth walking trajectory for 3D printing, and can also significantly reduce the storage space required to save nerve bundle information, so as to express the contour information of long nerve bundles with a small number of model parameters and ensure accuracy. And lay the foundation for the follow-up exploration of the regularity of neural bundles extending in space.

CONCLUSION

Constructing the contour of the nerve bundle can provide a positioning benchmark for peripheral nerve repair surgery. For this reason, based on constructing the nerve tract contour discrete point dataset, this paper explores a method suitable for constructing the neural tract contour mathematical model in the non-splitting and merging stage of peripheral nerve MicroCT images.

The main contributions of this paper are as follows: (1) Aiming at the modeling problem of nerve bundle contours in peripheral nerve MicroCT images, a modeling method based on the Fourier transform is proposed and compared with the classic B-spline curve modeling method. (2) Given the difficulty in evaluating the local description accuracy of the neural bundle contour mathematical model, the concept of the relative error of the Hausdorff distance is proposed. (3) Using the Dice coefficient as the evaluation index, we found the appropriate Fourier model order with the required accuracy and low complexity. (4) The statistical law of each parameter in the Fourier model of the nerve bundle profile was revealed.

Next, we will explore the correlation between model parameters and spatial extension.

DATA AVAILABILITY STATEMENT

The original contributions presented in the study are included in the article/supplementary materials, further inquiries can be directed to the corresponding author.

ETHICS STATEMENT

The studies involving human specimen were reviewed and approved by the Institutional Review Board of the Shenzhen Sixth People's Hospital.

AUTHOR CONTRIBUTIONS

SZ: conceptualization and writing—original draft preparation. SZ, YZ, and ZT: methodology. SZ and YZ: validation and funding acquisition. YZ and SS: writing—review and editing. All authors have read and agreed to the published version of the manuscript.

FUNDING

This research was funded by the National Natural Science Foundation of China (grant numbers 81801210, 61975248); Science and Technology Project of Guangzhou of China (grant numbers 202102020157, 202007040004); Natural Science Foundation Project of Guangdong Province, China (grant number 2018A0303130137); Major Science and Technology Project of Yunnan Province, China (grant number 202102AA100012).

REFERENCES

Albay, E., and Kamaşak, M. (2015). *Skin Lesion Classification Using Fourier Descriptors of Lesion Borders* (Piscataway, NJ: IEEE), 1–4. doi: 10.1109/TIPTEKNO.2015.7374547

Bahri, H., Chouchene, M., Khemiri, R., Sayadi, F., and Atri, M. (2018). *Fast Moving Human Detection Using Fourier and HOG Descriptors Based CUDA* (Piscataway, NJ: IEEE), 202–7. doi: 10.1109/SSD.2018.8570566

Chi, J., Wu, X., and Zhang, C. (2008). *Medical CT Image Preprocessing Based on Edge Detection and Spline Fitting* (Piscataway, NJ: IEEE), 709–14.

Kapoor, R., Gupta, R., and Kumar, R. (2019). Iris localization for direction and deformation independence based on polynomial curve fitting and singleton expansion. *Multimed. Tools Appl.* 78, 19279–19303. doi: 10.1007/s11042-019-7314-0

Kim, S. W., Bae, S. C., and Ahn, Y. J. (2016). An algorithm for G2 offset approximation based on circle approximation by G2 quadratic spline. *Comput.-Aided Des.* 73, 36–40. doi: 10.1016/j.cad.2015.11.003

Li, H. (2019). Multiple ellipse fitting of densely connected contours. *Inform. Sci.* 502, 330–345. doi: 10.1016/j.ins.2019.06.045

Roth, H. R., Oda, H., Zhou, X., Shimizu, N., Yang, Y., Hayashi, Y., et al. (2018). An application of cascaded 3D fully convolutional networks for medical image segmentation. *Comput. Med. Imaging Graph.* 66, 90–99. doi: 10.1016/j.compmedimag.2018.03.001

Serpa-Andrade, L., Robles-Bykbaev, V., González-Delgado, L., and Moreno, J. L. (2015). *An Approach Based on Fourier Descriptors and Decision Trees to Perform Presumptive Diagnosis of Esophagitis for Educational Purposes* (Piscataway, NJ: IEEE), 1–5. doi: 10.1109/ROPEC.2015.7395123

Sullivan, R., Dailey, T., Duncan, K., Abel, N., and Borlongan, C. V. (2016). Peripheral nerve injury: stem cell therapy and peripheral nerve transfer. *Int. J. Mol. Sci.* 17:122101. doi: 10.3390/ijms17122101

Zhong, Y., Li, J., Qi, F., Sun, S., Zhu, S., Wang, C., et al. (2021). Contours modeling of fascicular groups from micro-computed tomography images of peripheral nerves. *Microsc. Res. Techniq.* 84, 2811–2819. doi: 10.1002/jemt.23840

Zhong, Y., Luo, P., Zhang, Y., Li, F., and Zhu, S. (2020). Centroid of fascicular groups in micro-CT image of peripheral nerves. *J. Biomater. Tiss. Eng.* 10, 1757–1765. doi: 10.1166/jbt.2020.2494

Zhong, Y., Wang, L., Dong, J., Zhang, Y., Luo, P., and Qi, J. (2015). Three-dimensional reconstruction of peripheral nerve internal fascicular groups. *Sci. Rep.* 5, 1–13. doi: 10.1038/srep17168

Zhu, S., Zhu, Q., Liu, X., Yang, W., Jian, Y., and Zhou, X. (2016). Three-dimensional reconstruction of the microstructure of human acellular nerve allograft. *Sci. Rep.* 6, 1–07. doi: 10.1038/srep30694

Zhu, W., Tringale, K. R., Woller, S. A., You, S., Johnson, S., and Shen, H. (2018). Rapid continuous 3D printing of customizable peripheral nerve guidance conduits. *Mater. Today.* 21, 951–959. doi: 10.1016/j.mattod.2018.04.001

Zhuo, Z., Liu, Z., and He, Y. (2016). *High-Performance Image Contour Delineation Method Based on Piecewise Cubic Bezier Curves Fitting* (Piscataway, NJ: IEEE), 22–25. doi: 10.1109/SIPROCESS.2016.7888216

Conflict of Interest: The authors declare that the research was conducted in the absence of any commercial or financial relationships that could be construed as a potential conflict of interest.

Publisher's Note: All claims expressed in this article are solely those of the authors and do not necessarily represent those of their affiliated organizations, or those of the publisher, the editors and the reviewers. Any product that may be evaluated in this article, or claim that may be made by its manufacturer, is not guaranteed or endorsed by the publisher.

frontiers | Frontiers in Cellular Neuroscience

REVIEW
published: 28 June 2022
doi: 10.3389/fncel.2022.926222

Biomaterial-Based Schwann Cell Transplantation and Schwann Cell-Derived Biomaterials for Nerve Regeneration

Zilong Rao[1], *Zudong Lin*[2], *Panpan Song*[1], *Daping Quan*[1] *and Ying Bai*[1]*

[1] *Guangdong Engineering Technology Research Centre for Functional Biomaterials, School of Materials Science and Engineering, Sun Yat-sen University, Guangzhou, China,* [2] *PCFM Lab, GD HPPC Lab, School of Chemistry, Sun Yat-sen University, Guangzhou, China*

Schwann cells (SCs) dominate the regenerative behaviors after peripheral nerve injury by supporting axonal regrowth and remyelination. Previous reports also demonstrated that the existence of SCs is beneficial for nerve regeneration after traumatic injuries in central nervous system. Therefore, the transplantation of SCs/SC-like cells serves as a feasible cell therapy to reconstruct the microenvironment and promote nerve functional recovery for both peripheral and central nerve injury repair. However, direct cell transplantation often leads to low efficacy, due to injection induced cell damage and rapid loss in the circulatory system. In recent years, biomaterials have received great attention as functional carriers for effective cell transplantation. To better mimic the extracellular matrix (ECM), many biodegradable materials have been engineered with compositional and/or topological cues to maintain the biological properties of the SCs/SCs-like cells. In addition, ECM components or factors secreted by SCs also actively contribute to nerve regeneration. Such cell-free transplantation approaches may provide great promise in clinical translation. In this review, we first present the current bio-scaffolds engineered for SC transplantation and their achievement in animal models and clinical applications. To this end, we focus on the physical and biological properties of different biomaterials and highlight how these properties affect the biological behaviors of the SCs/SC-like cells. Second, the SC-derived biomaterials are also reviewed and discussed. Finally, the relationship between SCs and functional biomaterials is summarized, and the trends of their future development are predicted toward clinical applications.

Keywords: Schwann cells, cell transplantation, biomaterials, peripheral nerve injury, central nerve injury

OPEN ACCESS

Edited by:
Ji-Fan Hu,
Jilin University, China

Reviewed by:
Eduardo Martin Lopez,
Yale University, United States
Thomas Johnson,
Johns Hopkins University,
United States

***Correspondence:**
Ying Bai
baiy28@mail.sysu.edu.cn

Specialty section:
This article was submitted to Non-Neuronal Cells, a section of the journal Frontiers in Cellular Neuroscience

Received: *22 April 2022*
Accepted: *31 May 2022*
Published: *28 June 2022*

Citation:
Rao Z, Lin Z, Song P, Quan D and Bai Y (2022) Biomaterial-Based Schwann Cell Transplantation and Schwann Cell-Derived Biomaterials for Nerve Regeneration. Front. Cell. Neurosci. 16:926222. doi: 10.3389/fncel.2022.926222

INTRODUCTION

Central nervous system (CNS) and peripheral nervous system (PNS) constitute the large neural network in the human body. The CNS, which includes brain and spinal cord, communicates with other organs/tissues through the PNS, perceives and processes information from external environment and maintains the biological functions of living bodies. Neurons and glial cells are the main cell types in the nervous systems. Neurons can receive internal and external stimuli, conduct nerve impulses, and integrate information. Most neurons have multiple dendrites and one axon.

The axon conducts nerve impulses from the soma to the downstream neuron or effectors (such as myocytes). Meanwhile the dendrites receive information and transmit it to the soma. Glial cells, such as Schwann cells (SCs) in the PNS and oligodendrocytes in the CNS, wrap around axons and form insulating myelin structures, which facilitate rapid conduction of electrical impulses and protect neurons. Specific injuries in the nervous system (e.g., neurodegenerative disease, stroke, traumatic injury in the CNS, and peripheral nerve injury in the PNS) may disturb the interactions between neurons and glial cells, even result in complete impairment of the motor/sensory activities of the whole body.

Peripheral Nerve Injury

Peripheral nerve injury (PNI), which is usually caused by mechanical trauma (e.g., traffic accidents, tool injuries) and disease complications (e.g., tumorectomy), often results in long-term numbness, loss of motor/sensory function, neuropathic pain, or paralysis (Schmidt and Leach, 2003). Based on the degree of damage, peripheral nerve injuries are classified into three categories: neurapraxia, axonotmesis, and neurotmesis (Sunderland, 1951). Neurapraxia and axonotmesis are usually caused by compression, overstretch, and nerve crush, which exhibit moderate symptoms and better prognosis compared to neurotmesis. The basal lamina around axons/SCs and the connective neuronal stroma (endoneurium, perineurium, and epineurium) is preserved after neurapraxia and axonotmesis, leaving an intact and permissive environment for axonal regeneration. Unfortunately, most PNIs found in clinical practice are neurotmesis or nerve transection, in which the continuity of the peripheral nerve is disrupted, and the connective tissues are partially or completely damaged (Barrette et al., 2008). Between the proximal and distal stumps of the injured nerves, the physical guidance and biochemical support are lost, which was originally provided by basal lamina tubes and connective tissues, resulting in disorientation of the regenerating axons. Therefore, the main objective of PNI treatments is to bridge the nerve stumps and help guiding severed axons to reach their disconnected targets (Siemionow et al., 2010).

The most frequently used clinical treatment of PNI is either direct suture of the severed ends or bridging the proximal and distal stumps using autologous nerve grafts. However, these two methods have distinct limitations and drawbacks. The former is only effective for PNI injuries with small gaps (<1 cm) (Bassilios Habre et al., 2018). For long-distance (>1 cm) gaps, transplantation of autologous nerve grafts achieves significant repair effect, which serves as the gold standard for PNI repair. Large amount of SCs and basal lamina tubes remain in the autologous nerve grafts that provide sufficient physical guidance and neurotrophic factors to promote axonal regeneration (Jiang et al., 2010). However, autologous nerve transplantation requires harvest of healthy nerves, resulting in loss of sensory and motor function at the donor site, along with possible neuromas and scar formation. Moreover, the transplanted nerves are usually sensory nerves that might lead to mismatch against the nerve size of the recipient region or bundle branches, which is why only about 50% of the patients reached effective functional recovery after autologous nerve transplantation (Daly et al., 2012; Sabongi et al., 2014).

Artificial nerve grafts, also termed nerve guidance conduits (NGCs), often serve as the alternatives to autologous nerve grafts. Many FDA approved biocompatible and biodegradable polymers are used for NGCs fabrication, such as poly (L-lactic acid) (PLLA), poly (ε-caprolactone) (PCL), silk fibroin, alginate, and the extracellular matrix (ECM) derived materials, including collagen, hyaluronic acid, and fibrin (Gu et al., 2014b). The NGCs can be prepared by filling in or coating on specific topological structures (e.g., microgrooves and aligned fibers) to support and guide axonal regrowth (Sarker et al., 2018a; Yang et al., 2021). However, these engineered nerve grafts only achieved similar or lower outcomes in repairing small nerve gaps (<3 cm) compared to the autografts, but the functional recovery was still unsatisfying for long-distance nerve defects. The most significant drawback of these NGCs is the lack of cellular support within the conduits. Transplantation of SCs is a feasible treatment to provide sufficient cellular components in the injured sites, and ultimately support axonal regeneration. Within this context, Guenard et al. (1992) transplanted SCs in a rat sciatic nerve defect, which demonstrated enhanced axonal regeneration and myelin formation. In addition, autologous SCs can be isolated from the patient and expanded *in vitro* prior to implantation, which serve as functional cell type for auto-transplantation therapies.

Central Nerve Injury

The CNS possesses unique characteristics of structural and functional compositions compared to the PNS, and the pathological responses following central nerve injury (CNI) is also significantly different from PNI. The CNS is made up of gray matter and white matter, the gray matter mainly consists of neuronal somas, dendrites, and glial cells (astrocytes, microglia, and oligodendrocytes), and the white matter mainly consists of axons and glial cells (Assinck et al., 2017a). The gray matter forms a butterfly shape in the center of a spinal cord, which is wrapped around by the white matter or distributes on the periphery of the white matter in brain. Following CNI, large number of neurons and glial cells are dead and axons at the injury site are demyelinated. Unlike the PNS, myelin in the CNS is produced by oligodendrocytes rather than SCs. The myelin debris cannot be completely cleared after CNI due to apoptosis or silence of oligodendrocytes (Barres et al., 1993). The residual myelin debris and other inhibitory molecules further lead to inflammatory responses, including astrocyte proliferation and glial scar formation, resulting in a non-permissive microenvironment that prohibits neural stem cell differentiation into neurons and axonal regeneration (Cao et al., 2001; Pallini et al., 2005).

Facing with such a complex pathology after CNI, the treatment strategies usually require overcoming the specific pathological factors in the inhibitory microenvironment, which should reconstruct a favorable microenvironment for axonal regeneration (Pego et al., 2012). Therefore, current research on CNI treatment include blocking the inhibitory factors against axonal growth, such as Nogo-A, MAG, and CSPG that produced

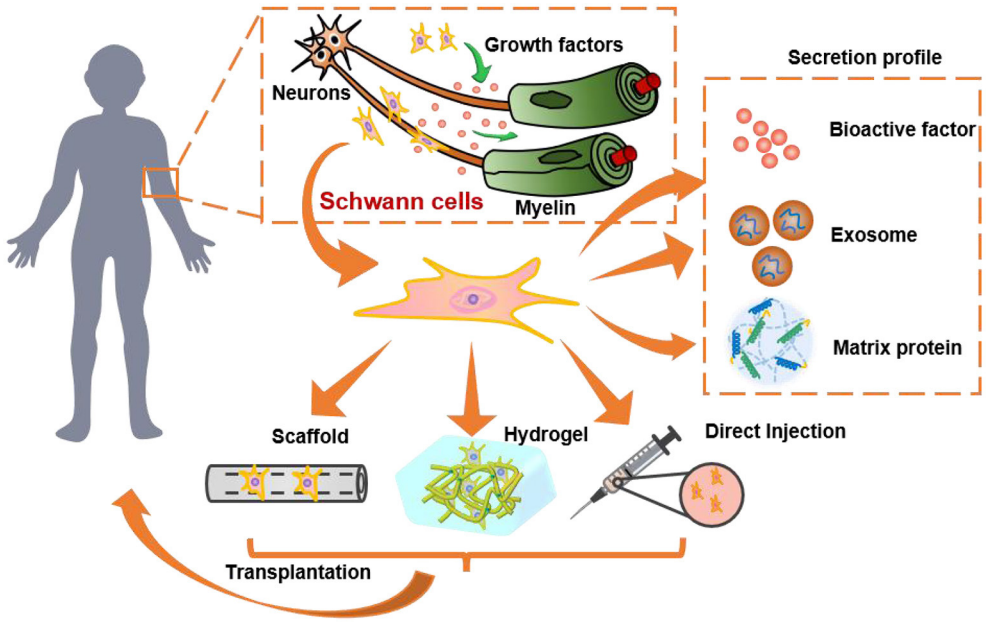

FIGURE 1 | The role and of SCs and SC-derived materials in nervous system and their transplantation for nerve regeneration. SCs secret growth factors to protect neurons, promote neurite growth, and wrap around axons to form myelin. They can be transplanted by direct injection into humans or pre-encapsulated in 3D hydrogels/scaffolds for transplantation. Besides, the secretion profile of SCs, such as the bioactive factors, exosomes, and extracellular matrix proteins, are also promising alternatives to SCs transplantation.

by myelin debris, or replacing ECM to activate the regeneration capacity of endogenous neurons. Anti-inflammatory drugs, such as minocycline, IL-10, indomethacin, and many neurotrophic factors, including nerve growth factor (NGF), neurotrophin-3 (NT-3), and brain-derived neurotrophic factor (BDNF) are also employed to alleviate inflammatory responses, promote neuron survival, and facilitate axonal regeneration (Cao et al., 2001; Sahni and Kessler, 2010). However, these strategies are mainly neuroprotective, aiming to prevent secondary cell death, minimize the extent of injury, or enhance neural plasticity by targeting only one inhibitory substance. Although their potential has been demonstrated by previous research, these single-target strategies cannot overcome the complex barriers toward regeneration, limiting their efficacy in promoting functional recovery. Therefore, a combinational approach is desired to resolve multiple issues after CNI.

Cell transplantation is considered to potentially ameliorate the injured environment in CNI treatments. The SCs and SC-like cells are the most promising cell lineages for cell-based therapies. As a cytokine bank in the PNS, SCs produce a variety of growth factors, including NGF, BDNF, and glial cell line-derived neurotrophic factors (GDNF), as well as some ECM proteins, such as laminin and fibronectin, which can stimulate the intrinsic capability of the damaged neurons to survive and facilitate axonal extension (Bixby et al., 1988). More importantly, considering that SCs can participate in myelin debris clearance and promote remyelination after PNI, which may provide viable solutions to those intractable problems caused by inactivity of oligodendrocytes after CNI. Furthermore, it was reported that SCs transplantation induced axon regeneration from retinal ganglion cells (RGCs) and peripheral-type myelination in a rat optic nerve injury model (Li et al., 2007). Therefore, SCs transplantation is potentially multi-functional for facilitating axonal regeneration and myelination in the CNI treatments (Hill et al., 2006).

The Role of Schwann Cells in Nerve Regeneration

After nerve injury, series of cellular and molecular changes occur at the injury site, including the changes of interaction between extracellular matrix and neural cells, which are potentially related to nerve regeneration (Gaudin et al., 2016). SCs play a pivotal role in several aspects of nerve regeneration, such as nerve fiber regeneration, myelination, and axonal guidance (**Figure 1**). For example, the damaged axons degenerate, and myelin sheath disintegrates after PNI (Touma et al., 2007), SCs lose contact with axons and result in radical changes of the signaling environment. Subsequently, SCs are activated and shift from a mature myelinating/non-myelinating state to a proliferating and repair phenotype, which is known as the plasticity of SCs (Ma and Svaren, 2018; Jessen and Mirsky, 2019). Along with macrophages, the dedifferentiated SCs participate in removal of cellular debris and myelination through autophagy (Zhao and Yi, 2019). This unique characteristic of SCs provides strong regeneration capacity in peripheral nerves. On the contrary, residual myelin debris usually remains uncleared at the injury site that leads to inhibitory microenvironment after CNI.

Once the myelin debris is cleared, series of regeneration-supporting neurotrophic factors and growth-inducing molecules, such as GDNF, BDNF, NGF, vascular endothelial growth factor (VEGF), and N-cadherin are secreted by SCs to promote neuron survival and axonal elongation (Ziegler et al., 2011; Wood and Mackinnon, 2015). The expression profile of different factors follows a temporal sequence that the protective factors (e.g., GDNF, NGF) are secreted earlier than the growth promoting factors (e.g., BDNF) (Gomez-Sanchez et al., 2017). Simultaneously, the dedifferentiated SCs begin to proliferate, elongate, and align within the residual endoneurial tube to form Büngner bands, which provides a growth pathway for the regenerating axons (Menorca et al., 2013; Sarker et al., 2018b). Following axonal regeneration, SCs wrap around the newborn axons to reconstruct myelin sheaths. This effect is considerably valuable for the treatments of both PNI and CNI, since the remyelination of regenerated axons is key to functional recovery of the injured nerves. Although SCs do not exist endogenously in the CNS, previous studies verified that some non-myelinating and myelinating SCs can be recruited from the PNS to promote myelin repair after CNI (Ma et al., 2018). Moreover, oligodendrocyte precursor cells (OPCs) in the CNS may differentiate into remyelinating SCs in response to demyelination and injury (Assinck et al., 2017b). These results strongly support the capacity of SCs to contribute in CNI repair.

Currently, the treatments that rely on the endogenous SCs are quite unsatisfactory, particularly for the long-distance peripheral nerve lesions. Although SCs are sensitive to environmental signals because of their plasticity, they cannot sustain their repair phenotype in long-term due to the gradually changing signals. Notably, it was evident that senescence-related SC markers (e.g., *SA-βgal*) is up-regulated in long-distance nerve injury and key regulators of the repair phenotype (e.g., *C-Jun*) is delayed, resulting in diminishing repairing effect (Saheb-Al-Zamani et al., 2013; Poppler et al., 2016; Chen et al., 2017). The transplantation of SCs may serve as an effective cell-based approach for the treatments of nerve injury.

Schwann Cells Transplantation for Nerve Injury Repair

Although the pathological responses in the PNS and CNS are quite different after injury, their repair strategies still share some common features. For example, researchers employed exogenous implants to improve the microenvironment of the injured area, stimulate the regenerative capacity of endogenous neural stem cells, guide axonal extension, and promote remyelination of the regenerated nerves. In recent years, numerous studies have been conducted using different therapeutic strategies, such as drugs, growth factors, and biomaterial scaffolds, for nerve injury repair (Gaudin et al., 2016; Sarker et al., 2018a). Although positive outcomes have been evident, the repair effects are still limited, especially for those severe nervous system injuries. The reason is that it is difficult to mimic the complex biochemical and physical characteristics of the native tissues, moreover, a long-lasting and favorable microenvironment is critical for nerve regeneration.

Cell-based therapies, especially SCs transplantation, are promising for the treatments of both PNI and CNI. As the most common glial cells in peripheral nerves, SCs are involved in the construction of extracellular matrix during peripheral nerve development, which can also actively participate in promoting nerve regeneration after PNI and CNI. However, there are two important issues that need to be addressed in SCs transplantation. First, the source of SCs is limited. Although the current technology allows extraction and purification of autologous SCs, it is difficult to obtain sufficient quantity and good quality of SCs for effective transplantation. The second issue is that the injection-based transplantation usually leads to significant shear-induced cell death. Furthermore, the injected cells are often rapidly lost at the injected region, resulting in unsatisfied survival *in situ*. On the other hand, most of the transplanted cells cannot transform into their regenerative phenotype spontaneously, but easily affected by the negative environmental factors and lose their regeneration capability at the injury site. Therefore, proper biomaterial-based cell carriers are highly desirable to address these two problems for the application prospects of SCs transplantation.

BIOMATERIAL-ASSISTED SCS TRANSPLANTATION

Transplantation of SCs and Schwann Cell-Like Cells

As the gold standard in treatments of peripheral nerve defects, transplantation of nerve autografts is the main approach to introduce autogenous SCs to the injury site after PNI, but the disadvantages of autografts are well-noticed as previously described. Meanwhile, scaffold implantation is only applicable to nerve lesions with gaps (El Seblani et al., 2020). Purified SCs can be obtained by *in vitro* culture and expansion techniques, which is potentially beneficial for exogenous SCs transplantation. The *in-situ* injection of autogenous SCs cause less damage to the injury sites and is more suitable for irregular nerve defects or demyelinating diseases. The cultured SCs also allow biological/chemical SCs induction to achieve a regenerative phenotype before implantation. However, the quality and repair capacity of the patient derived SCs may be affected by their physiological conditions, such as the age of donors (Painter et al., 2014; Bastidas et al., 2017). Moreover, SCs isolation requires surgical removal of healthy nerves and long-term cultivation to render adequate cell number for transplantation. Therefore, alternative resources of SCs are desirable for clinical applications.

Schwann cell-like cells (SCLCs) derived/differentiated from stem cells provide a great promise as the SCs substitution for nerve injury repair (Hopf et al., 2020). Numerous stem cell sources, such as embryonic stem cells (ESCs), adult stem cells, and induced pluripotent stem cells (iPSCs), can differentiate into SCLCs though biological/chemical inductions (Dezawa et al., 2001; Huang et al., 2017; Kim et al., 2017). Ziegler et al. obtained SCLCs with SC-like morphological and molecular properties through induced differentiation from human ESCs, they demonstrated that these SCLCs interacted with axons and

triggered myelination (Ziegler et al., 2011). Adult mesenchymal stem cell (MSCs), such as bone marrow stem cells (BMSCs) and adipose-derived stem cells (ADSCs), are also widely used in nerve injury therapies due to their high proliferation capability and multilineage differentiation potential (Park et al., 2010; Cai et al., 2017). Despite the capacity of direct differentiation into SCLCs, MSCs have also been identified to secret neurotrophic factors, cytokines, and immunomodulatory factors to support axonal growth and mediate immune response at the injury sites (Wang et al., 2009; Lin et al., 2012). MSCs secrete a variety of soluble factors, which include tumor necrosis factors (e.g., TNF-β1) and interleukins (e.g., IL-13 and IL-10) to exert anti-inflammatory potential and inhibit release of pro-inflammatory factors (such as TNF and IL-6), when transplanted into injured spinal cord (Sobacchi et al., 2017). Skin-derived precursors (SKPs) are another reliable source of SCLCs, since they originate from neural crest. SKP-differentiated SCLCs were identified to exhibit identical transcriptional signatures as in the primary SCs (Stratton et al., 2017). Unfortunately, these stem cells derived SCLCs have not yet progressed into clinical trials, because of heterogeneity, quality, and ethical restriction issues. SCLCs differentiated from iPSCs are currently more attractive, which may overcome the resource limitations of the ESCs and MSCs (Maherali et al., 2007). The iPSCs can be differentiated to neural crest cells and subsequently transformed into different neural cell lineages.

SCs and SCLCs can be delivered to the injured nerves through different ways. The simplest method is to prepare a suspension of the SCs and SCLCs in medium and then directly inject into the injury sites (Pinero et al., 2018; Mousavi et al., 2019; Assinck et al., 2020). Tomita et al. transdifferentiated ADSCs into SC phenotype, the cell suspension was then slowly injected into the distal region of the reconnected nerves. Compared to the allogenic SCs, ADSCs-derived SCs exhibited comparable capability in facilitating nerve regeneration after chronic denervation (Tomita et al., 2012). However, direct cell injection often has several serious drawbacks. First, the shear stress during needle-based microinjection causes irreversible damage to the cells. Second, the transplanted cells may disperse rapidly and lose their repair capacity due to the unfavorable microenvironment *in situ*. Especially for the stem cell-derived SCLCs, the SC-like phenotype is usually unstable and easily transformed into other cell types. The direct injection approach is also limited since the injury sites must be enclosed. Therefore, it is probably more applicable to the neurogenic diseases in brain, or injuries caused by contusions in spinal cord or peripheral nerve. To ensure high therapeutic efficacy after SCs or SCLCs transplantation, proper cell carriers are highly desired to reduce shear damage and provide physical and biological support for cell growth, retention, and nerve regeneration.

SCs Transplantation Using Injectable Hydrogels

To avoid severe damage to the cells during injection, the SCs or SCLCs can be pre-suspended in pre-gel solution for *in-situ* gelation or pre-encapsulated in hydrogel. Hydrogel is a hydrated polymer network with high water content (Drury and Mooney, 2003). It can provide a three-dimensional environment and similar structural/mechanical properties as the native tissues, thus has received considerable attentions in tissue engineering (Liu et al., 2020). Before gelation, the hydrogels present a liquid-like state (i.e., pre-gel solution), while cells can be mixed and encapsulated in the pre-gel solution. The polymer chains in the hydrogel can protect the cells from rupture and provide shear resistance during injection, resulting in promoted survival and viability of the transplanted cells. Following injection, the cells containing pre-gel solution can be induced to form hydrogel in response to temperature change or by exposure to light. The high porosity and permeability of the hydrogels allow the exchange of oxygen, nutrients, and cytokines with surrounding tissues to support cell survival and growth (Szabo et al., 2019).

In general, the hydrogels used for SCs or SCLSs transplantation need to meet some essential requirements. For instance, hydrogels must be biocompatible and non-toxic to the cells and host tissues. The pre-gel solution should exhibit low viscosity and gel quickly when delivered to the injured area, ensuring a rapid settlement and retention of the transplanted cells (Marquardt and Heilshorn, 2016). The implanted hydrogels are desired to resist compression and infiltration of the surrounding tissues, while providing suitable stiffness that allow attachment and functionalization of the SCs/SCLCs. Therefore, injectable hydrogel with mechanical strength ranging from 100 Pa to 10 kPa are often chosen to match with that of the native nerve tissue (Budday et al., 2017) and they are required to have adaptable stability to prevent degradation-induced loss of the transplanted cells. On the other hand, as regeneration progresses, hydrogels gradually degrade to allow impending tissue regrowth, and finally replaced by the ECM secreted by the surrounding cells, such as neurons and glial cells. Besides the physical properties, bioactivities that promotes revascularization are also desirable using hydrogels as transplantation carriers. It has been reported that the implanted cells can survive surrounded by blood vessels, otherwise they would be hard to obtain nutritional support. Therefore, rapid revascularization within hydrogels plays an important role in the survival of cell transplantation (Daly et al., 2020). Therefore, choosing a proper hydrogel with suitable mechanical and biological properties significantly influence the subsequent *in vivo* performance of the transplanted SCs/SCLCs for tissue repair.

Injectable hydrogels can be classified as natural and synthetic hydrogels, based on their origins (**Table 1**). Natural hydrogels derived from the ECM components in animals and plants are popular choices for SCs transplantation, due to their resemblance to the native nerves (Geckil et al., 2010; Li and Lepski, 2013). The most widely used natural hydrogels include proteins (e.g., collagen and fibrin) and polysaccharides (e.g., alginate and hyaluronic acid) (Gyles et al., 2017). They possess intrinsic amino acids or peptide domains that bind with cell receptors and typically contribute to cell adhesion and axonal growth in the native tissues, which make them biocompatible and bioactive in modulation of cellular functions (Catoira et al., 2019). Therefore, natural hydrogels have great advantages to serve as cell carriers, since they provide favorable

TABLE 1 | Hydrogels used for SCs/SCLCs transplantation.

	Biomaterial	Origin	Advantages	Disadvantages	Application
Protein-based hydrogel	Collagen	Animal tissues, a structural protein of the ECM	Easy to be isolated, purified, and can spontaneously form hydrogels Biocompatible and biodegradable Provide essential ECM molecules to support cellular functions Nanofibrous structures	Potential immunoreaction Inadequate mechanical property Rapid degradation *in vivo*	The raw material of FDA-approved nerve conduits Promote cellular survival, retention, and neurite regeneration as a cell carrier (Guan et al., 2013; Georgiou et al., 2015)
	Gelatin/GelMA	A product of hydrolyzed collagen	Good biocompatibility, degradability, low immunogenicity, and stable mechanical properties.	Potential damage to the transplanted cells during UV light crosslinking	The base of bio-ink in 3D bioprinting and cell encapsulation (Zhao et al., 2016; Sun et al., 2018; Xiao et al., 2019).
	Fibrin	An insoluble protein polymer of plasmic proteins	Highly compatible with blood and tissues Inhibit the expression of myelin and keep SCs in a non-myelin state to induce regeneration through ERK1/2 phosphorylation	Poor stiffness, fast degradation, and the risk of transmitting blood disease.	Enhanced SCs viability and nerve regeneration by introducing fibrin hydrogel (Schuh et al.) Promote EMSC differentiation into SCLCs (Chen et al., 2015).
Polysaccharides-based hydrogel	HA	Animal tissues, rich in eyes and joints, a glycosaminoglycan type of ECM content	Biocompatible and biodegradable Easy to be chemical functionalized Promote cell proliferation by binding to CD44 receptor on cell surface Shear-thinning	Poor cell attachment property due to the high-water retention rate	Combined with alginate hydrogel to promote SCs survival and proliferation (Wang et al., 2013) Provide injectability, printability, and bioactivity to protect SCs and SCLCs during transplantation (May et al., 2018; Ho et al., 2019)
	Alginate	A linear polysaccharide extracted from brown algae	Non-immunogenicity, slow degradation properties and high hydrophilicity Quickly and reversibly crosslinked by Ca^{2+}	Need biological modification	Bridging materials for both spinal cord and peripheral nerve injury repair (Mosahebi et al., 2002; Wu et al., 2020).
Decellularized matrix-based hydrogel	Tissue-derived dECM hydrogels	The native mammal tissues/organs	Retain large amount of ECM components, and recapitulate the biological characteristics of native ECM Biocompatible, biodegradable, and bioactive	Lower moduli, difficult to be modified Unknown immunoreaction in human	Peripheral nerve-derived dECM hydrogel significantly improved SCs survival and axonal remyelination (Cerqueira et al., 2018)
	Matrigel	Cultured EHS tumor cell lines	Excellent biological activity in promoting cell growth and proliferation.	Potential risk in clinical translation	Base material for cell culture (Kamada et al., 2005; Lopatina et al., 2011).
Synthetic hydrogels	PEG		Non-toxicity, good biocompatibility, low protein adsorption, and noninflammatory invasion. Reduces ROS to protect neurons.	Hydrophilic and biological inert Undegradable	Modified with RGD peptides or other functional peptides to support NSCs and SCs survival (Franco et al., 2011; Marquardt et al., 2020)
	PHEMA		Porosity and moduli are easily manipulated	Bio-inert	Supporting materials of the multicomponent hydrogels (Hejcl et al., 2010)

environment for the encapsulated cells and support their survival and proliferation.

Protein-Based Hydrogel

As the major protein components of the ECM in nerve tissues, collagen type I is one of the most commonly used natural biomaterials for nerve regeneration. Collagen can be easily isolated, purified, and spontaneously form hydrogel at temperature ∼37°C through adjusting the pH value (Silva et al., 2021). Collagen hydrogel not only provides essential ECM molecules to support cellular functions, but also mimics the nanofibrous structure of native nerves, which is beneficial for cell adhesion and proliferation. Marchand et al. injected a pre-cooled collagen I solution into a transected spinal cord injury rat model, the collagen self-assembled *in situ* and formed nanofibrous hydrogel. Eight days post-surgery, the host cells, such as fibroblasts, macrophages, and SCs were observed to penetrate into the hydrogel, and the regenerated axons were found crossing the injury boundary into the hydrogel after 3 months (Marchand and Woerly, 1990). Considering the positive cellular response, collagen has been widely used as the raw material in nerve conduits, as well as a popular cell carrier for SCs and SCLCs. It has been proven that when MSCs were transplanted using collagen gel, the survival and retention of the MSCs were increased compared to injection of MSCs alone (Guan et al., 2013). Georgiou et al. encapsulated both rat SCs and ADSCs-derived SCs (dADSCs) into collagen and induced cell alignment by plastic compression. The collagen supported the secretion of functional molecules and growth factors from the SCs and dADSCs, which guided neurite growth *in vitro*, and promoted nerve regeneration in a 15-mm rat sciatic nerve defect model cpmp (Georgiou et al., 2015). Due to the processability of hydrogel, collagen gel can be employed in many fabrication technologies, including lyophilization, 3D printing, and electrospinning, to expand its the clinical applicability. However, since collagen is derived from animal tissues, the implantation of collagen in human raises safety concerns that may cause immunoreaction (Friess, 1998).

Gelatin is a product of hydrolyzed collagen, which retains the amino acid sequences of collagen, such as the classic arginine-glycine-aspartate (RGD) peptide. Gelatin possesses good biocompatibility, degradability, and low immunogenicity, which supports cell infiltration, adhesion, and proliferation (Echave et al., 2017). However, gelatin becomes soluble at body temperature but gels at lower temperature, which makes it unsuitable for *in-situ* transplantation. To overcome this drawback, gelatin is frequently modified by crosslinking agents, or incorporate with other materials to ensure a stable state during implantation. Methacrylated gelatin (GelMA), produced by substituting amines in gelatin with methacrylamide, can form photocrosslinkable hydrogel with additional photoinitiator. Due to the rapid gelation and stable mechanical properties, GelMA has been broadly used for 3D bioprinting and cell encapsulation (Zhao et al., 2016; Sun et al., 2018; Xiao et al., 2019). Luo et al. encapsulated dental pulp stem cells (DPSCs) and bFGF in GelMA hydrogel to repair 15-mm long sciatic nerve defect in rats, which achieved functional recovery that comparable to nerve autograft (Luo et al., 2022). Wang et al. fabricated a bio-ink by mixing 10% GelMA solution with rat SCs and BMSCs, then underwent extrusion-based bioprinting to construct a bionic spinal cord stent. By changing the cellular components in the GelMA-based bioink, different spatial arrangement of SCs and BMSCs was achieved that facilitated motor function recovery after spinal cord injury (Wang et al., 2021).

Fibrin is derived from plasmic proteins and highly compatible with blood and tissues, which has received extensive attention in the field of wound healing, due to its capability in clotting and hemostatic properties (Mosesson, 2005). Moreover, fibrin also plays a special role in peripheral nerve regeneration. Following PNI, the blood-nerve barrier broke down and fibrinogen plasma can leak into the injured area, and then be cleaved by thrombin to form fibrin cables. The fibrin cables not only serve as physical guidance for SCs migration, but also interact with SCs to induce their regenerative phenotype by upregulating p75NGFR through ERK1/2 phosphorylation (Akassoglou et al., 2002; Petersen et al., 2018). Therefore, fibrin hydrogel can be viewed as a potential transplantation platform for SCs. Schuh et al. blended fibrin with collagen to form an engineered neural tissue, where fibrin was used as an activator for the transplanted SCs. It was confirmed that the addition of fibrin enabled significant enhancement of SCs viability and promoted nerve growth both *in vitro* and *in vivo*, compared to collagen (Schuh et al., 2018). Chen et al. confirmed that ectomesenchymal stem cells (EMSCs) grown on the fibrin hydrogel expressed myelination-related molecules such as myelin basic protein (MBP) and galactocerebrosides (GalCer), and secreted more neurotrophins compared to those grown on a plastic surface. They further demonstrated that fibrin hydrogel promoted EMSC differentiation into SCLCs (Chen et al., 2015). However, it should also be considered that the poor stiffness, fast degradation, and the risk of transmitting blood disease may limit the clinical applications of fibrin hydrogels.

Polysaccharides-Based Hydrogel

Polysaccharides are a sort of biopolymers consisting of monosaccharides or disaccharides, which can also be found easily in ECM (Russo et al., 2015). Polysaccharides play important roles in the composition of cell membranes, intercellular communication, and energy storage of living organisms in animals and plants. For example, hyaluronic acid (HA) is a linear, highly hydrated, non-sulfated anionic glycosaminoglycan (GAG) polymer consisting of β-1,4-D-glucuronide and β-1,3-N-acetylglucosamine. It is one of the most abundant components in the ECM of nervous tissues, which is involved in the regulation of many cellular functions, such as cell adhesion, proliferation, migration/maintenance of the connective tissue, and proteoglycan assembly (Zamboni et al., 2018). HA can specifically bind to CD44 receptor on cell surface and activate intracellular signaling pathways, such as the Ras-Raf-MEK-ERK pathway, to trigger cell proliferation (Ponta et al., 2003; Matsumoto et al., 2009). However, HA cannot be crosslinked directly and often exhibit poor cell attachment properties. Therefore, chemical modification to introduce functional groups onto HA chains, such as methacrylate or thiol groups, is required to endow gel formation capabilities. HA hydrogel

can be further mixed with other bioactive materials or undergo RGD peptide modification to promote cell adhesion. A hyaluronan/methylcellulose (HAMC)-based hydrogel was proven to be a versatile cell delivery system, which improved the survival and distribution of transplanted retinal stem cells (RSCs) and neural stem cells (NSCs) in stroke and spinal cord injury models (Ho et al., 2019). The HA component of the HAMC hydrogel is shear-thinning to endow injectability and exhibited enhanced tissue response, while the methylcellulose component underwent inversed thermal-gelling and formed physical crosslinking. May et al. encapsulated skin-derived precursor Schwann cells (SKP-SCs) in the HAMC hydrogel, and the survival of grafted SKP-SCs was improved when injected into spinal cord cavity. The modification by laminin and fibronectin further reduced cell spreading effect and anoikis compared to the HAMC hydrogel alone (May et al., 2018).

Alginate is a negative-charge linear polysaccharide extracted from the cell wall and intercellular mucilage of brown algae. Alginate consists of α-guluronic acid and β-D-mannuronic acid that can rapidly crosslink with multivalent cations to form an ionotropic hydrogel (Sun and Tan, 2013). In the past decade, alginate hydrogel has been widely used as bridging materials for both spinal cord and peripheral nerve injury repair. It can host exogenous SCs, stem cells, and neurotrophic factors. Mosahebi et al. transplanted allogeneic SCs pre-embedded in alginate hydrogel into a 10-mm sciatic nerve injury model. The SCs exhibited repair functions to promote sustained axonal regeneration compared to the alginate hydrogel without SCs (Mosahebi et al., 2002). Alginate hydrogel usually exhibits non-immunogenicity and slow degradation properties. However, some research studies reported that alginate prevents cell adhesion due to its high hydrophilicity, presents bioinert properties for nerve regeneration, or even inhibits neurite outgrowth (Novikova et al., 2006). Therefore, biological modifications are necessary for the application of alginate hydrogel as a platform for SCs transplantation. For example, Wu et al. formed a bioprinted 3D scaffold using a composite bio-ink consisting of gelatin and alginate with the presence of SCs, the content of gelatin facilitated SCs adhesion to the scaffold (Wu et al., 2020).

Decellularized Matrix-Based Hydrogel

Due to the complexity of organisms, single component biomaterials, such as proteins and polysaccharides, can only partially recapitulate the compositional and biological characteristics of the native ECM. ECM consists of a variety of proteins, proteoglycans, and glycosaminoglycans, which is secreted and constructed by the resident cells of tissues or organs, providing biological and topographical cues for cell growth (Hussey et al., 2018). In recent decades, decellularization have brought an alternative option to obtain ECM-mimicking biomaterials with tissue-specific properties by removing the cellular components from the native mammal tissues/organs. Compared to the single component materials, decellularized extracellular matrix (dECM) retains large amount of ECM components from natural tissues, including proteins, polysaccharides, and growth factors, which exhibit high biological activities. Collagen is the major component of ECM and mostly preserved in the dECM, which further enables the digested dECM to form nanofibrous hydrogel though self-assembly. These dECM hydrogels are highly biocompatible that may better recapitulate the 3D microenvironment in native tissues, which also can serve as promising cargos for cell transplantation.

Among the various dECM hydrogels, Matrigel has been commercialized and widely used as a base material for cell culture. Matrigel is a cell-derived dECM hydrogels extracted from cultured Englebreth-Holm-Swarm (EHS) tumor cell lines by proteolytic digestion (Hughes et al., 2010). Matrigel contains most of the components of the basement membrane (∼60% laminin, 30% IV collagen and 8% nestin, and cytokines, such as TGF-β, epidermal growth factor, and insulin-like growth factor) and shows excellent biological activity in promoting cell growth and proliferation. Therefore, Matrigel may serve as a good vehicle for the transplantation of SCs and stem cells (Kamada et al., 2005; Lopatina et al., 2011). Patel et al. encapsulated SCs into three different matrices, methylcellulose, mixture of laminin and collagen IV, and Matrigel, respectively. After transplantation into rat spinal cords, the SCs encapsulated within Matrigel enhanced SCs survival and facilitated angiogenesis and axonal in-growth (Patel et al., 2010). Williams et al. used Matrigel/allogenic SCs transplantation to treat transected spinal cord injury in rats. They found that the implantation of fluid Matrigel and SCs improved regeneration of brainstem axons across the rostral interface, compared to the pre-gelled Matrigel (Williams et al., 2015). Although Matrigel exhibits great biological activity as a 3D culture platform for many different cell types, its tumor-secreted nature leads to extremely high risk in clinical translation.

Unlike Matrigel, dECMs that harvested from animal tissues/organs and decellularized by chemical/physical methods are more clinically acceptable, which have become a hot topic of tissue engineering in recent years. The dECM scaffold can be enzymatically digested to obtain a decellularized matrix solution, and then neutralized to a physiological pH and gel at 37°C (Brightman et al., 2000). Particularly, similar to the natural environment of SCs, dECM hydrogel derived from peripheral nerves may serve as an excellent biomaterial carrier for SC transplantation. The bioactive molecules retained in the dECM hydrogel can synergistically maintain the viability and biological functions of the SCs. However, the utilization of nerve-derived dECM hydrogel on SCs or stem cell transplantation has been rarely reported. Cerqueira et al. (2018) used rat allogeneic peripheral nerve-derived dECM hydrogel (iPN) for SC transplantation into a rat spinal cord contusion model. They showed that the iPN significantly improved the survival of SCs after transplantation compared to Matrigel, and further promoted axonal myelination. On the other hand, the dECM hydrogels derived from various tissues, such as cardiac, liver, skin, and nerves have also shown great promise in cell delivery and regulation of cellular behaviors (Park et al., 2021; Xu et al., 2021). It is believed that the dECM hydrogels derived from the nervous system may serve as an optimal choice for SCs transplantation (Lin et al., 2018; Zou et al., 2018; Liu et al., 2021; Xu et al., 2021).

Synthetic Hydrogels

Natural hydrogels have shown their advantages in biocompatibility and bioactivity, but most natural hydrogels have relatively lower moduli ranging 100–1,000 Pa, which hardly resist the extrusion of surrounding tissues. The degradation of natural hydrogels is relatively fast due to the enzymatic environment *in vivo* and difficult to support a long-term nerve regeneration. Chemical-/photo-crosslinking is often employed to enhance the stiffness of natural hydrogels, but the modification of natural materials is difficult and might be harmful to their biological activities (Sionkowska, 2011). Synthetic polymers with biocompatibility and suitable biodegradability can also be used as cell carriers. The physical properties of the synthetic hydrogels, such as porosity, modulus, and degradation rate are easily manipulated. However, most of the synthetic materials lack bioactivity or specific binding sites for cellular interactions, making them unsuitable for cell adhesion or tissue attachment. To address these problems, the bioactivity of synthetic hydrogels is often introduced by immobilization of bioactive molecules, peptides, or blending with the natural polymers (Woerly et al., 2001).

Polyethylene glycol (PEG) based hydrogels are one of the most frequently used carriers for cell delivery due to its non-toxicity, biocompatibility, low protein adsorption, and non-inflammatory invasion (Pasut et al., 2016). More importantly, studies have shown that PEG can promote fusion of cell membranes and repair damaged membranes, which also reduces reactive oxygen species (ROS) to protect neurons (Shi, 2013). Once modified with acrylate, the resulting polyethylene glycol diacrylate (PEGDA) undergoes gelation under UV light. However, PEG hydrogel is usually highly hydrophilic and biological inert that is insufficient for cell adhesion, which makes PEG hydrogel alone unsuitable for cell transplantation. The bioactivity of PEG-based hydrogels can be improved through copolymerization with other polymers, modification with bioactive molecules, or blending with natural hydrogels. Franco et al. modified PEGDA with RGD peptides, and then microencapsulated neural stem cells within the PEG-RGD microspheres to repair a rat stroke model (Franco et al., 2011). Marquardt et al. designed a "SHIELD" hydrogel consisting of an 8-arm PEG polymer modified with proline-rich peptides, PNIPAM, and a recombinant engineering protein C7. This complex hydrogel matrix resulted in significant retention of the transplanted SCs compared to direct cell injection, and further improved functional recovery of spinal cord injury (Marquardt et al., 2020). Despite the nervous system, PEG-based hydrogels are extensively applied in encapsulating various cell types, such as islet cells, ESCs, and MSCs (Koffler et al., 2019).

There are also some other synthetic hydrogels that can potentially be used in SCs or SCLCs transplantation, such as poly (2-hydroxyethyl methacrylate) (PHEMA) and poly[N-(2-hydroxypropyl)-methacrylamide] (PHPMA) (Hejcl et al., 2010). Limited by the poor biological activities, synthetic hydrogels are not commonly used alone as cell carriers, but act as the supporting materials of the multicomponent hydrogels.

Overall, injectable hydrogels possess unique advantages in cell transplantation, since they can provide native-like 3D microenvironments that allow the transplanted cells to grow and proliferate (Alvarado-Velez et al., 2014). Meanwhile, cell transplantation using hydrogel-assisted injection is minimally invasive to patients and more clinically acceptable in the treatments of some neurodegenerative diseases.

SCs Transplantation Using Scaffolds

The injectable hydrogels only provide biological cues for the survival and functionalization of SCs, while topological cues in native nerves that guide SCs alignment and polarization are missing. The alignment of SCs plays a critical role in nerve regeneration, since endogenic SCs are induced to align by the residual endoneurium tubes or the fibrous matrix, forming the Büngner bands to guide neurite growth. However, introducing physical cues to the hydrogels is quite difficult, since SCs or SCLCs are often randomly distributed inside the bulk hydrogels. In addition to the hydrogels, cells can also be transplanted using preformed scaffolds, including the nerve guidance conduits. The good mechanical property and processability of synthetic polymers, such as PEG, poly (lactic acid) (PLA), polycaprolactone (PCL), and poly-3-hydroxybutyrate (PHB) play an important role in scaffold preparation for SC transplantation. Bio-scaffolds can be fabricated with different architectures, such as the aligned fibers and microchannels, to regulate cellular behaviors, sometimes more suitable for the treatments of nerve defects. The limitation of biomaterial scaffolds is that the transplanted SCs often grow only on the surface of the scaffolds, which is quite different from the 3D hydrogels.

Scaffolds Without Topological Cues

Many scaffolds that have been used for transplanting SCs and SCLCs were simply fabricated with isotropic architectures, such as nanofibrous or interconnected porous structures. These scaffolds are either fabricated by solvent evaporation from hydrogels or polymer solutions using lyophilization or vacuum drying. Polymer solutions can be dispersed in a defined mold, then dehydrated into a tubular shape. The medium suspensions of SCs and SCLCs are infused into the lumen of the dry tube, and the tube can absorb the medium and distend to form a hydrogel-like or hydrated scaffold. For example, a gelatin hydrogel tube was first made by dehydration, followed by injection of SCs or ADSCs suspension. After incubation in the medium, the hydrated gelatin tube was implanted into a 5 mm-sciatic nerve lesion. The results confirmed that SCs were retained in the gelatin tube after 8 weeks (Sowa et al., 2016). In fact, a significant number of the hydrogel-based grafts are used as the cargo for SCs transplantation. Berrocal et al. implanted an absorbable collagen based NeuraGen® tube that combined with autologous SCs for treatment of a critical sized gap (13 mm) in the sciatic nerve of Fischer rat (Berrocal et al., 2013). The transplanted SCs survived at least for 4 months post-surgery and significantly enhanced the regeneration of myelinated axons.

The scaffold-assisted cell transplantation allows the combination of robust synthetic polymers with bioactive natural hydrogels. For example, PCL is a biodegradable polymer that has low degradation rate and good processability. Babaloo et al. (2019) fabricated a PCL/gelatin nanofibrous scaffold and co-seeded with human SCs (hSCs) and human endometrial

stem cells (hEnSCs). The cell-laden PCL/gelatin scaffold was then transplanted into hemisected spinal cord. The co-cultured hEnSCs and hSCs successfully triggered hEnSCs differentiation into neuron-like cells and resulted in a better performance for SCI repair. Basically, the SCs are transplanted by adhering to the surface and the sponge-like pores of the scaffold, the microstructure of the scaffold may perform a positive impact on the cellular behaviors. Uz et al. (2017) constructed the 3D gelatin conduits with three different microstructures by thermally induced phase separation (TIPS). The results indicated that the gelatin conduits with microporous and ladder-like structures were beneficial for MSCs adhesion and proliferation, and the ladder-like structures were more favorable for MSCs differentiation into SC-like phenotypes than the microporous structures.

Scaffolds With Topological Cues

Given the tubular microstructure of the native nerve tissues and the directional connection between neurons and target tissues, anisotropic physical structures are crucial for SCs polarization, directed migration, and myelin formation. Introducing the oriented structures into the transplantation scaffolds allows the alignment of SCs, and the aligned SCs provide a direct pathway for neurite extension (Wang et al., 2015). For example, a significant difference was found when SCs were cultured on the aligned and randomly oriented poly (methyl methacrylate) (PMMA) nanofibers. When cultured on the aligned PMMA nanofibers, the SCs polarized and exhibited larger aspect ratio than those cultured on the non-aligned nanofibers, which were more likely to co-localize with neurites for further myelination (Xia et al., 2016). Electrospinning is a commonly used technique to prepare scaffolds with highly oriented nanofibrous structures. Lee et al. fabricated a polyvinylidene fluoride trifluoroethylene (PVDF-TrFE) membrane with aligned electrospun nanofibers, then rolled into a hollow conduit. By injection of SC-loaded Matrigel, the aligned PVDF-TrFE nanofibers were proven to be beneficial for SCs alignment *in vivo* and promoted axonal extension, compared to the randomly oriented nanofibers (Lee et al., 2017). Notably, electrospinning can hardly be used to process complex 3D architectures and the scaffolds are usually formed by rolling the electrospun meshes, which may diminish their orientation effect on the transplanted cells.

Unidirectional freeze-drying (UFD) is a unique approach to introduce longitudinally oriented microchannel structures inside the scaffold (Sridharan et al., 2015). Compared to the tubular conduits, scaffolds with 3D oriented structures prepared by UFD may possess larger specific surface area that allow SCs attachment. The resulting microchannels have been proven to guide SCs migration and neurite extension. Since the UFD technique utilizes the sublimation of unidirectional finger-like ice crystals to form microchannels, it is more applicable for the hydrogel-based natural materials, such as collagen, chitosan, and hyaluronic acid. Boecker et al. engineered a collagen conduit by UFD to transplant olfactory ensheathing cells (OECs), which is a type of glial cells that ensheaths olfactory axons to form myelin, similar to the SCs (Boecker et al., 2018). The suspension of OECs was perfused into the conduit and the cells aligned along the longitudinally oriented microchannels following conduit implantation. The OECs-containing conduits revealed local beneficial effects on axonal densities and myelination when compared to the empty scaffolds. Primary rat SCs were also transplanted with a UFD-prepared oriented collagen-chitosan conduit, which were observed to adhere and extend longitudinally along the microchannels (Zhang et al., 2013). The SCs-containing scaffolds closely resembled the microstructure and biological components of the native nerves, and provided a permissive microenvironment to promote axonal outgrowth and nerve regeneration.

In clinical practice, decellularized peripheral nerves are viewed as the most promising scaffolds for SCs transplantation (Han et al., 2019). Though the decellularized nerve grafts retain the longitudinally aligned tubular structures and most of the dECM compositions, the cellular components are removed from the native peripheral nerves, making them less effective in nerve regeneration compared to the autografts. The recellularization of SCs in the decellularized nerve grafts even more closely recapitulates the structure and bioactivity of the nerve autografts. Previous studies suggested that the decellularized nerves might support neuroregeneration in <30-mm peripheral nerve defects in non-human primates. Furthermore, Hess et al. (2007) combined the decellularized grafts with cultured autologous SCs which promoted remarkable regeneration in 6-cm ulnar nerve defects of macaca fascicularis. The decellularized allografts also provide pro-regenerative microenvironment for stem cells and induce their differentiation into SCLCs. Qiao et al. verified the SC-like differentiation of dental pulp stem cells (DPSCs) when cultured on a xenogeneic acellular nerve graft (ANG), which was further transplanted to repair 10-mm sciatic nerve defect in rat (Qiao et al., 2019). Immunohistochemical and electrophysiological assessments confirmed that the addition of DPSCs resulted in better functional recovery compared with the ANG scaffold. Recently, a study investigated the efficiency of introducing human ADSCs into commercialized human decellularized nerve grafts (Avance®), which further promoted the clinical application of SCs transplantation (Mathot et al., 2020). Although using decellularized nerves as the SCs carriers is promising, the limited source and potential risk of disease transmission still urges the development of advanced artificial implants for SCs transplantation.

Introducing Topological Cues Into Hydrogels

The main purpose of introducing oriented microstructures into the implanted scaffolds is to induce SCs polarization and alignment. However, the SCs or SCLCs usually attach to the surface of the aligned fibers/tubes, indicating that the cells are pre-cultivated bi-dimensionally. Following implantation, the cells need to transfer from surface to a 3D environment consisting of body fluids and ECM. With the rapid development of fabrication technologies, research studies have been focusing on introduction of oriented structures into hydrogels, in which the transplanted cells can grow three dimensionally. A representative approach was reported by B. Phillips et al. who incorporated different cell types, including SCs, ADCSs,

and DPSCs into collagen gel, respectively. The cell alignment was induced by plastic compression (Georgiou et al., 2013; Sanen et al., 2017; Schuh et al., 2018). They also fabricated an anisotropic SC-containing collagen hydrogel by a gel aspiration-ejection (GAE) system (Muangsanit et al., 2020). Through slowly aspirating the collagen hydrogel, the shear force conferred elongation and alignment of the SCs within the hydrogels. It was also noted that the alignment of SCs maintained for long periods, induced that the number of regenerated axons and extent of vascularization was superior to the empty conduits in a rat sciatic nerve injury model.

Bioprinting shows great potential in producing cell-encapsulated hydrogel scaffolds for tissue engineering, which allows manipulation of spatial arrangement/distribution of the transplanting cells. Ning et al. modified a low viscosity alginate using RGD peptide, then blended with HA and fibrin to form the stock solution, and rat primary SCs were also incorporated to generate a functional bioink (Ning et al., 2019). They found that nearly 80% of the bioprinted SCs were aligned along the axial direction when the moving speed of the printing nozzle was 9 mm/s. Wu et al. printed a 3D conduit with SCs-containing gelatin and sodium alginate hydrogel, resulting in upregulated secretion of some growth factors from the SCs, including NGF, BDNF, and GDNF. Besides the alignment of SCs, the spatial distribution of SCs within the scaffold is important since their cellular functions usually rely on the accurate cell positioning. Bi-printing provides unique advantages in precise design and controlling the cellular distribution in the 3D scaffolds to mimic the native tissues or to meet special requirements. Wang et al. encapsulated BMSCs and SCs in two different GelMA-based bioinks, then bioprinted 3D scaffolds with spatial arrangement of the cells, respectively (Wang et al., 2021). Compared to the homogeneous hydrogel encapsulated with both cells, the 3D-printed scaffold with spatial distribution resulted in better functional recovery after spinal cord injury.

Interestingly, the transplanted cells can also be controlled and re-arranged into pre-designed patterns by external stimulation, such as the introduction of electromagnetic fields. Acoustic stimulation can promote cell migration via the density differences between cells and the surrounding matrix, which has been employed to fabricate complex cell patterns either on 2D plate or in 3D hydrogel. Using a heptagon acoustic tweezer, Gesellchen et al. created a SCs-linear pattern on a cover slip, and dorsal root ganglion (DRG) neurites were proven to grow along the SCs (Gesellchen et al., 2014). Although have been applied in 3D SCs alignment, the acoustic stimulation was used to form neuro-progenitor cells (NPCs) 3D construct in a fibrin hydrogel, which showed a great potential in cell transplantation therapy (Bouyer et al., 2016). Integrating magnetic-responsive short electrospun fibers into the hydrogel is another promising method to obtain cellular alignment in 3D environment. Prior to electrospinning, superparamagnetic iron oxide nanoparticles (SPIONs) were mixed into the polymer solution. The obtained electrospun nanofibers were cut into short fibers, then incorporated into the hydrogel. In response to the magnetic stimulation, the short fibers spontaneously arranged along the direction of the magnetic field, and further provided an oriented guidance for DRG neurites (Johnson et al., 2019). These abovementioned techniques achieved the distribution of cells without changing the chemical and mechanical properties of the implanted scaffolds. More importantly, the induced cell patterns were formed within the hydrogel, which allowed 3D cell growth. The external stimulation can be introduced either pre or post transplantation. The cell transplantation using injectable hydrogels with pre-aligned cells may meet various clinical demands, including minimal invasive surgeries and other features to repair long-distance nerve defects.

SCHWANN CELL-DERIVED BIOMATERIALS

Nerve injury results in dysfunction of the innervated organs, which is hardly recovered unless proper surgical treatments are performed. Since SCs can support axonal regeneration, transplantation of SCs has been proven to be effective in nerve injury repair. Despite that cell transplantation has been proven repeatedly by animal experiments, clinical applications of cell therapy are scarce, due to the potential host rejection and risk of tumorigenesis (Cai and Huang, 2006). In fact, intercellular communication relies on the secretion of cells, such as cytokines, exosomes, and ECM, which can serve as the modulators in regulating cellular behaviors through paracrine pathways. It has been reported that the components of SCs secreted factors can actively support axonal maintenance and regeneration, some of which have already been employed in bioscaffolds (Gordon, 2009). Growth factors are cell-secreted proteins or peptides that can regulate numerous physiological processes, such as differentiation, migration, adhesion, and gene expression. The importance of SCs-derived growth factors (including NGF, GDNF and BDNF) in nerve injury repair has been well-established and reviewed and discussed, as well as the strategy of assembling these growth factors within the engineered nerve grafts (Deister and Schmidt, 2006). In this review, we emphasize on the properties of the other two types of secretions, exosomes and ECM proteins, which are discussed from the application prospect as SCs-derived biomaterials for nerve injury repair.

Transplantation of SCs-Derived Exosomes

Exosomes are nanoscale extracellular vesicles secreted by mammalian cells with a flattened spherical shape and diameters ranging from 30 to 150 nm (Thery et al., 2009). This nano-sized property of exosomes enables easy delivery through blood or other biological fluids. They also involve in many biological activities, such as immune regulation, metabolism, anti-oxidative stress, and tissue regeneration. Exosomes contain various functional proteins, mRNA, and micro-RNA (miRNA). Research studies have shown that exosomes can serve as an effective alternative to their origin cells in immunotherapy and regenerative medicine (Record et al., 2011). For example, glial cells in nervous systems secret exosomes with different functionalities. Lopez-Verrilli et al. (2013) first revealed that exosomes derived from SCs can be endocytosed by DRG axons, to promote the regrowth of transected DRG axons was

significantly enhanced by continuous supplement of the SCs-derived exosomes. By direct injection into the injury site of a rat crushed nerve injury model, the introduced SCs-derived exosomes significantly increased the rate of axonal regeneration, indicating their potential in nerve injury repair. Subsequent studies showed that the SCs exosomes can inhibit GTPase RhoA activity and modulate growth cone dynamics to promote axonal regeneration, which may be beneficial in delaying cell senescence and apoptosis through inhibiting the caspase-3 signaling pathway (Lopez-Verrilli et al., 2013). Proteomic analysis revealed that several pathways related to microenvironment regulation were enriched by SCs-derived exosomes, such as neurotrophin secretion and PI3K-Akt signaling pathway (Wei et al., 2019). The miRNAs and proteins in SC-derived exosomes can regulate axonal regeneration and enhance neuron survival, which may play a critical role in potential therapeutic applications against nervous system diseases.

Although some common components such as tetraspanin (CD63, CD81, and CD9) and heat shock proteins (Hsp70, Hsp90) are involved, different cell phenotypes secrete different exosomes that carry various types of biological substances (Tamkovich et al., 2016). Lopez-Leal et al. found that only the exosomes secreted by the SCs of repair phenotype can facilitate axonal regeneration after nerve injury, rather than those exosomes secreted by the differentiated SCs (i.e., the mature and myelinating SCs) (Lopez-Leal et al., 2020). Interestingly, although the exosomes of differentiated SCs failed in promoting axonal growth, further studies demonstrated that they may inhibit SCs migration through secreting specific miRNAs and promote myelinization (Sohn et al., 2020). This discovery strongly supports the hypothesis that exosomes can recapitulate the specific features of their donor cells. However, the functions of SCs-derived exosomes have been investigated for nerve regeneration only in recent years, and the components and features of such exosomes remain unclear. Considering the neuroprotective and neuroregeneration effects, the SCs-derived exosomes have become a promising biomaterial that may serve as SCs substitute for transplantation therapies and nerve regeneration. Compared to SCs or SCLCs, their secreted exosomes provide several advantages, such as convenient storage, easy modification, and low risk of tumorigenesis, which make them even more suitable for tissue engineering applications.

The exosome-based therapies have been progressing rapidly in recent years, but the application of SCs-derived exosomes is rarely reported. The commonly used transplantation strategy was to resuspend SCs-derived exosomes in culture medium or saline solution, then introduced to the injured area through direct injection. Wang et al. continuously infused SCs-derived exosomes through tail vein in mice every 2 weeks to treat diabetic peripheral neuropathy (DPN) within 8 weeks (Wang et al., 2020). They confirmed that the SCs-derived exosomes can improve the neurological function in DPN mice and increase the amount of intraepidermal nerve fibers by supplementing specific miRNAs (miR-21,−27a, and−146a). However, direct exosome injection limits their therapeutic effects due to the rapid clearance *in vivo*, and a sustained delivery system using hydrogels or scaffolds is highly desirable to maintain their stability and biological functions. In a recent study, Matrigel was used to first encapsulate SKP-SCs-derived exosomes and then perfused into a silicon tube to fabricate the artificial nerve graft (Yu et al., 2021). The release profile showed that the exosome encapsulated Matrigel underwent sustained release for at least 8 weeks. Although satisfactory results were achieved in sciatic nerve regeneration, the Matrigel-based transplantation is extremely risky. The potential application of various other bioactive materials may serve as the exosome carriers, such as collagen and fibrin, and their synergistic effects need to be explored extensively in nerve injury repair.

SCs-Derived Decellularized Extracellular Matrix

The ECM constitutes intrinsic physical and biochemical cues that can regulate cellular behavior and biological function in tissue development and regeneration. The composition and structure of ECM are determined by the type and function of the resident cells, which can be modified in response to various changes in the microenvironment, such as mechanical stimuli and nutrient concentrations. On the other side, ECM provides significant impact on the behaviors of the resident cells and maintains the biological functions of tissues/organs (Hussey et al., 2018). As the most important glial cells in peripheral nerves, ECM secreted from SCs contains a variety of macromolecules, such as collagens, laminins, and proteoglycans, during the development and regeneration process. These ECM components have been reported to be functional in inducing SCs alignment and proliferation. Therefore, materials extracted from the native ECM of peripheral nerves may serve as a promising alternative of SCs can be used as cell-free scaffolds for nerve regeneration (Khaing and Schmidt, 2012). Compared with individual ECM component, the compositional dECM reconstructs the 3D extracellular microenvironment that has been widely used in regenerative medicine. The dECM scaffolds derived from nerve tissues not only provide good platforms for SCs transplantation, but also possess great potential as the cell-free nerve grafts, due to their remarkable bioactivity and biocompatibility. During the past decades, decellularized nerve matrix has already been commercialized ("Avance," Axogen, USA and "hANGs," Guangzhou Zhongda Medical Device Company, China) for clinical applications, which becomes the most popular substitution of the nerve autografts. In the treatments of CNI, decellularized nerve grafts derived from peripheral nerves are also used. For example, Villegas-Perez et al. (1988) transplanted the decellularized nerve grafts to bridge the optic nerve defects and achieved a certain degree of tissue regeneration.

Furthermore, the hydrogels derived from the decellularized nerves also exhibit promising advantages in SCs regulation and nerve injury repair. Liu et al. (2021) prepared a porcine decellularized peripheral nerve matrix hydrogel, which exhibited high bioactivity in promoting axonal extension, SCs alignment, and nerve fiber remyelination. A consecutive study showed that the decellularized nerve matrix hydrogel coated electrospun PLLA nanofibers significantly promoted SCs migration and axonal extension (Chen et al., 2019; Deng et al., 2022). The

synergistic effects of the decellularized nerve matrix hydrogel and the aligned nanofibers were further confirmed *in vivo* regarding nerve fiber fasciculation, myelination, and functionalization (Zheng et al., 2021). The capacity of decellularized nerve matrix hydrogel was also assessed by Lin et al. *via* perfusion into a nerve guidance conduit and implantation into a rat 15-mm sciatic nerve injury model (Lin et al., 2018). Rao et al. further induced longitudinally oriented microchannel structures in the decellularized nerve matrix hydrogel by UFD. They showed that the introduction of topological guidance promoted neurite extension and SCs migration both *in vitro* and *in vivo* (Rao et al., 2021). The decellularized nerve matrix hydrogel with aligned topology resulted in functional recovery comparable to those using nerve autografts. These results indicate that the decellularized matrix derived hydrogel holds great potential in clinical translations.

Although the decellularized nerve matrix and its derivatives are beneficial in promoting nerve regeneration, some drawbacks still exist, including source tissue scarcity, host responses, and potential pathogen transfer through heterogenic or allogenic transplantation (Badylak et al., 2009). Alternatively, the cell-derived decellularized dECMs, especially those extracted from autogenic cells, often possess low immunogenicity and are free of pathogenic factors transfer. Particularly, SCs-derived dECM is more refined than the decellularized nerve matrix, which recapitulates the functions of native SCs (Lu et al., 2011). In consequence, the dECM scaffolds derived from cultured SCs have been used as bioactive materials for nerve regeneration. Gu et al. (2014a) cultured primary rat SCs for 14 days and then underwent decellularization. Fibronectin and laminin preserved in the SCs-derived dECM, was used to seed DRG neurons which sprouted much longer axons than those cultured on poly-lysine coated plates. The SCs were further cultured on a chitosan/silk fibroin conduit and decellularized to obtain dECM modified nerve conduit, which resulted in repair effect that was comparable to the decellularized nerves in 10-mm rat sciatic nerve injury. Considering the difficulty in acquiring adequate autologous SCs, the dECM derived from stem cell differentiated SCs (such as the SKP-SCs) can also be used in scaffold modification (Zhu et al., 2018). However, the cell-derived dECMs are barely used directly due to the relatively low yields of ECM secretion, which often serve as the bioactive supplements. Although production issues remain unsolved, such as the control of costs, batch differences, and large-scale production, the SCs-derived dECM based materials still hold great promise in neural tissue engineering.

CONCLUSION AND FUTURE PERSPECTIVES

SCs are the major glial cells in peripheral nervous system, which provide a permissive substrate for axonal growth, wrap around axons for myelination, and promote functional recovery after nerve injury. Transplantation of SCs has emerged as a promising cell-based therapy for treatments of nervous system diseases, such as long-distance peripheral defects, spinal cord injury, and neurodegenerative disorders. However, a few limitations still need to be overcome, including the insufficient sources of autogenous SCs, and poor cell survival upon injection to the injured area. The SCLCs differentiated from stem cells exhibit great promise as the SCs substitutes for nerve regeneration, but similar problems still exist.

Biomaterials can be used as cell carriers to assist SCs transplantation to the central and peripheral nervous system. These biomaterials, including hydrogels and scaffolds, not only provide cell substrates to avoid damages and anoikis during transplantation, but also can be engineered to promote cell viability, proliferation, and functionalization. Among these SCs transplantation platforms, it is highly desired to build a favorable microenvironment for SCs at both molecular and physiological levels. Additionally, the incorporation and spatial/temporal distributions of the stimulating factors (growth factors, exosomes, and other cells) that manipulate SCs phenotype are also valuable for SCs transplantation.

Although great advancements have been achieved in clinical applications, the cell-based therapy still faces serious limitations, such as the quantity of cells, timing of the treatment, high costs, and potential immune response. Therefore, alternative approaches using the secreta of SCs or SCLCs, such as their secreted exosomes and ECM have been actively developed and shown great promise in facilitating nerve regeneration. However, due to the complexity of exosomes and dECM, the specific roles of each component and the mechanisms on neural regeneration are barely investigated. Future studies focusing on understanding the role of SCs-derived exosomes and dECM can help evaluate the safety and effectiveness of these rapidly advancing biomaterials toward practical use in future clinical applications.

AUTHOR CONTRIBUTIONS

YB and DQ provided the idea for the review. ZR searched the literature, prepared the figures, and wrote the manuscript. ZL and PS participated in reviewing the literature. YB contributed to editing and approval of the final manuscript. All authors contributed to the article and approved the submitted version.

FUNDING

This work was supported by National Natural Science Foundation of China (51903255, 52073314, and 32171353), the Key Areas Research and Development Program of Guangdong (2020B1111150003), Natural Science Foundation of Guangdong (2022A1515011388), Science and Technology Program of Guangzhou (201904010364), and Science and Technology Projects in Guangzhou (202002020078).

REFERENCES

Akassoglou, K., Yu, W. M., Akpinar, P., and Strickland, S. (2002). Fibrin inhibits peripheral nerve remyelination by regulating schwann cell differentiation. *Neuron*. 33, 861–875. doi: 10.1016/S0896-6273(02)00617-7

Alvarado-Velez, M., Pai, S. B., and Bellamkonda, R. V. (2014). Hydrogels as carriers for stem cell transplantation. *IEEE T Bio-Med. Eng*. 61, 1474–1481. doi: 10.1109/Tbme.2014.2305753

Assinck, P., Duncan, G. J., Hilton, B. J., Plemel, J. R., and Tetzlaff, W. (2017a). Cell transplantation therapy for spinal cord injury. *Nat. Neurosci*. 20, 637–647. doi: 10.1038/nn.4541

Assinck, P., Duncan, G. J., Plemel, J. R., Lee, M. J., Stratton, J. A., Manesh, S. B., et al. (2017b). Myelinogenic plasticity of oligodendrocyte precursor cells following spinal cord contusion injury. *J Neurosci*. 37, 8635–8654. doi: 10.1523/JNEUROSCI.2409-16.2017

Assinck, P., Sparling, J. S., Dworski, S., Duncan, G. J., Wu, D., Liu, J., et al. (2020). Transplantation of skin precursor-derived schwann cells yields better locomotor outcomes and reduces bladder pathology in rats with chronic spinal cord injury. *Stem Cell Rep*. 15, 140–155. doi: 10.1016/j.stemcr.2020.05.017

Babaloo, H., Ebrahimi-Barough, S., Derakhshan, M. A., Yazdankhah, M., Lotfibakhshaiesh, N., Soleimani, M., et al. (2019). PCL/gelatin nanofibrous scaffolds with human endometrial stem cells/Schwann cells facilitate axon regeneration in spinal cord injury. *J. Cell Physiol*. 234, 11060–11069. doi: 10.1002/jcp.27936

Badylak, S. F., Freytes, D. O., and Gilbert, T. W. (2009). Extracellular matrix as a biological scaffold material: structure and function. *Acta Biomater*. 5, 1–13. doi: 10.1016/j.actbio.2008.09.013

Barres, B. A., Jacobson, M. D., Schmid, R., Sendtner, M., and Raff, M. C. (1993). Does oligodendrocyte survival depend on axons? *Curr. Biol*. 3, 489–497. doi: 10.1016/0960-9822(93)90039-q

Barrette, B., Hebert, M. A., Filali, M., Lafortune, K., Vallieres, N., Gowing, G., et al. (2008). Requirement of myeloid cells for axon regeneration. *J. Neurosci*. 28, 9363–9376. doi: 10.1523/JNEUROSCI.1447-08.2008

Bassilios Habre, S., Bond, G., Jing, X. L., Kostopoulos, E., Wallace, R. D., and Konofaos, P. (2018). The surgical management of nerve gaps: present and future. *Ann. Plast. Surg*. 80, 252–261. doi: 10.1097/SAP.0000000000001252

Bastidas, J., Athauda, G., De La Cruz, G., Chan, W. M., Golshani, R., Berrocal, Y., et al. (2017). Human schwann cells exhibit long-term cell survival, are not tumorigenic and promote repair when transplanted into the contused spinal cord. *Glia* 65, 1278–1301. doi: 10.1002/glia.23161

Berrocal, Y. A., Almeida, V. W., Gupta, R., and Levi, A. D. (2013). Transplantation of schwann cells in a collagen tube for the repair of large, segmental peripheral nerve defects in rats. *J. Neurosurg*. 119, 720–732. doi: 10.3171/2013.4.JNS121189

Bixby, J. L., Lilien, J., and Reichardt, L. F. (1988). Identification of the major proteins that promote neuronal process outgrowth on schwann cells in vitro. *J. Cell Biol*. 107, 353–361. doi: 10.1083/jcb.107.1.353

Boecker, A. H., Bozkurt, A., Kim, B. S., Altinova, H., Tank, J., Deumens, R., et al. (2018). Cell-enrichment with olfactory ensheathing cells has limited local extra beneficial effects on nerve regeneration supported by the nerve guide perimaix. *J. Tissue Eng. Regen. Med*. 12, 2125–2137. doi: 10.1002/term.2731

Bouyer, C., Chen, P., Guven, S., Demirtas, T. T., Nieland, T. J. F., Padilla, F., et al. (2016). A bio-acoustic levitational (bal) assembly method for engineering of multilayered, 3D brain-like constructs, using human embryonic stem cell derived neuro-progenitors. *Adv. Mater*. 28, 161–167. doi: 10.1002/adma.201503916

Brightman, A. O., Rajwa, B. P., Sturgis, J. E., McCallister, M. E., Robinson, J. P., and Voytik-Harbin, S. L. (2000). Time-lapse confocal reflection microscopy of collagen fibrillogenesis and extracellular matrix assembly in vitro. *Biopolymers* 54, 222–234. doi: 10.1002/1097-0282(200009)54:3<222::AID-BIP80>3.0.CO;2-K

Budday, S., Sommer, G., Birkl, C., Langkammer, C., Haybaeck, J., Kohnert, J., et al. (2017). Mechanical characterization of human brain tissue. *Acta Biomater*. 48, 319–340. doi: 10.1016/j.actbio.2016.10.036

Cai, S., Tsui, Y. P., Tam, K. W., Shea, G. K. H., Chang, R. S. K., Ao, Q., et al. (2017). Directed differentiation of human bone marrow stromal cells to fate-committed schwann cells. *Stem Cell Rep*. 9, 1097–1108. doi: 10.1016/j.stemcr.2017.08.004

Cai, Y., and Huang, S. L. (2006). Progress of research and application on hematopoietic stem cell transplantation by intra-bone marrow injection—review. *Zhongguo Shi Yan Xue Ye Xue Za Zhi*. 14, 179–182

Cao, Q. L., Zhang, Y. P., Howard, R. M., Walters, W. M., Tsoulfas, P., and Whittemore, S. R. (2001). Pluripotent stem cells engrafted into the normal or lesioned adult rat spinal cord are restricted to a glial lineage. *Exp. Neurol*. 167, 48–58. doi: 10.1006/exnr.2000.7536

Catoira, M. C., Fusaro, L., Di Francesco, D., Ramella, M., and Boccafoschi, F. (2019). Overview of natural hydrogels for regenerative medicine applications. *J. Mater. Sci-Mater*. 30, 1–10. doi: 10.1007/s10856-019-6318-7

Cerqueira, S. R., Lee, Y. S., Cornelison, R. C., Mertz, M. W., Wachs, R. A., Schmidt, C. E., et al. (2018). Decellularized peripheral nerve supports schwann cell transplants and axon growth following spinal cord injury. *Biomaterials*. 177, 176–185. doi: 10.1016/j.biomaterials.2018.05.049

Chen, Q., Zhang, Z. J., Liu, J. B., He, Q. H., Zhou, Y. P., Shao, G. B., et al. (2015). A fibrin matrix promotes the differentiation of emscs isolated from nasal respiratory mucosa to myelinating phenotypical schwann-like cells. *Mol. Cells*. 38, 221–228. doi: 10.14348/molcells.2015.2170

Chen, S. H., Du, Z. Y., Zou, J. L., Qiu, S., Rao, Z. L., Liu, S., et al. (2019). Promoting neurite growth and schwann cell migration by the harnessing decellularized nerve matrix onto nanofibrous guidance. *ACS Appl. Mater. Int*. 11, 17167–17176. doi: 10.1021/acsami.9b01066

Chen, W. A., Luo, T. D., Barnwell, J. C., Smith, T. L., and Li, Z. (2017). Age-dependent schwann cell phenotype regulation following peripheral nerve injury. *J. Hand Surg. Asian Pac*. 22, 464–471. doi: 10.1142/S0218810417500514

Daly, A. C., Riley, L., Segura, T., and Burdick, J. A. (2020). Hydrogel microparticles for biomedical applications. *Nat. Rev. Mater*. 5, 20–43. doi: 10.1038/s41578-019-0148-6

Daly, W., Yao, L., Zeugolis, D., Windebank, A., and Pandit, A. (2012). A biomaterials approach to peripheral nerve regeneration: Bridging the peripheral nerve gap and enhancing functional recovery. *J. R. Soc. Interf*. 9, 202–221. doi: 10.1098/rsif.2011.0438

Deister, C., and Schmidt, C. E. (2006). Optimizing neurotrophic factor combinations for neurite outgrowth. *J. Neural Eng*. 3, 172–179. doi: 10.1088/1741-2560/3/2/011

Deng, R. L., Luo, Z. L., Rao, Z. L., Lin, Z. D., Chen, S. H., Zhou, J., et al. (2022). Decellularized extracellular matrix containing electrospun fibers for nerve regeneration: a comparison between core-shell structured and preblended composites. *Adv. Fiber Mater*. 4, 503–519. doi: 10.1007/s42765-021-00124-5

Dezawa, M., Takahashi, I., Esaki, M., Takano, M., and Sawada, H. (2001). Sciatic nerve regeneration in rats induced by transplantation of in vitro differentiated bone-marrow stromal cells. *Eur. J. Neurosci*. 14, 1771–1776. doi: 10.1046/j.0953-816x.2001.01814.x

Drury, J. L., and Mooney, D. J. (2003). Hydrogels for tissue engineering: Scaffold design variables and applications. *Biomaterials*. 24, 4337–4351. doi: 10.1016/S0142-9612(03)00340-5

Echave, M. C., Burgo, L. S., Pedraz, J. L., and Orive, G. (2017). Gelatin as biomaterial for tissue engineering. *Curr. Pharm. Design*. 23, 3567–3584. doi: 10.2174/1381612823666170511123101

El Seblani, N., Welleford, A. S., Quintero, J. E., van Horne, C. G., and Gerhardt, G. A. (2020). Invited review: utilizing peripheral nerve regenerative elements to repair damage in the CNS. *J. Neurosci. Methods* 335, 108623. doi: 10.1016/j.jneumeth.2020.108623

Franco, C. L., Price, J., and West, J. L. (2011). Development and optimization of a dual-photoinitiator, emulsion-based technique for rapid generation of cell-laden hydrogel microspheres. *Acta Biomater*. 7, 3267–3276. doi: 10.1016/j.actbio.2011.06.011

Friess, W. (1998). Collagen—biomaterial for drug delivery. *Eur. J. Pharm. Biopharm*. 45, 113–136. doi: 10.1016/s0939-6411(98)00017-4

Gaudin, R., Knipfer, C., Henningsen, A., Smeets, R., Heiland, M., and Hadlock, T. (2016). Approaches to peripheral nerve repair: generations of biomaterial conduits yielding to replacing autologous nerve grafts in craniomaxillofacial surgery. *Biomed. Res. Int*. 2016, 3856262. doi: 10.1155/2016/3856262

Geckil, H., Xu, F., Zhang, X. H., Moon, S., and Demirci, U. (2010). Engineering hydrogels as extracellular matrix mimics. *Nanomedicine-UK*. 5, 469–484. doi: 10.2217/Nnm.10.12

Georgiou, M., Bunting, S. C. J., Davies, H. A., Loughlin, A. J., Golding, J. P., and Phillips, J. B. (2013). Engineered neural tissue for peripheral nerve repair. *Biomaterials*. 34, 7335–7343. doi: 10.1016/j.biomaterials.2013.06.025

Georgiou, M., Golding, J. P., Loughlin, A. J., Kingham, P. J., and Phillips, J. B. (2015). Engineered neural tissue with aligned, differentiated adipose-derived stem cells promotes peripheral nerve regeneration across a critical sized defect in rat sciatic nerve. *Biomaterials*. 37, 242–251. doi: 10.1016/j.biomaterials.2014.10.009

Gesellchen, F., Bernassau, A. L., Dejardin, T., Cumming, D. R., and Riehle, M. O. (2014). Cell patterning with a heptagon acoustic tweezer—application in neurite guidance. *Lab Chip*. 14, 2266–2275. doi: 10.1039/c4lc00436a

Gomez-Sanchez, J. A., Pilch, K. S., van der Lans, M., Fazal, S. V., Benito, C., Wagstaff, L. J., et al. (2017). After nerve injury, lineage tracing shows that myelin and remak schwann cells elongate extensively and branch to form repair schwann cells, which shorten radically on remyelination. *J. Neurosci*. 37, 9086–9099. doi: 10.1523/JNEUROSCI.1453-17.2017

Gordon, T. (2009). The role of neurotrophic factors in nerve regeneration. *Neurosurg. Focus*. 26, E3. doi: 10.3171/FOC.2009.26.2.E3

Gu, X., Ding, F., and Williams, D. F. (2014a). Neural tissue engineering options for peripheral nerve regeneration. *Biomaterials* 35, 6143–6156. doi: 10.1016/j.biomaterials.2014.04.064

Gu, Y., Zhu, J. B., Xue, C. B., Li, Z. M. Y., Ding, F., Yang, Y. M., et al. (2014b). Chitosan/silk fibroin-based, schwann cell-derived extracellular matrix-modified scaffolds for bridging rat sciatic nerve gaps. *Biomaterials* 35, 2253–2263. doi: 10.1016/j.biomaterials.2013.11.087

Guan, J., Zhu, Z. H., Zhao, R. C., Xiao, Z. F., Wu, C. X., Han, Q., et al. (2013). Transplantation of human mesenchymal stem cells loaded on collagen scaffolds for the treatment of traumatic brain injury in rats. *Biomaterials* 34, 5937–5946. doi: 10.1016/j.biomaterials.2013.04.047

Guenard, V., Kleitman, N., Morrissey, T. K., Bunge, R. P., and Aebischer, P. (1992). Syngeneic schwann cells derived from adult nerves seeded in semipermeable guidance channels enhance peripheral nerve regeneration. *J. Neurosci*. 12, 3310–3320. doi: 10.1523/jneurosci.12-09-03310.1992

Gyles, D. A., Castro, L. D., Silva, J. O. C., and Ribeiro-Costa, R. M. (2017). A review of the designs and prominent biomedical advances of natural and synthetic hydrogel formulations. *Eur. Polym. J*. 88, 373–392. doi: 10.1016/j.eurpolymj.2017.01.027

Han, G. H., Peng, J., Liu, P., Ding, X., Wei, S., Lu, S., et al. (2019). Therapeutic strategies for peripheral nerve injury: decellularized nerve conduits and schwann cell transplantation. *Neural Regen Res*. 14, 1343–1351. doi: 10.4103/1673-5374.253511

Hejcl, A., Sedy, J., Kapcalova, M., Toro, D. A., Amemori, T., Lesny, P., et al. (2010). HPMA-RGD hydrogels seeded with mesenchymal stem cells improve functional outcome in chronic spinal cord injury. *Stem Cells Dev*. 19, 1535–1546. doi: 10.1089/scd.2009.0378

Hess, J. R., Brenner, M. J., Fox, I. K., Nichols, C. M., Myckatyn, T. M., Hunter, D. A., et al. (2007). Use of cold-preserved allografts seeded with autologous schwann cells in the treatment of a long-gap peripheral nerve injury. *Plast. Reconstr. Surg*. 119, 246–259. doi: 10.1097/01.prs.0000245341.71666.97

Hill, C. E., Moon, L. D., Wood, P. M., and Bunge, M. B. (2006). Labeled schwann cell transplantation: cell loss, host schwann cell replacement, and strategies to enhance survival. *Glia*. 53, 338–343. doi: 10.1002/glia.20287

Ho, M. T., Teal, C. J., and Shoichet, M. S. (2019). A hyaluronan/methylcellulose-based hydrogel for local cell and biomolecule delivery to the central nervous system. *Brain Res. Bull*. 148, 46–54. doi: 10.1016/j.brainresbull.2019.03.005

Hopf, A., Schaefer, D. J., Kalbermatten, D. F., Guzman, R., and Madduri, S. (2020). Schwann cell-like cells: origin and usability for repair and regeneration of the peripheral and central nervous system. Cells-Basel. 9, 1990. doi: 10.3390/cells9091990

Huang, C. W., Huang, W. C., Qiu, X. F., da Silva, F. F. F., Wang, A. J., Patel, S., et al. (2017). The differentiation stage of transplanted stem cells modulates nerve regeneration. *Sci. Rep*. 7, 1–12. doi: 10.1038/s41598-017-17043-4

Hughes, C. S., Postovit, L. M., and Lajoie, G. A. (2010). Matrigel: A complex protein mixture required for optimal growth of cell culture. *Proteomics*. 10, 1886–1890. doi: 10.1002/pmic.200900758

Hussey, G. S., Dziki, J. L., and Badylak, S. F. (2018). Extracellular matrix-based materials for regenerative medicine. *Nat. Rev. Mater*. 3, 159–173. doi: 10.1038/s41578-018-0023-x

Jessen, K. R., and Mirsky, R. (2019). Schwann cell precursors; multipotent glial cells in embryonic nerves. *Front. Mol. Neurosci*. 12, 69. doi: 10.3389/fnmol.2019.00069

Jiang, X., Lim, S. H., Mao, H. Q., and Chew, S. Y. (2010). Current applications and future perspectives of artificial nerve conduits. *Exp. Neurol*. 223, 86–101. doi: 10.1016/j.expneurol.2009.09.009

Johnson, C. D. L., Ganguly, D., Zuidema, J. M., Cardina, T. J., Ziemba, A. M., Kearns, K. R., et al. (2019). Injectable, magnetically orienting electrospun fiber conduits for neuron guidance. *ACS Appl. Mater. Inter*. 11, 356–372. doi: 10.1021/acsami.8b18344

Kamada, T., Koda, M., Dezawa, M., Yoshinaga, K., Hashimoto, M., Koshizuka, S., et al. (2005). Transplantation of bone marrow stromal cell-derived schwann cells promotes axonal regeneration and functional recovery after complete transection of adult rat spinal cord. *J. Neuropath. Exp. Neur*. 64, 37–45. doi: 10.1093/jnen/64.1.37

Khaing, Z. Z., and Schmidt, C. E. (2012). Advances in natural biomaterials for nerve tissue repair. *Neurosci. Lett*. 519, 103–114. doi: 10.1016/j.neulet.2012.02.027

Kim, H. S., Lee, J., Lee, D. Y., Kim, Y. D., Kim, J. Y., Lim, H. J., et al. (2017). Schwann cell precursors from human pluripotent stem cells as a potential therapeutic target for myelin repair. *Stem Cell Rep*. 8, 1714–1726. doi: 10.1016/j.stemcr.2017.04.011

Koffler, J., Zhu, W., Qu, X., Platoshyn, O., Dulin, J. N., Brock, J., et al. (2019). Biomimetic 3d-printed scaffolds for spinal cord injury repair. *Nat. Med*. 25, 263–269. doi: 10.1038/s41591-018-0296-z

Lee, Y. S., Wu, S., Arinzeh, T. L., and Bunge, M. B. (2017). Enhanced noradrenergic axon regeneration into schwann cell-filled pvdf-trfe conduits after complete spinal cord transection. *Biotechnol. Bioeng*. 114, 444–456. doi: 10.1002/bit.26088

Li, J., and Lepski, G. (2013). Cell transplantation for spinal cord injury: A systematic review. *Biomed Res. Int*. 2013, doi: 10.1155/2013/786475

Li, Y., Li, D. Q., and Raisman, G. (2007). Transplanted Schwann cells, not olfactory ensheathing cells, myelinate optic nerve fibres. *Glia*. 55, 312–316. doi: 10.1002/glia.20458

Lin, C. S., Lin, G. T., and Lue, T. F. (2012). Allogeneic and xenogeneic transplantation of adipose-derived stem cells in immunocompetent recipients without immunosuppressants. *Stem Cells Dev*. 21, 2770–2778. doi: 10.1089/scd.2012.0176

Lin, T., Liu, S., Chen, S. H., Qiu, S., Rao, Z. L., Liu, J. H., et al. (2018). Hydrogel derived from porcine decellularized nerve tissue as a promising biomaterial for repairing peripheral nerve defects. *Acta Biomater*. 73, 326–338. doi: 10.1016/j.actbio.2018.04.001

Liu, H., Wu, M., Jia, Y. B., Niu, L. L., Huang, G. Y., and Xu, F. (2020). Control of fibroblast shape in sequentially formed 3d hybrid hydrogels regulates cellular responses to microenvironmental cues. *NPG Asia Mater*. 12, 1–12. doi: 10.1038/s41427-020-0226-7

Liu, S., Rao, Z. L., Zou, J. L., Chen, S. A., Zhu, Q. T., Liu, X. L., et al. (2021). Properties regulation and biological applications of decellularized peripheral nerve matrix hydrogel. *ACS Appl Bio Mater*. 4, 6473–6487. doi: 10.1021/acsabm.1c00616

Lopatina, T., Kalinina, N., Karagyaur, M., Stambolsky, D., Rubina, K., Revischin, A., et al. (2011). Adipose-derived stem cells stimulate regeneration of peripheral nerves: Bdnf secreted by these cells promotes nerve healing and axon growth de novo. *Plos ONE*. 6, 17899. doi: 10.1371/journal.pone.0017899

Lopez-Leal, R., Diaz-Viraque, F., Catalan, R. J., Saquel, C., Enright, A., Iraola, G., et al. (2020). Schwann cell reprogramming into repair cells increases mirna-21 expression in exosomes promoting axonal growth. *J. Cell Sci*. 133, 239004. doi: 10.1242/jcs.239004

Lopez-Verrilli, M. A., Picou, F., and Court, F. A. (2013). Schwann cell-derived exosomes enhance axonal regeneration in the peripheral nervous system. *Glia*. 61, 1795–1806. doi: 10.1002/glia.22558

Lu, H. X., Hoshiba, T., Kawazoe, N., Koda, I., Song, M. H., and Chen, G. P. (2011). Cultured cell-derived extracellular matrix scaffolds for tissue engineering. *Biomaterials*. 32, 9658–9666. doi: 10.1016/j.biomaterials.2011.08.091

Luo, L. H., He, Y., Jin, L., Zhang, Y. N., Guastaldi, F. P., Albashari, A. A., et al. (2022). Application of bioactive hydrogels combined with dental pulp stem cells for the repair of large gap peripheral nerve injuries. *Bioact. Mater*. 7, 2–2. doi: 10.1016/j.bioactmat.2021.04.034

Ma, D., Wang, B., Zawadzka, M., Gonzalez, G., Wu, Z., Yu, B., et al. (2018). A subpopulation of foxj1-expressing, nonmyelinating schwann cells of the peripheral nervous system contribute to schwann cell remyelination in the central nervous system. *J. Neurosci*. 38, 9228–9239. doi: 10.1523/JNEUROSCI.0585-18.2018

Ma, K. H., and Svaren, J. (2018). Epigenetic control of schwann cells. *Neuroscientist*. 24, 627–638. doi: 10.1177/1073858417751112

Maherali, N., Sridharan, R., Xie, W., Utikal, J., Eminli, S., Arnold, K., et al. (2007). Directly reprogrammed fibroblasts show global epigenetic remodeling and widespread tissue contribution. *Cell Stem Cell*. 1, 55–70. doi: 10.1016/j.stem.2007.05.014

Marchand, R., and Woerly, S. (1990). Transected spinal cords grafted with in situ self-assembled collagen matrices. *Neuroscience*. 36, 45–60. doi: 10.1016/0306-4522(90)90350-d

Marquardt, L. M., Doulames, V. M., Wang, A. T., Dubbin, K., Suhar, R. A., Kratochvil, M. J., et al. (2020). Designer, injectable gels to prevent transplanted schwann cell loss during spinal cord injury therapy. *Sci. Adv*. 6, aaz1039. doi: 10.1126/sciadv.aaz1039

Marquardt, L. M., and Heilshorn, S. C. (2016). Design of injectable materials to improve stem cell transplantation. *Curr. Stem Cell Rep*. 2, 207–220. doi: 10.1007/s40778-016-0058-0

Mathot, F., Rbia, N., Thaler, R., Bishop, A. T., van Wijnen, A. J., and Shin, A. Y. (2020). Introducing human adipose-derived mesenchymal stem cells to avance (r) nerve grafts and neuragen (r) nerve guides. *J. Plast. Reconstr. AES* 73, 1473–1481. doi: 10.1016/j.bjps.2020.03.012

Matsumoto, K., Li, Y. C., Jakuba, C., Sugiyama, Y., Sayo, T., Okuno, M., et al. (2009). Conditional inactivation of has2 reveals a crucial role for hyaluronan in skeletal growth, patterning, chondrocyte maturation and joint formation in the developing limb. *Development*. 136, 2825–2835. doi: 10.1242/dev.038505

May, Z., Kumar, R., Fuehrmann, T., Tam, R., Vulic, K., Forero, J., et al. (2018). Adult skin-derived precursor schwann cell grafts form growths in the injured spinal cord of Fischer rats. *Biomed. Mater*. 13, 0340101. doi: 10.1088/1748-605X/aa95f8

Menorca, R. M., Fussell, T. S., and Elfar, J. C. (2013). Nerve physiology: mechanisms of injury and recovery. *Hand Clin*. 29, 317–330. doi: 10.1016/j.hcl.2013.04.002

Mosahebi, A., Fuller, P., Wiberg, M., and Terenghi, G. (2002). Effect of allogeneic Schwann cell transplantation on peripheral nerve regeneration. *Exp. Neurol*. 173, 213–223. doi: 10.1006/exnr.2001.7846

Mosesson, M. W. (2005). Fibrinogen and fibrin structure and functions. *J. Thromb. Haemost*. 3, 1894–1904. doi: 10.1111/j.1538-7836.2005.01365.x

Mousavi, M., Hedayatpour, A., Mortezaee, K., Mohamadi, Y., Abolhassani, F., and Hassanzadeh, G. (2019). Schwann cell transplantation exerts neuroprotective roles in rat model of spinal cord injury by combating inflammasome activation and improving motor recovery and remyelination. *Metab. Brain Dis*. 34, 1117–1130. doi: 10.1007/s11011-019-00433-0

Muangsanit, P., Day, A., Dimiou, S., Atac, A. F., Kayal, C., Park, H., et al. (2020). Rapidly formed stable and aligned dense collagen gels seeded with Schwann cells support peripheral nerve regeneration. *J Neural Eng*. 17, 046036. doi: 10.1088/1741-2552/abaa9c

Ning, L. Q., Zhu, N., Mohabatpour, F., Sarker, M. D., Schreyer, D. J., and Chen, X. B. (2019). Bioprinting schwann cell-laden scaffolds from low-viscosity hydrogel compositions. *J. Mater. Chem. B*. 7, 4538–4551. doi: 10.1039/c9tb00669a

Novikova, L. N., Mosahebi, A., Wiberg, M., Terenghi, G., Kellerth, J. O., and Novikov, L. N. (2006). Alginate hydrogel and matrigel as potential cell carriers for neurotransplantation. *J. Biomed. Mater. Res. A*. 77a, 242–252. doi: 10.1002/jbm.a.30603

Painter, M. W., Lutz, A. B., Cheng, Y. C., Latremoliere, A., Duong, K., Miller, C. M., et al. (2014). Diminished schwann cell repair responses underlie age-associated impaired axonal regeneration. *Neuron*. 83, 331–343. doi: 10.1016/j.neuron.2014.06.016

Pallini, R., Vitiani, L. R., Bez, A., Casalbore, P., Facchiano, F., Di Giorgi Gerevini, V., et al. (2005). Homologous transplantation of neural stem cells to the injured spinal cord of mice. *Neurosurgery*. 57, 1014–1025. doi: 10.1227/01.NEU.0000180058.58372.4c

Park, H. W., Lim, M. J., Jung, H., Lee, S. P., Paik, K. S., and Chang, M. S. (2010). Human mesenchymal stem cell-derived schwann cell-like cells exhibit neurotrophic effects, via distinct growth factor production, in a model of spinal cord injury. *Glia*. 58, 1118–1132. doi: 10.1002/glia.20992

Park, Y., Ji, S. T., Yong, U., Das, S., Jang, W. B., Ahn, G., et al. (2021). 3d bioprinted tissue-specific spheroidal multicellular microarchitectures for advanced cell therapy. *Biofabrication*. 13, 045017. doi: 10.1088/1758-5090/ac212e

Pasut, G., Panisello, A., Folch-Puy, E., Lopez, A., Castro-Benitez, C., Calvo, M., et al. (2016). Polyethylene glycols: an effective strategy for limiting liver ischemia reperfusion injury. *World J. Gastroenterol*. 22, 6501–6508. doi: 10.3748/wjg.v22.i28.6501

Patel, V., Joseph, G., Patel, A., Patel, S., Bustin, D., Mawson, D., et al. (2010). Suspension matrices for improved schwann-cell survival after implantation into the injured rat spinal cord. *J. Neurotraum*. 27, 789–801. doi: 10.1089/neu.2008.0809

Pego, A. P., Kubinova, S., Cizkova, D., Vanicky, I., Mar, F. M., Sousa, M. M., et al. (2012). Regenerative medicine for the treatment of spinal cord injury: more than just promises? *J. Cell. Mol. Med*. 16, 2564–2582. doi: 10.1111/j.1582-4934.2012.01603.x

Petersen, M. A., Ryu, J. K., and Akassoglou, K. (2018). Fibrinogen in neurological diseases: mechanisms, imaging and therapeutics. *Nat. Rev. Neurosci*. 19, 283–301. doi: 10.1038/nrn.2018.13

Pinero, G., Usach, V., Soto, P. A., Monje, P. V., and Setton-Avruj, P. (2018). EGFP transgene: a useful tool to track transplanted bone marrow mononuclear cell contribution to peripheral remyelination. *Transgenic Res*. 27, 135–153. doi: 10.1007/s11248-018-0062-5

Ponta, H., Sherman, L., and Herrlich, P. A. (2003). CD44: from adhesion molecules to signalling regulators. *Nat. Rev. Mol. Cell Biol*. 4, 33–45. doi: 10.1038/nrm1004

Poppler, L. H., Ee, X., Schellhardt, L., Hoben, G. M., Pan, D., Hunter, D. A., et al. (2016). Axonal growth arrests after an increased accumulation of schwann cells expressing senescence markers and stromal cells in acellular nerve allografts. *Tissue Eng. Part A*. 22, 949–961. doi: 10.1089/ten.TEA.2016.0003

Qiao, W. L., Lu, L., Wu, G. X., An, X. L., Li, D., and Guo, J. (2019). Dpscs seeded in acellular nerve grafts processed by myroilysin improve nerve regeneration. *J. Biomater. Appl*. 33, 819–833. doi: 10.1177/0885328218812136

Rao, Z. L., Lin, T., Qiu, S., Zhou, J., Liu, S., Chen, S. H., et al. (2021). Decellularized nerve matrix hydrogel scaffolds with longitudinally oriented and size-tunable microchannels for peripheral nerve regeneration. *Mater. Sci. Eng. C-Mater*. 120, 111791. doi: 10.1016/j.msec.2020.111791

Record, M., Subra, C., Silvente-Poirot, S., and Poirot, M. (2011). Exosomes as intercellular signalosomes and pharmacological effectors. *Biochem. Pharmacol*. 81, 1171–1182. doi: 10.1016/j.bcp.2011.02.011

Russo, T., Tunesi, M., Giordano, C., Gloria, A., and Ambrosio, L. (2015). Hydrogels for central nervous system therapeutic strategies. *J. Eng. Med*. 229, 905–916. doi: 10.1177/0954411915611700

Sabongi, R. G., De Rizzo, L. A., Fernandes, M., Valente, S. G., Gomes dos Santos, J. B., Faloppa, F., et al. (2014). Nerve regeneration: is there an alternative to nervous graft? *J. Reconstruct. Microsurg*. 30, 607–616. doi: 10.1055/s-0034-1372477

Saheb-Al-Zamani, M., Yan, Y., Farber, S. J., Hunter, D. A., Newton, P., Wood, M. D., et al. (2013). Limited regeneration in long acellular nerve allografts is associated with increased schwann cell senescence. *Exp. Neurol*. 247, 165–177. doi: 10.1016/j.expneurol.2013.04.011

Sahni, V., and Kessler, J. A. (2010). Stem cell therapies for spinal cord injury. *Nat. Rev. Neurol*. 6, 363–372. doi: 10.1038/nrneurol.2010.73

Sanen, K., Martens, W., Georgiou, M., Ameloot, M., Lambrichts, I., and Phillips, J. (2017). Engineered neural tissue with schwann cell differentiated human dental pulp stem cells: potential for peripheral nerve repair? *J. Tissue Eng. Regener. Med*. 11, 3362–3372. doi: 10.1002/term.2249

Sarker, M., Naghieh, S., McInnes, A. D., Schreyer, D. J., and Chen, X. (2018b). Strategic design and fabrication of nerve guidance conduits for peripheral nerve regeneration. *Biotechnol. J*. 13, e1700635. doi: 10.1002/biot.201700635

Sarker, M. D., Naghieh, S., McInnes, A. D., Schreyer, D. J., and Chen, X. (2018a). Regeneration of peripheral nerves by nerve guidance conduits: Influence of design, biopolymers, cells, growth factors, and physical stimuli. *Prog. Neurobiol*. 171, 125–150. doi: 10.1016/j.pneurobio.2018.07.002

Schmidt, C. E., and Leach, J. B. (2003). Neural tissue engineering: strategies for repair and regeneration. *Annu. Rev. Biomed. Eng*. 5, 293–347. doi: 10.1146/annurev.bioeng.5.011303.120731

Schuh, C. M. A. P., Day, A. G. E., Redl, H., and Phillips, J. (2018). An optimized collagen-fibrin blend engineered neural tissue promotes peripheral nerve repair. *Tissue Eng. Pt A*. 24, 1332–1340. doi: 10.1089/ten.tea.2017.0457

Shi, R. Y. (2013). Polyethylene glycol repairs membrane damage and enhances functional recovery: a tissue engineering approach to spinal cord injury. *Neurosci. Bull.* 29, 460–466. doi: 10.1007/s12264-013-1364-5

Siemionow, M., Bozkurt, M., and Zor, F. (2010). Regeneration and repair of peripheral nerves with different biomaterials: review. *Microsurgery*. 30, 574–588. doi: 10.1002/micr.20799

Silva, D., Sousa, R. A., and Salgado, A. J. (2021). Hydrogels as delivery systems for spinal cord injury regeneration. *Mater. Today Biol*. 9, 100093. doi: 10.1016/j.mtbio.2021.100093

Sionkowska, A. (2011). Current research on the blends of natural and synthetic polymers as new biomaterials: review. *Prog. Polym. Sci*. 36, 1254–1276. doi: 10.1016/j.progpolymsci.2011.05.003

Sobacchi, C., Palagano, E., Villa, A., and Menale, C. (2017). Soluble factors on stage to direct mesenchymal stem cells fate. *Front. Bioeng. Biotech.* 5, 32. doi: 10.3389/fbioe.2017.00032

Sohn, E. J., Park, H. T., and Shin, Y. K. (2020). Exosomes derived from differentiated Schwann cells inhibit schwann cell migration via microRNAs. *Neuroreport*. 31, 515–522. doi: 10.1097/Wnr.0000000000001435

Sowa, Y., Kishida, T., Imura, T., Numajiri, T., Nishino, K., Tabata, Y., et al. (2016). Adipose-derived stem cells promote peripheral nerve regeneration *in vivo* without differentiation into schwann-like lineage. *Plast Reconstr Surg.* 137, 318e−330e. doi: 10.1097/01.prs.0000475762.86580.36

Sridharan, R., Reilly, R. B., and Buckley, C. T. (2015). Decellularized grafts with axially aligned channels for peripheral nerve regeneration. *J. Mech. Behav. Biomed. Mater*. 41, 124–135. doi: 10.1016/j.jmbbm.2014.10.002

Stratton, J. A., Kumar, R., Sinha, S., Shah, P., Stykel, M., Shapira, Y., et al. (2017). Purification and characterization of schwann cells from adult human skin and nerve. *ENEURO*. 4, ENEURO.0307-16.2017. doi: 10.1523/ENEURO.0307-16.2017

Sun, J. C., and Tan, H. P. (2013). Alginate-based biomaterials for regenerative medicine applications. *Materials*. 6, 1285–1309. doi: 10.3390/ma6041285

Sun, M. Y., Sun, X. T., Wang, Z. Y., Guo, S. Y., Yu, G. J., and Yang, H. Z. (2018). Synthesis and properties of gelatin methacryloyl (GelMA) hydrogels and their recent applications in load-bearing tissue. *Polymers-Basel.* 10, 1290. doi: 10.3390/polym10111290

Sunderland, S. (1951). A classification of peripheral nerve injuries producing loss of function. *Brain*. 74, 491–516. doi: 10.1093/brain/74.4.491

Szabo, L., Gonelle-Gisper, C., Montanari, E., Noverraz, F., Bornet, A., Buhler, L. H., et al. (2019). Cross-reactive alginate derivatives for the production of dual ionic-covalent hydrogel microspheres presenting tunable properties for cell microencapsulation. *ACS Appl. Polym. Mater*. 1, 1326–1333. doi: 10.1021/acsapm.9b00139

Tamkovich, S. N., Tutanov, O. S., and Laktionov, P. P. (2016). Exosomes: generation, structure, transport, biological activity, and diagnostic application. *Biochem. Suppl. Membr. Cell Biol.* 10, 163–173. doi: 10.1134/S1990747816020112

Thery, C., Ostrowski, M., and Segura, E. (2009). Membrane vesicles as conveyors of immune responses. *Nat. Rev. Immunol*. 9, 581–593. doi: 10.1038/nri2567

Tomita, K., Madura, T., Mantovani, C., and Terenghi, G. (2012). Differentiated adipose-derived stem cells promote myelination and enhance functional recovery in a rat model of chronic denervation. *J. Neurosci. Res*. 90, 1392–1402. doi: 10.1002/jnr.23002

Touma, E., Kato, S., Fukui, K., and Koike, T. (2007). Calpain-mediated cleavage of collapsin response mediator protein(CRMP)-2 during neurite degeneration in mice. *Eur. J. Neurosci*. 26, 3368–3381. doi: 10.1111/j.1460-9568.2007.05943.x

Uz, M., Buyukoz, M., Sharma, A. D., Sakaguchi, D. S., Altinkaya, S. A., and Mallapragada, S. K. (2017). Gelatin-based 3d conduits for transdifferentiation of mesenchymal stem cells into schwann cell-like phenotypes. *Acta Biomater*. 53, 293–306. doi: 10.1016/j.actbio.2017.02.018

Villegas-Perez, M. P., Vidal-Sanz, M., Bray, G. M., and Aguayo, A. J. (1988). Influences of peripheral nerve grafts on the survival and regrowth of axotomized retinal ganglion cells in adult rats. *J. Neurosci*. 8, 265–280. doi: 10.1523/jneurosci.08-01-00265.1988

Wang, J., Ding, F., Gu, Y., Liu, J., and Gu, X. S. (2009). Bone marrow mesenchymal stem cells promote cell proliferation and neurotrophic function of schwann cells in vitro and *in vivo*. *Brain Res.* 1262, 7–15. doi: 10.1016/j.brainres.2009.01.056

Wang, J. H., Kong, X. H., Li, Q., Li, C., Yu, H., Ning, G. Z., et al. (2021). The spatial arrangement of cells in a 3D-printed biomimetic spinal cord promotes directional differentiation and repairs the motor function after spinal cord injury. *Biofabrication* 13, 045016. doi: 10.1088/1758-5090/ac0c5f

Wang, L., Chopp, M., Szalad, A., Lu, X. R., Zhang, Y., Wang, X. L., et al. (2020). Exosomes derived from schwann cells ameliorate peripheral neuropathy in type 2 diabetic mice. *Diabetes* 69, 749–759. doi: 10.2337/db19-0432

Wang, M. D., Zhai, P., Schreyer, D. J., Zheng, R. S., Sun, X. D., Cui. F. Z., et al. (2013). Novel crosslinked alginate/hyaluronic acid hydrogels for nerve tissue engineering. *Front. Mater. Sci.* 7, 269–284. doi: 10.1007/s11706-013-0211-y

Wang, Y., Wang, W., Wo, Y., Gui, T., Zhu, H., Mo, X., et al. (2015). Orientated guidance of peripheral nerve regeneration using conduits with a microtube array sheet (MTAS). *ACS Appl. Mater. Interfaces*. 7, 8437–8450. doi: 10.1021/acsami.5b00215

Wei, Z. J., Fan, B. Y., Ding, H., Liu, Y., Tang, H. S., Pan, D. Y., et al. (2019). Proteomics analysis of schwann cell-derived exosomes: a novel therapeutic strategy for central nervous system injury. *Mol. Cell Biochem*. 457, 51–59. doi: 10.1007/s11010-019-03511-0

Williams, R. R., Henao, M., Pearse, D. D., and Bunge, M. B. (2015). Permissive schwann cell graft/spinal cord interfaces for axon regeneration. *Cell Transpl.* 24, 115–131. doi: 10.3727/096368913x674657

Woerly, S., Pinet, E., de Robertis, L., Van Diep, D., and Bousmina, M. (2001). Spinal cord repair with phpma hydrogel containing RGD peptides (neurogel (TM)). *Biomaterials* 22, 1095–1111. doi: 10.1016/S0142-9612(00)00354-9

Wood, M. D., and Mackinnon, S. E. (2015). Pathways regulating modality-specific axonal regeneration in peripheral nerve. *Exp. Neurol*. 265, 171–175. doi: 10.1016/j.expneurol.2015.02.001

Wu, Z. X., Li, Q., Xie, S., Shan, X. F., and Cai, Z. G. (2020). In vitro and *in vivo* biocompatibility evaluation of a 3d bioprinted gelatin-sodium alginate/rat schwann-cell scaffold. *Mater. Sci. Eng. C-Mater*. 109, 110530. doi: 10.1016/j.msec.2019.110530

Xia, H., Sun, X., Liu, D., Zhou, Y., and Zhong, D. (2016). Oriented growth of rat schwann cells on aligned electrospun poly(methyl methacrylate) nanofibers. *J. Neurol. Sci*. 369, 88–95. doi: 10.1016/j.jns.2016.07.061

Xiao, S. N., Zhao, T. F., Wang, J. K., Wang, C. G., Du, J. N., Ying, L. W., et al. (2019). Gelatin methacrylate (GELMA)-based hydrogels for cell transplantation: an effective strategy for tissue engineering. *Stem Cell Rev. Rep*. 15, 664–679. doi: 10.1007/s12015-019-09893-4

Xu, Y. W., Zhou, J., Liu, C. C., Zhang, S., Gao, F. L., Guo, W. J., et al. (2021). Understanding the role of tissue-specific decellularized spinal cord matrix hydrogel for neural stem/progenitor cell microenvironment reconstruction and spinal cord injury. *Biomaterials* 268, 120596. doi: 10.1016/j.biomaterials.2020.120596

Yang, C. Y., Huang, W. Y., Chen, L. H., Liang, N. W., Wang, H. C., Lu, J., et al. (2021). Neural tissue engineering: the influence of scaffold surface topography and extracellular matrix microenvironment. *J. Mater. Chem. B* 9, 567–584. doi: 10.1039/d0tb01605e

Yu, M. M., Gu, G. H., Cong, M., Du, M. Z., Wang, W., Shen, M., et al. (2021). Repair of peripheral nerve defects by nerve grafts incorporated with extracellular vesicles from skin-derived precursor schwann cells. *Acta Biomater*. 134, 190–203. doi: 10.1016/j.actbio.2021.07.026

Zamboni, F., Vieira, S., Reis, R. L., Oliveira, J. M., and Collins, M. N. (2018). The potential of hyaluronic acid in immunoprotection and immunomodulation: Chemistry, processing and function. *Prog. Mater. Sci*. 97, 97–122. doi: 10.1016/j.pmatsci.2018.04.003

Zhang, Y. G., Sheng, Q. S., Qi, F. Y., Hu, X. Y., Zhao, W., Wang, Y. Q., et al. (2013). Schwann cell-seeded scaffold with longitudinally oriented micro-channels for reconstruction of sciatic nerve in rats. *J. Mater. Sci-Mater. Med*. 24, 1767–1780. doi: 10.1007/s10856-013-4917-2

Zhao, L., and Yi, S. (2019). Transcriptional landscape of alternative splicing during peripheral nerve injury. *J. Cell Physiol*. 234, 6876–6885. doi: 10.1002/jcp.27446

Zhao, X., Liu, S., Yildirimer, L., Zhao, H., Ding, R. H., Wang, H. N., et al. (2016). Injectable stem cell-laden photocrosslinkable microspheres fabricated using microfluidics for rapid generation of osteogenic tissue constructs. *Adv. Funct. Mater*. 26, 2809–2819. doi: 10.1002/adfm.201504943

Zheng, C. S., Yang, Z. H., Chen, S. H., Zhang, F., Rao, Z. L., Zhao, C. L., et al. (2021). Nanofibrous nerve guidance conduits decorated with decellularized matrix hydrogel facilitate peripheral nerve injury repair. *Theranostics* 11, 2917–2931. doi: 10.7150/thno.50825

Zhu, C. L., Huang, J., Xue, C. B., Wang, Y. X., Wang, S. R., Bao, S. X., et al. (2018). Skin derived precursor schwann cell-generated acellular matrix modified chitosan/silk scaffolds for bridging rat sciatic nerve gap. *Neurosci. Res*. 135, 21–31. doi: 10.1016/j.neures.2017.12.007

Ziegler, L., Grigoryan, S., Yang, I. H., Thakor, N. V., and Goldstein, R. S. (2011). Efficient generation of schwann cells from human embryonic stem cell-derived neurospheres. *Stem Cell Rev. Rep*. 7, 394–403. doi: 10.1007/s12015-010-9198-2

Zou, J. L., Liu, S., Sun, J. H., Yang, W. H., Xu, Y. W., Rao, Z. L., et al. (2018). Peripheral nerve-derived matrix hydrogel promotes remyelination and inhibits synapse formation. *Adv. Funct. Mater*. 28, 1705739. doi: 10.1002/adfm.201705739

Conflict of Interest: The authors declare that the research was conducted in the absence of any commercial or financial relationships that could be construed as a potential conflict of interest.

Publisher's Note: All claims expressed in this article are solely those of the authors and do not necessarily represent those of their affiliated organizations, or those of the publisher, the editors and the reviewers. Any product that may be evaluated in this article, or claim that may be made by its manufacturer, is not guaranteed or endorsed by the publisher.

frontiers | Frontiers in Cellular Neuroscience

TYPE Mini Review
PUBLISHED 10 August 2022
DOI 10.3389/fncel.2022.948454

OPEN ACCESS

EDITED BY
Ji-Fan Hu,
Jilin University, China

REVIEWED BY
Gonzalo Rosso,
Max Planck Institute for the Science of Light, Germany
Laura Fontenas,
University of Virginia, United States

*CORRESPONDENCE
Anthi Ranella
ranthi@iesl.forth.gr

SPECIALTY SECTION
This article was submitted to Non-Neuronal Cells, a section of the journal Frontiers in Cellular Neuroscience

RECEIVED 19 May 2022
ACCEPTED 14 July 2022
PUBLISHED 10 August 2022

CITATION
Manganas P, Kavatzikidou P, Kordas A, Babaliari E, Stratakis E and Ranella A (2022) The role of mechanobiology on the Schwann cells response: A tissue engineering perspective. Front. Cell. Neurosci. 16:948454. doi: 10.3389/fncel.2022.948454

The role of mechanobiology on the Schwann cell response: A tissue engineering perspective

Phanee Manganas[1], Paraskevi Kavatzikidou[1,2], Antonis Kordas[1,3], Eleftheria Babaliari[1,2], Emmanuel Stratakis[2] and Anthi Ranella[1]*

[1]Tissue Engineering, Regenerative Medicine and Immunoengineering Laboratory, Institute of Electronic Structure and Laser, Foundation for Research and Technology-Hellas (IESL-FORTH), Heraklion, Greece, [2]Ultrafast Laser Micro and Nano Processing Laboratory, Institute of Electronic Structure and Laser, Foundation for Research and Technology-Hellas (IESL-FORTH), Heraklion, Greece, [3]Department of Materials Science and Technology, University of Crete, Heraklion, Greece

Schwann cells (SCs), the glial cells of the peripheral nervous system (PNS), do not only form myelin sheaths thereby insulating the electrical signal propagated by the axons, but also play an essential role in the regeneration of injured axons. SCs are inextricably connected with their extracellular environment and the mechanical stimuli that are received determine their response during development, myelination and injuries. To this end, the mechanobiological response of SCs is being actively researched, as it can determine the suitability of fabricated scaffolds for tissue engineering and regenerative medicine applications. There is growing evidence that SCs are sensitive to changes in the mechanical properties of the surrounding environment (such as the type of material, its elasticity and stiffness), different topographical features provided by the environment, as well as shear stress. In this review, we explore how different mechanical stimuli affect SC behaviour and highlight the importance of exploring many different avenues when designing scaffolds for the repair of PNS injuries.

KEYWORDS

mechanobiology, Schwann cells, neural tissue engineering, mechanical properties, topography, shear stress

Introduction

The nervous system of vertebrates consists of the central nervous system (CNS) and the peripheral nervous system (PNS). Both are made up of neurons and glial cells, with neurons being responsible for receiving and transmitting electrical and chemical signals and glial cells providing the necessary support and protection for neurons. In the PNS, the glial cells are known as Schwann cells (SCs) and are responsible for the creation of myelin sheaths that protect and insulate the axons of peripheral neurons (Belin et al., 2017). They are also essential and indispensable for axon regeneration in the event of injury (Rosso et al., 2017) and as such, their role and function are under much investigation.

One of the main differences between the CNS and PNS is their capacity for regeneration. Injuries in the PNS are more easily repaired, as broken myelin sheaths can be phagocytosed and removed from the area of injury

(Yao and Priyadarshani, 2018), while in the CNS, there are a number of limiting factors—including glial scar formation and the presence of inhibitory molecules—that make regeneration next to impossible (Huebner and Strittmatter, 2009). In the case of the PNS, when an injury is quite small, it can be repaired by suturing the two ends of the severed nerve together. Autografts have been considered the standard method of countering PNS injuries with slightly larger gap lengths, while commercially available nerve guides have been successful for nerve gaps of 20 mm or more (Bell and Haycock, 2012). However, despite the fact that there are treatments available for PNS injuries, there are still factors that limit their application, such as donor nerve shortage or immunological issues, and they have displayed moderate success (Millesi and Tsolakidis, 2005; Vindigni et al., 2009; Mahumane et al., 2018). As a result, there is a constant ongoing effort to find alternative treatment options by utilising the principles of tissue engineering.

Neural tissue engineering takes advantage of a large number of different biofabrication techniques, as well as biomaterials in order to create three-dimensional scaffolds and structures that can be used to facilitate regeneration (Boni et al., 2018; Papadimitriou et al., 2020; Doblado et al., 2021; Scaccini et al., 2021). The aim when creating scaffolds for such purposes is to mimic the physiological environment as closely as possible and provide the necessary cues to promote repair while ensuring that no localised toxicity or immune reaction is induced (Crupi et al., 2015; Doblado et al., 2021). It is well known that SCs are inextricably connected to their extracellular environment (Rosso et al., 2017). Characteristics of their physiological microenvironment include—but are not limited to—specific mechanical properties (such as elasticity and stiffness), different topographical features, as well as shear stress. All these factors are taken into account when designing scaffolds targeting PNS injuries, either individually or collectively.

Mechanobiology is related to how cells, tissues and organs sense the surrounding mechanical and physical signals and how are these signals converted into specific cellular responses such as adhesion, spreading, migration, gene expression, and cell-cell interactions in multiple cell types (Jansen et al., 2015; Belin et al., 2017). Mechanobiology relies on two main players within the cell: (i) mechanosensors, that allow cells to sense the mechanical signals provided by their environment; and; (ii) mechanotransducers, which enable cells to convert mechanical cues into biochemical signals. Various mechanosensors and mechanotransducers from both intra- and extracellular compartments have already been identified (Jansen et al., 2015). In the case of peripheral nerves and SCs, their identities are still emerging, with research focusing on how physical signals can be transmitted in SCs through the extracellular matrix (ECM), cell adhesion molecules (CAMs) and internal structures, such as the cortical cytoskeleton and the nucleus.

In this review, we explore how the different extracellular stimuli affect SC behaviour and highlight the importance of exploring many different avenues when designing scaffolds for the repair of PNS injuries.

The effect of the microenvironment on Schwann cell behaviour

The effect of mechanical properties

Schwann cells in peripheral nerves are physiologically exposed to mechanical stimuli such as shear and compressive and tensile stress, which can occur due to injuries or diseases, as well as during development and adulthood (Zhang et al., 2015; Belin et al., 2017). Peripheral nerves possess great elasticity in order to propagate action potentials throughout developmental growth (Simpson et al., 2013), mechanical compression and stretches while performing daily activities (Phillips et al., 2004). SCs are very sensitive to the surrounding stiffness and possess great plasticity. In case of injury of the peripheral nerves, myelinated SCs can dedifferentiate and guide the regeneration of peripheral axons (Jessen and Mirsky, 2016; Boerboom et al., 2017). Generally, in peripheral nerves, myelinated fibres are surrounded by 6–15 layers of connective tissue, which shield the SCs and the axons from mechanical forces originating from the external environment. It is known that the relative elasticity or stiffness of the peripheral nerves can affect the mechanical cues that the SCs are exposed to, while SC architecture and basal lamina integrity play key roles in the SC response to mechanical stress (Belin et al., 2017). *In vitro* studies have shown that mechanical stimulation at low levels may activate SC mitogenic pathways, independently of the regulation occurring between SCs and axons after axonal injury (Salzer and Bunge, 1980).

The mechanical properties of the ECM are defined mainly by elastin and collagen fibres that provide resilience (elasticity) and tensile strength. In peripheral nerves, there are more collagen fibres in comparison to elastin fibres (Sunderland, 1965), which contribute to the elastic properties of peripheral nerves. The main mechanotransducers that have been identified in SCs are responsible for the transmission of signals through the ECM and the SC basal side. Various studies report that SCs interact with axons on their apical side, where the biochemical signals from neurons are critical for SC migration, proliferation, survival, polarisation, differentiation, and gene expression (Monk et al., 2015; Salzer, 2015). SC function depends on the formation of adhesion complexes (through CAMs) between SCs with both axons and the ECM. All these stimuli are then transduced into biological responses, by YAP/TAZ, MRTF or LINC (Poitelon et al., 2016). In addition, forces such as mechanical compression can act on the actin cytoskeleton, leading to deformation of the nucleus

and influencing chromatin organisation (Hernandez et al., 2016), while the nuclear envelope and the actin cytoskeleton work as mechanotransducers between the inner membrane of the cell and the nucleus (Plessner et al., 2015). Rosso et al. (2022) showed that the intrinsic physiological plasticity of SCs, which change their phenotype in response to physiological and patho-physiological changes in their microenvironment, in conjunction with their demonstrated mechanosensitivity, render them powerful targets for cell-based regenerative therapies.

In the field of peripheral nerve engineering, there is a wide range of biomaterials, both natural and synthetic, applied to the supporting cells involved in the repair process, such as neurons, SCs, macrophages, and blood vessels (Gregory and Phillips, 2021; Powell et al., 2021). Synthetic polymers are popular as their mechanical properties can be fine-tuned and they can be adapted to improve cell adhesion (Shahriari et al., 2017). Natural materials (typically derived from ECM components and found in hydrogel form) give the benefit of structural integrity for supporting regenerating axons, whilst maintaining the materials' viscoelastic properties and their capability to further improve function (Bhatnagar et al., 2016). They can also be adapted to possess additional functionalities, such as controlled drug release to *in situ* gel formation. They can also be easily adjusted to fit defects with complicated geometries, such as that of the spinal cord. Multiple biomaterials such as chitosan (Li et al., 2014), collagen (Dalamagkas et al., 2016; Yeh et al., 2020), hyaluronic acid (Thomas et al., 2017), polycaprolactone (PCL; Chew et al., 2008; Mobasseri et al., 2014), poly (lactic acid; PLA; Miller et al., 2001; Mobasseri et al., 2014), poly (lactide-co-glycolide; PLGA; Babaliari et al., 2018a), and others (Gu et al., 2011; Bell and Haycock, 2012; Lotfi et al., 2019) have been assessed for scaffold fabrication. One of the most common materials used for hybrid polymeric conduits is gelatin/polycaprolactone (PCL), which has been shown to provide great support for *in vitro* neurite outgrowth and SC proliferation (Boni et al., 2018).

The surrounding ECM and microenvironment play a significant role in peripheral nerve tissue regeneration. Studies have shown that the regularity of a scaffold surface can guide migration and promote the maturation of SCs, and consequently direct the growth of dorsal root ganglion (DRG) neuritis (Ning et al., 2018; Petcu et al., 2018). In another study, Chen and co-workers evaluated the effects of cyclic tensile stimulation on the neural differentiation capabilities of human SCs. The auxetic hydrogels were found to withstand up to 20% tensile strain without tears, while only losing about 10% weight after being immersed for 14 days. The tensile forces were able to enhance cell viability and proliferation compared to static culture (Chen et al., 2020). Mechanical stimuli can also affect the remyelination of injured axons, with factors such as surface area, porosity, and surface structuring playing an important role in supporting and regulating SCs and directly influencing myelin-related gene expression (Liu et al., 2019; Park et al., 2021).

From the above, it can be seen that when it comes to assessing scaffold requirements for peripheral nerve tissue engineering, one must always take into account: (a) the static mechanical properties of the scaffolds whose aim is to imitate nerve tissue stiffness; (b) the dynamic nature of the nerve tissue; and (c) the time-varying mechanics relating to the stress gradient responses in the native tissue.

The effect of topography

The effect of topography —the surface spatial features of tissues or biomaterials—on SCs has attracted a lot of attention in the fields of neuron regeneration and regenerative medicine (Lotfi et al., 2019). Topographical cues in the micro-and nano-scale affect key SC responses such as migration, alignment, proliferation, and differentiation. The importance of these effects is highlighted by the fact that SCs provide structural support, remove debris, and direct axon regrowth in diseases associated with the PNS. Researchers attempt to mimic the natural environment of SCs to provide all the necessary cues that will enhance SC performance when developing strategies to counter neurodegenerative diseases, trauma, and disorders (Gu et al., 2011; Bell and Haycock, 2012; Lotfi et al., 2019). Fabrication of suitable scaffolds for SC seeding is gaining more popularity as a means to develop grafts that can be used as transplants for SC culture and neuron regeneration for *in vivo* trials (Gu et al., 2011; Deng et al., 2021).

Various topographical features have been investigated in literature (Lotfi et al., 2019). These features include but are not limited to, micro- and nano-scale surface topography and patterning (Miller et al., 2001; Schmalenberg and Uhrich, 2005; Li et al., 2014; Yiannakou et al., 2017; Angelaki et al., 2020), cell imprinted topography (Moosazadeh Moghaddam et al., 2019), scaffold geometry (grooves, filaments, wells, pillars etc.; Schmalenberg and Uhrich, 2005; Chew et al., 2008; Mitchel and Hoffman-Kim, 2011; Mobasseri et al., 2014; Tonazzini et al., 2015; Chen et al., 2019), hydrophilicity (Mobasseri et al., 2014), and roughness (Simitzi et al., 2015; Babaliari et al., 2021; Huang et al., 2021) and porosity (Li et al., 2014). Moreover, topographical characteristics are not investigated in a qualitative manner exclusively. For instance, grooves of different dimensions and spacing have been reported to have different effects on SCs (Schmalenberg and Uhrich, 2005; Li et al., 2014; Tonazzini et al., 2015). It has been shown that surface coating further mimics the ECM, which in turn boosts SC performance in axon regeneration. In 2001, Miller et al. (2001) seeded SCs and DRGs on laminin-coated poly(D, L-lactic acid) micropatterned grooves with varied groove spacing and depth and reported the effects of topography alongside the benefit of SC presence as a biological cue for neurite outgrowth and alignment. Another study reports the use of laminin-coated poly (dimethylsiloxane; PDMS)

grooves for SC alignment as a means of directing neuron regeneration (Schmalenberg and Uhrich, 2005). Mobasseri et al. (2014) developed PCL/PLA films as scaffolds and reported the combined effect of different groove geometries and shapes along with scaffold wettability on SC interactions. Ahmed and Brown have also reported differential SC responses such as adhesion, alignment and migration on fibronectin fibres by comparing different combinations of substrates of fibronectin, laminin, and poly (L-lysine) and highlighting the directed orientation and enhanced speed, cell extension and cell area SCs exhibited on fibronectin fibres compared to the respective responses on non-topographical substrates (Ahmed and Brown, 1999).

Although the importance of topography cannot be understated, it is more common to investigate the topographical effects alongside other stimuli, such as electrical conductivity, shear stress, and use of growth factors, and examine their synergistic or antagonistic effects on SC behaviour. For instance, Huang et al. (2021) have developed reduced graphene oxide electrospun fibres that exhibit electrical conductivity and are suitable for SC electrical stimulation (ES). In another study, SCs combined with glial-derived neurotrophic factor (GDNF) on laminin-coated filaments exhibited significant and unidirectional axonal growth in the graft environment, reducing the inflammatory response, astrogliosis and tissue damage compared to non-coated filaments or coated filaments lacking SCs/GDNF. This demonstrated that the combination of laminin-coating and the use of SCs/GDNF was key to the success of the approach (Deng et al., 2021).

Another point of interest pertains to studies that have focused on co-culturing neurons alongside SCs since the nervous system is very complicated and multiple parameters should be taken into account for the successful application of scaffolds as *in vivo* transplants (Angelaki et al., 2020; Kordas et al., 2022). One such study utilised a substrate with combined morphology including both micro-cones and nano-ripples for the co-culture of SCs and neuronal cells. The authors were able to show that SCs adhesion was affected by the underlying pattern, which in turn also influenced neuronal cell behaviour (Angelaki et al., 2020).

Additionally, the focus has been directed not only on morphology, directionality and axon regeneration, but also on other key responses such as remyelination, myelin-related gene, and neurotrophic factor regulation, and examination of markers of immature or aged SCs. For example, Chew et al. (2008) used electrospun fibrous scaffolds to study SC alignment and investigate the regulation of various selected genes, myelin-specific proteins and immature SC markers. Follow-up work also highlighted the importance of topography on the spatial organisation of SCs, which in turn influenced myelination as well as neurite alignment (Siddiqui et al., 2021). Another study also used electrospun scaffolds and investigated topographical effects on myelin-related genes such as myelin-associated glycoprotein (MAG) and myelin protein zero (P0) *via* qRT-PCR, enabling the creation of a gene expression profile during the myelination process on scaffolds with specific alignment (Radhakrishnan et al., 2015).

It is evident that topography is one of the major factors that influence SC behaviour and plays a pivotal role in nerve regeneration applications. Topography can influence major cell responses such as adhesion, migration, alignment, and proliferation, while also affecting the regulation of multiple genes related to myelination and neurodegenerative diseases. As such, it is essential that it is taken into account and integrated into potential solutions.

The effect of shear stress

When studying cell-material interactions, more often than not conventional cell culture techniques are used, which means that the cells are cultured in flasks, Petri dishes, and other surfaces under static conditions (Coluccio et al., 2019), where they also have limited cell-cell interactions. However, within a multicellular organism, cells interact with a number of materials with different mechanical properties and topographical characteristics and are surrounded by fluid and nutrients (Zhang and Van Noort, 2011; Babaliari et al., 2018b). In order to better understand biological problems, it is important to assess cellular behaviour under conditions that reflect more closely the *in vivo* conditions with cell-cell, cell-matrix, and cell-soluble factor interactions (Hui and Bhatia, 2007). To achieve a more realistic environment for biological research, microfluidic devices are routinely used, as they can offer precise control over the microenvironment that influences biochemical and mechanical factors in a cell and, thus, cell functionality, such as changes in the flow-induced shear stress, the pH or O_2 levels (Zhang and Van Noort, 2011).

Although shear stress—the external force acting on an object or surface parallel to the slope or plane in which it lies—is a critical component of the natural environment for the regeneration of axons (Chafik et al., 2003), the use of such systems for the study of neuronal cell behaviour is not widespread and there are very few studies available. One such study investigated the use of different substrate coatings for the use of SCs in microfluidic culturing environments, as shear stress significantly affected the effectiveness of surface coatings (Chafik et al., 2003). Gupta and co-workers studied the effect of shear stress on SC proliferation and genetic expression profiles and were able to find that under constant laminar fluid flow SCs had increased proliferation rates but displayed downregulation of MAG and myelin basic protein (MBP; Gupta and Steward, 2003; Gupta et al., 2005). Babaliari et al. (2021) have studied the combined effect of

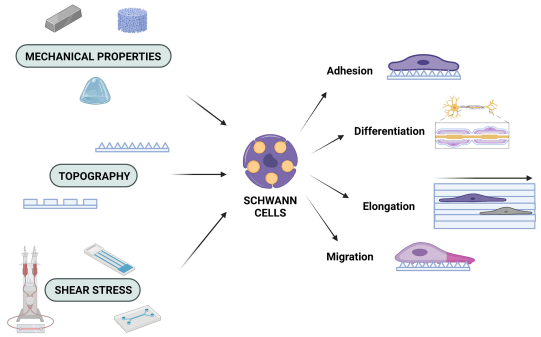

FIGURE 1
Mechanobiology and the Schwann cell response. SCs are affected by the mechanical properties of the engineered microenvironment, the underlying topography, and shear stress forces, which can determine their adhesion profiles, their ability to migrate and/or elongate, as well as their capacity to differentiate. Created with BioRender.com.

shear stress and topography on SC behaviour under dynamic culture conditions attained *via* continuous flow. Experiments using a precise flow-controlled microfluidic system which incorporated laser-microstructured microgrooved polyethylene terephthalate (PET) substrates revealed that, depending on the relation of the direction of the flow with respect to the topographical features (parallel or perpendicular), wall shear stress gradients act in a synergistic or antagonistic manner to topography in promoting a guided morphological cell response (Babaliari et al., 2021).

It is thus evident that flow-induced shear stress also affects neuronal behaviour. As a result, the necessity of developing *in vitro* biomimetic cell culture systems simulating shear stress, together with the micro/nano topography of the *in vivo* environment is mandatory. By utilising such systems to study the mechanobiology of peripheral glial cells, there would be a great benefit for various applications, including the creation of autologous graft substitutes for nerve tissue regeneration.

Conclusion and future perspectives

Over the past decades, there has been great interest in trying to understand the function of SC cells in order to fully utilise their potential in tissue engineering. As with all cells, SC function is inextricably connected to the microenvironment and it must not be ignored when attempting to understand PNS injury and disease. In this review, it has been highlighted how different aspects of the microenvironment (mechanical properties, topography and shear stress) can influence SC behaviour (**Figure 1**). It must be noted that all of these properties are so interconnected that integral parts of the process can be missed when they are not all taken into account. Due to the complexity of the nervous system, it is more beneficial to assess and investigate all cues provided by the natural microenvironment and apply this knowledge to the fabrication of biomimetic scaffolds. By integrating different mechanobiological aspects into scaffold design, potential synergistic, or antagonistic effects that could affect scaffold performance can be investigated. In addition, by using a multifaceted approach in scaffold design, the immunogenicity can also be modulated. By selecting materials with appropriate chemical and mechanical characteristics, as well as carefully designing the 3D architecture of the scaffolds, the immune response could be controlled and thus, lead to the reduction of adverse effects, such as scar formation (Crupi et al., 2015; Andorko and Jewell, 2017). Scaffolds that combine such features are gaining more ground as candidate conduits for *in vivo* PNS regeneration (Bell and Haycock, 2012; Liu et al., 2021). Hence, by choosing the appropriate materials, as well as topographical, mechanical, and chemical properties for potential scaffolds, while also utilising stimuli such as electrical stimulation and shear stress, more comprehensive solutions can be offered, which will pave the way for future state-of-the-art scaffolds to counter injuries and neurodegenerative diseases (Tupone et al., 2021).

Author contributions

PM, PK, AK, and EB wrote the manuscript. PM created the figure. ES revised the manuscript. AR designed and revised the manuscript. All authors contributed to the article and approved the submitted version.

Funding

This work was funded by the projects "BioCombs4Nanofibers" (Horizon 2020 FET Open Programme—GA862016), "NeuroStimSpinal" (Horizon 2020 Research and Innovation Programme—GA829060), and by the Stavros Niarchos Foundation within the framework of the project ARCHERS ("Advancing Young Researchers' Human Capital in Cutting Edge Technologies in the Preservation of Cultural Heritage and the Tackling of Societal Challenges"; Reference Number 2019_1193).

Conflict of interest

The authors declare that the research was conducted in the absence of any commercial or financial relationships that could be construed as a potential conflict of interest.

Publisher's note

References

Ahmed, Z., and Brown, R. A. (1999). Adhesion, alignment and migration of cultured Schwann cells on ultrathin fibronectin fibres. *Cell Motil. Cytoskeleton* 42, 331–343. doi: 10.1002/(SICI)1097-0169(1999)42:4<331::AID-CM6>3.0.CO;2-7

Andorko, J. I., and Jewell, C. M. (2017). Designing biomaterials with immunomodulatory properties for tissue engineering and regenerative medicine. *Bioeng. Transl. Med.* 2, 139–155. doi: 10.1002/btm2.10063

Angelaki, D., Kavatzikidou, P., Fotakis, C., Stratakis, E., and Ranella, A. (2020). Laser-induced topographies enable the spatial patterning of co-cultured peripheral nervous system cells. *Mater. Sci. Eng. C Mater. Biol. Appl.* 115:111144. doi: 10.1016/j.msec.2020.111144

Babaliari, E., Kavatzikidou, P., Angelaki, D., Chaniotaki, L., Manousaki, A., Siakouli-Galanopoulou, A., et al. (2018a). Engineering cell adhesion and orientation via ultrafast laser fabricated microstructured substrates. *Int. J. Mol. Sci.* 19:2053. doi: 10.3390/ijms19072053

Babaliari, E., Petekidis, G., and Chatzinikolaidou, M. (2018b). A precisely flow-controlled microfluidic system for enhanced pre-osteoblastic cell response for bone tissue engineering. *Bioengineering (Basel)* 5:66. doi: 10.3390/bioengineering5030066

Babaliari, E., Kavatzikidou, P., Mitraki, A., Papaharilaou, Y., Ranella, A., and Stratakis, E. (2021). Combined effect of shear stress and laser-patterned topography on Schwann cell outgrowth: synergistic or antagonistic? *Biomater. Sci.* 9, 1334–1344. doi: 10.1039/d0bm01218a

Belin, S., Zuloaga, K. L., and Poitelon, Y. (2017). Influence of mechanical stimuli on schwann cell biology. *Front. Cell. Neurosci.* 11:347. doi: 10.3389/fncel.2017.00347

Bell, J. H. A., and Haycock, J. W. (2012). Next generation nerve guides: materials, fabrication, growth factors and cell delivery. *Tissue Eng. Part B Rev.* 18, 116–128. doi: 10.1089/ten.TEB.2011.0498

Bhatnagar, D., Simon, M., and Rafailovich, M. H. (2016). "Hydrogels for Regenerative Medicine," in *Recent Advances in Biopolymers*, ed F. K. Parveen (London: Intech Open), 105–123. doi: 10.5772/62044

Boerboom, A., Dion, V., Chariot, A., and Franzen, R. (2017). Molecular mechanisms involved in schwann cell plasticity. *Front. Mol. Neurosci.* 10:38. doi: 10.3389/fnmol.2017.00038

Boni, R., Ali, A., Shavandi, A., and Clarkson, A. N. (2018). Current and novel polymeric biomaterials for neural tissue engineering. *J. Biomed. Sci.* 25:90. doi: 10.1186/s12929-018-0491-8

Chafik, D., Bear, D., Bui, P., Patel, A., Jones, N. F., Kim, B. T., et al. (2003). Optimization of Schwann cell adhesion in response to shear stress in an *in vitro* model for peripheral nerve tissue engineering. *Tissue Eng.* 9, 233–241. doi: 10.1089/107632703764664701

Chen, S., Du, Z., Zou, J., Qiu, S., Rao, Z., Liu, S., et al. (2019). Promoting neurite growth and schwann cell migration by the harnessing decellularized nerve matrix onto nanofibrous guidance. *ACS Appl. Mater. Interfaces* 11, 17167–17176. doi: 10.1021/acsami.9b01066

Chen, Y. W., Wang, K., Ho, C. C., Kao, C. T., Ng, H. Y., and Shie, M. Y. (2020). Cyclic tensile stimulation enrichment of Schwann cell-laden auxetic hydrogel scaffolds towards peripheral nerve tissue engineering. *Mater. Des.* 195:108982. doi: 10.1016/j.matdes.2020.108982

Chew, S. Y., Mi, R., Hoke, A., and Leong, K. W. (2008). The effect of the alignment of electrospun fibrous scaffolds on Schwann cell maturation. *Biomaterials* 29, 653–661. doi: 10.1016/j.biomaterials.2007.10.025

Coluccio, M. L., Perozziello, G., Malara, N., Parrotta, E., Zhang, P., Gentile, F., et al. (2019). Microfluidic platforms for cell cultures and investigations. *Microelectronic Eng.* 208, 14–28. doi: 10.1016/j.mee.2019.01.004

Crupi, A., Costa, A., Tarnok, A., Melzer, S., and Teodori, L. (2015). Inflammation in tissue engineering: the Janus between engraftment and rejection. *Eur. J. Immunol.* 45, 3222–3236. doi: 10.1002/eji.201545818

Dalamagkas, K., Tsintou, M., and Seifalian, A. (2016). Advances in peripheral nervous system regenerative therapeutic strategies: a biomaterials approach. *Mater. Sci. Eng. C Mater. Biol. Appl.* 65, 425–432. doi: 10.1016/j.msec.2016.04.048

Deng, L. X., Liu, N. K., Wen, R., Yang, S. N., Wen, X., and Xu, X. M. (2021). Laminin-coated multifilament entubulation, combined with Schwann cells and glial cell line-derived neurotrophic factor, promotes unidirectional axonal regeneration in a rat model of thoracic spinal cord hemisection. *Neural Regen. Res.* 16, 186–191. doi: 10.4103/1673-5374.289436

Doblado, L. R., Martínez-Ramos, C., and Pradas, M. M. (2021). Biomaterials for neural tissue engineering. *Front. Nanotechnol.* 3:643507. doi: 10.3389/fnano.2021.643507

Gregory, H., and Phillips, J. B. (2021). Materials for peripheral nerve repair constructs: natural proteins or synthetic polymers? *Neurochem. Int.* 143:104953. doi: 10.1016/j.neuint.2020.104953

Gu, X., Ding, F., Yang, Y., and Liu, J. (2011). Construction of tissue engineered nerve grafts and their application in peripheral nerve regeneration. *Prog. Neurobiol.* 93, 204–230. doi: 10.1016/j.pneurobio.2010.11.002

Gupta, R., and Steward, O. (2003). Chronic nerve compression induces concurrent apoptosis and proliferation of Schwann cells. *J. Comp. Neurol.* 461, 174–186. doi: 10.1002/cne.10692

Gupta, R., Truong, L., Bear, D., Chafik, D., Modafferi, E., and Hung, C. T. (2005). Shear stress alters the expression of myelin-associated glycoprotein (MAG) and myelin basic protein (MBP) in Schwann cells. *J. Orthop. Res.* 23, 1232–1239. doi: 10.1016/j.orthres.2004.12.010

Hernandez, M., Patzig, J., Mayoral, S. R., Costa, K. D., Chan, J. R., and Casaccia, P. (2016). Mechanostimulation promotes nuclear and epigenetic changes in oligodendrocytes. *J. Neurosci.* 36, 806–813. doi: 10.1523/JNEUROSCI.2873-15.2016

Huang, Z., Sun, M., Li, Y., Guo, Z., and Li, H. (2021). Reduced graphene oxide-coated electrospun fibre: effect of orientation, coverage and electrical stimulation on Schwann cells behavior. *J. Mater. Chem. B* 9, 2656–2665. doi: 10.1039/d1tb00054c

Huebner, E. A., and Strittmatter, S. M. (2009). "Axon regeneration in the peripheral and central nervous systems," in *Cell Biology of the Axon. Results and Problems in Cell Differentiation*, Vol. 48, ed E. Koening (Berlin, Heidelberg: Springer), 309–360.

Hui, E. E., and Bhatia, S. N. (2007). Micromechanical control of cell-cell interactions. *Proc. Natl. Acad. Sci. U S A* 104, 5722–5726. doi: 10.1073/pnas.0608660104

Jansen, K. A., Donato, D. M., Balcioglu, H. E., Schmidt, T., Danen, E. H. J., and Koenderink, G. H. (2015). A guide to mechanobiology: where biology and physics meet. *Biochim. Biophys. Acta* 1853, 3043–3052. doi: 10.1016/j.bbamcr.2015.05.007

Jessen, K. R., and Mirsky, R. (2016). The repair Schwann cell and its function in regenerating nerves. *J. Physiol.* 594, 3521–3531. doi: 10.1113/JP270874

Kordas, A., Manganas, P., Selimis, A., Barmparis, G. D., Farsari, M., and Ranella, A. (2022). Development of an oriented co-culture system using 3D scaffolds fabricated via non-linear lithography. *Materials (Basel)* 15:4349. doi: 10.3390/ma15124349

Li, G., Zhao, X., Zhao, W., Zhang, L., Wang, C., Jiang, M., et al. (2014). Porous chitosan scaffolds with surface micropatterning and inner porosity and their effects on Schwann cells. *Biomaterials* 35, 8503–8513. doi: 10.1016/j.biomaterials.2014.05.093

Liu, S., Niu, C., Xu, Z., Wang, Y., Liang, Y., Zhao, Y., et al. (2019). Modulation of myelin formation by combined high affinity with extracellular matrix structure of electrospun silk fibroin nanoscaffolds. *J. Biomater. Sci. Polym. Ed.* 30, 1068–1082. doi: 10.1080/09205063.2019.1621244

Liu, F., Xu, J., Wu, L., Zheng, T., Han, Q., Liang, Y., et al. (2021). The influence of the surface topographical cues of biomaterials on nerve cells in peripheral

nerve regeneration: a review. *Stem Cells Int.* 2021:8124444. doi: 10.1155/2021/8124444

Lotfi, L., Khakbiz, M., Moosazadeh Moghaddam, M., and Bonakdar, S. (2019). A biomaterials approach to Schwann cell development in neural tissue engineering. *J. Biomed. Mater. Res. A* 107, 2425–2446. doi: 10.1002/jbm.a.36749

Mahumane, G. D., Kumar, P., du Toit, L. C., Choonara, Y. E., and Pillay, V. (2018). 3D scaffolds for brain tissue regeneration: architectural challenges. *Biomater. Sci.* 6, 2812–2837. doi: 10.1039/c8bm00422f

Miller, C., Jeftinija, S., and Mallapragada, S. (2001). Micropatterned Schwann cell-seeded biodegradable polymer substrates significantly enhance neurite alignment and outgrowth. *Tissue Eng.* 7, 705–715. doi: 10.1089/107632701753337663

Millesi, H., and Tsolakidis, S. (2005). End-to-side coaptation: an important tool in peripheral nerve surgery. *Eur. Surg.* 37, 228–233. doi: 10.1007/s10353-005-0171-2

Mitchel, J. A., and Hoffman-Kim, D. (2011). Cellular scale anisotropic topography guides Schwann cell motility. *PLoS One* 6:e24316. doi: 10.1371/journal.pone.0024316

Mobasseri, S. A., Terenghi, G., and Downes, S. (2014). Schwann cell interactions with polymer films are affected by groove geometry and film hydrophilicity. *Biomed. Mater.* 9:055004. doi: 10.1088/1748-6041/9/5/055004

Monk, K. R., Feltri, M. L., and Taveggia, C. (2015). New insights on Schwann cell development. *Glia* 63, 1376–1393. doi: 10.1002/glia.22852

Moosazadeh Moghaddam, M., Bonakdar, S., Shokrgozar, M. A., Zaminy, A., Vali, H., and Faghihi, S. (2019). Engineered substrates with imprinted cell-like topographies induce direct differentiation of adipose-derived mesenchymal stem cells into Schwann cells. *Artif. Cells Nanomed. Biotechnol.* 47, 1022–1035. doi: 10.1080/21691401.2019.1586718

Ning, L., Sun, H., Lelong, T., Guilloteau, R., Zhu, N., Schreyer, D. J., et al. (2018). 3D bioprinting of scaffolds with living Schwann cells for potential nerve tissue engineering applications. *Biofabrication* 10:035014. doi: 10.1088/1758-5090/aacd30

Papadimitriou, L., Manganas, P., Ranella, A., and Stratakis, E. (2020). Biofabrication for neural tissue engineering applications. *Mater. Today Bio* 6:100043. doi: 10.1016/j.mtbio.2020.100043

Park, S. E., Ahn, J., Jeong, H. E., Youn, I., Huh, D., and Chung, S. (2021). A three-dimensional *in vitro* model of the peripheral nervous system. *NPG Asia Mater.* 13:2. doi: 10.1038/s41427-020-00273-w

Petcu, E. B., Midha, R., McColl, E., Popa-Wagner, A., Chirila, T. V., and Dalton, P. D. (2018). 3D printing strategies for peripheral nerve regeneration. *Biofabrication* 10:032001. doi: 10.1088/1758-5090/aaaf50

Phillips, J. B., Smit, X., De Zoysa, N., Afoke, A., and Brown, R. A. (2004). Peripheral nerves in the rat exhibit localized heterogeneity of tensile properties during limb movement. *J. Physiol.* 557, 879–887. doi: 10.1113/jphysiol.2004.061804

Plessner, M., Melak, M., Chinchilla, P., Baarlink, C., and Grosse, R. (2015). Nuclear F-actin formation and reorganization upon cell spreading. *J. Biol. Chem.* 290, 11209–11216. doi: 10.1074/jbc.M114.627166

Poitelon, Y., Lopez-Anido, C., Catignas, K., Berti, C., Palmisano, M., Williamson, C., et al. (2016). YAP and TAZ control peripheral myelination and the expression of laminin receptors in Schwann cells. *Nat. Neurosci.* 19, 879–887. doi: 10.1038/nn.4316

Powell, R., Eleftheriadou, D., Kellaway, S., and Phillips, J. B. (2021). Natural biomaterials as instructive engineered microenvironments that direct cellular function in peripheral nerve tissue engineering. *Front. Bioeng. Biotechnol.* 9:674473. doi: 10.3389/fbioe.2021.674473

Radhakrishnan, J., Kuppuswamy, A. A., Sethuraman, S., and Subramanian, A. (2015). Topographic cue from electrospun scaffolds regulate myelin-related gene expressions in schwann cells. *J. Biomed. Nanotechnol.* 11, 512–521. doi: 10.1166/jbn.2015.1921

Rosso, G., Wehner, D., Schweitzer, C., Möllmert, S., Sock, E., Guck, J., et al. (2022). Matrix stiffness mechanosensing modulates the expression and distribution of transcription factors in Schwann cells. *Bioeng. Transl. Med.* 7:e10257. doi: 10.1002/btm2.10257

Rosso, G., Young, P., and Shahin, V. (2017). Implications of Schwann cells biomechanics and mechanosensitivity for peripheral nervous system physiology and pathophysiology. *Front. Mol. Neurosci.* 10:345. doi: 10.3389/fnmol.2017.00345

Salzer, J. L. (2015). Schwann cell myelination. *Cold Spring Harb. Perspect. Biol.* 7:a020529. doi: 10.1101/cshperspect.a020529

Salzer, J. L., and Bunge, R. P. (1980). Studies of Schwann cell proliferation. I. An analysis in tissue culture of proliferation during development, Wallerian degeneration and direct injury. *J. Cell Biol.* 84, 739–752. doi: 10.1083/jcb.84.3.739

Scaccini, L., Mezzena, R., De Masi, A., Gagliardi, M., Gambarotta, G., Cecchini, M., et al. (2021). Chitosan micro-grooved membranes with increased asymmetry for the improvement of the Schwann cell response in nerve regeneration. *Int. J. Mol. Sci.* 22:7901. doi: 10.3390/ijms22157901

Schmalenberg, K. E., and Uhrich, K. E. (2005). Micropatterned polymer substrates control alignment of proliferating Schwann cells to direct neuronal regeneration. *Biomaterials* 26, 1423–1430. doi: 10.1016/j.biomaterials.2004.04.046

Shahriari, D., Shibayama, M., Lynam, D. A., Wolf, K. J., Kubota, G., Koffler, J. Y., et al. (2017). Peripheral nerve growth within a hydrogel microchannel scaffold supported by a kink-resistant conduit. *J. Biomed. Mater. Res. A* 105, 3392–3399. doi: 10.1002/jbm.a.36186

Siddiqui, A. M., Brunner, R., Harris, G. M., Miller, A. L., Waletzki, B. E., Schmeichel, A. M., et al. (2021). Promoting neuronal outgrowth using ridged scaffolds coated with extracellular matrix proteins. *Biomedicines* 9:479. doi: 10.3390/biomedicines9050479

Simitzi, C., Efstathopoulos, P., Kourgiantaki, A., Ranella, A., Charalampopoulos, I., Fotakis, C., et al. (2015). Laser fabricated discontinuous anisotropic microconical substrates as a new model scaffold to control the directionality of neuronal network outgrowth. *Biomaterials* 67, 115–128. doi: 10.1016/j.biomaterials.2015.07.008

Simpson, A. H., Gillingwater, T. H., Anderson, H., Cottrell, D., Sherman, D. L., Ribchester, R. R., et al. (2013). Effect of limb lengthening on internodal length and conduction velocity of peripheral nerve. *J. Neurosci.* 33, 4536–4539. doi: 10.1523/JNEUROSCI.4176-12.2013

Sunderland, S. (1965). The connective tissues of peripheral nerves. *Brain* 88, 841–854. doi: 10.1093/brain/88.4.841

Thomas, R. C., Vu, P., Modi, S. P., Chung, P. E., Landis, R. C., Khaing, Z. Z., et al. (2017). Sacrificial crystal templated hyaluronic acid hydrogels As biomimetic 3D tissue scaffolds for nerve tissue regeneration. *ACS Biomater. Sci. Eng.* 3, 1451–1459. doi: 10.1021/acsbiomaterials.7b00002

Tonazzini, I., Jacchetti, E., Meucci, S., Beltram, F., and Cecchini, M. (2015). Schwann cell contact guidance versus boundary -interaction in functional wound healing along nano and microstructured membranes. *Adv. Healthc. Mater.* 4, 1849–1860. doi: 10.1002/adhm.201500268

Tupone, M. G., d'Angelo, M., Castelli, V., Catanesi, M., Benedetti, E., and Cimini, A. (2021). A state-of-the-art of functional scaffolds for 3D nervous tissue regeneration. *Front. Bioeng. Biotechnol.* 9:639765. doi: 10.3389/fbioe.2021.639765

Vindigni, V., Cortivo, R., Iacobellis, L., Abatangelo, G., and Zavan, B. (2009). Hyaluronan benzyl ester as a scaffold for tissue engineering. *Int. J. Mol. Sci.* 10, 2972–2985. doi: 10.3390/ijms10072972

Yao, L., and Priyadarshani, P. (2018). "Application of Schwann cells in neural tissue engineering," in *Glial Cell Engineering in Neural Regeneration*, (Cham: Springer), 37–57. doi: 10.1007/978-3-030-02104-7_3

Yeh, J. Z., Wang, D. H., Cherng, J. H., Wang, Y. W., Fan, G. Y., Liou, N. H., et al. (2020). A collagen-based scaffold for promoting neural plasticity in a rat model of spinal cord injury. *Polymers (Basel).* 12:2245. doi: 10.3390/polym12102245

Yiannakou, C., Simitzi, C., Manousaki, A., Fotakis, C., Ranella, A., and Stratakis, E. (2017). Cell patterning via laser micro/nano structured silicon surfaces. *Biofabrication* 9:025024. doi: 10.1088/1758-5090/aa71c6

Zhang, C., and Van Noort, D. (2011). Cells in microfluidics. *Top. Curr. Chem.* 304, 295–321. doi: 10.1007/128_2011_147

Zhang, L., Yang, X., Yue, Y., Ye, J., Yao, Y., Fu, Y., et al. (2015). Cyclic mechanical stress modulates neurotrophic and myelinating gene expression of Schwann cells. *Cell Prolif.* 48, 59–66. doi: 10.1111/cpr.12151

frontiers | Frontiers in Cellular Neuroscience

TYPE Original Research
PUBLISHED 20 December 2022
DOI 10.3389/fncel.2022.1065557

OPEN ACCESS

EDITED BY
Ji-Fan Hu,
Jilin University, China

REVIEWED BY
Qianru He,
Nantong University, China
Susu Mao,
Nantong University, China
Joseph Rosen,
Dartmouth College, United States

*CORRESPONDENCE
Xiaofeng Lin
linxf22@mail.sysu.edu.cn

†These authors have contributed equally to this work and share first authorship

SPECIALTY SECTION
This article was submitted to Non-Neuronal Cells, a section of the journal Frontiers in Cellular Neuroscience

RECEIVED 09 October 2022
ACCEPTED 29 November 2022
PUBLISHED 20 December 2022

CITATION
Chen Y, Pan Z, Meng F, Yu X, Xu Q, Huang L, Liang Q, Wu Y and Lin X (2022) Magnetic resonance imaging assessment of the therapeutic effect of combined electroacupuncture and stem cells in acute peripheral nerve injury.
Front. Cell. Neurosci. 16:1065557.
doi: 10.3389/fncel.2022.1065557

Magnetic resonance imaging assessment of the therapeutic effect of combined electroacupuncture and stem cells in acute peripheral nerve injury

Yueyao Chen[1†], Zhongxian Pan[1†], Fanqi Meng[1], Xuewen Yu[2], Qian Xu[1], Leyu Huang[1], Qiumei Liang[1], Yanglei Wu[3] and Xiaofeng Lin[4*]

[1]Department of Radiology, Shenzhen Traditional Chinese Medicine Hospital (The Fourth Clinical Medical College of Guangzhou University of Chinese Medicine), Shenzhen, China, [2]Department of Pathology, Shenzhen Traditional Chinese Medicine Hospital (The Fourth Clinical Medical College of Guangzhou University of Chinese Medicine), Shenzhen, China, [3]Siemens Healthineers, Beijing, China, [4]Department of Nuclear Medicine, The Seventh Affiliated Hospital, Sun Yat-sen University, Shenzhen, China

Objectives: This study aimed to evaluate the therapeutic effect of a combination of Bone Mesenchymal stem cells (BMSCs) transplantation and Electroacupuncture (EA) for acute sciatic nerve injury in rats using magnetic resonance.

Methods: Ninety-two male adult healthy Sprague-Dawley rats were randomly divided into the EA+BMSCs group, EA group, MSCs group, and PBS group (control). Electroacupuncture was performed on a rat receiving EA treatment at Huantiao (GB30) and Zusanli (ST36). T2 values and diffusion tensor imaging (DTI) derived from multiparametric magnetic resonance imaging (MRI), histological assessments, and immunohistochemistry was used to monitor nerve regeneration. Walking track analysis was used to assess nerve functional recovery. Repeated-measures one-way analysis of variance was used to evaluate the significance of T2, DTI, and SFI values among the four groups. One-way analysis of variance was used for comparing the histological characteristics. Bonferroni test was used for multiple pairwise comparisons at each time point.

Abbreviations: AD, axial diffusion; ADC, apparent diffusion coefficient; BMSC, bone mesenchymal stem cells; DOMF, diameter of myelinated fiber; DTI, diffusion tensor imaging; EA, electroacupuncture; EIT, experimental intermediary toe spread; EPL, experimental print length; ETS, experimental toe spread; FA, fractional anisotropy; IOD, integrated optical density; MRI, magnetic resonance imaging; NIT, normal intermediary toe spread; NPL, normal print length; NTS, normal toe spread; PBS, phosphate-buffered saline; PNI, peripheral nerve injury; POAA, percentage of axon area; POMA, percentage of myelin area; POMDA, percentage of myelin debris area; RD, radial diffusivity; ROI, region of interest; SD, standard deviation; SFI, sciatic functional index; TOM, thickness of myelin.

Results: In terms of FA, the EA+BMSCs and EA groups had faster recovery than PBS (control) in all time points after surgery, and the EA+BMSCs group recovered better than the BMSCs group at 3 weeks ($P \leq 0.008$). FA values were higher in the EA group than in the BMSCs group at 4 weeks ($P \leq 0.008$). In terms of RD, the EA+BMSCs group recovered better than the BMSCs group at 2 and 4 weeks ($P \leq 0.008$). Immunofluorescence staining for axon guidance molecule netrin-1 revealed that it was significantly higher in the EA+BMSCs subgroup and EA subgroup than it was in the control (PBS) subgroup at 1–3 weeks ($P < 0.001$). Immunofluorescence staining for S100 showed the continuity of nerve fibers recovered more quickly in the EA+BMSCs subgroup than in the BMSCs subgroup.

Conclusion: Our research revealed that a combination of MSCs and EA can provide both topological and biomolecular guidance to promote axonal extension, myelin regeneration, and functional recovery after PNI. EA not only promotes nerve repair on its own, but also enhanced the beneficial effects of stem cell treatment and the secretion of netrin 1, a guidance regeneration factor, and promotes the orderly growth of nerve fibers. These PNI repairs could be monitored non-invasively and *in situ* by MRI. The FA and RD values derived from MRI could be sensitive biomarkers to reflect the PNI repair process.

KEYWORDS

magnetic resonance imaging, diffusion tensor imaging, electroacupuncture, mesenchymal stem cells, netrin-1, peripheral nerve injury

Introduction

Peripheral nerve injury (PNI) is a clinical condition characterized by sensory and motor deficits. Bone mesenchymal stem cell (BMSC) transplantation has emerged as a promising candidate strategy for the treatment of PNI due to their multipotency, regeneration promotion, secretion of paracrine factors, immunomodulatory properties, and ease of isolation and expansion (Dun and Parkinson, 2017; Yu et al., 2019). Many animal studies and preliminary clinical trials have investigated the efficacy of BMSCs in PNI therapy. Recent clinical trials have indicated that the therapeutic benefit of BMSCs for treating PNI patients remains limited, despite the success of BMSCs in improving nerve injury outcomes in animals (Mathot et al., 2019). In addition, due to abnormal stimulation of axonal buds, BMSC transplantation may result in atypical, non-linear nerve growth patterns (Sullivan et al., 2016).

Electroacupuncture (EA) combines conventional acupuncture with low-voltage electricity. It has been widely utilized for PNI rehabilitation due to its relative simplicity, affordability, and safety compared to conventional therapies (Wu et al., 2021). In addition, increasing evidence has shown that EA can play a beneficial therapeutic role in peripheral neuropathy by rapidly improving nerve function, reducing edema, down-regulating inflammation, and exerting analgesic effects (Ahn et al., 2019).

Notably, studies on cerebral ischemic disease have revealed that grafted BMSCs and EA treatment significantly enhanced the functional recovery of motor and cognitive deficits compared to BMSCs or EA treatment alone. Furthermore, treatment with EA could promote the differentiation of BMSCs into neuron-like cells and migration to injured areas following tissue damage, and enhance growth factor and cytokine expression, as well as cell survival (Emelyanov et al., 2016; Salazar et al., 2017; Ahn et al., 2019). Therefore, EA plus electromagnetic therapy could effectively repair neural and nerve injuries.

Netrin-1 was the first axon guidance molecule discovered in vertebrates and has a strong chemotropic role in axon guidance, cell migration, morphogenesis, and angiogenesis (Dun and Parkinson, 2017). Recent research has shown that the netrin-1 mRNA and protein are expressed in the adult rat sciatic nerve and that Schwann cells are the predominant cell type that secretes netrin-1 (Madison et al., 2000; Dun and Parkinson, 2020). In addition, it is upregulated in distal nerve segment Schwann cells after peripheral nerve injury. Thus, netrin-1 plays a positive role in promoting peripheral nerve regeneration. Whether BMSCs and EA intervention can promote the secretion of netrin-1, thus promoting nerve regeneration and improving function, is an innovation proposed in this study.

Monitoring the fate of therapeutic cells and modalities is typically performed through postmortem histological analysis

at predetermined time points, which is laborious and invasive and cannot reflect the longitudinal changes or effect of nerve repair in the same living organism. MRI is a powerful non-invasive diagnostic tool for evaluating PNI and nerve tissue regeneration through direct visualization of peripheral nerve changes (Zheng et al., 2021). Quantitative MRI parameters, such as T2 values and diffusion tensor imaging (DTI) metrics, can detect axonal and myelin information during recovery at multiple time points (Chen et al., 2017; Martín et al., 2017; Zheng et al., 2018). In this study, rat sciatic nerve repair was evaluated using multiparametric MRI, T2 mapping, and DTI. It was hypothesized that combining BMSCs and EA could provide topological and biomolecular guidance to promote axonal extension, myelin regeneration, and functional recovery following PNI. MRI could also be used to monitor PNI repair non-invasively and *in situ*.

Materials and methods

Animals and surgery

All interventions and animal care procedures were performed following the Guangzhou University of Traditional Chinese Medicine's (Guangzhou, China) Guidelines and Policies for Animal Surgery. They were approved by the Institutional Animal Use and Care Committee. The Animal Core Facility of Jennio Biotech Co., Ltd. (Guangzhou, China) supplied 92 adult Sprague-Dawley rats weighing 220 g each. The rats were housed in a conventional animal facility with a 12-h on/off light cycle and free access to conventional food and water. All rats sustained an acute crush injury to the left sciatic nerve. Each animal's right sciatic nerve, serving as control, was examined without damaging it.

After administering sodium pentobarbital intraperitoneally at a dose of 30 mg per kilogram of body weight (Sigma-Aldrich; St. Louis, MO), animals were placed in the prone position and the left sciatic nerve was exposed using a blunt splitting technique. A 5-mm-long crush injury was made in the middle of the nerve trunk using hemostatic forceps (Jinzhong Medical Devices Company, Shanghai, China), which were closed to the tightest gear and held in place for 1 min with a holding force of approximately 150 *g* to ensure that all nerve fascicles were completely disrupted with an intact epineurium, as observed under a stereomicroscope (Chen et al., 2017).

After surgery, the animals were randomly divided into four groups: A, EA + BMSCs group; B, EA group; C, BMSCs group; and D, PBS group (control). Each group was separated into two subgroups for functional assessment (A1, B1, C1, and D1; $n = 8$ in each subgroup) and histological analysis (A2, B2, C2, and D2; $n = 15$ in each subgroup). SD rat adolescent bone marrow MSCs were collected and grown as previously described (Chen et al., 2017). On the second day following injury, animals in groups A and B underwent electroacupuncture by stimulating Huantiao (GB30) and Zusanli (ST36; Perreault et al., 2021; Yu et al., 2022). In addition, at the time of modeling, animals in groups A and C received subepidermal microinjections of 5×10^5 BMSCs suspended in phosphate-buffered saline (PBS) with a final volume of 3.0 μl. In contrast, animals in group D received the same volume of PBS as the controls.

As previously described, microinjections were administered in the epicenter of the lesion using a Hamilton 32-G needle attached to a 10-L syringe (Hamilton Company; Reno, NV). To collect longitudinal MR data, animals in subgroups A1, B1, C1, and D1 underwent serial MR imaging before surgery (0 weeks) and one (cell transplantation), 2, 3, and 6 weeks after surgery. In addition, animals from subgroups A2, B2, C2, and D2 were used to collect histological data; at each time point of 1, 2, 3, 4, and 6 weeks following MR imaging, three from each subgroup were chosen at random and sacrificed for histological analysis. The study design is shown in **Figure 1**.

EA treatment

For groups A and B that underwent electroacupuncture treatment, acupuncture needles (0.18 mm and 13 mm) were placed into the acupoints 1 day after the modeling. Groups C and D were minimally restrained in the same manner as the acupuncture group, but needles were not inserted. Connecting a global pulse treatment device (Model G6805-C; Shanghai Huayi Medical Instrument Co., LTD, Shanghai, China) with a frequency of 2/15 Hz, a 20-mA current was used to stimulate acupoints with disperse-dense waves. Mild contraction of the hindlimb muscles was appropriate for this type of stimulus. The positive pole was linked to Huantiao (GB30) on the damaged side of the rats. On the wounded side, Zusanli was connected to the negative pole (ST36). Each of the treatments mentioned above was administered daily for 15 min for 1 week, for six consecutive courses, with 2 days of rest between each course.

MR imaging

Rats were scanned at 3T after being put to sleep with 7% chloralhydrate (5 ml/kg, intraperitoneal injection; MAGNETOM Prisma, Siemens Healthcare, Erlangen, Germany). Each rat was prone in a rat coil (6-cm diameter, 8-channel, Suzhou Medcoil Healthcare Co., Ltd.), and its limbs were secured with medical adhesive tape to prevent further movement. Both hind limbs were symmetrically positioned.

Parameters of acquisition: Coronal FS T2WI was obtained with repetition time (TR) = 3,000 ms, echo time (TE) = 67 ms, resolution = 100 × 100, field of view (FOV) = 80 mm × 80 mm, Average = 1, slice thickness = 1.0 mm, slices = 20, and voxel

size = 0.2 mm × 0.2 mm × 1.0 mm. Coronal T2-mapping was obtained using a multi-slice, multi-echo spin-echo sequence with TR = 1,400 ms, TE = 17–80 ms, resolution = 256 × 256, FOV = 80 mm × 80 mm, Average = 1, slice thickness = 1.0 mm, slices = 10, and voxel size = 0.3 mm × 0.3 mm × 1.0 mm. Axial DTI was obtained using an echo planar imaging (EPI) sequence with the following acquisition parameters: TR = 3,500 ms, TE = 72 ms, slice thickness = 1.5 mm, slices = 20, *b*-value = 0, 800 s/mm^2, FOV = 70 mm × 70 mm, Average = 3, voxel size = 0.3 mm × 0.3 mm × 1.5 mm; resolution = 100 × 100, EPI factor = 100, flip angle = 90, diffusion mode: MDDW, and diffusion directions = 20. Twenty slices were acquired to cover the damaged sciatic nerve, including the proximal stump, crush lesion, and distal stump. The plane's center was placed near the epicenter of the lesion. Finally, the total DTI scan time was 4 min and 6 s.

Imaging analysis

Nerve morphological changes were observed on fat-suppressed T2WI in a blinded manner by two authors in consensus (*** and *** with 10 and 8 years of experience with musculoskeletal MR imaging, respectively). The size of the diameter of the distal stumps of the nerve is measured so that the degree of nerve edema can be recorded. At the same time these two authors independently measured T2 relaxation times of the distal stumps on T2-mapping in a blinded manner using the region of interest (ROI) technique, as previously described (Liao et al., 2012; Chen et al., 2017). In brief, a rectangular ROI with a minimal size of 40 pixels covering a 6-mm proximal segment of the distal stump was placed within the nerve and along the course of the nerve. An effort was made to avoid including fatty tissue, edema, or muscle in the measured volume. The average values from the two datasets were used for analysis.

DTI data were uploaded to the workstation (Syngo Via 2, Siemens) and examined by two authors (*** and ***, each with 10 years of experience with DTI) while isolated and blinded. The diffusion tensor was generated and diagonalized on a pixel-by-pixel basis to provide the eigenvectors and values from which the FA, AD, and RD values were derived for each voxel (Lehmann et al., 2010; Chen et al., 2014). Using ROI data, the DTI metrics of the distal stumps were determined quantitatively. Transverse DTI data were fused with coronal T2-weighted images to confirm that ROIs in the distal stump were positioned correctly and consistently.

A 6-mm-long stump distal to the crushing edge on the three adjacent slices was manually outlined within the ROIs. Three measurements were averaged, and the two mean dataset values were used for analysis. The ROIs were positioned as precisely as possible to minimize the partial volume impact. Tractography was obtained using the fiber tracking analysis software accessible on the same machine. Reconstruction of diffusion tensor tractography (DTT) was performed using a multiple ROI technique (Breitenseher et al., 2015). Briefly, at least two ROIs were manually established at various slice sites along the damaged sciatic nerve on the DTI axial images. One was placed at the proximal stump slice and the other at the distal

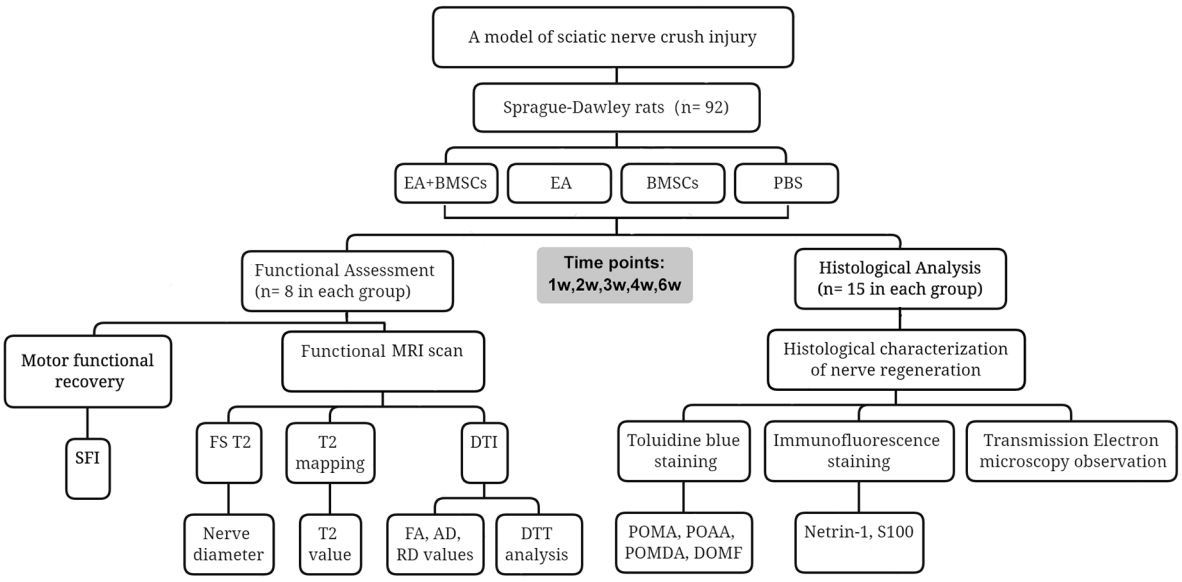

FIGURE 1
Study timeline and flowchart.

stump slice. The passage of fibers *via* various ROIs was also seen. FA was set to 0.12, the maximum fiber angle was 50 degrees, and the minimum fiber length was 15 mm (Takagi et al., 2009).

Motor functional assessment

The motor functional recovery of the sciatic nerve was evaluated blind and in consensus in groups A1, B1, C1, and D1 using walking track analysis performed at each time point prior to MR imaging by two authors (*** and ***, each with 3 years of experience with sciatic nerve functional assessment). As a measure of nerve locomotor dysfunction, the sciatic functional index (SFI) was established (Bain et al., 1989).

Histology

After MR imaging at specific periods, animals in groups A2, B2, C2, and D2 were euthanized by transcardial perfusion with PBS followed by 4% paraformaldehyde in 0.1 M PBS (pH 7.4). The central and distal stumps of the damaged nerves were removed, fixed in 4% paraformaldehyde for 1 h, and maintained in 20% sucrose solution until examination. Transverse semi-thin sections (2 μm thickness) were prepared from the distal end of the tissue specimens and stained with toluidine blue to detect nerve degeneration (Feirabend et al., 1998). Contiguous 15-μm-thick longitudinal sections were obtained at the proximal end of the tissue specimens and processed for netrin-1, and S100 immunofluorescence staining occurred to assess axonal regeneration, as previously described (Zhang et al., 2014; Salameh et al., 2018). For netrin-1, an objective magnification of ×400 was used to obtain digital images of the entire cross-sectional area of the nerve (1,388 × 1,040 pixels, 3.9 pixels/μm) on a microscope (Olympus BX60; Japan) for detailed histological quantification. Of these images, five randomly selected images (585 × 468 pixels, 3.9 pixels/μm) were analyzed. Image Pro Plus software was used to perform an analysis to determine the integrated optical density (IOD) of netrin-1 (Sun et al., 2017; Huang et al., 2021). The final value used for statistical analysis represented the mean of five measured images per nerve segment and animal.

To quantify toluidine blue staining, sections of the distal stumps were analyzed morphometrically. In brief, an objective magnification of ×1,000 was used to obtain digital images of the entire cross-sectional area of the nerve (1,920 × 1,080 pixels, 13.7 pixels/μm) on a microscope (Olympus BX60; Japan) for detailed histological quantification. Of these images, five randomly selected measured images (1,644 × 959 pixels, 13.7 pixels/μm) were analyzed. ImageJ software was used to determine the percentage of axon area (POAA), percentage of myelin area (POMA), percentage of myelin debris area (POMDA), and diameter of myelinated fiber (DOMF). The final value used for statistical analysis represented the mean of five measuring images per nerve segment and animal.

To observe the microstructural changes of the axon and myelin sheath during the regeneration of the injured rat sciatic nerve in different subgroups, transmission electron microscopy (TEM) was performed (Liu et al., 2019).

Statistical analysis

Repeated-measures one-way analysis of variance (ANOVA) was used to evaluate the significance of DTI and SFI values among the four groups in the first subgroup of animals who underwent MRI and functional recovery assessments. The DTI and SFI values were compared between these subgroups using a Bonferroni test for multiple pairwise comparisons at each time point (zero to about 6 weeks post-surgery) to determine the effects of EA. Histological characterization was compared between subgroups in the second group of animals, who were subjected to histologic analysis, using one-way analysis of variance followed by a Bonferroni *post-hoc* test for multiple pairwise comparisons. Statistical analyses were performed using SPSS version 22.0. All data were presented as means ± standard deviation. A two-sided *P*-value of 0.05 or less indicated a significant difference, and the significance level was $P \leq 0.008$ (0.05/6) for *post-hoc* Bonferroni test (six comparisons were made between these four groups).

Results

MRI monitoring of PNI repair *in vivo*

Nerve diameter and T2 values

After surgery, the injured sciatic nerves in the EA + BMSCs, EA, BMSCs, and PBS subgroups were visualized by FS-T2WI (**Figures 2A–D**). The contralateral side (right side) shows T2 images of normal sciatic nerves. In the 1st week after surgery, the edema of the damaged and distal stumps of the damaged nerves was severe, displaying an enlarged nerve diameter and hyperintense T2 signals in all groups. Subsequently, as the edema gradually subsided, the nerve diameter decreased. For repeated-measures ANOVA, there was a significant interaction between time, treatment, and time*group for nerve diameter (all $P < 0.001$) and T2 values ($P < 0.001$ for time, $P = 0.003$ for treatment, and $P < 0.001$ for time*treatment). At 3 and 4 weeks, the groups treated with EA and EA + BMSCs showed a more rapid reduction in swelling. At 1 week, the nerve diameter of the EA subgroup was less than that of the BMSCs ($P \leq$

0.008) and PBS groups ($P \leq 0.008$). At 4 weeks, the nerve diameter of the EA + BMSCs group was significantly smaller than that of the PBS grouping ($P \leq 0.008$). Six weeks later, the morphology of all nerves had been restored. In addition, a smaller nerve diameter was detected in the PBS group compared to the contralateral side due to nerve atrophy after chronic injury (**Figure 2E**, **Table 1**).

The T2 signals of all subgroups reverted to normal (comparable to the contralateral side) 6 weeks after surgery. However, the temporal dependency of T2 values in the distal stumps of the wounded nerves differed across the EA + BMSCs, EA, BMSCs, and PBS subgroups (**Figure 2F**). After 1 week, the T2 readings of all groups climbed fast and peaked at similar levels. Then, they declined gradually but at varying rates (slopes are given in **Figure 2F**). At 2 weeks, both groups treated with electroacupuncture recovered quicker than other subgroups (both $P \leq 0.008$). In addition, at 2 weeks, the T2 levels of the EA subgroup were lower than those of the BMSCs subgroup ($P \leq 0.008$; **Table 2**).

DTI metrics of nerves

For repeated-measures ANOVA, there was a significant interaction between time, treatment, and time*group for FA (all $P < 0.001$) and RD (all $P < 0.001$). For AD, there was a significant interaction between time ($P < 0.001$) and treatment ($P < 0.001$), but not between time*group ($P = 0.077$). Two to 6 weeks following surgery, the FA levels rose (**Figure 3E**), indicating axonal regeneration in the damaged nerves. The FA values of the injured nerves gradually normalized. Both subgroups treated with EA exhibited larger FA values than the EA-untreated group ($P \leq 0.008$) in the 2nd week after surgery. Among all the groups, the EA + BMSCs group maintained the most significant FA values at 3, 4, and 6 weeks post-operation, followed by the EA group, but the FA values of the PBS group were the lowest. Among them, the EA + BMSCs and EA groups had faster recovery than the PBS (control) group at all time points after surgery in terms of FA. The EA + BMSCs group recovered better than the BMSCs group at 3 weeks ($P \leq 0.008$). FA values were higher in the EA group than in the BMSCs group at 4 weeks ($P \leq 0.008$). The FA values of the EA + BMSCs group were higher than the other groups at 6 weeks ($P \leq 0.008$).

Furthermore, the EA and BMSCs groups had a lower RD value than the PBS (control) group (both $P \leq 0.008$) approximately 2–4 weeks after surgery. The EA + BMSCs group recovered better than the BMSCs group ($P \leq 0.008$) at 2 and 4 weeks. In addition, the RD values were lower in the EA + BMSCs group than in the PBS (control) group ($P \leq 0.008$) at 3 and 4 weeks. AD values were higher in the EA + BMSCs group than in the PBS group ($P \leq 0.008$) at 3 and 4 weeks, and the AD values of the BMSCs group were higher than in PBS (control) groups ($P \leq 0.008$) at 6 weeks (**Table 2**).

Comparing the preoperative measurements, the FA of the EA + BMSCs group value recovered and was higher ($P = 0.028$) at the 6th week, and the AD value recovered to the preoperative level ($P = 0.332$). In the EA group, the FA value recovered to the preoperative level ($P = 0.326$), and the AD value was close to the preoperative level, but there were still differences (0.645 ± 0.020 vs. 0.646 ± 0.054, $P = 0.017$). In the BMSCs group, the FA value had not recovered to the preoperative level ($P < 0.001$), and the AD value recovered to the preoperative level ($P = 0.126$). In the PBS group, neither FA nor AD recovered to the preoperative level (both $P < 0.05$).

DTT of nerves

Compared with the uninjured contralateral nerves, the number of projected injured nerve fibers decreased 2 weeks after surgery, as characterized by DTT analysis (**Figure 3**). The EA + BMSCs and EA groups showed more nerve fibers and more significant trajectories than those implanted without EA treatment at 2–6 weeks after surgery.

Histological characterization of nerve regeneration

One to 2 weeks after surgery, toluidine blue staining of the distal stumps of the damaged nerves indicated extensive myelin loss and axonal degeneration (**Figure 4A**). All groups demonstrated considerable improvement in myelin debris clearing (**Figure 4C**), axonal regeneration, and remyelination 2 and 6 weeks after surgery (**Figure 4A**). Statistically, the EA + BMSCs group displayed the greatest number of regenerated myelinated fibers (**Figures 4B,D,E**) at 3 and 6 weeks and the greatest myelinated nerve fiber diameter (**Figure 4F**) at the distal stumps, followed by the EA group (**Table 3**). TEM revealed ultrastructural modifications after the healing of the sciatic nerve (**Figure 5**).

Comparing the preoperative measurements, the POAA recovered to the preoperative level in the EA + BMSCs subgroup and EA subgroup at the 6th week (all $P > 0.05$). In the BMSCs group, the POAA had not recovered to the preoperative level ($P = 0.002$). In the PBS group, the POAA recovered to the preoperative level ($P < 0.001$).

Immunofluorescence staining for netrin-1 showed that the IOD of netrin-1 in all groups was significantly increased at 1–2 weeks, with a peak at 2 weeks, followed by a rapid decrease at 3 weeks and a gradual decrease to a normal level. As shown in **Table 4**, the IOD of netrin-1 in the EA + BMSCs and EA subgroups was significantly higher than in the control (PBS) subgroup at 1–3 weeks ($P < 0.001$). In addition, the IOD in the EA + BMSCs subgroup was markedly higher

10.3389/fncel.2022.1065557

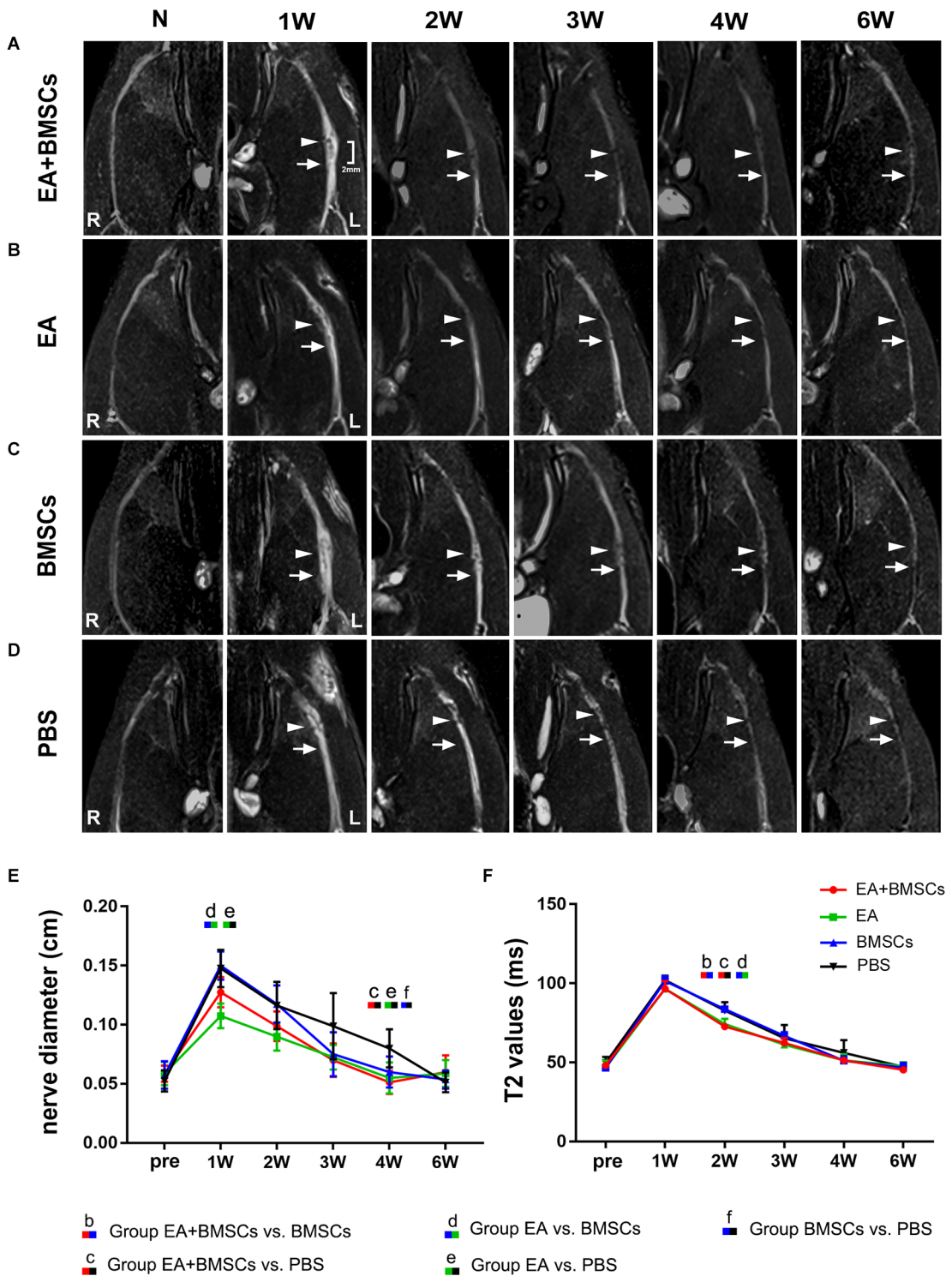

FIGURE 2
Sequential FS-T2WI of injured and uninjured contralateral sciatic nerves in rats. **(A–D)** MRI images depicting the injured nerves on the left side of the EA + BMSCs, EA, BMSCs, and PBS subgroups and the uninjured nerves (control group) on the opposite side. Injured nerves in all subgroups exhibited enlarged and hyperintense signals in the proximal and distal portions, which decreased gradually. BMSCs were injected into the crushed section (indicated by arrowheads). R: right, L: left, W: week. **(E)** Nerve diameter in the distal stumps of the injured nerves of four subgroups up to 6 weeks post-surgery. **(F)** T2 values in the distal stumps of the injured nerves of four subgroups up to 6 weeks post-surgery. The nerve diameter and T2 values of acquisition points within groups were compared by using repeated-measures one-way ANOVA with Bonferroni *post-hoc* testing, and statistically significant differences are listed in Tables 1, 2 respectively.

TABLE 1 Nerve diameter in EA + BMSCs, EA, BMSCs, and PBS [M (P25, P75)].

MRI	Time points (weeks)	EA + BMSCs	EA	BMSCs	PBS	$P \leq 0.008$
Nerve diameter	Pre	0.06 (0.05, 0.06)	0.06 (0.05, 0.06)	0.06 (0.05, 0.06)	0.06 (0.04, 0.06)	-
	1	0.13 (0.12, 0.14)	0.11 (0.10, 0.11)	0.15 (0.14, 0.16)	0.14 (0.14, 0.16)	de
	2	0.10 (0.09, 0.11)	0.09 (0.08, 0.10)	0.12 (0.11, 0.13)	0.12 (0.10, 0.14)	-
	3	0.07 (0.06, 0.08)	0.08 (0.06, 0.08)	0.07 (0.06, 0.09)	0.09 (0.08, 0.13)	-
	4	0.06 (0.04, 0.06)	0.06 (0.04, 0.06)	0.06 (0.05, 0.06)	0.08 (0.07, 0.09)	cef
	6	0.06 (0.05, 0.06)	0.06 (0.05, 0.06)	0.06 (0.05, 0.06)	0.05 (0.04, 0.06)	-

MRI, magnetic resonance imaging; EA, electroacupuncture; BMSCs, bone mesenchymal stem cells; PBS, phosphate-buffered saline; $P \leq 0.008$, *post-hoc* analysis with Bonferroni correction. Statistically significant difference between: [a]Group EA + BMSCs vs. EA. [b]Group EA + BMSCs vs. BMSCs. [c]Group EA + BMSCs vs. PBS. [d]Group EA vs. BMSCs. [e]Group EA vs. PBS. [f]Group BMSCs vs. PBS.

TABLE 2 MRI values in EA + BMSCs, EA, BMSCs, and PBS (mean ± SD).

MRI	Time points (weeks)	EA + BMSCs	EA	BMSCs	PBS	$P \leq 0.008$
T2	Pre	48.21 ± 2.0	46.84 ± 4.32	46.51 ± 1.75	49.65 ± 3.77	-
	1	96.55 ± 4.91	96.50 ± 6.04	101.43 ± 3.08	102.04 ± 2.73	-
	2	72.31 ± 1.52	74.33 ± 3.22	83.73 ± 1.43	82.81 ± 5.31	bcd
	3	62.30 ± 3.19	61.21 ± 5.53	66.78 ± 2.36	65.32 ± 8.36	-
	4	51.75 ± 1.38	51.26 ± 3.89	51.11 ± 2.91	56.05 ± 8.01	-
	6	45.83 ± 1.20	47.68 ± 2.41	45.92 ± 2.38	47.19 ± 2.90	-
FA	Pre	0.637 ± 0.005	0.625 ± 0.014	0.633 ± 0.004	0.627 ± 0.014	-
	1	0.409 ± 0.016	0.405 ± 0.012	0.406 ± 0.016	0.397 ± 0.013	-
	2	0.454 ± 0.018	0.447 ± 0.016	0.433 ± 0.014	0.412 ± 0.015	ce
	3	0.508 ± 0.025	0.492 ± 0.023	0.472 ± 0.018	0.455 ± 0.019	bce
	4	0.530 ± 0.006	0.525 ± 0.028	0.499 ± 0.006	0.492 ± 0.014	bcde
	6	0.644 ± 0.005	0.618 ± 0.009	0.614 ± 0.004	0.599 ± 0.013	abcef
RD	Pre	0.643 ± 0.009	0.646 ± 0.054	0.655 ± 0.024	0.653 ± 0.031	-
	1	0.867 ± 0.020	0.880 ± 0.021	0.880 ± 0.021	0.889 ± 0.018	-
	2	0.764 ± 0.022	0.797 ± 0.027	0.810 ± 0.029	0.843 ± 0.029	bef
	3	0.726 ± 0.021	0.745 ± 0.032	0.747 ± 0.024	0.788 ± 0.031	cef
	4	0.711 ± 0.011	0.722 ± 0.014	0.731 ± 0.017	0.753 ± 0.013	bcef
	6	0.639 ± 0.015	0.645 ± 0.020	0.648 ± 0.015	0.658 ± 0.016	-
AD	Pre	2.088 ± 0.073	2.071 ± 0.039	2.080 ± 0.043	2.072 ± 0.049	-
	1	1.835 ± 0.072	1.822 ± 0.062	1.825 ± 0.062	1.819 ± 0.041	-
	2	1.886 ± 0.080	1.811 ± 0.041	1.859 ± 0.039	1.826 ± 0.053	-
	3	1.924 ± 0.073	1.867 ± 0.035	1.904 ± 0.044	1.829 ± 0.061	c
	4	1.946 ± 0.030	1.903 ± 0.090	1.920 ± 0.059	1.870 ± 0.043	c
	6	2.053 ± 0.049	1.966 ± 0.070	2.025 ± 0.064	1.894 ± 0.083	cf

EA, electroacupuncture; BMSCs, bone mesenchymal stem cells; SD, standard deviation; $P \leq 0.008$, *post-hoc* analysis with Bonferroni correction; FA, fractional anisotropy; RD, radial diffusivity; AD, axial diffusion; PBS, phosphate-buffered saline. Statistically significant difference between: [a]Group EA + BMSCs vs. EA. [b]Group EA + BMSCs vs. BMSCs. [c]Group EA + BMSCs vs. PBS. [d]Group EA vs. BMSCs. [e]Group EA vs. PBS. [f]Group BMSCs vs. PBS.

than in the BMSCs subgroup ($P = 0.000$). At 1 and 3 weeks, the netrin-1 expression of the EA subgroup was higher than in the BMSCs subgroup ($P = 0.001$; $P < 0.001$; Figure 6, Table 4).

Immunofluorescence staining for S100 showed that the continuity of nerve fibers of the injured nerves decreased 1 week post-operation, followed by a gradual recovery in all four subgroups. At 3 weeks post-surgery, the continuity of the injured nerve fibers improved. At 6 weeks post-operation, the continuity of the injured site nerve fibers in the EA + BMSCs and EA subgroups showed almost a full recovery, but not in the BMSCs and control (PBS) subgroups. In addition, the continuity of nerve fibers recovered more quickly in the EA + BMSCs than in the BMSCs subgroup. Finally, the control subgroup (PBS) showed the slowest recovery of the continuity of nerve fibers (Figure 7).

Motor functional recovery

The recovery of motor function in injured rats was examined using walling track analysis and SFI. The footprints of the wounded rats' rear paws were documented (Figures 8A–C). For repeated-measures ANOVA, there was a significant interaction between time ($P < 0.001$), group ($P < 0.001$), and time*group ($P < 0.001$) for SFI. According to the SFI formula (Figure 8C), the normal sciatic nerve function index tends to be zero before the injury. The injured animals exhibited a rapid decrease in SFI within the 1st week following surgery, which recovered progressively (Figure 8D). At 2–5 weeks following surgery, the EA + BMSCs group had the highest SFI value, followed by the EA group alone. The SFI values of the EA group were −30.38 ± 8.72 and −20.75 ± 3.66 at 3 and 4 weeks, respectively (Table 5), whereas those of the EA + BMSCs group were

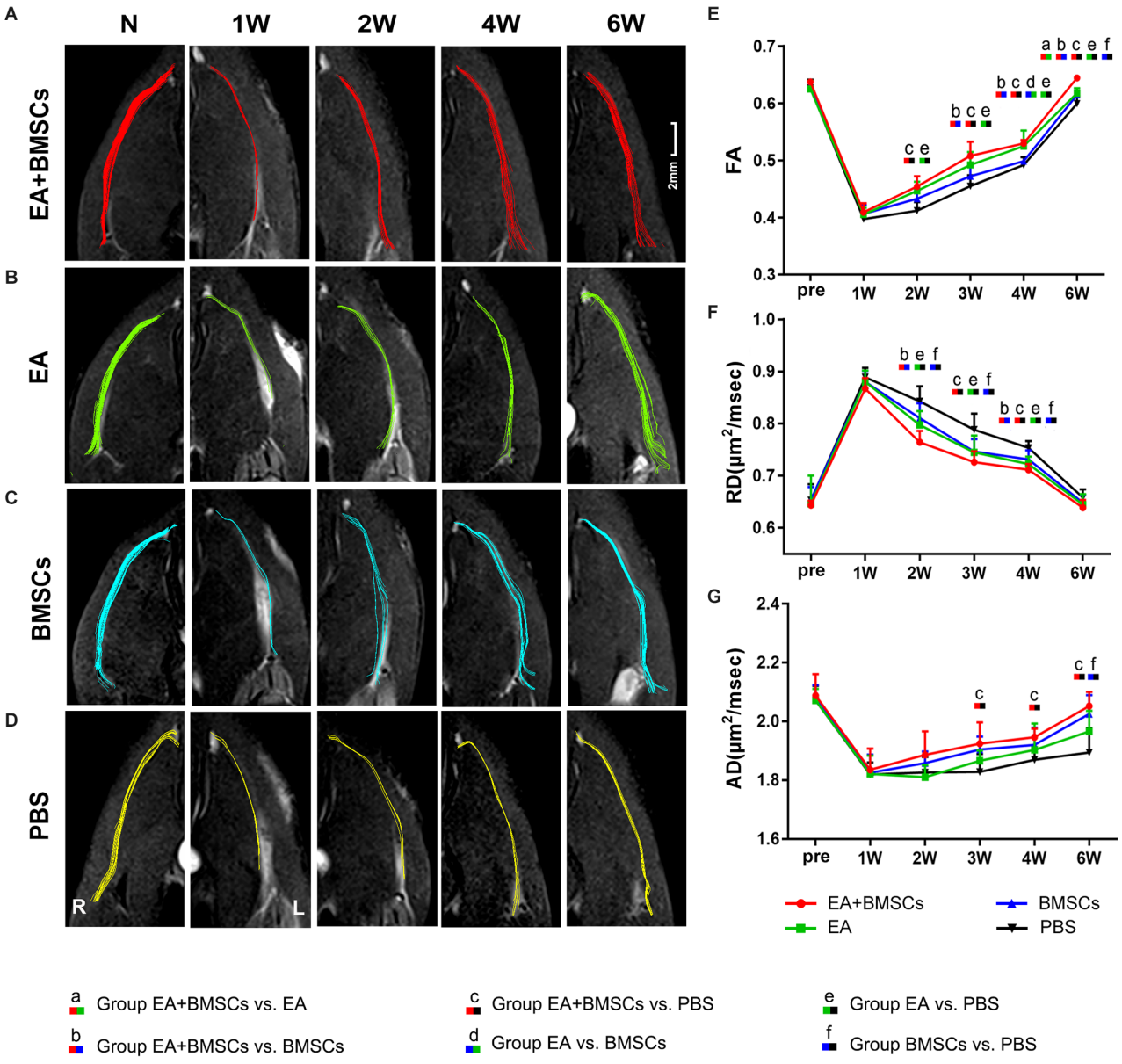

FIGURE 3
DTI of injured sciatic nerves in rats. **(A–D)** DTT of injured sciatic nerves compared to uninjured contralateral nerves after surgery. Images depicting the injured nerves in the EA + BMSCs, EA, BMSCs, and PBS subgroups on the left and the uninjured nerves (control group) on the right. R: right, L: left, W: week. **(E–G)** Six weeks after surgery, FA, RD, and AD values in the distal stumps of all injured nerves were compared to their respective control values. The FA, RD, and AD values of acquisition points within groups were compared by using repeated-measures one-way ANOVA with Bonferroni *post hoc* testing, and Table 2 lists statistically significant differences. DTI, diffusion tensor imaging; DTT, diffusion tensor tractography; EA, electroacupuncture; BMSCs, bone mesenchymal stem cells; PBS, phosphate-buffered saline; FA, fractional anisotropy; RD, radial diffusivity; AD, axial diffusion.

−34.57 ± 4.92 and −24.50 ± 4.08, respectively. The respective SFI values of these two groups were higher than those of the BMSCs (−57.69 ± 10.11 and −39.72 ± 5.29) and PBS groups (−61.13 ± 12.23 and −44.47 ± 4.21). In addition, the SFI values of the EA + BMSCs group were higher than those of the BMSCs group at 2 weeks and the PBS group at 6 weeks. These results indicated that the injured nerve with EA or EA + BMSCs treatment provided a more rapid functional restoration at 2–6 weeks post-surgery.

Correlation coefficients between MRI and histological/functional indexes of the distal stumps of injured nerves were shown in Table 6. Among several noninvasive MR parameters, FA (r = 0.901–0.989, $P < 0.05$) and RD (r = −0.928– −0.983, $P < 0.05$) had higher correlation

10.3389/fncel.2022.1065557

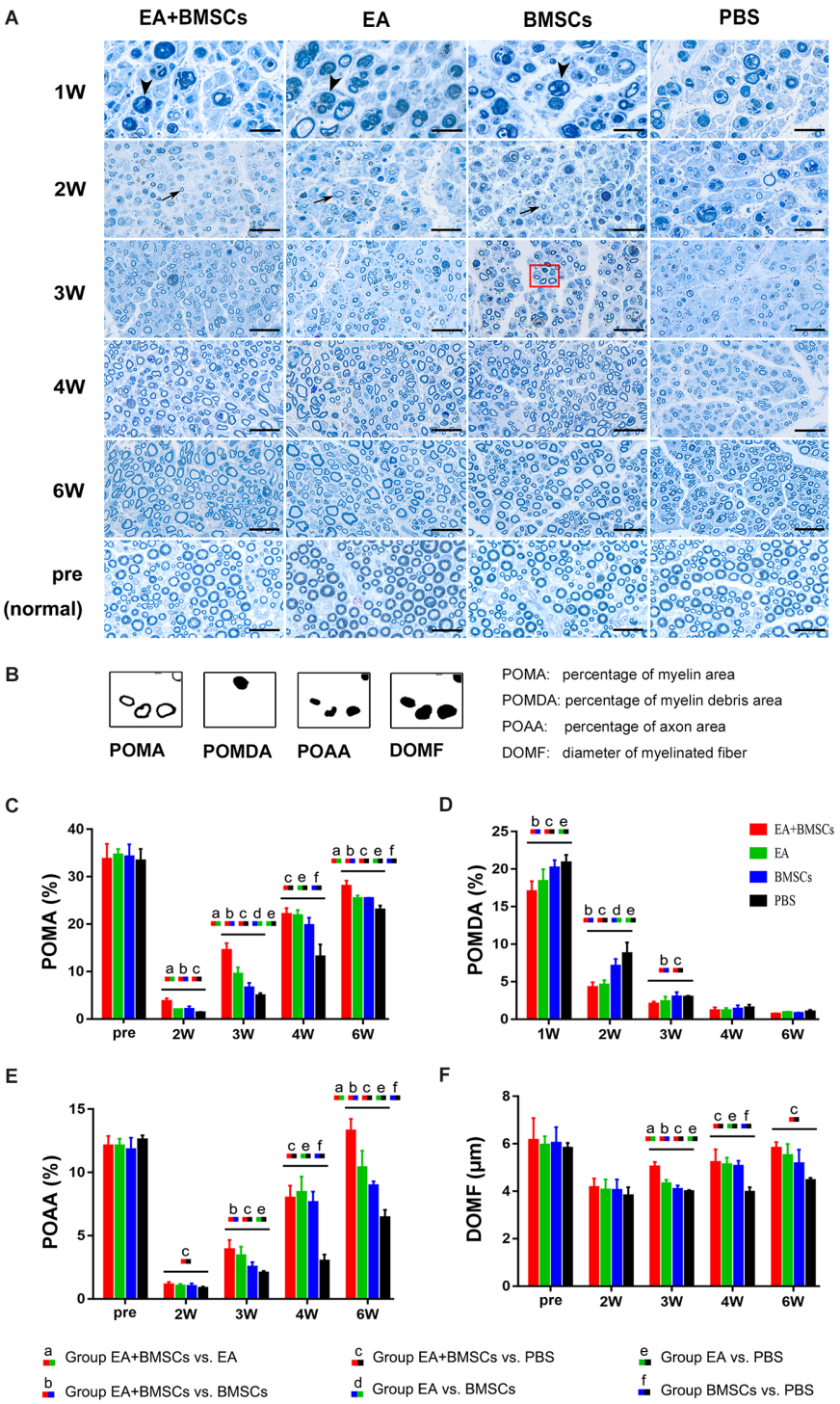

FIGURE 4
Toluidine blue staining of the distal stumps of injured and uninjured contralateral nerves. **(A)** Representative cross-sectional micrographs exhibiting axonal degeneration and myelin disintegration at 1 and 2 weeks post-surgery. The arrowheads denote the myelin debris, which was removed with nerve repaired. By the second week, new myelin sheaths begin to appear, which were thin and small (arrows). Pronounced axonal regeneration and remyelination were observed at 6 weeks post-operation. W: week. Scale bars = 20 μm. **(B)** Semi-quantitative analysis of the four pathological indicators. **(C–F)** Percentage of myelin area (POMA), percentage of myelin debris area (POMDA), percentage of axon area (POAA), and diameter of myelinated nerve fibers (DOMF) in the distal stumps of the injured nerves of all groups compared to their contralateral uninjured nerves (control group) at about 2–6 weeks post-surgery. The POMA, POMDA, POAA, and DOMF values of acquisition points within groups were compared by using one-way ANOVA with Bonferroni *post-hoc* testing, and statistically significant differences are listed in **Table 3**.

TABLE 3 Histological characterizations in EA + BMSCs, EA, BMSCs, and PBS (mean ± SD).

Histology of the injured nerves	Time points (weeks)	EA + BMSCs	EA	BMSCs	PBS	$P \leq 0.008$
POMA	Pre	33.68 ± 3.23	34.57 ± 1.27	34.19 ± 2.63	33.31 ± 2.53	-
	2	3.72 ± 0.62	1.97 ± 0.09	2.04 ± 0.61	1.30 ± 0.20	abc
	3	14.46 ± 1.52	9.42 ± 1.45	6.56 ± 1.05	4.89 ± 0.55	abcde
	4	22.05 ± 1.33	21.8 ± 1.17	19.7 ± 1.58	13.08 ± 2.64	cef
	6	27.99 ± 1.15	25.3 ± 0.67	25.3 ± 0.17	22.98 ± 0.94	abcef
POAA	Pre	12.09 ± 0.79	12.09 ± 0.58	11.80 ± 0.94	12.59 ± 0.35	-
	2	1.30 ± 0.20	1.00 ± 0.18	0.98 ± 0.24	0.84 ± 0.13	c
	3	3.88 ± 0.78	3.42 ± 0.71	2.50 ± 0.41	2.04 ± 0.16	bce
	4	7.97 ± 0.98	8.42 ± 1.25	7.64 ± 0.85	2.98 ± 0.53	cef
	6	13.27 ± 0.97	10.38 ± 1.32	8.95 ± 0.34	6.41 ± 0.64	abcef
POMDA	1	17.00 ± 1.39	20.85 ± 1.59	20.18 ± 1.01	20.85 ± 1.05	bce
	2	4.24 ± 0.69	4.58 ± 0.62	7.08 ± 0.96	8.74 ± 1.48	bcde
	3	2.01 ± 0.33	2.36 ± 0.65	2.98 ± 0.63	2.96 ± 0.18	bc
	4	1.16 ± 0.41	1.16 ± 0.33	1.36 ± 0.49	1.51 ± 0.42	-
	6	0.69 ± 0.09	0.89 ± 0.11	0.75 ± 0.13	1.00 ± 0.23	-
DOMF	Pre	6.14 ± 0.94	5.95 ± 0.37	6.02 ± 0.68	5.81 ± 0.23	-
	2	3.98 ± 0.10	4.26 ± 0.45	4.04 ± 0.45	3.81 ± 0.36	-
	3	5.03 ± 0.21	4.32 ± 0.17	4.08 ± 0.17	3.98 ± 0.07	abce
	4	5.21 ± 0.55	5.10 ± 0.31	5.05 ± 0.23	3.96 ± 0.21	cef
	6	5.81 ± 0.26	5.51 ± 0.49	5.16 ± 0.55	4.46 ± 0.11	c

EA, electroacupuncture; BMSCs, bone mesenchymal stem cells; PBS, phosphate-buffered saline; SD, standard deviation; $P \leq 0.008$, *post-hoc* analysis with Bonferroni correction; POMA, percentage of myelin area; POAA, percentage of axon area; POMDA, percentage of myelin debris area; DOMF, diameter of myelinated fiber. Statistically significant difference between: [a]Group EA + BMSCs vs. EA. [b]Group EA + BMSCs vs. BMSCs. [c]Group EA + BMSCs vs. PBS. [d]Group EA vs. BMSCs. [e]Group EA vs. PBS. [f]Group BMSCs vs. PBS.

coefficients with pathological and functional findings than the other MRI indexes.

Discussion

In a rat model of sciatic nerve crush damage, we found that combined BMSCs and EA therapy synergistically improved axon and myelin regeneration. Moreover, the combined therapy significantly decreased post-injury nerve edema, improved the axon guiding factor, and expedited motor function recovery. These longitudinal alterations can be evaluated quantitatively and morphologically *in vivo* by MRI. These findings expand our understanding of the neurogenic mechanisms mediated by EA-BMSCs as a potential treatment target for PNI and provide vital information for treating this disease in humans in the future.

BMSCs may exert therapeutic effects in experimental PNI models by multiple pathways, including stimulation of angiogenesis and neurogenesis, generation of neuroprotective and neurotrophic chemicals, differentiation into repair-relevant cell types, and modulation of the immune system (Moattari et al., 2018; Lavorato et al., 2021). According to our data, however, even untreated injury-model rats (PBS group) displayed nerve self-healing potential. The BMSCs alone treatment group did not demonstrate a substantial functional recovery advantage. Similar results were obtained in our previous study, showing that the BMSCs group promoted regeneration only at the early stage and then exhibited a similar trend to the control group (Chen et al., 2017).

Several factors may contribute to the inadequate efficacy of stem cell therapy in PNI. A small percentage of the transplanted BMSCs survived for up to 8 weeks. Several of the surviving cells developed into Schwann cells. BMSCs might exert their therapeutic effect *via* paracrine factors rather than *in vivo* transdifferentiation into the target cell (Duan et al., 2017). Furthermore, BMSCs could elicit a humoral and cellular immune response *in vivo* and promote inflammation when the immune system is under-activated (Ankrum et al., 2014; Jiang and Xu, 2020). This might explain the slower rate of edema reduction and debris removal in the stem cell-alone group.

In our investigation, combining BMSCs with EA yielded the most effective therapeutic outcomes, including optimal myelin and axonal regeneration and recovery of nerve function. The combination suggests that EA not only increases the regeneration of myelin and axons on its own but also enhances the efficacy of stem cells by improving their survival, migration, paracrine function, and neural differentiation. In terms of several histological parameters of nerve fiber regeneration and the sciatic nerve function index, the EA-only group demonstrated superior or equal efficacy compared to the stem cell-only group. It also demonstrates that electroacupuncture has distinct benefits in treating peripheral neuropathy, is non-invasive and inexpensive, and should be promoted as a therapy approach.

Netrin-1 has a significant chemotropic role in axon guidance, cell migration, morphogenesis, and angiogenesis. It was the first axon guidance molecule found in vertebrates. Schwann cells, the cell bodies of sensory neurons, and the axons of both motor and sensory neurons express netrin-1

10.3389/fncel.2022.1065557

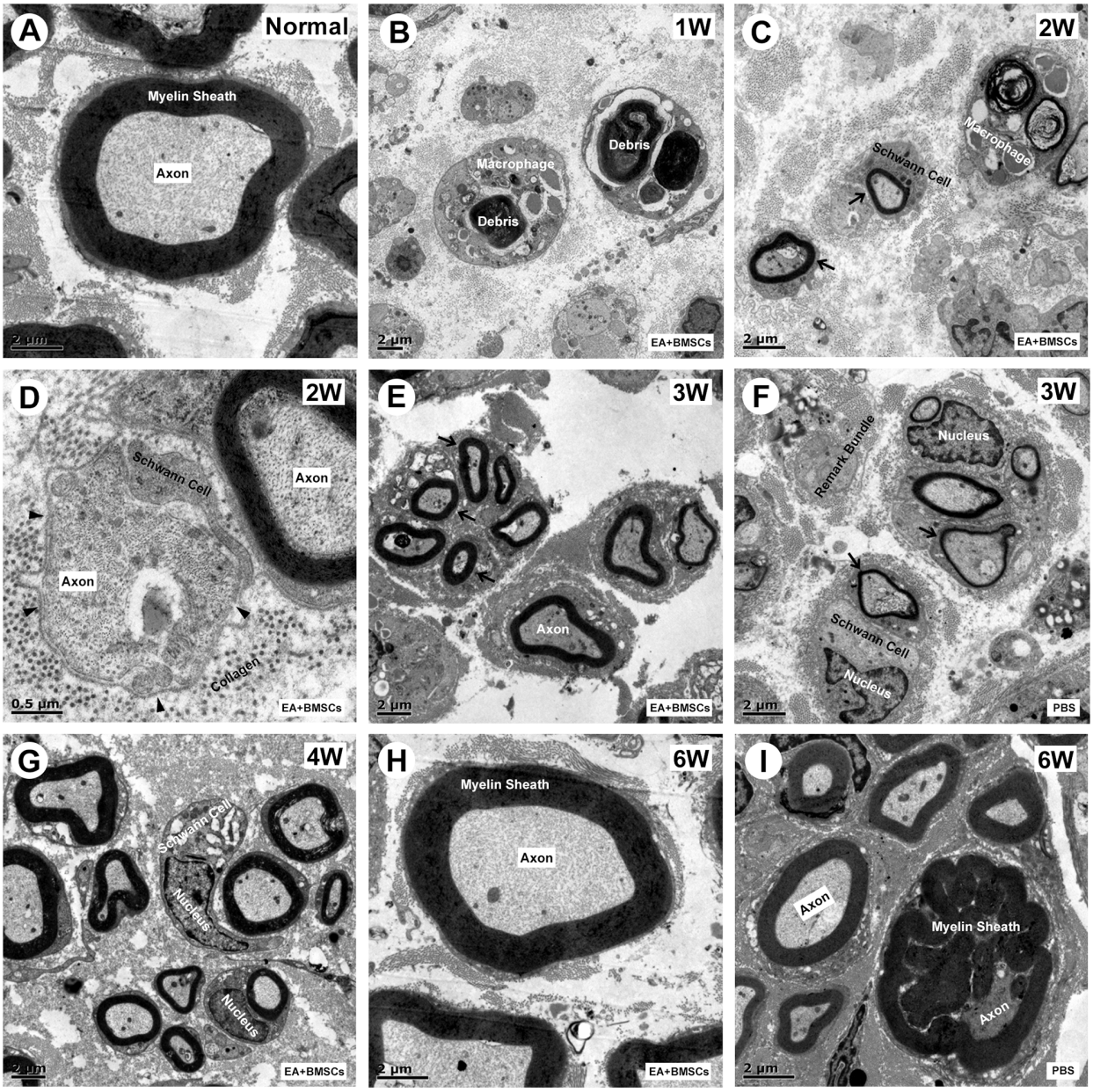

FIGURE 5
Transmission electron microscopy (TEM) images of cross-sections of the sciatic nerve. **(A)** Cross-section of a myelinated axon of a normal adult mouse sciatic nerve. The central axon (Ax) is surrounded by the myelin sheath (MS), with a thickness of 1.2 to 2 μm. **(B)** At 1-week post-operation, the myelin sheath became creased, strangled, and fell off into fragments. Massive myelin debris was phagocytosed and cleared by the macrophages. **(C,D)** Most debris was cleared at 2 weeks post-operation. The Schwann cells thrived, and their synapses wrapped around the axons to form new myelin sheaths, which were thin in myelin sheaths (< 0.5 μm; black arrow) and small in diameter. In addition, some unmyelinated fibers (black arrowhead) could be seen, with surrounding collagen tissue serving as a scaffold for the extension and winding of Schwann cells during myelin formation **(D)**. **(E,G)** During the period from 3 to 4 weeks after surgery, the number of myelinated nerve fibers, myelin thickness, and the degree of maturity of regenerating nerve fibers in EA + BMSCs group were superior to that in the PBS group **(F)**. **(H,I)** At 6 weeks post-operation, nerve fibers of EA + BMSCs group **(H)** recovered with regenerated axons and myelin sheaths comparable to those of the normal nerves **(A)**, as well as superior fiber diameter and myelin thickness to that of the PBS subgroup **(I)**. Some malformed regenerated fibers were observed in the PBS subgroup, with abnormally thickened myelin sheaths that are convex in the lumen. The axons are compressed and narrow.

receptors in the peripheral nervous system. Schwann cells direct regenerated axons to their targets by nerve gap migration and the formation of nerve bridges. Without Schwann cell guidance, regenerated axons lack directionality and travel along ectopic paths following peripheral nerve transection injury (Dun and Parkinson, 2017). Given the evidence from many studies

10.3389/fncel.2022.1065557

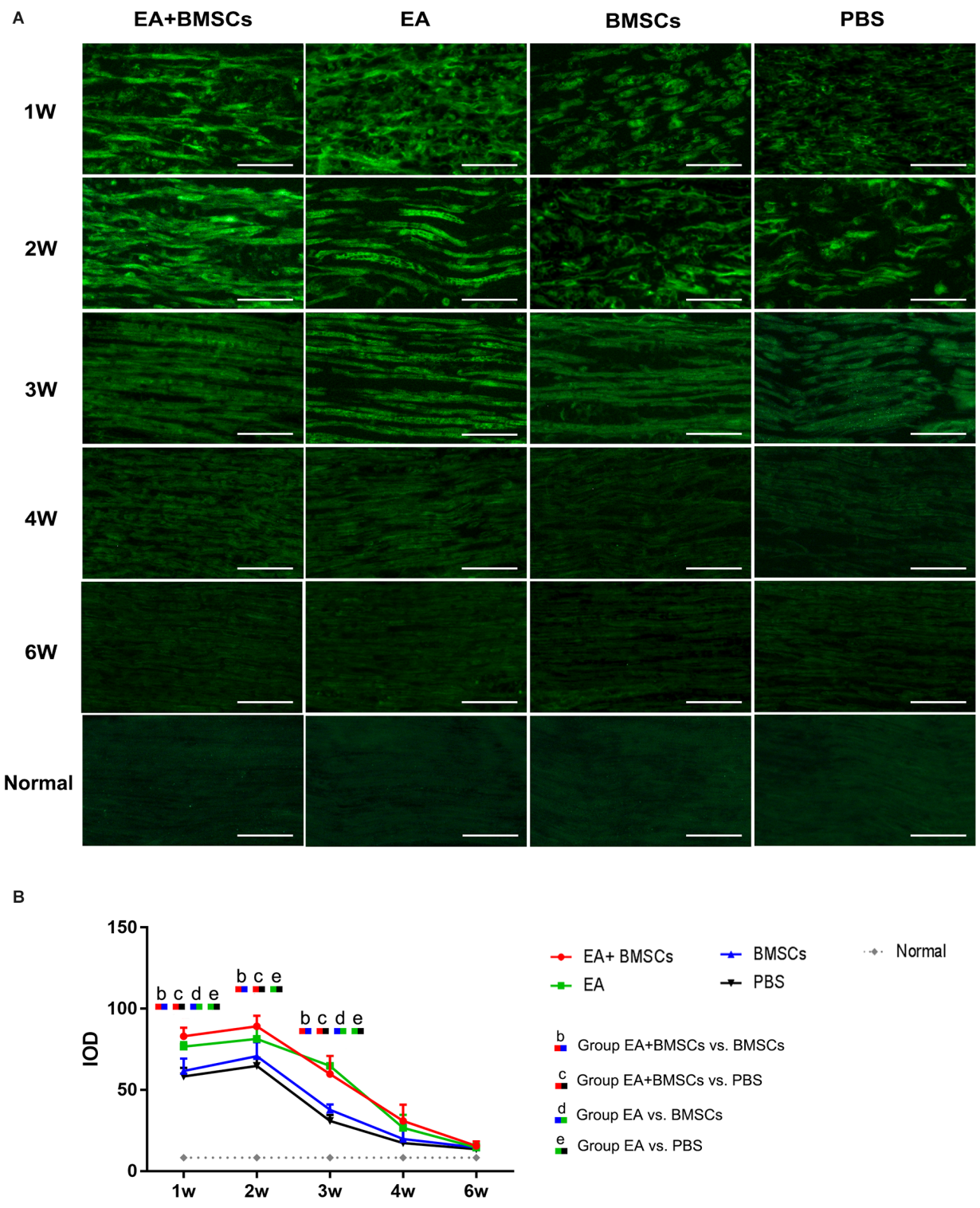

FIGURE 6
Histology of netrin-1 expression of the injured nerves. Immunofluorescence staining shows that netrin-1 is present in the myelin sheath composed of Schwann cells, therefore when it is secreted, the myelin sheath is colored and outlined **(A)**. The expression of netrin-1 of all subgroups significantly increased in 1–2 weeks. The EA+BMSCs and EA subgroups had higher netrin-1 expression (green) than the BMSCs and control subgroups (PBS treatment) in 1–3 weeks **(B)**. In addition, 4 and 6 week figures had a darker degree of staining with the loss of fiber textures **(A)**, which could be judged as a negative expression of the netrin-1 protein. Scale bar = 50 μm; W: week. The IOD of acquisition points within groups were compared by using one-way ANOVA with Bonferroni *post-hoc* testing, and **Table 4** lists statistically significant differences. IOD, integrated optical density.

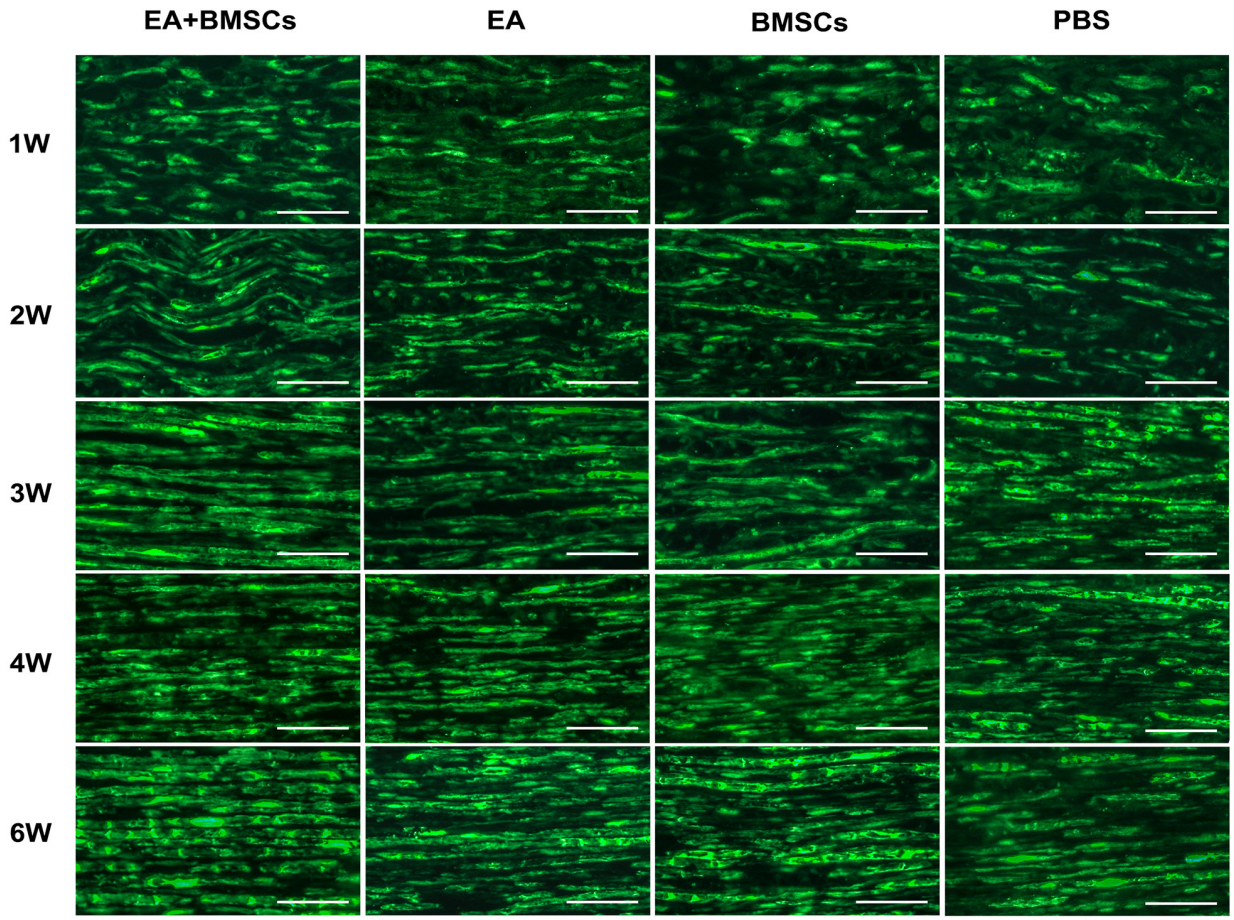

FIGURE 7
S100 staining of the distal stumps of injured nerves. Immunohistochemical staining of S100 observed under the fluorescence microscope (400×) showed the continuity of the restored, damaged sciatic nerve. In terms of neural regeneration connections, compared with the PBS subgroup, the EA + BMSCs subgroup recovered best. In addition, the EA subgroup was better than the BMSC subgroup. Scale bar = 50 μm; W: week.

showing that netrin-1 is associated with Schwann cells and undergoes a regeneration-related increase, netrin-1's influence on peripheral nerve regeneration will be complex.

Netrin-1 protein is expressed in the myelin sheath composed of Schwann cells, therefore when it is secreted, the corresponding myelin is colored and outlined. In the present study, the netrin-1 protein expression was upregulated 1 and 2 weeks after rat sciatic nerve injury, followed by a rapid decrease at 3 weeks, then a gradual decrease to a normal level, consistent with available reports (Lee et al., 2007). The substantial rise in netrin-1 expression might be connected with the proliferation of Schwann cells. These cells are the primary source of netrin-1 protein in the peripheral nerve (Madison et al., 2000; Ellezam et al., 2001; Webber et al., 2011). Notably, netrin-1 can promote Schwann cell proliferation and migration (Lee et al., 2007; Lv et al., 2015). As the degree of sciatic nerve injury increases, netrin-1 secretion also does. In a study comparing a crush injury and a transection injury model, netrin-1 protein could not become detectable 2 weeks after a crush injury, inconsistent with our results. The reason was that our crush injury model had a more severe degree of damage (Madison et al., 2000). Additionally, we found that netrin-1 in the EA + BMSCs and EA groups was higher than in the BMSCs and control (PBS) groups at 1–3 weeks; all groups tended to be at a normal level at 4 and 6 weeks.

The results suggested that EA treatment could promote netrin-1 secretion, which decreased with recovery from the injury. It has been reported that EA promotes nerve regeneration and functional recovery. The mechanism might be associated with the enhancement of Schwann cell proliferation and the upregulation of nerve growth factors (Hu et al., 2018). Moreover, our data showed that at 1–3 weeks, the expression of netrin-1 was significantly increased in combined BMSCs and EA treatment compared to controls or BMSCs alone, and this was likely because EA treatment enhances BMSCs to secrete netrin-1, thereby

TABLE 4 IOD values in EA + BMSCs, EA, BMSCs, and PBS (mean ± SD).

Time points (weeks)	EA + BMSCs	EA	BMSCs	PBS	Normal	$P \leq 0.008$
1	83.04 ± 5.31	76.72 ± 2.78	61.65 ± 7.62	58.31 ± 5.21	8.33 ± 2.01	bcde
2	89.24 ± 6.60	80.90 ± 6.61	70.82 ± 8.60	64.77 ± 5.11	8.33 ± 2.01	bce
3	59.81 ± 11.26	64.75 ± 6.28	37.86 ± 3.34	30.88 ± 3.63	8.33 ± 2.01	bcde
4	30.94 ± 9.96	26.63 ± 8.07	19.86 ± 8.96	17.34 ± 7.84	8.33 ± 2.01	-
6	15.61 ± 2.85	14.60 ± 2.29	14.56 ± 1.88	13.56 ± 2.24	8.33 ± 2.01	-

IOD, integrated optical density; EA, electroacupuncture; BMSCs, bone mesenchymal stem cells; SD, standard deviation; $P \leq 0.008$, *post-hoc* analysis with Bonferroni correction. Statistically significant difference between: [a]Group EA + BMSCs vs. EA. [b]Group EA + BMSCs vs. BMSCs. [c]Group EA + BMSCs vs. PBS. [d]Group EA vs. BMSCs. [e]Group EA vs. PBS. [f]Group BMSCs vs. PBS.

improving the viability of BMSCs (Ke et al., 2015). The above results indicated that EA and BMSCs have a synergistic effect.

The amount of *in situ* axonal regeneration was evaluated using multiparametric MRI. T2 FA and RD values can serve as sensitive indicators for detecting peripheral nerve injury and non-invasive instruments for monitoring nerve regeneration. T2 hyperintensity of the distal degenerating nerves is caused by an increase in water content, myelin turnover, vascular permeability, inflammatory mediators, and axonal and myelin degradation products (Shen et al., 2010; Chen et al., 2015). In this study, the rapid recovery of T2 values and nerve diameter in injured nerves treated with EA at 2–3 weeks indicated that fewer nerves developed post-injury inflammatory edema during the early stages of nerve injury, which might be associated with the treatment of EA. Simultaneously, histological assessments showed that a higher debris removal rate was evident within the EA and EA + BMSCs subgroups. The result indicated that EA and stem cell therapy were anti-inflammatory and optimized the regenerative environment. More importantly, EA may have reduced graft rejection after stem cell transplantation while enhancing the function of stem cells in immune regulation.

Quantitative DTI metrics such as FA and RD values can be further compared with histological results and behavioral assessments for a fuller picture of nerve regeneration (Chen et al., 2017). Compared to BMSCs alone and the control group (PBS), the FA and RD values of injured nerves treated with EA and EA + BMSCs indicated rapid nerve tissue repair in this study. As histological evaluations revealed thicker myelin, thicker axons, and a higher concentration of the axon guidance molecule (netrin-1) in regenerating nerve fibers of the EA + BMSCs group compared to the EA or BMSCs-alone group, the rapid recovery of FA and RD values were likely attributable to enhanced axonal regeneration. Furthermore, FA values, which are the most important quantitative parameters of DTI, correlate more strongly with axon packing density and diameter than with axon diameter alone (Takagi et al., 2009).

In addition, FA assesses the degree of anisotropic diffusion, which represents the degree of cell alignment in nerve fiber pathways (Chen et al., 2017). In our study, the FA value began to grow 2 weeks after sciatic nerve injury, with the most significant increase occurring between weeks 2 and 4 in the EA + BMSCs group. The EA + BMSCs group exhibited denser and more uniformly distributed new myelin sheaths than the other groups, with the EA group next. RD values show myelin integrity and correlate most strongly with myelin thickness and axon regeneration (Martín et al., 2017). At week 2, we found that RD recovered faster than FA, probably because of the more sensitive RD value, on the one hand, reflecting the efficacy of electroacupuncture combined with stem cells in promoting myelin regeneration at the early stage of nerve regeneration on the other (Chen et al., 2017, 2022).

Axial diffusivity (AD) characterizes the mean diffusion coefficient of water molecules diffusing parallel to the tract in the voxel of interest (Song et al., 2003). We discovered that AD was not the same at week 6 as other MRI parameters, which did not return to normal at week 6, in contrast to pathological indicators and SFI. Although toluidine blue staining at week 6 suggested that fiber diameter and myelin thickness were substantially restored, electron microscopic ultrastructure revealed that the PBS group had more aberrantly regenerated myelinated fibers, displaying wrinkling, and central axon occlusion, which may have contributed to the failure of AD to recover (Mirzakhani et al., 2018; Liu et al., 2019). This was consistent with the trend of the percentage of axon area, further demonstrating that AD was closely related to axons and AD can respond to axonal regeneration.

Among these DTI metrics, FA and RD had higher correlation coefficients with pathological and functional findings than the others. Thus FA and RD might be more sensitive and stable biomarkers to evaluate nerve repair.

Our study had several limitations. First, SFI primarily reflected the recovery of motor function, whereas neurosensory recovery could not be described in animals, and thermal withdrawal latency should be added in the future. Second, due to the very small specimen volume of the injured nerve and low expression of netrin-1 protein, the protein quantitative assay such as Western blot was difficult to succeed. Third, due to the high cost of TEM photographs, we were unable to analyze a large number of TEM images in this study. Future research will be required to determine the significance of changes in TEM ultrastructure for the interpretation of MRI parameter changes.

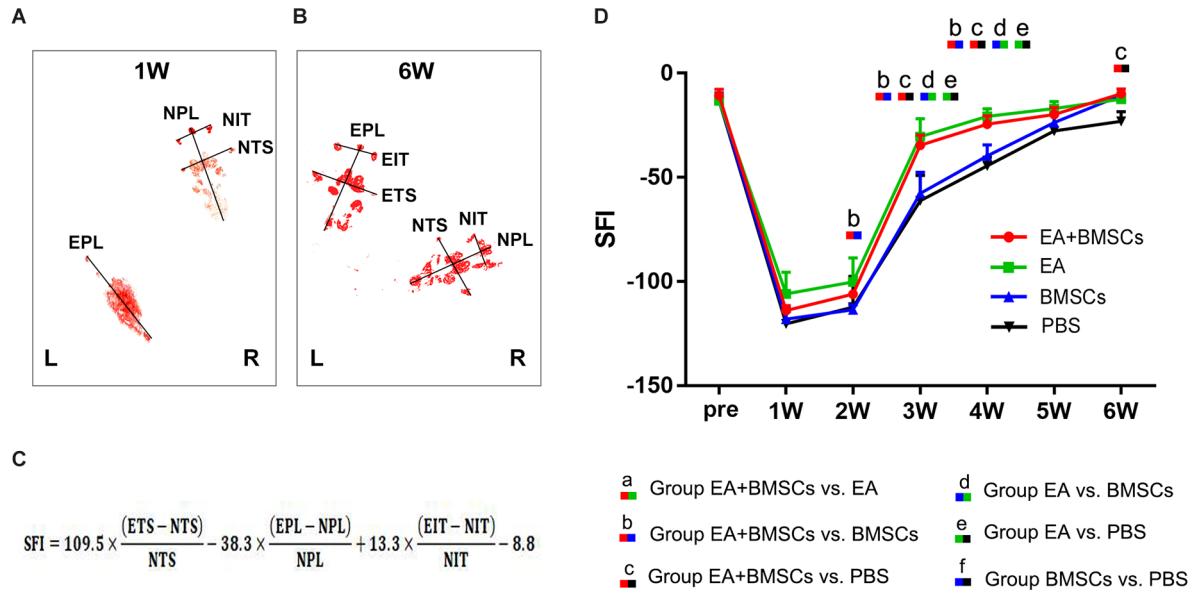

FIGURE 8
Walking track analysis of the sciatic nerve-injured rats. **(A,B)** Hind paw footprints of the EA + BMSCs subgroup at 1 and 6 weeks post-surgery. **(C)** The formula to calculate the sciatic functional index (SFI) is shown as derived by multiple linear regression (EPL, experimental print length; NPL, normal print length; ETS, experimental toe spread; NTS, normal toe spread; EIT, experimental intermediary toe spread; and NIT, normal intermediary toe spread). **(D)** Sciatic nerve function index (SFI) of the injured side compared with the uninjured contralateral side post-surgery in the four sub-groups. The SFI of acquisition points within groups were compared by using one-way ANOVA with Bonferroni *post-hoc* testing, and statistically significant differences are listed in Table 5.

TABLE 5 SFI values in EA + BMSCs, EA, BMSCs, and PBS (mean ± SD).

MRI	Time points (weeks)	EA + BMSCs	EA	BMSCs	PBS	$P \leq 0.008$
SFI	Pre	−10.70 ± 3.07	−13.17 ± 3.16	−12.59 ± 3.15	−13.12 ± 3.00	-
	1	−113.97 ± 2.06	−105.9 ± 10.43	−118.10 ± 5.91	−120.33 ± 5.95	-
	2	−106.08 ± 1.35	−100.20 ± 11.55	−113.52 ± 2.42	−112.33 ± 14.80	b
	3	−34.57 ± 4.92	−30.38 ± 8.72	57.69 ± 10.11	−61.13 ± 12.23	bcde
	4	−24.50 ± 4.08	−20.75 ± 3.66	−39.72 ± 5.29	−44.47 ± 4.21	bcde
	5	−19.85 ± 3.39	−16.88 ± 3.47	−23.66 ± 3.67	−27.68 ± 8.26	-
	6	−9.79 ± 2.32	−12.41 ± 2.68	−10.62 ± 1.33	−23.06 ± 4.62	c

SFI, sciatic functional index; EA, electroacupuncture; BMSCs, bone mesenchymal stem cells; SD, standard deviation; MRI, magnetic resonance imaging. $P \leq 0.008$, *post-hoc* analysis with Bonferroni correction. Statistically significant difference between: [a]Group EA + BMSCs vs. EA. [b]Group EA + BMSCs vs. BMSCs. [c]Group EA + BMSCs vs. PBS. [d]Group EA vs. BMSCs. [e]Group EA vs. PBS. [f]Group BMSCs vs. PBS.

TABLE 6 Correlation coefficient between MRI and histological indexes of the distal stumps of injured nerves.

	FA	RD	AD	ADC	T2
POAA	0.974	−0.973	0.913	−0.612	−0.901
	(0.000)	(0.000)	(0.000)	(0.004)	(0.000)
POMA	0.970	−0.983	0.929	−0.492	−0.920
	(0.000)	(0.000)	(0.000)	(0.027)	(0.000)
POMDA	−0.989	0.978	−0.872	0.912	0.985
	(0.000)	(0.000)	(0.000)	(0.000)	(0.000)
TOM	0.901	−0.928	0.908	−0.430	−0.750
	(0.000)	(0.000)	(0.000)	(0.059)	(0.000)
DOMF	0.921	−0.945	0.911	−0.463	−0.797
	(0.000)	(0.000)	(0.000)	(0.040)	(0.000)
SFI	0.960	−0.968	0.868	−0.838	−0.955
	(0.000)	(0.000)	(0.000)	(0.000)	(0.000)

In the four subgroups, there is a good correlation between the T2, FA, fractional anisotropy; RD, radial diffusivity; AD, axial diffusion; ADC, apparent diffusion coefficient; POAA, values of the distal segments of injured nerves with the percentage of axonal area; POMA, percentage of myelin area; POMDA, percentage of myelin debris area; TOM, thickness of myelin; DOMF, diameter of myelinated fibers; and SFI, sciatic functional index.

To summarize, our findings indicated that BMSCs combined with EA treatment provided a good treatment option for peripheral nerve repair. EA treatment promotes the orderly regeneration of nerves and enhances the therapeutic effect of stem cells. Multiparametric MRI, including T2-mapping and DTI, was used to monitor the extent of nerve regeneration dynamically and evaluate *in vivo* different therapeutic effects.

Data availability statement

The original contributions presented in the study are included in the article, further inquiries can be directed to the corresponding author.

Ethics statement

The animal study was reviewed and approved by Animal Care and Use Committee of Jennio Biotech Co., Ltd.

Author contributions

YC: data collection and analysis, experiment design, and writing of the manuscript. ZP: statistical analysis of data and creation of statistical charts. FM: rat MRI scan, sequence optimization, and technical assistance. QX: pathological staining and analysis. LH: image processing. QL: MRI data acquisition. XY: pathological staining. YW: discussion and revision of the manuscript. XL: full access to all the data in the study and responsible for the integrity of the data and the accuracy of the data analysis. All authors contributed to the article and approved the submitted version.

Funding

This research was supported by the National Natural Science Foundation of China (Grant Code: 81903960) and the Natural Science Foundation of Guangdong Province (Grant Code: 2020A1515010732).

Conflict of interest

YW was employed by Siemens Healthcare (China).

The remaining authors declare that the research was conducted in the absence of any commercial or financial relationships that could be construed as a potential conflict of interest.

Publisher's note

All claims expressed in this article are solely those of the authors and do not necessarily represent those of their affiliated organizations, or those of the publisher, the editors and the reviewers. Any product that may be evaluated in this article, or claim that may be made by its manufacturer, is not guaranteed or endorsed by the publisher.

References

Ahn, S. M., Kim, Y. R., Shin, Y.-I., Ha, K. T., Lee, S.-Y., Shin, H. K., et al. (2019). Therapeutic potential of a combination of electroacupuncture and TrkB-expressing mesenchymal stem cells for ischemic stroke. *Mol. Neurobiol.* 56, 157–173. doi: 10.1007/s12035-018-1067-z

Ankrum, J. A., Ong, J. F., and Karp, J. M. (2014). Mesenchymal stem cells: immune evasive, not immune privileged. *Nat. Biotechnol.* 32, 252–260. doi: 10.1038/nbt.2816

Bain, J. R., Mackinnon, S. E., and Hunter, D. A. (1989). Functional evaluation of complete sciatic, peroneal, and posterior tibial nerve lesions in the rat. *Plast. Reconstr. Surg.* 83, 129–138. doi: 10.1097/00006534-198901000-00024

Breitenseher, J. B., Kranz, G., Hold, A., Berzaczy, D., Nemec, S. F., Sycha, T., et al. (2015). MR neurography of ulnar nerve entrapment at the cubital tunnel: a diffusion tensor imaging study. *Eur Radiol.* 25, 1911–1918. doi: 10.1007/s00330-015-3613-7

Chen, Y. Y., Lin, X. F., Zhang, F., Zhang, X., Hu, H. J, Wang, D. Y., et al. (2014). Diffusion tensor imaging of symptomatic nerve roots in patients with cervical disc herniation. *Acad Radiol.* 21, 338–344. doi: 10.1016/j.acra.2013.11.005

Chen, Y., Pan, Z., Meng, F., Li, Z., Hu, Y., Yu, X., et al. (2022). Performance of single-shot echo-planar imaging in diffusion tensor imaging in rat sciatic nerve compared with readout-segmented echo-planar imaging. *Front. Neurosci.* 16:844408. doi: 10.3389/fnins.2022.844408

Chen, P., Piao, X., and Bonaldo, P. (2015). Role of macrophages in Wallerian degeneration and axonal regeneration after peripheral nerve injury. *Acta Neuropathol.* 130, 605–618. doi: 10.1007/s00401-015-1482-4

Chen, Y.-Y., Zhang, X., Lin, X.-F., Zhang, F., Duan, X.-H., Zheng, C.-S., et al. (2017). DTI metrics can be used as biomarkers to determine the therapeutic effect of stem cells in acute peripheral nerve injury. *J. Magn. Reson. Imaging* 45, 855–862. doi: 10.1002/jmri.25395

Duan, X., Lu, L., Wang, Y., Zhang, F., Mao, J., Cao, M., et al. (2017). The long-term fate of mesenchymal stem cells labeled with magnetic resonance imaging-visible polymersomes in cerebral ischemia. *Int. J. Nanomed.* 12, 6705–6719. doi: 10.2147/IJN.S146742

Dun, X. P., and Parkinson, D. B. (2017). Role of netrin-1 signaling in nerve regeneration. *Int. J. Mol. Sci.* 18:491. doi: 10.3390/ijms18030491

Dun, X.-P., and Parkinson, D. B. (2020). Classic axon guidance molecules control correct nerve bridge tissue formation and precise axon regeneration. *Neural Regen. Res.* 15, 6–9. doi: 10.4103/1673-5374.264441

Ellezam, B., Selles-Navarro, I., Manitt, C., Kennedy, T. E., and McKerracher, L. (2001). Expression of netrin-1 and its receptors DCC and UNC-5H2 after axotomy and during regeneration of adult rat retinal ganglion cells. *Exp. Neurol.* 168, 105–115. doi: 10.1006/exnr.2000.7589

Emelyanov, A. N., Borisova, M. V., and Kiryanova, V. V. (2016). Model acupuncture point: bone marrow-derived stromal stem cells are moved by a weak electromagnetic field. *World J. Stem Cells* 8, 342–354. doi: 10.4252/wjsc.v8.i10.342

Feirabend, H. K., Choufoer, H., and Ploeger, S. (1998). Preservation and staining of myelinated nerve fibers. *Methods* 15, 123–131. doi: 10.1006/meth.1998.0615

Hu, L. N., Tian, J. X., Gao, W., Zhu, J., Mou, F. F., Ye, X. C., et al. (2018). Electroacupuncture and moxibustion promote regeneration of injured sciatic nerve through Schwann cell proliferation and nerve growth factor secretion. *Neural Regen. Res.* 13, 477–483. doi: 10.4103/1673-5374.228731

Huang, Q., Cai, Y., Zhang, X., Liu, J., Liu, Z., Li, B., et al. (2021). Aligned graphene mesh-supported double network natural hydrogel conduit loaded with netrin-1 for peripheral nerve regeneration. *ACS Appl. Mater. Interfaces* 13, 112–122. doi: 10.1021/acsami.0c16391

Jiang, W., and Xu, J. (2020). Immune modulation by mesenchymal stem cells. *Cell Prolif.* 53:e12712. doi: 10.1111/cpr.12712

Ke, X., Li, Q., Xu, L., Zhang, Y., Li, D., Ma, J., et al. (2015). Netrin-1 overexpression in bone marrow mesenchymal stem cells promotes functional recovery in a rat model of peripheral nerve injury. *J. Biomed. Res.* 29, 380–389. doi: 10.7555/JBR.29.20140076

Lavorato, A., Raimondo, S., Boido, M., Muratori, L., Durante, G., Cofano, F., et al. (2021). Mesenchymal stem cell treatment perspectives in peripheral nerve regeneration: systematic review. *Int. J. Mol. Sci.* 22:572. doi: 10.3390/ijms22020572

Lee, H. K., Seo, I. A., Seo, E., Seo, S. Y., Lee, H. J., and Park, H. T. (2007). Netrin-1 induces proliferation of Schwann cells through Unc5b receptor. *Biochem. Biophys. Res. Commun.* 362, 1057–1062. doi: 10.1016/j.bbrc.2007.08.143

Lehmann, H. C., Zhang, J., Mori, S., and Sheikh, K. A. (2010). Diffusion tensor imaging to assess axonal regeneration in peripheral nerves. *Exp. Neurol.* 223, 238–244. doi: 10.1016/j.expneurol.2009.10.012

Liao, C. D., Zhang, F., Guo, R. M., Zhong, X. M., Zhu, J., Wen, X. H., et al. (2012). Peripheral nerve repair: monitoring by using gadofluorine M-enhanced MR imaging with chitosan nerve conduits with cultured mesenchymal stem cells in rat model of neurotmesis. *Radiology* 262, 161–171. doi: 10.1148/radiol.11110911

Liu, B., Xin, W., Tan, J. R., Zhu, R. P., Li, T., Wang, D., et al. (2019). Myelin sheath structure and regeneration in peripheral nerve injury repair. *Proc. Natl. Acad. Sci. U S A* 116, 22347–22352. doi: 10.1073/pnas.1910292116

Lv, J., Sun, X., Ma, J., Ma, X., Zhang, Y., Li, F., et al. (2015). Netrin-1 induces the migration of Schwann cells via p38 MAPK and PI3K-Akt signaling pathway mediated by the UNC5B receptor. *Biochem. Biophys. Res. Commun.* 464, 263–268. doi: 10.1016/j.bbrc.2015.06.140

Madison, R. D., Zomorodi, A., and Robinson, G. A. (2000). Netrin-1 and peripheral nerve regeneration in the adult rat. *Exp. Neurol.* 161, 563–570. doi: 10.1006/exnr.1999.7292

Martín, N. T., Barousse, R., Socolovsky, M., and Luna, A. (2017). Quantitative magnetic resonance (MR) neurography for evaluation of peripheral nerves and plexus injuries. *Quant. Imaging Med. Surg.* 7, 398–421. doi: 10.21037/qims.2017.08.01

Mathot, F., Shin, A. Y., and Van Wijnen, A. J. (2019). Targeted stimulation of MSCs in peripheral nerve repair. *Gene* 710, 17–23. doi: 10.1016/j.gene.2019.02.078

Mirzakhani, N., Farshid, A. A., Tamaddonfard, E., Imani, M., Erfanparast, A., and Noroozinia, F. (2018). Carnosine improves functional recovery and structural regeneration after sciatic nerve crush injury in rats. *Life Sci.* 215, 22–30. doi: 10.1016/j.lfs.2018.10.043

Moattari, M., Kouchesfehani, H. M., Kaka, G., Sadraie, S. H., and Naghdi, M. (2018). Evaluation of nerve growth factor (NGF) treated mesenchymal stem cells for recovery in neurotmesis model of peripheral nerve injury. *J. Craniomaxillofac. Surg.* 46, 898–904. doi: 10.1016/j.jcms.2018.03.015

Perreault, T., Fernández-de-Las-Peñas, C., Cummings, M., and Gendron, B. C. (2021). Needling interventions for sciatica: choosing methods based on neuropathic pain mechanisms-a scoping review. *J. Clin. Med.* 10:2189. doi: 10.3390/jcm10102189

Salameh, S., Nouel, D., Flores, C., and Hoops, D. (2018). An optimized immunohistochemistry protocol for detecting the guidance cue Netrin-1 in neural tissue. *MethodsX* 5, 1–7. doi: 10.1016/j.mex.2017.12.001

Salazar, T. E., Richardson, M. R., Beli, E., Ripsch, M. S., George, J., Kim, Y., et al. (2017). Electroacupuncture promotes central nervous system-dependent release of mesenchymal stem cells. *Stem Cells* 35, 1303–1315. doi: 10.1002/stem.2613

Shen, J., Zhou, C. P., Zhong, X. M., Guo, R. M., Griffith, J. F., Cheng, L. N., et al. (2010). MR neurography: T1 and T2 measurements in acute peripheral nerve traction injury in rabbits. *Radiology* 254, 729–738. doi: 10.1148/radiol.09091223

Song, S.-K., Sun, S.-W., Ju, W.-K., Lin, S.-J., Cross, A. H., and Neufeld, A. H. (2003). Diffusion tensor imaging detects and differentiates axon and myelin degeneration in mouse optic nerve after retinal ischemia. *Neuroimage* 20, 1714–1722. doi: 10.1016/j.neuroimage.2003.07.005

Sullivan, R., Dailey, T., Duncan, K., Abel, N., and Borlongan, C. V. (2016). Peripheral nerve injury: stem cell therapy and peripheral nerve transfer. *Int. J. Mol. Sci.* 17:2101. doi: 10.3390/ijms17122101

Sun, Y. Y., Zhang, W. J., Dong, C. L., Zhang, X. F., Ji, J., Wang, X., et al. (2017). Baicalin alleviates nitroglycerin-induced migraine in rats via the trigeminovascular system. *Phytother. Res.* 31, 899–905. doi: 10.1002/ptr.5811

Takagi, T., Nakamura, M., Yamada, M., Hikishima, K., Momoshima, S., Fujiyoshi, K., et al. (2009). Visualization of peripheral nerve degeneration and regeneration: monitoring with diffusion tensor tractography. *Neuroimage* 44, 884–892. doi: 10.1016/j.neuroimage.2008.09.022

Webber, C. A., Christie, K. J., Cheng, C., Martinez, J. A., Singh, B., Singh, V., et al. (2011). Schwann cells direct peripheral nerve regeneration through the Netrin-1 receptors, DCC and Unc5H2. *Glia* 59, 1503–1517. doi: 10.1002/glia.21194

Wu, Q., Chen, J., Yue, J., Ying, X., Zhou, Y., Chen, X., et al. (2021). Electroacupuncture improves neuronal plasticity through the A2AR/cAMP/PKA signaling pathway in SNL rats. *Neurochem. Int.* 145:104983. doi: 10.1016/j.neuint.2021.104983

Yu, F. T., Liu, C. Z., Ni, G. X., Cai, G. W., Liu, Z. S., Zhou, X. Q., et al. (2022). Acupuncture for chronic sciatica: protocol for a multicenter randomised controlled trial. *BMJ Open* 12:e054566. doi: 10.1136/bmjopen-2021-054566

Yu, Z., Xu, N., Zhang, N., Xiong, Y., Wang, Z., Liang, S., et al. (2019). Repair of peripheral nerve sensory impairments via the transplantation of bone marrow neural tissue-committed stem cell-derived sensory neurons. *Cell. Mol. Neurobiol.* 39, 341–353. doi: 10.1007/s10571-019-00650-2

Zhang, X., Zhang, F., Lu, L., Li, H., Wen, X., and Shen, J. (2014). MR imaging and T2 measurements in peripheral nerve repair with activation of toll-like receptor 4 of neurotmesis. *Eur. Radiol.* 24, 1145–1152. doi: 10.1007/s00330-014-3134-9

Zheng, C., Yang, Z., Chen, S., Zhang, F., Rao, Z., Zhao, C., et al. (2021). Nanofibrous nerve guidance conduits decorated with decellularized matrix hydrogel facilitate peripheral nerve injury repair. *Theranostics* 11, 2917–2931. doi: 10.7150/thno.50825

Zheng, C.-S., Zhang, X., Chen, Y.-Y., Zhang, F., Duan, X.-H., Chen, M.-W., et al. (2018). Assessment of the synergic effect of immunomodulation on nerve repair using multiparametric magnetic resonance imaging. *Muscle Nerve* 57, E38–E45. doi: 10.1002/mus.25674

Frontiers in
Cellular Neuroscience

Leading research in cellular mechanisms underlying brain function and development

Part of the world's most cited neuroscience journal series that advances our understanding of the cellular mechanisms underlying cell function in the nervous system across all species.

Discover the latest Research Topics

See more →

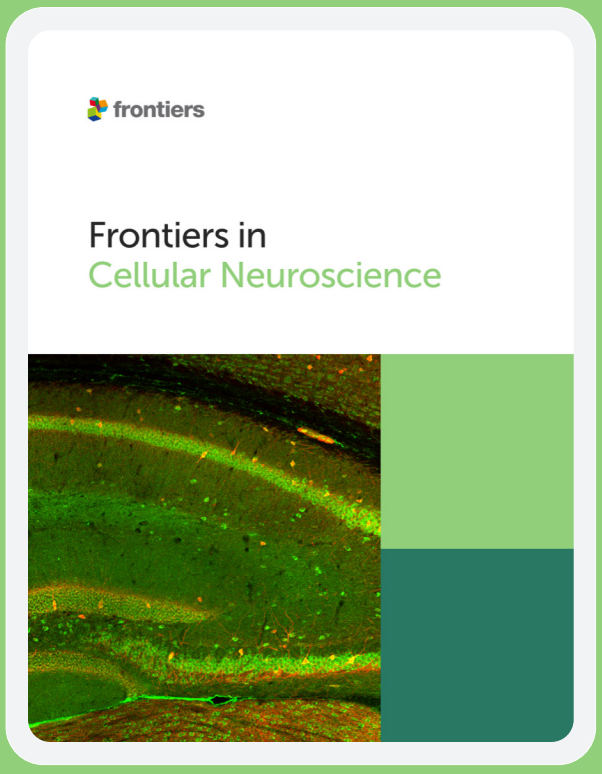

Frontiers

Avenue du Tribunal-Fédéral 34
1005 Lausanne, Switzerland
frontiersin.org

Contact us

+41 (0)21 510 17 00
frontiersin.org/about/contact